INTERACTION PHENOMENA IN COMPOSITE BEAMS AND PLATES

Thesis presented for the Degree of Ph.D.(Engineering)
in the University of London

- by -

Sailadhar Gogoi, B.E., D.I.C.

Imperial College of Science and Technology,
London

February 1964

ABSTRACT

Interaction Phenomena in Composite Beams and Plates

The thesis deals with the interaction between steel and concrete in composite beams and plates; stud shear connectors were used with varying degrees of roughness at the interface.

Methods are presented for calculating the interface shear in T-beams and plated beams for incomplete interaction in the elastic stage and for complete interaction in the elasto-plastic stage. An attempt has been made to obtain the interface shear in a composite plate for incomplete interaction. A method based on the yield line concept of failure is presented for obtaining the total interface shear in a composite plate for complete interaction. A theoretical analysis giving the pressure distribution on stud shear connectors is presented. An attempt has been made to explain the uplift phenomenon which occurs in T-beams.

Tests were carried out on small scale T-beams and plated beams with plain and roughened steel surfaces at the interface and varying numbers of connectors. A small scale composite plate (spanning in two directions) was tested to study its general behaviour. Push-out specimens, some with roughened flanges, and pull-out specimens were tested to correlate the connector behaviour with that in beams.

Correlation between theory and experiments is reasonably good. A very high degree of interaction was achieved in specimens with roughened flanges. The calculated ultimate moment was attained in T-beams with fewer connectors than required to resist the nominal total horizontal shear, but this was not the case in plated beams. The ultimate capacity of connectors obtained from beam tests agrees well with push-out results.

ACKNOWLEDGEMENTS

The work described in this thesis was carried out in the Civil Engineering Department of Imperial College under the direction of Dr. J. C. Chapman as part of the research programme into composite construction. The author is greatly indebted to Dr. Chapman for his constant guidance and valuable advice.

The author is also deeply grateful to Professor S. R. Sparkes for the opportunity to take part in this research programme.

The author wishes to thank Messrs. J. Neale, N. D. Scott and all the members of the laboratory and workshop staff for their assistance with the experimental work.

Special thanks are due to Miss G. Blake for typing the thesis, to Miss J. Gurr for taking the photographs, and to Mr. S. P. Sarna and Mr. P. Krishna for their help in tracing the drawings.

The author wishes to record his deep debt of gratitude to the Government of Assam (India) for granting him the leave and scholarship which enabled his postgraduate studies and research at the Imperial College, London.

CONTENTS

		Page
CHAPTER I:	INTRODUCTION	1
1.1	General	
1.2	A brief survey of researches on composite beams and plates	3
1.3	Objects of this investigation	9
CHAPTER II:	THEORY	
2.1	Horizontal shear at the interface in composite beams (a) Complete interaction within the elastic limit (b) Complete interaction in the elasto-plastic stage (c) Incomplete interaction within the elastic limit	11
2.2	Horizontal shear at the interface in composite plates and plated beams (a) Complete interaction within the elastic limit (b) Complete interaction at plastic collapse (c) Incomplete interaction within the elastic limit	25
2.3	Uplift	47
2.4	Embedded cantilever theory for stud shear connectors	57
CHAPTER III:	PUSH-OUT AND PULL-OUT EXPERIMENTS	
3.1	Push-out tests (a) Purpose of tests (b) Description and preparation of specimens (c) Testing procedure (d) Test results (e) Discussion of test results	65

Page

3.2 Pull-out tests 85
(a) Introduction
(b) Description and preparation of specimens
(c) Testing procedure
(d) Test results
(c) Discussion of test results

CHAPTER IV: EXPERIMENTS ON COMPOSITE BEAMS

4.1 Quarter scale composite beams 96
(a) Purpose of tests
(b) Description and preparation of specimens
(c) Loading
(d) Measurements
(e) Testing procedure
(f) Test results
(g) Discussion of test results

4.2 Half scale composite beams 125
(a) Purpose of tests
(b) Description and preparation of specimens
(c) Loading
(d) Measurements
(e) Testing procedure
(f) Test results
(g) Discussion of test results

CHAPTER V: EXPERIMENTS ON COMPOSITE PLATES

5.1 Pilot tests on plated beams 136
(a) Purpose of tests
(b) Description and preparation of specimens
(c) Loading
(d) Measurements
(e) Testing procedure
(f) Test results
(g) Discussion of test results

5.2 Plated beams 141
(a) Purpose of tests
(b) Description and preparation of specimens
(c) Loading
(d) Measurements
(e) Testing procedure
(f) Test results
(g) Discussion of results

Page

5.3 Composite plate 153
(a) Purpose of test
(b) Description and preparation of specimens
(c) Loading
(d) Measurements
(e) Testing procedure
(f) Test results
(g) Discussion of test results

CHAPTER VI: CORRELATION OF RESULTS 162

CHAPTER VII: DESIGN 190

CHAPTER VIII: CONCLUSIONS 197

APPENDIX I: Horizontal shear distribution over the depth of a section in elasto-plastic stage

APPENDIX II: Calculation of deflections in composite beams

REFERENCES

LIST OF FIGURES

LIST OF TABLES

FIGURES

TABLES

CHAPTER I

INTRODUCTION

I.1 General Introduction

Any structural member composed of two or more different materials may be termed composite. In recent years, however, the term "composite" has been applied particularly to a system of construction in which steel sections are shear connected to a concrete slab to form a composite member. In this thesis, the term "composite" is used in this restricted sense.

The merit of composite construction lies in the fact that the concrete slab, besides performing its primary function of carrying and transferring the external load to the supporting beams also acts as a part of the beam itself. This gives greater stiffness and an increased shape factor, with consequent higher permissible stresses for a given deflection limit and load factor.

A composite beam requires less steel than the corresponding non-composite steel beam, and this leads to some saving in cost. Further savings result from the reduction in depth of the beam, due to reduced column heights and vertical runs for services. With the reduction in floor heights made possible by the use of composite design, it is often possible to gain an extra floor of usable space and still keep the overall height of the building within the same limit. Alternatively a greater column spacing may be used with a composite beam than with a conventional beam of equal depth. By making composite an existing non-composite structure the allowable loading can be increased.

A major advantage of the composite plate lies in the utilisation of the steel plate as shuttering for the concrete, in addition to its being used as tensile reinforcement. Besides spanning between the stringers or main girders to form the deck slab, it may also act as the tension or compression flange of the main girder. In the case of battle-deck construction a concrete wearing surface will be utilised to stiffen the deck plate. At the expense of some increase in total weight, the deck plate could be reduced in thickness and the stringer spacing could be increased.

The composite action between beams and slabs is taken into account in reinforced concrete designs. But then, the material in the slab and the rib is the same, which makes composite action easier to achieve than in the case of steel beam and concrete slab, where there is a plane of weakness at the junction. To achieve composite action, therefore, it is necessary to strengthen this plane of weakness by some means, unless the beam is encased in concrete where natural bond may be sufficient to ensure composite action. Where the beam is not encased mechanical shear connectors are provided; these transmit the horizontal shear at the interface and prevent vertical separation. It is suggested that the performance of shear connectors can be enhanced by providing some form of roughness at the beam flange; in this event the horizontal shear might be transmitted by the roughness, but connectors would still be required to prevent vertical separation.

This thesis is primarily concerned with the mechanism of stee-concrete interaction in uncased composite beams and in composite plates.

I.2 A Brief Survey of Researches on Composite Beams and Plates

The early studies were concerned with encased beams in which the interaction between steel and concrete was provided primarily by bond. Some of the first recorded tests were made at the National Physical Laboratory in England in 1922-3 [1]. These tests were mainly on filler joist floor panels and indicated clearly that a gain in strength was obtained when the steel was embedded in concrete.

At about the same time in Canada, a series of tests was reported by Mackay, Gillespie and Leluau [2]. Later,[3] Mackay tested seven simply supported T-beams, four fully encased, two partially encased and one fully encased but with bond absent on the top flange. On the basis of these tests Mackay recommended a working bond stress of 240p.s.i. for fully encased beams.

Tests on six composite T-beams were reported in 1929 by Caughey [4]. On the basis of these tests and on the tests reported in the literature prior to 1929, Caughey concluded that "Composite beams may be designed safely on the basis of elementary principles of design", and recommended an allowable bond stress of 0.03 f'_c (f'_c = cylinder strength).

The most comprehensive experimental study of composite beams relying primarily on natural bond was reported by Batho, Lash and Kirkham [5] in 1939. Out of a total of fifteen beams, three of which could be described as reinforced concrete beams, nine had the I-beam fully encased while the other three had only the top flange encased in concrete; one of each type was provided with

mechanical connectors. The authors concluded that the theory for reinforced concrete is applicable to composite beams as long as bond is present. A lower limit of ultimate bond stress of 240 p.s.i. was accepted for a fully encased beam and with a factor of safety of four, the authors recommended an allowable bond stress of 60 p.s.i. for fully encased beam and 50 p.s.i. for partially encased beam.

V. Lapsins [6] tested four T-beams with the top flange roughened by chiseling out small projections spaced at about $\frac{1}{4}$ in. Slip between the beams and the slab was absent practically up to failure. The specimens failed abruptly by separation of the slab from the beams at loads lower than those carried by companion specimens with mechanical connectors.

Wastlund and Ostlund [7] tested three T-beams. A plain steel plate was welded to the top flange in the first, a chequered plate was welded to the top flange in the second and the third had a chequered plate with four shear connectors, welded to the top flange. The test specimens and results are summarised in Table 1. Max_m bond stress was found to be only 90 p.s.i. in the first and 334 p.s.i. and ~~556~~ 455 p.s.i. in the second and third respectively. In the second, the slab lifted from the steel after the bond broke.

The first systematic studies with mechanical connectors were made in Switzerland, with spiral shear connectors. Tests on five beams and 36 push-out specimens with spiral connectors were rported by Vollemy in 1935-6[8]. Out of these four beams were tested under repetitive loading. Spiral shear connectors were also used in tests on composite beams carried out at Columbia University [9]. Push-out

specimens with spirals, flexible angles, flexible channels and stiff H-sections were tested at Lehigh University [10]. Viest [11] tested six push-out specimens with spirals to obtain data comparable to those available for stud and channel shear connectors. Connectors made from reinforcing bars in the form of hooks or loops and stiff connectors made from rectangular bars or from rolled shapes were used by investigators in Europe.

Tests on stiff connectors made with Tees and angles welded on end, some combined with hooked bars attached to the connectors, were reported by Ros [12] in 1944. The investigation included static tests of 21 push-out specimens and two T-beams and fatigue tests of four push-out specimens and three T-beams. The author concluded that full interaction existed in the T-beams until the failure of bond; that the T-beams developed their fully plastic moments; and that good concrete and very good welds were needed when fatigue loading was involved.

Another extensive investigation of stiff connectors was reported by Graf [13],[14]. The study, including 22 push-out specimens, six T-beams and three sets of bar connectors, employed stiff connectors combined with bar anchorages. Connectors were either square bars or flat bars welded across the flange. All specimens failed by crushing of concrete behind the connectors at pressures equal to between 1.7 and 3.2 times the cube-strength of concrete. Similar connectors were used by Fuchs [15] in his tests of two double T-beams with prestressed slab. Very good interaction between the slab and the steel was observed up to the failure.

Tests on channel and angle connectors were first reported in 1943, carried out in Lehigh University [10]. Two extensive investigations of channel shear connectors were carried out at the University of Illinois in the 1940's. The first study [16] included static tests of 64 push-out specimens, static tests of three T-beams and fatigue tests of 85 T-beams. All specimens were small scale models. The second study [17] included four T-beams and 43 push-out specimens. It was found that in all but two beams, the slip was very small. The fully plastic flexural capacity was reached in all but two beams, where the shear connection was very weak. In a few T-beams the bond between the slab and the beam was effective during a part or even full duration of the repeated load tests. The fatigue strength of these beams was increased appreciably over that of the beams without bond.

Studies of stud shear connectors began in 1954. Static and fatigue tests of push-out specimens using headed studs of diameters ranging from $\frac{1}{2}$ in. to $1\frac{1}{4}$ in. were carried out in Illinois University [18],[19],[20]. Fatigue and static test of a double T-beam using $\frac{1}{2}$ in. diameter bent and $\frac{3}{4}$ in. diameter headed studs was reported by Thürlimann [21]. Static and fatigue tests of push-out specimens for studs of the types used in the test of a double T-beam were also reported by Thürlimann [22].

Tests on composite beams with bent and headed stud shear connectors along with push-out tests were carried out in Lehigh University [23],[24],[25],[26]. The programme included the study of (a) interaction created by bond and friction alone; (b) influence of slip on ultimate strength of beams; (c) strength and spacing of connectors and (d) the feasibility of designing continuous composite beams by the ultimate load method. Two point loads were used in most of the tests and the spacing between the loads was increased until failure of the connectors occurred.

Investigation into composite beams and shear connectors was carried out in Imperial College by Wong [27], Adekola [28] and Balakrishnan [29]. Wong tested 14 push-out specimens using $\frac{7}{8}$ in. diameter plain and headed studs; the main variation was in the number of connectors per flange. A T-beam with a larger bottom flange and $\frac{7}{8}$ in. diameter headed studs was tested under a central point load.

Thirty-five small scale push-out specimens using plain and headed studs, vertical and splayed bent studs and idealised tension studs were tested by Adekola. The variations were in the diameter, pitch and number of connectors per flange. Thirteen small scale T-beams, three of which were encased, were tested with varying numbers of studs. Three T-beams using castella beams were also tested. $\frac{3}{16}$ in. diameter studs bent or headed with a central point load were used for all these beams.

Twelve push-out specimens using T-connectors with holding-down hoops, $\frac{3}{4}$ in. and $\frac{1}{2}$ in. diameter headed studs of different lengths and $\frac{3}{4}$ in. diameter bent studs 4.75 in. long were tested by Balakrishnan. Four small scale push-out tests using $\frac{3}{16}$ in. diameter bent and headed studs were also carried out. Tests on seventeen full scale T-beams, twelve of which were under a central point load and the rest under an approximate uniformly distributed load were carried out in this investigation. Different parameters used in these beam tests were (a) type of connectors namely, T-connectors, bent and headed studs; (b) length and diameter of studs; (c) number of connectors and (d) distribution of connectors (triangular or uniform). In addition, eleven small scale T-beams using $\frac{3}{16}$ in. diameter bent and headed studs were tested under a central point load with varying numbers of connectors.

The first investigation on plated beams was reported in 1957 by Casillas, Khachaturian and Siess [30]. The programme included tests on plated beams under point and distributed loads. Shear connectors employed were wire-meshes welded to the steel plate and headed studs of $\frac{3}{4}$ in. and $\frac{5}{8}$ in. diameters. In the beams with wire-mesh as shear connectors, failure occurred either by weld failure or by crushing of concrete behind the transverse wires or by diagonal tension after the slab had separated from the plate. Maximum bond stress was found to vary from 170 p.s.i. to about 250 p.s.i. With stud shear connectors, the plated beams mostly failed by bond shear. The bond shear at a slip of 0.0005in. varied from 69 p.s.i. to 200 p.s.i. The test specimens and the results are summarised in Table 2.

1.3 Objects of this investigation

It is evident that a good interaction between the concrete and the steel is necessary to exploit the full economy of composite construction. The degree of interaction depends mainly on the amount of slip, i.e. the relative movement between the steel and concrete and also on the separation of concrete slab from the steel, here called "uplift". The horizontal shear distribution at the interface which causes slip and also the cause and amount of uplift, therefore, need to be investigated. An adequate shear connection at the interface must then be provided, and the degree of interaction will depend on the behaviour of the shear connection.

The objects of this investigation are to study analytically:

1. The horizontal shear distribution at the interface in composite beams and plates in both elastic and plastic conditions;
2. The cause and amount of uplift and uplift force at the interface;
3. The deformation of stud shear connectors;

and to investigate experimentally:

1. The comparative behaviour of beams with stud shear connectors spaced uniformly and spaced according to the inelastic interface shear distribution at collapse;
2. The effect on interaction of the following forms of roughness at the compression flange:
   (a) triangular transverse grooves
   (b) resin bonded aggregates
   (c) Durbar plate;

3. Effect of pitch, diameter and length of studs on the general behaviour of plated beams;

4. Behaviour of plated beams with varying number of stud shear connectors;

5. Comparative behaviour of plated beam with Durbar plate and plain steel plate and also of plain steel plate with and without natural bond;

6. General behaviour of composite plate with uniform spacing of studs in either direction;

7. Comparative behaviour of threaded (with or without head) and plain headed studs in push-out and pull-out specimens;

8. Comparative push-out behaviour of plain headed studs when welded to plain and roughened plate;

9. Effect of stud length in pull-out tests;

10. The ultimate carrying capacity of stud shear connectors used in this investigation.

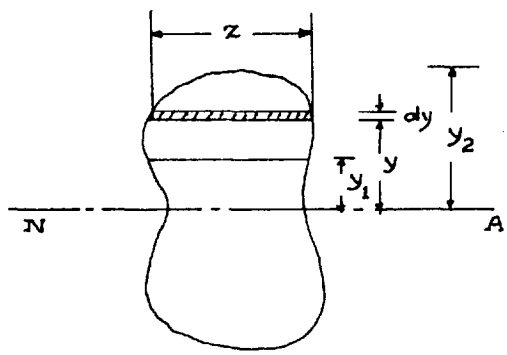
CHAPTER II

THEORY

2.1 Horizontal shear at the interface in composite beams

(a) Complete interaction within the elastic limit

The horizontal shear at the interface is calculated on the basis of an equivalent section. The moduli of elasticity, E_s, E_c, and modular ratio m are assumed to be constant; the equivalent section is obtained by dividing the slab width by m.



The horizontal shear per unit length in any plane distant y_1 from the neutral axis (figure above) is given by

$$q = \frac{V \int_{y_1}^{y_2} yz\, dy}{I}$$

$$= \frac{V M'}{I} \qquad \ldots (1)$$

where V = Total vertical shear at the section

I = Moment of inertia of the section

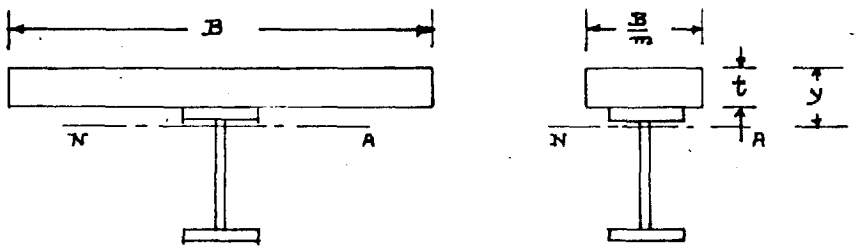
M′ = Moment of area above the plane about N.A.

q = horizontal shear per unit length.

Applying this relation to a composite section, the horizontal shear q per unit length at the interface is given by

$$q = \frac{VM'}{I_{cs}}$$

$$= \frac{V}{I_{cs}}\left[\frac{B}{m} \cdot t \cdot \left(y - \frac{t}{2}\right)\right] \qquad \ldots (2)$$



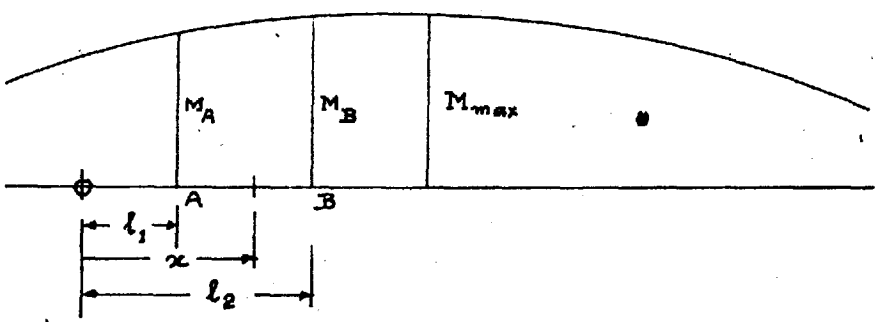
COMPOSITE SECTION EQUIVALENT SECTION

where t = thickness of slab

B = width of slab

y = distance of top surface of slab from N.A.

I_{cs} = moment of inertia of equivalent section.



The total horizontal shear at the interface between two points A and B on a beam of uniform section is given by:

$$Q = \int_{x=l_1}^{x=l_2} \frac{VM'}{I}\, dx$$

$$= \frac{M'}{I} \int_{x=l_1}^{x=l_2} V\, dx$$

$$= \frac{M'}{I} \left[M_B - M_A \right]$$

. . . (3)

where Q = total horizontal shear at the interface between B and A.

M_B and M_A are bending moments at B and A.

Also

$$Q = \frac{M'}{I} \left[M_B - M_A \right]$$

$$= \int_{y_1}^{y_2} \frac{M_B}{I}\, yz\, dy - \int_{y_1}^{y_2} \frac{M_A}{I}\, yz\, dy$$

$$= \int_{y_1}^{y_2} f_B z\, dy - \int_{y_1}^{y_2} f_A z\, dy$$

$$= F_B - F_A \qquad \text{. . . (4)}$$

where F_B = total axial force in concrete or in steel at B

F_A = total axial force in concrete or in steel at A.

(i) Complete interaction in the elasto-plastic stage

An expression for obtaining horizontal shear distribution across the depth of a section in the elasto-plastic stage is given below. The solution for this expression is given in the Appendix. Two cases are considered:

Case I: The section is of homogeneous material having a trapezoidal stress-strain curve. Horizontal shear per unit length "q" is given by

$$q = \frac{VM'_e}{I_e} \qquad \ldots (5)$$

where V = total vertical shear at the section

I_e = moment of inertia of the elastic part of the section about N.A.

M'_e = moment of the elastic area of the section above the surface under consideration about N.A.

Case II: The section is a composite section fully interconnected, composed of two materials, each having a trapezoidal stress-strain curve with different yield stresses and yield strains. Horizontal shear "q" is given by a similar expression,

$$q = \frac{VM'_{ee}}{I_{ee}} \qquad \ldots (6)$$

where V = total vertical shear at the section

I_{ee} = moment of inertia of the elastic part of the equivalent section about N.A.

M'_{ee} = moment of the elastic part of the area of the equivalent section above the surface under consideration about N.A.

It may be mentioned here that in both these cases, no horizontal shear exists in the part of the section where the material is fully plastic.

These expressions cannot be applied to a composite section of steel and concrete, as concrete has a non-linear stress-strain curve and has limited tensile strength. A numerical method, therefore, is outlined below for obtaining horizontal shear distribution at the interface of a composite beam.

It is assumed that:

1. The concrete has a stress block similar to Hognestad's stress block for concrete in compression.
2. The steel has an idealised trapezoidal stress block.
3. Concrete does not take any tension.

The first step in the calculation is to assume a strain distribution across the depth of the section. The stresses in the concrete slab and the steel beam are derived from the appropriate stress blocks and assumed strain distribution. The total tensile and compressive forces are then calculated. These forces must be equal for equilibrium. If the total tension is not equal to the total compression, another strain distribution is assumed using the first assumption as a guide. This process is repeated till the two forces are equal. Moment of resistance for the cross section is then calculated. Equating this moment of resistance to the external moment for known loading, the position of the section abng the length of the beam is obtained. Total axial force in the steel beam is then calculated. The force "F" at a particular section along the length of the beam is thus obtained.

Similar procedure is then adopted to obtain the value of the axial force F at different sections along the length of the beam. These values of F are then plotted along the length and joined by a smooth curve. The slope of this curve at any point gives the horizontal shear per unit length "q" at the interface.

Figures 5 and 6 show the variations of "F" and "q" along the length of a small scale composite beam of simple span 60 in. and subjected to a central point load P and a uniformly distributed load w respectively.

The assumed concrete and steel stress blocks and also the properties of the idealised cross-section are given in Figure 3. A concrete cylinder strength of 4000 lb./in.^{2} and a steel yield stress of 16 tons/in.^{2} are assumed.

(c) Incomplete interaction within the elastic limit

A theory for partial interaction giving slip and horizontal shear at the interface along the length of the beam was presented by Newmark. The following assumptions were made:

1). The shear connection between the slab and the I-beam is continuous and uniform along the length of the beam.

$$\text{i.e.} \quad \frac{k}{s} = \text{constant}$$

where k_c is the so-called modulus of the connector and s is the spacing between the connectors.

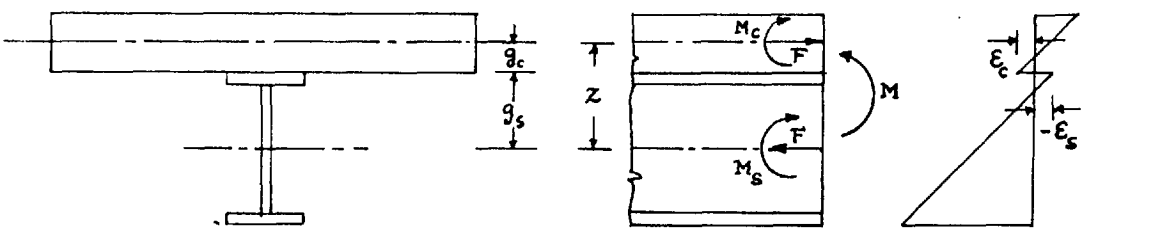
2). The amount of slip "r" permitted by the shear connection is directly proportional to the load transmitted.

$$\text{i.e.} \quad r = \frac{q}{k}$$

where q is the load transmitted by the connector.

3). The strain distributions in the slab and in the beam are respectively linear. The concrete does not crack.

4). The I-beam and the slab deflect equally at all points along the beam.



Composite T-beam with incomplete interaction

The relative movement between the slab and the beam (slip) is given by

$$r = \frac{Q}{k} = \frac{qs}{k}$$

$$= \frac{s}{k} \cdot \frac{dF}{dx}$$

$$\therefore \quad \frac{dr}{dx} = \frac{s}{k} \cdot \frac{d^2F}{dx^2} \qquad \ldots (7)$$

where q is the horizontal shear per unit length.

The rate of change of slip along the length of beam is equal to the strain difference between slab and beam at the interface.

$$\text{i.e.} \quad \frac{dr}{dx} = \varepsilon_s - \varepsilon_c \qquad \ldots (8)$$

where

$$\varepsilon_s = \frac{F}{E_s A_s} - \frac{M_s q_s}{E_s I_s} \qquad \ldots (9a)$$

$$\varepsilon_c = \frac{F}{E_c A_c} + \frac{M_c q_c}{E_c I_c} \qquad \ldots (9b)$$

From assumption (4) we have

$$\frac{M_s}{E_s I_s} = \frac{M_c}{E_c I_c} = \frac{M_s + M_c}{E_s I_s + E_c I_c} = \frac{M - Fz}{E_s I_s + E_c I_c} \qquad \ldots (10)$$

Equating (7) and (8) and substituting from equations (9) and (10) and then rearranging, we have

$$\frac{d^2F}{dx^2} - F \cdot \frac{k}{s} \cdot \frac{\overline{EI}}{\overline{EA}\ \sum EI} = -\frac{k}{s} \cdot \frac{Mz}{\sum EI} \qquad \ldots (11)$$

where

$$\sum EI = E_s I_s + E_c I_c$$

$$\overline{EI} = \sum EI + \overline{EA}\, z^2$$

$$\frac{1}{\overline{EA}} = \frac{1}{E_s A_s} + \frac{1}{E_c A_c}$$

E_s, E_c, I_s, I_c and A_s, A_c are the elastic moduli, moments of inertia and areas of cross-section of steel and concrete respectively

Solution of the above equation with an appropriate expression for bending moment M, and appropriate boundary conditions, gives F, from which q, r and ε at any section can be obtained.

(i) Point Load

This solution is due to Newmark and is as follows. For a concentrated load P acting on a simply supported beam of span L at a distance u from the left support, the boundary conditions are:

$$\text{at } x = 0 \quad F_L = 0$$
$$\text{at } x = L \quad F_R = 0$$
$$\text{at } x = u \quad F_L = F_R \text{ and } \frac{dF_L}{dx} = \frac{dF_R}{dx}$$

where F_L and F_R are the axial forces in the beam to the left and right of the point load.

Substituting the appropriate expressions for the bending moments in equation (11) and solving for F_L and F_R, we have

For $x < u$

$$F_L = \frac{\overline{EA}\,z}{\overline{EI}} \cdot PL\left\{\left(1-\frac{u}{L}\right) - \frac{\sqrt{c}}{\pi} \cdot \frac{\sinh\left[\frac{\pi}{\sqrt{c}}\left(1-\frac{u}{L}\right)\right]}{\sinh\frac{\pi}{\sqrt{c}}} \cdot \sinh\left(\frac{\pi}{\sqrt{c}}\cdot\frac{x}{L}\right)\right\} \quad \ldots (12a)$$

and for $x > u$

$$F_R = \frac{\overline{EA}\,z}{\overline{EI}} \cdot PL\left\{\frac{u}{L}\left(1-\frac{x}{L}\right) - \frac{\sqrt{c}}{\pi} \cdot \frac{\sinh\left(\frac{\pi}{\sqrt{c}}\cdot\frac{u}{L}\right)}{\sinh\frac{\pi}{\sqrt{c}}} \cdot \sinh\left[\frac{\pi}{\sqrt{c}}\left(1-\frac{x}{L}\right)\right]\right\} \quad \ldots (12b)$$

where $$C = \frac{s}{k} \cdot \frac{\pi^2\,\overline{EA}\,\sum EI}{L^2\,\overline{EI}}$$

and for $x < u$

$$q_L = \frac{dF_L}{dx} = \frac{\overline{EA}\,z}{\overline{EI}} P\left\{\left(1-\frac{u}{L}\right) - \frac{\sinh\left[\frac{\pi}{\sqrt{c}}\left(1-\frac{u}{L}\right)\right]}{\sinh\frac{\pi}{\sqrt{c}}} \cosh\left(\frac{\pi}{\sqrt{c}}\,\frac{x}{L}\right)\right\} \quad \ldots (13a)$$

and for $x > u$

$$q_R = \frac{dF_R}{dx} = \frac{\overline{EA}\,z}{\overline{EI}} p\left\{-\frac{u}{L} + \frac{\sinh\left(\frac{\pi}{\sqrt{c}}\cdot\frac{u}{L}\right)}{\sinh\frac{\pi}{\sqrt{c}}}\cosh\left[\frac{\pi}{\sqrt{c}}\left(1-\frac{x}{L}\right)\right]\right\} \quad \ldots (13b)$$

Slip at any point is:

For $x < u$ $\qquad r_L = \frac{s}{k}\cdot q_L$

For $x > u$ $\qquad r_R = \frac{s}{k}\cdot q_R$

(ii) Uniformly distributed load

This solution is given by Adekola [28] and is as follows. For a simply supported composite beam of span L with uniformly spaced shear connectors and subjected to uniformly distributed load "w", the boundary conditions are:

at $x = 0$ $\quad F = 0$

at $x = L$ $\quad F = 0.$

Substituting the appropriate expression for the bending moment in equation (11) and solving for F, we have

$$F = \frac{\overline{EA}\,z}{\overline{EI}}\cdot wL^2\left[\frac{c}{\pi^2}\cdot\cosh\frac{\pi x}{\sqrt{c}L} + \frac{c}{\pi^2}\cdot\frac{\left(1-\cosh\frac{\pi}{\sqrt{c}}\right)}{\sinh\frac{\pi}{\sqrt{c}}}\cdot\sinh\frac{\pi x}{\sqrt{c}L} - \frac{1}{2}\left(\frac{x}{L}\right)^2 + \frac{1}{2}\left(\frac{x}{L}\right) - \frac{c}{\pi^2}\right] \quad \ldots (14)$$

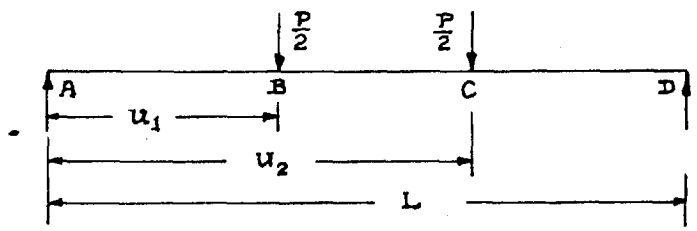
and

$$q = \frac{dF}{dx} = \frac{\overline{EA}\,z}{\overline{EI}}\cdot wL\left[\frac{\sqrt{c}}{\pi}\cdot\sinh\frac{\pi x}{\sqrt{c}L} - \frac{\sqrt{c}}{\pi}\tanh\frac{\pi}{2\sqrt{c}}\cosh\frac{\pi x}{\sqrt{c}L} - \frac{x}{L} + \frac{1}{2}\right] \quad \ldots (15)$$

Figures 7a and 7b show respectively the interface shear distribution for a point load P at midspan and for uniformly distributed load "w" over the entire span. The beam is the quarter scale composite beam with studs designed at 100% of the ultimate capacity. Spacing of connectors is 2.73in. in pairs and the connector modulus is assumed to be 200 tons per in.

(iii) Two point loads

For a composite beam of simple span L subjected to two point loads of equal magnitude at distances u_1 and u_2 from the left hand support, the axial force can be obtained from equation (12) using the method of superimposition.



If F_L, F_C, and F_R are the axial forces for lengths A-B, B-C and C-D respectively (fig. above), then by superimposition, and using equation (12), we have

for $x < u_1$

$$F_L = \frac{\overline{EA}\,z}{\overline{EI}} \cdot \frac{PL}{2}\left[\left(2 - \frac{u_1+u_2}{L}\right)\frac{x}{L} - \frac{\sinh\frac{\pi}{\sqrt{c}}\frac{x}{L}}{\frac{\pi}{\sqrt{c}}\sinh\frac{\pi}{\sqrt{c}}}\left\{\sinh\frac{\pi}{\sqrt{c}}\left(1-\frac{u_1}{L}\right) + \sinh\frac{\pi}{\sqrt{c}}\left(1-\frac{u_2}{L}\right)\right\}\right] \quad \ldots \text{(16a)}$$

for $u_1 < x < u_2$

$$F_C = \frac{\overline{EA}\,z}{\overline{EI}} \cdot \frac{PL}{2}\left[\frac{u_1}{L} + \left(1-\frac{u_1+u_2}{L}\right)\frac{x}{L} - \frac{1}{\frac{\pi}{\sqrt{c}}\sinh\frac{\pi}{\sqrt{c}}}\left\{\sinh\frac{\pi u_1}{\sqrt{c}\,L}\cdot\sinh\frac{\pi}{\sqrt{c}}\left(1-\frac{x}{L}\right) + \sinh\frac{\pi}{\sqrt{c}}\left(1-\frac{u_2}{L}\right)\cdot\sinh\frac{\pi x}{\sqrt{c}\,L}\right\}\right] \quad \ldots \text{(16b)}$$

for $x > u_2$

$$F_R = \frac{\overline{EA}\,z}{\overline{EI}} \cdot \frac{PL}{2}\left[\frac{u_1+u_2}{L}\left(1-\frac{x}{L}\right) - \frac{\sinh\frac{\pi}{\sqrt{c}}\left(1-\frac{x}{L}\right)}{\frac{\pi}{\sqrt{c}}\sinh\frac{\pi}{\sqrt{c}}}\left\{\sinh\frac{\pi\,u_1}{\sqrt{c}\,L} + \sinh\frac{\pi\,u_2}{\sqrt{c}\,L}\right\}\right] \quad \ldots (16c)$$

In a particular case where these two loads are applied symmetrically, we have

$$u_1 = L - u_2 = u \text{ (say)}$$

and the expressions reduce to

For $x < u$

$$F_L = \frac{\overline{EA}\,z}{\overline{EI}} \cdot \frac{PL}{2}\left[\frac{x}{L} - \frac{\sinh\frac{\pi}{\sqrt{c}}\frac{x}{L}}{\frac{\pi}{\sqrt{c}}\sinh\frac{\pi}{\sqrt{c}}}\left\{\sinh\frac{\pi}{\sqrt{c}}\left(1-\frac{u}{L}\right) + \sinh\frac{\pi}{\sqrt{c}}\frac{u}{L}\right\}\right] \quad \ldots (17a)$$

For $u < x < L - u$

$$F_C = \frac{\overline{EA}\,z}{\overline{EI}} \cdot \frac{PL}{2}\left[\frac{u}{L} - \frac{\sinh\frac{\pi}{\sqrt{c}}\frac{u}{L}}{\frac{\pi}{\sqrt{c}}\sinh\frac{\pi}{\sqrt{c}}}\left\{\sinh\frac{\pi}{\sqrt{c}}\left(1-\frac{x}{L}\right) + \sinh\frac{\pi}{\sqrt{c}}\frac{x}{L}\right\}\right] \quad \ldots (17b)$$

For $x > (L - u)$

$$F_R = \frac{\overline{EA}\,z}{\overline{EI}} \cdot \frac{PL}{2}\left[\left(1-\frac{x}{L}\right) - \frac{\sinh\frac{\pi}{\sqrt{c}}\left(1-\frac{x}{L}\right)}{\frac{\pi}{\sqrt{c}}\sinh\frac{\pi}{\sqrt{c}}}\left\{\sinh\frac{\pi}{\sqrt{c}}\frac{u}{L} + \sinh\frac{\pi}{\sqrt{c}}\left(1-\frac{u}{L}\right)\right\}\right] \quad \ldots (17c)$$

and for $x < u$

$$q_L = \frac{\overline{EA}\,z}{\overline{EI}} \cdot \frac{P}{2}\left[1 - \frac{\cosh\frac{\pi}{\sqrt{c}}\frac{x}{L}}{\sinh\frac{\pi}{\sqrt{c}}}\left\{\sinh\frac{\pi}{\sqrt{c}}\left(1-\frac{u}{L}\right) + \sinh\frac{\pi}{\sqrt{c}}\frac{u}{L}\right\}\right] \quad \ldots (18a)$$

for $u < x < (L - u)$

$$q_c = \frac{\overline{EA}\, z}{\overline{EI}} \cdot \frac{P}{2}\left[\frac{\sinh \frac{\pi}{\sqrt{c}} \frac{u}{L}}{\sinh \frac{\pi}{\sqrt{c}}}\left\{\cosh \frac{\pi}{\sqrt{c}}\left(1-\frac{x}{L}\right) - \cosh \frac{\pi}{\sqrt{c}} \frac{x}{L}\right\}\right]$$

. . . (18b)

for $x > (L - u)$

$$q_R = \frac{\overline{EA}\, z}{\overline{EI}} \cdot \frac{P}{2}\left[-1 + \frac{\cosh \frac{\pi}{\sqrt{c}}\left(1-\frac{x}{L}\right)}{\sinh \frac{\pi}{\sqrt{c}}}\left\{\sinh \frac{\pi}{\sqrt{c}} \frac{u}{L} + \sinh \frac{\pi}{\sqrt{c}}\left(1-\frac{u}{L}\right)\right\}\right]$$

. . . (18c)

Figure 8 shows the calculated interface shear distribution for the quarter scale composite beam with studs designed at 100% ultimate capacity, subjected to two symmetrical point loads. It is seen that even though there is no external vertical shear in the central zone, there is interface horizontal shear. The slope of the interface shear curve at midspan, however, decreases as the two loads move further apart.

An expression for strain difference at the interface can be obtained from equations (7), (8) and (18). In the central zone of the composite beam subjected to two symmetrical point loads, we have

$$\varepsilon_s - \varepsilon_c = \frac{s}{k} \frac{dq_c}{dx}$$

$$= -\frac{s}{k} \cdot \frac{\overline{EA}\, z}{\overline{EI}} \cdot \frac{P}{2L} \cdot \frac{\pi}{\sqrt{c}}\left[\frac{\sinh \frac{\pi}{\sqrt{c}} \frac{u}{L}}{\sinh \frac{\pi}{\sqrt{c}}}\left\{\sinh \frac{\pi}{\sqrt{c}}\left(1-\frac{x}{L}\right) + \sinh \frac{\pi}{\sqrt{c}} \frac{x}{L}\right\}\right]$$

. . . (19)

For $x = \frac{L}{2}$

$$\varepsilon_s - \varepsilon_c = -\frac{s}{k} \cdot \frac{\overline{EA}\, z}{\overline{EI}} \cdot \frac{P}{2L} \cdot \frac{\pi}{\sqrt{c}}\left[\frac{\sinh \frac{\pi}{\sqrt{c}} \frac{u}{L}}{\cosh \frac{\pi}{2\sqrt{c}}}\right] \quad \text{. . . (20)}$$

Using equation (20), the variation of strain difference at midspan with variation of u is shown in Figure 9. The beam used is the quarter scale composite beam with studs designed at 100 per cent of the ultimate capacity.

2.2 Horizontal shear at the interface in composite plates and plated beams

(a) Complete interaction within the elastic limit

1. Composite plate

In this analysis, the ordinary theory of flexure of plates is used to compute the deflections in the composite plate, and moments and the magnitude and direction of the resultant shear at the interface.

It is assumed that:

1. The stresses acting on any cross-section have no resultant force in the direction of the plane of the plate.
2. The plate is loaded only by forces normal to its plane
3. The plate is of constant thickness of homogeneous, elastic and isotropic material.
4. The distribution of strains is linear through the depth of the composite plate.

The following notation is used:

w = vertical deflection; taken positive downward

V_x = vertical shear per unit width on a section perpendicular to the x-axis

V_y = the same, on a section perpendicular to the y-axis

M_x = bending moment per unit width on a section perpendicular to the x-axis

M_y = the same, on a section perpendicular to the y-axis

M_{xy} = twisting moment per unit width on sections perpendicular to x and y axes

μ = Poisson's ratio

D = $\frac{EI}{1-\mu^2}$

I = equivalent moment of inertia per unit width of section

jd = lever arm of the section

On the basis of the assumptions made, the relations between the bending moments, twisting moments and deflections are:

$$M_x = -D\left(\frac{\partial^2 w}{\partial x^2} + \mu \frac{\partial^2 w}{\partial y^2}\right) \quad \ldots (18a)$$

$$M_y = -D\left(\frac{\partial^2 w}{\partial y^2} + \mu \frac{\partial^2 w}{\partial x^2}\right) \quad \ldots (18b)$$

$$M_{xy} = -M_{yx} = D(1-\mu)\frac{\partial^2 w}{\partial x\, \partial y} \quad \ldots (18c)$$

and the relations between shears and deflections are

$$V_x = -D\frac{\partial}{\partial x}\left(\frac{\partial^2 w}{\partial x^2} + \frac{\partial^2 w}{\partial y^2}\right) = \frac{\partial M_x}{\partial x} + \frac{\partial M_{yx}}{\partial y} \quad \ldots (19a)$$

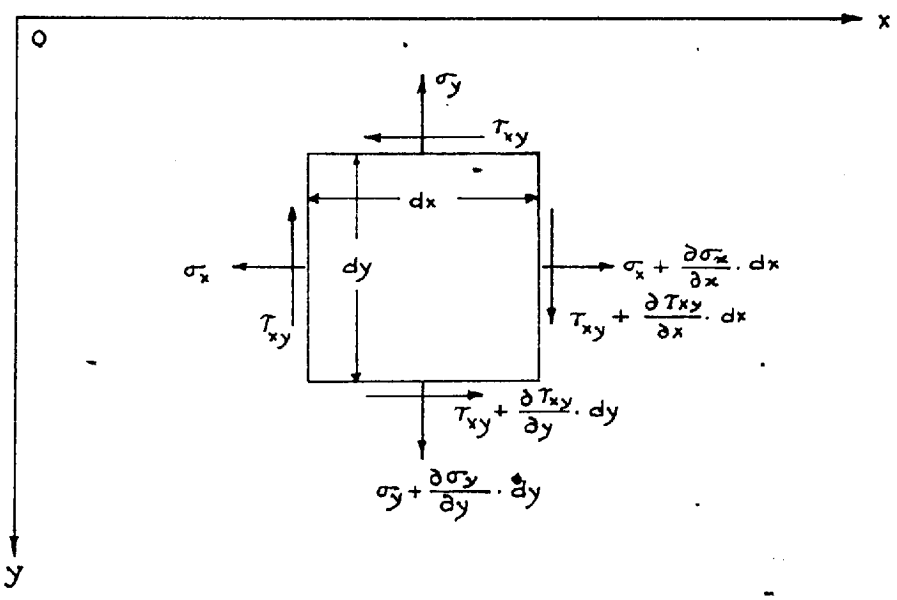
$$V_y = -D\frac{\partial}{\partial y}\left(\frac{\partial^2 w}{\partial x^2} + \frac{\partial^2 w}{\partial y^2}\right) = \frac{\partial M_y}{\partial y} + \frac{\partial M_{yx}}{\partial x} \quad \ldots (19b)$$

and the basic equation for the deflection surface is:

$$\frac{\partial^4 w}{\partial x^4} + 2\frac{\partial^4 w}{\partial x^2\, \partial y^2} + \frac{\partial^4 w}{\partial y^4} = \frac{1}{D} \cdot p(x,y) \quad \ldots (20)$$

Solution of equation (20) with appropriate expression for load distribution gives "w" from which M_x, M_y, M_{xy}, V_x, V_y, etc. can be evaluated.

In a composite plate, the horizontal shear at the interface can be related to vertical shear as follows:(30)



A rectangular element of the steel plate

Consider an element of the steel plate with dimensions dx by dy and thickness t. The stresses acting on the plate are shown in fig. above. The net normal forces in the x and y directions are:

$$\Delta F_x = \frac{\partial \sigma_x}{\partial x} \cdot dx.dy.t + \frac{\partial \tau_{xy}}{\partial y} \cdot dx.dy.t \qquad \ldots (21a)$$

$$\Delta F_y = \frac{\partial \sigma_y}{\partial y} \cdot dx.dy.t + \frac{\partial \tau_{xy}}{\partial x} \cdot dx.dy.t \qquad \ldots (21b)$$

These net forces must be transferred from the steel plate to the concrete by means of horizontal shear stresses which may be expressed as follows:

$$q_x = \frac{\Delta F_x}{dx.dy} = \left(\frac{\partial \sigma_x}{\partial x} + \frac{\partial \tau_{xy}}{\partial y} \right) t \qquad \ldots (22a)$$

$$q_y = \frac{\Delta F_y}{dx.dy} = \left(\frac{\partial \sigma_y}{\partial y} + \frac{\partial \tau_{xy}}{\partial x}\right) t \qquad \ldots (22b)$$

where q_x and q_y are horizontal shear stresses in the x and y directions respectively.

The stresses in the steel plate can also be expressed in terms of the bending moments and cross-sectional properties as follows:

$$\sigma_x = \frac{M_x}{jd.t} \qquad \ldots (23a)$$

$$\sigma_y = \frac{M_y}{jd.t} \qquad \ldots (23b)$$

$$\tau_{xy} = \frac{M_{xy}}{jd.t} \qquad \ldots (23c)$$

Substituting these expressions into the equations for q_x and q_y and observing the expressions (19a) and (19b), we have:

$$q_x = \left(\frac{\partial M_x}{\partial x} + \frac{\partial M_{xy}}{\partial y}\right) \frac{1}{jd} = \frac{V_x}{jd} \qquad \ldots (24a)$$

$$q_y = \left(\frac{\partial M_y}{\partial y} + \frac{\partial M_{xy}}{\partial x}\right) \frac{1}{jd} = \frac{V_y}{jd} \qquad \ldots (24b)$$

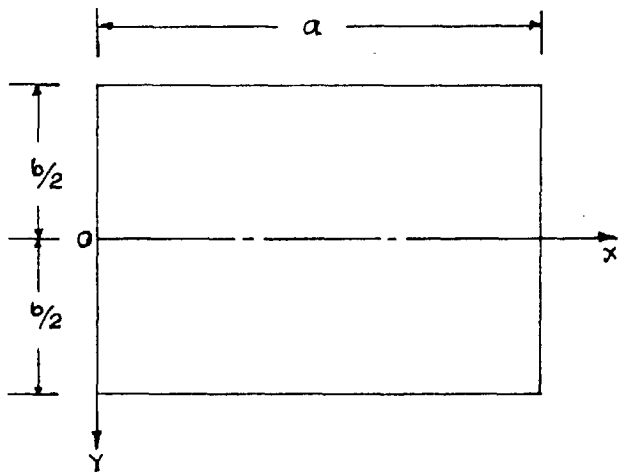
Thus it has been found that the relation between vertical and horizontal shear in the composite plate is the same as that for Reinforced Concrete beams.

The resultant horizontal shear stress at any point x, y is given by

$$q = \sqrt{q_x^2 + q_y^2} = \frac{\sqrt{V_x^2 + V_y^2}}{jd} \qquad \ldots (25)$$

(i) Simply supported rectangular composite plate

From the solution of equation (20) with appropriate expression for the intensity of load, the deflections, bending moments and shear forces can be evaluated. Levy's solution gives rapidly converging expressions for V_x and V_y for simply supported rectangular plates with uniform load of intensity p.
The expressions for w, V_x and V_y are as follows:



$$w = \frac{4pa^4}{\pi^5 D} \sum_{m=1,3,5\cdots}^{\infty} \frac{1}{m^5} \left(1 - \frac{\alpha_m \tanh \alpha_m + 2}{2 \cosh \alpha_m} \cosh \frac{2\alpha_m y}{b} + \frac{\alpha_m}{2 \cosh \alpha_m} \cdot \frac{2y}{b} \sinh \frac{2\alpha_m y}{b} \right) \sin \frac{m\pi x}{a} \quad \cdots \cdots \cdots (26)$$

$$V_x = \frac{p(a-2x)}{2} - \frac{4pa}{\pi^2} \sum_{m=1,3,5\cdots}^{\infty} \frac{\cosh \frac{m\pi y}{a}}{m^2 \cosh \alpha_m} \cdot \cos \frac{m\pi x}{a} \quad \cdots \cdots (27a)$$

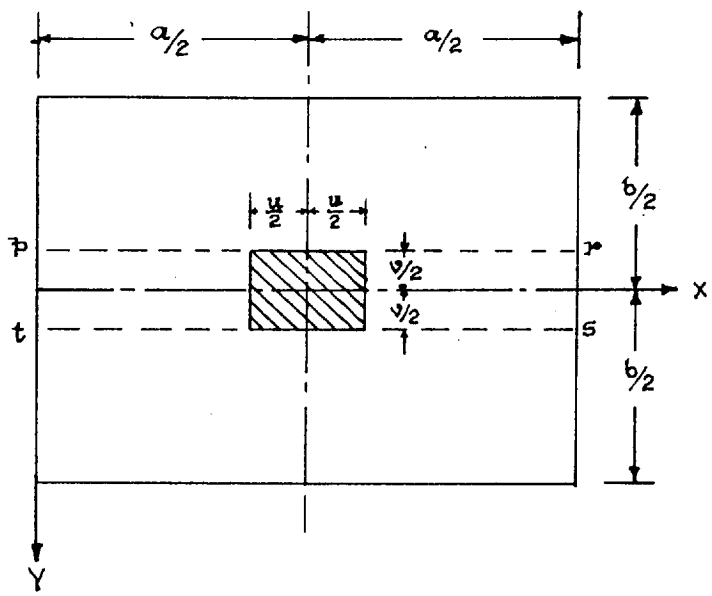
$$V_y = -\frac{4pa}{\pi^2} \sum_{m=1,3,5\cdots}^{\infty} \frac{\sinh \frac{m\pi y}{a}}{m^2 \cosh \alpha_m} \cdot \sin \frac{m\pi x}{a} \quad \cdots \cdots \cdots (27b)$$

where $\alpha_m = \frac{m\pi b}{2a}$

Figure 10 shows the distribution of q_x and q_y for a square composite plate of size a x a.

(ii) Partially loaded simply supported rectangular plate

The solution is given by Timoshenko [31]. This solution can also be applied for a point load assuming the load to be uniformly distributed over an area as shown in Figure below.



A uniform load p is distributed over the rectangle with sides u and v. The load for the portion p r s t can be represented by

$$\frac{4p}{\pi}\sum_{m=1,3,5\cdots}^{\infty}\frac{(-1)^{\frac{m-1}{2}}}{m}\sin\frac{m\pi u}{2a}\sin\frac{m\pi x}{a} \qquad \ldots (28)$$

And the expressions for w as given by Timoshenko are as follows:

For the portion prst

$$w = \sum_{m=1,3,5\cdots}^{\infty} \left(a_m + A_m \cosh \frac{m\pi y}{a} + B_m \frac{m\pi y}{a} \sinh \frac{m\pi y}{a} \right) \sin \frac{m\pi x}{a} \qquad \ldots (29a)$$

and for the portion below the line ts

$$w = \sum_{m=1,3,5\cdots}^{\infty} \left(A'_m \cosh \frac{m\pi y}{a} + B'_m \frac{m\pi y}{a} \sinh \frac{m\pi y}{a} + C'_m \sinh \frac{m\pi y}{a} + D'_m \frac{m\pi y}{a} \cosh \frac{m\pi y}{a} \right) \sin \frac{m\pi x}{a} \qquad \ldots (29b)$$

Differentiating expressions (29) and then substituting in equations (19), the shear forces V_x and V_y are obtained. These are:

For the portion prst

$$V_x = D \sum_{m=1,3,5\cdots}^{\infty} \frac{m^3\pi^3}{a^3} \left(a_m - 2 B_m \cosh \frac{m\pi y}{a} \right) \cos \frac{m\pi x}{a} \qquad \ldots (30a)$$

$$V_y = -D \sum_{m=1,3,5\cdots}^{\infty} \frac{m^3\pi^3}{a^3} \left(2 B_m \sinh \frac{m\pi y}{a} \right) \sin \frac{m\pi x}{a} \qquad \ldots (30b)$$

and for the portion below the line ts

$$V_x = -D \sum_{m=1,3,5\cdots}^{\infty} \frac{2m^3\pi^3}{a^3} \left(B'_m \cosh \frac{m\pi y}{a} + D'_m \sinh \frac{m\pi y}{a} \right) \cos \frac{m\pi x}{a} \qquad \ldots (31a)$$

$$V_y = -D \sum_{m=1,3,5\cdots}^{\infty} \frac{2m^3\pi^3}{a^3} \left(B'_m \sinh \frac{m\pi y}{a} + D'_m \cosh \frac{m\pi y}{a} \right) \sin \frac{m\pi x}{a} \qquad \ldots (31b)$$

where

$$a_m = \frac{4pa^4}{\pi^5 m^5 D}(-1)^{\frac{m-1}{2}} \sin\frac{m\pi u}{2a}$$

$$A'_m = a_m\left[\tanh\alpha_m\left(\sinh 2r_m - r_m\cosh 2r_m\right) + \alpha_m\frac{\sinh 2r_m}{2\cosh^2\alpha_m}\right]$$

$$B'_m = -\frac{a_m}{2}\tanh\alpha_m \sinh 2r_m$$

$$C'_m = a_m\left[r_m\cosh 2r_m - \sinh 2r_m\right]$$

$$D'_m = \frac{a_m}{2}\sinh 2r_m$$

$$A_m = -\frac{a_m}{\cosh\alpha_m}\left[\cosh\left(\alpha_m - 2r_m\right) + r_m\sinh\left(\alpha_m - 2r_m\right) + \alpha_m\frac{\sinh 2r_m}{2\cosh\alpha_m}\right]$$

$$B_m = \frac{a_m}{2\cosh\alpha_m}\cdot\cosh\left(\alpha_m - 2r_m\right)$$

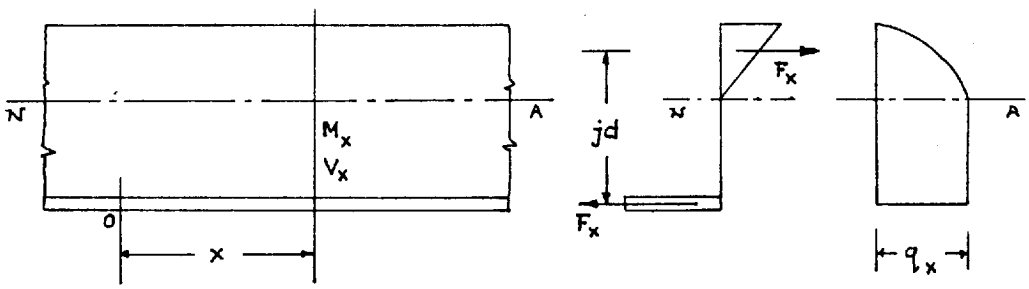
$$\alpha_m = \frac{m\pi b}{2a} \qquad r_m = \frac{m\pi v}{4a}$$

Figure 11 shows the horizontal shear distribution at the interface of a square composite plate of side "a", subjected to a central point load assumed to be distributed over an area u x u where $u = \frac{a}{11}$.

2. Plated Beams

The simple reinforced concrete beam theory is used to compute the deflection, stress distribution and horizontal shear stress at the interface between steel plate and the concrete slab.

The usual assumptions of reinforced concrete are also made here.



(a) beam (b) bending stress (c) Shear stress

Stress distributions in plated beam

Consider any section at a distance x, subjected to external moment M_x and vertical shear V_x. The total tension T or compression C are:

$$T = C = F_x = \frac{M_x}{jd} \qquad \ldots (32)$$

$$q_x = \frac{dF_x}{dx} = \frac{d}{dx}\cdot\frac{M_x}{jd} = \frac{V_x}{jd} \qquad \ldots (33)$$

and

where q is the horizontal shear per unit length at a distance x, and jd is the lever arm of the section.

The total horizontal shear at the interface between any two sections A and B is

$$Q = \int_A^B q_x\,dx = \frac{1}{jd}\left[M_B - M_A\right] = F_B - F_A \qquad \ldots (34)$$

(b) Complete interaction at plastic collapse

For calculating the number of shear connectors on an elastic basis the horizontal shear distribution at the interface must be known. This distribution can be obtained if the solution of the plate under the given load is known. In most of the cases this solution is not known, and even if it is known, the computation of horizontal shear distribution involves such numerical calculations as to render it impracticable for the design office.

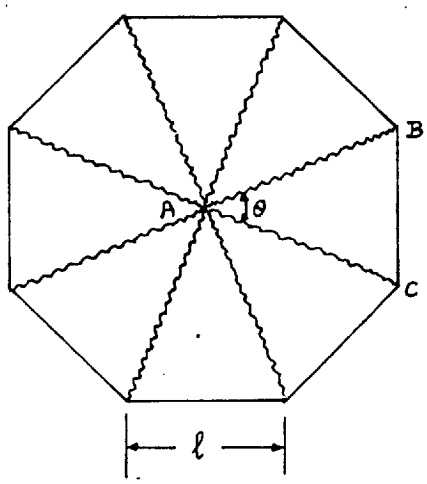
The theory which follows gives a very simple expression for the total horizontal shear to be transmitted by the shear connectors in a simply supported plate at plastic collapse. The theory is based on the yield line concept of failure of plates.

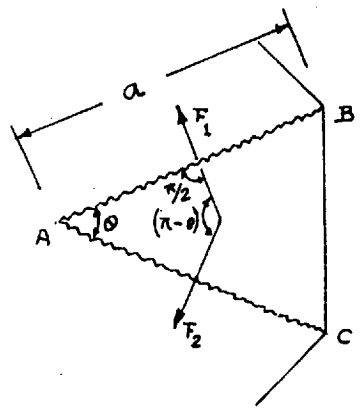
(i) Simply supported plates of regular shape subjected to uniformly distributed load

It is assumed that

1. The stresses acting on any section have no resultant force in the direction of the plane of the plate.

2. Plastic failure occurs on yield lines as shown below.





Yield lines at plastic failure of a regular simply supported plate under uniformly distributed load

Consider a composite plate of "n" sides, each side of length "l", simply supported on all sides. The yield lines at collapse are shown as above. Taking a sector ABC, the total tensile forces at AB and AC in the steel plate of thickness "t" and yield stress f_y, are:

$$F_1 = F_2 = f_y \cdot t \cdot a \qquad \ldots(35)$$

where $a = \dfrac{\ell}{2 \sin \theta/2}$

The resultant of these two forces is the total resultant horizontal shear which must be transmitted by the shear connectors in the sector.

$$\therefore \; F_R = \sqrt{F_1^2 + F_2^2 + 2 F_1 F_2 \cos(\pi - \theta)}$$

$$= 2 f_y \cdot t \cdot a \sin \frac{\theta}{2}$$

$$= f_y \cdot t \cdot \ell \qquad \ldots(36)$$

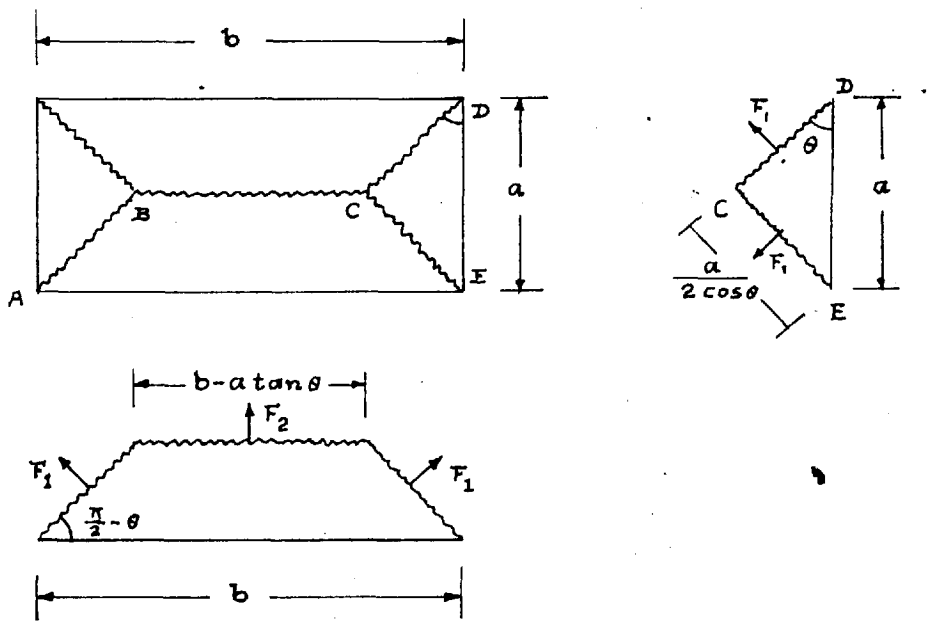
where F_R is the total horizontal shear for the sector ABC; and the total horizontal shear H at the interface is:

$$H = f_y.t.\sum l$$
$$= f_y.t.L \qquad \ldots (36a)$$

where L is the length of the boundary.

(ii) Simply supported rectangular plates subjected to uniformly distributed load

The same principle can be used for evaluating total horizontal shear at the interface at plastic collapse for a rectangular composite plate of sides a by b assuming the yield lines at failure as shown below. It should be noted that although the angle θ varies depending on the a/b ratio, the total horizontal shear H does not vary with θ.



Yield lines at plastic failure of a simply supported rectangular plate under uniformly distributed load

we have:

$$F_1 = f_y.t.\frac{a}{2\cos\theta} \quad \ldots (37a)$$

$$F_2 = f_y.t.\left(b - a\tan\theta\right) \quad \ldots (37b)$$

For the sector CDE

$$F_{R1} = \sqrt{F_1^2 + F_1^2 + 2F_1^2\cos 2\theta} = f_y.t.a \quad \ldots (38a)$$

$$F_{R2} = F_2 + \sqrt{F_1^2 + F_1^2 + 2F_1^2\cos\left(\pi - 2\theta\right)} = f_y.t.b \quad \ldots (38b)$$

$\therefore$ Total horizontal shear H =

$$H = 2\left[F_{R1} + F_{R2}\right]$$

$$= f_y.t.\ 2\left(a+b\right) = f_y.t.L \quad \ldots (39)$$

where L is the length of the boundary.

It should be noted that when the plate is not supported along the sides of length b, this length can be neglected and the expression of 'H' equals $2f_y ta$, which is the total horizontal shear for a plated beam of width a and plate thickness t.

(c) Incomplete interaction within the elastic limit

1. Composite plate

A theory for incomplete interaction giving slip and horizontal shear at the interface of a composite plate is presented below. The theory is developed in a similar way to that for a composite T-beam.

It is assumed that

(1) The shear connection between concrete slab and steel plate is continuous in both x and y directions.

i.e. $\frac{k}{s}$ = constant in both directions

(2) The amount of slip permitted by the shear connection is directly proportional to the load transmitted.

i.e. $r = \frac{Q}{k}$

(3) The strain distribution in the concrete slab and in the steel plate is linear.

(4) The twisting moments M_{xy} and M_{yx} do not produce any longitudinal strains in the x and y directions.

(5) The curvatures for the steel plate and the concrete slab are the same at all points in both the x and y directions.

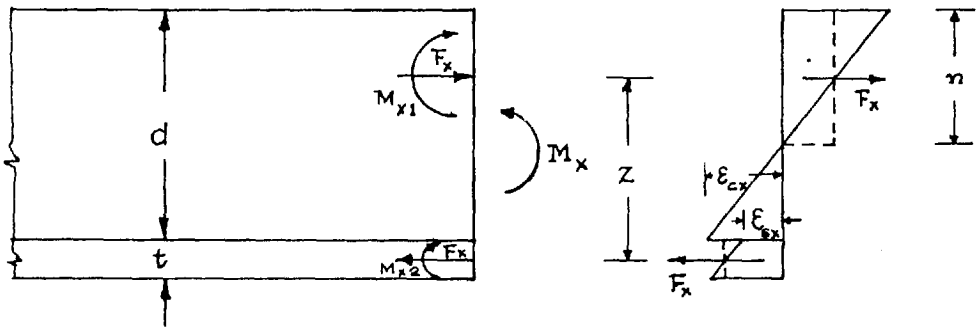
The following notation, in addition to that on page 25 is used:

F_x = total axial force either in steel plate or in concrete slab per unit width on a section perpendicular to x-axis

F_y = the same, on a section perpendicular to the y-axis

r_x and r_y = slips in the x and y directions

n = distance of neutral axis from the top of the slab.



(a) forces (b) Strain distribution

A longitudinal strip of unit width along the x-direction of a composite plate

The relative movement between concrete slab and steel plate (slip) is given by:

$$r_x = \frac{q_x s}{k} = \frac{s}{k}\frac{\partial F_x}{\partial x} \qquad \ldots (40)$$

$$\therefore \frac{\partial r_x}{\partial x} = \frac{s}{k}\cdot\frac{\partial^2 F_x}{\partial x^2} \qquad \ldots (41a)$$

Similarly,

$$\frac{\partial r_y}{\partial y} = \frac{s}{k}\cdot\frac{\partial^2 F_y}{\partial y^2} \qquad \ldots (41b)$$

where q_x and q_y are horizontal shears and r_x and r_y are slips in the x and y directions respectively.

The rate of change of slip is equal to the strain difference between concrete slab and steel plate at the interface

$$\text{i.e.} \quad \frac{\partial r_x}{\partial x} = \varepsilon_{sx} - \varepsilon_{cx} \qquad \ldots (42)$$

where

$$\varepsilon_{sx} = \frac{F_x}{E_s A_s} - \frac{\mu F_y}{E_s A_s} - \frac{M_{x2}}{E_s I_s}\cdot\frac{t}{2} + \frac{\mu M_{y2}}{E_s I_s}\cdot\frac{t}{2} \qquad \ldots (43a)$$

and

$$\varepsilon_{cx} = \left[\frac{F_x}{E_c A_c} - \frac{\mu F_y}{E_c A_c} + \frac{M_{x1}}{E_c I_c} \cdot \frac{n}{2} - \frac{\mu M_{y1}}{E_c I_c} \cdot \frac{n}{2} \right] \frac{d-n}{n} \qquad \ldots (43b)$$

where E_s and E_c are moduli of elasticity for steel and concrete respectively

I_s and I_c are respectively the moments of inertia of the steel plate per unit width, and of the concrete slab of depth n per unit width.

Substituting equations (43) and (41a) in equation 42, we have

$$\frac{\partial^2 F_x}{\partial x^2} \cdot \frac{s}{k} = F_x \left(\frac{1}{E_s A_s} - \frac{d-n}{n E_c A_c} \right) - \mu F_y \left(\frac{1}{E_s A_s} - \frac{d-n}{n E_c A_c} \right)$$

$$- \frac{d-n}{2 E_c I_c} \left(M_{x1} - \mu M_{y1} \right) - \frac{t}{2 E_s I_s} \left(M_{x2} - \mu M_{y2} \right) \qquad \ldots (44)$$

From statics,

$$M_x = M_{x1} + M_{x2} + F_x z \qquad \ldots (45a)$$

$$M_y = M_{y1} + M_{y2} + F_y z \qquad \ldots (45b)$$

From assumption (5)

$$\frac{1}{R_{xc}} = \frac{1}{R_{xs}}$$

where $\frac{1}{R_{xc}}$ and $\frac{1}{R_{xs}}$ are the curvatures of concrete slab and steel plate in the x-direction.

$$\frac{1}{R_{xc}} = \frac{M_{x1} - \mu M_{y1}}{E_c I_c} \qquad \ldots (46a)$$

$$\frac{1}{R_{xs}} = \frac{M_{x2} - \mu M_{y2}}{E_s I_s} \qquad \ldots (46b)$$

$$\therefore \quad \frac{M_{x1} - \mu M_{y1}}{E_c I_c} = \frac{M_{x2} - \mu M_{y2}}{E_s I_s} = \frac{M_{x1} + M_{x2} - \mu \left(M_{y1} + M_{y2} \right)}{E_c I_c + E_s I_s}$$

$$= \frac{\left(M_x - F_x z \right) - \mu \left(M_y - F_y z \right)}{E_c I_c + E_s I_s} \qquad \ldots (47)$$

Substituting equation (47) in equation (44) and rearranging, we have

$$\frac{\partial^2 F_x}{\partial x^2} = \left[\left(F_x - \mu F_y\right)\left\{\frac{(d-n+t)z}{2\sum EI} - \frac{d-n}{n E_c A_c} + \frac{1}{E_s A_s}\right\} - \frac{d-n+t}{2\sum EI}\left(M_x - \mu M_y\right)\right]\frac{k}{s}$$

$$= A F_x - A\mu F_y - B\left(M_x - \mu M_y\right) \qquad \ldots (48)$$

where $$A = \frac{k}{s}\left[\frac{d-n+t}{2\sum EI}\cdot z - \frac{d-n}{n E_c A_c} + \frac{1}{E_s A_s}\right]$$

$$B = \frac{d-n+t}{2\sum EI}\cdot\frac{k}{s}$$

$$\sum EI = E_c I_c + E_s I_s$$

A and B are constants and depend on the properties of the section.

Similarly it can also be shown that

$$\frac{\partial^2 F_y}{\partial y^2} = A F_y - A\mu F_x - B\left(M_y - \mu M_x\right) \qquad \ldots (49)$$

Differentiating equation (48) twice with respect to y and then substituting equation (49), we have, after rearranging

$$\frac{\partial^4 F_x}{\partial x^2 \partial y^2} - A\left(\frac{\partial^2 F_x}{\partial y^2} + \frac{\partial^2 F_x}{\partial x^2}\right) + A^2\left(1-\mu^2\right)F_x$$

$$= -B\left(\frac{\partial^2 M_x}{\partial y^2} - \mu\frac{\partial^2 M_y}{\partial y^2}\right) + AB\left(1-\mu^2\right)M_x \qquad \ldots (50a)$$

Similarly, differentiating equation (11) twice with respect to x and then substituting equation (10), we have

$$\frac{\partial^4 F_y}{\partial x^2 \partial y^2} - A\left(\frac{\partial^2 F_y}{\partial x^2} + \frac{\partial^2 F_y}{\partial y^2}\right) + A^2\left(1-\mu^2\right) F_y$$

$$= -B\left(\frac{\partial^2 M_y}{\partial x^2} - \mu \frac{\partial^2 M_x}{\partial x^2}\right) + AB\left(1-\mu^2\right) M_y$$

. . . (50b)

The solution of the equation (50) with appropriate expressions for M_x and M_y, together with appropriate boundary conditions, gives the value of axial forces F_x and F_y, from which, after differentiation, the values of q_x and q_y, the horizontal shear at the interface in the x and y directions, can be found.

There is apparently no exact solution available for equation (50), but a solution may be obtained by finite differences or by numerical integration.

2. Plated beams

The general differential equation for F_x in a plated beam for incomplete interaction can be directly obtained from that of a composite plate, by observing that, for a plated beam,

$$M_y = 0 \qquad F_y = 0$$

$$\frac{\partial M_x}{\partial y} = 0 \qquad \frac{\partial F_x}{\partial y} = 0$$

$$\mu = 0$$

and the equation (50a) reduces to

$$-A\frac{\partial^2 F_x}{\partial x^2} + A^2 F_x = AB\,M_x$$

or,

$$\frac{\partial^2 F_x}{\partial x^2} - A F_x = -B M_x \qquad \ldots (51)$$

Solution of this equation with an appropriate expression for M_x along with appropriate boundary conditions gives the value of F_x, from which q_x, the horizontal shear, can be found after differentiation.

It may be noted that the equation (51) is similar to the equation ontained by Newmark for incomplete interaction in a composite beam.

(i) Point load

For a simply supported plated beam of span L subjected to a concentrated load P at a distance u from the left support, the differential equations are:

for $x < u$

$$\frac{d^2 F_L}{dx^2} - A F_L = -BP\left(1 - \frac{u}{L}\right)x \qquad \ldots (52a)$$

for $x > u$

$$\frac{d^2 F_R}{dx^2} - A F_R = -BP\frac{u}{L}\left(L - x\right) \qquad \ldots (52b)$$

where F_L and F_R are the axial forces in the beam to the left and right of the loaded points

The differential equations can be solved for the known boundary conditions, which are:

$$\text{at } x = 0 \quad F_L = 0$$
$$\text{at } x = L \quad F_R = 0$$
$$\text{at } x = u \quad F_L = F_R \text{ and } \frac{dF_L}{dx} = \frac{dF_R}{dx}$$

The solutions for the force F are:

for $x < u$

$$F_L = \frac{B}{A} P \left[x\left(1 - \frac{u}{L}\right) - \frac{L}{\sqrt{c}} \cdot \frac{\sinh\left\{\sqrt{c}\left(1 - \frac{u}{L}\right)\right\}}{\sinh\sqrt{c}} \sinh\left(\sqrt{c}\,\frac{x}{L}\right) \right] \quad \ldots (53a)$$

for $x > u$

$$F_R = \frac{B}{A} P \left[u\left(1 - \frac{x}{L}\right) - \frac{L}{\sqrt{c}} \cdot \frac{\sinh\left(\sqrt{c}\,\frac{u}{L}\right)}{\sinh\sqrt{c}} \sinh\left\{\sqrt{c}\left(1 - \frac{x}{L}\right)\right\} \right] \quad \ldots (53b)$$

where $c = AL^2$, a dimensionless constant, introduced for convenience.

The horizontal shear per unit length:

for $x < u$

$$q_L = \frac{dF_L}{dx}$$
$$= \frac{B}{A} P \left[\left(1 - \frac{u}{L}\right) - \frac{\sinh\left\{\sqrt{c}\left(1 - \frac{u}{L}\right)\right\}}{\sinh\sqrt{c}} \cdot \cosh\left(\sqrt{c}\,\frac{x}{L}\right) \right] \quad \ldots (54a)$$

for $x > u$

$$q_R = \frac{dF_R}{dx}$$
$$= \frac{B}{A} P \left[-\frac{u}{L} + \frac{\sinh\left(\sqrt{c}\,\frac{u}{L}\right)}{\sinh\sqrt{c}} \cdot \cosh\left\{\sqrt{c}\left(1 - \frac{x}{L}\right)\right\} \right] \quad \ldots (54b)$$

(ii) Uniformly distributed load

For a simply supported plated beam of span L subjected to a uniformly distributed load "w" per unit length, the differential equation is:

$$\frac{d^2F}{dx^2} - AF = -B\left(\frac{wLx}{2} - \frac{wx^2}{2}\right) \qquad \ldots (55)$$

and the boundary conditions are:

at $x = 0$ $\quad F = 0$

at $x = L$ $\quad F = 0$

The solution of equation (55) after substituting the values of arbitrary constants evaluated from the boundary conditions is:

$$F = \frac{B}{A} wL^2\left[\frac{1}{C}\cosh\left(\sqrt{C}\,\frac{x}{L}\right) + \frac{1}{C}\cdot\frac{\left(1-\cosh\sqrt{C}\right)}{\sinh\sqrt{C}}\cdot\sinh\left(\sqrt{C}\,\frac{x}{L}\right) + \left\{\frac{1}{2}\frac{x}{L} - \frac{1}{2}\left(\frac{x}{L}\right)^2 - \frac{1}{C}\right\}\right] \qquad \ldots (56)$$

where $C = AL^2$, a dimensional constant.

Differentiating F with respect to x gives the horizontal shear per unit length:

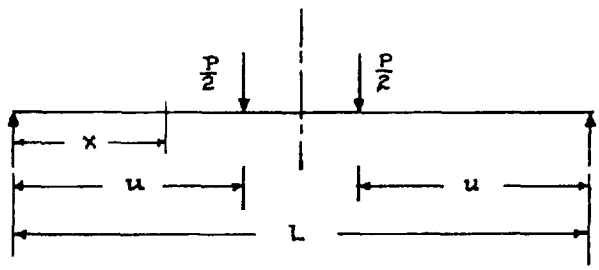
$$q = \frac{dF}{dx}$$

$$= \frac{B}{A} wL\left[\frac{1}{\sqrt{C}}\sinh\left(\sqrt{C}\,\frac{x}{L}\right) + \frac{1}{\sqrt{C}}\cdot\frac{1-\cosh\sqrt{C}}{\sinh\sqrt{C}}\cdot\cosh\left(\sqrt{C}\,\frac{x}{L}\right) + \left(\frac{1}{2} - \frac{x}{L}\right)\right] \qquad \ldots (57)$$

The figures 12a and 12b show the variation of horizontal shear along the length of plated beams subjected to a central point load and a uniformly distributed load respectively.

(iii) Two point loads

For a simply supported plated beam of span L subjected to two point loads, the horizontal shear at the interface can be obtained from equation (54), using the method of superposition.



When the two point loads are applied symmetrically about the midspan, the expression for q, the horizontal shear at the interface is as follows:

For $0 < x < u$

$$q = \frac{B}{A}\frac{P}{2}\left[1 - \frac{\cosh\sqrt{c}\left(1-\frac{2u}{L}\right)}{\cosh\frac{\sqrt{c}}{2}} \cdot \cosh\sqrt{c}\,\frac{x}{L}\right] \quad \ldots (58a)$$

For $u > x > \frac{L}{2}$

$$q = \frac{B}{A}\frac{P}{2}\left[\frac{\sinh\sqrt{c}\,\frac{u}{L}}{\cosh\frac{\sqrt{c}}{2}} \cdot \sinh\frac{\sqrt{c}}{2}\left(1-\frac{2x}{L}\right)\right] \quad \ldots (58b)$$

2.3 Uplift

An important phenomenon in composite beams is the tendency of the concrete slab to separate from the steel beam. This tendency, which will be called uplift, is associated with the slip. As the slip begins, the slab also begins to lift from the beam. Bending and axial strains in the shear connectors which are associated with the slip and uplift then develop. Uplift produces differential curvatures in the slab and the beam, and could initiate corrosion by exposing the interface to the atmosphere. The uplift forces may be quite considerable, and if the shear connectors are not sufficiently anchored, they may eventually pull out of the slab, so losing their shear carrying capacity.

Uplift may be caused by one or more of the following.

(1) As the slip begins, the natural undulations on the top of the flange, although small, force the slab to lift from the beam. This phenomenon is particularly important when the top surface of the flange is deliberately deformed to augment the bond resistance at the interface. The holding down action of the shear connectors then resists the lifting tendency, and axial forces develop in the shear connectors.

(2) With the advent of slip between the slab and the beam, there will be deformation in the shear connector and in the surrounding concrete. As the shear increases, the pressure in the concrete behind the connector, particularly at the root, also increases and local crushing of the concrete occurs. The slab then may tend to ride over the crushed portion of the concrete and so cause uplift.

(3) When a beam, supported on an elastic foundation, is subjected to a load, the distribution of re-action between the beam and the foundation depends on the 'foundation modulus' of the elastic foundation. In a composite beam, where the concrete slab is supported on the steel beam, any transmission of load from the slab to the beam takes place at the interface and the distribution of this load then depends on the foundation modulus at the interface. This foundation modulus mainly depends on the extensibility of connectors and the compressibility of concrete just underneath the connector head. This is effective only when the slab tries to separate from the beam and not when the slab tries to move down on the beam. The distribution of vertical loads at the interface due to this effect of foundation modulus is believed to be one of the reasons that cause uplift.

A theoretical approach for evaluating the last type of uplift and uplift force in a composite beam is given below. The formulation of the theory is due to Chapman [32], who used this for the interaction between a ship's hull and superstructure.

It is assumed that:

1. The concrete slab and the steel beam are two separate elements, interconnected by a cohtinuous shear connection and each element acts as an elastic foundation for the other.

2. The foundation modulus, defined as the load per unit length per unit separation, is assumed to be the same in both upward and downward directions, and is given by

$$\frac{2W}{s} \times \frac{1}{0} = \frac{w(x)}{\delta} = k_s$$

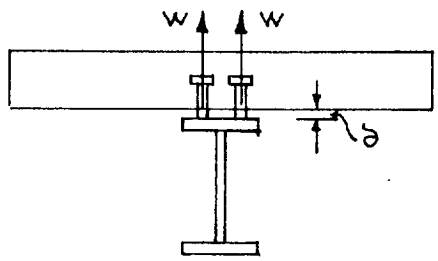
where k_s = foundation modulus

W = vertical force per connector

s = spacing of connectors

δ = separation or uplift between the slab and the beam

$w(x)$ = vertical force per unit length at the interface.

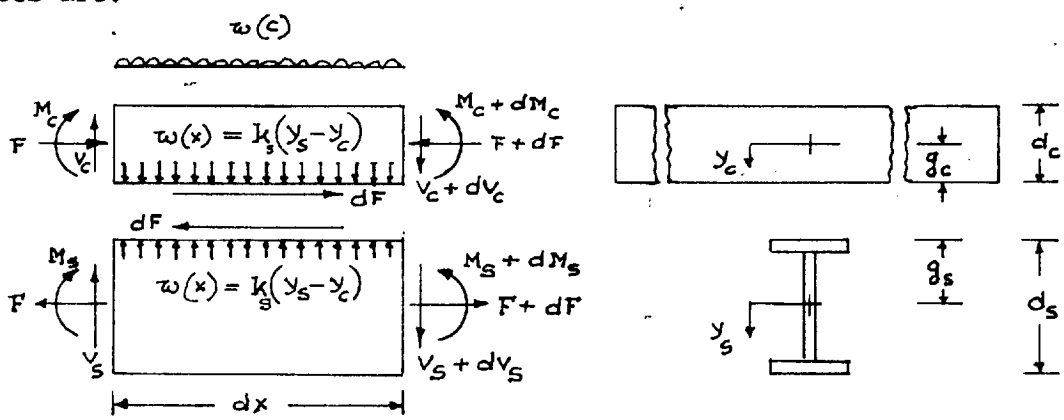


$$\text{Foundation modulus} = \frac{\frac{2W}{s}}{\delta}$$

3. For the present purpose it is assumed that full interaction exists between the slab and the beam, i.e. the strains at the bottom of the slab and at the top of the beam are equal.

4. The strain distribution across the depth of the slab and the beam are each linear.

Consider a short length of the composite beam. The internal forces are:



Forces in an element of composite beam

Considering the rotational equilibrium of the slab and neglecting the second order terms,

$$d M_c = V_c\, dx - g_c\, dF \qquad \ldots (59a)$$

Differentiating equation (59a),

$$\frac{d^2 M_c}{dx^2} = \frac{dV_c}{dx} - g_c \frac{d^2 F}{dx^2} \qquad \ldots (59b)$$

From vertical equilibrium,

$$\frac{dV_c}{dx} = -\omega(c) - \omega(x)$$
$$= -\omega(c) - k_s(y_s - y_c) \qquad \ldots (60)$$

Substituting equation (60) in equation (59b),

$$\frac{d^2 M_c}{dx^2} = -k_s(y_s - y_c) - \omega(c) - g_c \frac{d^2 F}{dx^2} \qquad \ldots (61a)$$

Similarly for the steel beam,

$$\frac{d^2 M_s}{dx^2} = +k_s(y_s - y_c) - g_s \frac{d^2 F}{dx^2} \qquad \ldots (61b)$$

From strain compatibility, i.e. assumption 3,

$$\frac{M_c}{E_c I_c} g_c - \frac{F}{E_c A_c} = -\frac{M_s}{E_s I_s} g_s + \frac{F}{E_s A_s} \qquad \ldots (62)$$

Differentiating equation, and then rearranging,

$$\frac{d^2 F}{dx^2} = A'\left[\frac{m g_c}{I_c} \cdot \frac{d^2 M_c}{dx^2} + \frac{g_s}{I_s} \cdot \frac{d^2 M_s}{dx^2}\right] \qquad \ldots (63)$$

where $$A' = \frac{A_s A_c}{m A_s + A_c}$$

$$m = \frac{E_s}{E_c} \quad , \text{ the modular ratio.}$$

Substituting equation (63) in equations (61a) and (61b), and writing $E_c I_c \frac{d^4 y_c}{dx^4}$ and $E_s I_s \frac{d^4 y_s}{dx^4}$ for $\frac{d^2 M_c}{dx^2}$ and $\frac{d^2 M_s}{dx^2}$ respectively, and then rearranging,

$$\frac{d^4 y_c}{dx^4}\left[\frac{I_c}{m} + A' g_c^2\right] - \frac{k_s}{E_s}\left(y_s - y_c\right) + A' g_c g_s \frac{d^4 y_s}{dx^4} - \frac{\omega(c)}{E_c} = 0 \qquad \ldots (64a)$$

$$\frac{d^4 y_s}{dx^4}\left[I_s + A' g_s^2\right] + \frac{k_s}{E_s}\left(y_s - y_c\right) + A' g_c g_s \frac{d^4 y_c}{dx^4} = 0 \qquad \ldots (64b)$$

Rearrangement and subraction give

$$\frac{d^4 y_s}{dx^4} - \frac{d^4 y_c}{dx^4} + \frac{k_s}{E_s}\left(\beta_c + \beta_s\right)\left(y_s - y_c\right) + \frac{\beta_c}{E_s}\omega(c) = 0 \qquad \ldots (65)$$

where $\lambda_c = \dfrac{A' g_c g_s}{\frac{I_c}{m} + A' g_c^2}$ $\qquad \lambda_s = \dfrac{A' g_c g_s}{I_s + A' g_s^2}$

$$\beta_c = \frac{1}{\frac{I_c}{m} + A' g_c^2} \cdot \frac{1 + \lambda_s}{\left(1 - \lambda_c \lambda_s\right)} \qquad \beta_s = \frac{1}{I_s + A' g_s^2} \cdot \frac{1 + \lambda_c}{\left(1 - \lambda_c \lambda_s\right)}$$

λ and β depend only on the sectional properties of the composite beam. The equation (65) can be rewritten as

$$\frac{d^4 \bar{y}}{dx^4} + \frac{\beta_c + \beta_s}{E_s} \cdot k_s \bar{y} + \frac{\beta_c}{E_s}\omega(c) = 0 \qquad \ldots (66)$$

where $\bar{y} = \left(y_s - y_c\right)$

The solution of equation (66) with appropriate boundary conditions gives $\bar{y}$, i.e. the uplift and the uplift force is obtained by multiplying $\bar{y}$ with the foundation modulus k.

The shearing forces in the slab and the beam respectively are:

$$V_c = \frac{dM_c}{dx} + g_c \frac{dF}{dx} \qquad \ldots (67a)$$

$$V_s = \frac{dM_s}{dx} + g_s \frac{dF}{dx} \qquad \ldots (67b)$$

and substituting for F, M_c and M_s leads to

$$V_c = -E_s\left(\frac{I_c}{m} + A'g_c^2\right)\left(\frac{d^3y_c}{dx^3} + \lambda_c \frac{d^3y_s}{dx^3}\right) \qquad \ldots (68a)$$

$$V_s = -E_s\left(I_s + A'g_s^2\right)\left(\frac{d^3y_s}{dx^3} + \lambda_s \frac{d^3y_c}{dx^3}\right) \qquad \ldots (68b)$$

(a) Central point load

For a composite beam of span 2L subjected to a concentrated load P at midspan, the equation (66) reduces to

$$\frac{d^4\bar{y}}{dx^4} = -\frac{\beta_c + \beta_s}{E_s} k_s \bar{y} \qquad \ldots (67)$$

The general solution of this equation is

$$\bar{y} = A \cosh ax.\ \sin ax + B \sinh ax\ \cos ax + C \cosh ax.\ \cos ax + D \sinh ax.\ \sin ax \qquad \ldots (68)$$

where $$a = \sqrt[4]{\frac{k_s(\beta_c + \beta_s)}{4E_s}}$$

Taking the origin at the midspan, by symmetry A = B = 0. Hence the general solution takes the form:

$$\bar{y} = C \cosh ax \cos ax + D \sinh ax . \sin ax \quad \ldots (69)$$

where C and D are the arbitrary constants to be evaluated from the boundary conditions.

As the slab is connected to the beam by a continuous foundation, the shear in the slab $V_c = 0$ at the support, and hence $V_s = -V$ where V is the external shear at the support.

From equations (68a) and (68b)

$$\frac{d^3 y_c}{dx^3} + \lambda_c \frac{d^3 y_s}{dx^3} = 0 \quad \ldots (70a)$$

$$\frac{d^3 y_s}{dx^3} + \lambda_s \frac{d^3 y_c}{dx^3} = - \frac{V}{E_s (I_s + A' g_s^2)} \quad \ldots (70b)$$

from which

$$\frac{d^3 \bar{y}}{dx^3} = + \frac{\beta_s}{E_s} V \quad \text{at the support.} \quad \ldots (71)$$

Hence the boundary conditions are:

at $x = L$ $\qquad \frac{d^2 \bar{y}}{dx^2} = 0$

at $x = L$ $\qquad \frac{d^3 \bar{y}}{dx^3} = \frac{\beta_s}{E_s} \frac{P}{2}$

and the arbitrary constants are

$$C = - \frac{\beta_s}{E_s} \frac{P}{2a^3} \cdot \frac{\cos aL . \cosh aL}{\sin 2aL + \sinh 2aL}$$

$$D = - \frac{\beta_s}{E_s} \frac{P}{2a^3} \cdot \frac{\sin aL . \sinh aL}{\sin 2aL + \sinh 2aL}$$

(b) Uniformly distributed load

For a simply supported composite beam of span L carrying a uniformly distributed load w per unit length, the basic equation (66) remains the same.

$$\frac{d^4\bar{y}}{dx^4} + \frac{\beta_c+\beta_s}{E_s} k_s \bar{y} + \frac{\beta_c}{E_s} w = 0$$

The general solution of this equation is

$$\bar{y} = A \cosh ax . \sin ax + B \sinh ax . \cos ax + C \cosh ax . \cos ax + D \sinh ax . \sin ax - \frac{\beta_c}{\beta_c+\beta_s} \frac{w}{k_s} \quad \ldots (72)$$

where $$a = \sqrt[4]{\frac{k_s(\beta_c+\beta_s)}{4 E_s}}$$

Taking the origin at the midspan, by symmetry A = B = 0. Hence the general solution takes the form:

$$\bar{y} = C \cosh ax . \cos ax + D \sinh ax . \sin ax - \frac{\beta_c}{\beta_c+\beta_s} \frac{w}{k_s} \quad \ldots (73)$$

where C and D are arbitrary constants to be evaluated from the boundary conditions.

From equations (68a) and (68b) and observing that $V_c = 0$ and $V_s = -V$ at the support, we have

$$\frac{d^3\bar{y}}{dx^3} = \frac{\beta_s}{E_s} wL \qquad \text{at} \quad x = L$$

Hence the boundary conditions are

$$\text{at } x = L \qquad \frac{d^2\bar{y}}{dx^2} = 0$$

$$\text{at } x = L \qquad \frac{d^3\bar{y}}{dx^3} = \frac{\beta_s}{E_s}\omega L$$

and the arbitrary constants are

$$C = -\frac{\beta_s}{E_s}\cdot\frac{\omega L}{a^3}\cdot\frac{\cos aL.\cosh aL}{\sin 2aL + \sinh 2aL}$$

$$D = -\frac{\beta_s}{E_s}\cdot\frac{\omega L}{a^3}\cdot\frac{\sin aL.\sinh aL}{\sin 2aL + \sinh 2aL}$$

The extensional modulus of a connector is obtained from pull-out tests. The foundation modulus appropriate to the beam is then derived. If K_e is the modulus of connector, s is the spacing of connectors in pairs, $w(x)$ is the uplift force per unit length, W is the uplift load per connector, and $\bar{y}$ is the uplift at any point along the beam, then the foundation modulus k_s is given by

$$k_s = \frac{w(x)}{\bar{y}} = \frac{w(x)\cdot\frac{s}{2}}{\bar{y}}\cdot\frac{2}{s}$$

$$= \frac{W}{\bar{y}}\cdot\frac{2}{s} = \frac{2K_e}{s}$$

It should be noted that this extensibility of connectors is effective only when the slab tries to move up from the beam and not when it tries to move down on the beam. However it is assumed for the present exploratory calculations that it operates in both directions.

Figure 13 shows the variation of uplift and uplift force at the interface of a full scale and a half scale composite beam respectively. For the full scale beam having $\frac{3}{4}$ in. diameter and 3in. long studs at 8.5 centres in pairs, the value of K_e is obtained from the slope of the load-separation curves in pull-out tests, and is taken to be 446 tons/inch. A proportional value of 223 tons/inch for $\frac{3}{8}$ in. diameter and $1\frac{1}{2}$ in. long studs is taken for the half scale beam.

Neglecting the steel reinforcement in the slab, the properties of the steel beam and concrete slab are:

(a) for full scale beam

A_c = 288 in.^{2} g_c = 3in. I_c = 864 in.^{4} d_c = 6in.

A_s = 13 in.^{2} g_s = 6in. I_s = 317 in.^{4} d_s = 12in.

E_c = 4.5 x 10^6 p.s.i. E_s = 13000 t.s.i. A' = 9.993 in.^{2}

λ_c = 0.819 β_c = 7.371 x 10^{-3} in.$^{-4}$

λ_s = 0.266 β_s = 3.437 x 10^{-3} in.$^{-4}$

K_e for $\frac{3}{4}$ in. stud = 446 T/in.

spacing = 8.5in. span = 2L = 216in.

(b) for half scale beam

The sectional properties are calculated from the idealised section shown in Figure 4. E_s, E_c, K_e, 2L and spacing are taken as 13,000 t.s.i., 4.5 x 10^6 p.s.i., 223 T/in., 108in. and 3.86in. respectively.

2.4 Embedded Cantilever Theory for Stud Shear Connectors

Theoretical investigation on the behaviour of stud shear connectors, carried out by earlier investigators [27],[28], was based on the assumption that the connector was embedded in an elastic medium of concrete and that deflection due to shear could be neglected; the analysis was then similar to that of a cantilever beam in elastic foundation. A study of these theoretical results shows that:

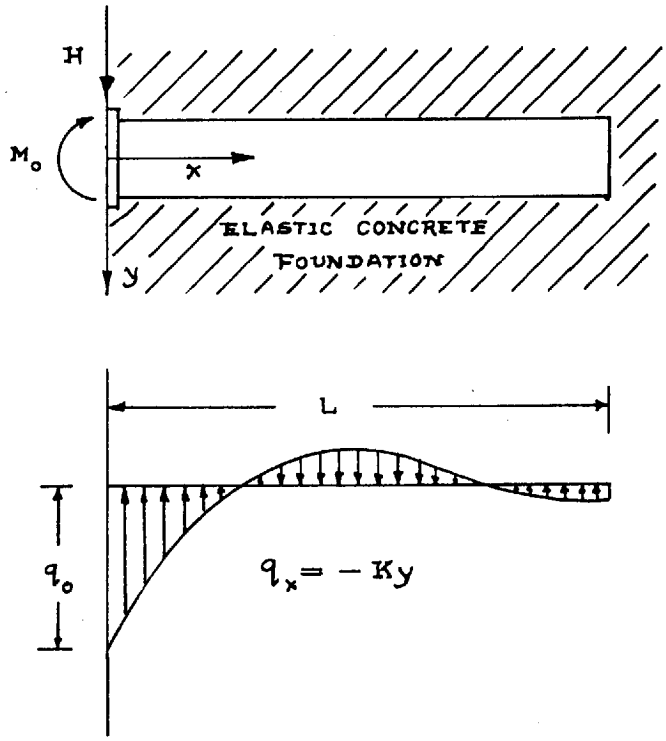
1. The bending moment distribution along the length of the stud does not agree well with the results obtained from experiments. In fact, the bending strains, measured experimentally at a height of $\frac{7}{8}$ in. from the flange in a $\frac{3}{4}$ in. diameter and 4in. long stud, is of sign opposite to that given by theory.

2. The theoretically obtained bending stress at the root of the stud is very high. For a $\frac{3}{4}$ in. diameter stud, it is about 12.0 tons per sq. in. per one ton shear. This appears to be too high considering that the ultimate capacity of a $\frac{3}{4}$ in. dia. stud is about 12.5 tons.

As the connectors are comparatively short and the shear to be resisted is very high, it was considered that the deflection due to shear might be as important as that due to bending. In the following analysis, therefore, shear deflection is taken into consideration. This analysis, otherwise, is based on similar assumptions, i.e.:

1) The stud behaves as a cantilever in the elastic foundation of concrete.

2) The foundation modulus "K", defined as the load per unit length per unit deflection is constant.



Stud connector in elastic foundation

The following notation is used:

y_s = deflection due to shear

y_m = deflection due to bending

y = $(y_s + y_m)$ = total deflection

AG = torsional rigidity of the stud

EI = flexural rigidity of the stud

K = foundation modulus

If q_x be the load per unit length on the connector at a distance x from the origin, then

$$q_x = -K(y_s + y_m) = -Ky \qquad \ldots (74)$$

The curvature at any point due to shear only:

$$\frac{d^2y_s}{dx^2} = \frac{\alpha}{AG} q_x \qquad \ldots (75)$$

Total curvature at any point distant x from origin:

$$\frac{d^2y}{dx^2} = \frac{d^2y_m}{dx^2} + \frac{d^2y_s}{dx^2} \qquad \ldots (76)$$

Substituting equations (74) and (75) in equation (76),

$$\frac{d^2y}{dx^2} = \frac{d^2y_m}{dx^2} - \frac{\alpha K}{AG} y \qquad \ldots (77)$$

Differentiating equation (77) twice with respect to x, and observing that

$$EI \frac{d^4y_m}{dx^4} = q_x = -Ky$$

we have

$$\frac{d^4y}{dx^4} = -\frac{K}{EI} y - \frac{\alpha K}{AG} \cdot \frac{d^2y}{dx^2} \qquad \ldots (78)$$

The equation can be rewritten as

$$\frac{d^4y}{dx^4} + \frac{\alpha K}{AG} \frac{d^2y}{dx^2} + \frac{K}{EI} y = 0 \qquad \ldots (79)$$

The solution of this equation with appropriate boundary conditions gives y, from which pressure distribution, shear and bending deflections, bending moments, etc., can be evaluated.

The general solution of the equation is

$$y = e^{ax}\left[A \cos bx + B \sin bx\right] + e^{-ax}\left[C \cos bx + D \sin bx\right] \qquad \ldots (80)$$

where

$$a = \sqrt[4]{\frac{K}{4EI}}\left[1 - \frac{\frac{\alpha K}{2AG}}{\sqrt{\frac{K}{EI}}}\right]^{\frac{1}{2}}$$

$$b = \sqrt[4]{\frac{K}{4EI}}\left[1 + \frac{\frac{\alpha K}{2AG}}{\sqrt{\frac{K}{EI}}}\right]^{\frac{1}{2}}$$

The boundary conditions are:

$$\text{at } x = 0 \qquad \frac{dy}{dx} = -\frac{\alpha H}{AG}$$

$$\text{at } x = 0 \qquad \frac{d^3y_m}{dx^3} = \frac{H}{EI}$$

$$\text{at } x = L \qquad \frac{d^2y_m}{dx^2} = 0$$

$$\text{at } x = L \qquad \frac{d^3y_m}{dx^3} = 0$$

The expression for $\frac{d^2y_m}{dx^2}$ is obtained by substituting y and $\frac{d^2y}{dx^2}$ from equation (80) in equation (77).

The arbitrary constants are

$$A = \frac{H}{EI}\cdot\frac{\left(1+\frac{\alpha}{AG}\sqrt{KEI}\right)}{2ab\left(a^2+b^2\right)}\left[\frac{-ab\cos bL\sinh bL - b^2\cosh aL\sinh aL + a^2\cos^2 bL + b^2\cosh^2 aL}{a\sin 2bL + b\sinh 2aL}\right.$$
$$\left. - \frac{1}{2ab}\cdot\frac{\alpha H}{AG}\left\{\frac{\frac{3\alpha K}{4AG} + 2a^2\cos^2 bL}{a\sin 2bL + b\sinh 2aL}\right\}\right]$$

$$B = \frac{H}{EI}\cdot\frac{\left(1-\frac{\alpha}{AG}\sqrt{KEI}\right)}{2ab\left(a^2+b^2\right)}\left[\frac{a^2\cos bL\sinh bL + ab\cosh aL\sinh aL + ab\cos^2 bL - ab\cosh^2 a}{a\sin 2bL + b\sinh 2aL}\right.$$
$$\left. - \frac{\alpha H}{2AG}\left\{\frac{3-2\cos^2 bL}{a\sin 2bL + b\sinh 2aL}\right\}\right]$$

$$C = \frac{H}{EI}\cdot\frac{\left(1+\frac{\alpha}{AG}\sqrt{KEI}\right)}{2ab\left(a^2+b^2\right)}\left[\frac{ab\cos bL\sinh bL + b^2\cosh aL\sinh aL + a^2\cos^2 bL + b^2\cosh^2 aL}{a\sin 2bL + b\sinh 2aL}\right.$$
$$\left. - \frac{1}{2ab}\cdot\frac{\alpha H}{AG}\left\{\frac{\frac{3\alpha K}{4AG} + 2a^2\cos^2 bL}{a\sin 2bL + b\sinh 2aL}\right\}\right]$$

$$D = \frac{H}{EI}\cdot\frac{\left(1-\frac{\alpha}{AG}\sqrt{\kappa EI}\right)}{2ab\left(a^2+b^2\right)}\left[\frac{a^2\cos bL\,\sin bL + ab\cosh aL\,\sinh aL - ab\cos^2 bL + ab\cosh^2 aL}{a\sin 2bL + b\sinh 2aL}\right.$$

$$\left. - \frac{\alpha H}{2AG}\left\{\frac{2\cos^2 bL - 3}{a\sin 2bL + b\sinh 2aL}\right\}\right]$$

The deflected shape and the bending moments are given by

$$y = e^{ax}\left\{A\cos bx + B\sin bx\right\} + e^{-ax}\left\{C\cos bx + D\sin bx\right\} \quad \ldots (80a)$$

$$EI\frac{d^2y_m}{dx^2} = EI\left[\frac{\alpha\kappa}{2AG}\cdot e^{ax}\left\{A\cos bx + B\sin bx\right\} - 2ab\cdot e^{ax}\left\{A\sin bx - B\cos bx\right\}\right.$$

$$\left. - \frac{\alpha\kappa}{2AG}\cdot e^{-ax}\left\{C\cos bx + D\sin bx\right\} + 2ab\cdot e^{-ax}\left\{C\sin bx - D\cos bx\right\}\right] \quad \ldots (81a)$$

When the deflection due to shear is neglected, the term $\frac{\alpha}{AG}$ becomes equal to zero and $a = b = \sqrt[4]{\frac{\kappa}{4EI}}$. The deflected shape and the bending moment distribution are then given by the following expressions:

$$y = e^{ax}\left\{A\cos ax + B\sin ax\right\} + e^{-ax}\left\{C\cos ax + D\sin ax\right\} \quad \ldots (80b)$$

$$EI\frac{d^2y_m}{dx^2} = -EI\,2a^2\left[e^{ax}\left\{A\sin ax - B\cos ax\right\}\right.$$

$$\left. - e^{-ax}\left\{C\sin ax - D\cos ax\right\}\right] \quad \ldots (81b)$$

The arbitrary constants are:

$$A = \frac{Ha}{K}\left[\frac{-\cos aL.\ \sin aL - \cosh aL.\ \sinh aL + \cos^2 aL + \cosh^2 aL}{\sin 2aL + \sinh 2aL}\right]$$

$$B = \frac{Ha}{K}\left[\frac{\cos aL.\ \sin aL + \cosh aL.\ \sinh aL + \cos^2 aL - \cosh^2 aL}{\sin 2aL + \sinh 2aL}\right]$$

$$C = \frac{Ha}{K}\left[\frac{\cos aL.\ \sin aL + \cosh aL.\ \sinh aL + \cosh^2 aL + \cos^2 aL}{\sin 2aL + \sinh 2aL}\right]$$

$$D = \frac{Ha}{K}\left[\frac{\cos aL.\ \sin aL + \cosh aL.\ \sinh aL - \cos^2 aL + \cosh^2 aL}{\sin 2aL + \sinh 2aL}\right]$$

At the welded end of the stud (i.e. $x = 0$), the deflection is

(a) Considering shear deflection

$$y_o = \frac{H}{EI}\cdot\frac{1+\frac{\alpha}{AG}\sqrt{KEI}}{ab\,(a^2+b^2)}\left[\frac{a^2\cos^2 bL + b^2\cosh^2 aL}{a\sin 2bL + b\sinh 2aL}\right] - \frac{1}{ab}\cdot\frac{\alpha H}{AG}\left\{\frac{\frac{3\alpha K}{4AG} + 2a^2\cos^2 bL}{a\sin 2bL + b\sinh 2aL}\right\} \quad \ldots (82a)$$

(b) Neglecting shear deflection

$$y_o = \frac{Ha}{K}\cdot\frac{\cos 2aL + \cosh 2aL + 2}{\sin 2aL + \sinh 2aL} \quad \ldots (82b)$$

The deflection y_o is the relative movement between the concrete and the steel beam. In the push-out tests, this relative movement (defined as slip) is measured, and from the known applied shear, H, and the measured slip, a suitable value of "k" can be estimated.

If the value of κ is known, the deflected shape of the stud, the moment and stress along the length of the stud, the concrete pressure, etc., can be determined from equations (80), (81) and (74).

Figures 14 and 15 show the deflected shape and the moment distribution along the length of a $\frac{3}{4}$ in. diameter and 4in. long stud. The foundation modulus of the concrete, κ, is obtained from the average slope of the load-slip curves for $\frac{3}{4}$ in. x 4in. long plain headed studs, given in Figure 27.

The re-active concrete load under the welds, q_o, can be calculated from equations (74) and (82) and is 2290 lb./in. per ton load when sheardeflection is neglected, and 3780 lb./in. when shear deflection is considered. For a $\frac{3}{4}$ in. diameter stud, this gives a concrete stress of approximately 3050 lb./in.^{2} and 5050 lb./in.^{2} respectively per one ton shear. No attempt is made to develop a practical formula by using the criterion of maximum stress in the concrete, as it is difficult to generalise the behaviour of concrete under the triaxial stress which exists at the root of the studs.

Maximum bending stress occurs at the welded end when shear deflection is neglected and is 11.8 tons/in.^{2} per ton shear. This gives a yield load per connector of only 2.55 tons for a yield stress of 30 tons/in.^{2}. This is evidently too low, when compared with the useful capacity of such connectors.

In the case where shear deflection is considered, the maximum bending stress occurs at a distance of $\frac{7}{8}$ in. from the base, and is about 4.9 tons/in.^{2}; it should also be noted that at this

section of maximum bending moment, the shear is zero. At the welded end the maximum bending stress is 3.9 tons/in.^{2}, and the maximum shear stress on the axis of the stud is 3.0 tons/in.^{2} It is possible, therefore, that the failure may occur either at the section of maximum B.M. by bending or at the welded end by a combination of bending and shear. As the bending stress at the section of maximum bending moment is more than the maximum stress at the base, it is believed that the failure by yield first occurs at a distance of $\frac{7}{8}$ in. from the base. After this yielding, more load is thrown into the portion of the stud nearer the root, and eventual failure occurs at the root by a combination of bending and shear. The fractures, observed by Thürlimann [22] at the base and also at approximately $\frac{3}{4}$ in. from the base of a $\frac{1}{2}$ in. by $2\frac{1}{4}$ in. long L-stud under fatigue loading, can also be explained with the help of this theory, although the reason given by Thürlimann is different.

Taking the failure by bending at the section of maximum bending moment as the criterion for failure, the yield load of a $\frac{3}{4}$ in. diameter by 4in. long stud is given by 0.205 f_y, where f_y is the yield stress of the material. For a normal stud material, having a yield stress of 30 tons/in.^{2}, this gives a yield load of 6.2 tons. The yield load of connectors of different diameter and different concrete strength can also be estimated after obtaining the slope of load-slip curves from push-out tests.

For equal strength, it will be reasonable to design the number of shear connectors such that the yield load is reached at each connector when the beam reaches the yield. Taking the yield load and ultimate load as 6.0 T and 13.0 T respectively, it can be shown for a beam with neutral axis at the interface, that this design is equivalent to a design where the number of connectors are designed to reach 90 per cent of their ultimate capacity when the beam reaches its ultimate load.

CHAPTER III

PUSH-OUT AND PULL-OUT EXPERIMENTS

3.1 Push-out Tests

(a) Purpose of tests

The main purpose of these tests was to study the behaviour of stud shear connectors under a known load and to obtain experimentally the ultimate capacity and the useful capacity of the connectors. The useful capacity of a connector is defined as the load per connector at a residual slip of 0.003in. Another purpose was to study the effect on the general behaviour of stud shear connectors when the flange to which the connectors are welded is mechanically or otherwise roughened. The influence of roughening the stud shank was also studied.

As the slip begins, the concrete slab tries to ride over the undulations on the roughened flange and produces axial strains in the connectors. This axial force holds down the slab and thus helps the projections to resist shear. The larger the cross-sectional area of a connector, the greater will be the holding down force and so the more effective will be the projections in resisting shear. Tests were, therefore, carried out to study the effect of stud diameter on the resistance of a roughened (Durbar) flange.

All the types of connector used in the beam and plate experiments were also tested in push-out specimens.

(b) Description and preparation of specimens

Each small scale push-out specimen was designated by two numbers and two capital letters, as, for example, P3C2. In these symbols the numbers and letters have the following meaning:

The first letter P represents small scale push-out specimen. The first number expresses the diameter of studs in sixteenths of an inch.

The second letter designates the nature of the flange surface: A stands for $\frac{1}{8}$ in. x $\frac{1}{16}$ in. grooved flange; B stands for $\frac{1}{16}$ x $\frac{1}{32}$ in. grooved flange; C stands for $\frac{1}{32}$in. x $\frac{1}{64}$ in. grooved flange; D stands for plain flange with natural bond; and E stands for Durbar plated flange.

The second number is used to distinguish between similar specimens.

Each of these push-out specimens had eight studs, four on each flange except specimen P2E2, which had four studs, two on each flange. All these studs were 1in. long and headed.

Two half-scale push-out specimens, designated as P6D1 and P6D2, each having four $\frac{3}{8}$ in. diameter x $1\frac{1}{2}$ in. long headed studs, two on each flange (plain flange with natural bond) were tested.

Four full scale push-out specimens, designated as P12D(TH), P12D(T), P12E1 and P12E(DE) were tested. Specimen P12D(TH) had four $\frac{3}{4}$ in. diameter x 4 in. long threaded studs with head, and specimen P12D(T) had four $\frac{3}{4}$ in. diameter x 4in. long threaded studs without head. Each had two studs on each flange (plain flange with natural bond). A Durbar flanged steel beam was used for specimens P12E1 and P12E(DE). Specimen P12E1 had eight $\frac{3}{4}$ in. diameter x 3in. long headed studs, four on each flange. Specimen P12E(DE) was a

double ended push-out specimen with sixteen $\frac{3}{4}$ in. diameter x 4in. long headed studs, four on each flange.

Figures 16 and 17 and Tables 5 and 6 give the details of all push-out specimens.

The small scale push-out specimen consisted of a 4in. x $1\frac{3}{4}$ in. I section 10in. long with two concrete slabs $1\frac{1}{2}$in. thick and 6in. wide by 8in. long, one on each flange. Two layers of reinforcement, similar to those used in quarter scale beams were provided in each slab. Concrete was made using Ferrocrete rapid hardening cement, sand and $\frac{3}{16}$ in. aggregate. Aggregate cement ratio and water cement ratio respectively were 3.25 and 0.55 all by weight. The slabs were cast in a vertical position using a steel mould, cured for a week under wet sacking covered with polythene sheet and tested two weeks after casting.

A 12in. x 5in. I section 3ft. long with two concrete slabs 6in. thick and 12in. wide by 18in. long, one on each flange, was used for half scale and full scale push-out specimens. For specimens P12E1 and P12E(DE), the I section was made up using $\frac{5}{8}$ in. thick Durbar plate as flanges. The reinforcement in the slab was as shown in Figure 17. Concrete was made using Ferrocrete rapid hardening cement. An aggregate cement ratio of 4.5 with $\frac{3}{8}$ in. aggregate was used in half scale specimens, whereas an aggregate cement ratio of 5.5 with $\frac{3}{4}$ in. aggregate was used for full scale specimens. The water cement ratio was 0.55 for all the specimens. The slabs were cast on top of the flanges in a horizontal position. Specimens were cured for a week under wet sacking covered with polythene sheet and tested two weeks after casting.

Two 4in. cubes and one 12in. x 6in. cylinder were cast for each of the slabs for all the specimens.

(c) Testing procedure

Small scale push-out specimens were set up on specially machined bases as shown in Figure 16. Load was applied through a 30 ton hydraulic jack, operated by a hand pump and was measured with a 25 ton capacity proving ring dynamometer. Two 0.0001in. dial gauges were used to measure slip.

Half scale and full scale specimens were set up as shown in Figure 17. The slabs were bedded in ciment fondu. Load was applied through a hydraulic jack in specimens P6D1, P6D2 and P12E1 and was measured with a calibrated pressure gauge. Specimens P12D(TH), P12D(T), and P12E(DE) were tested in a 200,000 lb. screw loading testing machine. Slip was measured using 0.0001in. dial gauges. In a few specimens, separation between the slab and the steel beam was measured using 0.0001in. dial gauges. Strains in studs at a distance of $\frac{7}{8}$ in. from the base were measured in specimens P12E1 and P12E(DE), using special single filament resistance gauges 1in. long and also $\frac{1}{4}$ in. long foil gauges.

The general procedure of testing was as follows. An increment of load was applied and stabilised; readings were taken at all dials including the strain gauges. The load was then released to zero and another set of readings was taken. This procedure was continued until the failure occurred. At high loads the jack was pumped occasionally to prevent the load from falling due to creep.

(d) Test Results

1. Small scale push-out specimens

Slips and residual slips for all the small scale push-out specimens are shown in Figures 19 to 24. A summary of the test results with a brief description of specimens and strength of concrete appear in Table 5. The results of the tests are also described separately, as follows:

(i) Specimen POA1. This specimen was without any stud connectors. The only shear connection provided was by $\frac{1}{8}$ in. x $\frac{1}{16}$ in. triangular grooves on the flange. The specimen failed before it could be tested. One of the concrete slabs fell off while the slip measuring device was being fixed.

(ii) Specimens P3A1 and P3A2. The load slip curve was almost linear in specimen P3A1 up to a load of 1.69 tons per stud; a small cracking sound was heard at this load and slip increased rapidly thereafter. In specimen P3A2, slip was almost proportional to load up to 1.50 tons per stud. The maximum load attained in specimen P3A1 was 1.84 tons per stud at a slip of 0.0136 in. After this, slip increased very rapidly, load started faliing and finally all the eight studs were sheared off with a banging sound. Failure was similar in specimen P3A2, where the maximum load reached was 1.97 tons per stud. The maximum slip that could be recorded before failure was 0.0147in. at 1.94 tons per stud for this specimen. Residual slip was first observed at 0.30 ton per stud in specimen P3A1 and at load 0.25 ton per stud in specimen P3A2. Residual slip recorded before failure was 0.0021 in. after a load of 1.75 tons per stud in specimen P3A1 and 0.0095 in. after a load of 1.94 tons per stud in specimen P3A2.

(iii) Specimens P3B1 and P3B2. Slip was almost proportional to load up to 1.0 ton per stud in both the specimens, and thereafter increased rapidly with load. The maximum load reached in specimen P3B1 was 1.56 tons per stud, when slip increased very rapidly, load started falling and all the eight studs were sheared off at a slip of 0.0645in. In specimen P3B2, the maximum load reached was 1.50 tons per stud. Failure was similar to the specimen P3B1 and occurred at a slip of 0.076in. Residual slip started at a load of 0.25 ton per stud in both the specimens. The maximum residual slip recorded before failure was 0.0102in. after a load of 1.50 tons per stud in specimen P3B1 and 0.0046in. after a load of 1.44 tons per stud in specimen P3B2.

(iv) Specimen P3C1. The load-slip curve was nearly a straight line up to 0.25 tons per stud and thereafter slip increased rapidly with load. A small cracking sound was heard at a load of 0.94 ton per stud and separation between the slab and steel was visible at 1.06 tons per stud. The maximum load attained was 1.25 tons per stud at a slip of 0.0375in. Slip increased very rapidly after this, load started dropping and finally all the eight studs were sheared off. Residual slip started at 0.374 ton per stud and the maximum residual slip recorded before failure was 0.0141in. after a load of 1.19 tons per stud.

(v) Specimens P3D1 and P3D2. Slip started from the first application of load in both specimens and then increased progressively with load. Residual slip started at 0.125 tons per stud in both specimens. A very small cracking sound was heard in specimen P3D2 at 0.7 ton per stud. At the same load separation between the slab and steel was observed in specimen P3D1. The maximum load attained was 1.08 tons per stud in both specimens. Failure occurred by shearing of all four studs on one slab after slip had

increased considerably after the maximum load had been reached. The maximum slip recorded before failure was 0.0561in. in specimen P3D1 and 0.0684in. in specimen P3D2. Maximum residual slip recorded before failure was 0.0310 in. after a load of 1.02 tons per stud in specimen P3D1 and 0.0350in. after a load of 1.05 tons per stud in specimen P3D2.

(vi) Specimen P3E1. Slip and residual slip both started from the first application of load. Separation between the slab and steel was observed on both sides at 1.25 tons per stud. At 1.50 tons per stud, the separation became very clear. Slip started increasing very rapidly at 1.63 tons per stud, which was also the maximum load reached. Failure occurred by shearing of all four studs on one slab. The maximum slip and residual slip recorded before failure were 0.0452 in. at 1.63 tons per stud and 0.0225in. at 1.62 tons per stud respectively.

(vii) Specimen P4E1. Slips and separations are shown in Figures 23, 24 and 37. Slip started from the first application of load, whereas residual slip was first observed at a load of 0.25 tons per stud. Separation of the slab from the steel was also first recorded at this load. The slip-separation relationship was nearly linear up to a load of 1.13 tons per stud and thereafter separation increased more rapidly. The maximum load reached was 2.0 tons per stud at a slip of 0.0410in. Thereafter slip increased rapidly, the load started falling, and finally all four studs in one slab were sheared off at a load of 1.625 tons per stud and at an approximate slip of 0.09in. The residual slip recorded just before maximum load was 0.0250in.

(viii) Specimens P2E1 and P2E2. Specimen P2E2 had four studs, whereas specimen P2E1 had eight studs (Figure 16). In both the specimens slip started from the first application of load and residual slip started at a total load of 0.5 ton. Separation between the slab and steel was clearly visible in specimen P2E2, separation was measured and is shown in Figure 37. The slip-separation relationship was almost linear up to the failure load. The maximum load attained in specimen P2E1 was 0.94 ton per stud. Failure was due to shearing of all four studs in one slab. The maximum slip and residual slip recorded before failure were 0.0620in. and 0.0262in. respectively. In specimen P2E2, the maximum load reached was 1.25 tons per stud. Slip increased very rapidly after this load, failure was imminent and the test was stopped to prevent the gauges from being damaged. Slip and residual slip recorded at 1.25 tons per stud were 0.0303in. and 0.0260in. respectively. The average separation recorded at 1.19 tons per stud was 0.0080in.

(ix) Specimen P4D1. Total slips and residual slips for this specimen are shown in Figures 21 and 22. Slip started from the first application of load whereas residual slip was not observed until a load of 0.15 ton per stud was applied. The maximum load attained was 1.75 tons per stud at a slip of 0.0820in. Slip increased very rapidly thereafter, the load started falling and failure occurred at a load of 1.70 tons per stud at an approximate slip of 0.11in. The maximum residual slip recorded was 0.0715in. just after maximum load. Failure was by shearing of four studs in one slab. A horizontal crack at the level of the upper pair of studs was observed on the outside of the concrete slab at failure. On the inside of the slab cracks were observed starting from the location of the studs and spreading towards the corners.

(x) Specimen P2D1. Figures 21 and 22 show total and residual slips for this specimen. Both total and residual slips started from the first application of load. The maximum load attained was 0.51 ton per stud at a slip of 0.0657in. Thereafter slip increased very rapidly and eventually failure occurred by shearing of four studs on one slab. The maximum residual slip recorded was 0.0270in. after a load of 0.50 ton per stud.

2. Half scale push-out tests

(i) Specimens P6D1 and P6D2. Total slips and residual slips for both specimens are shown in Figure 25 and 26. Slips and residual slips started at a load of 0.45 ton per stud and 0.75 ton per stud respectively in both the specimens. Greater slips were recorded for specimen P6D1 in the early stages of loading up to 2.25 tons per stud, and thereafter both slip curves were almost identical. Q_{useful} was the same for both specimens and was 2.28 tons per stud. The maximum load reached was 2.99 tons per stud in specimen P6D1 and 3.01 tons per stud in specimen P6D2. Failure was similar in both specimens. Slip increased very rapidly after the maximum load had been reached, load started failing and failure occurred by shearing of all four studs. The maximum slips recorded were 0.1259in. in specimen P6D1 and 0.0823in. in specimen P6D2.

3. Full scale push-out tests

(i) Specimens P12D(TH) and P12D(T). Slips and residual slips for both the specimens are shown in Figures 27 and 28. Slips and residual slips both started at 1.32 tons per stud in specimen P12D(TH) (with head) and at 0.48 ton per stud in specimen P12D(T) (without head). Load-slip curves were almost identical up to a load of 7.0 tons per stud and thereafter greater slips were recorded for specimen P12D(T) until failure. Horizontal cracks

on the inside of the slabs were observed at the stud level at 12.4 tons per stud in specimen P12D(TH). The maximum load reached in this specimen was 13.4 tons per stud, whereas in specimen P12D(T), this was 12.5 tons per stud. Failure was similar in both cases and was by shearing of both studs on one slab. The maximum average slip recorded before failure was 0.0869in. in specimen P12D(TH) at 12.7 tons per stud and 0.0744in. in specimen P12D(T) at 11.9 tons per stud.

In both these specimens, cracks starting from near the locations of studs and spreading towards the corners of the slab, occurred on the inside of slabs at failure. Figure 40 shows a typical close-up view of these crack patterns.

(ii) Specimens P12E1 and P12E(DE). Slips and separations for both these specimens are shown in Figure 29 to 32. Figure 33 shows the bending and axial components of the stud strains. Slip-bending strains and separation-axial strain relationships are shown in Figure 35 and 34.

In specimen P12E1, slips, residual slips and separations all started at the same load of 2.27 tons per stud. Separation became clearly visible at 11.35 tons per stud. Load at residual slip of 0.003in. was 11.72 tons per stud. Cracks on the inside of both slabs were observed at a load of 14.0 tons per stud. The maximum load per stud reached was 14.75 tons. The average slip, residual slip and separation recorded at maximum load were 0.0586in., 0.0452in. and 0.0190in. respectively. Slip increased very rapidly after the maximum load had been reached, load started falling off and the upper pairs of studs were sheared off; the load dropped to 41.75 tons and remained there. On further pumping, the load dropped still further, cracks became wider and the test was stopped when

slip was about $\frac{3}{4}$in. It was later found that the lower two pairs of studs had also failed but had not been completely detached. A slight horizontal force was sufficient to remove the studs from the steel beam.

The upper pairs of studs were sheared off at sections just outside the weld fillet, whereas the lower pairs brought some parent metal from the steel flange with them. Figure 41 shows a close-up view of one of the slabs after failure.

In specimen P12E(DE), slips, residual slips and separation all started at a load of 1.70 tons per stud. Separation cracks were visible at 9.0 tons per stud. The test was stopped at a load of 11.25 tons per stud, that is, at a total load of 90 tons which was very close to the maximum capacity of the testing machine. The failure load of the specimen, therefore, could not be obtained. For the same load slip and separation were greater in this specimen than in P12E1. The average total slip, residual slip and separation at 11.25 tons per stud were 0.0152in. 0.0068in. and 0.0053in. respectively.

(e) Discussion of Test Results

(i) Effect of flange roughening on carrying capacity of connectors:

Figures 19 and 20 give total slips and residual slips for eight specimens with $\frac{3}{16}$ in. diameter studs and having varying degrees of flange roughening. The studs were from the same stock having a yield stress of 31.1 t.s.i. and an ultimate stress of 35.1 t.s.i. The concrete cube strengths varied from 6360 p.s.i. to 6890 p.s.i.

The ultimate capacity varied from 1.08 tons per stud on a specimen with plain flange and natural bond, to 1.94 tons per stud on a specimen with $\frac{1}{8}$ in. x $\frac{1}{16}$ in. grooved flange. The average ultimate capacity was 1.89 tons for specimens with $\frac{1}{8}$ in. x $\frac{1}{16}$ in. grooves, 1.53 tons for specimens with $\frac{1}{16}$ in. x $\frac{1}{32}$ in. grooves and 1.25 tons for the specimen with $\frac{1}{32}$ in. x $\frac{1}{64}$ in. grooves. In the Durbar flanged specimen the ultimate capacity was 1.63 tons. The useful capacity similarly varied from 0.63 ton in the plain flanged specimen to 1.75 tons in specimens with $\frac{1}{8}$ in. x $\frac{1}{16}$ in. grooved falnge. The ratio $\frac{Q_{uc}}{Q_{use}}$ was between 1.1 and 1.3 in grooved flanged specimens, about 1.6 in plain flanged specimens and 1.8 in specimens with Durbar flanges.

The load-slip characteristics are different in specimens having different types of flange roughening. The specimens with grooved flanges, the slip is very small and proportional to load at early stages of loading. The limit of proportionality increases with the increase in the size of the grooves, and is 0.63 ton per stud in the specimen with $\frac{1}{32}$ x $\frac{1}{64}$in. grooves, 1.0 ton per stud in specimens with $\frac{1}{16}$in. x $\frac{1}{32}$ in. grooves and 1.5 tons per stud in specimens with $\frac{1}{8}$ in. x $\frac{1}{16}$ in. grooves. Beyond the limit of proportionality slip increases very rapidly until failure occurs.

In the case of specimens with Durbar flanges slip increases rather gradually and final failure occurs when the slip becomes excessive.

The difference in behaviour can probably be explained as follows. In specimens with grooved flange, the concrete within the grooves provides a mechanical key and resists shear. The larger the groove, the greater is the mechanical keying action and the load carrying capacity. As the shear is resisted all over the contact area, the deformation of concrete is smaller and so is the slip. But once the shear per unit area exceeds a certain limit, which depends on the size of groove, the concrete in the grooves starts shearing, slip starts increasing very rapidly, load is thrown mostly to the studs and immediate failure occurs. In case of specimens with Durbar flanges, the small projections resist shear in conjunction with the studs. The deformation of concrete under the studs and the projections is greater as the projecting area is less than in the case of specimens with grooved flange. At higher loads, concrete under the studs and projections crushes, slip increases rapidly and failure occurs by shearing of studs when slip becomes excessive.

In grooved flanged specimens, failure occurs primarily due to shearing of concrete, whereas in Durbar flanged specimens it is the excessive slip that causes failure. The former is comparable to a very rigid shear connector and in the latter the projections appear to act as flexible connectors.

(ii) Effect of shank roughening on carrying capacity of stud shear connectors

Figures 27 and 28 show total and residual slips for two specimens P12D(TH) and P12D(T) with $\frac{3}{4}$ in. diameter and 4in. long threaded studs with and without heads respectively. Similar curves for a specimen with $\frac{3}{4}$ in. diameter and 4in. long plain headed studs tested by Balakrishnan [29] are also shown.

Slip curves are almost identical for all the specimens up to a load of 1.8 tons per stud and thereafter slip in the specimen with plain headed studs increases more rapidly. In specimens with threaded studs, load-slip curves intermingle up to a load of 7.0 tons per stud, beyond which slip is greater in the specimen with studs without heads.

Plain headed studs failed at 12.7 tons per stud whereas a maximum load of 13.4 tons per stud was reached in the specimen with threaded and headed studs. The difference may be due to the threads, which provide slightly better holding down and hence contain the concrete more effectively. Higher concrete strength (6,230 p.s.i. against 5,500 p.s.i.) may be another reason. A lower ultimate load of 12.5 tons per stud was reached in the specimen with threaded studs without heads.

Residual slip curves are nearly the same for all the specimens up to 8.4 tons per stud. The useful capacity was 6.75 tons for threaded and headed studs, 6.50 tons for threaded studs without heads and 6.75 tons for plain headed studs.

The threaded studs appear to give better performance with less total slip for the same load than plain studs, although there is not much difference either in useful or in ultimate capacity in the three types of studs tested.

(iii) Effect of variation of stud diameter on the shear resisting capacity of a roughened flange

Figures 23 and 24 give total and residual slips for four Durbar flanged specimens P4E1, P3E1, P2E1 and P2E2. The total area of the Durbar flange in contact with concrete was 28 in.^{2}, and the total cross-sectional area of the studs was varied from 0.049in.^{2} in specimen P2E2 to 0.393in.^{2} in specimen P4E1. The concrete strength for specimens P4E1 and P2E2 was 5450 p.s.i. against 6360 p.s.i. for specimens P3E1 and P2E1.

Ultimate loads as well as useful loads are considerably increased in these specimens over those specimens with plain flanges. Ultimate capacity was 2.0 tons for $\frac{1}{4}$ in. dia. studs in specimen P4E1, 1.63 tons for $\frac{3}{16}$ in. dia. studs in specimen P3E1, 0.94 ton for $\frac{1}{8}$ in. dia. studs in specimen P2E1 and 1.25 tons for $\frac{1}{8}$ in. dia. studs in specimen P2E2. Percentage increases over corresponding ultimate loads in specimens with plain flanges are 14, 52, 84 and 145 respectively. Percentage increases in useful capacity are 22, 37, 45 and 52 respectively. It is thus seen that the percentage increase in the useful or ultimate capacity of studs decreases with increasing stud diameter.

If it is assumed that the difference in ultimate load between a Durbar flanged specimen and a plain flanged specimen having identical studs, is due to the shear resistance offered by the projections of the Durbar flange, then the shear per sq. in. resisted by Durbar flange at ultimate load in the four specimens are 160, 350, 270 and 240 lb. respectively. In the full scale specimen P12 E1 with $\frac{3}{4}$ in. dia. x 3in. long studs the shear resistance offered by the durbar flange is 495 p.s.i. There is no comparable push out specimen on Durbar flange tested with

$\frac{3}{8}$ in. diameter studs. But the average value of shear resistance offered by the Durbar flange obtained from beam D1 near ultimate load is 453 p.s.i. The shear resistance offered by the projections of Durbar plate increases with increasing stud area (Figure 43) except for specimen P4E1 with $\frac{1}{4}$ in. diameter studs where this value is rather low.

In specimen P12E1 with $\frac{3}{4}$ in. diameter x 3in. long studs, the percentage increase in useful and ultimate capacity of studs over the corresponding values obtained by Balakrishnan from P.O. specimens with plain flanges, are 102 and 46 respectively. When compared to the quarter scale specimens these percentage increases appear to be high, presumably because the area of Durbar plate per stud provided in specimen P12E1 was 20in.^{2}, against 3.5in.^{2} per stud in quarter scale specimens. Also, the 4in. cube strength of concrete in specimen P12E1 was much higher, 8960 p.s.i., against 5000 p.s.i. in Balakrishnan's specimen.

(iv) The influence of flange roughening on stud strain

Figure 33 shows the strains in specimens P12E1 and P12E(DE). The axial component of strain which is associated with separation of the slab from the beam is plotted against separation in Figure 34, and the bending component, which is associated with slip, is plotted against slip in Figure 35.

Strains are plotted for loads in excess of 3.78 tons per stud for specimen P12E1 and in excess of 2.26 tons per stud for specimen P12E(DE). Strain readings for smaller loads are very small and scattered.

The axial component of the measured strain is quite high and even higher than the bending component. Only near the ultimate load did the bending component become greater than the axial

component. Both axial and bending components are smaller in specimen P12E1 than in P12E(DE). This is probably because the partial fixity at the base of the single ended specimen P12E1 restricts the horizontal movement of the slab, whereas in the double ended specimen P12E(DE), the slabs are free to separate from the flange. This free movement allows more separation and hence more slip and produces greater strains in specimen P12E(DE).

At earlier stages of loading, separation is proportional to the axial component, in both the specimens. In specimen P12E(DE) slip is very nearly proportional to the bending component but in specimen P12E1, the relationship is linear only up to a slip of 0.0030in., which corresponds to a load of 8.25 tons per stud.

If the separation is assumed to be equal to the total extension of the stud (excluding the head), then the slope of the separation-axial strain curve will be 2.5in. and 3.5in. for studs 3in. and 4in. long respectively. The values obtained experimentally at earlier stages of loading are 2.8in, for specimen P12E1 with 3in. long studs, and 3.4in. for specimen P12E(DE) with 4in. long studs. At higher loads, however, the ratios are much greater, presumably because at higher loads the concrete under the head deforms.

(v) Relation between slip and separation

Figures 36 and 37 show separation-slip curves for specimens P12E1, P12E(DE) and P4E1 and P2E2 respectively. A separation-slip curve for a plain flanged push-out specimen with $4\text{-}\frac{3}{4}$ in. diameter plain headed studs 4in. long, tested by [33] Teraszkiewicz is also shown in Figure 36.

Separation is proportional to slip; and in both the specimens P12E1 and P12E(DE), separation-slip curves are almost identical, although the specimen P12E1 was a single ended specimen

with 3in. long studs and the specimen P12E(DE) was a double-ended specimen with 4in. long studs. The slope of this curve, however, is much greater than the corresponding curve of the plain flanged specimen.

Separation is proportional to slip in the small scale specimen P2E2 at all stages of loading but in specimen P4E1 the separation-slip curve deviates from the line of proportionality at a slip of about 0.01 in. In the proportional range, the separation for specimen P4E1 is smaller than that for specimen P2E2 for the same slip. This may be attributed to the greater stiffness of studs in specimen P4E1 which had 8-$\frac{1}{4}$ in. diameter studs, than that in specimen P2E2 which was provided with only 4-$\frac{1}{8}$ in. diameter studs.

(vi) Effect of stud diameter

Figures 21 and 22 show total and residual slips for specimens P4D1, P3D1, P3D2 and P2D1, each having eight 1 in. long studs of diameters $\frac{1}{4}$ in., $\frac{3}{16}$, $\frac{3}{16}$ and $\frac{1}{8}$ in. respectively. Only one curve is shown for total slip and another for reisdual slip for specimens P3D1 and P3D2. Average values of the results from these two specimens are taken for this purpose. Concrete strength varied from 6490 to 6570 p.s.i.

If the capacity is assumed to be proportional to the stud cross-sectional area, then the capacities of $\frac{1}{4}$ in. and $\frac{3}{16}$in. diameter studs should be 4 and 2.25 times the capacity of a $\frac{1}{8}$ in. diameter stud. But the ultimate capacities of $\frac{1}{4}$ in. and $\frac{3}{16}$ in. diameter studs were found to be only 3.43 and 2.12 times that of $\frac{1}{8}$ in. diameter studs. Similarly, the useful capacities of $\frac{1}{4}$ in. and $\frac{3}{16}$ in. diameter studs were 2.79 and 2.03 times that of $\frac{1}{8}$ in. diameter studs. The ratios $\frac{Q_{uc}}{Q_{use}}$ are 1.90, 1.61 and 1.55 for $\frac{1}{4}$ in., $\frac{3}{16}$ in. and $\frac{1}{8}$ in. diameter studs respectively.

Figure 44 shows the variation of average shear at ultimate load with the stud diameter. The results for $\frac{1}{2}$ in. and $\frac{3}{4}$ in. diameter studs 4in. long are taken from tests carried out by Balakrishnan[29]. The comparatively lower value for $\frac{3}{8}$ in. diameter studs may be due to the shorter length of the studs and the comparatively lower concrete strength.

It is observed that the average shear stress in the studs at ultimate load decreases with increasing stud diameter. For the same total cross-sectional area, therefore, studs of smaller diameter show better performance.

(vii) Nature of failure

All the small scale specimens falied by shearing of studs. In the grooved flanged specimens, failure was initiated by shearing of concrete in the grooves followed by sudden and rapid increase in slip and finally fialure occurred by shearing of studs. In the other specimens, the increase in slip was gradual and when slip became excessive failure occurred due to shearing of studs. Failure was similar in all the full scale specimens where failure occurred by shearing of studs after excessive slip.

In most cases failure of studs occurred at a section just outside the weld fillet. Only in specimen P12E1, which was a single ended Durbar flanged specimen with eight $\frac{3}{4}$ in. diameter, 3in. long studs, the lower pairs of studs brought some parent metal from the flange at failure.

No crack in the concrete was observed in small scale specimens with studs of $\frac{3}{16}$ in. diameter or below. Only in specimen P4D1 with eight $\frac{1}{4}$ in diameter studs, horizontal cracks were observed on the outside of the slab at the level of the upper pairs of studs.

On the inside, cracks were observed starting from near the location of the studs and extending to the four corners. Similar concrete cracks occurred in all full scale specimens with $\frac{3}{4}$ in. diameter studs. No crack was, however, observed in specimens with $\frac{3}{8}$ in. diameter studs. This is because the $\frac{3}{8}$ in. diameter studs were tested in a full sized push-out specimen with a bigger concrete slab, whereas the $\frac{1}{4}$ in diameter studs were tested in a small scale push-out specimen. Crushing of concrete behind the studs and also behind the projections of Durbar flanged specimens was observed in all specimens.

3.2. Pull-out Tests

(a) Introduction

Tests on composite beams have shown that, as the slip begins, the slab also begins to separate from the steel beam. The shear connectors are then called upon to resistthis separation. As a result, axial forces are produced in the shear connectors in addition to bending stresses caused by slip. In order to study the relationship between the separation and the axial force in the connectors, pull-out tests were planned. A known axial load was applied to the connectors and the behaviour was studied.

The main purpose of these tests was to study the pull-out behaviour of stud shear connectors, having varying lengths. Another objective was to study the effect of shank roughening on the pull-out behaviour of stud shear connectors.

(b) Description and preparation of specimens

Figure 18 shows a pull-out specimen. The specimen consisted of a 12in. x 12in. x 18in. concrete block with two 12in. x 6in. x 24in. long rolled I sections, one on each side of the concrete block. One flange of each I section was removed and on the other, shear connectors were welded. The form and dimensions of the specimen were such that:

(a) the specimen could be accommodated in the testing machine,
(b) the load could be easily applied,
(c) the effect of adhesion of the concrete to the flange could be observed, and
(d) the area of slab exceeds the anticipated failure cone.

The concrete block was unreinforced; this represented the least favourable condition in the slab. Ferrocrete rapid hardening cement was used for the concrete. An aggregate cement ratio of 5.5 by weight, with 60 per cent of $\frac{3}{4}$ in. aggregate and 40 per cent of sand, was used. The water cement ratio was 0.55. Casting was done using a timber mould with the steel beams standing on edge. An immersion vibrator was used for compacting the concrete. The formwork was struck one day after casting and the specimens were cured for a week under wet sacking covered with polythene sheet. Two 4in. cubes and one 12in. x 6in. cylinder were cast for each of the specimens.

Five specimens were tested altogether. These were designated as PL1, PL2 . . . P15. Specimens PL1, PL2 and PL3 each had four $\frac{3}{4}$ in diameter plain headed studs; the studs were 4in. long in specimen PL1, 3in. long in specimen PL2 and 2in. long in specimen PL3. Specimen PL4 had four $\frac{3}{4}$ in. diameter 4in. long threaded studs with heads, whereas specimen PL5 had four $\frac{3}{4}$ in. diameter 4in. long threaded studs without heads. Table 7 gives the details of the specimens.

(c) Testing procedure

The specimens were tested in a 200,000 lb. screw loading testing machine; the arrangement of the specimen is shown in Figure 18. Separation between the concrete and the steel on the centre line was measured using four 0.0001 in. dial gauges. The total separation between the two steel beams at both ends was also measured using 0.0001 in. dial gauges. A demountable mechanical gauge of 8in. gauge length was used to measure concrete strains at both ends.

Load was applied in increments of 1000 lb. After each application of load, a set of readings was taken; the load was released and another set of readings was taken at zero load. The procedure was continued until failure occurred.

(d) Test Results

Separations and residual separations for all the specimens are shown in Figures ~~38~~ 44 and ~~39~~ 45. A summary of test results including the concrete strength appears in Table 7. The results of each test are described separately in the following paragraphs.

(i) Specimen PL1: 4-$\frac{3}{4}$in. diameter 4in. long plain headed studs

Separation between concrete and steel was first observed at a load of 0.59 ton, an average separation of 0.0001in. was recorded at this load. This load is equivalent to an axial force of 12.3 lb./in.^{2} of contact area. Residual separation also started at the same load. Thereafter separation increased progressively with the loads. A low sound was heard at 1.35 tons. Separation became visible at both top and bottom at 3.11 tons. Maximum load attained was 6.80 tons at an average separation of 0.0164 in. Horizontal cracks in the concrete were observed at this load, at about $2\frac{1}{4}$ in. from the top interface and extending for about 3in. on either side of the stud centre line. Thereafter load started falling. A vertical crack along the stud line, which extended from the top and later joined the horizontal cracks, developed at failure.

Separations between the two flanges at both ends increased equally up to 0.86 ton. Thereafter separation at one end increased more rapidly than at the other. These tended to be equal after the maximum load had been reached.

(ii) Specimen PL2. $4\text{-}\frac{3}{4}$ in. diameter and 3in. long plain headed studs

Separation between concrete and steel was first observed at load 0.46ton when an average separation of 0.00015in. was recorded. This load is equivalent to an axial force of 9.5 lb./in.^{2} of contact area. Residual separation started at 0.94 ton. Thereafter separation increased progressively with load. Separation became clearly visible at 3.91 tons. A small cracking sound was heard at 5.52 tons. The maximum load attained was 6.25 tons. An average separation of 0.0077in. was recorded at 5.80 tons. Cracks in the concrete block started at maximum load and thereafter load started falling off. A horizontal crack at about 2in. from the top, followed by a Y-shaped vertical crack extending from the top on the stud centre line and later joining the horizontal crack, developed at failure.

Separation between the two steel flanges increased more rapidly at one end than at the other from the beginning of the test. These, however, tended to be equal after the maximum load had been reached.

(iii) Specimen PL3. $4\text{-}\frac{3}{4}$ in. diameter 2in. long plain headed studs

Separation at the interface was first observed at a load of 0.42 ton when an average separation of 0.00006in. was recorded. This load is equivalent to an axial force of 8.6 lb./in.^{2} of contact area. Residual slip started at 0.74 ton. A low cracking sound was heard at this load. Thereafter separation increased progressively with load. At 2.45 tons, separation started to increase rapidly, and the load-separation curve became nearly horizontal after a load of 2.66 tons. The maximum load carried by the specimen was 2.68 tons at an average separation of 0.0068in. The concrete started cracking at this load and the load started

falling off. Inclined cracks starting from near the location of the studs on the top were observed to spread outward and downward at failure.

Separations between the two steel flanges were nearly equal at both ends up to a load of 2.05 tons, after which separation at one end increased more rapidly than at the other.

(iv) Specimen PL4. $4\text{-}\frac{3}{4}$ in. diameter 4in. long threaded studs with heads.

Separation between concrete and steel was first observed at a load of 0.37 ton which was equivalent to an axial force of 7.7 lb./in.^{2} of contact area. An average separation of 0.0001 in. was recorded at this load. Residual separation also started at this load. The load separation curve was nearly a straight line up to 2.46 tons. A low cracking sound occurred at this load; the load dropped off, followed by a sudden increase in separation at the following increment of load. Separation increased progressively with load thereafter. The maximum load attained was 7.25 tons at an average separation of 0.0062in. A cracking sound, followed by horizontal cracks in the concrete block, occurred at this load, after which load started falling off. A wide crack across the concrete block along the line of the studs was observed on top of the block. This crack extended to the horizontal crack at failure.

Separations between the two steel flanges at both ends indicated an increase in relative inclination between the flanges during the test.

(v) Specimen PL5. $4\text{-}\frac{3}{4}$ in. diameter 4in. long threaded studs without heads

Separation was first observed at 0.29 ton; the average separation recorded at this load was 0.0001 in. This load is equivalent to an axial force of 6.0 lb./in.^{2} of contact area. Residual separation started at a load of 0.61 ton. The load-separation curve was nearly a straight line up to a load of 1.52 tons. A sudden increase in separation occurred at 1.82 tons. The maximum load reached was 5.47 tons at an average separation of 0.022in. Thereafter the separation started increasing very rapidly and the load started falling. Maximum separation recorded was 0.068in. Final failure occurred by the top pair of studs pulling out from the concrete block.

Observed end separation between the steel flanges indicated an increase in relative inclination between the flanges with loads up to a load of 2.41 tons. Thereafter the two separations were nearly the same.

(e) Discussion of test results

(i) General behaviour of pull-out specimens:

The first separation between concrete and steel was recorded at loads varying from 0.29 ton to 0.59 ton. It is believed that this signified the failure of natural adhesion between steel and concrete. Assuming this adhesion to be uniform over the contact surface, this gives an adhesion strength of 6.0 p.s.i. to 12.3 p.s.i. It is likely that this adhesion is not uniform over the contact surface; partly because of shrinkage of concrete and partly because of the possibility of this adhesion being broken down while handling, this may have a lower value on the outer periphery of the contact surface than at the centre. The wider variation in the adhesion strength may, therefore, be attributed to this.

After the adhesion breaks, separation occurs and in most cases remains proportional to load up to a certain limit, beyond which the load-separation curve becomes non-linear. Near the ultimate load separation increases rapidly, horizontal cracks develop in the concrete block, followed by a vertical crack along the line of studs, and then final failure occurs. This behaviour can probably be explained as follows:

After the breaking of adhesion, the load is taken wholly by the studs and is transmitted to the concrete through the bond around the studs and by direct compression under the head. Separation then depends on the extension of the stud and subsequently on the deformation of concrete under the head. At small loads, therefore, separation is proportional to load, but at higher load, when concrete under the head deforms non-linearly, the load-separation curve also becomes non-linear. The compression in the concrete under the head, which gradually decreases and becomes equal to zero at the free surface, is transmitted to the surrounding concrete through shear. At higher loads, tension cracks may develop just under and at the outer periphery of the head, due to this shear and also the stress concentration that may exist there. With load, these cracks become wider and spread all round. Separation increases more rapidly. A void within the concrete may be created by widening of these tension cracks, which then produces upward curvature at the centre of the concrete block. Vertical tension cracks then develop across the concrete at the top, and final failure occurs.

(ii) Effect of stud length

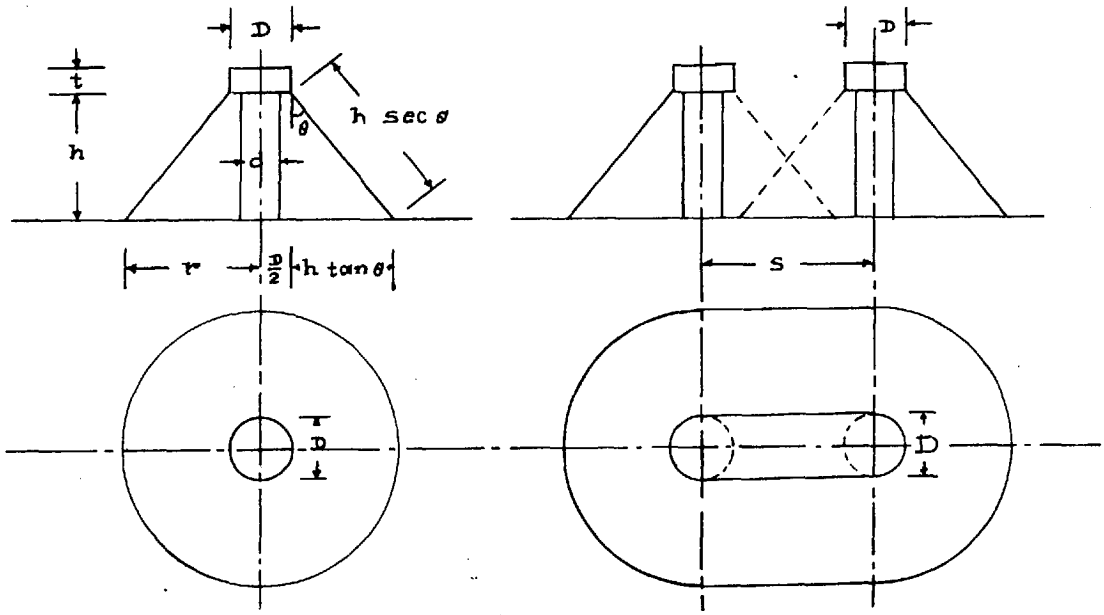
Specimens PL1, PL2 and PL3 had $\frac{3}{4}$ in. diameter plain headed studs 4in., 3in. and 2in. long respectively. Figures 44 and 45 show total and residual separation for these three specimens.

Separation curves for specimens PL1 and PL2 intermingle up to a load of 2.6 tons and thereafter separation in specimen PL1 with 4in. long studs increases more rapidly. In specimen PL3 with 2in. long studs, the separation is much smaller at early stages of loading. At small loads separation may be mainly due to the extension of studs and the elastic deformation of concrete under the head. With shorter studs, therefore, the separation may be expected to be smaller. But at high loads separation will depend mainly on the inelastic deformation of concrete under the head and also on the tension cracks that may develop just under the periphery of the connector head.

It is difficult to give a general expression for failure load of a pull out specimen. But if it is assumed that the failure occurs due to failure of concrete in a conical surface as shown below, then the failure load which will depend on surface area of the cone and tensile strength of concrete will be proportional to

$$(h \tan \theta + \frac{D}{2})\, h. \sec \theta.\, f_{cu}$$

where f_{cu} is the concrete strength and h, D and θ are as shown in Figure (a) below.



(a) Single stud (b) A pair of studs

Assumed conical failure of pull-out specimens

In many composite beams the transverse spacing of studs is such that the assumed failure surfaces overlap; in such cases, a failure surface as shown in Figure(b) may be assumed, and the failure load will then be proportional to

$$h.\ \sec\theta\ (h\ \tan\theta + \frac{D}{2} + 2s)f_{cu}$$

Assuming $\theta = 45^{o}$, the failure loads for 2in., 3in. and 4in. long studs with s = 3in. will be in the ratio of 1 : 2.03 : 3.03. The maximum loads per stud attained in specimens PL3, PL2 and PL1 are 1.34 tons, 3.13 tons and 3.40 tons respectively, a ratio of 1 : 2.34 : 2.54. This ratio is reasonably close to the calculated ratio. The comparatively lower value for specimen PL1, with 4in. long studs, may be due to the limited size of the concrete block.

(iii) Effect of threading the stud shank

Specimens PL4 and PL5 had 4in. long threaded studs with and without head respectively. In specimen PL5, separation is proportional to load up to 1.5 tons and thereafter separation increases very rapidly. Within this range load is transmitted to the concrete through bond in the threaded length of the stud. Assuming the bond stress to be uniform over the threaded length, this attains a value of 360 p.s.i. at 1.50 tons load. It is likely that the bond starts failing at this load which results in a rapid increase in separation and eventual failure by pulling out from the concrete block. When compared with specimen PL1 having 4in. long plain headed studs, specimen PL5 shows a smaller separation up to 1.7 tons, after which separation in specimen PL5 increases more rapidly than in specimen PL1.

In specimen PL4 (with threaded and headed studs), separation is smaller than in either specimens PL5 or PL1 at all stages of loading. Separation is proportional to load up to 2.5 tons, when a sudden increase in separation occurs. The reason may be the failure of bond in the threaded length of the stud at this load. The separation at which the bond failure occurs is almost the same in both the specimens PL4 and PL5.

The maximum loads carried were 3.63 tons in specimen PL4, 2.73 tons in specimen PL5 and 3.43 tons in specimen PL1. Failure in specimens PL1 and PL4 was similar and occurred by failure of concrete. The slightly higher ultimate load in specimen PL4 may be due to the higher concrete strength of 7000 p.s.i. against 6000 p.s.i. in specimen PL1.

Although there is not much difference in the ultimate load, the specimen with threaded and headed stud shows much better load-separation characteristic than the specimen with plain headed

studs. Even the specimen with threaded studs without heads shows less separation at smaller loads than the specimen with plain headed studs.

If the shank is threaded for its entire length, the pull-out force is most likely to be resisted by the mechanical bond surrounding the thread nearest to the interface. If the conical failure described earlier is assumed here, the failure will occur at a much lower load as the surface area of the cone will be very small. The situation will be further aggravated when the stud is subjected to horizontal shear from alternate directions. Failure of concrete around the nearest threading will throw the pull-out force to the next upper threadings, and the process may continue.

CHAPTER IV

EXPERIMENTS ON COMPOSITE BEAMS

4.1 Quarter Scale Composite Beams

(a) Purpose of tests

The main purpose of these tests was to study the interaction in composite beams having varying degrees of roughness on the top flange surface. "V" grooves of various sizes were cut in the transverse direction on the top surface of the steel beam for this purpose. In one beam the top flange was replaced by a Durbar plate. In another, $\frac{3}{16}$ in. aggregate was bonded with resin to the top flange of the steel beam before the slab was cast.

Another purpose was to study the effect of three particular shear connector spacings. The connectors were spaced:

(a) To reach 100 per cent of their ultimate capacity when the beam reached its ultimate moment, the shear being calculated according to the elastic theory.

(b) As (a), but the shear being calculated from the assumed fully plastic stress distribution at mid span. The connectors were uniformly spaced.

(c) As (b), but the connectors were spaced according to the shear distribution at collapse, assuming full interaction.

In case (a), the ratio $\frac{\text{ultimate capacity of connector}}{\text{nominal load per connector}}$ at working load will be the same as the load factor for the beam; but then at ultimate load the total number of connectors will be much less than the number required to resist the total horizontal shear. In cases (b) and (c), however, the total number will be the

same as required to resist the total horizontal shear at ultimate load, but the ratio $\frac{\text{ultimate capacity of connector}}{\text{nominal load per connector}}$ at working load will be greater than the load factor for the beam. In case (a) the nominal load per connector at ultimate load is found to be 138 per cent of its ultimate capacity for the quarter scale beams tested.

All the beams were tested under a central point load except one, where a two-point load 6in. apart was used. The purpose of the latter test was to find whether there was any essential difference in behaviour of the beam due to the absence of a contained area of concrete under the load at the centre of the beam.

The cross-section of the beams was kept constant, so that a comparative study of behaviour could be made.

(b) Description and preparation of specimens

Steel beams 4in. x $1\frac{3}{4}$ in. x 5 lb. B.S.B. were used for all the specimens except one, where the top flange was replaced by a $1\frac{3}{4}$ in. x $\frac{3}{16}$ in. thick Durbar plate. The shear connectors used were $\frac{3}{16}$ in. diameter x$\frac{7}{8}$in. long headed studs welded in pairs 1in. apart transversely.

The reinforced concrete slab was $1\frac{1}{2}$ in. thick and 60in. long by 20in. wide. Two layers of reinforcements, one at the top and one at the bottom, covering the whole width of slab were provided. 3in. x 1in. x 0.104in. weld mesh, with wires at 3in. spacing placed longitudinally was used as reinforcement. A steel mould was used for casting the slab. Concrete was made using Ferrocrete rapid hardening cement, sand and $\frac{3}{16}$ in. aggregate. The aggregate cement ratio by weight was 3.25 with 50 per cent aggregate and 50 per cent sand, and the water cement ratio was 0.55.

Three 4in. cubes and two 12in. x 6in. cylinders were cast for each of the slabs. Concrete was compacted using a Kango vibrator and the formwork was struck one day after casting. Curing was done for a week under wet sacking covered with polythene sheet.

Altogether 14 beams were tested, Group A consisted of five beams, A1 to A5, each having 32 studs, spaced uniformly. The number of connectors was obtained as follows. The horizontal shear at the interface at the theoretical collapse load was calculated in the elastic region of the beam. The spacing of the connectors was then estimated, using 100 per cent of the ultimate connector capacity. The spacing so botained was then used throughout the length of the beam.

In addition to studs, the beams A1, A2 and A3 had transverse "V" grooves onthe top flange. The grooves were $\frac{1}{8}$ in. wide and $\frac{1}{16}$ in. deep in beam A1, $\frac{1}{16}$ in. x $\frac{1}{32}$ in. in beam A2 and $\frac{1}{32}$ in. x $\frac{1}{64}$ in. in beam A3. A length of $\frac{5}{8}$ in. was kept plain for stud welding (Figure 47). In beam A4, no special treatment was given to the steel beam except brushing with a stiff wire brush to remove loose scale or rust. In beam A5, the natural bond between the slab and the beam was destroyed by painting with a resin varnish and using grease on the top surface of the steel beam before casting.

Group B consisted of eight beams, designated as B1 to B8, each having 44 studs spaced uniformly. The number of studs was obtained as follows. The total horizontal shear at the interface at theoretical collapse load was calculated. This is equal to $A_s \times f_y$, where A_s is the area of cross-section of the steel beam and f_y is the yield stress. The number of studs was then calculated using 100 per cent of the ultimate connector capacity.

In addition to stud connectors, the beams B1 and B2 had triangular grooves $\frac{1}{16}$ in. x $\frac{1}{32}$ in. and $\frac{1}{32}$ in. x $\frac{1}{64}$ in. respectively on the top flanges. A length of $\frac{1}{2}$ in. was kept plain for stud welding (Figure 47). In beam B3, no special treatment was given to the steel beam except brushing with a stiff wire brush to remove the loose scale or rust. In beam B4 the natural bond was destroyed by using the same procedure as in A5.

$\frac{3}{16}$ inch aggregate was bonded with resin to the top flange of beam B5. On the follwoing day, when the resin had hardened, the slab was cast on top of the beam (Figure 78). In beam B6, the top flange of the steel beam was cut off and a Durbar plate $1\frac{3}{4}$ in. wide by $\frac{3}{16}$ in. thick was welded in its place, keeping the overall dimensions the same. No special preparation was given to the steel beam of beam B7, but the roots of the studs were covered with flexible latex up to a height of $\frac{1}{2}$ in. (Figure 80) to prevent the studs from resisting shear at the base. Beam B8 was similar to B3 and was tested with two point loads 6in. apart.

Beam C1 had 44 studs. The studs in this beam were spaced according to the theoretical shear diagram at the interface at collapse, the studs being loaded at 100 per cent of their ultimate strength. The theoretical shear diagram at collapse was obtained by numerical calculation as outlined in Chapter 2.1. No special preparation was given to the steel beam except brushing with a stiff wire brush.

The age at which the beams were tested varied from two to four weeks.

(c) Loading

Point load at midspan was applied through a 30 ton hydraulic jack, operated by a hand pump. The point load was spread over the concrete slab by a 3in. diameter steel block. In the case of two point loading, a steel beam supported on a free roller at one end and on a spherical seating at the other over a span of 6in. was used.

Load was measured by a proving ring dynamometer of 10 tons capacity. All the beams were tested over a span of 60in., supported on a fixed roller at one end and on a free roller at the other.

(d) Measurements

Deflection at midspan, end slip, and slip and uplift at quarter span, were measured using dial gauges. In a few beams slips at a number of locations along the span were measured using a demountable mechanical gauge of 2in. gauge length. Another demountable mechanical gauge was used to measure the strains in concrete and steel at the midspan section.

(e) Testing procedures

Beams. The point load at midspan was applied in 0.5 ton increments up to 5.5 tons, and thereafter the increment in load was governed by the increment in deflection. After each application of load a set of readings was taken, the load was then released and another set of readings was taken at zero load. At loads higher than yield load, the beam creeps under the applied load and so the load falls off. In order to maintain a constant load, the jack was pumped up repeatedly until steady conditions were obtained.

Materials

(i) Steel: Two flat specimens $1\frac{1}{2}$ in. wide by 24in. long, one from the web and the other from the flange, were cut from each length of 4in. x $1\frac{3}{4}$ in. R.S.J. The specimens were tested in a 25 ton universal testing machine using an autographic extension recorder.

(ii) Concrete: Cubes and culinders were tested in a 200 ton compression testing machine. Load was applied axially to the cubes at the rate of approximately 2000 lb./in.^{2} per minute, in accordance with C.P.114 (1957). 12in. x 6in. cylinders were tested to find cylinder strength and also the Young's modulus. Stress and strain at a load of 10 tons were used to calculate Young's modulus.

(iii) Studs: Specimens were turned from the base of unused studs wherever possible and were tested in a Hounsfield Tensometer to find the yield and ultimate stress of the stud material.

(f) Test Results

1. Beams of Group A

Summaries of results of the beam tests and the material tests appear separately in Tables 8 and 9. Deflection, end slip, slip and uplift at quarter span are shown in Figures 49 to 53. The test results of each beam are discussed below.

(i) Beam A1. Shear connection: 32 studs with $\frac{1}{8}$ in. x $\frac{1}{16}$ in. grooves on top flange.

Deflections were proportional to load up to 4.0 tons and thereafter deviated from the proportional line. Transverse tension cracks were visible at the bottom of the slab at midspan at 6.5 tons.

Spalling of concrete was observed near the loading pad after a load of 7.0 tons at an approximate strain of 0.0040. Failure occurred by crushing of concrete. The maximum load reached was 7.9 tons at a deflection of 1.24in. After this, load began to fall off, crushing of concrete became more extensive and the test was finally stopped at 5.50 tons and at a deflection of 3.34in. A residual deflection of 2.96in. was recorded after the load was finally released to zero.

The interaction was nearly complete. The average end slip at maximum load was 0.0007in. The end slip, however, continued increasing after the maximum load had been reached and attained a maximum value of 0.0020in. at load 6.04 tons, after which there was no further increase. The residual slip, after the load was finally released to zero was 0.0009in.

(ii) Beam A2. Shear Connection: 32 studs with $\frac{1}{16}$ in. x $\frac{1}{32}$ in. grooves on top flange.

Non-linearity of the load-deflection curve started at a load of 4.0 tons. Transverse tension cracks at the bottom of the slab were observed at midspan at 6.0 tons. Spalling of concrete started at 6.5 tons at an approximate strain of 0.0054. The maximum load attained was 6.7 tons at a deflection of 0.84in. After this, the slip increased very rapidly, followed by a bond-breaking sound, and the load dropped to 5.7 tons. On increasing deflection, the load started falling and at 5.03 tons there occurred a loud sound which indicated shearing of the studs on one half of the beam. After failure of the shear connectors the beam carried a load of 3.68 tons at a

deflection of 1.99in. The residual deflection after this load was released was 1.67in.

The interaction was very good up to a load of 6.5 tons, when the average end slip was 0.0019in. The average slip and uplift at quarter span at this load were 0.0067in. and 0.0046in. respectively. The maximum end slip recorded before failure of the studs was 0.083in.

(iii) Beam A3. Shear connection: 32 studs with $\frac{1}{32}$ in. x $\frac{1}{64}$ in. grooves on top flange

Deflections were proportional to load up to 4.0 tons and thereafter deviated from the proportional line. Transverse tension cracks at the bottom of the slab at midspan were visible at 6.5 tons. The maximum load attained was 7.2 tons at a deflection of 0.57in. After this, slip increased very rapidly followed by breaking of bond and the load dropped to 6.25 tons. On increasing deflection, the load also increased and the beam was able to carry a load of 6.86 tons at a deflection of 0.72in. Spalling of concrete near the loading pad was observed at this load. A slight increase in pressure was followed by a loud sound and the studs on one half of the beam sheared off, after which the load dropped to 4.40 tons. On increasing deflection, the load started falling and the beam carried a load of 4.20 tons at a deflection of 1.48in. A residual deflection of 1.17in. was recorded after the load was finally released to zero.

The interaction was very good up to a load of 7.0 tons, when the average end slip was 0.0007in. The slip and uplift at quarter span at this load were 0.0024in. and 0.0027in respectively. Slip started increasing rapidly after this load (from 0.0007in at 7.0 tons to 0.0169in. at 7.2 tons) followed by loss of interaction. The maximum end slip recorded before failure of the studs occurred was 0.024in.

(iv) Beam A4. Shear connection: 32 studs with natural bond

Deflections were proportional to load up to 2.63 tons and deviated from the line of proportionality at 3.0 tons. This was due to incomplete interaction and not to yielding of the beam. The first bond breaking sound was heard at load 2.63 tons followed by slip in the left half of the beam. A second sound occurred at a load of 3.0 tons, when slip in the other half was observed. Transverse tension cracks at the bottom of the slab were visible at midspan at a load of 6.25 tons. After 6.4 tons, the right end slip started increasing more rapidly and at 6.5 tons, which was also the maximum load, there occurred a loud sound and some studs in the right half of the beam sheared off. The load dropped to 5.40 tons. Another stud-breaking sound followed and the load dropped to 4.68 tons. Further increase in deflection did not increase the load and the beam carried a load of 4.33 tons at a deflection of 1.79in. The residual deflection after the load was released, was 1.47in.

Slip increased progressively with load after breaking of bond. The maximum end slip recorded before failure of the studs was 0.061in. All the studs in the right half, except the first

pair from the midspan and two other pairs from the end, sheared off. A big tension crack right across the bottom of the slab developed near midspan at failure. No crushing of concrete was, however, observed.

(v) Beam A5. Shear connection: 32 studs with natural bond destroyed.

Non-linearity of the load-deflection curve started from load 3.0 tons. This was due to incomplete interaction and not to yielding of the beam. Slip started from the first application of load, but residual slip was not observed until a load of 3.0 tons. Transverse tension cracks at the bottom of the slab at midspan became visible at 6.0 tons. The maximum load attained was 6.1 tons at a deflection of 0.88in. A slight increase in pressure was followed by a loud sound and the studs in the left half of the beam sheared off. The load dropped to 3.90 tons. The beam carried a load of 4.30 tons at a deflection of 1.98in. A residual deflection of 1.62in. was recorded after the load was released.

All the studs in the left half of the beam sheared off. The maximum end slip, recorded before stud failure, was 0.052in. A big tension crack right across the bottom of the slab developed at midspan at failure. There was complete separation of the slab from the beam in the left half. No crushing of concrete was observed.

The strain and stress distribution at the midspan section at or near ultimate load for the beams of this group are shown in Figure 72. Yielding penetrated the whole depth of the beam A1 with strain hardening occurring in the bottom flange and a part of the web.

In beam A2, yielding did not occur at the extreme top fibres for a depth of about 0.1in., and in beam A3 yielding penetrated almost up to the top of the web. Strain hardening occurred in the bottom flange of this beam. The top flange and a part of the web were in compression in beams A4 and A5 with strain hardening occurring in the bottom flange of beam A4.

2. Beams of Group B

The test results for the beams, and the material tests for this series are summarised in Tables 8 and 9. Deflection, end slip, slip and uplift at quarter span are shown in Figures 54 to 67. The behaviour of each beam is described in the following pages.

(i) Beam B1. Shear connection: 44 studs with $\frac{1}{16}$ in. x $\frac{1}{32}$ in. grooves on top flange

Deflections were proportional to load up to 3.5 tons and deviated from the proportional line at 4.0 tons. Small tensile cracks at the bottom of the slab, starting from near the steel beams, were observed at midspan at 6.5 tons. Separation cracks between the slab and the beam started from these tension cracks at the same load. Spalling of concrete was visible around the loading pad at 6.8 tons. At this load, a central longitudinal crack on top of the slab was observed near midspan. The maximum load attained was 7.5 tons and the corresponding deflection was 1.52in. The load was then released and on re-loading, a bond breaking sound was heard at 6.9 tons, followed by a loud sound at 7.22 tons when the studs in the right half of the beam sheared off. After failure of the connectors the beam carried a load of 3.90 tons at a deflection of 2.02in. A residual deflection of 1.71in. was recorded after the load was finally released to zero.

Interaction was nearly complete up to a load of 7.3 tons; the average end slip at this load was 0.0011in. The slip and uplift at quarter span were 0.0079in. and 0.0039in. respectively. The maximum end slip recorded before failure of studs was 0.022in.

(ii) Beam B2. Shear connection: 44 studs with $\frac{1}{32}$ in x $\frac{1}{64}$ in. grooves on top flange

Non-linearity of the load-deflection curve started at 4.0 tons. Transverse tension cracks at the bottom of the slab at midspan were observed at the edges and near the steel beam at a load of 6.3 tons. Separation cracks between the slab and the beam started from the tension cracks developed near the steel beam at a load of 6.7 tons. A central longitudinal crack on top of the slab was observed to the left of midspan at a load of 6.9 tons. At the same load, spalling of concrete was observed near the loading pad. Failure was due to crushing of concrete and the maximum load attained was 7.4 tons at a deflection of 1.40 in. On increasing deflection, load gradually fell off and at 6.9 tons, the left end slip started increasing rapidly. Further increase in deflection was followed by a loud sound and the studs in the left hal of the beam sheared off at a load of 6.6 tons; the load dropped to 3.4 tons. Thereafter, the slab started shifting horizontally in a transverse direction, the beam became unstable and the test was stopped.

Interaction was nearly complete up to the maximum load of 7.4 tons. The average end slip at this load was 0.0011in; the average slip and uplift at quarter span were 0.0056in. and 0.0072in. respectively. The maximum end slip recorded before failure was 0.034 in.

(iii) Beam B3. Shear connection: 44 studs with natural bond

Deflections were proportional to load up to 3.45 tons, when the first slip sound was heard. Slip occurred in the left half of the beam at this load. The second slip sound occurred at 3.8 tons, followed by slip in the right half of the beam. Transverse tension cracks at the bottom of the slab were visible at midspan at 6.0 tons. The maximum load reached was 6.5 tons at a deflection of 1.04in. Two consecutive stud breaking sounds occurred at this load. Studs on the left half of the beam sheared off. After failure of the studs the beam carried a load of 3.61 tons at a deflection of 1.87 in. The residual deflection after the load was released to zero was 1.56in.

The interaction was complete until the bond broke and thereafter slip increased progressively with load. The maximum end slip recorded before stud failure was 0.034in. A big tension crack right across the bottom of the slab developed at midspan at failure. No crushing of concrete was observed.

(iv) Beam B4. Shear connection: 44 studs with natural bond destroyed

Deflections were proportional to load up to 3.5 tons and thereafter deviated from the proportional line. Slip started from the first application of load, but no residual slip was observed until a load of 3.5 tons was reached. Transverse tension cracks at the bottom of the slab were visible at midspan at 6.1 tons, and developed across the full width of the slab at 5.25 tons. The maximum load carried by this beam was 6.3 tons at a deflection of 1.06in. At this load, the left end slip started increasing very rapidly, followed by a loud sound and the studs in the left half of the beam sheared off. After failure of the connectors the beam

carried a load of 3.80 tons at a deflection of 1.60in. A residual deflection of 1.29in. was recorded after the load was released to zero.

The maximum end slip recorded before stud failure was 0.058in. A big tension crack right across the bottom of the slab developed at midspan at failure. There was complete separation of the slab from the steel beam in the left half. No crushing of concrete was observed.

(v) Beam B5. Shear connection: 44 studs with $\frac{3}{16}$ aggregate bonded to the top flange

Deflections were proportional to load up to 3.5 tons and thereafter deviated from the porportional line. Transverse tension cracks at the bottom of the slab were observed at midspan at 6.1 tons and extended to the full width of the slab at 6.3 tons. Spalling of concrete was observed near the loading pad at 6.5 tons. A separation crack between the slab and the beam was observed at this load. The maximum load reached was 6.6 tons. Before this load could be stablilised, there occurred a loud sound and the load dropped to 5.6 tons. Another sound followed and the studs on the right half of the beam sheared off; the load dropped to 4.30 tons. The beam carried a load of 4.15 tons at a deflection of 1.71 in. A residual deflection of 1.39 in. was recorded after the load was finally released to zero.

Slip started from the first application of load and was almost proportional to load up to 3.5 tons. Thereafter slip increased progressively with load. No residual slip was, however, observed until a load of 4.5 tons was reached. A small cracking sound was heard at load 4.0 tons, followed by an increase in slip. No other slip sound was heard. The maximum slip recorded before failure of the studs was 0.033 in.

(vi) Beam B6. Shear connection: 44 studs with Durbar plate as top flange

Deflections were proportional to load up to 3.0 tons and deviated from the proportional line at 3.5 tons. Yielding of the beam started at this load. Small tension cracks at the bottom of the slab developed near midspan at 5.8 tons and extended to the full width of the slab at 6.1 tons. Slight spalling of concrete was observed near the loading pad at 6.7 tons. Separation cracks between the slab and the beam became visible near midspan at 6.4 tons, extended up to about 20in. on either side of midspan at 6.7 tons and over the whole span at 7.0 tons. At 7.05 tons, which was also the maximum load attained, slip in the right half of the beam increased very rapidly. This was followed by a loud sound and the studs in this half of the beam sheared off; the load dropped to 3.0 tons. The deflection at the maximum load was 1.49in. After failure of the connectors the beam carried a load of 3.40 tons at a deflection of 1.80in. A residual deflection of 1.49in. was recorded after the load was finally released to zero.

Interaction was nearly complete up to a load of 2.9 tons, when a faint slip sound was heard, and an average end slip of 0.0001in. was registered in the slip gauges. No residual end slip was observed until a load of 4.5 tons was reached. The maximum end slip recorded before stud failure was 0.039in. Crushing of concrete and shearing of studs occurred almost simultaneously in this beam.

(vii) Beam B7. Shear connection: 44 studs with Latex rubber covering the root of the studs

The load-deflection curve was linear up to 1.75 tons and thereafter became non-linear, due to loss of interaction. No slip was observed up to 1.5 tons, when there occurred a slip sound, followed by breaking of bond on the left half of the beam, and a slip of 0.0012in. was recorded at the left end. A louder slip sound occurred at 1.75 tons and the slip at the left end increased to 0.0039in.; load dropped to 1.68 tons. At 2.0 tons, there occurred another slip sound; the bond on the right half of the beam broke and a slip of 0.0045ub, was recorded at the right end. Thereafter slip increased progressively with load.

Transverse tension cracks at the bottom of theslab were visible at midspan at 4.3 tons and extended to the full width of the slab at 4.5 tons. Crushing of concrete was observed near the loading pad at 6.25 tons at a strain of 0.0097. The maximum load attained was 6.50 tons at a deflection of 2.16in. Two consecutive stud breaking sounds occurred at this load and the studs in the left half of the beam were sheared off; the load dropped to 4.75 tons. The final load carried by the beam was 4.60 tons at a deflection of 2.39in. Residual deflection after the load was released to zero was 2.04in.

Interaction was nearly complete until the bond broke; thereafter there was practically no interaction until a load of 5.25 tons was reached, when the load-deflection curve became steeper. The average end slip at this load was 0.085in., compared to the latex cover around the studs of 0.094in. Apparently the studs started resisting slip at this load. The maximum end slip recorded before stud failure was 0.131in.

(viii) Beam B8. Shear connection: 44 studs with natural bond

Deflections were proportional to load up to 3.5 tons, and thereafter deviated from the proportional line. A small slip sound was heard at a load of 2.5 tons, followed by a loud sound at 3.0 tons, and the bond broke in both halves of the beam. Small tension cracks at the bottom of the slab were visible at midspan at 6.3 tons and extended to the full width of the slab at 6.8 tons. The maximum load attained was 6.9 tons at a deflection of 1.25 in. Two consecutive stud breaking sounds occurred at this load, the studs on the left half of the beam sheared off, and the load dropped to 4.2 tons. The beam carried a load of 4.4 tons at a deflection of 1.85in. A residual deflection of 1.53in. was recorded after the load was released to zero.

Slip increased progressively after bond broke. No residual end slip was observed until a load of 4.5 tons was reached. The maximum end slip recorded before stud failure was 0.049in. No crushing of concrete was observed. A big tension crack across the full width of slab developed near midspan at failure.

The strain and stress distribution at midspan of beams of group B at or near ultimate load are shown in Figure 73. Yielding penetrated the whole depth of the steel section in beams B1, B2 and B6. Extensive strain hardening occurred at the bottom flange in these beams. In beams B3, B4, B5 and B8, yielding occurred almost up to the top of the web with a part of the top flange in compression. In beam B7 yielding in compression occurred in the top flange and a part of the web, whereas extensive strain hardening occurred at the bottom flange and a part of the web at the bottom.

3. Beam C1

The shear connection consisted of 44 studs spaced according to the theoretical interface shear diagram at collapse. The test results for the beam and materials are summarised in Tables 8 and 9. Deflections, end slips, slips and uplifts at quarter span are shown in Figures 61, 62, 66 and 67. For convenience of comparison these are plotted along with those of beam B3.

Deflections were proportional to load up to 3.0 tons and thereafter deviated from the proportional line, due to loss of interaction. A comparatively loud slip sound occurred at 3.2 tons, followed by two more, and the load dropped to 3.1 tons. The first sound was accompanied by slip in the left half of the beam, while the others initiated slip in the right half. Transverse tension cracks at the bottom of the slab were visible at midspan at 5.8 tons and extended to the full width of the slab at 6.1 tons. Separation between the slab and the beam was clearly visible at this load along the whole length of the beam. The maximum load attained was 6.25 tons at a deflection of 0.89in. At this load there occurred three consecutive sounds, the studs in the left half of the beam sheared off and the load dropped to 4.53 tons. Increase in deflection did not increase the load. The beam carried a load of 4.2 tons at a deflection of 1.41in. A residual deflection of 1.11in. was recorded after the load was finally released to zero.

Slip increased progressively after bond had broken. An elliptical crack at the bottom of the slab and around a pair of studs was observed at about 9in. to the left of midspan. The maximum end slip recorded before stud failure was 0.051in. No crushing of concrete was observed. A big tension crack across the full width of the slab developed near midspan at failure.

The stress distribution at midspan at 6.1 tons is shown in Figure 73. The top flange up to a depth of 0.21in. was in compression whereas extensive strain hardening occurred in the bottom flange.

(g) Discussion of test results

1. Effect of "V" grooves on interaction

A very high degree of interaction is obtained in all the beams with V-grooves. The bigger the size of the grooves, the better is the interaction achieved. This can be seen from the apparent load per connector at ultimate load in beams A1, A2 and A3 (Table 8), and also from the stress distribution in the steel section of these beams at ultimate load (Figure 72). In beam A3 with $\frac{1}{32}$ in. x $\frac{1}{64}$ in. grooves, yielding penetrated almost up to the top of the web. In beam A2, with $\frac{1}{16}$ in. x $\frac{1}{32}$ in. grooves, a part of the top flange also yielded, whereas in beam A1 with $\frac{1}{8}$ in x $\frac{1}{16}$ in. grooves, full plasticity was obtained and interaction was almost complete until failure occurred by crushing of concrete. The apparent load per connector at ultimate load is 1.98 tons, 1.84 tons and 1.58 tons in beams A1, A2 and A3 respectively.

No definite slip sound was heard in these tests. At the first measured slip, to reach 0.0005in., the average shear stresses at the interface were 853 p.s.i., 800 p.s.i. and 708 p.s.i. in beams A1. A2 and A3 respectively. The maximum shear stresses, however, can be much higher than these average stresses, as yielding had already occurred.

The ultimate load carried by beam A2 is comparatively lower, that is, 6.7 tons as against 7.9 tons in beam A1, and 7.0 tons in beam A3. Beam A2 also shows larger deflection and greater slip for the same load in the inelastic stage than beams A1 and A3. This can be attributed to the variation in quality of steel.

A tension test on a coupon from the flange of beam A2 shows a very large plastic range, $\varepsilon_{sh}/\varepsilon_y$ being about twelve (Table 3), whereas in beams A1 and A3, strain hardening occurs soon after the yield strain. Beyond the yield load, therefore, beams A1 and A3 can carry higher loads at a smaller additional deflection, and can develop a greater moment than beam A2 for the same strain gradient. On the other hand, to develop the same moment, the strain gradient will have to be greater in beam A2, and this decreases the lever arm and so increases the axial force. For the same load, therefore, beam A2 will have larger deflection, greater axial force and hence greater slip.

Interaction produced by V-grooves improves with increase in the number of studs. Beams B1 and B2, having grooves similar to beams A2 and A3 but with a greater number of studs, show even better interaction. Full plasticity was obtained at ultimate load in both beams and maximum end slips recorded at or near ultimate load were 0.0012in. and 0.0014in. in beams B1 and B2 respectively. At the first significant slip, calculated average mechanical bond stresses were 860 p.s.i. and 1009 p.s.i. respectively. The higher value in B2 may be due to its higher concrete cylinder strength (5650 p.s.i., against 4650 p.s.i. for beam B1).

If H is the total horizontal shear at the interface, H_c is the total horizontal shear resisted by the connectors, then it is reasonable to assume that $H - H_c = H_B$, where H_B is the total horizontal shear resisted by mechanical bond at the interface. At a particular load, H can easily be estimated from measured strains at midspan and corresponding stress-strain curves. If the slip distribution along the length of the beam is known, then the load taken by each connector and hence H_c can be calculated using the load-slip curve for the connector as obtained from a push-out test. H_B is then obtained using the above relation.

H_B is calculated for various loads and the maximum value of H_B is obtained. These maximum values of H_B and the corresponding average mechanical bond stress for the three different grooved flanges are shown below.

Beam	Nature of flange surface	W (tons)	H (tons)	H_B (tons)	Av. mech. bond stress (p.s.i.)	$\frac{H_B}{H} \times 100\%$
A1	$\frac{1}{8}$in. x $\frac{1}{16}$in. grooves	7.64	30.80	23.91	1020	77.6%
B1	$\frac{1}{16}$in. x $\frac{1}{32}$in. grooves	6.50	29.75	21.30	910	71.6%
B2	$\frac{1}{32}$in. x $\frac{1}{64}$in. grooves	6.50	28.72	20.75	885	72.2%

Since the loads at which these values are obtained are close to the ultimate loads and since the horizontal shear distribution at ultimate load is far from uniform, the maximum shear being about 3 times the average shear (Figure), the maximum values of bond stress for these grooved surfaces may be much higher than the average values given in the table. It may also be pointed out that not more than 30% of the total shear is carried by the connectors.

The shear resistance provided by the grooves is due to their mechanical keying action; the bigger the grooves, the better is the keying action and therefore greater is the interaction achieved. When the shear is sufficiently high, concrete starts shearing at the plane on top of the grooves; shear resistance reduces to a very great extent and the load is mostly thrown on to the studs. As the total shear obtained from measured strains at midspan is much greater than the total capacity of the studs, immediate failure of studs occurs. In beams A2, A3, B1 and B2, failure of studs occurred immediately after the ultimate load had been reached.

2. Effect of Durbar flange of interaction

Slip is due to the deformation of concrete behind the projections of the Durbar plate and the studs. The overriding effect is more pronounced in this case than in the "V" grooved flange and so also is the uplift. However, given sufficient hodling down, these small projections act as connectors and greatly increase the interaction between the concrete slab and the steel beam.

In beam B6, where the top flange was replaced by a Durbar plate, very good interaction was obtained. Full plasticity was obtained in the steel section (Figure 73) at ultimate load. The ratio of experimental ultimate load to calculated ultimate load is 1.16, as against 1.03 for beam B3 with natural bond. Slip was higher in this beam than in beams with V-grooves, but smaller than in beam B3. At the first faint slip sound, which is also the load at first significant slip, the calculated average bond stress in beam B6 was 493 p.s.i.

Beam B6 shows a larger deflection than beam B3. The top Durbar plated flange was $\frac{3}{16}$ in. thick against an average flange thickness of $\frac{1}{4}$in. in beam B3. Yield stresses of the top flange and web of beam B6 are also slightly smaller than those of beam B3. The smaller concrete cylinder strength of 4000 p.s.i. for beam B6 as against 5500 p.s.i. for beam B3 may also contribute to the larger deflection of beam B6.

The apparent load per connector at ultimate load in beam B6 was 1.29 tons against the ultimate push-out capacity of 1.08T with natural bond and 1.63T with the Durbar plated flange. The lower strength of stud in the beam test with respect to the corresponding push-out test result with similar flange may be due to the smaller area of Durbar plate per connector in the beam (36 per cent less)

than in the push-out specimen.

The maximum value of H_B and the corresponding average mechanical bond stress is given below. The corresponding load was 4.60T and is higher than the yield load. It can, therefore, be argued that the maximum shear resistance of the Durbar flange will be higher than this average value.

Beam	Flange surface	H (tons)	H_B (tons)	Av. mech. bond stress (p.s.i.)	$\frac{H_B}{H} \times 100\%$
B6	Durban flange	19.24	13.13	560	68.2%

3. Effect of resin-bonded aggregate on top surface of steel flange

$\frac{3}{16}$ in. aggregates were glued with resin (Polyester resin plus 0.1% hardener) to the surface of the top flange of beam B5. The concrete slab was cast after the resin had hardened.

The results obtained are not satisfactory. Slip occurred from the first application of load and was higher at all stages of loading than the slip in beam B3 (with natural bond). Resin when hardened leaves a smooth surface on top. Concrete when cast on top of this surface may not bond properly with the resin. This may account for the occurrence of slip from the first application of load. On the other hand it is possible that the resin behaved elastically and caused slip.

The calculated bond stress at the first significant slip is 358 p.s.i. A very faint cracking sound was heard at load 4.0 tons. No definite slip sound was heard in this beam which would have indicated the failure of the resin bonded joint at the interface.

The degree of interaction obtained was by no means better than beam B3. Ultimate load was 6.60 tons as compared with 6.50 tons in beam B3. The maximum end slips recorded at 6.50 tons were 0.034in. and 0.033in. in beams B5 and B3 respectively. The ultimate capacity of connectors obtained from beam B5 and B3 are 1.0 ton and 1.1 tons respectively. A part of the top flange was in compression in both beams at ultimate load (Figure 73).

Results of tension tests on coupons from these two beams do not differ very much. The concrete cube strengths are very nearly the same. This test indicates therefore that no improvement in interaction can be obtained by using resin bonded aggregates to the surface of the steel flange.

4. Effect of natural bond on interaction

It is known that in uncased beams bond alone cannot be relied upon to produce any interaction between the concrete slab and the steel beam. In most cases bond breaks down even before the specimen can be tested. In order to help bond develop, it is necessary to provide sufficient mechanical connectors. Having done that, bond plays a very important part in producing interaction in composite beams; and in fact interaction is complete until bond fails.

Failure of bond in composite beams is often indicated by a slip sound accompanied by sudden occurrence of slip, but in some cases slip is recorded even before such a sound is heard. Table 8 shows the bond stress at first slip sound and also at the first significant slip.

The bond stress obtained from the test of beam B7 is of particular interest. In this beam, the roots of the studs were covered with flexible latex up to a height of about $\frac{1}{2}$ in. from the base so as virtually to prevent the studs from resisting any shear whilst at the same time holding down the slab to the steel beam. The horizontal shear, therefore, was resisted almost entirely by natural bond until bond broke. The first slip sound was heard at 1.50 tons, which corresponded to a bond stress of 228 p.s.i. Slip was first observed at this load, and thereafter increased very rapidly. That the bond resists the whole of the shear and creates complete interaction until it fails is very well brought out in this test. Complete interaction was obtained in this beam up to this load.

Bond stress was found to vary rather widely, ranging from 228 p.s.i. to 512 p.s.i., a variation from 0.045 f'_c to 0.117 f'_c when expressed in terms of concrete cylinder strength.

After bond failure, the friction appears to provide a certain amount of shear resistance at the interface. This frictional resistance, which is greater near the supports, may be a reason for smaller slip at the ends than at the quarter span region in beams where bond was not destroyed.

Slip is generally greater in beams without bond than in beams with bond, even after the failure of bond. This may be attributed to the frictional resistance at the interface in beams where bond was not destroyed. This may also explain the greater average load per connector obtained at ultimate load in beams with bond than in beams without bond.

5. Comparative behaviour of beams with studs spaced uniformly and according to horizontal shear diagram at interface at ultimate load (Beams B3 and C1)

If the number of shear connectors is chosen on the basis of total horizontal shear at the interface at ultimate load, then it can be argued that the connectors could be spaced according to the distribution of interface shear at that load. The results of this method of connector spacing can be seen from a comparative study of the behaviour of beams C1 (studs spaced according to interface shear) and B3 (studs spaced uniformly).

A study of slip curves (Figure 62) shows that the slip is approximately the same for both beams up to a load of 3.0 tons. Thereafter, the slip in beam C1 increases more rapidly than in beam B3. As this load is below yield load, the interface shear (for complete interaction) is still uniform and higher slips at the ends and at quarter span points in beam C1 are presumably due to the greater spacing of studs in this region. This argument, however, does not hold good after yield. The much lower concrete cylinder strength of beam C1 (3920 p.s.i. against 5500 p.s.i. for beam B3) may be a reason for greater slip in beam C1.

If slip is an indication of the degree of interaction achieved, then interaction in beam C1 is less complete than in beam B3. This, together with lower concrete strength may account for slightly larger deflection at loads greater than 3.0 tons in beam C1 (there is not much difference in the steel properties).

The ratio of the experimental ultimate load to the calculated ultimate load is nearly the same in both the beams. The average load per connector at ultimate load is 1.1 tons for beam B3 and 0.97 ton in beam C1. The maximum end slips recorded at or near ultimate load were 0.034 in. and 0.037 in. in beams B3 and C1

respectively. At ultimate load a greater depth of the top flange was in compression in beam C1, than in beam B3, showing a slightly better interaction in beam B3 than in beam C1.

In view of the above observations and the enormous numerical calculations involved in estimating the interface shear distribution at ultimate load (even when the effect of slip is ignored), it could be concluded that no useful purpose will be served by spacing the connectors according to the interface shear at ultimate load.

6. Nature of failure

Beam A1 failed by crushing of concrete. Connectors did not fail in this beam. In beams A2 and B1 spalling of concrete had been observed before the maximum load was attained; final failure occurred at the maximum load by studs shearing off. Beam A3 failed by shearing of concrete at the interface at the maximum load, followed by studs shearing off. Beam B2 failed by crushing of concrete; studs sheared off after the maximum load had been reached. Crushing of concrete and shearing of studs occurred almost simultaneously in beam B6. All other beams failed by studs shearing off at maximum load.

The loads the beams were able to carry after failure of the studs, except beams A1, B7 and B8, ranged from 3.61 tons to 4.33 tons. In the case of beam A1 the test was stopped at 5.50 tons at a deflection of 3.34in., after extensive crushing of concrete had taken place. Beam B7 carried a load of 4.60 tons after failure of studs. This higher load was due to extensive strain hardening which had occurred in both top and bottom flanges of the steel beam.

Beam B8, which was tested under two point loads, carried a load of 4.42 tons after stud failure. The collapse load of the bare steel beam is 3.02 tons, based on f_y = 20.98 t.s.i. (average experimental yield stress).

Transverse tension cracks at the bottom of the slab at or near midspan were seen at loads ranging from 5.8 tons to 6.5 tons, except beam B7, where a crack was observed at 4.3 tons. These cracks, except those in grooved flanged beams, extended right across the slab within a load increase varying from 0.15 ton to 0.45 ton from the load of their first appearance.

In most of the beams, tension cracks started from the edge of the slab. The decreasing compression towards the edge, due to shear lag in the slab, may cause larger tensile strains at the edge which eventually cause tension cracks to develop there. But in beams with grooved flanges, tension cracks were found to start from the centre. In beam B2 tension cracks were observed both at the edge and near the centre at the same load. In these beams interaction was very high and since the loads at which these cracks occurred were much higher than yield load, the interface horizontal shear near midspan was also very high. Due to this high shear and stress concentration which may exist at the ends of flange serration, it is possible that concrete cracks occur there and then spread outward. This effect was very clearly seen in the Durban flanged beam B6, where these cracks started from the side of the pips facing midspan.

Crushing of concrete was observed near the loading pad at loads varying from 6.5 to 7.0 tons in grooved flanged beams and also in beam B6. Approximate concrete strains at crushing varied from 0.0040 to 0.0054. Spalling of concrete was also observed in beam B7 at load 6.25 tons at a concrete strain of 0.0097. No crushing of concrete was observed in other beams. A very wide

tension crack right across the bottom of the slab near midspan, however, occurred in these beams at failure (Figure 83).

In beams B1 and B2, a central longitudinal crack, similar to those observed by Adekola [28], occurred near midspan at loads of 6.8 tons and 6.9 tons respectively.

In grooved flanged beams, failure is initiated by shearing of concrete at the interface. A muffled sound is often heard when this failure occurs. Slip increases very rapidly thereafter, and the eventual failure occurs by shearing of studs. In all other beams slip increases gradually, and the rate of increase increases with load until an end slip of about 0.03in. to 0.04in. is recorded. Thereafter the increase is extremely rapid and final failure of studs occurs at an end slip of about 0.06in.

4.2 Half Scale Composite Beams

(a) Purpose of tests

The main purpose of these tests was to study the behaviour of composite beams where the steel beam was provided with small projections formed on the top surface of the top flange. It was thought that these small projections would strengthen the shear connection by resisting the interface shear and preventing the slip. Another purpose was to estimate experimentally the axial forces which would be introduced in the stud shear connectors, due to the concrete slab riding over these small projections as the slip began.

Two beams were tested; one having the top flange provided with these small projections while the other had a plain top flange. The cross-section of both the beams were kept the same, so that a comparative study of the behaviour could be made.

(b) Description and preparation of specimens

Steel beams were made from 9in. x 4in. at 21 lb. A.S.B. The top flange was replaced by a 4in x $\frac{3}{8}$ in. thick Durban plate, making an overall dimension of $8\frac{3}{16}$ in. x 4in. (Figure 85). The Durban plate was welded to the web with the plain surface facing the web in beam D1, whereas in beam D2, the surface having the projections was facing the web.

56-$\frac{3}{8}$ in, diameter x $1\frac{1}{2}$ in. long headed studs were welded to each beam in pairs at uniform spacing longitudinally and 2in. apart transversely. The number of connectors was chosen to resist the total horizontal shear at the interface at collapse using 100%

of the connector capacity. No special preparation was given to the steel beams, except brushing with a stiff wire brush to remove loose scale or rust.

The reinforced concrete slab was 3in. thick and 9' 4" long by 3' 0" wide. Transverse reinforcement consisted of $\frac{3}{8}$ in. diameter mild steel bars placed at $4\frac{1}{2}$ in. centres at the top and at 9 in. centres at the bottom. Reinforcement in the longitudinal direction consisted of $\frac{1}{4}$ in. diameter bars at 10in. centres at both top and bottom. A timber mould was used for casting the slab. The beam and the mould rested on the floor while casting. Concrete was made using Ferrocrete rapid hardening cement, sand and $\frac{3}{8}$ in. aggregates. The aggregate cement ratio by weight was 4.5 with 60 per cent aggregate and 40 per cent sand, and the water cement ratio was 0.55. The concrete was compacted by an immersion vibrator. Eight 4in. cubes and four 12in. x 6in. cylinders were cast for each of the slabs. Curing lasted a week under wet sacking covered with polythene sheet.

(c) Loading

Point load at midspan was applied through a 50 ton hydraulic jack operated by an electric pump. A hand pump was used in conjunction with the electric pump to control the applied load accurately. The point load was spread over the concrete slab by a 6in. x 5in. x $\frac{5}{8}$ in. thick steel plate. In order to distribute the pressure uniformly a thin plywood board was used under the loading plate.

Load was measured by a proving ring dynamometer of 50 ton capacity. Both the beams were tested over a span of 9' 0", supported at both ends on free rollers of 4in. diameters as shown in Figure 85.

(d) Measurements

Deflection at midspan, slips and uplifts at a number of locations along the span were measured using dial gauges. A demountable mechanical gauge of 8in. gauge length was used to measure the strains in concrete and steel at the midspan section. Strains in studs at a number of points in one half and at the quarter span point in the other half of the beam, were measured using foil strain gauges of $\frac{1}{4}$ in. gauge length. Figure 86 shows the arrangements for measurement of slips, strains, etc.

(e) Testing procedures

Beams: The point load at midspan was applied in 2.5 ton increments up to 10 tons, then in 2.0 ton increments up to 20 tons and thereafter in 1 ton increments. After each application of load a set of readings was taken, the load was released and another set of readings was taken at zero load. At loads higher than yield load, the jack was pumped repeatedly to obtain steady conditions before the readings were taken.

Materials:

(a) Steel. Flat specimens $1\frac{1}{2}$ in. wide by 24in. long were cut from both top and bottom flanges of each beam and tested as explained in section 4.1.

(b) Concrete. Concrete was tested as explained in section 4.1.

(c) Studs. Specimens were turned from $\frac{3}{8}$ in. dia. x $1\frac{1}{2}$ in. long studs and tested as explained in section 4.1.

(f) Test results

(i) Beam D1. Shear connection: 56-$\frac{3}{8}$ in. dia. x 1$\frac{1}{2}$ in. long headed studs with projections of Durbar plate

Midspan deflections are shown in Figure 88. Deflections are proportional to load up to 17.0 tons and thereafter deviate from the proportional line. Transverse tension cracks at the bottom of the slab at midspan started from near the steel beam at 22.0 tons, and extended to the full width of the slab at 24.0 tons. Spalling of concrete was observed near the loading pad at 29,0 tons at a strain of 0.0039. Horizontal cracks at the bottom of the slab starting from the front of each projection were observed at 30 tons at approximately 12in. on either side of midspan. The maximum load carried was 31.3 tons and the corresponding deflection was 1.59in. Thereafter the crushing of concrete became more extensive, transverse tension cracks became wider and the load started falling. At load 30 tons a cracking sound was heard, and a big lump of concrete broke off from the edge of the slab. A central longitudinal crack, extending from near the loading pad to about 24in. on either side, was observed at this load. Horizontal splitting on the edge of the slab at midspan was also observed at the same load. The beam carried a load of 23.06 tons at a deflection of 2.24in. A residual deflection of 1.86in. was recorded after the load was finally released to zero.

Slips at the end, at quarter span and along the span at various loads are shown in Figures 89 to 92. Slip started from the beginning of the test and was almost proportional to load up to 24.0 tons. The average total end slip at this load was 0.0024in. and average residual end slip was 0.0007in. The maximum end slip recorded at the maximum load was 0.0115in. Slip, however, continued increasing after the maximum load had been reached.

Separation of the slab from the beam at quarter span and also along the whole span at various loads are shown in Figures 93 and 94. Up to a load of 22.0 tons uplift was very small and negative at all points except at the right hand support and at midspan. Thereafter uplift became positive at all points and started increasing rapidly with load. Up to a load of 28.0 tons, the maximum uplift recorded was smaller than the maximum slip for the same load; but thereafter the maximum uplift was greater than the maximum slip. The maximum uplift recorded at the maximum load was 0.056in. and was at a distance of $6\frac{3}{4}$ in. from midspan.

The stress distribution at the midspan section at a load of 31.3 tons is shown in Figure 98. Yield had penetrated up to the top of the steel beam and extensive strain hardening had occurred in the bottom flange and the web.

Figures 100 and 101 show the extensive crushing at the top of the slab, the wide tension crack at the bottom and the horizontal splitting of the slab at the edge.

(ii) Beam D2. Shear Connection: 56-$\frac{3}{8}$ in. dia. x $1\frac{1}{2}$ in. long studs with plain flange and natural bond

Midspan deflections are shown in Figure 88. Deflections are proportional to load up to 12.0 tons and thereafter increase rapidly with load. This is due to loss of interaction and not to yielding of the beam. Transverse tension cracks at the bottom of the slab were observed at midspan at 18.0 tons. Two more tension cracks developed, one on either side of midspan, at 22 tons and the separation between the slab and the beam started from these cracks. Crushing of concrete was observed near the loading pad at a load of 25 tons at a strain of 0.0048. The maximum load carried by the beam was 26 tons at a deflection of 1.58in. Thereafter crushing of concrete became more extensive, the tension cracks became wider,

and the load started falling. At 23.2 tons the slip on the left half started increasing more rapidly and at 22.0 tons the beam collapsed by failure of concrete around the studs (Figure 102). Only two studs near the left support sheared off. A horizontal splitting of the slab at midspan was observed just before final failure. The load dropped to 13.4 tons; the corresponding deflection was 3.03in.

Slips at the end, at quarter span and along the span at various loads are shown in Figures 89 to 92. A faint slip sound was heard at 10 tons, when end slips were first recorded. Two consecutive loud sounds occurred at 14.0 tons, followed by considerable slip on both sides. Thereafter slip increased progressively with load. The maximum end slip at ultimate load was 0.039in. and the maximum slip before failure was 0.070in., both recorded at the left end.

Separation of slab from beam at quarter span and also along the length at various loads is shown in Figures 94 and 95. First uplift was recorded at $6\frac{3}{4}$ in. from midspan on either side, at the same load at which the first end slip was recorded, and thereafter increased progressively with load. The maximum uplift at the ultimate load was 0.037in., recorded at $6\frac{3}{4}$ in. to the left of midspan.

The axial strains in the studs at points along the beam are shown for various loads in Figure 97. The stress distribution at the midspan section at 26 tons is shown in Figure 98. Yield had penetrated up to about half the depth of the top flange. Strain hardening had occurred in the bottom flange and part of the web. The failure of concrete around the studs is shown in Figure 103.

(g) Discussion of test results

1. Deflection

Figure 88 shows midspan deflections for both beams. Deflections are the same up to a load of 14.0 tons, after which beam D2 shows larger deflections for the same load. This marked difference in deflections can be explained as follows. Concrete strengths for both beams are nearly the same; so also the properties of the top flange, which is a $\frac{3}{8}$ in. thick Durbar plate in both cases. The main difference is in the steel properties of web and bottom flange in the two beams. Tension tests on coupons show a higher yield stress of 20.3 t.s.i. and a lower $\varepsilon_{sh}/\varepsilon_y$ ratio of 1.9 in beam D1, compared to a yield stress of 17.7 t.s.i. and $\varepsilon_{sh}/\varepsilon_y$ ratio of 14.1 in beam D2. Besides having a higher yield load, beam D1 can, therefore, carry a higher load at a smaller additional deflection. The slightly larger deflection in beam D2 below yield load is due to greater loss of interaction.

2. Ultimate load

The calculated ultimate loads for beams D1 and D2 are 28.27 tons and 25.05 tons respectively; the ultimate loads obtained from experiments are 31.3 tons and 26.0 tons, an increase of 11 per cent and 4 per cent respectively. The higher increase in beam D1 is due to (a) smaller $\varepsilon_{sh}/\varepsilon_y$ ratio of stress-strain curve for web and bottom flange, which increases the load carrying capacity of the beam and (b) better interaction achieved due to shear resistance of the pips of Durbar plate. Full plasticity was obtained at ultimate load in beam D1, whereas in beam D2 yielding did not occur in part of the top flange.

3. Effect of Durbar plated flange on interaction

(a) Slip. Figures 89 to 92 show end slips, quarter span point slips and slips along the beam at various loads. Slip started from the first application of load in beam D1 and was greater up to a load of 15.0 tons. This may be attributed to the original painting on the Durbar plate as supplied, which makes the surface smooth and prevents bonding of the concrete slab to steel beam. No slip sound was, therefore, heard in this beam.

After 15.0 tons, slip in beam D2 increased more rapidly than in beam D1. Because of the difference in the properties of steel, it is expected that beam D2 will have a greater axial force at midspan, with greater total horizontal shear and so greater slip for the same load beyond yield. Nevertheless, slip in beam D2 is much higher than in beam D1. At 26.0 tons, which is the ultimate load of beam D2, the maximum end slip in beam D1 was 0.0035in. compared to 0.038 in. in beam D2. The maximum end slip recorded in beam D1 at the ultimate load of 31.3 tons was 0.0116in.

(b) Uplift. Uplift at the quarter span point and along the beam at various loads are shown in Figures 93 and 94. Because of the presence of projections on the Durbar plate of beam D1, it would be reasonable to expect a greater uplift in beam D1 than in beam D2. But the uplift curves show that at all stages of loading, uplift is smaller in beam D1 than in beam D2 for the same load.

Uplift is also shown against slip in Figure 95 for both beams at quarter span. Except when both uplift and slip are small, uplift in beam D1 is found to be much greater than in beam D2 for the same slip. It can also be seen that the uplift-slip curve is not very far from linear, with a bigger gradient for beam D1. It can, therefore, be concluded that uplift is more related to slip than to the external load applied.

(c) Strain in studs. Strains in studs at various locations along the beam were measured using E.R. foil gauges (Figure 86). Unfortunately, some of these gauges in beam D1 did not function properly, perhaps being damaged during casting of the slab. However, axial and bending components of measured strains in studs at quarter span point for both beams and variation of axial strains along the beam D2 at various loads are shown in Figures 96 and 97. The axial strain is more or less equal to the bending strain in beam D2, whereas in beam D1, the axial strain is much higher than the corresponding bending strain.

The variation of axial strain along beam D2 is similar to the theoretical uplift force curve and isishown in Figure 97.

(d) Load per connector at ultimate loads. The load per connector at ultimate load, as obtained from measured strains at midspan, is 4.38 tons in beam D1 and 3.66 tons in beam D2. The ultimate capacity of a $\frac{3}{8}$ in. dia. x $1\frac{1}{2}$ in. long headed stud as obtained from push-out tests with natural bond is 3.00T. The higher ultimate strength obtained in beam D2 can be explained as follows. The concrete cylinder strength in beam D2 was 4850 p.s.i. as compared with 3530 p.s.i. in the push-out specimen. If it is assumed that the ultimate capacity of a stud varies directly as the square root of the concrete cylinder strength, then the ultimate capacity of a stud for a concrete strength of 4850 p.s.i. will be 3.52T, which is quite close to the ultimate capacity obtained in beam D2.

The even higher ultimate stud capacity obtained in beam D1 is, however, due to the extra shear resistance offered by the projections on the Durbar plate. It may also be pointed out that the connectors did not fail in beam D1, the failure of the beam was due to crushing of concrete. It is therefore possible that the apparent ultimate capacity of the connector could be even higher.

(e) Bond stress. The calculated bond stress at first significant slip is 237 p.s.i. in beam D1. Due to the painting on the surface of the Durbar plate, this figure does not give a true mechanical bond value for this type of surface. The maximum value of H_B calculated on the basis described earlier and the corresponding average mechanical bond stress are given below.

Beam	Flange surface	W (tons)	H (tons)	H_B (tons)	Av. mech. bond stress (p.s.i.)	$\frac{H_B}{H}$ x 100%
D1	Durbar flange	29.4	113.37	50.14	520	44.2%

This value is very close to the value obtained in the quarter scale beam. As the load on the beam is very close to the ultimate load, the maximum mechanical bond stress could be higher than this average value.

The bond stress in beam D2 is found to be 334 p.s.i. (Table 8).

4. Type of failure

Beam D1 failed due to crushing of concrete which started at a load of 29.0 tons at an approximate concrete strain of 0.0039. Crushing became more extensive after the maximum load of 31.3 tons had been reached and finally a big lump of concrete broke off from the concrete slab at 30.0 tons and the load dropped to 23.0 tons. Initial failure of beam D2 was also due to crushing of the slab which started at 25.0 tons at an approximate concrete strain of 0.0048. Thereafter slip started increasing more rapidly, load started falling after a maximum load of 26.0 tons had been reached, and final failure occurred at a load of 22.0 tons due to failure of concrete around the studs. Two studs near the left support sheared off.

The failure of concrete around the studs in beam D2 is of particular significance. Considering an individual stud, if it is assumed that the failure occurs in the same way as has been described on page 93 , then assuming that

$$T = (h \tan \theta + \frac{D}{2})\, h \sec \theta .\ f_t$$

where T = total tension in the stud

f_t = tensile stress in concrete,

for $\theta = 45^{\circ}$

$$f_t = \frac{T}{\sqrt{2}\, h\, (h + \frac{D}{2})}$$

The maximum strain was recorded in a stud at quarter span. At 24.0 tons, the value of f_t, estimated using the above relation for this stud, is 340 p.s.i. At the maximum load of 26.0 tons, this stress may be still higher and so sufficient to cause failure. Since the transverse and longitudinal spacing of studs in beam D2 is 2in. and 3.86in. respectively, it is quite possible that the failure surfaces overlap and this may account for the nature of the failure in beam D2 (Figure 102).

CHAPTER V

EXPERIMENTS ON COMPOSITE PLATES

5.1 Pilot tests on quarter scale plated beams

(a) Purpose of Tests

The main purpose of these tests was to make a preliminary study of the behaviour of plated beams to obtaine information which would help in the planning and carrying out of further tests. The interaction produced by natural bond, by natural bond with stud shear connectors and by stud shear connectors without natural bond was studied in these tests.

(b) Description and preparation of specimens

Three beams were tested, each consisting of a $2\frac{1}{4}$ in. deep and 6in. wide by 36in. long concrete slab shear connected to a mild steel plate $\frac{1}{8}$ in. thick and 6in. wide by 44in. long (Figure 103). No reinforcement was provided in the concrete slab.

The beams were designated as PB1, PB2 and PB3. Shear connection in PB1 was provided only by natural bond, whereas beams PB2 and PB3 each had 24-$\frac{3}{16}$ in. diameter by 1in. long (100 per cent design) headed studs welded to the steel plate at 3in. centres in both directions. Natural bond was destroyed in PB3 by using resin and grease on the steel plate, whereas in PB2 natural bond was allowed to develop.

Concrete was made using rapid hardening cement, sand and $\frac{3}{16}$ in. aggregate. The aggregate cement ratio by weight was 3.25 with 50 per cent aggregate and 50 per cent sand, and the water cement ratio was 0.55. A steel mould was used for casting. The

steel plate was continuously supported while casting. Three 4in. cubes and two 12in. x 6in. cylinders were cast for each of the slabs. Concrete was compacted with an immersion vibrator and the curing was done for a week under wet sacking covered with polythene sheet.

(c) Loading

The beams were tested under a central point load over a simple span of 36in. The load was applied through a 30 ton hydraulic jack operated by a hand pump, and was measured by a proving ring dynamometer of 5 ton capacity. The beams were supported on a free roller at one end and on a fixed roller at the other (Figure 103).

(d) Measurements

Deflections at midspan and slips at both ends were measured using dial-gauges. Strains in concrete and steel at the midspan section and in steel at the bottom of the plate at a number of locations along the span were measured by a demountable mechanical gauge of 2in. gauge length. Figure 104 shows the general arrangement for measuring slips, strains, etc.

(e) Testing Procedure

The point load at midspan was applied in 0.25 ton increments until failure. After each application of load a set of readings was taken, the load was released and another set of readings was taken at zero load. This procedure was continued until the end of the test.

Steel, concrete and stud material were tested as explained in section 4.1.

(f) Test results

(i) Beam PB1. Shear connection: Natural bond

This beam could not be tested, as the bond was broken before the beam could be lifted to the test frame. A cracking sound was heard during handling, the bond broke down and the steel plate separated from the concrete slab on one half of the beam. The bond failure appeared to have started from all round; and it is possible that the shear produced at the interface due to shrinkage of concrete is the main cause that initiated the breaking of bond.

(ii) Beam PB2. Shear connection: 24-$\frac{3}{16}$ in. diameter by 1in. long headed studs with natural bond

Midspan deflections and end slips are shown in Figures 105, 106 and 107. Deflections were proportional to load up to 1.0 ton. No slip was observed up to this load. At this load a cracking sound was heard and the bond broke at both ends. This was accompanied by dropping of load and increase in deflection. Thereafter both deflection and slips increased rapidly with load. The calculated bond stress at this load was 102 p.s.i. The separation between the slab and the plate was visible at a load of 1.50 tons and at 1.75 tons vertical tension cracks developed near midspan. A diagonal tension crack appeared at the bottom of the slab at a distance of $6\frac{1}{2}$ in. from the midspan at 2.40 tons, progressed rapidly upwards and finally broke off the concrete at the top, at a distance of about $2\frac{1}{4}$ in. from midspan. The maximum load attained was 2.47 tons. The maximum strains recorded at midspan at 2.40 tons were 0.0046 in the concrete and 0.0010 in the steel plate. The greater end slip at this load was 0.014in.

(iii) Beam PB3. Shear connection: 24-$\frac{3}{16}$ in. diameter by 1in. long headed studs, without natural bond.

Midspan deflections and end slips are shown in Figures 105, 106 and 107. Slip started from the first application of load and increased with load. Vertical tension cracks were visible at midspan at a load of 1.75 tons. At 2.25 tons, a diagonal tension crack, similar to the one in beam PB2, appeared at the bottom of t the slab at about 7in. from midspan, spread rapidly upwards until finally the concrete broke off at the top near midspan. The maximum load reached was 2.25 tons. The maximum strains recorded at midspan at 2.25 tons were 0.0037 in concrete and 0.0011 in steel. The greater end slip at this load was 0.015in.

(g) Discussion of test results

It is evident from beam PB1 that the natural bond alone cannot be relied upon to produce any interaction and that mechanical connectors are necessary to produce it.

Both the beams PB2 and PB3 failed before the calculated ultimate load was reached. The maximum steel stresses reached were 13.0 t.s.i. in beam PB2 and 14.3 t.s.i. in beam PB3. The beam with natural bond, i.e. PB2, failed at a slightly higher load but at a lower steel stress than the beam without bond. This shows that a slightly better interaction is obtained with natural bond than without it. This is probably due to friction that existed at the interface after bond had broken.

The mode offailure was similar in both the beams. The failure was due to shear failure of concrete in diagonal tension. The calculated shear stresses at failure were 244 p.s.i. and 228 p.s.i. in beams PB2 and PB3 respectively. It was also observed

that the diagonal tension cracks followed a path that did not intersect any studs. It was therefore believed that if the crack could have been intercepted by connectors, either by decreasing the spacing or by increasing the length, the diagonal tension failure might have been delayed. Alternatively, shear reinforcement would be necessary.

Heavy local bending of the steel plate was observed after failure near the lowest point of the diagonal tension crack. This was due to shearing displacement as the sudden failure of concrete had caused the steel plate to resist the full shearing force momentarily before the load fell off.

5.2 Small scale plated beams

(a) Purpose of tests

The main purpose of these tests was to study the behaviour of plated beams having varying numbers of shear connectors. Headed stud shear connectors were used and the number was so varied that the nominal load per connector at theoretical collapse load would vary from 50 to 150 per cent of the ultimate strength of the connector. The longitudinal pitch was kept constant and was equal to the elastic lever arm of the composite section. The variation of number was achieved by varying the transverse spacing.

Another purpose was to study the effect on interaction of roughness on the top surface of the steel plate. A Durban plate was used for this purpose.

(b) Description and preparation of specimens

Three plated beams were used to study the effect of varying the number of connectors. They were designated as PB4, PB5 and PB6. Each consisted of a $2\frac{1}{2}$ in. thick and 6in. wide by 3ft. 6in. long concrete slab shear connected to a $\frac{1}{8}$ in. thick mild steel plate 6in. wide by 4ft. 2in. long.

Beam PB4 had 36-$\frac{1}{8}$ in. diameter by 2in. long headed studs, beam PB5 had 54 and beam PB6 had 108, all welded to the steel plate at 2in. longitudinal pitch. Transverse spacings were 3in., 2in. and 1in. in beams PB4, PB5 and PB6 respectively. Figure 103 shows the arrangement of studs in the three beams.

To study the effect of plate roughness, two beams were tested and were designated as PB7 and PB8. Each consisted of a $3\frac{3}{4}$ in. deep and 9in. wide by 4ft. 8in. long concrete slab shear connected to a Durbar plate $\frac{3}{16}$ in. thick and 9in. wide by 5ft. 4in.

long. In beam PB8 the slab was cast on the rough side of the Durbar plate, whereas in beam PB7 the slab was cast on the smooth side.

Each beam had 36-$\frac{1}{4}$ in. diameter by $3\frac{1}{2}$ in. long headed studs welded at 3in. centres in the longitudinal direction and $4\frac{1}{2}$ in. apart transversely (Figure 103). The number was such that the nominal load per connector at collapse load would be equal to the ultimate strength of the connector.

No reinforcement was provided in the concrete slab. Rapid hardening cement was used for all beams. $\frac{3}{8}$ in. aggregate with an aggregate cement ratio of 4.5 was used for beams PB4, PB5 and PB6 and $\frac{3}{4}$ in. aggregate with an aggregate cement ratio of 5.5 was used for beams PB7 and PB8. The proportion of coarse to fine aggregate was 60 to 40 for all the beams, and the water cement ratio was 0.55. A steel mould was used for casting and the steel plate was supported during casting and curing. Three 4in. cubes and two 12in. x 6in. cylinders were cast for each of the slabs. Concrete was compacted using an immersion vibrator and the slab was cured for a week under wet sacking covered with polythene sheet.

(c) Loading

The beams PB4, PB5 and PB6 were tested under two point loads 4in. apart over a simple span of 3ft. 4in. The beams PB7 and PB8 were tested under a central point load over a simple span of 4ft. 6in. The beams were supported on a free roller at one end and on a fixed roller at the other.

The load was applied through a hydraulic jack of 30 ton capacity, operated by a hand pump. A proving ring dynamometer of 5 ton capacity was used for measuring the loads in beams PB4, PB5 and PB6, whereas in beams PB7 and PB8 a proving ring of 10 ton capacity was used.

(d) Measurements

Deflections at midspan and slips at both ends were measured using dial gauges. Slips, uplifts and bottom steel strains at a number of locations along the span were measured using a demountable mechanical gauge of 2in. gauge length. Strains in concrete and steel at midspan section were measured using a demountable mechanical gauge of 4in. gauge length. Figure 104 shows the general arrangement for measuring slips, strains, etc.

(e) Testing procedure

The total load at midspan was applied in 0.25 ton increments in the case of beams PB4, PB5 and PB6 and in 0.50 ton increments in the case of beams PB7 and PB8. This was followed until the failure load was approached, when the increment was governed by the increment in deflection. After each application of load a set of readings was taken, the load was released and another set of readings was taken at zero load.

(f) Test results

(i) Beam PB4. Shear connection: $36\text{-}\frac{1}{8}$ in. diameter by 2in. long headed studs at 2in. centres longitudinally and 3in. centres transversely

Midspan deflections and end slips are shown in Figures 109 and 110. The first slip sound was heard at a load of 0.9 ton; bond broke on both sides and slips and uplifts were observed all along the span. Vertical tension cracks at the bottom of the slab were observed at midspan at 1.50 tons. The maximum load attained was 2.05 tons at a deflection of 0.28in. After this, the load was released to zero. On reloading, a loud sound was heard at 1.95 tons;

seven studs from the fixed roller end sheared off and a length of concrete slab containing these studs broke off; the load dropped to 0.60 ton. The maximum end slip before failure, recorded at 2.05 tons, was 0.029in. The maximum strains in concrete and steel at 2.05 tons were 0.0024 and 0.0011 respectively.

(ii) Beam PB5. Shear connection: 54-$\frac{1}{8}$ in. diameter by 2in. long headed studs at 2in. centres both ways

Midspan deflections and end slips are shown in Figures 109 and 110. The first slip sound occurred at a load of 1.0 ton; bond broke at both ends and slips and uplifts were observed all along the span. Vertical tension cracks at the bottom of the slab were visible at midspan at a load of 2.25 tons. The maximum load reached was 2.97 tons at a deflection of 0.43in. A loud sound was heard at this load before the readings could be taken and eight studs from the fixed roller end sheared off, accompanied by breaking of the concrete slab. A small diagonal tension crack was observed at the bottom of the slab at a distance of 5in. from the fixed roller end before failure.

A longitudinal crack on the top of the slab along one of the end longitudinal rows of studs was observed before failure. The maximum end slip recorded before failure, i.e. at 2.90 tons, was 0.019in. The maximum strains at the midspan section in concrete and steel at 2.90 tons were 0.0031 and 0.0015 respectively.

(iii) Beam PB6. Shear connection: 108-$\frac{1}{8}$ in. dia. by 2in. long headed studs at 2in. centres longitudinally and 1in. centres transversely

Midspan deflections and end slips are shown in Figures 109 and 110. Slips and uplifts were recorded near quarter span at

a load of 1.0 ton, although the first slip sound was heard at 1.5 tons, followed by slip at both ends. Vertical tension cracks in the concrete slab were visible at midspan at 2.75 tons. Spalling of concrete was observed at midspan at a load of 3.5 tons at a concrete strain of 0.0043. The steel appeared to have yielded at the same load. The maximum load attained was 3.75 tons at a deflection of 0.38in. Thereafter crushing of concrete became more extensive and the carrying capacity of the beam started falling. The beam was able to carry a load of 3.17 tons at a deflection of 0.66in. A residual deflection of 0.36in. was recorded after the load was finally released to zero.

Interaction was very good almost up to the failure of the beam. The maximum end slip recorded was 0.0028in. The failure was by flexure; the concrete had crushed and the steel had yielded.

(iv) Beam PB7. Shear connection: 36-$\frac{1}{4}$ in. dia. by $3\frac{1}{2}$ in. long headed studs at 3in. centres longitudinally and $4\frac{1}{2}$ in. apart transversely (Durbar plate reversed)

Midspan deflections and end slips are shown in Figures 115 and 116. The first slip sound was heard at a load of 3.3 tons, when bond on the half having the fixed roller support broke, followed by another sound at load 3.5 tons, when bond on the other half broke. Thereafter slip increased rapidly with load. Small tension cracks at the bottom of the slab at midspan appeared at a load of 3.5 tons. The maximum load carried by the beam was 5.45 tons. Before any reading could be taken at this load, a loud sound was heard and three studs from the fixed roller end were sheared off. The concrete slab broke off (Figure 123) and the load dropped to 0.67 ton. The deflection was 0.45 in. The maximum end slip recorded at 5.0 tons was 0.012in. The strains in concrete and steel at midspan at 5.0 tons were 0.0026 and 0.0012 respectively.

(v) Beam PB8. Shear connection: 36-$\frac{1}{4}$ in. diameter by $3\frac{1}{2}$ in. long headed studs at 3in. centres longitudinally and $4\frac{1}{2}$ in. apart transversely (Durbar plate)

Midspan deflections and end slips are shown in Figures 115 and 116. Slip was first observed at about 9in. from midspan towards the fixed roller end at a load of 2.0 tons, whereas end slip was not observed until a load of 3.5 tons was reached. No definite slip sound was heard in this beam. Vertical tension cracks at the bottom of the slab were observed at midspan at 4.5 tons. Spalling of concrete was observed near the loading pad at 7.5 tons at a concrete strain of 0.0038. The maximum load attained was 7.8 tons at a deflection of 0.40 in. Thereafter the crushing of concrete became extensive and the load started falling off. The beam was able to carry a load of 6.6 tons at a deflection of 0.69in. A residual deflection of 0.30in. was recorded after the load was released.

A high degree of interaction was achieved. The greater end slip recorded at maximum load was 0.0028in. The end slip, however, continued increasing after the maximum load; the maximum end slip recorded at the last application of load was 0.0064in. The top concrete and bottom steel strains at maximum load were 0.0052 and 0.0025 respectively.

Figure 124 shows a general view of the beam after failure.

(g) Discussion of test results

1. Effect of variation of the amount of shear connection (PB4, PB5 and PB6)

The steel plates used in these beams were from the same stock having a yield stress of 22.7 T/in^2. Concrete cylinder strengths varied from 3450 p.s.i. to 3880 p.s.i., the average being 3660 p.s.i., a maximum variation of $\pm$6 per cent. Similarly the maximum variation in the 4in. cube strength of concrete is $\pm$5 per cent with an average strength of 6110 p.s.i. Since the strengths of steel and concrete are consistent, the difference in behaviour of these beams may be attributed mainly to the variation in the number of shear connectors.

Midspan deflections, end slips and slips at quarter span and uplift near quarter span are shown in Figures 109 to 113.

The first slip sound occurred at 0.9 ton, 1.0 ton and 1.5 tons in beams PB4, PB5 and PB6 respectively. Loads at first significant slip were 0.9 ton, 1.0 ton and 1.25 tons respectively. Corresponding bond stresses are 80 p.s.i., 89 p.s.i. and 111 p.s.i. respectively. Load at first slip sound, and so the bond strength appears to increase with the increase in the number of shear connectors.

The increase in slip was more rapid in beam PB4 than in beam PB5. This is expected in view of the greater number of connectors in beam PB5. The maximum end slips recorded in beams PB4 and PB5 at or near ultimate load were, however, very nearly the same (0.028in. and 0.029in. in beams PB4 and PB5 respectively). In beam PB6, which had the greatest number of shear connectors, the slip was the smallest; maximum end slip recorded at ultimate load was only 0.0026in.

The growth of slip at quarter span was similar to that at the ends. Quarter span slip was, however, greater than end slip at all stages of loading.

If slip is an indication of the degree of interaction achieved, then it can be said that a very high degree of interaction is achieved in beam PB6 and that the degree of interaction decreases with the decrease in the number of connectors.

Uplift at quarter span started at a load of 0.5 ton in all these beams. The growth of uplift was very similar to the growth of slip. Uplift was found to be greatest near the quarter span point in beams PB4 and PB5, whereas in beam PB6 the greatest uplift was recorded at a point 3in. from midspan. The maximum uplifts recorded at or near ultimate loads were 0.0126in., 0.0090in. and 0.0036in. in beams PB4, PB5 and PB6 respectively.

Deflections at midspan intermingle up to a load of 0.9 ton; and thereafter the difference in deflections increases greatly. Beams with fewer connectors are expected to show larger deflection because of the lesser degree of interaction achieved. But the very wide difference in deflection of these beams is mainly due to the fact that the greater loss of interaction in beams with fewer connectors produces greater tensile strains at the bottom of the slab, causing tension cracks to develop at a much lower load. These cracks then reduce the effective thickness of slab and so reduce the stiffness of the beam.

The most striking difference, however, is in the ultimate loads obtained. Ultimate loads, which increased with increase in the number of studs, were 2.05 tons, 2.97 tons and 3.75 tons in beams PB4, PB5 and PB6 respectively. The ratio of experimental ultimate load to calculated ultimate load based on the Whitney distribution, are 0.70, 1.06 and 1.23 respectively.

Beams PB4 and PB5 failed by shearing of studs; failure occurred much before the yielding of steel. This is expected, in view of the fact that the experimental yield stress of the steel plate was 22.7 t.s.i. compared to 16.0 t.s.i. which had been assumed in design. The average loads per connector at failure were 0.49 ton and 0.54 ton in beams PB4 and PB5 respectively; the push-out ultimate capacity of connectors was 0.51 ton.

Both crushing of concrete and yielding of steel occurred in beam PB6 at ultimate load. The average load per connector at ultimate load was o.31 T, that is, 0.61 times the ultimate capacity as obtained from a push-out test.

At failure, seven studs of the first four rows from one end sheared off in beam PB4; the length of concrete slab containing these studs broke off from the rest. Failure was similar in beam PB5, where eight studs of the first three rows from one end sheared off. A small diagonal tension crack starting from the bootom of the slab was seen in beam PB5 at a distance of about 8in. from the support at load prior to failure. It is therefore thought that the failure of the slab and shearing of studs from this section might be initiated by this tension crack.

2. Effect of projections of Durbar plate
(Comparison of beams PB7 and PB8)

The properties of steel and of concrete are very nearly the same in both these beams. The yield stress of the Durbar plate used in both beams was 19.8 t.s.i. The concrete cylinder strength was 3560 p.s.i. in beam PB7 and 3500 p.s.i. in beam PB8. The 4in. cube strength was 6200 p.s.i. and 6600 p.s.i. respectively. The number of studs used was the same in both beams. In view of this and in view of the similar properties of materials used, the difference in behaviour of the two beams is attributed mainly to

the difference in the steel surface at the interface.

Midspan deflections, end slips and slips and uplifts at a distance of 10in. from midspan are shown in Figures 115 to 119. Top concrete and bottom steel strains are shown in Figure 122.

The first slip sound occurred at a load of 3.3 tons in beam PB7; the load at first significant slip was 3.0 tons. The corresponding bond stress was 117 p.s.i. No slip sound was heard in beam PB8. The load at first significant slip was 3.0 tons at a bond stress of 116 p.s.i. End slip, however, did not start in beam PB8 until a load of 3.5 tons was reached.

A study of the slip curves clearly shows the effect of the Durbar plate in resisting slip. Both end slip and slip at a point 10in. from midspan are very much smaller in beam PB8 than in beam PB7. A maximum end slip of 0.0028in. was recorded at ultimate load in beam PB8, whereas the same was 0.0119in. in beam PB7 at 5.0 tons (the ultimate load of beam PB7 was 5.45 tons).

The total horizontal shear H and the total horizontal shear resisted by the surface of the Durban plate, H_B, in beam PB8 at the ultimate load of 7.8 tons, are given below.

Beam	Surface	Load (tons)	H (tons)	H_B (tons)	Av. mech. bond stress (p.s.i.)	$\frac{H_B}{H} \times 100\%$
PB8	Durban plate	7.8	42.98	27.51	254	64%

H is calculated assuming a lever arm of 2.46in. (based on Whitney, using cylinder strength and yield stress) and external moment. H_B is calculated using the method described in chapter 4.1 (g). It is seen that at ultimate load 64% of the total horizontal shear is resisted by the Durbar plate. It is also found that the average value of mechanical bond was still increasing at ultimate load.

A much higher ultimate load of 7.8 tons was attained in beam PB8, compared to 5.45 tons in beam PB7. The ratio of experimental ultimate load to calculated ultimate load (based on Whitney) is 0.89 and 1.29 in beam PB7 and PB8 respectively. Beam PB7 also shows much larger deflection than beam PB8. This is partly due to greater loss of interaction in beam PB7, and mainly due to occurrence of tension cracks at the bottom of the slab at a much lower load caused by its greater loss of interaction.

Beam PB7 failed by shearing of studs; three studs at one end sheared off and the portion of the concrete slab containing these studs broke off. Beam PB8 failed by crushing of concrete; full yielding of the steel plate occurred at ultimate load.

The average load per connector at ultimate load calculated on the basis of a lever arm of 2.46in. was 1.66 tons in beam PB7 and 2.38 tons in beam PB8. The ultimate capacity of connectors obtained from a push-out test was 1.75 tons.

These observations clearly show the great effectiveness of Durbar plate in resisting shear and producing interaction in composite plated beams.

4. Effect of spacing and length of studs.

The effect of spacing and length of studs on the general behaviour of plated beams can be seen from a comparative study of beams PB2 and PB5. The connectors were designed at 100 per cent of their Q_{uc} in both beams. Beam PB2 was provided with $\frac{3}{16}$ in. dia. by 1in. long studs at 3in. centres, whereas beam PB5 was provided with $\frac{1}{8}$ in. dia. by 2in. long studs at 2in. centres. The steel strength was very nearly the same; the concrete cylinder strength was 4310 p.s.i. for beam PB2 and 3450 p.s.i. for beam PB5.

The difference in the nature of failure of these two beams is significant. Failure in beam PB2 was by diagonal tension at a calculated shear stress of 244 p.s.i., whereas beam PB5 failed by shearing of studs when the load per connector exceeded its ultimate capacity. The calculated shear stress at failure in beam PB5 was 256 p.s.i. When related to cylinder strength, the shear stresses at ultimate load are 0.057 f'_c and 0.074 f'_c in beams PB2 and PB5 respectively. In spite of a 30 per cent increase in relative shear stress, beam PB5 did not fail by shear.

The spacing and length of studs in beam PB5 was approximately equal to the elastic lever arm of the section, a spacing which is specified as a maximum spacing for stirrups in reinforced concrete design. In the beams considered, this spacing and length prevented the premature shear failure of the beams.

5.3 Small Scale Composite Plate

(a) Purpose of test

The main purpose of this test was to study the behaviour of a composite plate with welded stud shear connectors. $\frac{1}{8}$in. dia. and 2in. long studs, with nuts to serve as heads were welded to the steel plate at 2in. centres in both directions. The length and the spacing of studs were equal to the elastic lever arm of the section.

It was intended to study the possibility of utilising the wearing surface of a battledeck as a structural part of the deck. A simulated wheel load, therefore, was used to test the specimen. Near failure, however, the load was spread over a bigger area to prevent local failure of concrete.

(b) Description and preparation of specimen

The specimen consisted of a $\frac{1}{8}$in. thick mild steel plate 6' 4" by 6' 4" overall, shear connected to a concrete slab $2\frac{1}{2}$in. thick and 5' 8" square. A layer of 3in. x 3in. x 0.104in. weld mesh reinforcement was provided on the top surface over the whole area of the slab.

The specimen was supported on four sides over a panel of 5' 6" square on $\frac{1}{4}$in. thick and 20in. deep steel plates; the latter were welded at the corners to form a box section. These supporting plates were lightly welded to the steel plate of the specimen to ensure contact at all stages of loading. The box frame was then supported at the four corners on concrete blocks through 8in. x 8in. x $\frac{5}{8}$in. thick steel plates welded to the box frame at each corner. The $\frac{1}{4}$in. thick side plates were intended to be flexible enough in the horizontal direction to allow horizontal and rotational freedom of the specimen at the edges and at the same time sufficiently rigid in the vertical direction to resist the reactive pressure

without any siginificant deflection. A practically simply supported condition at the edges would thereby be obtained. Calculations based on relations given by Young [34] shows that at the centre of the edge, the stiffness of the supporting plate is only 3 per cent of the stiffness of the specimen.

Ferrocrete rapid hardening cement was used. The aggregate consisted of 60 per cent of $\frac{3}{8}$in. gravels and 40 per cent of sand. An aggregate cement ratio of 4.5 and a water cement ratio of 0.55, both by weight, were used. Concrete was compacted using an immersion vibrator. Eight 4in. cubes and four 12in. x 6in. cylinders were cast along with the slab. Curing lasted a week under wet sacking covered with polythene sheet.

(c) Loading

Load was applied through a 60 ton hydraulic jack operated by an electric pump. A hand pump was used in conjunction with the electric pump to control the applied load accurately. To simulate the wheel load, the load was spread over an area $7\frac{1}{2}$in. x $1\frac{1}{2}$in. through a steel plate of the same size and a thin plywood strip. Near failure, the load was spread over a greater area using a 6in. x 6in. steel plate and a thin plywood board of the same size to reduce the local stresses in the concrete.

Load was measured using a proving ring dynamometer of 50 ton capacity.

(d) Measurements

Deflections at the centre, at the quarter point of one major axis and at the quarter point of one diagonal, were measured using 0.0001in. dial gauges. End slips and slips and uplifts at a number of locations in the panel were measured using 0.0001in. dial gauges. $\frac{1}{2}$in. dia. holes were made in the steel plate for this purpose. A demountable mechanical gauge of 4in. gauge length was used to measure concrete strains at vaious . . . .

locations. Steel strains at the centre, at the quarter point of one major axis and at the quarter point of one diagonal were measured using $\frac{1}{2}$in. foil resistance strain gauges. In the failure test, the slope at the centre of one of the edges was measured using an electronic level. Figure 126 shows the arrangements for measurement of slips, strains, etc.

(e) Testing procedure

The specimen was tested under five different load conditions. In the first condition load was applied at the centre of the panel, referred to as position A, in 2.5 ton increments up to a maximum load of 20 tons. In the second condition load was applied at the quarter point of a major axis, referred to as position B, in increments of 2.5 tons up to a maximum load of 20 tons. In the third condition load was applied at the quarter point of one diagonal, referred to as position C, in increments of 2.5 tons up to a load of 17.5 tons, with a final increment of 18.38 tons. In the fourth condition, the load position, referred to as position B1, was diametrically opposite to position B. The load increment was in 5.0 tons up to a load of 15.0 tons, with further increments to 17.5 tons and 18.7 tons. In the fifth condition, load was applied at position A in 5.0 ton increments up to a load of 15.0 tons and then in 2.5 ton increments until failure occurred. The size of the loading pad was changed from $7\frac{1}{2}$in. x $1\frac{1}{2}$in. to 6in. x 6in. after a load of 20.0 tons was reached.

After each application of load, a set of readings was taken, the load was released and another set of readings was taken at zero load.

Materials:

(a) Steel: A flat specimen $1\frac{1}{2}$in. wide by 20 in. long was cut from the steel plate and was tested as explained in section 4.1.

(b) Concrete: 4in. cubes and 6in. cylinders were tested as explained in section 4.1.

(f) Test results

Deflections at positions A, B and C for different load positions are shown in Figures 127 to 129. Slips along the edges and slips and uplifts at various locations for different load positions are shown in Figures 130 to 134. Figure 125 shows the key diagram.

With the load at the centre of the panel, deflections at positions A, B and C were all proportional to load up to about 5.0 tons and thereafter deviated from the line of proportionality. The load deflection relationship became linear again after 10 tons and remained so up to the maximum load of 20 tons. A faint cracking sound was heard at a load of 12.5 tons and the sounds became louder and more numerous at 17.5 tons. Corner cracks on the surface of the slab were first observed at this load.

At 20 tons, the maximum principal strain calculated from measured steel strains at the centre was 1120×10^{-6}. As this was quite close to the yield strain of the plate, load was not increased any further.

In the second condition, with the load at position B, the deflection was proportional to load up to 10 tons at B and up to 12.5 tons at A and C. The maximum load was 20 tons. The maximum slip observed at this load was very large and to avoid overstressing the shear connectors the load was not further increased.

In the third condition, with the load at position C, the load-deflection curve at A was fairly linear up to the maximum load of 18.38 tons. At positions B and C, however, the deflection was proportional to load up to 10 tons and thereafter deviated from the

line of proportionality. At 18.38 tons, the maximum principal strain calculated from measured steel strains was 905 x 10^{-6}; but the rate of increase in slip was very high and so the load was not increased any further.

In the fourth condition, the load was applied at position B1 which was diametrically opposite to position B. This was done primarily to break the bond symmetrically before the failure test. Slip and uplift readings could also be obtained at those points where readings could not be obtained in the second loading condition. The maximum load applied at this position was 18.7 tons.

In the failure test with the load at the centre, load-deflection curves were fairly linear at all three positions up to a load of 17.5 tons and thereafter became non-linear. Numerous cracking sounds were heard at this load. The loading pad was changed from $7\frac{1}{2}$in. x $1\frac{1}{2}$in. to 6in. x 6in. after a load of 20 tons to provide for a bigger area in order to avoid local failure of the slab. The maximum load attained was 26.0 tons, when a sudden local shear failure occurred. The load dropped to 12.65 tons and remained fairly stable. The plane at which the concrete failed was found to be inclined at approximately 30° to the horizontal.

End slips at the four edges are shown in Figure 130 for various loads. With few exceptions end slip was generally higher at the centre of each edge and gradually decreased towards the corners.

Both uplifts and slips in the panel started from the first application of load. The magnitude and direction of slips and uplifts at a number of locations are shown in Figure 137. These were greater near the load position, decreasing gradually towards the edges.

The maximum principal strain calculated from the measured steel strains are shown plotted against load in Figure 136. The

relationship is fairly linear throughout. At a load of 25 tons the maximum principal strain was 1405 x 10^{-6}, compared to the uniaxial yield strain of 1374 x 10^{-6} obtained from the coupon test.

Other results of the test are summarised in the table overleaf. Concrete properties are shown in Table 11.

(g) Discussion of test results

The deflection measured under the load for each load condition was proportional to load at early stages of loading; at higher loads the deflection increases more rapidly than the load. This can be explained by tensile cracking and by a diminution in the tangent modulus of the concrete. An increase in the modular ratio from 7.5 to 15 decreases the moment of inertia of the section by about 31 per cent (Figure 15$\frac{4}{5}$). The breaking of bond, resulting in loss of interaction also produces greater deflection at higher loads.

In the failure test, the load deflection curve is fairly linear up to 17.5 tons. This is expected because of the stress-strain characteristic of concrete which follows a linear path on reloading so long as the maximum stress is within the critical range. The slope is however smaller than the slope of the linear portion of the load-deflection curve in the first load condition. This is presumably due to loss of interaction due to breaking of bond all over the plate, corner cracks, developed earlier in the first load condition, and extensive cracking of the concrete due to application of load at various positions.

The observed end slip was very small in the first load condition. The highest slip was recorded at the third points, which were the measurement points nearest to the centre. Slip decreased from these points outward and became very small at the edges.

		Load Condition A			Load Condition B		
		Load (tons)	Gauge	Magnitude (in.)	Load (tons)	Gauge	Magnitude (in.)
First significant slip	End	17.5	7_e		15.0	7_e	
	Panel	7.5	17		5.0	7 15	
Max. slip at max. load	End	20.0	2_e	0.0010	20.0	8_e	0.0107
	Panel	20.0	17	0.0089	20.0	5	0.0162
First uplift recorded	Panel	7.5	27	0.0005			
Max. uplift at max. load	Panel	20.0	28	0.0037			
Max. residual slip after max. load had been released	End		2_e	0.0009		8_e	0.0084
	Panel		17	0.0036		5	0.0095
Max. principal strain in steel plate at max. load		20.0	A	1120×10^{-6}	20.0	B	806×10^{-6}
Deflection at maximum load		20.0	A	0.357	20.0	A	0.165
			B	0.184		B	0.238
			C	0.120		C	0.111
Residual deflection after maximum load had been released			A	0.074		A	0.009
			B	0.031		B	0.045
			C	0.018		C	0.014

Results of the composite plate for different load conditions

		Load Condition C			Failure test Load at position A		
		Load tons	Gauge	Magnitude in.	Load tons	Gauge	Magnitude in.
First significant slip	End	12.5	8_e 9_e		10.0	8_e	
	Panel	2.5	16		At first application of load (i.e., 5.0 tons)		
Max. slip at max. load	End	18.4	9_e	0.0056	25.0	2_e	0.0021
	Panel	18.4	13	0.0090	25.0	17	0.0216
First uplift recorded	Panel	5.0	25	0.0002	At first application of load (i.e., 5.0 tons)		
Max. uplift at max. load	Panel	18.4	25	0.0031	25.0	28	0.0066
Max. residual slip after release of max. load	End		9_e	0.0043		2_e	0.0016
	Panel		13	0.0057		17	0.0098
Max. principal steel strain at max. load		18.4	C	905×10^{-6}	25.0	A	1405×10^{-6}
Deflection at max. load		18.4	A	0.106	25.0	A	0.560
			B	0.106		B	0.258
			C	0.100		C	0.166
Residual deflection after release of max. load			A	0.005		A	0.115
			B	0.006		B	0.033
			C	0.027		C	0.017

RESULTS OF THE COMPOSITE PLATE TEST FOR DIFFERENT LOAD CONDITIONS

Similar results were observed in the failure test, but with greater slips at all points. This is due to breaking of bond at all points in the earlier phases of loading. The slip distribution is generally similar to the interface shear distribution for full interaction.

In the second load condition with the load at position B, slip was highest near the load and decreased gradually towards the edges (Figures 138 and 139). The end slips along the edge nearest to the load had a very high value at the centre with little or no slip at the corners (Figure 132).

A study of the end slip curves along edges bc and cd with the load at position C, shows that at points nearest to the load position where the interface shear is expected to be high, slip is also high and then decreases on either side. On the other edges which are furthest from the load, slip is almost zero at all points.

The uplift distribution was similar to the slip distribution (Figures 137, 140 and 142), with high values near the load position decreasing gradually towards the edges. With the load at positions B and C, the uplift was almost zero at points near the edges which were furthest from the load position.

No crushing of concrete was observed. It appeared from the maximum principal strain of 1405×10^{-6}, calculated from the measured strains at 25.0 tons, that yielding had occurred (the uniaxial yield strain of the plate was 1374×10^{-6}). Failure occurred by local shear at the loading pad (Figure 145) at a load of 26.0 tons. Such a failure may occur by diagonal tension. When the shear stress in concrete is sufficiently high, diagonal cracks occur at the bottom of the slab, which then extend upward and towards the load position. This occurred in plated beams PB2 and PB3. In this case the plane of failure was inclined at about 30° to the horizontal. The shear connectors did not fail.

CHAPTER VI

CORRELATION OF RESULTS

6.1. Deflection

(a) Composite beams: The elastic deflection for complete interaction has been claculated using the transformed area method. The area of reinforcement in the concrete slab was neglected, as this forms less than one per cent of the slab area.

Bending deflection has been calculated on the basis of simple bending theory using experimental values of Young's modulus for steel and concrete. To calculate shear deflection, the portion of the total shear resisted by the steel beam was first estimated using equation (13) of Appendix II. Shear deflection was then calculated as for a simple I-beam assuming the shear stress to be distributed uniformly over the web area. Average values of E_s and E_c of all the quarter scale beams were used for calculating shear deflection for these beams. Similarly, average values of E_s and E_c were used for calculating shear deflection of the half scale beams.

The deflection for incomplete interaction was calculated on the basis of the elastic theory for incomplete interaction. Deflection due to bending was calculated using equation (17) of Appendix II, whereas shear deflection was assumed to be the same as for complete interaction. This is sufficiently accurate, as the shear resisted by a steel beam in incomplete interaction is very close to that for complete interaction. The additional bending deflection for incomplete interaction is given by the second term of equation (17) of Appendix II; the first term represents the deflection due to bending for full interaction. The values of E_s and E_c used for calculating shear deflection are used for calculating additional bending deflection due to incomplete interaction.

The table overleaf shows the calculated bending and shear deflections per one ton load for complete interaction, and the additional bending deflection per one ton load for incomplete interaction for some of the composite beams. The experimental deflection for these beams per one ton load is also given in the table. An average value of deflections per one ton load for loads from 1 ton to 3 tons is taken as the experimental value for each of these beams. Additional deflection due to incomplete interaction is not considered while calculating the total deflection for beams A1, A2, A3, B1 and B2 (where the top flange surface was provided with "V" grooves), because the interaction was very good almost up to failure.

The agreement between theoretical and experimental deflections is good. Except for beams A2 and B1, the variation is withing $\pm$ 5 per cent. In the quarter scale beams the shear deflection is about 14 per cent of the deflection due to bending for complete interaction, whereas the additional deflection due to incomplete interaction, with shear connectors designed at 100 per cent of capacity, is about 16 per cent of the bending deflection for complete interaction.

The bending deflection in the inelastic range can be calculated by numerical integration if the moment curvature relationship is known. There is no known method for calculating shear deflection as the shear distribution in the inelastic stage is not easily obtained.

The moment curvaure relationship for quarter scale beams for complete interaction obtained by using the method set out in section 2.1 is shown in Figure 146. Idealised stress blocks for concrete and steel with f_y = 20.98 t.s.i. and f'_c = 4700 p.s.i. are used. These are the average of experimental values of all the quarter scale beams. The curvatures obtained from experiments for beams of group B are shown in the same figure. The experimental curvature is generally

higher than the calculated values even in the beams where slip was negligible up to failure. This may be due to the actual shape of the stress-strain curves for steel and concrete which may be different from the idealised curves.

Beam	$\delta_{bending}$ in.x 10^{-3}	δ_{shear} in.x10^{-3}	Additional $\delta_{bending}$ - incomplete interaction in.x10^{-3}	δ_{total} in.x10^{-3}	$\delta_{expt.}$ in.x10^{-3}
A1	27.56	3.74		31.30	32.50
A2	27.46	3.74		31.20	34.07
A3	26.96	3.74		30.70	29.61
A4	27.26	3.74	6.33	37.33	30.62 *
A5	27.11	3.74	6.33	37.18	37.05
B1	26.67	3.74		30.41	35.77
B2	27.49	3.74		31.23	31.82
B3	26.39	3.74	4.06	34.19	32.42
B4	26.56	3.74	4.06	34.36	35.88
B5	26.66	3.74	4.06	34.46	35.61
C1	26.61	3.74	4.06	34.41	33.67
D1	9.22	1.62	0.88	11.72	10.74
D2	9.15	1.62	0.88	11.65	11.32

* deflection before bond broke

(b) Plated beams: The elastic deflection is calculated using the transformed area method. Two methods were employed to calculate flexural rigidities. In the first, the whole depth of the section is used, whereas in the second the depth of concrete in the tensile zone is neglected. Shear deflection is neglected because the shear stress in the slab, which resists almost the whole of the vertical shear, is very small and the shear deflection is found to be less than 2 per cent of the bending deflection. Average experimental values of E_s and E_c for the beams having the same cross-section area were used for calculating bending deflections.

The calculated elastic deflections are shown along with the experimental deflections in Figures 105, 109 and 115. At smaller loads the experimental deflection follows fairly closely the calculated deflection, but as the load increases, the deflection increases more rapidly. This is due to the stress-strain characteristic of concrete and to the cracking at the bottom of the concrete slab at higher loads.

The increase in deflection due to incomplete interaction can be calculated using the theory for incomplete interaction as outlined in section 2.2, but this deflection is very small compared to the total deflection and has, therefore, been neglected.

(c) Composite plate: The elastic deflection for a patch load at the centre is calculated using expressions (29a) given in section 2.2, after substituting appropriate values for u, v, x and y. Poisson's ratio is assumed to be the same for both steel and concrete and is taken to be equal to 0.3. Experimental values of Young's modulus for steel and concrete are used. The value of D was calculated for both uncracked and cracked sections and deflections calculated accordingly.

The elastic central deflection for load at the centre based on D of the uncracked section is shown along with the experimental deflection in Figure 127. At smaller loads, the experimental deflection is very close to the calculated deflection, but as the load increases deflection increases more rapidly due to cracking of concrete, non-linearity of stress strain relationship of concrete and the decrease in vlaue of D with increase in modular ratio.

In the failure test the central deflection is equal to the theoretical elastic deflection based on the plate stiffness of the cracked section and m = 15.

6.2 Ultimate Moment

(a) Composite beams: Two methods are used to calculate the ultimate moment. In the first, the stress distribution in the concrete at failure is assumed to be equivalent to a constant compressive stress of 0.85 times the measured cylinder strength of concrete, and in the second the stress is assumed to be equivalent to a constant compressive stress of four-ninths of the measured cube strength. The steel is assumed to be at its measured yield stress in both methods. The first method is based on Whitney's distribution and the second is as recommended in the draft CP117. The plastic neutral axis may lie in the concrete slab or in the steel beam. Figure 2 shows the assumed stress distributions and also the expression for ultimate moments for all cases.

The ultimate moments of the composite beams were calculated using the above methods. Dead load was neglected in calculating the ultimate load as this produces less than 0.6 per cent of the ultimate moment. The calculated and experimental ultimate loads for each beam are shown in Table 8. The ratios $\frac{\text{Experimental}}{\text{Calculated}}$ ultimate load are also shown in the table.

The ultimate moments based on Whitney are slightly higher than those calculated according to CP117. Except for grooved and Durbar flanged beams and beam B3, the ratio of experimental to calculated ultimate load based on CP117 varies from 0.99 to 1.06. It should, however, be remembered that all these beams except A1 and D1 failed by failure of shear connectors, which were designed on the basis of the nominal yield stress of the beam. When based on the actual yield stress of the steel, the nominal load per connector at ultimate load was 176 per cent of the ultimate connector capacity in beams of group A and 123 per cent in beams of groups B and C. The calculated ultimate load was, nevertheless, obtained. In the roughened flanged beams crushing of concrete had occurred before the maximum load was reached.

Higher ultimate loads achieved in grooved and Durbar flanged beams may be attributed partly to the better interaction achieved in these beams. The considerably higher ultimate loads attained in beams A1, A3, A4, B6 and D1 is due to the stress-strain characteristic of the steel. The ratio $\varepsilon_{sh}/\varepsilon_y$ for the bottom flange of these beams is very small so that strain hardening occurs soon after the yield strain and so increases the carrying capacity of these beams.

In beam B7, where the studs were covered with flexible latex at the base to prevent them from resisting any shear, the calculated ultimate moment was attained by virtue of strain hardening. It can, therefore, be said that in composite beams the calculated ultimate moment can generally be attained even with the minimum number of shear connectors. A higher ultimate moment can, however, be achieved with better interaction.

(b) Plated beams: The methods used for composite beams are also used for calculating ultimate moments in plated beams, using experimental values of yield stress for steel and cube and cylinder strengths of concrete. The calculated and experimental ultimate loads along with the ratios of experimental to calculated ultimate load for each beam are given in Table 10.

The ultimate moments calculated using the two methods differ considerably. In beam PB2, which is the extreme case, the calculated moment based on cube strength is 31 per cent lower than the calculated moment based on cylinder strength. This variation is considered to be mainly due to the variations in the ratio of experimental cube strength to cylinder strength of concrete. To obtain the same ultimate moment from these two methods the ratio $\frac{\text{cylinder strength}}{\text{cube strength}}$ will have to be equal to 0.52 which apparently is low. It should, however, be remembered that four-ninths of the cube strength is chosen to put a higher safety factor on the concrete than on the steel. The experimental ultimate load in PB2 was 2.4 tons against calculated ultimate load of 1.89 tons, based on cube strength, and 2.74 tons, based on cylinder strength. The maximum stress in steel estimated from measured strain was 13.0 t.s.i. at a load of 2.40 tons. Assuming a linear variation of steel stress with load, this would give a stress of 10.2 t.s.i. at ultimate load based on cube strength, and 14.8 t.s.i. at ultimate load based on cylinder strength. For the beams considered here, ultimate moments based on cylinder strength will therefore be used for comparison.

In beams PB2 and PB3, experimental ultimate loads were 0.88 and 0.86 times the respective calculated ultimate loads. Failure in these beams was due to shear failure of concrete in diag diagonal tension. In all other beams with increased length of studs spaced at distances equal to the lever arm of the section, this premature shear failure was prevented. In beams PB4, PB5 and PB6,

with shear connectors designed at 150, 100 and 50 per cent of their ultimate capacity respectively, the ratios of experimental to calculated ultimate load were 0.70, 1.06 and 1.23 respectively. It is thus seen in plated beams that at least a sufficient number of connectors to resist the total horizontal shear is necessary to attain the calculated ultimate moment. In beam PB8, where the rough face of Durbar plate was in contact with the concrete slab, the ratio of experimental to calculated ultimate load was 1.29 as against 0.89 in beam PB7 which had the same number of connectors but with the Durbar plate inverted. A better interaction is, therefore, found to increase the ultimate load.

(c) Composite plate: The theoretical collapse load in a simply supported isotropic square plate subjected to a point load at the centre is $2\pi M_p$ where M_p is the ultimate moment per unit width of the section. M_p has been calculated in the same way as for plated beams using experimental values of uniaxial yield stress of steel and uniaxial cube and cylinder strengths of concrete. The ultimate load so calculated is 26.1 tons when based on cube strength and 26.9 tons when based on cylinder strength. The experimental ultimate load was 26 tons, but failure was due to local shear failure of the concrete at the loading pad, so that the flexural failure load was not determined.

6.3 Slip

(a) Composite beams: Elastic distribution of slip for incomplete interaction is calculated using equation (13) given in section 2.1. Figure 147 shows the slip distribution at loads of 1.5, 2.5 and 4.0 tons in the quarter scale beams having studs designed at 100 per cent of capacity. The values of E_s, E_c and k used were 13.400 t.s.i, 3.64×10^6 p.s.i. and 200 tons per in. respectively.

Slips measured at the end and at quarter span in beam B4 (without bond) at the same loads are shown for comparison. There is good agreement between experimental and theoretical slips up to 2.5 tons, but at higher loads the experimental slip is relatively higher. This is due to the decrease in k as the load increases.

A revised slip distribution at 4.0 tons using a connector modulus which will approximately correspond to the average load per connector at this load is shown in dotted lines in the same figure. This was obtained as follows. The axial force F at midspan for incomplete interaction at 4.0 tons was calculated using k = 200 tons per in. and the average load per connector was then obtained. From the load-slip curve obtained from the push-out test the slip corresponding to this load per connector was estimated, and a new value of connector modulus was obtained. Using this new value of k a revised slip distribution was obtained which agrees fairly well with experimental values.

A study of the experimental slip distributions in beams B1, B6, B5 and B4 (Figures 68 to 71) shows that the slip distribution is fairly uniform along the beam up to the yield load of 4.0 tons. Beams B4, B5, B6 and B1 show gradually smaller slips in that order. As the load increases beyond yield, the shape of the slip curve along the beam also changes and at ultimate load the slip distribution in beam B1 with V-grooved flange becomes very similar to the interface shear distribution for complete interaction, whereas in beam B4 (without bond) the slip distribution still remains fairly uniform except at the central portion. It may therefore be said that as the degree of interaction increases, the slip distribution along the beam approaches the shape of the interface shear distribution for full interaction.

If slip is an indication of the load carried by a connector, then the load distribution between connectors in beam B4 is nearly uniform at all stages of loading, including the ultimate load.

It appears that there is redistribution of shear due to flexibility of the connectors until the shear resisted by each connector is nearly the same. It follows, therefore, that when flexible connectors are used, the total number of connectors is more important than their distribution. This was also brought out by the similar behaviour of beams tested by Balakrishnan [29] under uniformly distributed load having uniform and triangular distribution of connectors.

When the degree of interaction achieved is very high, such as is obtained in V-grooved flanges, the slip is very small. For small slip the interface shear will not be much different from interface shear for complete interaction. If it is assumed that the interface shear is the same as that for complete interaction in beams with V-grooved flanges, then assuming a constant modulus k, the slip distribution along the beam can be calculated at ultimate load from the known interface shear for complete interaction at that load. The slip distribution so calculated is shown in Figure 148. The interface shear at the calculated ultimate load of 6.35 tons is calculated using the method set out in section 2, using f_y = 20.98t.s.i. and f'_c = 4700 p.s.i., which are the average of experimental values for all the quarter scale beams. A value of k = 550 tons per in. obtained from push-out tests (Figure 19) for $\frac{3}{16}$ in. dia. studs on V-grooved flanges is used. The measured slips in beam B1 at 6.5 tons are shown for comparison, The experimental slips agree reasonably well with the calculated values, considering that the calculated connector load for a length of about 9in. from midspan is higher than the limit of proportionality of the load-slip curve of the appropriate push-out test.

Slip causes a strain difference between the concrete slab and steel beam at the interface. This strain difference then reduces the resisting moment of the composite section. Calculations show, however, that the reduction in resisting moment due to strain difference

in a normal composite beam with adequate shear connectors is small. Considering beam B3 with studs designed at 100 per cent (natural bond) the maximum strain difference recorded near the ultimate load was 54×10^{-4}. Using this maximum strain difference, a strain distribution across the composite section can be obtained using the idealised stress blocks for concrete and steel (Figure 3) with $f_y = 20.98$ t.s.i. and $f'_c = 4700$ p.s.i., such that the resultant axial force is equal to zero. The resisting moment of the section is then obtained from this calculated strain distribution. The resisting moment obtained from such a calculation is 11 per cent smaller than the resisting moment for full interaction for the same top concrete strain. The reduction in total axial tension, however, is 39 per cent. This smaller loss in resisting moment is possible because the centre of gravity of the tension in the steel beam moves down, thereby increasing the lever arm and compensating for the smaller axial force.

The reduction in the total axial tension in the steel beam reduces the load per connector by the same percentage. Because of this reduction, the small loss in resisting moment due to loss of interaction, and the effect of strain hardening, beams A4 and A5 attained their calculated ultimate moments before failure of shear connectors occurred, in spite of the design load of the shear connectors being as high as 176 percent of their ultimate capacity when based on the actual yield stress of the steel beam.

It may also be mentioned here that in a simple composite beam with two point loads applied symmetrically about the midspan, there exists interface shear in the "no shear" zone due to incomplete interaction, and slips are observed in this zone.

(b) Plated beams: The elastic slip distribution for incomplete interaction has been calculated using equation (58) given in section 2.2. Figure 149 shows the theoretical slip distribution at various loads for plated beams PB4, PB5 and PB6 with studs designed at 150, 100 and 50 per cent respectively. Values of E_s, E_c and k (obtained from push-out test for appropriate stud diameter) used are 13,400 t.s.i., 3.64×10^6 p.s.i. and 150 tons per in. respectively. Slips obtained from experiments at various locations are also shown for comparison. At lower loads, the experimental values agree reasonably well with the calculated values but at higher loads the experimental values are found to be higher than the calculated values. The decreased connector modulus at higher loads may be a reason for this. In addition, the experimental slips near midspan are greater than those near the support. The tension cracks developed near midspan may cause greater slip to be recorded in the central portion of the beam.

Theoretical slip distributions for incomplete interaction along with experimental slips for beams PB7 and PB8 are shown in Figure 150. Values of E_s, E_c and k used are 13,400 t.s.i., 3.64×10^6 p.s.i. and 290 tons per in. The experimental values are much scattered in both these specimens with smaller values in PB8 (due to Durbar plate projections) than in PB7. Like PB4, PB5 and PB6, the experimental slips are higher near midspan than near the supports.

(c) Composite plate: There is no theoretical solution available for calculating the slip distribution for incomplete interaction in a composite plate. However, if it is assumed that the interface shear for incomplete interaction is the sameas the interface shear for full interaction, and assuming the slip to be proportional to the interface shear, then it is possible to calculate the slip distribution in the composite plate if the interface shear distribution for complete interaction is known.

For the composite plate tested under a central load distributed over an area $7\frac{1}{2}$in. x $1\frac{1}{2}$in., the interface shear is calculated using equations (30), (31) and (24) and a lever arm equal to 2in. The slip distribution along the two major axes is then calculated using a value of k equal to 150 tons per in. The slip distribution so obtained for a load of 10 tons is shown in Figure 151 together with the experimental values. It will be appreciated that the slip distribution calculated in this way will be only approximate since there will be some redistribution of shear due to incomplete interaction.

The general agreement is reasonably good, considering the approximate nature of the calculation. The observed slip along AP (Figure 151) is higher than the calculated values. The estimated load per connector at one-third span based on the interface shear distribution for complete interaction is 0.28 ton, which corresponds to a connector modulus of 105 tons per in. (Figure 21), compared to the assumed value of k = 150 tons per in. There is also the possibility of the interface shear curve moving away from the centre due to incomplete interaction, which will then result in a greater shear at one-third span and hence greater slip.

The distribution of slip along the edge is shown in Figure 152. The general shape is very similar to the interface shear, although the experimental slips are lower than the calculated values.

6.4 Uplift

A theoretical expression for differential deflection between the slab and the beam (uplift) has been given in section 2.3. The uplift in beam D2 calculated on the basis of this theory for a point load at midspan is shown in Figure 13. A value of 115.5 tons per sq. in. is assumed as the foundation modulus in this calculation. It has been assumed in this investigation that the foundation modulus is constant and operates in both directions. But in actual practice, the slab can not have a greater deflection than the beam and hence there may not be any negative uplift in the portions AB and CD of the beam. Uplift will occur in the portio portion BC of the beam. Uplift readings from experiments confirm the general shape of the curve. The recording of negative uplift near the supports may be due to initial separation of the end of the slab from the beam due to shrinkage, followed by the gap closing under load.

If $\bar{y}$ is the uplift at any point along the beam, k is the foundation modulus, s is the spacing of studs in pairs, then the uplift force or the axial force per connector is equal to $\frac{\bar{y}ks}{2}$; and the axial strain in the connector is equal to $\frac{\bar{y}ks}{2AE_s}$ where A is the area of cross-section of the connector. The axial strain in studs along the beam D2 for a load of 10 tons at midspan was calculated using the above expression and the theoretical uplift distribution. The axial strains so calculated are shown in Figure 153. Strains were measured on studs at several locations along the beam D2 using $\frac{1}{4}$in. long resistance strain gauges. If the strains in a pair of gauges on a stud are ε_1 and ε_2, then the axial and bending components of the measured strain are $\frac{\varepsilon_1 + \varepsilon_2}{2}$ and $\frac{\varepsilon_1 - \varepsilon_2}{2}$ respectively. The axial strains so obtained from measured strains are also shown in Figure 152. The experimental strains also confirm the general shape of the theoretical strain curve, with compressive

strain near midspan, compressive strains near the supports and tensile strains in between these two regions.

6.5 Ultimate capacity of connectors (beam and push-out tests)

The ultimate capacity of a connector in a beam test has been calculated assuming that all connectors carry equal loads just before failure. This assumption is reasonable for beams with or without natural bond, as the slip distribution along such beams is nearly uniform at or near ultimate load (Figure 71). The total load carried by the connectors just before failure is equal to the total axial tension in the steel beam at midspan and is calculated from the strains measured across the section just before failure. The appropriate stress strain curve obtained from coupon tests is used for this purpose. The ultimate capacity of the connectors is then obtained by dividing this axial tension by the total number of connectors in one half of the beam. The ultimate capacity of $\frac{3}{16}$in. dia. x 1in. long headed studs obtained from beams with or without natural bond is given below. The ultimate capacity of such connectors obtained from push-out tests is 1.08 tons per stud with bond and 1.00 tons per stud without bond [29].

Beam	Flange Surface	Q_{uc} (beam) (tons)	Q_{uc} (P.O) (tons)	$\frac{Q_{uc}(\text{beam})}{Q_{uc}(\text{P.O.})}$
A4	Natural bond	0.96	1.08	0.89
A5	Bond destroyed	0.88	1.00	0.88
B3	Natural bond	1.10	1.08	1.02
B4	Bond destroyed	0.93	1.00	0.93
B5	Resin and aggregate	1.00	1.08	0.93
B8	Natural bond	1.11	1.08	1.03
C1	Natural bond	0.97	1.08	0.90

The strains at midspan were measured using a demountable mechanical gauge of 8in. gauge length. This gauge length was rather long compared to the span of 60in. The actual strain at the midspan could, therefore, be higher than measured; this would result in a slightly greater axial tension and a higher $\frac{Q_{uc\ (beam)}}{Q_{uc\ (P.O.)}}$ ratio. However, the agreement between the ultimate capacities obtained from beam tests and push-out tests appears to be reasonably good.

In the beams with grooved flanges, the degree of interaction achieved is very high so that the interface shear distribution is more similar to the interface shear for complete interaction. The apparent load per connector at failure is, therefore, much greater near midspan than in the rest of the beam length. This results in a lower value of Q_{uc} (beam) when calculated in the way described earlier than the actual maximum value. Nevertheless a study of the results in the table below shows that the ultimate capacity obtained from beam tests is higher than the ultimate capacity obtained from corresponding push-out tests. This may be due to the fact that in push-out tests with grooved flange surfaces, where the slip is very small up to about 80 per cent of the ultimate load, the load may be resisted mostly by the grooves and the studs in the top half of the specimen with very little or no resistance offered by the lower half, so that the average Q_{uc} obtained is again smaller than the maximum value.

In the Durbar flanged beam, where the interaction was fairly good, the value of Q_{uc} (beam) obtained using the above method will also be smaller than the maximum value of Q_{uc} (beam). But the much lower $\frac{Q_{uc\ (beam)}}{Q_{uc\ (P.O.)}}$ ratio is due to the fact that the area of Durbar plate per connector provided in the beam is 36 per cent less than the area provided in the corresponding push-out specimen.

Beam	Flange surface	Q_{uc}(beam) (tons)	Q_{uc}(P.O.) (tons)	$\frac{Q_{uc}(beam)}{Q_{uc}(P.O.)}$
A2	$\frac{1}{16}$in. x $\frac{1}{32}$in. grooves	1.84	1.53	1.20
A3	$\frac{1}{32}$in. x $\frac{1}{64}$in. grooves	1.56	1.25	1.25
B1	$\frac{1}{16}$in. x $\frac{1}{32}$in. grooves	1.51	1.53	0.99
B2	$\frac{1}{32}$in. x $\frac{1}{64}$in. grooves	1.48	1.25	1.18
B6	Durbar plate	1.29	1.63	0.79

The ultimate capacity of $\frac{3}{8}$in. dia. x $1\frac{1}{2}$in. long headed studs as obtained from beam D2 was 3.66 tons against 3.0 tons obtained from the push-out test. This higher Q_{uc}(beam) to Q_{uc}(P.O.) ratio is mainly due to the difference in concrete strength, as discussed in section 4.2.

The table below gives the ultimate capacities of connectors obtained from plated beam tests and corresponding push-out tests. The ultimate capacity of a connector in a plated beam test is obtained in the same way as in composite T-beams. It may be mentioned that the lengths of studs used in the plate beams were different from those used in the push-out tests.

Specimen	Nature of Interface	Dia. of stud (in.)	Q_{uc}(beam) (tons)	Q_{uc}(P.O.) (tons)	$\frac{Q_{uc}(beam)}{Q_{uc}(P.O.)}$
PB4	Plain face and natural bond	$\frac{1}{8}$	0.49	0.51	0.96
PB5		$\frac{1}{8}$	0.54	0.51	1.06
PB7		$\frac{1}{4}$	1.66	1.75	0.95

The agreement between the ultimate capacities obtained from plated beam and push-out tests is good, within $\pm$ 6 per cent. The ultimate capacity of a connector does not appear to be much affected by the cracking of concrete, although greater slips were recorded near midspan in plated beams due to cracking.

The table below shows the maximum end slips recorded in beams in the load increment immediately before failure. Alongside is also shown the average slip at which the load was fairly stable before failure in push-out tests. Figures within brackets give the percentage of ultimate load at which the given slips were recorded. The results are for $\frac{3}{16}$in. dia. x 1in. long headed studs.

Beam	Max. end slip in beams (inches)	Slip in P.O. test (inches)	P.O. specimen
A4	0.0341 (98.5)	0.0369 (95.4)	P3D1
A5	0.0374 (98.4)	0.0409 (97.8)	P3D2
B3	0.0337 (100)		
B4	0.0338 (99.2)		
B5	0.0326 (98.5)		
B6	0.0254 (99.4)		
B8	0.0337 (97.5)		
C1	0.0373 (97.6)		

Near the ultimate load the slip increases at a very rapid rate so that the slip at actual failure could not be recorded. Maximum end slips recorded in load increments immediately before failure are failry consistent and agree fairly well with push-out results.

6.6 Bond Stress

Failure of natural bond in a composite T-beam is often indicated by a slip sound accompanied by the sudden occurrence of slip; but in some cases slip is recorded even before such a sound is heard. In such cases a slip of 0.0005in. is taken as the slip at which the bond is considered to have failed. In either case the failure of bond occurs before the beam reaches the yield load, so that the bond stress can be calculated on an elastic basis using the transformed area method.

The bond stress at any point at the interface is equal to the shear stress and is given by:

$$f_b = \frac{VM'}{Ib}$$

where f_b = calculated bond stress

V = total vertical shear at that section

M' = moment of the transformed slab area about N.A.

I = moment of inertia of the transformed section

and b = width of the steel flange.

In a plated beam, the bond stress is similarly given by:

$$f_b = \frac{V}{jd \times b}$$

where jd = elastic lever arm of the section

b = width of the steel plate

The values of bond stress calculated using above expression in composite T-beams for loads at first slip sound and at first significant slip are given in Table 8. The smaller of these two values may be taken as the effective bond stress, and is given below.

Beam	Number of studs	Load at bond failure (tons)	Bond stress (psi.)	$\frac{\text{bond stress}}{\text{cylinder strength}}$
A4	32	2.63	401	0.085
B3	44	3.45	527	0.096
B7 *	44	1.50	228	0.045
B8	44	2.50	378	0.083
C1	44	3.00	473	0.117
D2	56- $\frac{3}{8}$in. x $1\frac{1}{2}$in.	10.00	317	0.065

(A4, B3, B7*, B8, C1: $\frac{3}{16}$in. x 1in.)

* stud roots covered with latex

Except for beam B7, where the base of the studs was covered with flexible latex, the calculated bond stress varies from 317 to 527 p.s.i. The concrete cylinder strength of these beams varied from 4550 to 5500 p.s.i. These results agree reasonably well with the results obtained by Balakrishnan [29]. Of twelve full scale composite T-beams tested under a central point load, a slip sound was not heard in three, one showed very low bond stress, whereas the rest showed a bond stress varying from 286 to 403 p.s.i., a variation from 0.067 f'_c to 0.117 f'_c, where f'_c is the concrete cylinder strength. The cylinder strength for these beams varied from 2650 to 4740 p.s.i. In the four composite T-beams tested at Lehigh University [24] under two point loads applied symmetrically, the bond stress at first slip sound was found to vary from 236 to 298 p.s.i., a variation from 0.067 f'_c to 0.084 f'_c. The average cylinder strength was 3540 p.s.i.

Considering these results an ultimate bond stress of 0.065 f'_c for concretes having cylinder strength varying from 3000 p.s.i. to 5500 p.s.i. may be accepted for composite T-beams with an adequate number of shear connectors.

In the case of plated beams, the load at first significant slip is found to be either equal to or smaller than the load at the first slip sound. The bond stress, therefore, is calculated only for loads at first significant slip using the expression described earlier, and is given below.

Beam	Studs	Load at first significant slip (tons)	Bond stress (psi.)	$\frac{\text{Bond stress}}{\text{Cylinder strength}}$
PB2	24 - $\frac{3}{16}$in. x 1in.	1.0	102	0.024
PB4	36 - $\frac{1}{8}$in. x 2in.	0.9	80	0.022
PB5	54 - $\frac{1}{8}$in. x 2in.	1.0	89	0.026
PB6	108 - $\frac{1}{8}$in. x 2in.	1.25	111	0.029
PB7	36 - $\frac{1}{4}$in. x $3\frac{1}{2}$in.	3.0	117	0.033

The bond stress in plated beams is found to vary from 80 to 117 p.s.i., a variation from 0.022 f'_c to 0.033 f'_c, where f'_c is the concrete cylinder strength. This is much smaller than the bond stress in composite T-beams. The fact that the concrete is in tension near the interface may be a reason for this. These values compare very well with the findings of the University of Illinois [30] plated beam tests. The calculated bond stress at first significant slip which was also taken as a slip of 0.0005in. for ten plated beams using studs of diameters $\frac{1}{2}$in., $\frac{5}{8}$in. and $\frac{3}{4}$in. was found to vary between 81 p.s.i. and 121 p.s.i., a variation from 0.016 f'_c to 0.039 f'_c.

In beams with mechanical bond such as is provided by Durbar plate or V-grooved flanges, no definite slip sound was heard. Load at first significant slip is, therefore, taken as the load at failure of bond. This load was, however, found to be greater than the yield load in the grooved flanged beams, so that the elastic method based on transformed area can no longer be applied to

calculate the bond stress. The total axial tension in the steel section at midspan is calculated using the appropriate stress strain curve and the bond stress is evaluated by dividing this total axial tension by the interface area on one half of the beam. The bond stress so calculated in V-grooved flanged beams is given below. The same method is used in Durbar flanged beams, even though the loads at first significant slip in these beams are lower than the yield loads. The load carried by the studs is neglected for this purpose.

Beam	Flange surface	Studs	load (tons)	Mech. bond stress (psi.)	Mech. bond stress / Cylinder strength
A1	$\frac{1}{8}$in x $\frac{1}{16}$in grooves	32-$\frac{3}{16}$in x 1in	5.50	853	0.190
A2	$\frac{1}{16}$in x $\frac{1}{32}$in grooves	32-$\frac{3}{16}$in x 1in	4.50	800	0.170
A3	$\frac{1}{32}$in x $\frac{1}{64}$in grooves	32-$\frac{3}{16}$in x 1in	5.00	708	0.156
B1	$\frac{1}{16}$in x $\frac{1}{32}$in grooves	44-$\frac{3}{16}$in x 1in	5.00	860	0.185
B2	$\frac{1}{32}$in x $\frac{1}{64}$in grooves	44-$\frac{3}{16}$in x 1in	5.8	1009	0.179
B6	$\frac{3}{16}$in. Durbar plate	44-$\frac{3}{16}$in x 1in	2.9	493	0.123
D1	$\frac{3}{8}$in. Durbar plate	56- $\frac{3}{8}$in x $1\frac{1}{2}$in	7.5	293	0.046

A study of the bond values obtained from beams A1, A2 and A3 shows that the bond stress increases with the increase in size of grooves, but the increase is not in proportion to the size of the grooves. An increase in the total number of studs also increases the bond value. The bond stress is lower in beam B1 than in B2, but compared to the cylinder strength the bond value in beam B1 is relatively higher. The bond stress obtained from the Durbar flanged beams is rather low. The projections behave more as shear connectors. The effective shear resistance of the Durbar plate is much higher, as will be shown later.

The maximum shear resistance offered by the different types of mechanical bond is calculated as described on page 115. taking account of the resistance of the shear connectors. The values so obtained are given below.

Beam	Flange Surface	Studs	Max. total shear resistance (tons)	Average mechanical bond (psi.)
A1	$\frac{1}{8}$in x $\frac{1}{16}$in grooves	32-$\frac{3}{16}$in x 1in	23.91	1020
B1	$\frac{1}{16}$in x $\frac{1}{32}$in grooves	44-$\frac{3}{16}$in x 1in	21.30	910
B2	$\frac{1}{32}$in x $\frac{1}{64}$in grooves	44-$\frac{3}{16}$in x 1in	20.75	885
B6	$\frac{3}{16}$in. Durbar plate	44-$\frac{3}{16}$in x 1in	13.13	560
D1	$\frac{3}{8}$in. Durbar plate	56- $\frac{3}{8}$in x 1$\frac{1}{2}$in	50.14	520

The actual maximum shear resistance could be much higher than the average values given above, since the loads at which these maximum values occur are very near the ultimate loads (except the Durbar plated beams).

6.7 Shear and Punching Shear Stress

The shear stress in plated beams was calculated on the basis of simple theory for reinforced concrete design. The elastic lever arem based on experimental values of E_s and E_c was used for this purpose. The shear stress so calculated is given below.

Beam	Studs	Max. shear stress at ult. load lb./in.^{2}	Shear stress / Cylinder strength
PB2	24 - $\frac{3}{16}$in. x 1in. (Natural bond)	244	0.057
PB3	24 - $\frac{3}{16}$in. x 1in. (Bond destroyed)	228	0.057
PB4	36 - $\frac{1}{8}$in. x 2in. (Natural bond)	183	0.050
PB5	54 - $\frac{1}{8}$in. x 2in. (Natural bond)	256	0.074
PB6	108 - $\frac{1}{8}$in. x 2in. (Natural bond)	323	0.086
PB7	36 - $\frac{1}{4}$in. x $3\frac{1}{2}$in. (Natural bond)	212	0.060
PB8	36 - $\frac{1}{4}$in. x $3\frac{1}{2}$in. (Durbar plate)	302	0.086

Shear failure occurred in beams PB2 and PB3. In all other beams which were provided with studs of length and longitudinal pitch equal to the elastic lever arm of the section, shear failure did not occur.

In the composite plate, the shear stress per unit area is calculated using expressions (30), (31) and (24) given in section 2.2, after substituting appropriate values for u, v, x, y and p. The lever arm jd is calculated using experimental values of E_s and E_c.

At a central load of 26 tons spread over an area 6in. x 6in., the maximum shear stress so calculated occurs at the face of the loading pad and along either of the major axes and is equal to 1040 p.s.i. The maximum shear could be smaller due to incomplete interaction.

If the connectors are assumed to act as shear reinforcement then the stress in the connectors obtained using equation (13) given in CP 114, clause 316, are as follows. In this equation the shear resistance of concrete has been neglected.

Specimen	Tensile stress in stud at ult. load (t.s.i.)
PB2	34.8
PB3	32.5
PB4	39.9
PB5	37.2
PB6	24.2
PB7	37.0
PB8	25.0

A similar figure for the composite plate in a stud subjected to the maximum shear outside the loading pad for complete interaction is 125 t.s.i. The actual value, however, could be much smaller, due to incomplete interaction. It may, however, be pointed out that the above figures are the same as the average shear stress in the connectors calculated from the load carried by them at ultimate load.

The punching shear stress in the composite plate is calculated using the expression $f_p = \frac{w^*}{\Sigma bxd}$

where b is the effective periphery and d is the effective depth of the punching resisting surface. Taking $\sum b$ equal to the periphery of the loading pad and d equal to the full depth of the concrete slab, the calculated punching shear stress at failure (26 tons) is found to be 971 p.s.i.

6.8 Criterion of Failure in Plates

To predict when failure will occur in a material with complicated stress conditions, various strength theories have been developed. By failure of the material is meant either yielding or actual rupture, whichever occurs first. A brief description of the various strength theories is given below. In this discussion tension is considered positive, compression negative and the principal stresses by which the stress condition in a body can be completely determined are considered to be algebraically such that $\sigma_1 > \sigma_2 > \sigma_3$.

(a) The maximum stress theory considers the maximum or minimum principal stress as the criterion of failure. For a ductile material this means that the failure occurs when

$$\sigma_1 = \sigma_y \quad \text{or} \quad |\sigma_3| = \sigma'_y$$

where σ_y = yield stress in tension and

σ'_y = yield stress in compression.

(b) The maximum strain theory considers the maximum (maximum tensile) and minimum (maximum compressive) strains as the criterion of failure. Equating the maximum and minimum strains to the corresponding yield strains, the criteria of failure are:

$$\sigma_1 - \mu(\sigma_2 + \sigma_3) = \sigma_y$$
$$\sigma_3 - \mu(\sigma_1 + \sigma_2) = \sigma'_y.$$

(c) The maximum shear theory assumes that yielding begins when the maximum shear stress in the material becomes equal to the maximum shear stress at the yield point in a simple tension test. The criterion of failure, therefore, is:

$$\tau_{max} = \frac{\sigma_1 - \sigma_3}{2} = \frac{\sigma_y}{2}$$

$$\sigma_1 - \sigma_3 = \sigma_y$$

(d) In the maximum strain energy theory, the quantity of strain energy per unit volume of the material is used as the basis for determining failure. Equating this energy to the energy at yielding in simple tension, the criterion for yielding becomes

$$\frac{1}{2E}(\sigma_1^2 + \sigma_2^2 + \sigma_3^2) - \frac{\mu}{E}(\sigma_1\sigma_2 + \sigma_2\sigma_3 + \sigma_3\sigma_1) = \frac{\sigma_y^2}{2E}$$

or, $$\sigma_1^2 + \sigma_2^2 + \sigma_3^2 - 2\mu(\sigma_1\sigma_2 + \sigma_2\sigma_3 + \sigma_3\sigma_1) = \sigma_y^2$$

(e) Another strength theory, first proposed by Huber, is based on the strain energy of distortion. Equating the distortion energy to the strain energy at yielding in a simple tension test, the condition for yielding becomes

$$(\sigma_1 - \sigma_2)^2 + (\sigma_2 - \sigma_3)^2 + (\sigma_3 - \sigma_1)^2 = 2\sigma_y^2$$

This theory based on the distortion energy is the one most commonly used for determining failure of ductile material having a pronounced yield point stress in simple tension.

In the composite plate subjected to a central load spread over an area 6in. x 6in., the principal stresses in the steel plate at the centre are:

$$\sigma_1 = \sigma_2 \text{ (from symmetry) and } \sigma_3 = 0.$$

The conditions for yielding from different theories are:

(a) Maximum stress theory $\sigma_1 = \sigma_y = \sigma_y$

(b) Maximum strain theory $\sigma_1 = \frac{\sigma_y}{1-\mu} = 1.4286\ \sigma_y$

(c) Maximum shear theory $\sigma_1 = \sigma_y = \sigma_y$

(d) Maximum energy theory $\sigma_1 = \frac{\sigma_y}{\sqrt{2(1-\mu)}} = 0.8452\ \sigma_y$

(e) Distortion energy theory $\sigma_1 = \sigma_y = \sigma_y$

where Poisson's ratio μ is taken to be equal to 0.3.

It appears that the theories (a), (c) and (e) give the same value of failure load, theory (d), i.e. the maximum energy theory, gives a lower failure load, whereas the theory (b), the maximum strain theory, gives a much higher value of load at which yielding will occur.

The loads at which yielding will occur according to different theories are given below. These are calculated on an elastic basis using the experimental yield stress and the experimental value of modular ratio.

Maximum stress theory	16.99 tons
Maximum strain theory	24.28 tons
Maximum shear theory	16.99 tons
Maximum energy theory	14.36 tons
Distortion energy theory	16.99 tons.

The experimental maximum principal strain was equal to the yield strain at 23.5 tons but was almost linear with load up to 25 tons (Figure 136). It is therefore not clear whether yielding had occurred. It appears however that the calculated value according to the maximum strain theory shows better correlation than the other theories.

CHAPTER VII

DESIGN

7.1 Composite Beams

In the design of composite beams the span and the spacing of beams and the thickness of slab will be known beforehand. The problem is only to design the steel beam and the shear connection. Basically there are two approaches, elastic and plastic. In either approach, full interaction can be assumed and the steel reinforcement in the slab neglected.

(a) Elastic method. This method is based on permissible stress in steel and concrete. The recommendation of the draft CP117 is considered reasonable. A smaller value of modular ratio than 15, recommended in the draft Cp117, may however be considered for transient live load in view of the values of m obtained from T-beam tests (the experimental values of m varied from 6.2 to 8.3). A larger value of m should then be used for sustained load.

(b) Plastic method. The plastic design method recommended in the draft CP117 with a load factor of 1.75 and a maximum allowed elastic steel stress at working load of 0.9 times the specified yield stress is considered satisfactory in view of the high reserve strength of a composite section. No limit for concrete stress is however specified in the draft CP117. It is thought that in a composite section having a larger bottom steel flange and a relatively thin and narrow concrete slab, the maximum concrete stress could be very high when the steel stress reaches 0.9 times the specified yield stress. A limit for the concrete stress is probably necessary.

(c) Design of shear connectors. The ultimate load method may be used for designing the shear connection, and this has been proposed in the draft CP117.

The effect of natural bond should be neglected, although the natural bond produces very good interaction until bond breaks. The shear connectors may be designed to transmit the whole of the horizontal shear using 100 per cent of the ultimate capacity. This is considered safe up to the calculated ultimate moment because of the reduction in total axial force at the section of maximum moment due to loss of interaction. The draft CP117, which uses 80 per cent of capacity, appears to be conservative in this respect.

Composite beams with grooved flanges are presumably not a practical proposition. Such beams were tested only to explore the effect of flange roughening. In Durbar flanged beams an ultimate shear resistance of 500 p.s.i. for the Durbar plate was obtained with $\frac{\text{stud area}}{\text{Durbar plate area}}$ ratio of not less than 0.022 (**Figure** 39). In view of the test results, a design for shear connectors using 120 per cent of the ultimate capacity appears to be satisfactory up to the calculated moment, provided the area of the Durbar plate is less than 45 times the area of the studs.

7.2 Composite Plate

In the design of a composite plate for a bridge deck or similar structure, the size of the panel and the boundary conditions will be known beforehand. The actual design, therefore, is reduced to the design of thickness of the concrete slab and the steel plate and the number of shear connectors. Like a composite beam, the composite plate may be designed assuming complete interaction. Two approaches, elastic and plastic, may be used for designing a composite plate.

Design of slab (a) elastic method. The ordinary theory for reinforced concrete design may be used for designing a composite plate. The design dead load and live load moment is calculated based on elastic theory for isotropic plates for assumed boundary conditions.

When unpropped, the dead load, that is, the weight of wet concrete, is considered to be resisted by the steel plate alone and the live load by the composite section. Stresses due to live load in composite section is calculated by the transformed area method using a suitable modular ratio. The stresses so calculated together with the stress in the steel plate due to dead load should be within the permissible stresses for steel and concrete (B.S. 449 and CP114). It will, however, be seen that the thickness of the steel plate will be governed by its capacity to carry the weight of the wet concrete. Considering a simply supported panel of 12 ft. be 12 ft. with a concrete slab of 9in. thick, the plate thickness required for an elastic balanced design is about 0.8 per cent of the slab thickness (that is, 0.072in.), whereas a plate thickness of 0.432in. is necessary to carry the wet concrete at a steel stress of 10.5 t.s.i. (small deflection theory). It is possible to reduce the plate thickness required to carry the wet concrete by making smaller panels using temporary supports while casting. In such cases the composite section may be designed to take both dead and live load.

(b) Plastic method. Two cases may be considered. In the first the total design moment is calculated on an elastic basis and the required ultimate moment is obtained using a suitable load factor. In the second case, the total collapse load of the desired section is first obtained using a suitable load factor from the known total design load and then the required ultimate moment is calculated from the known plastic solution of the slab. Unfortunately, plate

solutions by plastic theory are known only for very simple cases. A greater load factor is, however, necessary in the second case than in the first, because of the higher value of $\frac{w_p}{w_y}$ (w_p = the collapse load and w_y = the yield load) than the shape factor of the section.

Having found the required ultimate moment, a section is obtained by trial and error such that the calculated ultimate moment of the section equals the desired ultimate moment. The ultimate moment per unit width of a composite section is calculated as shown in Figure 2 . As the ultimate moment is independent of any intial deformation or stress, design by plastic method can be done without considering the stress in the plate due to wet concrete. The stress in the steel plate before the concrete has hardened should however be within permissible limits.

For a normal composite plate subjected to uniform load, the maximum shear stress is quite small; but when subjected to a point or patch loads the maximum shear stress could be quite high. In such cases the maximum shear stress needs to be investigated.

Design of shear connectors. For designing the number of shear connectors in a composite plate the horizontal shear at the interface must be known. The theory in section 2.2 gives a method for calculating the total horizontal shear at collapse load at the interface for a simply supported n-sided regular composite plate and also for a simply supported rectangular composite plate when subjected to a uniformly distributed load of intensity p. If H_p represents the total horizontal shear at collapse load and Q_{uc} represents the ultimate capacity of connectors, then the number of connectors, N_p, when designed at 100 per cent, is given by

$$N_p = \frac{H_p}{Q_{uc}} = \frac{L.f_y.t}{Q_{uc}}$$

where L = freely supported boundary

t = thickness of the steel plate

f_y = yield stress of the steel plate

and N_p = number of connectors when designed on plastic basis

In cases where plastic solutions are not known the horizontal shear distribtuion at the interface is calculated using elastic theory. The following procedure may be adopted. The composite plate may be divided into a number of smaller panels and the resultant horizontal shear stress q is calculated at the centre of each panel using equation (25) of section 2.2. Assuming this q to be uniform over the area of the panel, the total horizontal shear for the panel is calculated and will be equal to q x panel area. The number of shear connectors for the panel is then obtained by dividing this total resultant horizontal shear by the design capacity of the connectors. A similar procedure is adopted for all other panels and the total number of shear connectors obtained.

A study of the number of connectors obtained from plastic and elastic method where both plastic and elastic solutions are known, leads to the following results.

Consider a simply supported square composite plate of side "a" and steel plate thickness "t" subjected to a uniformly distributed load of intensity p. The total horizontal shear at the interface at collapse is, from equation (36a), $4a.f_y.t.$, so that the number of connectors when designed at 100 per cent is

$$N_p = \frac{4a.f_y.t}{Q_{uc}} .$$

The number of shear connectors when designed on an elastic basis is obtained using the methods set out earlier. The composite plate has been divided into 64 square panels and the value of q_r is obtained at the centre of each panel using equation (25) and Levy's solution as outlined in section 2.3. The number of connectors so calculated when designed at 100 per cent is found to be

$$N_e = 0.1734 \frac{pa^3}{Q_{uc} jd}$$

and at yield load, the number of connectors

$$N_y = 0.1734 \frac{P_y a^3}{Q_{uc} jd_y}$$

where p_y = intensity of yield load

jd_y = lever arm of the section at yield moment.

The maximum moment for a simply supported square plate subjected to a uniformly distributed load obtained from Levy's solution[31] is

$$M_{max} = 0.0479\ pa^2$$

so that at yield load

$$W_y = p_y a^2 = \frac{M_y}{0.0479} = 20.88\ M_y$$

and $$N_y = \frac{0.1734 \times 20.88\ M_y xa}{Q_{uc} \cdot jd_y} = \frac{3.62 \times f_y . a . t}{Q_{uc}}$$

Hence

$$\frac{Np}{Ny} = \frac{4}{3.62} = 1.10$$

This shows that the number of connectors obtained at collapse load from plastic design is only 10 per cent higher than the number of connectors obtained at yield load from elastic design. If it is assumed that the plastic lever arm is equal to the lever arm at yield, then

$$M_p = M_y \text{ and the ratio } \frac{W_p}{W_y} = \frac{24\ M_p}{20.88 M_y} = 1.14.$$

This compares reasonably well with the ratio N_p to N_y. Subject to further checks in other types of composite plates, the method of calculating total horizontal shear at collapse, given in section 2.2, and the design of shear connectors therefrom appears to be reasonable.

It is therefore proposed that the total horizontal shear at the interface to be transmitted by the shear connectors be calculated using the method given in section 2.2 for simply supported regular or rectangular composite plateswhen subjected to uniformly distributed load. For other composite plates the total horizontal shear may be calculated using method outlined earlier from known elastic solution at yield load. The number of connectors are then designed using a suitable design load per connector.

CHAPTER VIII

CONCLUSIONS

(1) The calculated ultimate moment, based on the experimental yield stress and $\frac{4}{9}$ of the concrete cube strength, was attained in all quarter scale composite T-beams except one in which the experimental ultimate moment was 99 per cent of the calculated value. Natural bond was destroyed in this beam and the shear connectors were designed at 138 per cent of their ultimate capacity. In the beam with $\frac{1}{8}$ in. x $\frac{1}{16}$ in. grooves and a 138 per cent design for studs, the connectors did not fail and the calculated ultimate moment was exceeded by 36 per cent. In all other beams failure occurred by studs shearing off and the experimental ultimate moment was greater than the calculated ultimate moment by amounts varying from 0 to 20 per cent (Table 8).

(2) In the half scale composite T-beam with Durbar plate projections at the interface, the connectors did not fail and the experimental ultimate moment was 11 per cent greater than the calculated value. In the other half scale beam with the plain face of Durbar plate at the interface the experimental ultimate moment exceeds the calculated value by 6 per cent. Failure was due to failure of concrete around the studs; only two studs sheared off. Both beams had 100 per cent shear connector design (Table 8).

(3) The quarter scale T-beam with $\frac{1}{8}$ in. x $\frac{1}{16}$ in. grooves and 138 per cent design for studs recorded tensile yielding over the full depth of the steel beam. Full plasticity in the steel beam was obtained in the quarter scale T-beams with $\frac{1}{16}$in. x $\frac{1}{32}$ in. and $\frac{1}{32}$in. x $\frac{1}{64}$ in. grooves and 100 per cent design for studs. Tensile yielding over the full depth of the steel beam also occurred in the

quarter scale and the half scale beam with the Durbar flange and 100 per cent design for shear connectors. All the quarter scale T-beams with or without natural bond and resin bonded aggregate at the interface recorded compression at the top flange. In the beam where the studs were covered with latex at the base, compression yielding and tensile yielding occurred in the top and bottom flange respectively (Figures 72 and 73).

(4) Strain hardening occurred in the bottom flange of all the T-beams except two; the tensile test on coupons from the flange of these two beams shows a very high $\frac{\varepsilon_{sh}}{\varepsilon_y}$ ratio (Table 3).

(5) At working load the stress distribution and load-deflection characteristic of a T-beam are affected only to a small extent by the loss of interaction due to slip.

(6) The ultimate carrying capacity and the load-deflection characteristic beyond yield load of a T-beam depends more on the properties of the material than on the loss of interaction. The load per connector at ultimate load, however, is greatly affected by the loss of interaction.

(7) A very high degree of interaction was obtained in T-beams with grooved flanges. A lesser degree of interaction was obtained in the Durbar flanged T-beams, whereas in the beam with resin bonded aggregate at the interface, interaction was no better than the interaction obtained in a similar beam with natural bond.

(8) In beams where bond has been destroyed the slip distribution along the length, at loads lower than yield load, agrees well with that obtained from incomplete interaction theory. In beams

where natural bond has not been destroyed, there is little or no slip until bond breaks; after the bond has broken, the slip is greater near the quarter span region than at the ends, presumably because of greater frictional resistance at the supports. At loads higher than yield load the slip distribution is fairly uniform in beams where bond has been destroyed (Figure 71). With better interaction, the shape of the slip distribution curve gradually approaches the shape of the interface shear curve and when the degree of interaction is very high, in beams with grooved flanges, the slip distribution at ultimate load becomes very similar to the interface shear distribution for complete interaction at collapse (Figure 68).

(9) Uplift in a T-beam is generally greater in the quarter span region. Negative uplift was also observed in the half scale beams, presumably because of the initial separation of the slab from the beam at the ends due to shrinkage, followed by the gap closing under load.

(10) Uplift appears to be associated more with slip than with the external load. At quarter span in the half scale beams, uplift is proportional to slip (Figure 95), with greater uplift in the Durbar flange than in the plain flange for the same slip. Similar results were observed in both small and full scale push-out tests, where separation was proportional to slip with greater slope for the separation-slip curve in specimens with Durbar flange than with plain flange (Figures 36 and 37).

(11) The calculated ultimate moment, based on the experimental yield stress and 0.85 times the concrete cylinder strength was exceeded by 6 per cent in the plated beam with 100 per cent design

for shear connectors, by 23 per cent in the plated beam with 50 per cent design for shear connectors and by 29 per cent in the Durbar plated beam with 100 per cent design for shear connectors. Shear connectors did not fail in the last two beams. The length and longitudinal spacing of shear connectors in these beams were equal to the elastic lever arm of the section. In all other plated beams failure occurred either by shear failure of concrete or by studs shearing off at loads smaller than the calculated ultimate load.

(12) The loss of interaction greatly affects the ultimate carrying capacity of a plated beam. Unlike T-beams, at least a sufficient number of connectors to resist the total horizontal shear at ultimate load is necessary to attain the ultimate moment. Better interaction created by the projections of a Durbar plate increases the ultimate carrying capacity.

(13) The shear resistance of the concrete slab in a plated beam is increased by using the shear connectors at pitch and length equal to the lever arm of the section.

(14) In the plated beams tested, slip is often greater near midspan, presumably because of tension cracks which develop at the bottom of the concrete slab near midspan.

(15) The ultimate value of bond stress obtained from plated beam tests is about 30 per cent of the corresponding values obtained from T-beam tests.

(16) The ultimate flexural failure did not occur in the composite plate. Failure occurred by local shear failure at 26.0 tons. The calculated ultimate load is 26.1 tons. based on $\frac{4}{9}$ of the concrete cube strength and 26.9 tons based on 0.85 times the concrete cylinder strength.

(17) Slip distribution at the interface in the composite plate follows the general pattern of the interface shear distribution based on complete interaction.

(18) The experimental yield load in the composite plate agrees better with the yield load given by the maximum strain theory.

(19) The ultimate capacity of connectors obtained from tests in T-beams (with or without natural bond) and plated beams (with natural bond) is very nearly the same as obtained from push-out tests (Tables 8 and 10).

(20) For the same total cross sectional area, studs of smaller diameter have greater ultimate capacity (Figure 39).

(21) For the same diameter and length, there appears to be no difference either in useful or in ultimate capacity of threaded studs with heads, threaded studs without heads, and plain headed studs; the threaded studs, however, produce less total slip for the same load. For headed studs of equal length and diameter, the threaded studs show less total separation in pull-out tests than the plain studs.

(22) The limit of proportionality of load-slip curve in a push-out specimen with grooved flange increases with the size of the grooves. In push-out specimens, otherwise identical, the ultimate load increases with increasing size of grooves (Figure 19).

(23) Holding down is needed to mobilise the shear resistance of a roughened flange. The shear resistance of a Durbar flange increases in a non-linear fashion with the increase in the total cross-sectional area of studs (Figure 38).

(24) In small scale push-out specimens with studs of diameter $\frac{3}{16}$in. or below, no crack in the concrete slab was observed; cracks in the concrete slab, however, occurred with $\frac{1}{4}$in. diameter studs. In full scale push-out specimens with $\frac{3}{4}$in. diameter studs, cracks occurred in the concrete slab; no concrete crack was observed in full scale specimens with $\frac{1}{2}$in. or $\frac{3}{8}$in. diameter studs.

(25) In the pull-out specimens with headed studs, failure occurred due to concrete failure, whereas in the specimen with threaded studs without heads, failure occurred due to pulling out of the studs from the concrete block.

(26) The failure load in a pull-out specimen with headed studs appears to be proportional to the area of the conical failure surface (figure on page 93) and the tensile strength of the concrete.

(27) For all practical purposes, there is no significant difference between the behaviour of T-beams with studs spaced uniformly, and spaced according to the theoretical interface shear distribution at collapse.

(28) A 100 per cent design for shear connectors in T-beams with natural bond and a 120 per cent design for shear connectors in T-beams with Durbar flange or grooved flange appear to be quite safe up to the calculated ultimate moment. But failure may occur due to studs shearing off if the beam is subjected to moments greater than the calculated moment.

(29) The bending strain in studs calculated on the basis of a theoretical solution taking shear deflection into consideration appears to agree reasonably well with the experimental values. The inclusion of shear also explains why studs do not yield below the ultimate capacity.

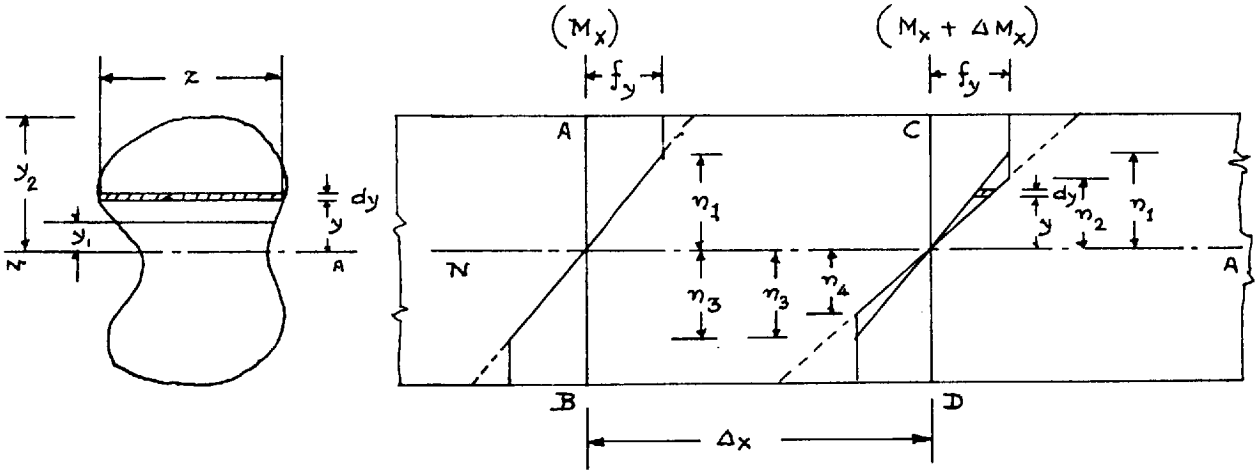
APPENDIX I

Horizontal shear distribution over the depth of a section in elasto-plastic stage

An expression is obtained here for calculating horizontal shear distribution over the depth of a section when the material of the section is partly elastic and partly plastic. Two cases are considered.

Case I

The section is of homogeneous material having a trapezoidal stress-strain relationship.



Consider two sections AB and CD, Δx apart and subjected to external moments M_x and $M_x + \Delta M_x$ respectively. Let n_1 and n_2 be distances from N.A. up to which the material is elastic.

Total horizontal shear to be resisted over an area b x Δx at distance y_1 from N.A.

$$= \int_{y_1}^{n_1} \left(f_y - \frac{f_y}{n_1} y \right) z \, dy - \int_{y_1}^{n_2} \left(f_y - \frac{f_y}{n_2} y \right) z \, dy$$

$$= \int_{n_2}^{n_1} \left(f_y - \frac{f_y}{n_1} y \right) z \, dy + \int_{y_1}^{n_2} \left(\frac{f_y}{n_2} - \frac{f_y}{n_1} \right) y z \, dy \qquad \ldots (1)$$

so that the horizontal shear per unit length

$$q = \frac{1}{\Delta x} \left[\int_{n_2}^{n_1} \left(f_y - \frac{f_y}{n_1} y \right) z \, dy + \int_{y_1}^{n_2} \left(\frac{f_y}{n_2} - \frac{f_y}{n_1} \right) y z \, dy \right.$$

In the limit when $\Delta x \to 0$ $n_1 \to n_2$ and the first term can be neglected

$$\therefore \quad q = \frac{1}{dx} \int_{y_1}^{n_2} \left(\frac{f_y}{n_2} - \frac{f_y}{n_1} \right) y z \, dy \qquad \ldots (2)$$

Observing that

$$\int_{n_2}^{n_1} \left(f_y - \frac{f_y}{n_1} y \right) y z \, dy + \int_{n_4}^{n_3} \left(f_y - \frac{f_y}{n_3} y \right) y z \, dy + \int_{0}^{n_2} \left(\frac{f_y}{n_2} - \frac{f_y}{n_1} \right) y^2 z \, dy$$

$$+ \int_{0}^{n_4} \left(\frac{f_y}{n_4} - \frac{f_y}{n_3} \right) y^2 z \, dy = \Delta M_x$$

when $\Delta x \to 0$ $n_1 \to n_2$ and $n_3 \to n_4$, the first two terms can be neglected, and hence

$$\int_0^{n_2}\left(\frac{f_y}{n_2}-\frac{f_y}{n_1}\right)y^2z\,dy+\int_0^{n_4}\left(\frac{f_y}{n_4}-\frac{f_y}{n_3}\right)y^2z\,dy = d M_x \qquad \ldots (3)$$

Now observing that $n_1 = n_3$
and $n_2 = n_4$ for any section,
we have

$$\left(\frac{f_y}{n_2}-\frac{f_y}{n_1}\right)\left[\int_0^{n_2}y^2z\,dy+\int_0^{n_4}y^2z\,dy\right] = d M_x \qquad \ldots (4)$$

The term $\left[\int_0^{n_2}y^2z\,dy+\int_0^{n_4}y^2z\,dy\right]$ is really the moment of inertia of the section between n_2 and n_4, i.e. M. of I. of the elastic portion of the section. Representing this by I_e, we have

$$\left(\frac{f_y}{n_2}-\frac{f_y}{n_1}\right)I_e = d M_x$$

$$\therefore \quad \left(\frac{f_y}{n_2}-\frac{f_y}{n_1}\right) = \frac{d M_x}{I_e} \qquad \ldots (5)$$

Substituting equation (5) in equation (2), we have

$$q = \frac{dM_x}{dx}\cdot\frac{1}{I_e}\int_{y_1}^{n_2} y z\,dy$$

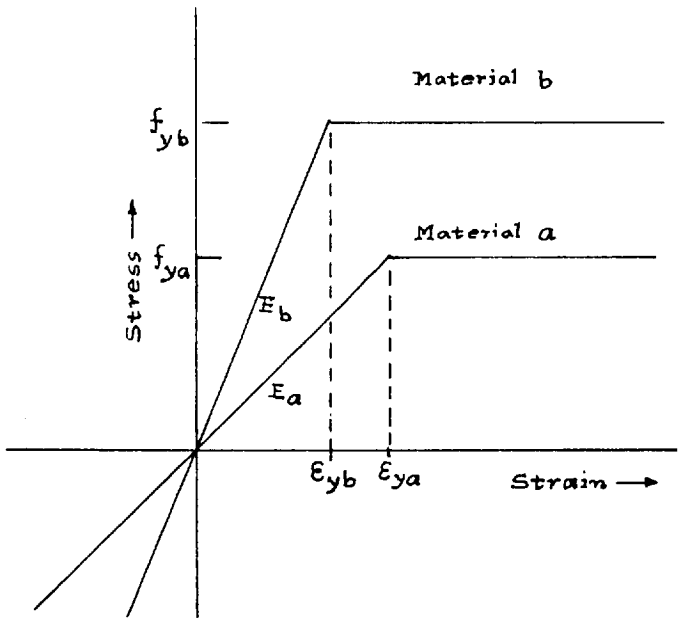
$$= \frac{V M'_e}{I_e} \qquad \ldots (6)$$

where v = Total vertical shear at the section
I_e = Moment of inertia of the elastic part of the section
M'_e = Moment about N.A. of the elastic area of the section above the surface under consideration
q = horizontal shear/unit length on the surface at the section.

The above equation is valid for any section of homogeneous material with a trapezoidal stress block. The value of "n" can be calculated directly by equating the internal and the external moment.

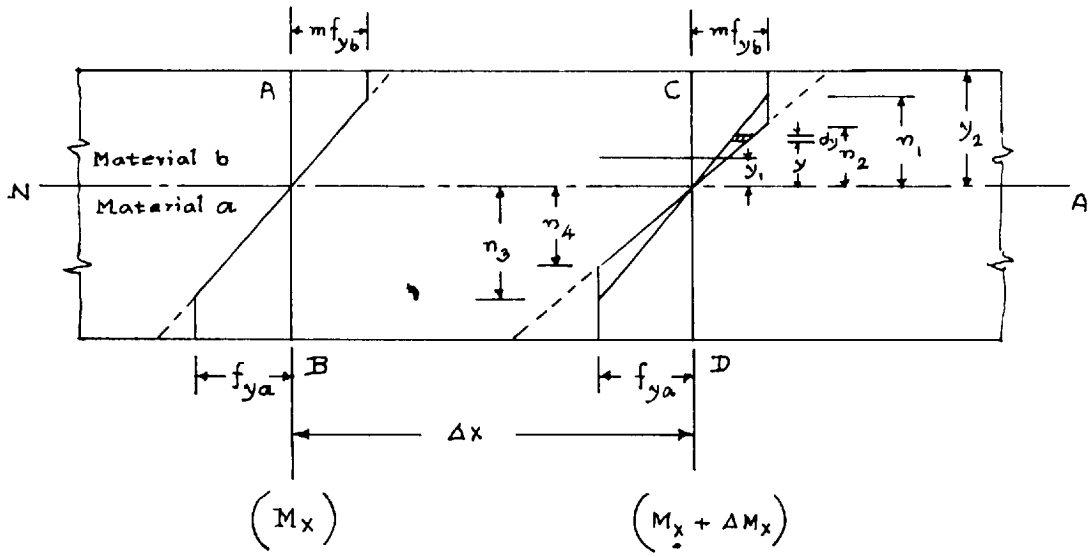
Case II

The section is a composite section fully interconnected and composed of two materials a and b, both having trapezoidal stress-strain relationship, but with different yield stresses and yield strains as shown below



$$\frac{E_b}{E_a} = m$$

$$\frac{\varepsilon_{yb}}{\varepsilon_{ya}} = \alpha$$



Stress and strain distribution at two sections AB and CD, Δx apart, on the basis of equivalent section in terms of material a are shown in the above figure.

The expression for "q" after rewriting equation (2)

$$q = \frac{1}{dx}\int_{y_1}^{n_2}\left(\frac{m f_{yb}}{n_2} - \frac{m f_{yb}}{n_1}\right) y z\, dy \qquad \ldots (7)$$

The expression (3) after rewriting:

$$\int_0^{n_2}\left(\frac{m f_{yb}}{n_2} - \frac{m f_{yb}}{n_1}\right) y^2 z\, dy + \int_0^{n_4}\left(\frac{f_{ya}}{n_4} - \frac{f_{ya}}{n_3}\right) y^2 z\, dy = d M_x$$

Here $n_1 \neq n_3$

$n_2 \neq n_4$

But $$\frac{\frac{m f_{yb}}{Eb}}{n_2} = \frac{\frac{f_{ya}}{Ea}}{n_4} = \frac{1}{R_{CD}}$$

$$\therefore \quad \frac{m f_{yb}}{n_2} = \frac{f_{ya}}{n_4}$$

Similarly, $$\frac{m f_{yb}}{n_1} = \frac{f_{ya}}{n_3}$$

$$\therefore \quad \frac{m f_{yb}}{n_2} - \frac{m f_{yb}}{n_1} = \frac{f_{ya}}{n_4} - \frac{f_{ya}}{n_3}$$

Hence the expression reduces to

$$\left(\frac{m f_{yb}}{n_2} - \frac{m f_{yb}}{n_1}\right)\left[\int_0^{n_2} y^2 z\, dy + \int_0^{n_4} y^2 z\, dy\right] = dM_x \qquad \ldots (8)$$

The expression $\left[\int_0^{n_2} y^2 z\, dy + \int_0^{n_4} y^2 z\, dy\right]$ is the moment of inertia of the equivalent section between n_2 and n_4, i.e., the moment of inertia of the elastic portion of the section. Representing this expression by I_{ee}, we have

$$q = \frac{dM_x}{dx} \cdot \frac{1}{I_{ee}} \int_0^{n_2} y z\, dy$$

$$= \frac{V M'_{ee}}{I_{ee}} \qquad \ldots (9)$$

where V = total vertical shear

I_{ee} = moment of inertia of the elastic part of the equivalent section about N.A.

M'_{ee} = moment of the elastic part of the equivalent section above the surface under consideration about N.A.

It may be noted that the expressions for q, the horizontal shear in a plane at a section when the section is partly elastic and partly plastic, is similar to that when the section is fully elastic.

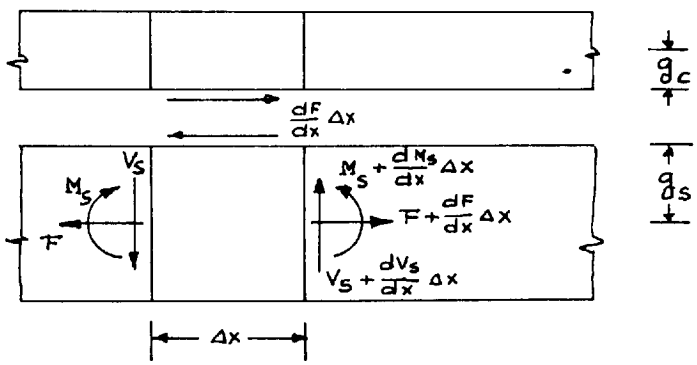
APPENDIX II

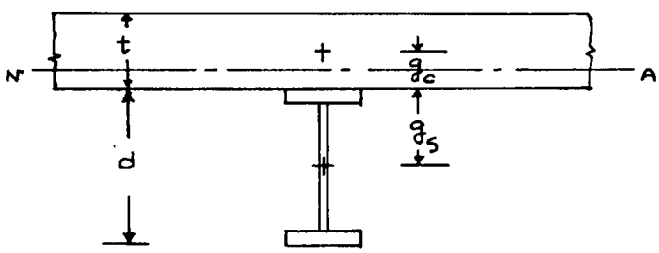
Calculation of deflections in composite beams

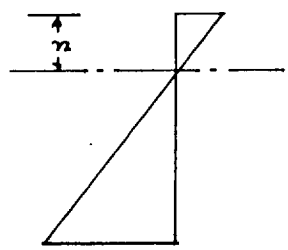
1. Complete interaction

(a) Deflection due to bending: Bending deflection is calculated using simple theory for bending based on transformed area method. The transformed section of the concrete slab is obtained by dividing the slab width by the modular ratio, m.

(b) Deflection due to shear: Shear deflection is calculated only for the shear resisted by the steel beam. The shear force resisted by the steel beam is calculated as follows:







Considering the equilibrium of an element of the steel beam of length Δx,

$$\frac{dM_s}{dx}\Delta x + V_s \cdot \Delta x + \frac{dV_s}{dx}\cdot\Delta x \cdot \Delta x + \frac{dF}{dx}\Delta x \cdot g_s = 0$$

Neglecting the second order terms we have

$$\frac{dM_s}{dx} + V_s + \frac{dF}{dx}\cdot g_s = 0$$

$$\text{or,} \qquad -V_s = \frac{dM_s}{dx} + \frac{dF}{dx}\cdot g_s$$

$$\text{or numerically,} \qquad V_s = \frac{dM_s}{dx} + \frac{dF}{dx} g_s \qquad \ldots (10)$$

Considering the composite section subjected to external moment M,

$$\frac{M}{E_s I_{cs}} = \frac{M_s}{E_s I_s} = \frac{M_c}{E_c I_c}$$

$$\therefore \qquad M_s = M.\frac{I_s}{I_{cs}} \qquad \ldots (11)$$

The axial force F in the steel beam and in the concrete slab, which are numerically the same, is

$$F = \frac{M}{I_{cs}}\left(t + g_s - n\right)\cdot A_s \qquad \text{(in the steel beam)}$$

$$= \frac{M}{I_{cs}}\left(n - t + g_c\right)\cdot \frac{A_c}{m} \qquad \text{(in the concrete slab)}$$

from which, after simplification,

$$F = \frac{M}{I_{cs}} \cdot \frac{\frac{A_c}{m}\cdot A_s}{A_s + \frac{A_c}{m}} \cdot z \qquad \ldots (12)$$

Substituting for F and M_s in equation (10),

$$V_s = \frac{d}{dx}\frac{M}{I_{cs}}\left[I_s + \frac{\frac{A_c}{m}\cdot A_s}{A_s + \frac{A_c}{m}} \cdot z \cdot g_s\right]$$

$$= \frac{V}{I_{cs}}\left[I_s + \frac{\frac{A_c}{m}\cdot A_s}{A_s + \frac{A_c}{m}} \cdot z \cdot g_s\right] \qquad \ldots (13)$$

Where V = total external shear force

I_{cs} = moment of inertia of the transformed composite section

I_s = moment of inertia of the steel section

A_c and A_s are the cross-sectional areas of the slab and the steel beam.

Shear deflection is then calculated assuming the shear to be resisted uniformly by the web. For a beam subjected to a central point load, the shear deflection at midspan will be given by

$$\delta_s = \frac{V_s \cdot \frac{L}{2}}{A_w \cdot G} \qquad \ldots (14)$$

where A_w = cross-section area of the web

G = shear modulus taken as 5410 t.s.i. for all calculations.

2. Incomplete interaction

(a) Deflection due to bending: The bending deflection in a composite beam for incomplete interaction is calculated using Newmark's theory for incomplete interaction.

The expression for the curvature of a composite beam may be obtained from equation (10), given in section 2.1 as

$$\frac{d^2y}{dx^2} = -\frac{M}{\Sigma EI} + \frac{Fz}{\Sigma EI} \qquad \ldots (15a)$$

After substituting for F from equation (11) of section 2.1 and then rearranging, the equation (15a) gives

$$\frac{d^2y}{dx^2} = -\frac{M}{\overline{EI}} + \frac{s}{k}\cdot\frac{\overline{EA}\,z}{\overline{EI}}\cdot\frac{d^2F}{dx^2} \qquad \ldots (15b)$$

Integrating the above equation twice with respect to x, after substituting the appropriate expression for M, the deflection of a composite beam is obtained using the approporiate boundary conditions.

For a composite beam of span L subjected to a point load P at midspan, the boundary conditions are:

$$\text{at } x = 0 \quad y = 0 \quad \text{and } F = 0$$

$$\text{at } x = \frac{L}{2} \quad \frac{dy}{dx} = 0 \quad \text{and } \frac{dF}{dx} = 0,$$

and the deflection for $0 < x < \frac{L}{2}$,

$$y = \frac{P}{48\overline{EI}}\left(3L^2x - 4x^3\right) + \frac{s}{k}\left(\frac{\overline{EA}}{\overline{EI}}\cdot z\right)^2 \frac{PL}{2}\left(\frac{x}{L} - \frac{\sinh \frac{\pi}{\sqrt{c}}\cdot\frac{x}{L}}{\frac{\pi}{\sqrt{c}}\cosh\frac{\pi}{2\sqrt{c}}}\right) \quad \ldots (16)$$

at $x = \frac{L}{2}$,

$$y = \frac{PL^3}{48\overline{EI}} + \frac{s}{k}\left(\frac{\overline{EA}}{\overline{EI}}\cdot z\right)^2 \frac{PL}{2}\left[\frac{1}{2} - \frac{2\sqrt{c}}{\pi}\tanh\frac{\pi}{2\sqrt{c}}\right] \quad \ldots (17)$$

It should be noted that the first term of the expression for deflection in equations (16) and (17) represents the deflection of the composite beam for complete interaction, and the second term represents the additional deflection due to incomplete interaction.

The notation used above is the same as that in section 2.1.

(b) Deflection due to shear. In a composite beam with an adequate number of shear connectors, the shear resisted by the steel beam for incomplete interaction is very close to that for complete interaction. The shear deflection for incomplete interaction, therefore, is taken as the same for complete interaction.

REFERENCES

1. Test of Steel Beams in Concrete in National Physical Laboratory
Published by Redpath Brown and Co. Ltd., London 1924

2. H. M. Mackay, P. Gillespie and C. Leluau
Report on the Strength of Steel I-Beams Haunched with Concrete
Engineering Journal, Eng. Inst. of Canada,
vol. 6, No.8, pp. 365-369, 1923

3. H. M. Mackay
Steel I-Beams Haunched in Concrete
Bulletin No.5, Section 2, University of Toronto, 1925

4. R. A. Caughey
Composite Beams of Concrete and Structural Steel
Proceedings, 41st Annual Meeting, Iowa Engineering Society
pp. 96-104, 1929

5. C. Batho, S. D. Lash and R. H. H. Kirkham
The Properties of Composite Beams, Consisting of Steel Joists Encased in Concrete, under Direct and Sustained Loading
Journal, I.C.E., vol.11, No.4, pp. 61-114, 1939

6. V. Lapsins
A Comparative Study of Composite Action in Structural Steel and Concrete Beams
Thesis presented to the State University of Iowa in 1953, in partial fulfilment of the requirements for the degree of Master of Science

7. G. Wastlund and L. Ostlund
Studies of Composite Beams
International Association of Bridge and Structural Engineers
IVth Congress, 1952, pp. 557-569

8. A. Voellmy
Strength of Alpha Composite Sections under Static and Dynamic Stresses
Unpublished report, Swiss Federal Mat. Test. Lab., EMPA, Zürich, 1936

9. Tests Made on Four Floor Panels Designed According to the Alpha System
Porete Mfg. Co., North Arlington, N.J., 1937

10. Report of Tests of Composite Steel and Concrete Beams
Unpublished report, Fritz Engineering Laboratory, Lehigh University, 1943

11. I. M. Viest
Tests of Spiral Shear Connectors
Engineering Test Data, Nelson Stud Welding, Loraine, Ohio

12. M. Ros
Träger in Verbundbauweise
Report No.149, Swiss Federal Mat. Test. Lab., EMPA, Zürich, 1944

13. O. Graf
Versuche über den Verschiebewiderstand von Dubeln für Verbundträger
Der Bauingenieur, Berlin, vol.25, No.8, pp.297-303, 1950

14. O. Graf
Über Versuche mit Verbundträgern
Abhandlungen aus dem Stahlbau, Heft 10, Stahl-Tagung Karlsruhe, pp.74-90, 1951

15. D. Fuchs
Versuche mit Spannbeton-Verbundträgern
Der Bauingenieur, Berlin, vol.25, No.8, pp. 289-294, 1950

16. C. P. Siess, I. M. Viest, N. M. Newmark
Studies of Slab and Beam Highway Bridges, Part III - Small Scale Tests of Shear Connectors and Composite T-Beams
Bulletin 396, Univ. of Illinois Eng. Experiment Station, 1952

17. I. M. Viest, C. P. Siess, J. H. Appleton and N. M. Newmark
Studies of Slab and Beam Highway Bridges, Part IV - Full Scale Tests of Channel Shear Connectors and Composite T-Beams
Bull. 405, Univ. of Illinois Eng. Experiment Station, 1952

18. I. M. Viest
Investigation of Stud Shear Connectors for Composite Concrete and Steel T-Beams
Journal, A.C.I., vol.27, No.8, pp.875-891, 1956

19. G. M. Sinclair
Fatigue Strength of $\frac{3}{4}$in. Welded Stud Shear Connectors
Engineering Test Data, Nelson Stud Welding, Lorain, Ohio

20. I. M. Viest
Tests on Stud Shear Connectors, Parts I, II, III and IV
Engineering Test Data, Nelson Stud Welding, Lorain, Ohio

21. B. Thürlimann
Composite Beams with Stud Shear Connectors
Bulletin 174, Highway Research Board, Washington D.C.,
pp. 18-38, 1958

22. B. Thürlimann
Fatigue and Static Strength of Stud Shear Connectors
Journal, A.C.I., vol.30, No.12, pp.1287-1302, 1959

23. C. Culver and R. Coston
Tests of Composite Beams with Stud Shear Connectors
Fritz Eng. Laboratory Report No.354.1, April 1959

24. C. Culver, P. J. Zarzeczny and G. C. Driscoll
Tests of Composite Beams for Buildings
Fritz Eng. Laboratory Report No. 279.2, June 1960

25. C. Culver, P. J. Zarzeczny and G. C. Driscoll
Tests of Composite Beams for Buildings
Fritz Eng. Laboratory Report No.279.6, January, 1961

26. R. G. Slutter and G. C. Driscoll
Test Results and Design Recommendations for Composite Beams
Fritz Eng. Laboratory Report No.279.10, January, 1962

27. K. C. F. Wong
The Behaviour of Building Frames of Composite Construction
Thesis presented to the University of London for the
degree of Ph.D., 1957

28. A. O. Adekola
Interaction between Steel Beams and a Concrete Floor Slab
Thesis presented to the University of London for the
degree of Ph.D., 1959

29. S. Balakrishnan
The Behaviour of Composite Steel and Concrete Beams with
Welded Stud Shear Connectors
Thesis presented to the University of London for the
degree of Ph.D., 1963

30. J. Casillas G. de L., N. Khachaturian and C. P. Siess
Studies of Reinforced Concrete Beams and Slabs Reinforced with Steel Plates
Civil Eng. Studies, Structural Research Series No.134, University of Illinois, 1957

31. S. Timoshenko and S. Woinowsky-Krieger
Theory of Plates and Shells

32. J. C. Chapman
The Interaction between a Ship's Hull and a Long Superstructure
Trans. I.N.A., 1957, vol.99

33. J. S. Teraszkiewicz
Ph.D. Thesis to be submitted to the University of London

34. D. Young
Bending Moments in the Walls of Rectangular Tanks
Proceedings of American Soc. of Civil Engineers
vol.67, No.9, November 1941, pp.1683-1696

35. R. H. Wood
Plastic and Elastic Design of Slabs and Plates

36. I. M. Viest, R. S. Fountain and C. P. Siess
Development of the new AASHO Specifications for Composite Steel and Concrete Bridges
Bulletin 174, Highway Research Board, Washington D.C. 1957, pp. 1-17

37. Tentative Recommendations for Design of Composite Beams and Girders for Buildings
Journal of the American Concrete Institute, vol.32 No.6 December 1960, pp. 609-628

38. I. M. Viest
Review of Research on Composite Steel-Concrete Beams
Journal of the Structural Division, Proc. A.S.C.E., June 1960

LIST OF FIGURES

Figure No.

1. Summary of tension test curves

2. Assumed stress distribution at ultimate load
   (a) T-beam
   (b) Plated beam

3. Idealised stress strain curves for concrete and steel

4. Idealised sections for the T-beams

5. Axial force in steel beam and interface shear at collapse
   — T-beam with central point load (complete interaction)

6. Axial force in steel beam and interface shear at collapse
   — T-beam with U.D.L. (complete interaction)

7. Interface shear for elastic incomplete interaction
   — T-beam with (a) central point load and (b) U.D.L.

8. Interface shear for elastic incomplete interaction
   — T-beam with two equal point loads

9. Influence line for strain difference at the interface at midspan: T-beam with two equal point loads

10. Interface shear in a simply supported square composite plate under U.D.L. (complete interaction)

11. Interface shear in a simply supported square composite plate under a central patch load (complete interaction)

12. Interface shear for elastic incomplete interaction
    — Plated beam with (a) central point load and (b) U.D.L.

13. Separation between slab and beam
    — T-beams with central point load

14. Deflected shape of a $\frac{3}{4}$in. dia. x 4in. long stud

15. Bending moment distribution along a $\frac{3}{4}$in. dia. x 4in. long stud

Figure No.

16. Details of quarter scale push-out specimens

17. Details of full scale push-out specimens

18. Pull-out specimen

19. Total slips: quarter scale push-out specimens with varying flange roughness

20. Residual slips: quarter scale push-out specimens with varying flange roughness

21. Total slips: push-out specimens P2D1, P3D1, P3D2 and P4D1

22. Residual slips: push-out specimens P2D1, P3D1, P3D2 and P4D1

23. Total slips: push-out specimens P2E1, P2E2, P3E1 and P4E1

24. Residual slips: push-out specimens P2E1 and P2E2, P3E1 and P4E1

25. Total slips: push-out specimens P6D1 and P6D2

26. Residual slips: push-out specimens P6D1 and P6D2

27. Total slips: push-out specimens P12D(TH) and P12D(T)

28. Residual slips: push-out specimens P12D(TH) and P12D(T)

29. Total slips: push-out specimens P12E1 and P12E(DE)

30. Residual slips: push-out specimens P12E1 and P12E(DE)

31. Total separations: push-out specimens P12E1 and P12E(DE)

32. Residual separations: push-out specimens P12E1 and P12E(DE)

33. Stud strains: push-out specimens P12E1 and P12E(DE)

34. Separation-axial strain curves: push-out specimens P12E1 and P12E(DE)

Figure No.

35. Slip-bending strain curves: push-out specimens P12E1 and P12E(DE)

36. Separation-slip curves: push-out specimens P12E1 and P12E(DE)

37. Separation-slip curves: push-out specimens P2E2 and P4E1

38. Shear stress at ultimate load in plain headed studs with varying stud diameter

39. Shear resistance of Durbar plate with varying cross-sectional area of studs

40. Photograph of crack patterns in the concrete slab of a full scale push-out specimen with $\frac{3}{4}$ in. dia. studs

41. Photograph of crack patterns in the concrete slab of push-out specimen P12E1 after failure

43. Photograph of a pull-out specimen

44. Total separations: pull-out specimens

45. Residual separations: pull-out specimens

47. Details of quarter scale T-beams

48. General arrangement for measurement in quarter scale T-beams

49. Midspan deflections: Beams of group A

50. Average end slips: Beams of group A

51. Average residual end slips: Beams of group A

52. Average slips at quarter span: Beams of group A

53. Average uplifts at quarter span: Beams of group A

54. Mispan deflections: Beams of group B

Figure No.

55. Average end slips: Beams of group B

56. Average residual end slips: Beams of group B

57. Average slips at quarter span: Beams of group B

58. Average uplift at quarter span: Beams of group B

59. Midspan deflections: Beams B3 and B8

60. Average end slips: Beams B3 and B8

61. Midspan deflections: Beams B3 and C1

62. Average end slips: Beams B3 and C1

63. Midspan deflections: Beams B3 and B7

64. Average end slips: Beams B3 and B7

65. Average residual end slips: Beams B3, B7 B8 and C1

66. Average slips at quarter span: Beams B3, B7, B8 and C1

67. Average uplifts at quarter span: Beams B3, B7, B8 and C1

68. Slips along the length: Beam B1

69. Slips along the length: Beam B6

70. Slips along the length: Beam B5

71. Slips along the length: Beam B4

72. Strains at midspan and corresponding stress distribution in the steel beam at or near ultimate load: group A

73. Strains at midspan and corresponding stress distribution in the steel beam at or near ultimate load: group B

74. Strains at midspan: Beam B1

75. Strains at midspan: Beam B3

Figure No.

76. Strains at midspan: Beam B7

77. Photograph of a beam with grooved flange

78. Photographs of the beam with resin bonded aggregates on top flange

79. Photograph of the Durbar flanged quarter scale beam

80. Photograph of the beam with latex cover around the studs

82. Photograph of crushing of concrete: Beam A1

83. Photograph of transverse tension cracks at the bottom of the slab: Beam B4

84. Photograph of a typical failure of stud in T-beam

85. Details of half scale T-beam

86. General arrangement for measurement in half scale T-beam

87. Photograph of set-up for half scale T-beams

88. Midspan deflections: Beams D1 and D2

89. Average end slips: Beams D1 and D2

90. Average residual end slips: Beams D1 and D2

91. Average slips at quarter span: Beams D1 and D2

92. Slips along the length: Beams D1 and D2

93. Average uplifts at quarter span: Beams D1 and D2

94. Uplifts along the length: Beams D1 and D2

95. Uplift-slip curves at quarter span: Beams D1 and D2

96. Strains in studs at quarter span: Beams D1 and D2

97. Axial strain in studs along the length: Beam D2

Figure No.

98. Strains at midspan and corresponding stress distribution in the steel beam at ultimate load: Beams D1 and D2

99. Strains at midspan: Beams D1 and D2

100. Photograph of curshing of concrete at failure of beam D1

101. Photograph of horizontal splitting and tension cracks of the slab at midspan in beam D1

102. Photograph of concrete failure around studs in beam D2

103. Details of plated beams

104. General arrangement for measurement in plated beams

105. Midspan deflections: plated beams PB2 and PB3

106. Average end slips: plated beam PB2 and PB3

107. Average residual end slips: plated beams PB2 and PB3

108. Strains at midspan: plated beams PB2 and PB3

109. Midspan deflections: plated beams PB4, PB5 and PB6

110. Average end slips: plated beams PB4, PB5 and PB6

111. AVerage residual end slips: plated beams PB4, PB5 and PB6

112. Average slips at quarter span: plated beams PB4, PB5 and PB6

113. Average uplfits at quarter span: plated beams PB4, PB5 and PB6

114. Slips along the length of plated beam PB5 and PB6

115. Midspan deflections: plated beams PB7 and PB8

116. Average end slips: plated beams PB7 and PB8

117. Average residual end slips: plated beams PB7 and PB8

Figure No.

118. Average slips near one-third span: plated beams PB7, PB8

119. Average uplifts near one-third span: plated beams PB7 and PB8

120. Slips along the length: plated beams PB7 and PB8

121. Strains at midspan: plated beams PB4, PB5 and PB6

122. Strains at midspan: plated beams PB7 and PB8

123. Photograph of plated beam PB7 after failure

124. Photograph of plated beam PB8 after failure

125. Details of the composite plate

126. General arrangement for measurement in the composite plate

127. Central deflections: composite plate

128. Deflections at B: composite plate

129. Deflections at C: composite plate

130. End slips: composite plate for central loads

131. End slips: composite plate for load at position C

132. End slips: composite plate for load at position B

133. Maximum end slips: composite plate for different load positions

134. Maximum slips in the panel: composite plate for different load positions

135. Maximum uplifts: composite plate for different load positions

136. Maximum principal strains: composite plate

137. Slips and uplifts: composite plate for various central loads

Figure No.

138. Slips: composite plate for various loads at position B

139. Slips along RS: composite plate for loads at position B

140. Uplifts: composite plate for various loads at position B

141. Slips: composite plate for various loads at position C

142. Uplifts: composite plate for various loads at position C

143. Photograph of set-up for the compostie plate

144. Underside of the composite plate showing slip, uplift and deflection gauges

145. Photograph of the local failure of the composite plate

146. Moment curvature relationship: quarter scale T-beams

147. Theoretical and experimental slip distribution along length: Beam B4

148. Approximate theoretical and experimental slip distribution at theoretical ultimate load: Beam B1

149. Theoretical and experimental slip distribution in plated beams PB4, PB5 and PB6

150. Theoretical and experimental slip distribution in plated beam PB7 and PB8

151. Approximate theoretical and experimental slip distribution along the major axes in the composite plate

152. Approximate theoretical and experimental end slip distribution in the composite plate

153. Theoretical and experimental axial strains in studs along beam D2

154. Variation of moment of inertia per unit width of a plated beam with modular ratio

Notation for specimens are shown in Figures 16, 17, 47, 85 and 103.

LIST OF TABLES

Table No.	
1	Summary of the results of composite beams tested by Wastlund and Ostlund
2	Summary of the results of some of the plate beams tested in the University of Illinois
3	Tension test results
4	Properties of stud material
5	Small scale push-out test results
6	Half scale and full scale push-out test results
7	Full scale pull-out test results
8	Summary of test results of composite beams
9	Summary of results of material tests for composite beams
10	Summary of test results of plated beams
11	Summary of results of material tests for plated beams and composite plate

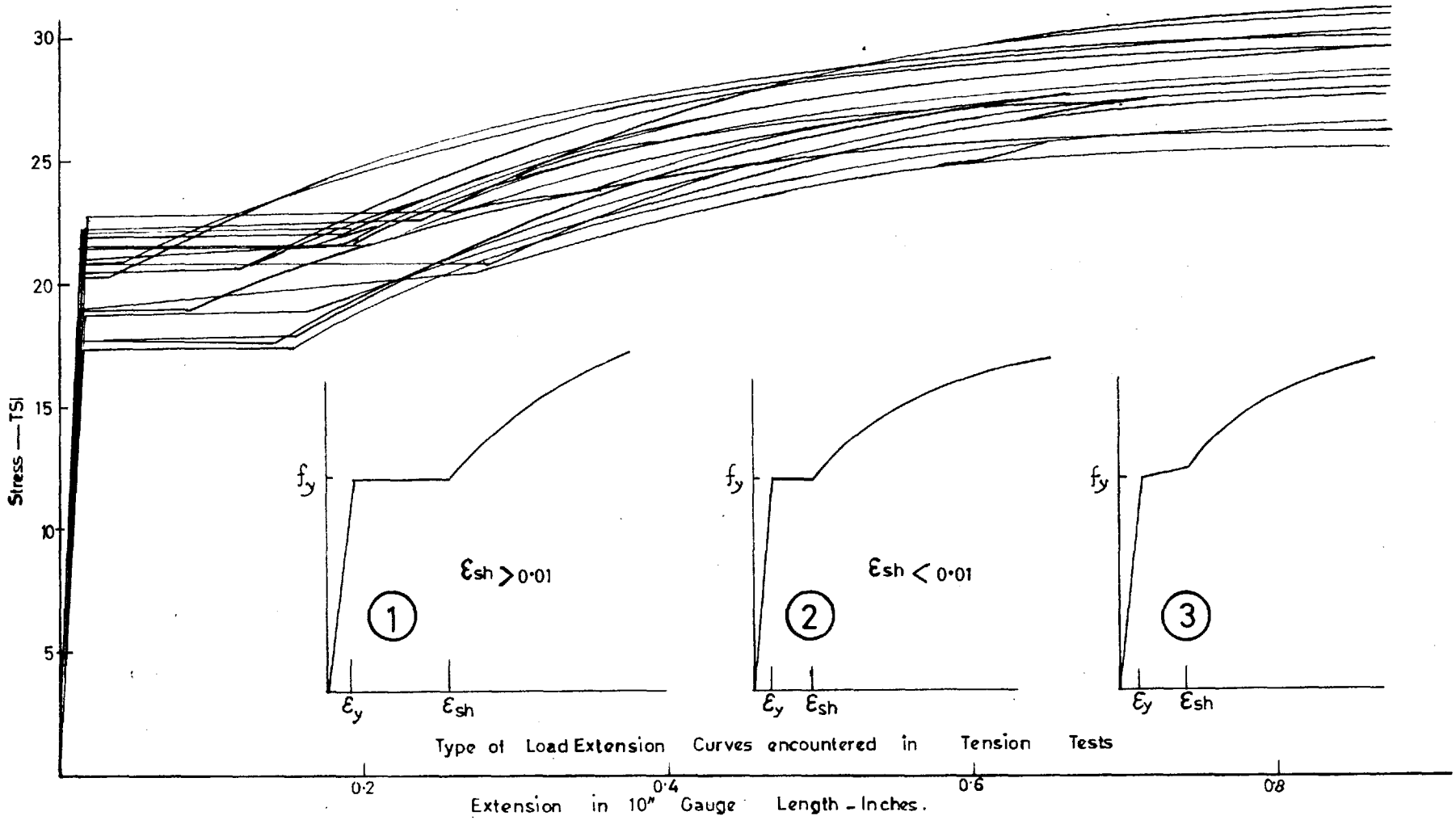
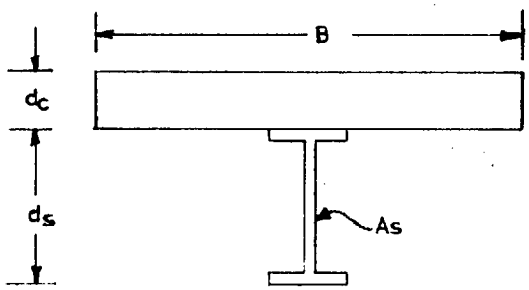
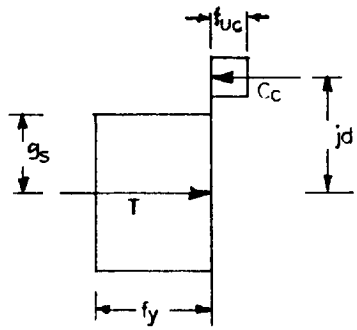


Fig. 1 TENSION TEST CURVES

(a) COMPOSITE BEAMS

Case(1) Neutral Axis in the Concrete Slab

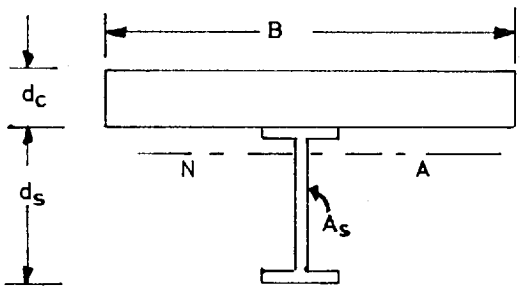


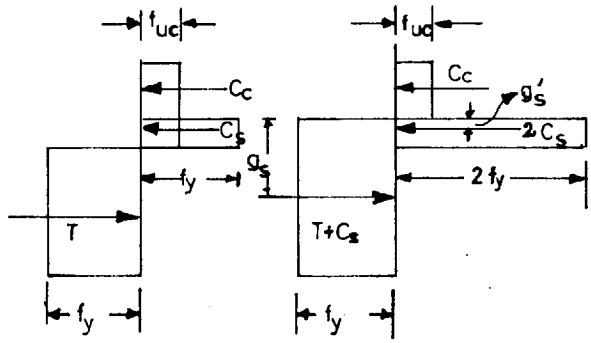


Assumed Stress Distribution at Ultimate Moment

$$M_u = A_s \cdot f_y \left\{ g_s + d_c - \frac{A_s \cdot f_y}{2B \cdot f_{uc}} \right\}$$

Case(2). Neutral Axis in the Steel Beam



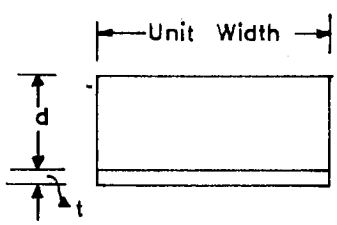


Assumed Stress Distribution at Ultimate Moment

Equivalent Stress Distribution

$$M_u = A_s \cdot f_y \left\{ g_s + \frac{d_c}{2} \right\} - 2C_s \left\{ \frac{d_c}{2} + g'_s \right\}$$

(b) PLATED BEAMS AND COMPOSITE PLATE

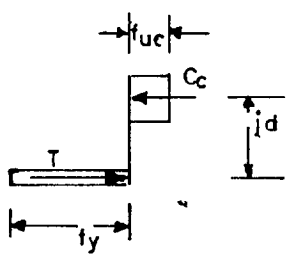


$$M_u \text{ per unit width} = t.f_y.\left\{ d_c + \frac{t}{2} - \frac{f_y \cdot t}{f_{uc}} \right\}$$

Where $f_{uc} = 4/9\, Cu$ or $0{\cdot}85\, f'_c$

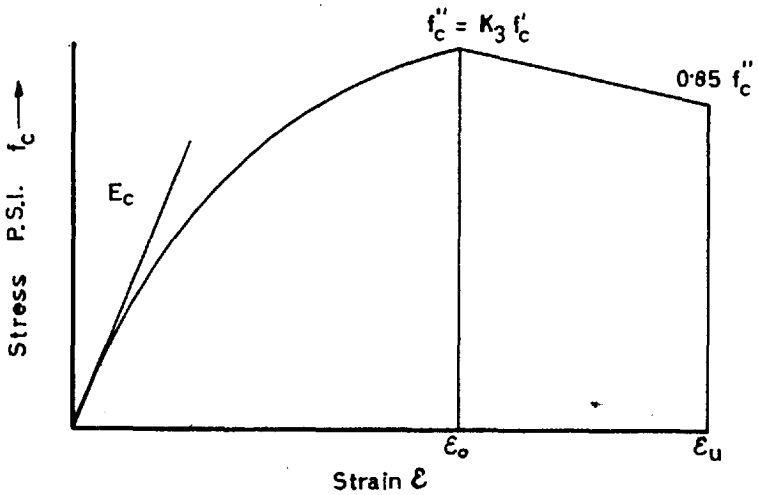
Cu = Actual Cube Strength

f'_c = Actual Cylinder Strength



Assumed Stress Distribution at Ultimate Moment.

Fig. 2. ASSUMED STRESS DISTRIBUTION AT ULTIMATE MOMENT



f_c' = Cylinder Strength in P.S.I.

$E_c = 1{\cdot}8 \times 10^6 + 460\ f_c'$

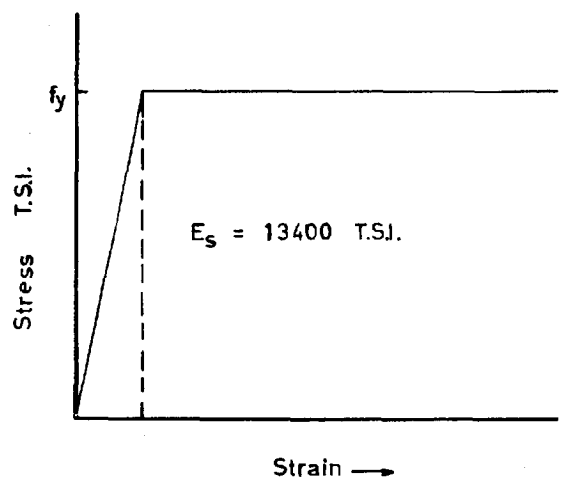
$\varepsilon_o = 2\ \dfrac{f_c''}{E_c}$

$\varepsilon_u = 0{\cdot}004 - \dfrac{f_c'}{6{\cdot}5 \times 10^6}$

$K_3 = \dfrac{3900 + 0{\cdot}35\ f_c'}{3000 + 0{\cdot}82 f_c' - \dfrac{f_c'^2}{26000}}$

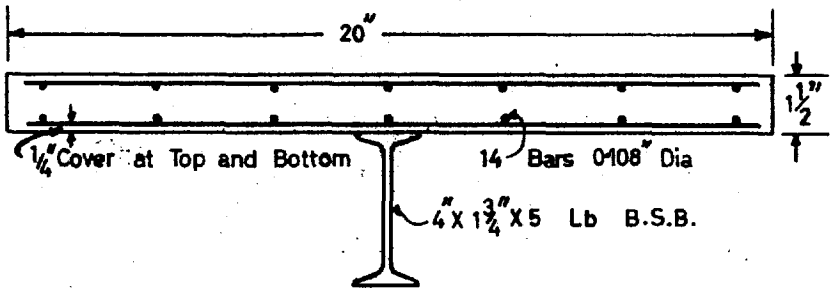
$f_c' = f_c''\left[2\left(\dfrac{\varepsilon_c}{\varepsilon_o}\right) - \left(\dfrac{\varepsilon_c}{\varepsilon_o}\right)^2\right]$

(a) Hognestad's Idealised Stress Strain Diagram for Concrete

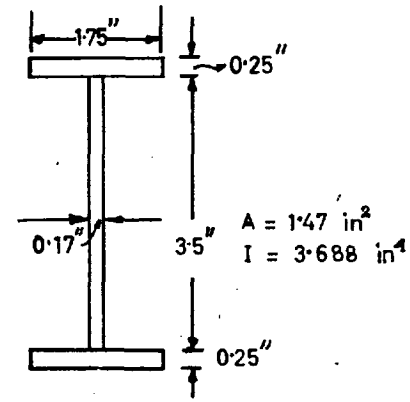


(b) Idealised Stress Strain Curve for Steel

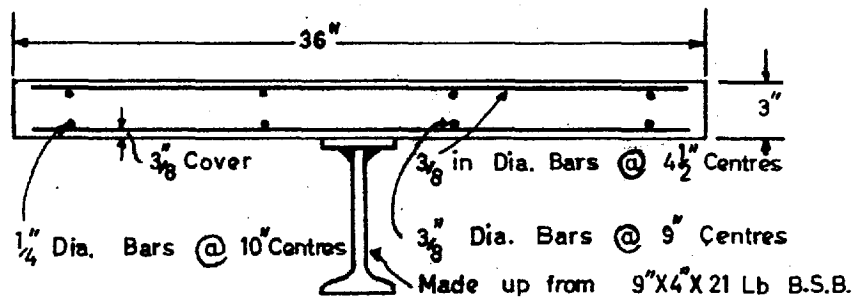
Fig. 3 IDEALISED STRESS STRAIN CURVES FOR CONCRETE AND STEEL



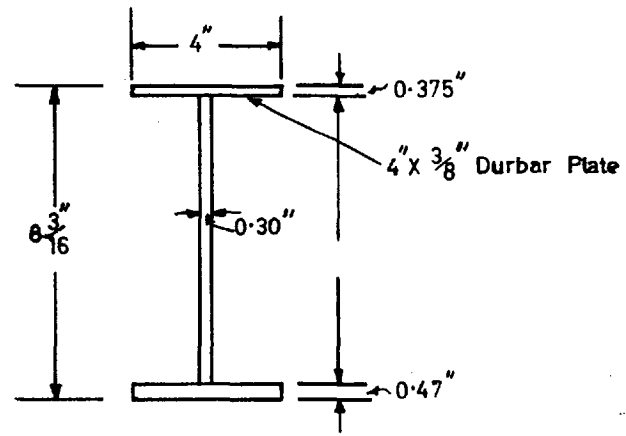
(a) Cross Section of the Quarter Scale Composite Beam



(b) Idealised I Section of the Quarter Scale Composite Beam

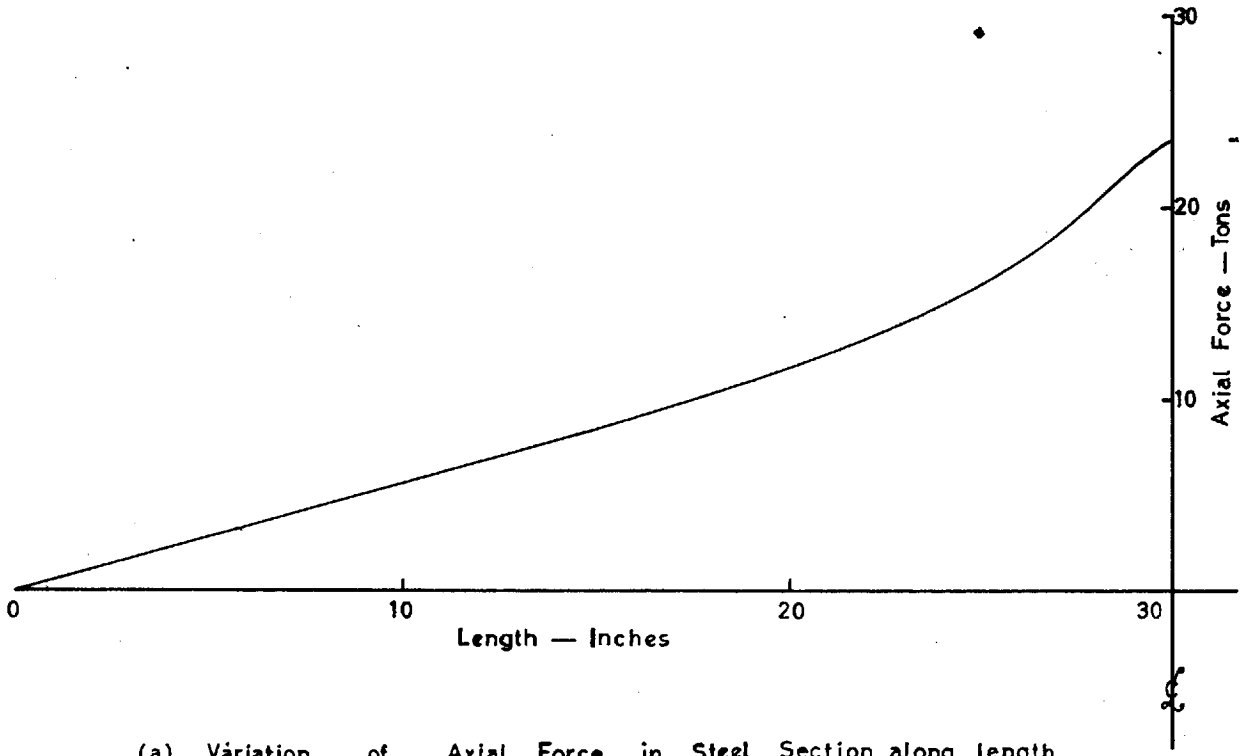


(c) Cross Section of Half Scale Composite Beam

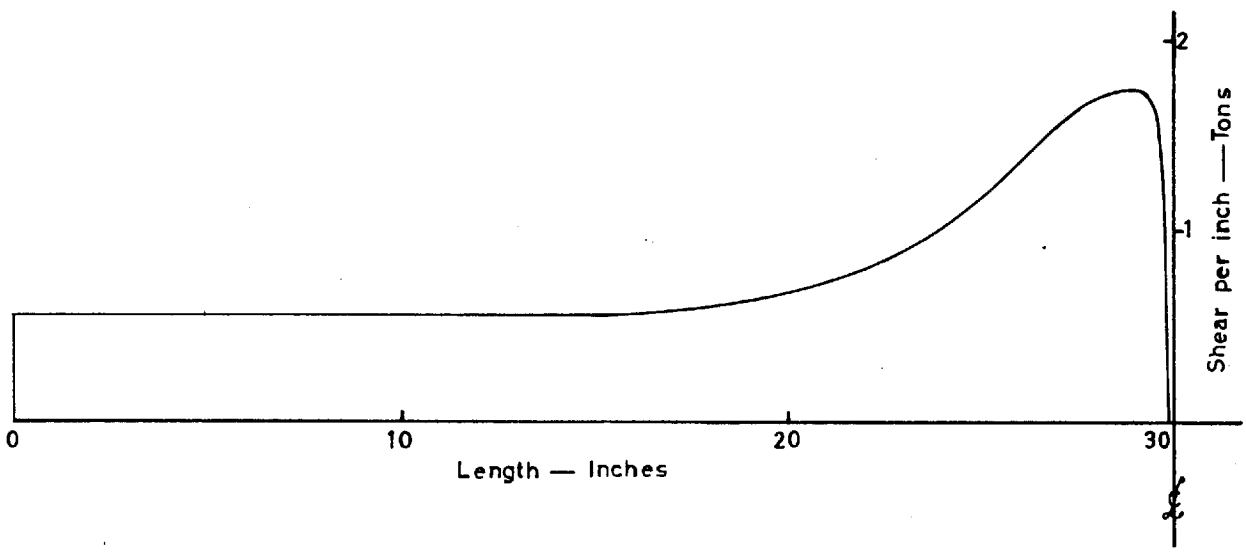


(d) Idealised Steel Section for the Half Scale Composite Beam

Fig. (4) IDEALISED SECTIONS FOR THE QUARTER SCALE AND THE HALF SCALE COMPOSITE BEAMS

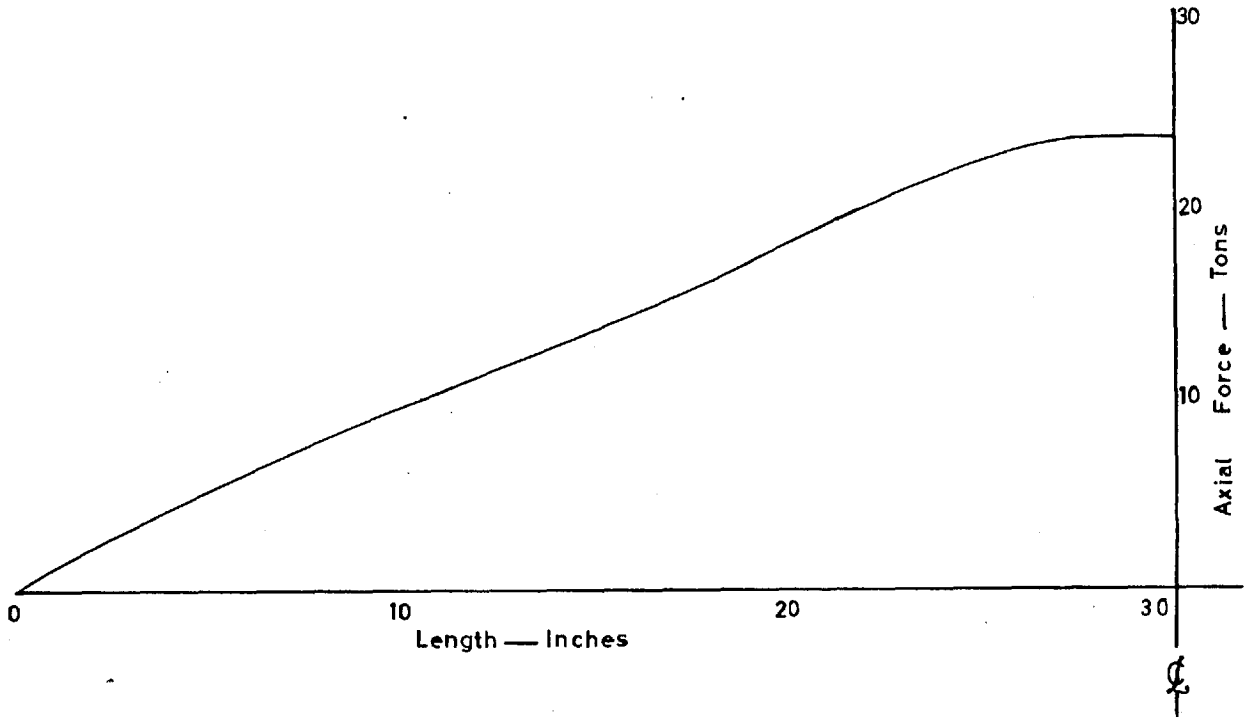


(a) Variation of Axial Force in Steel Section along length

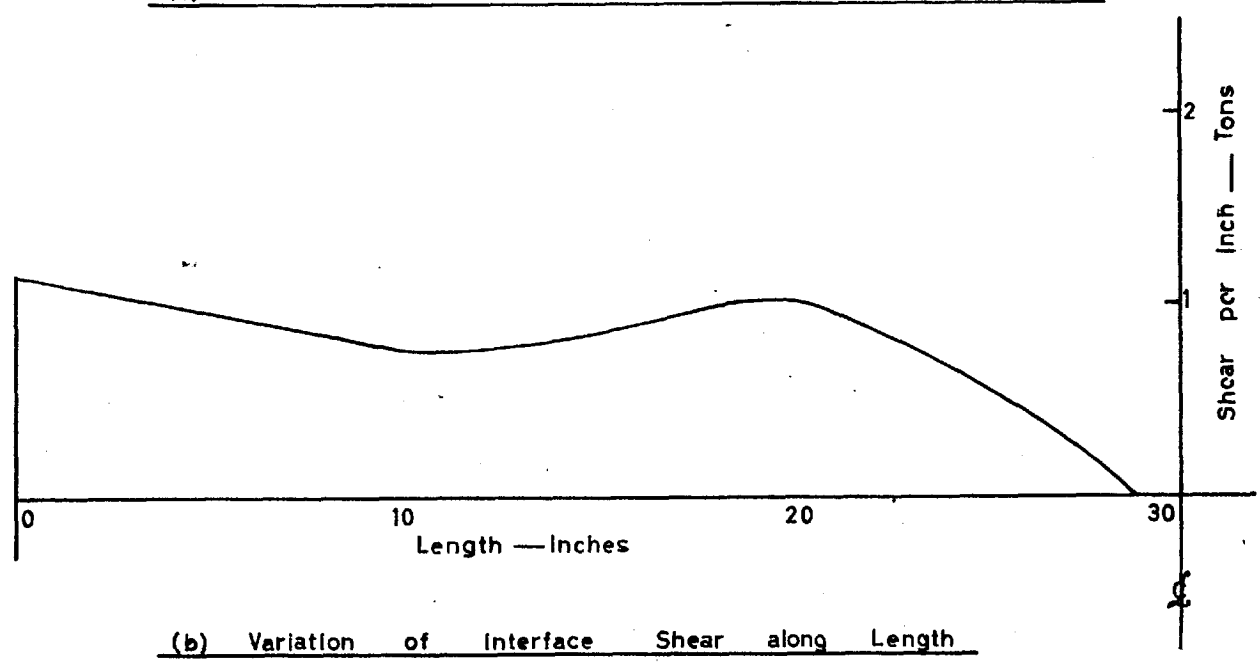


(b) Variation of Interface Shear along length

Fig.5. AXIAL FORCE IN STEEL BEAM AND INTERFACE SHEAR AT COLLAPSE — QUARTER SCALE T-BEAM WITH CENTRAL POINT LOAD (Complete Interaction, Idealised Beam Section and Idealised Stress-Strain curves for Concrete and Steel with $f'_c = 4000$ psi and $f_y = 16$ tsi assumed.)

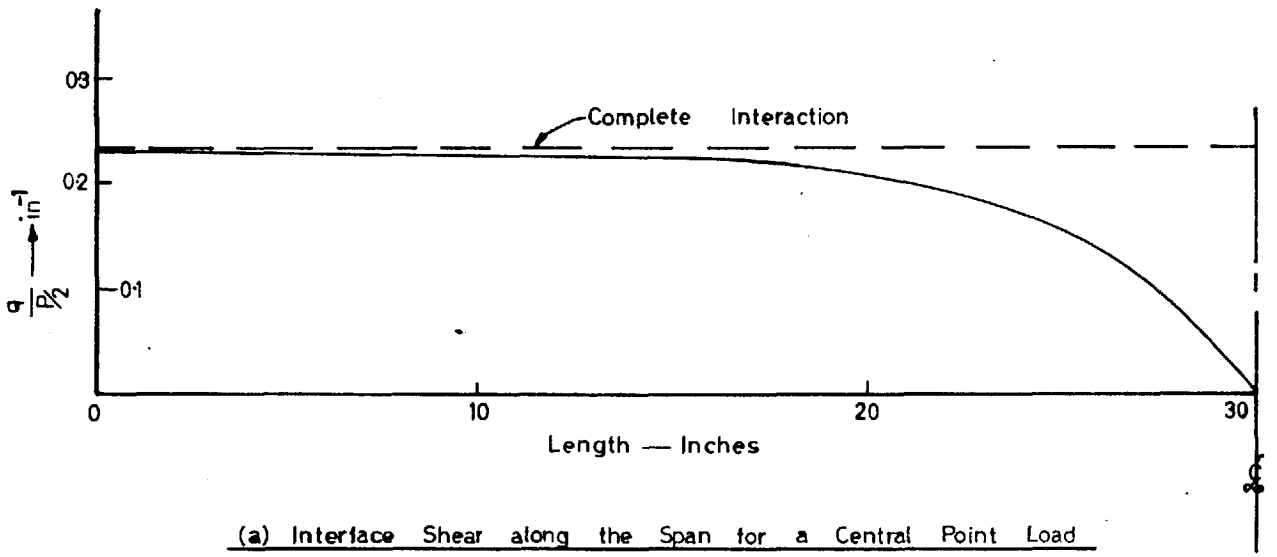


(a) Variation of Axial Force in Steel Section along length

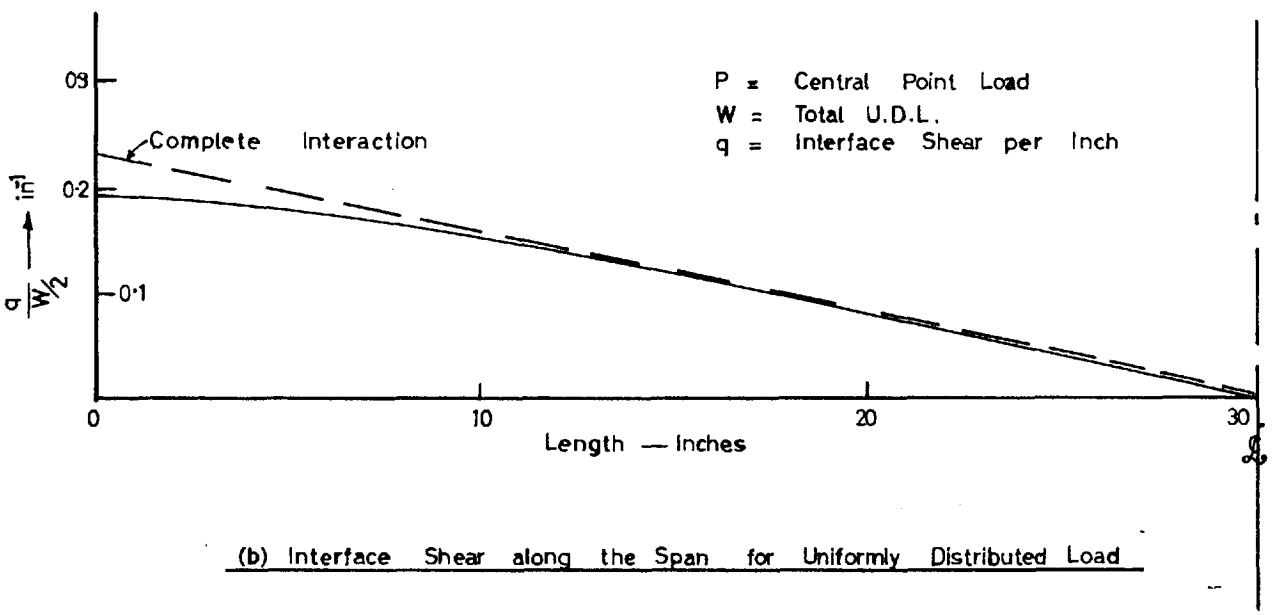


(b) Variation of Interface Shear along Length

Fig. 6. AXIAL FORCE IN STEEL BEAM AND INTERFACE SHEAR AT COLLAPSE — QUARTER SCALE T BEAM WITH UNIFORMLY DISTRIBUTED LOAD (Complete Interaction, Idealised Beam Section and Idealised Stress-Strain curves for Concrete and Steel with $f_c' = 4000$ psi and $f_y = 16$ tsi assumed.)



(a) Interface Shear along the Span for a Central Point Load



(b) Interface Shear along the Span for Uniformly Distributed Load

Fig. 7. INTERFACE SHEAR FOR ELASTIC INCOMPLETE INTERACTION WITH STUDS AT 100% STRENGTH [Quarter Scale T Beam with (a) Central Point Load and (b) Uniformly Distributed Load (Pitch Constant)]

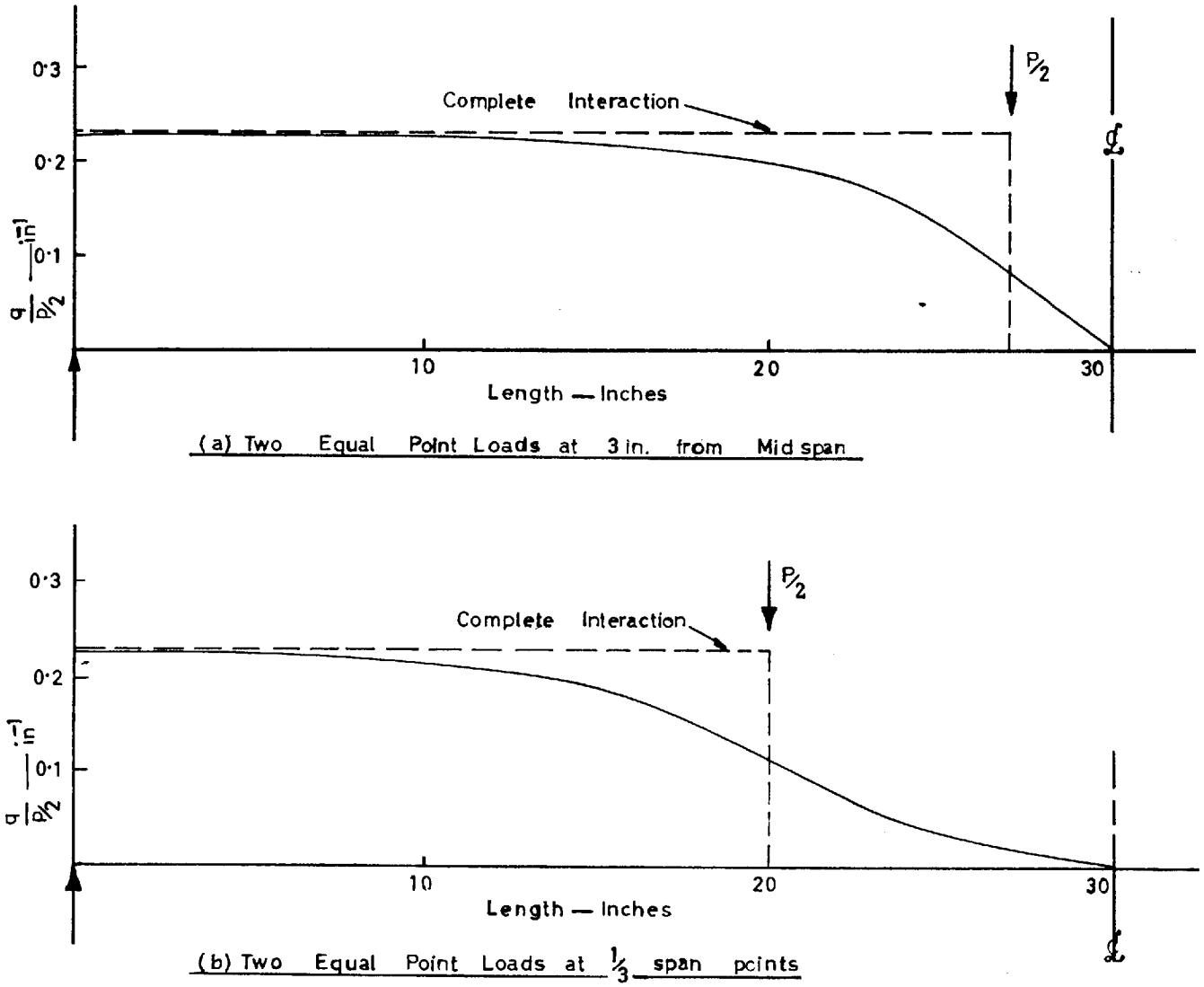


Fig.(8). INTERFACE SHEAR FOR ELASTIC INCOMPLETE INTERACTION WITH STUDS AT 100% STRENGTH — QUARTER SCALE T BEAMS WITH TWO EQUAL POINT LOADS SYMMETRICALLY PLACED.

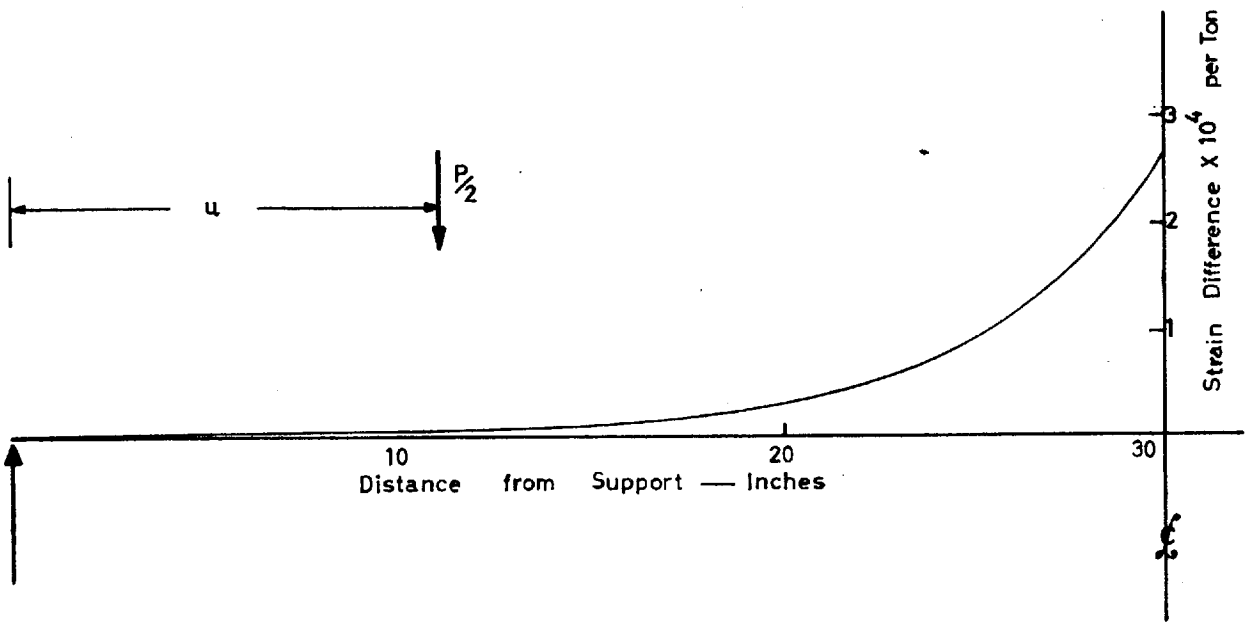


Fig.9. INFLUENCE LINE FOR STRAIN DIFFERENCE AT THE INTERFACE AT MIDSPAN — QUARTER SCALE T BEAM WITH STUDS AT 100% STRENGTH. (Two Equal Point loads at Equal Distance from Mid span)

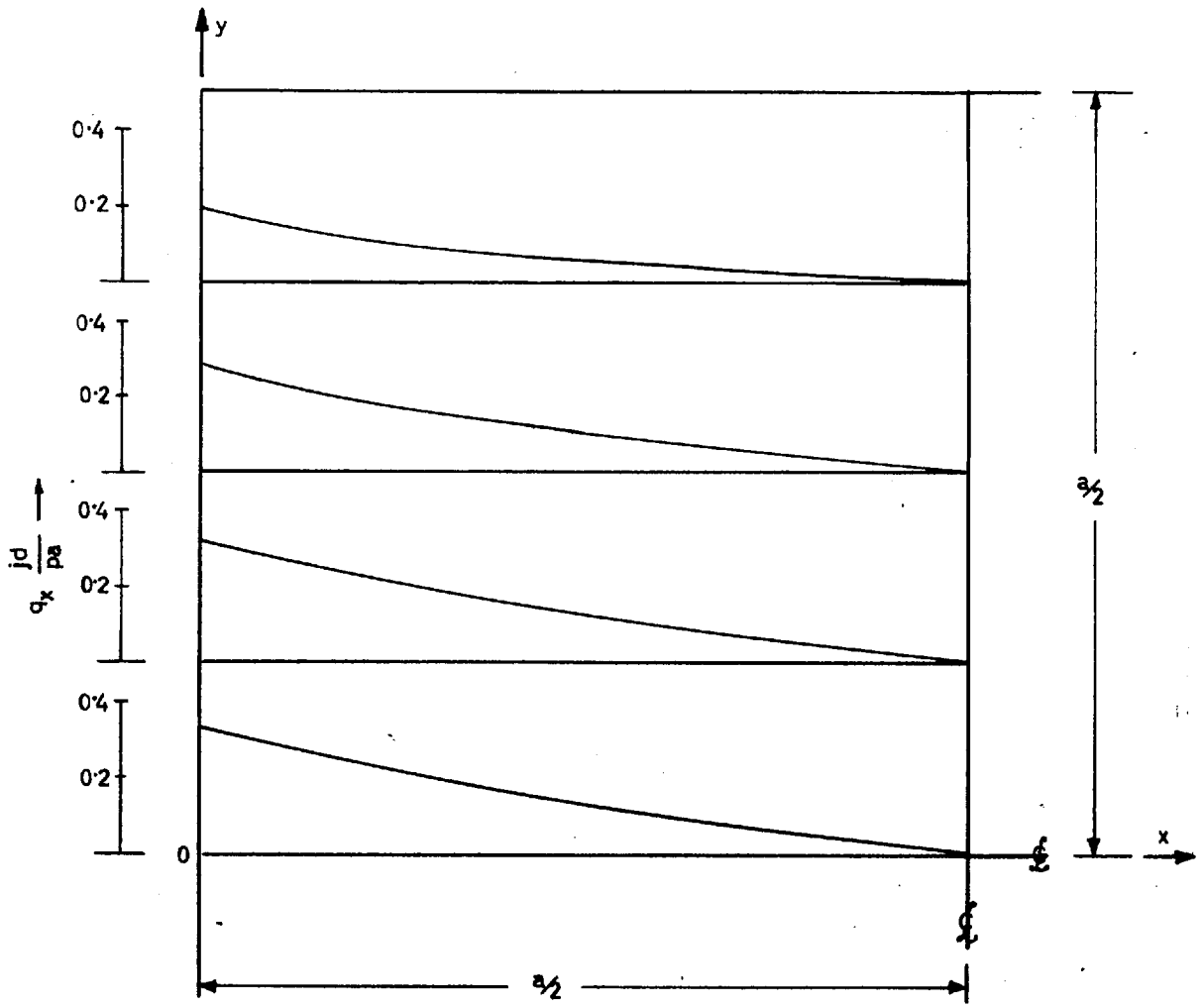


Fig.10. DISTRIBUTION OF HORIZONTAL SHEAR AT INTERFACE IN A SIMPLY SUPPORTED SQUARE PLATE OF SIDE a UNDER UNIFORMLY DISTRIBUTED LOAD p FOR COMPLETE INTERACTION.

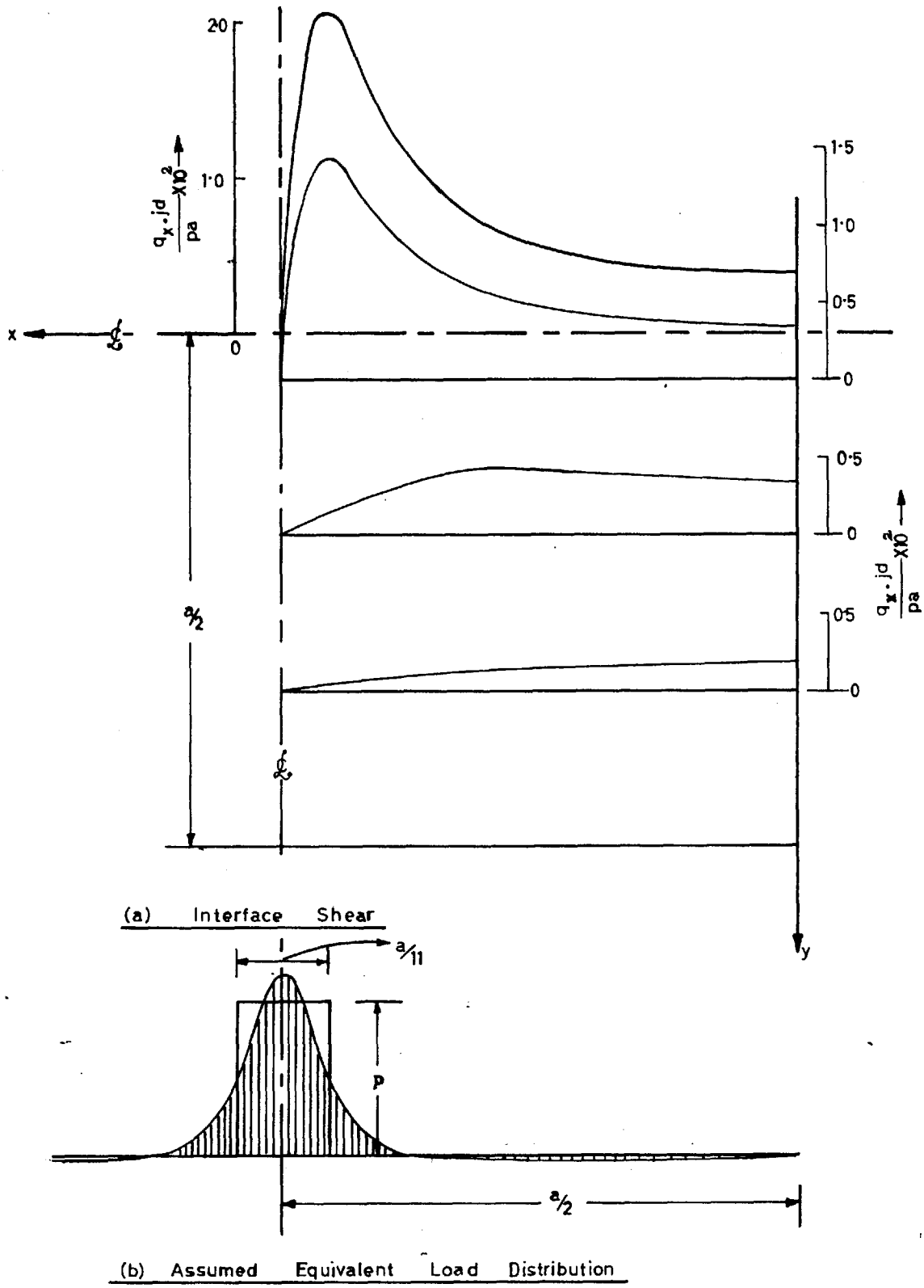
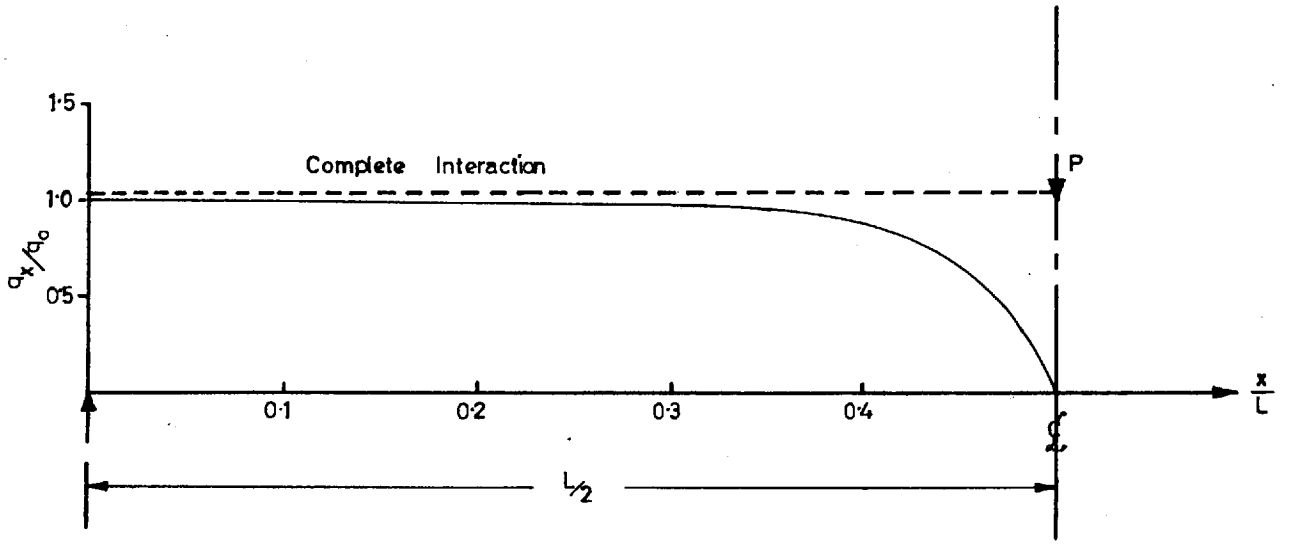
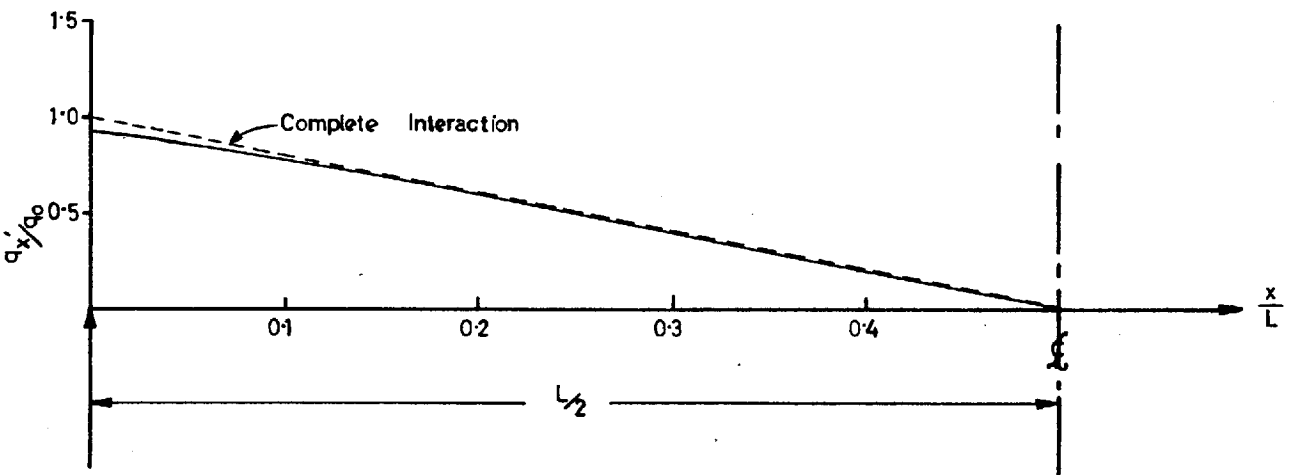


Fig. 11. HORIZONTAL SHEAR AT THE INTERFACE IN A SIMPLY SUPPORTED SQUARE COMPOSITE PLATE UNDER A UNIFORMLY DISTRIBUTED CENTRAL SQUARE PATCH LOAD OF INTENSITY p —— COMPLETE INTERACTION



(a) For a Central Point Load



(b) For Uniformly Distributed Load

Fig.12. HORIZONTAL SHEAR DISTRIBUTION AT INTERFACE IN A PLATED BEAM FOR INCOMPLETE INTERACTION

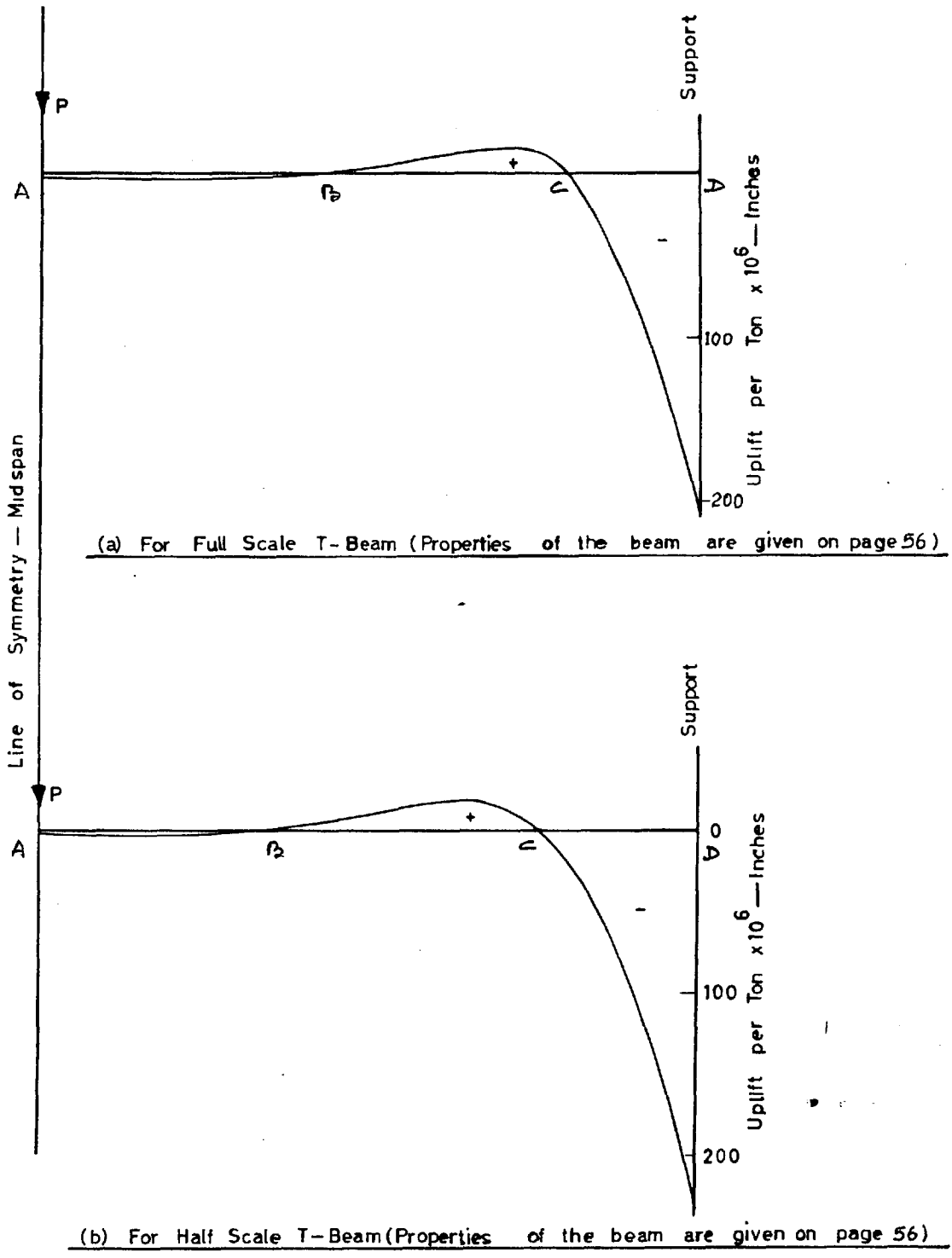


Fig. 13. SEPARATION BETWEEN SLAB AND BEAM (Point Load at Midspan)

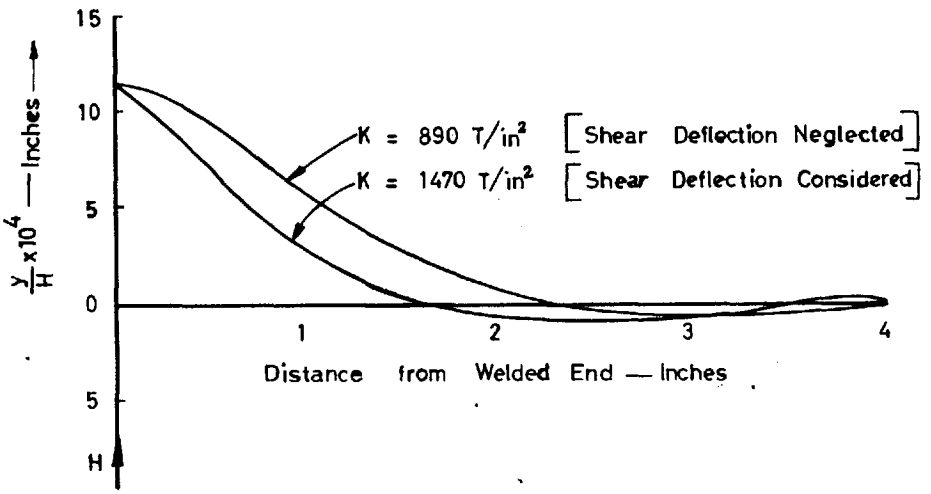


Fig. 14. DEFLECTED SHAPE OF A 3/4" DIAMETER AND 4" LONG STUD

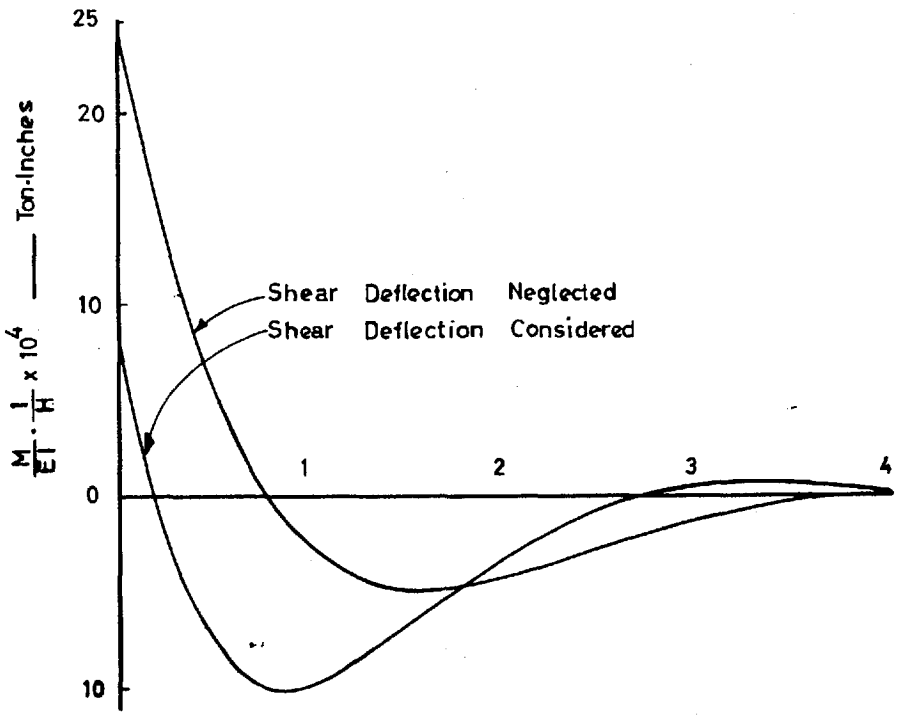


Fig. 15. BENDING MOMENTS ALONG THE LENGTH OF 3/4" DIAMETER AND 4" LONG STUD

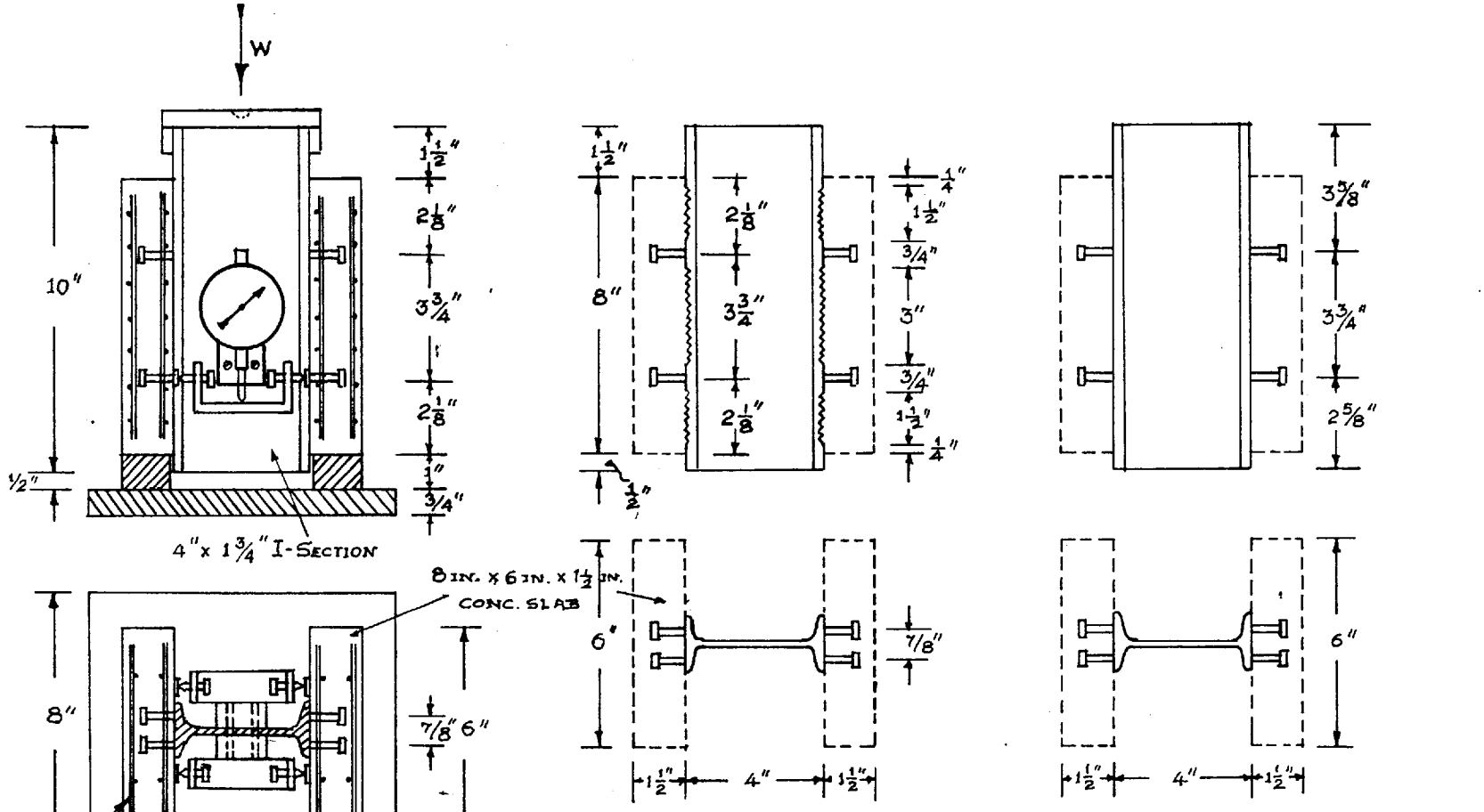
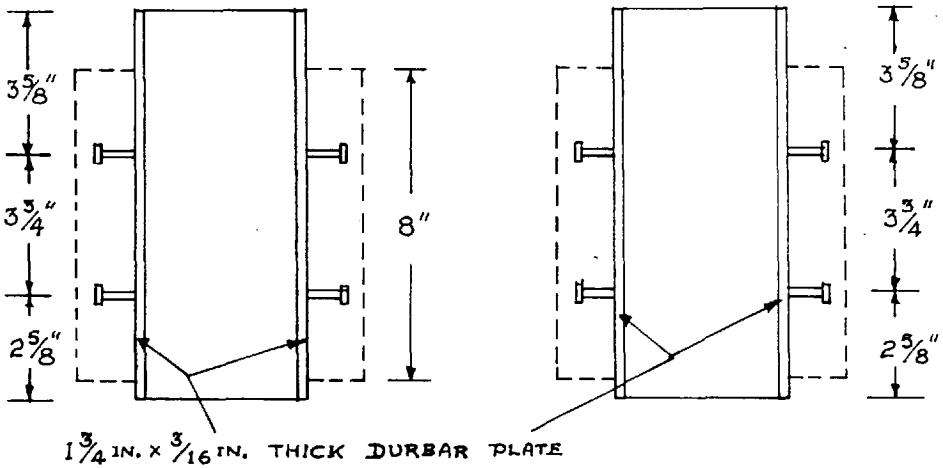
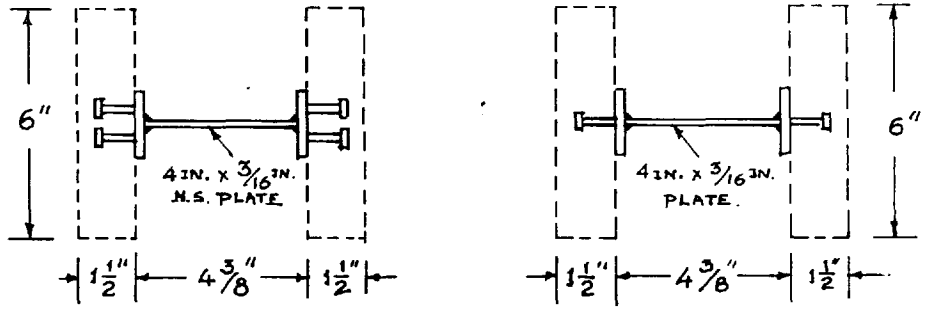


FIG. 16 DETAILS OF QUARTER SCALE PUSH-OUT SPECIMENS



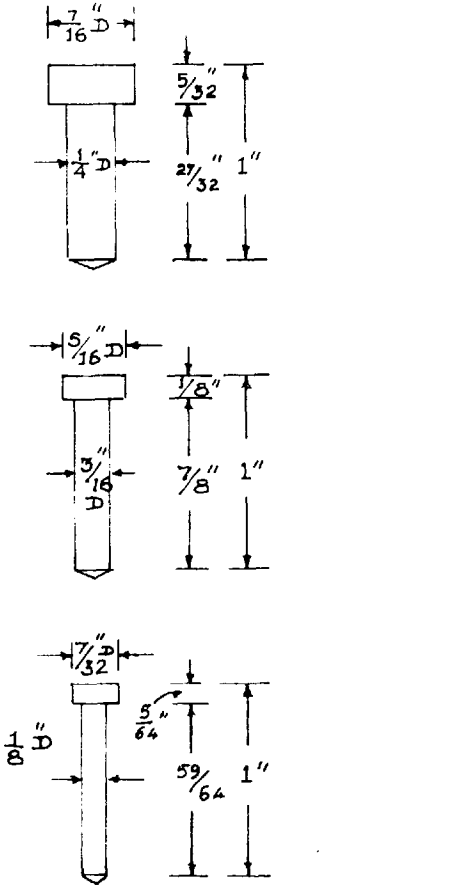


(d) SPECIMENS

P4E1 - 8-1/4 IN. DIA STUDS
P3E1 - 8-3/16 IN. DIA STUDS
P2E1 - 8-1/8 IN. DIA STUDS

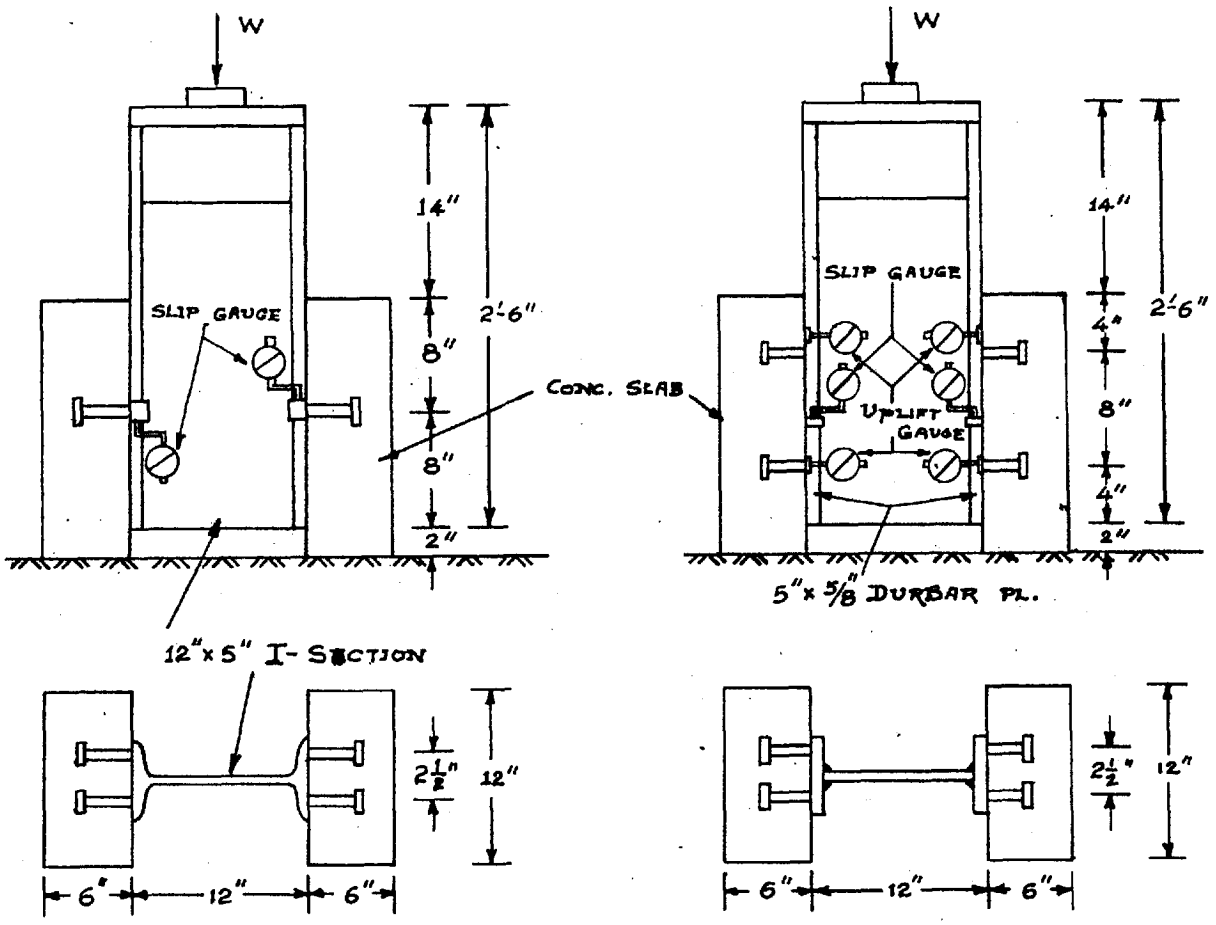
(e) SPECIMEN P2E2

4 - 1/8 IN. DIA. STUDS



(f) 1/4 IN., 3/16 IN. AND 1/8 IN. DIA. HEADED STUDS 1 IN. LONG.

FIG. 16 (CONTD) DETAILS OF QUARTER SCALE PUSH-OUT SPECIMENS



(a) SPECIMENS –

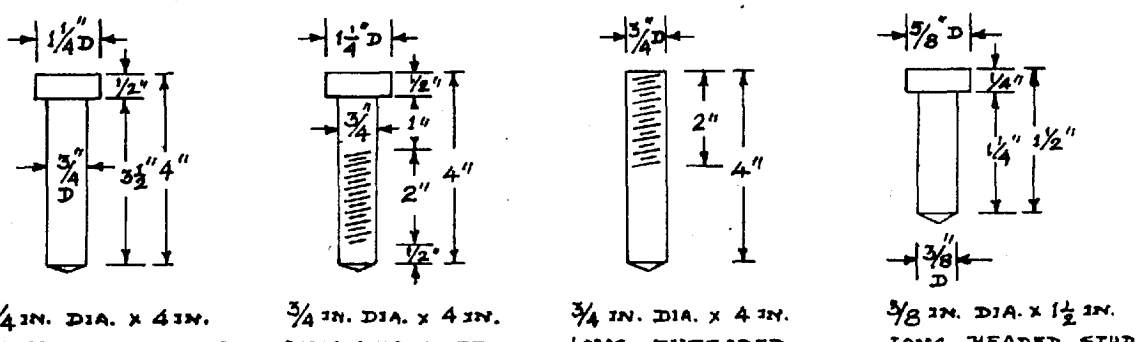
P6D1, P6D2 – ⅜" DIA. x 1½" LONG HEADED STUDS.

P12D(T) – ¾" DIA. x 4 IN. LONG THREADED STUDS WITHOUT HEAD

P12D(TH) – ¾" x 4" THREADED STUDS WITH HEAD.

(b) SPECIMEN P12E1

¾ IN. DIA. x 3 IN. LONG HEADED STUDS



¾ IN. DIA. x 4 IN. LONG HEADED STUD

¾ IN. DIA. x 4 IN. LONG THREADED STUD WITH HEAD

¾ IN. DIA. x 4 IN. LONG THREADED STUD WITHOUT HEAD.

⅝ IN. DIA. x 1½ IN. LONG HEADED STUD.

FIG. 17 FULL SCALE PUSH-OUT SPECIMENS

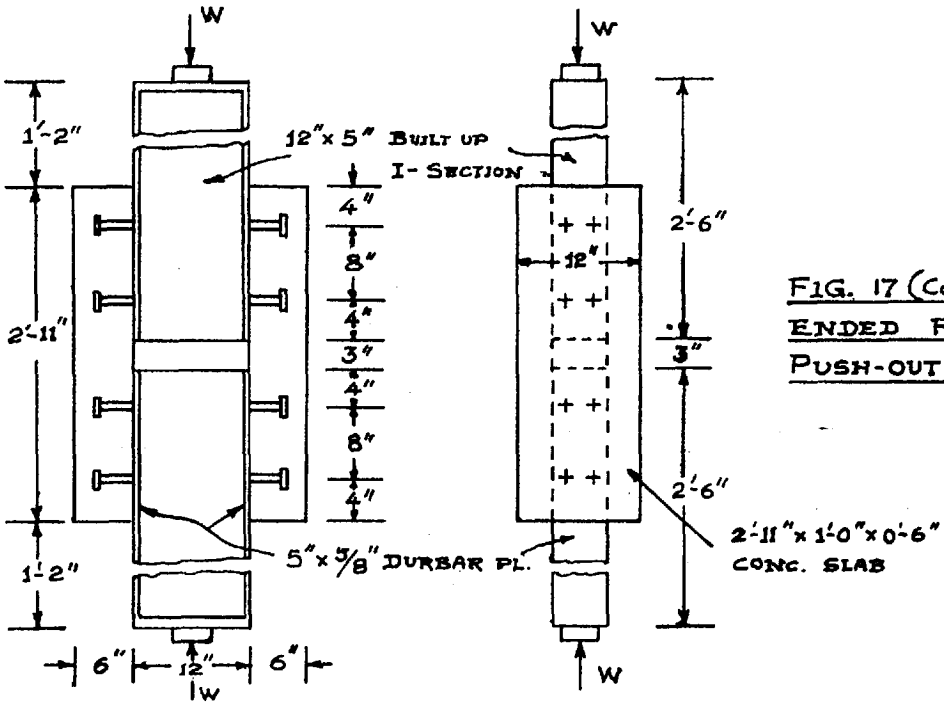


FIG. 17 (CONTD) DOUBLE-ENDED FULL SCALE PUSH-OUT SPECIMEN

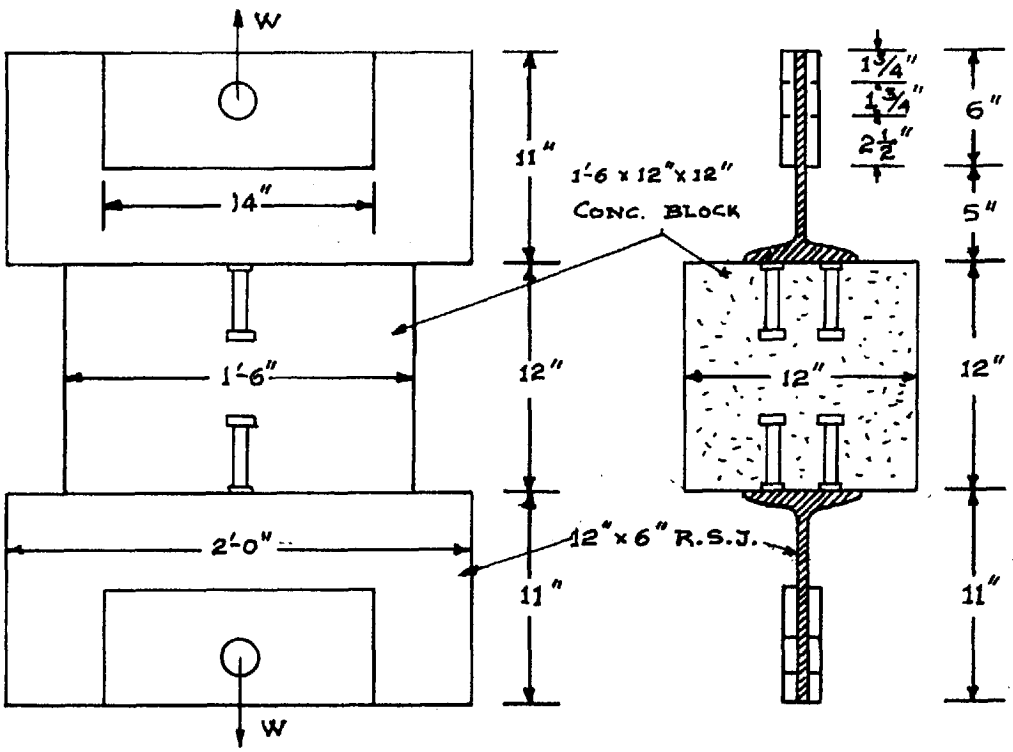
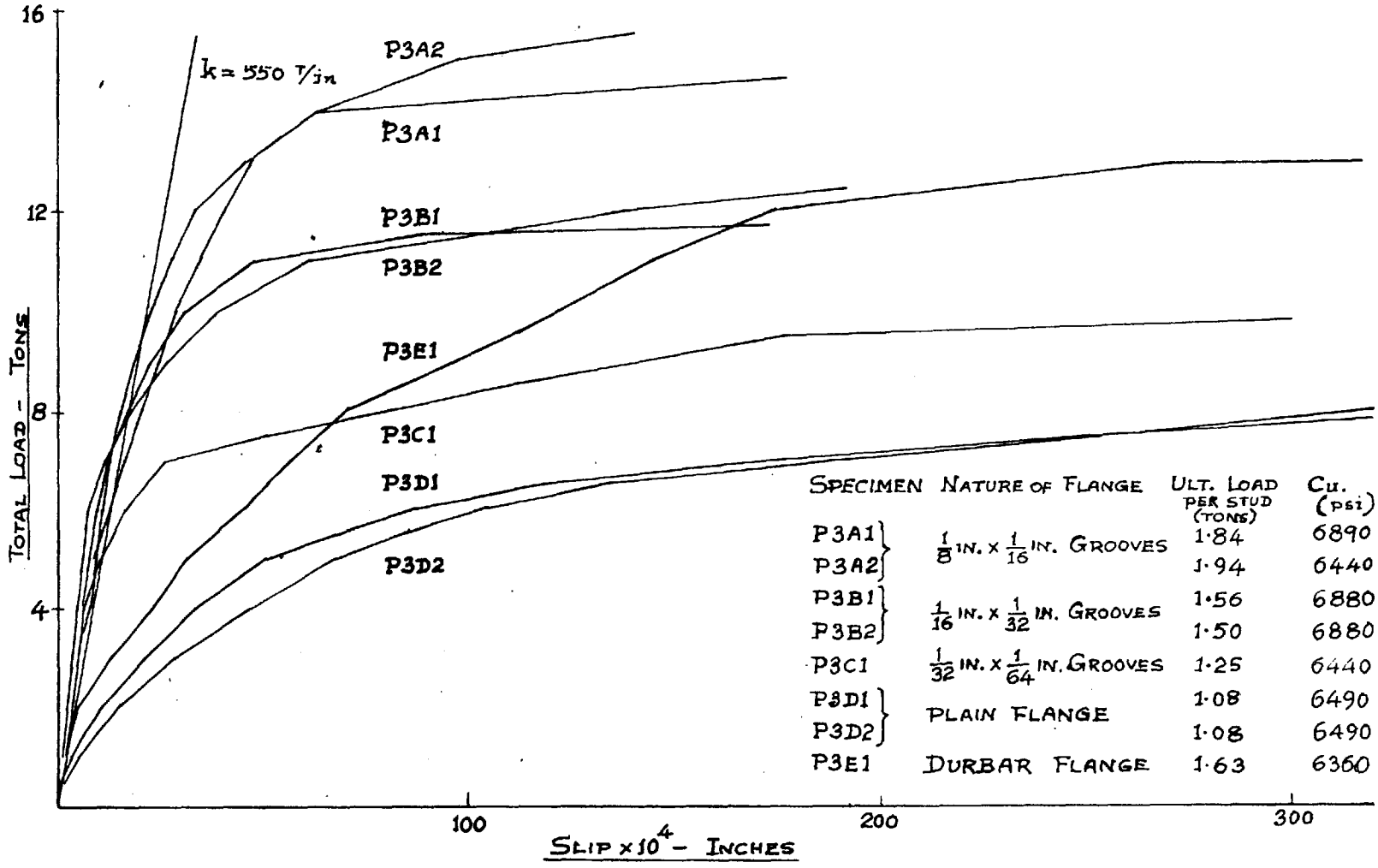


FIG. 18 PULL OUT SPECIMEN



SPECIMEN	NATURE OF FLANGE	ULT. LOAD PER STUD (TONS)	Cu. (psi)
P3A1	$\frac{1}{8}$ IN. x $\frac{1}{16}$ IN. GROOVES	1·84	6890
P3A2		1·94	6440
P3B1	$\frac{1}{16}$ IN. x $\frac{1}{32}$ IN. GROOVES	1·56	6880
P3B2		1·50	6880
P3C1	$\frac{1}{32}$ IN. x $\frac{1}{64}$ IN. GROOVES	1·25	6440
P3D1	PLAIN FLANGE	1·08	6490
P3D2		1·08	6490
P3E1	DURBAR FLANGE	1·63	6360

FIG. 19 TOTAL SLIPS - PUSH-OUT SPECIMENS WITH 8 - $\frac{3}{16}$ IN. DIA. 1 IN. LONG H-STUDS AND VARYING FLANGE ROUGHNESS

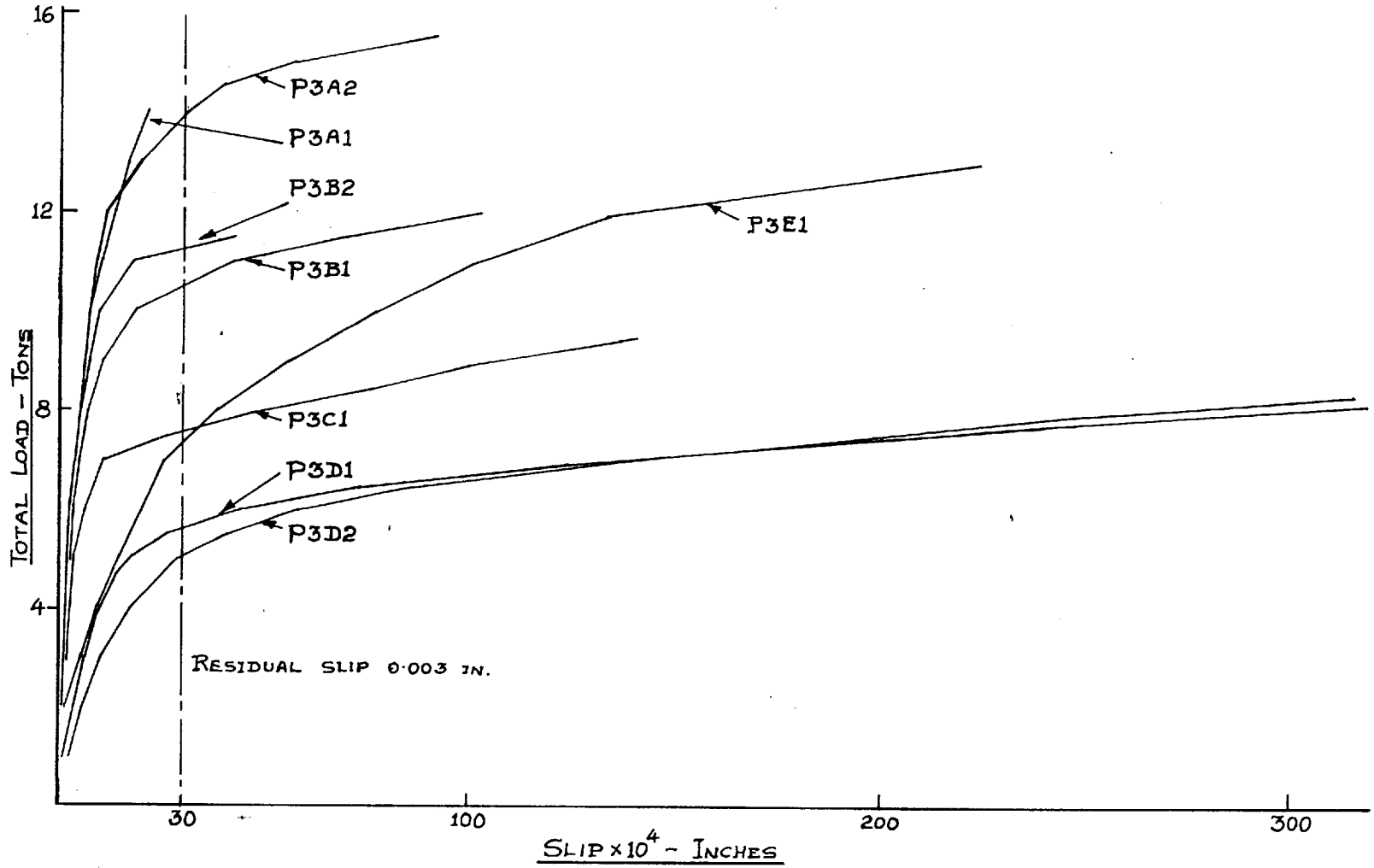
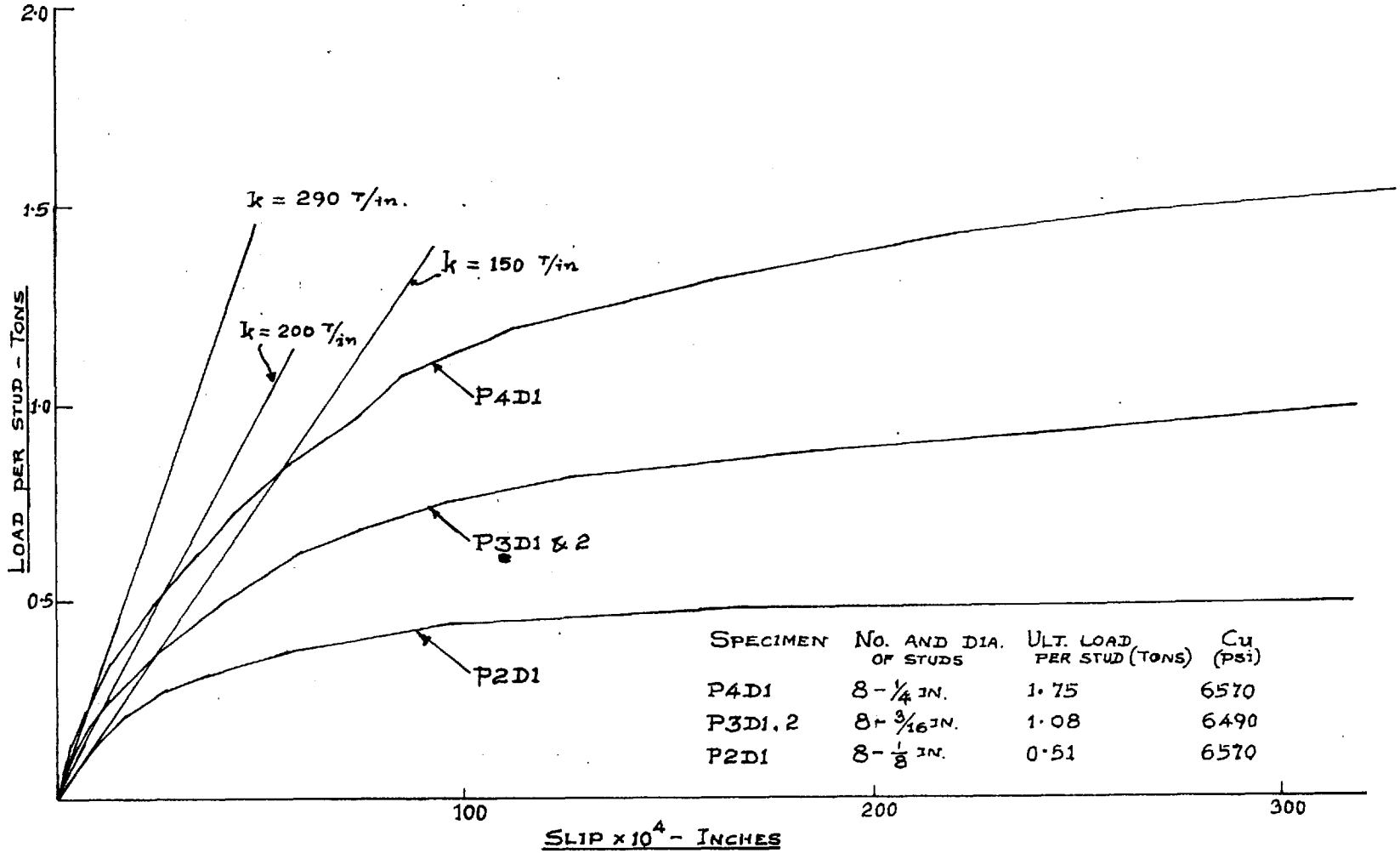
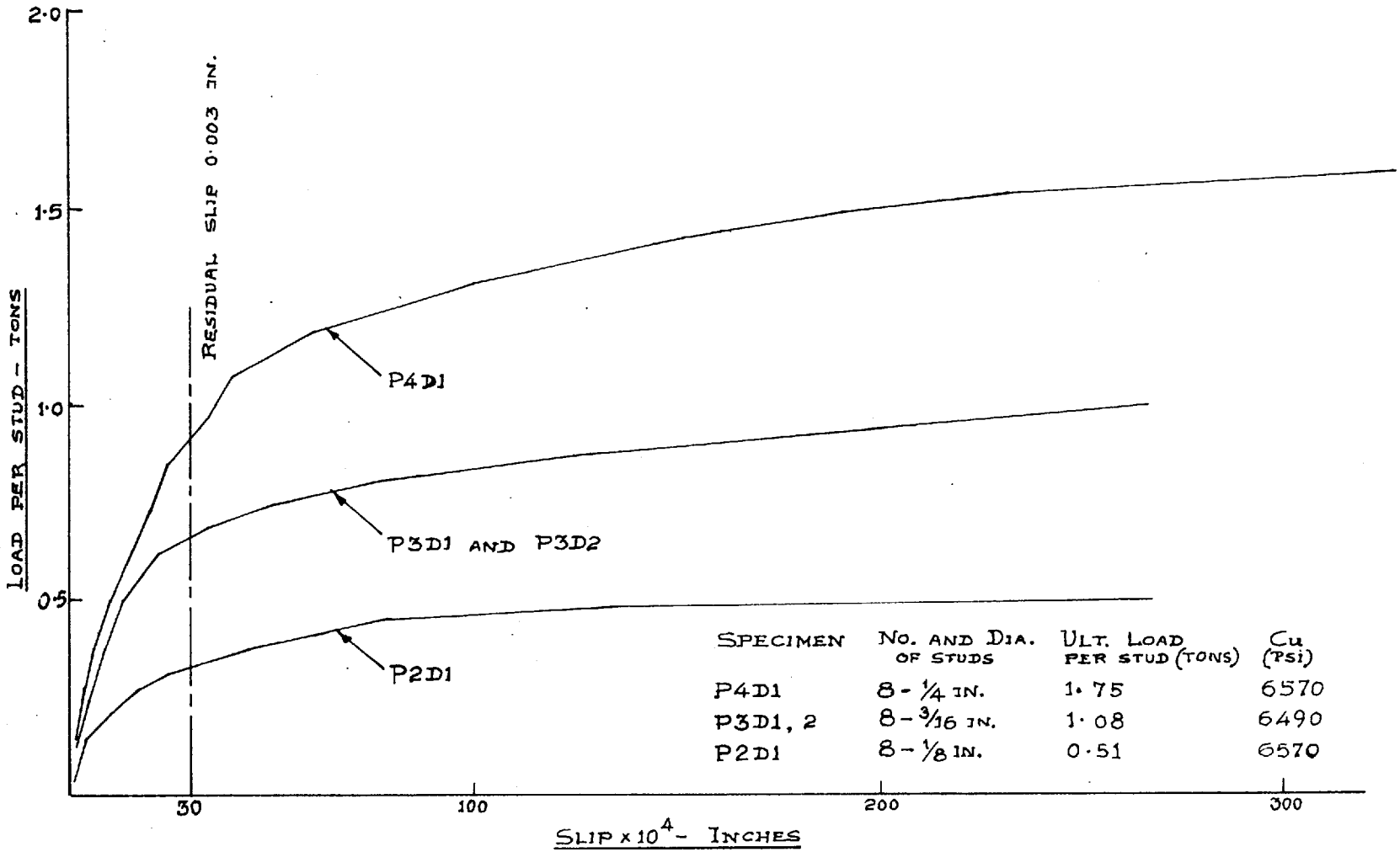


FIG. 20 RESIDUAL SLIPS - PUSH-OUT SPECIMENS WITH 8-3/16 IN. DIA. 1 IN. LONG H-STUDS AND VARYING FLANGE ROUGHNESS



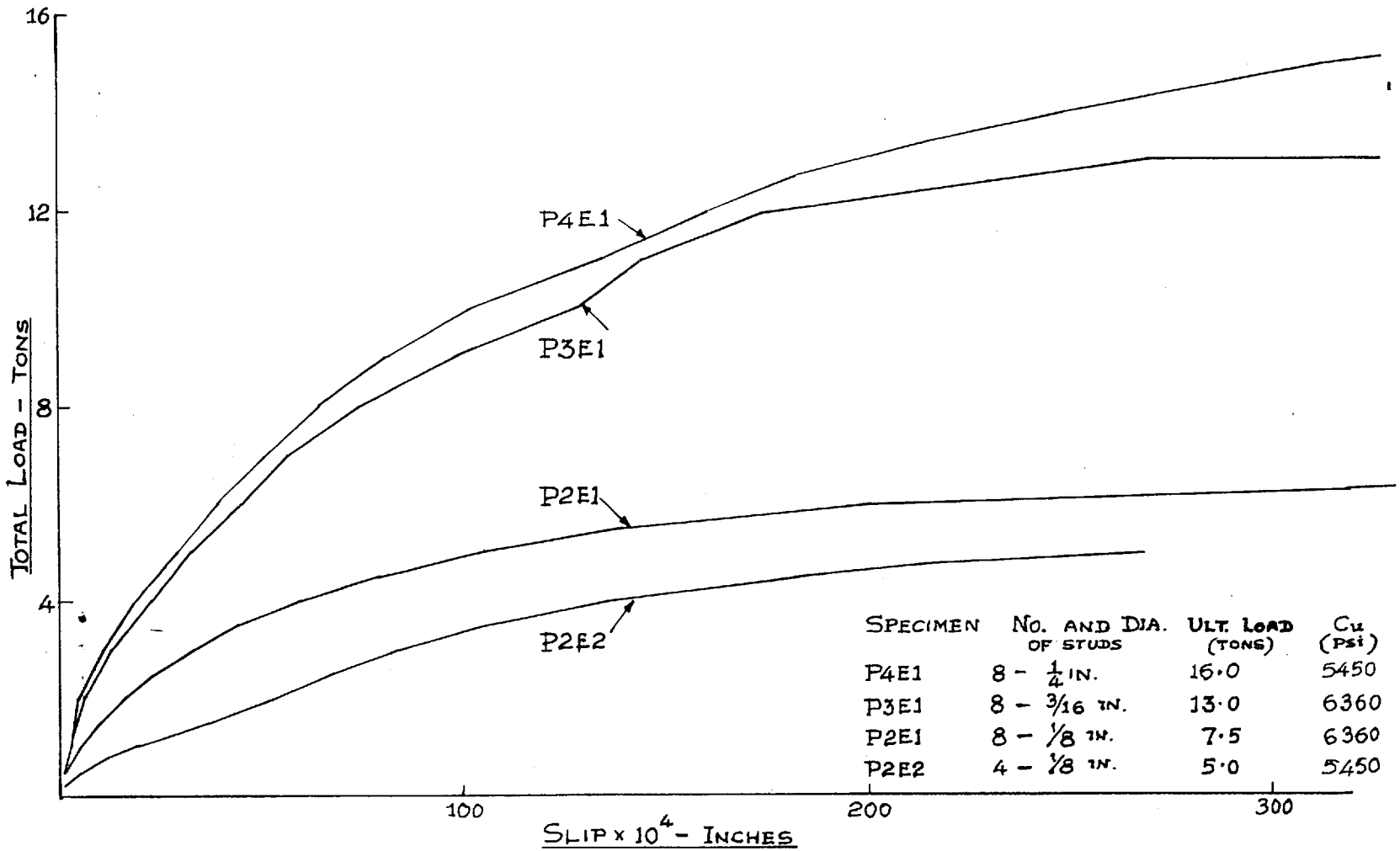
SPECIMEN	NO. AND DIA. OF STUDS	ULT. LOAD PER STUD (TONS)	Cu (psi)
P4D1	8 - 1/4 IN.	1·75	6570
P3D1, 2	8 - 3/16 IN.	1·08	6490
P2D1	8 - 1/8 IN.	0·51	6570

FIG. 21 TOTAL SLIPS - PUSH-OUT SPECIMENS WITH 1/4 IN., 3/16 IN. AND 1/8 IN. DIA. HEADED STUDS 1 IN. LONG



SPECIMEN	NO. AND DIA. OF STUDS	ULT. LOAD PER STUD (TONS)	Cu (PSI)
P4D1	8 – ¼ IN.	1·75	6570
P3D1, 2	8 – 3/16 IN.	1·08	6490
P2D1	8 – ⅛ IN.	0·51	6570

FIG. 22 RESIDUAL SLIPS – PUSH-OUT SPECIMENS WITH ¼ IN., 3/16 IN. AND ⅛ IN. DIA. HEADED STUDS 1 IN. LONG



SPECIMEN	NO. AND DIA. OF STUDS	ULT. LOAD (TONS)	Cu (Psi)
P4E1	8 - 1/4 IN.	16·0	5450
P3E1	8 - 3/16 IN.	13·0	6360
P2E1	8 - 1/8 IN.	7·5	6360
P2E2	4 - 1/8 IN.	5·0	5450

FIG. 23 TOTAL SLIPS - DURBAR FLANGED PUSH-OUT SPECIMENS WITH VARYING TOTAL CROSS-SECTIONAL AREA OF STUDS

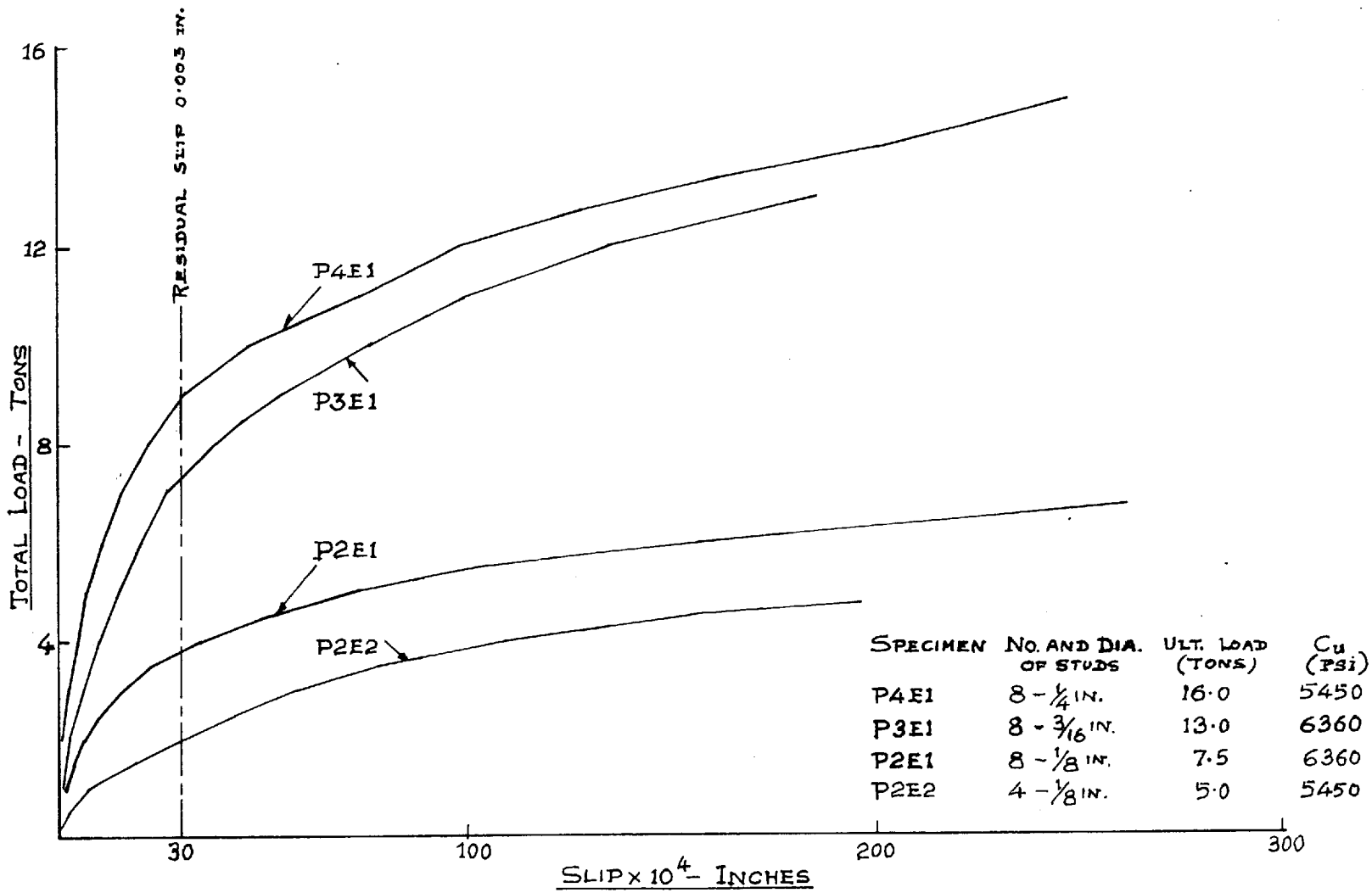


FIG. 24 RESIDUAL SLIPS - DURBAR FLANGED PUSH-OUT SPECIMENS WITH VARYING TOTAL CROSS-SECTIONAL AREA OF STUDS.

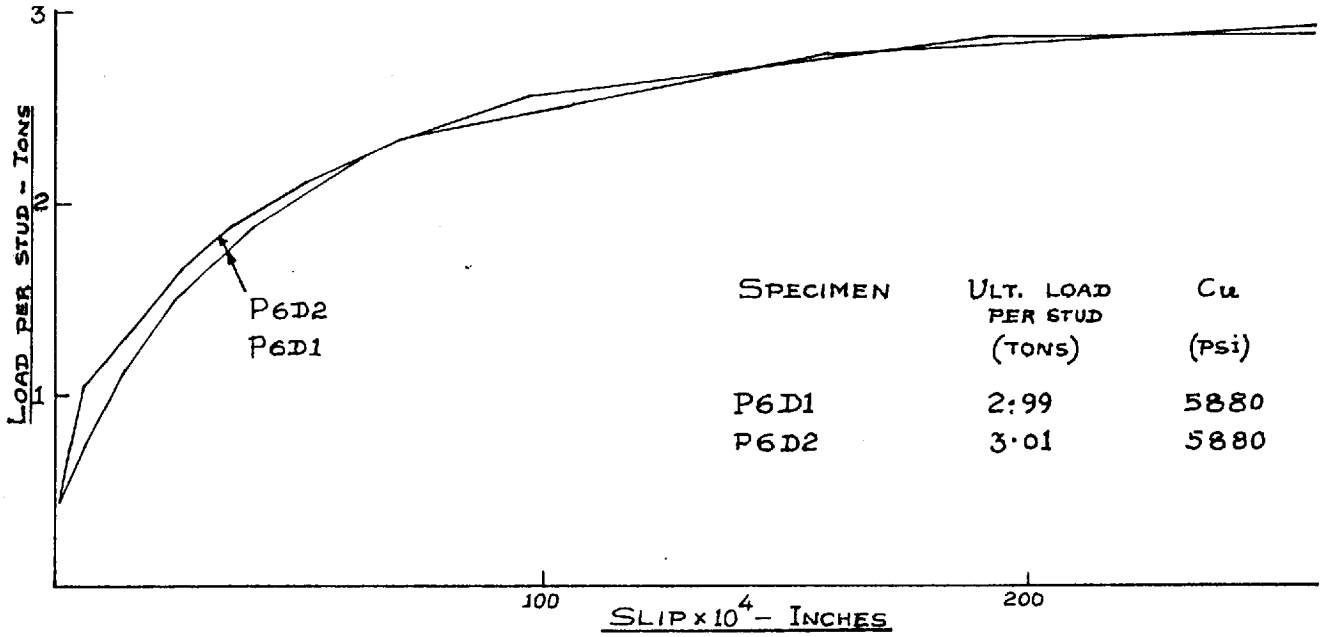


FIG. 25 TOTAL SLIPS - PUSH-OUT SPECIMENS WITH 3/8 IN. DIA. HEADED STUDS 1½ IN. LONG

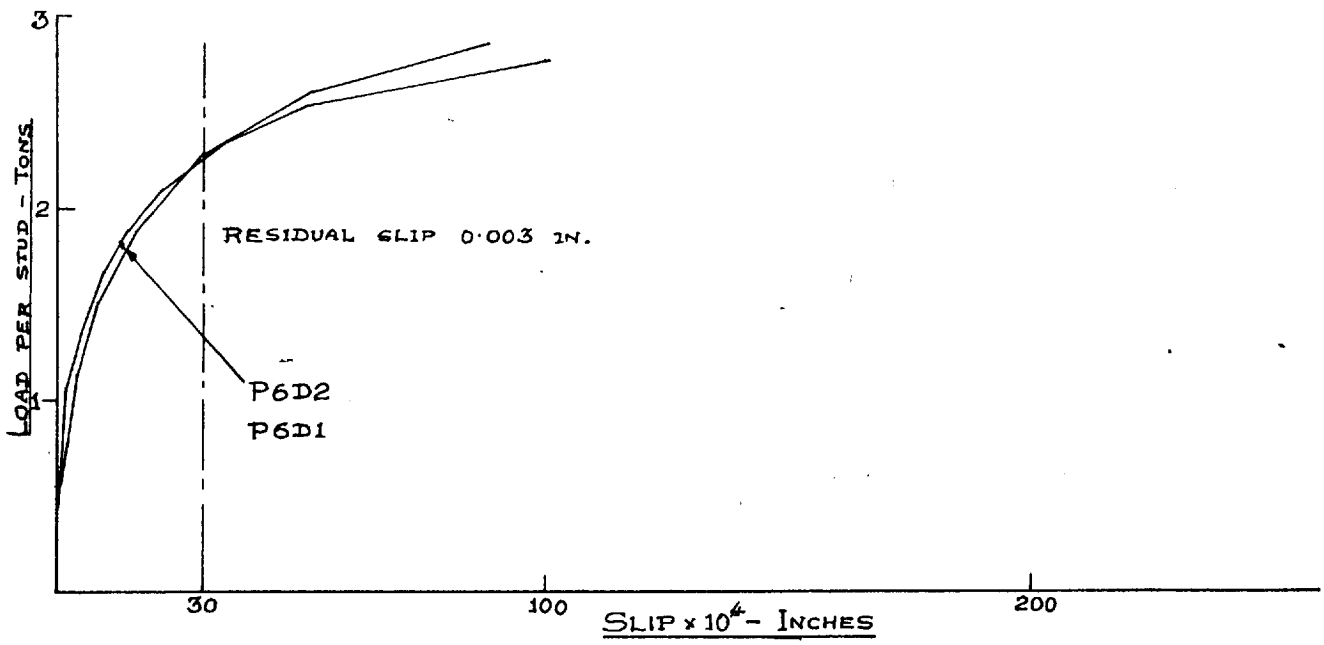
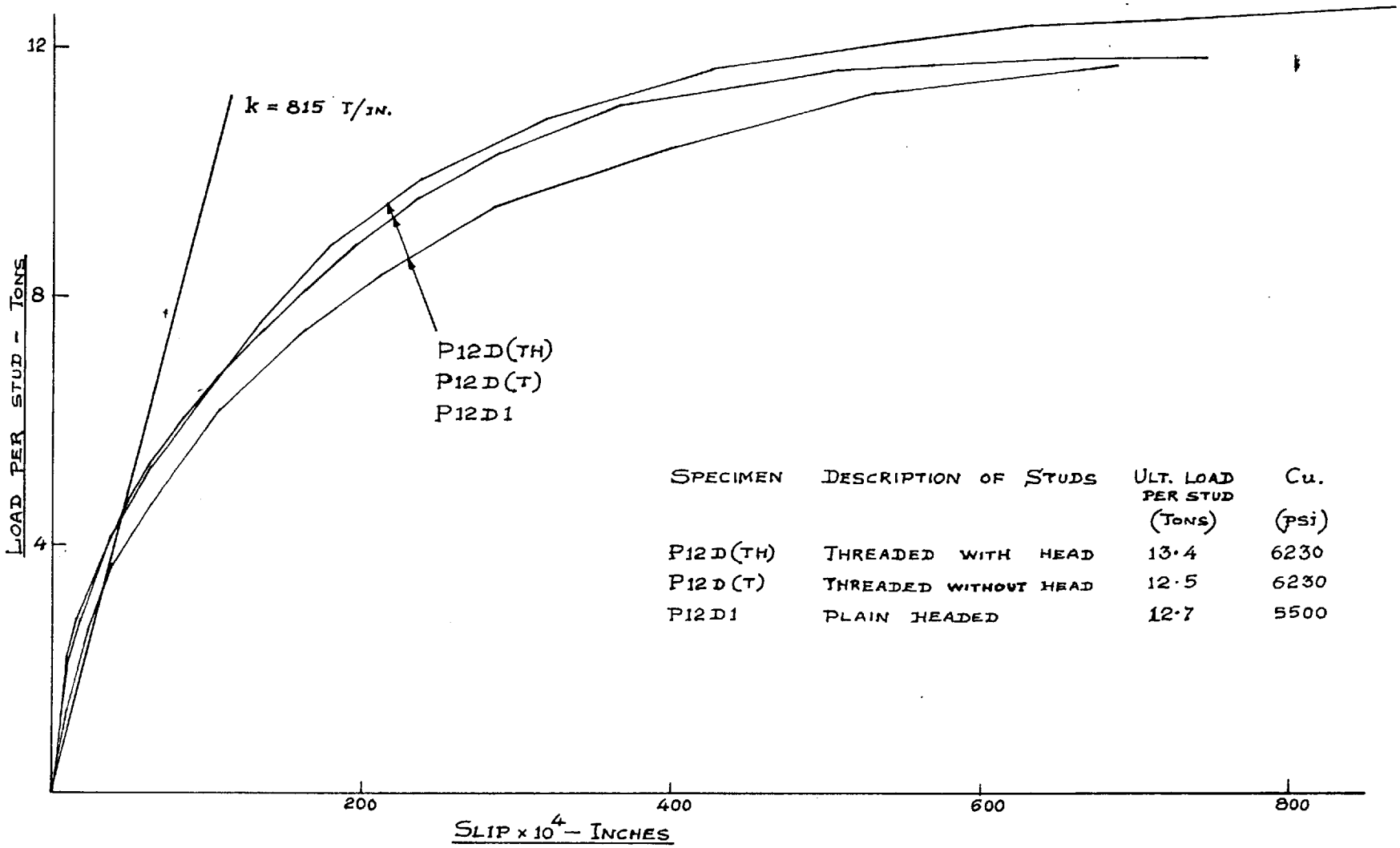
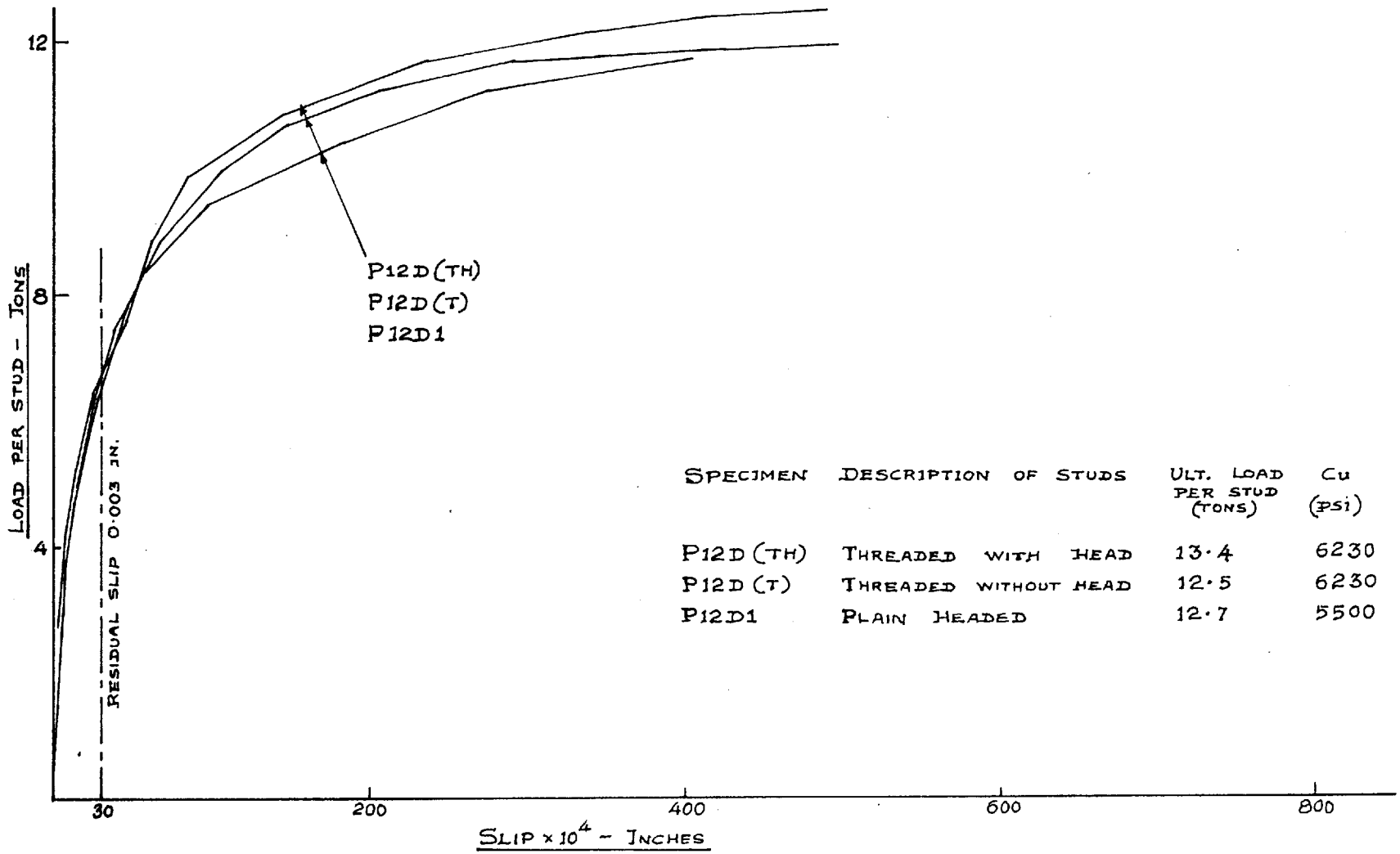


FIG. 26 RESIDUAL SLIPS - PUSH-OUT SPECIMENS WITH 3/8 IN. DIA. HEADED STUDS 1½ IN. LONG



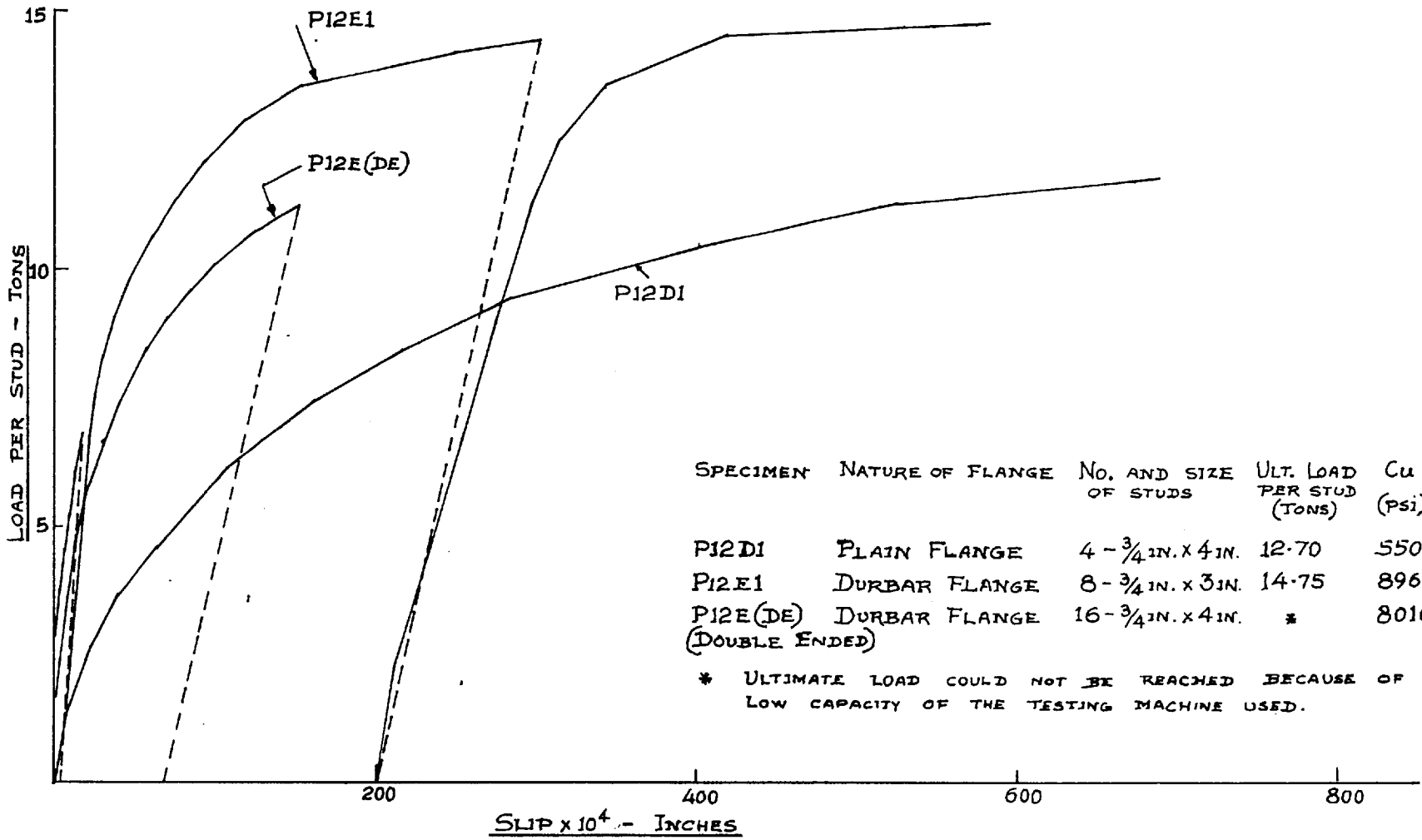
SPECIMEN	DESCRIPTION OF STUDS	ULT. LOAD PER STUD (TONS)	Cu. (psi)
P12D(TH)	THREADED WITH HEAD	13·4	6230
P12D(T)	THREADED WITHOUT HEAD	12·5	6230
P12D1	PLAIN HEADED	12·7	5500

FIG. 27 TOTAL SLIPS - PUSH OUT SPECIMENS WITH 3/4 IN. DIA. STUDS 4 IN. LONG.



SPECIMEN	DESCRIPTION OF STUDS	ULT. LOAD PER STUD (TONS)	Cu (psi)
P12D (TH)	THREADED WITH HEAD	13·4	6230
P12D (T)	THREADED WITHOUT HEAD	12·5	6230
P12D1	PLAIN HEADED	12·7	5500

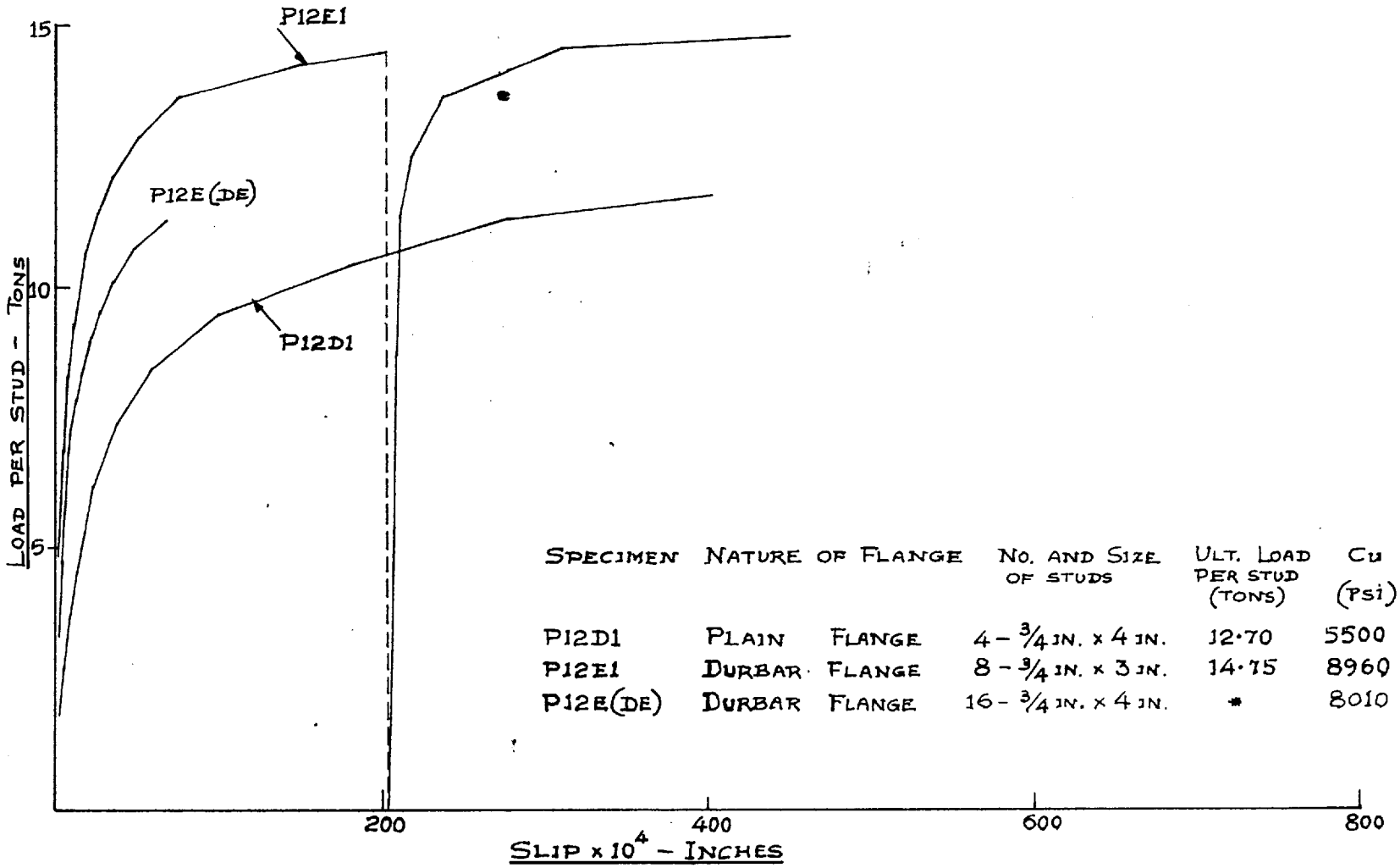
FIG. 28 RESIDUAL SLIPS – PUSH-OUT SPECIMENS WITH 3/4 IN. DIA. STUDS 4 IN. LONG



SPECIMEN	NATURE OF FLANGE	NO. AND SIZE OF STUDS	ULT. LOAD PER STUD (TONS)	Cu (psi)
P12D1	PLAIN FLANGE	4 - 3/4 IN. x 4 IN.	12·70	5500
P12E1	DURBAR FLANGE	8 - 3/4 IN. x 3 IN.	14·75	8960
P12E(DE) (DOUBLE ENDED)	DURBAR FLANGE	16 - 3/4 IN. x 4 IN.	*	8010

* ULTIMATE LOAD COULD NOT BE REACHED BECAUSE OF LOW CAPACITY OF THE TESTING MACHINE USED.

FIG. 29 TOTAL SLIPS - DURBAR FLANGED PUSH-OUT SPECIMENS WITH 3/4 IN. DIA. HEADED STUDS



SPECIMEN	NATURE OF FLANGE	NO. AND SIZE OF STUDS	ULT. LOAD PER STUD (TONS)	Cu (psi)
P12D1	PLAIN FLANGE	4 – 3/4 IN. x 4 IN.	12·70	5500
P12E1	DURBAR FLANGE	8 – 3/4 IN. x 3 IN.	14·75	8960
P12E(DE)	DURBAR FLANGE	16 – 3/4 IN. x 4 IN.	*	8010

FIG. 30 RESIDUAL SLIPS – DURBAR FLANGED PUSH-OUT SPECIMENS WITH 3/4 IN. DIA. HEADED STUDS

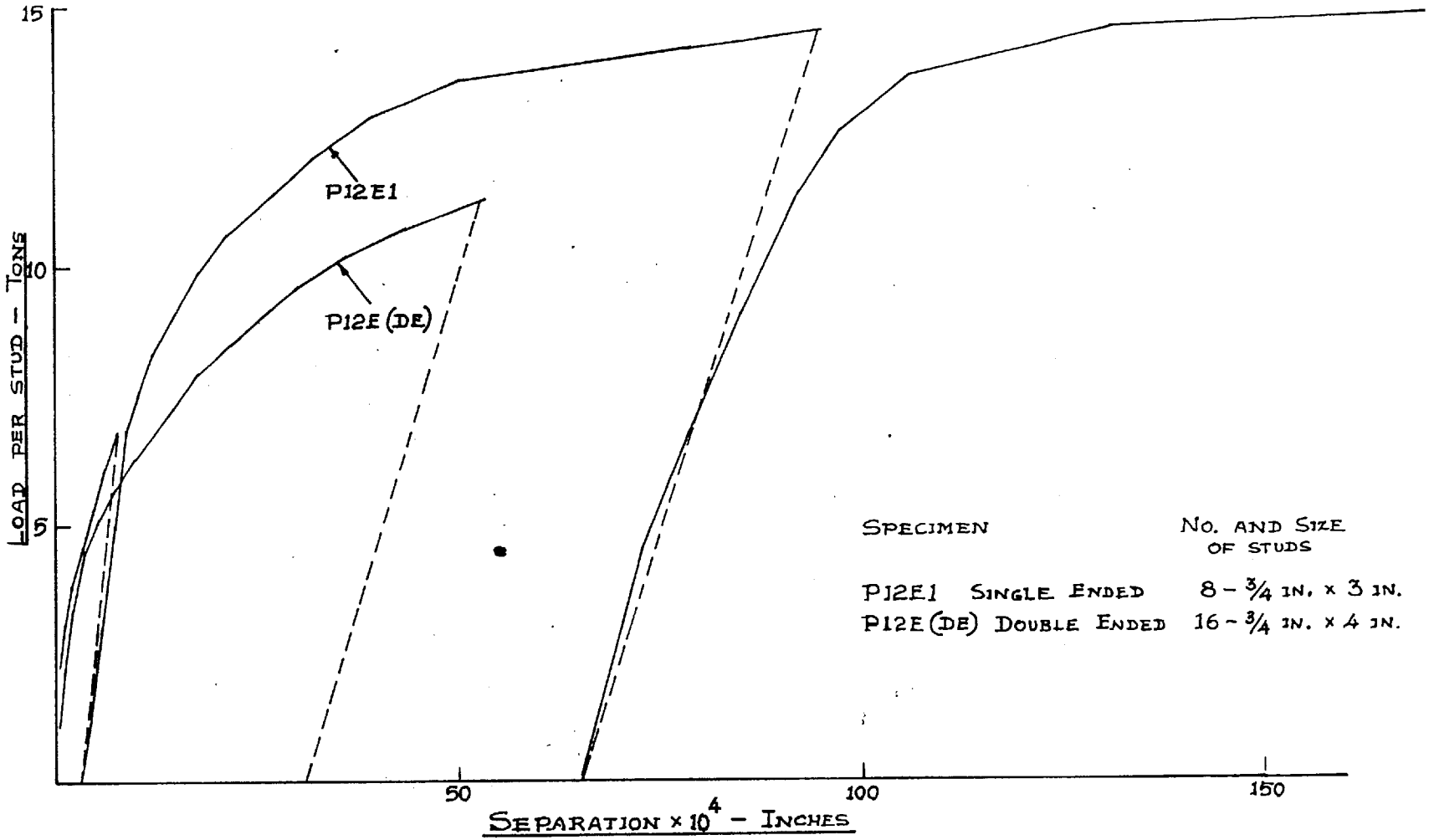


FIG. 31 TOTAL SEPARATIONS – DURBAR FLANGED PUSH-OUT SPECIMENS WITH 3/4 IN. DIA. HEADED STUDS

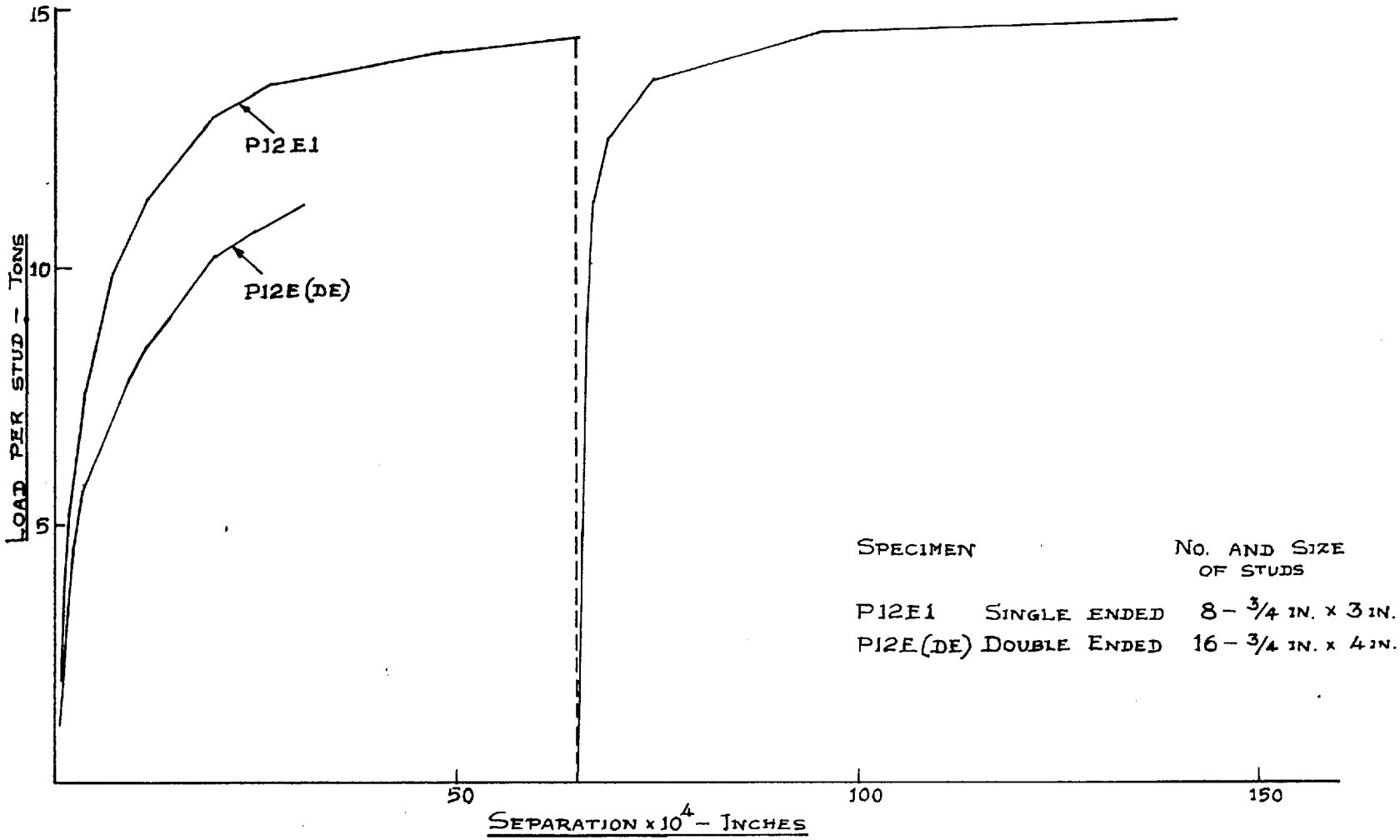


FIG. 32 RESIDUAL SEPARATIONS – DURBAR FLANGED PUSH-OUT SPECIMENS WITH 3/4 IN. DIA. HEADED STUDS

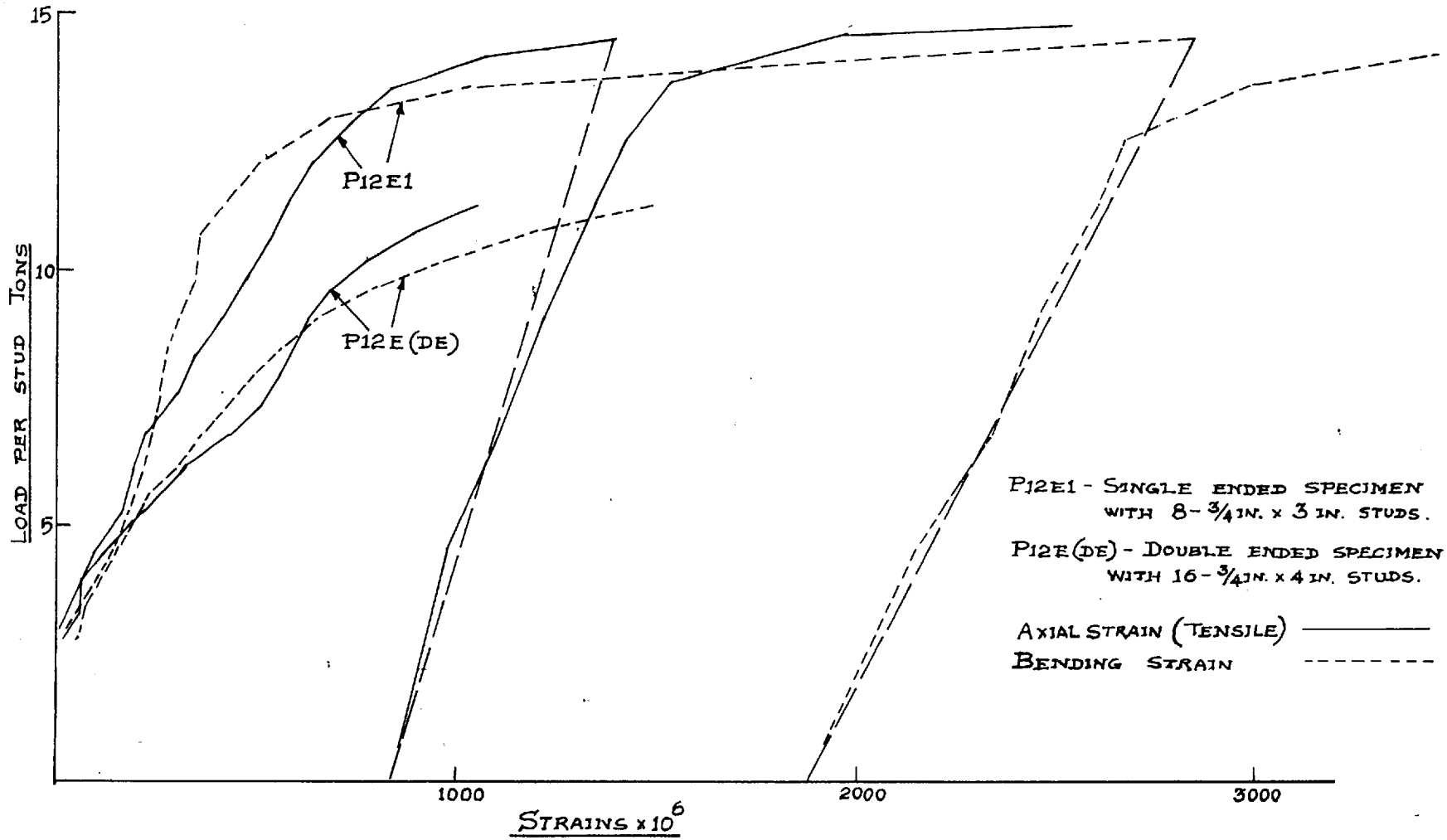


FIG 33 STUD STRAINS - DURBAR FLANGED PUSH-OUT SPECIMENS WITH 3/4 IN. DIA. HEADED STUDS

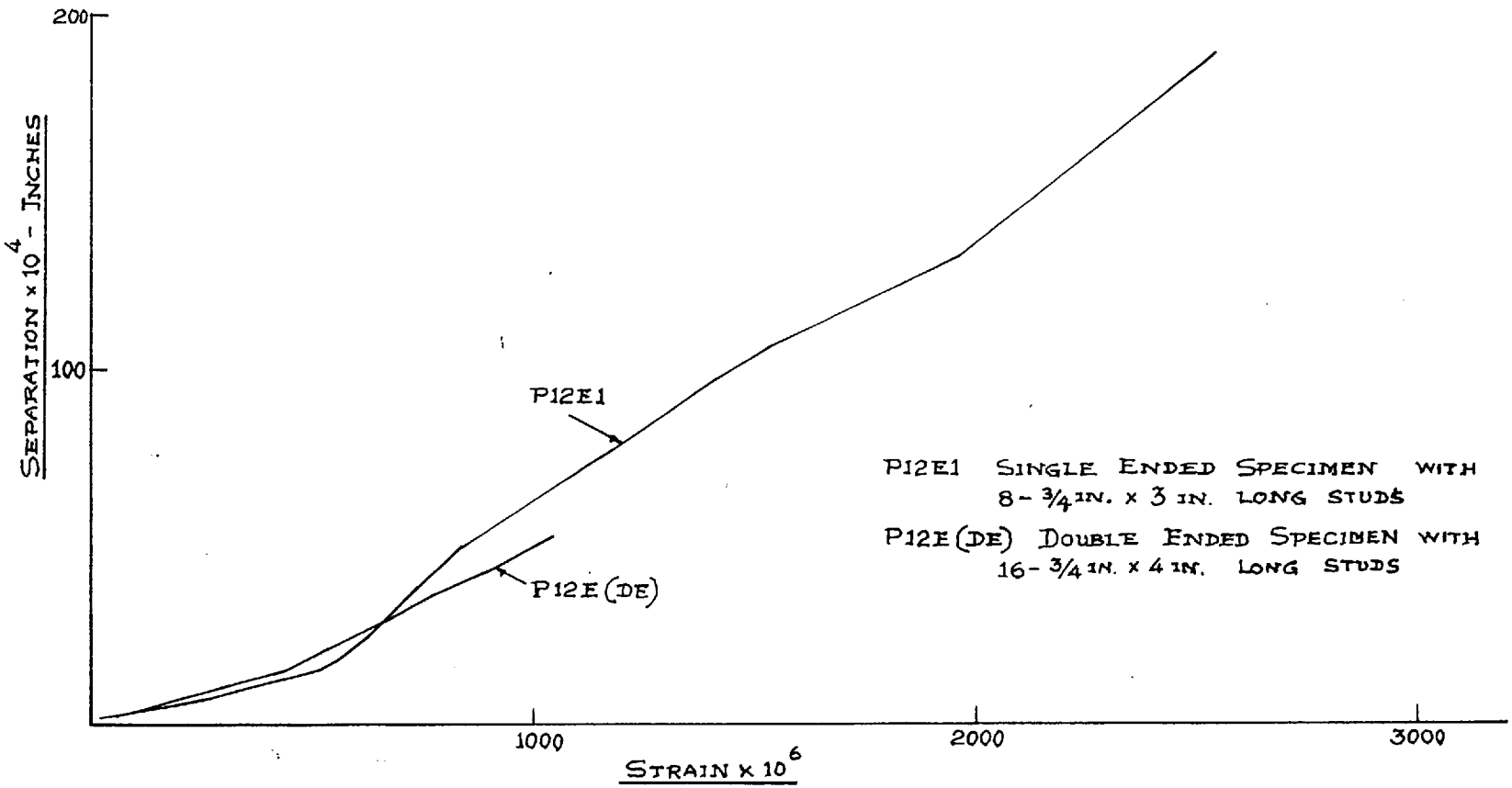


FIG. 34 SEPARATION - AXIAL STRAINS - DURBAR FLANGED PUSH-OUT SPECIMENS WITH 3/4 IN. DIA. HEADED STUDS

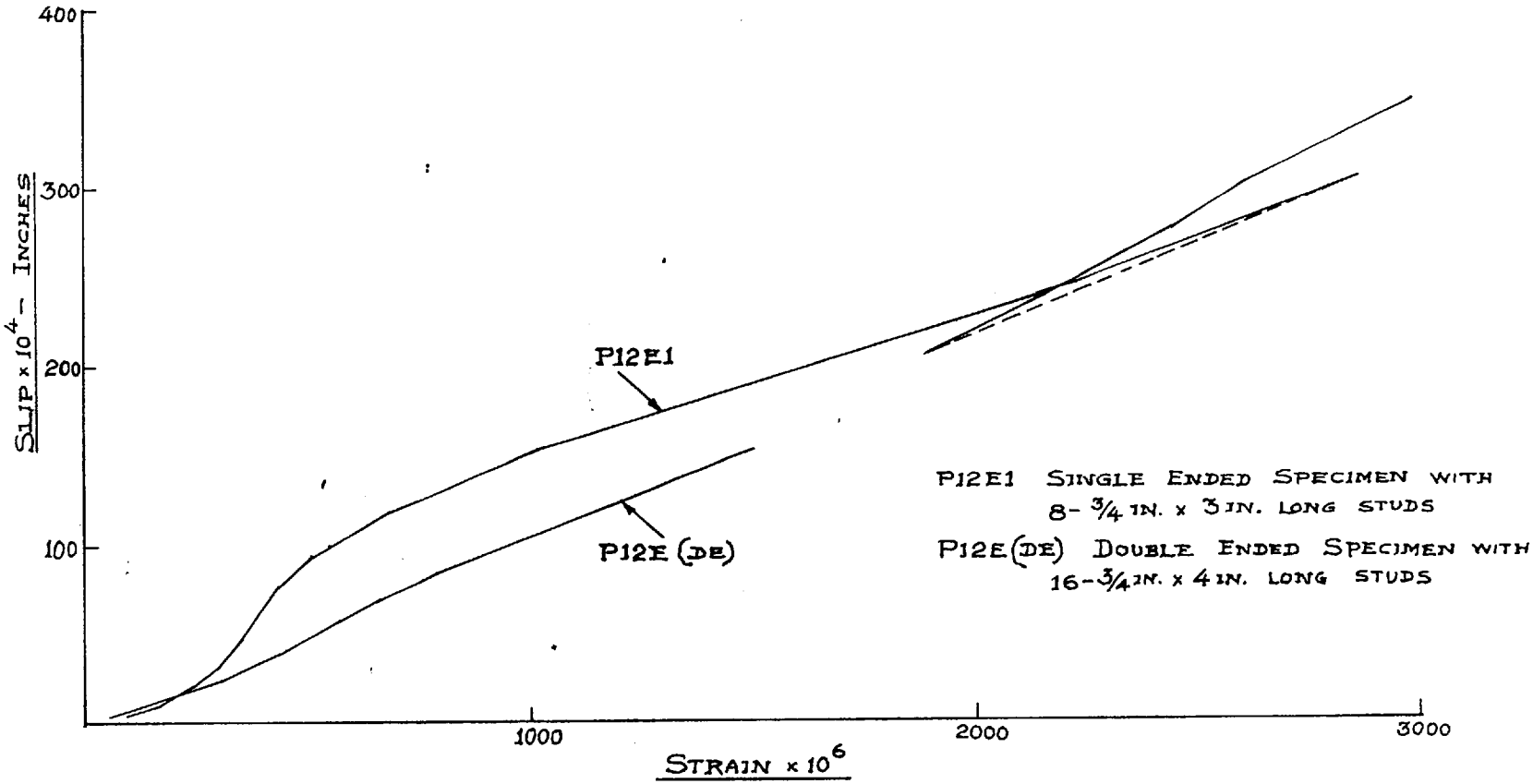


FIG. 35 SLIP - BENDING STRAINS - DURBAR FLANGED PUSH-OUT SPECIMENS WITH 3/4 IN. DIA. HEADED STUDS

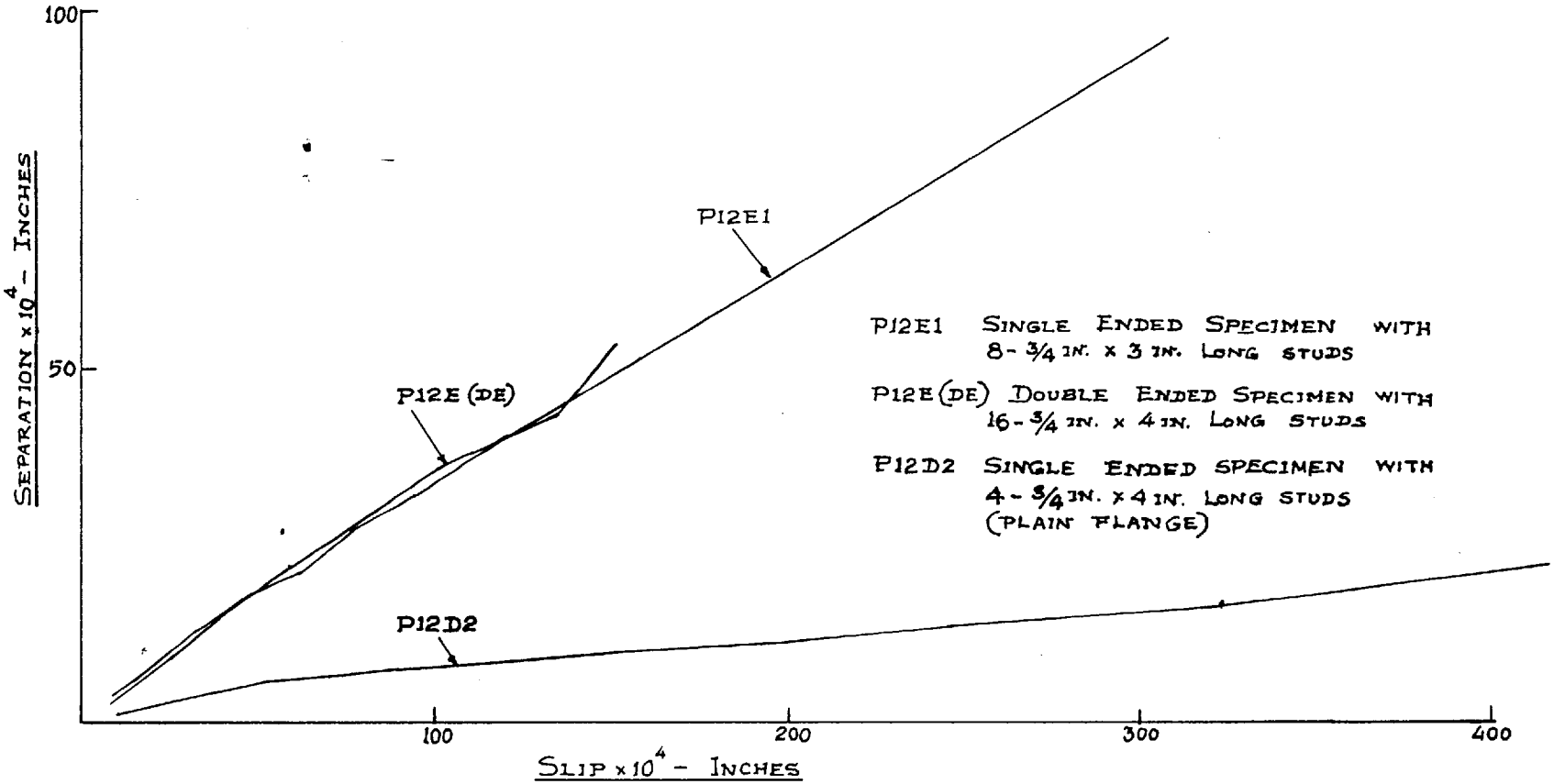


FIG. 36 SEPARATION - SLIPS - DURBAR FLANGED PUSH-OUT SPECIMENS WITH 3/4 IN. DIA. HEADED STUDS

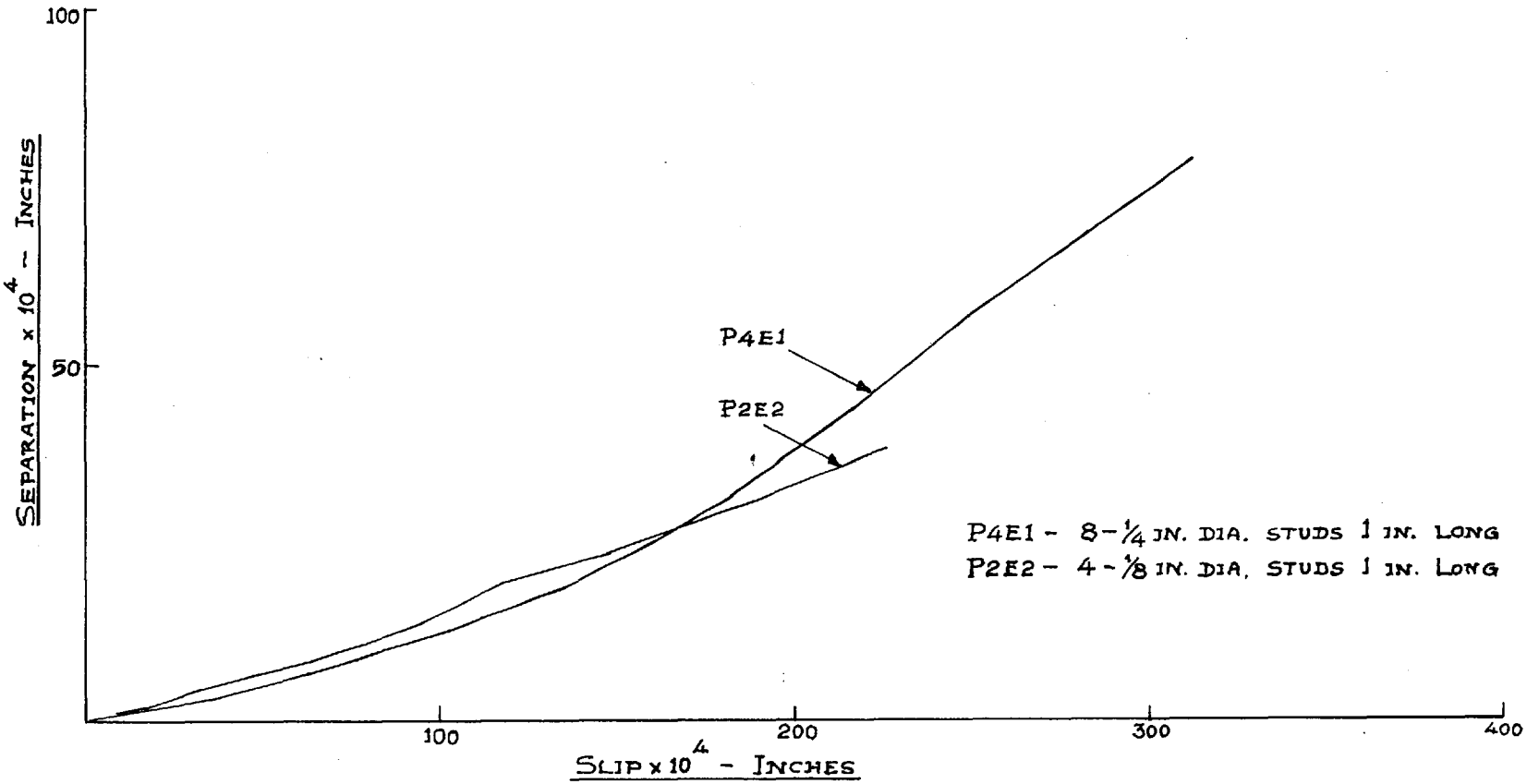


FIG. 37 SEPARATION - SLIPS - DURBAR FLANGED PUSH-OUT SPECIMENS WITH 1/4 IN. AND 1/8 IN. DIA. HEADED STUDS

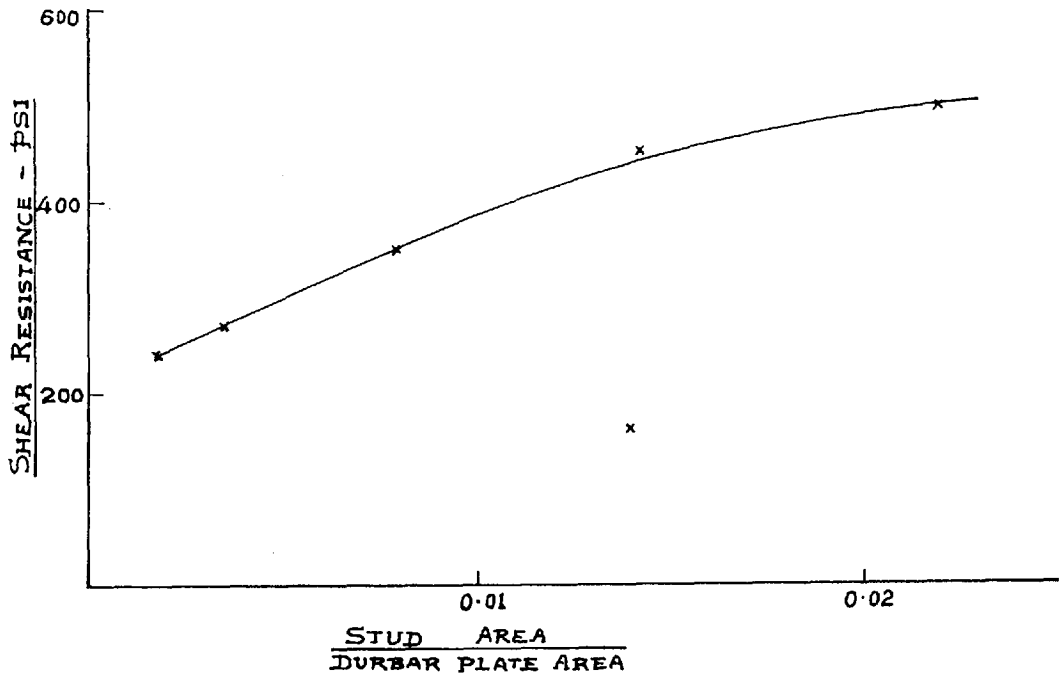


FIG. 39 SHEAR RESISTANCE OF DURBAR PLATE WITH VARYING CROSS-SECTIONAL AREA OF STUDS

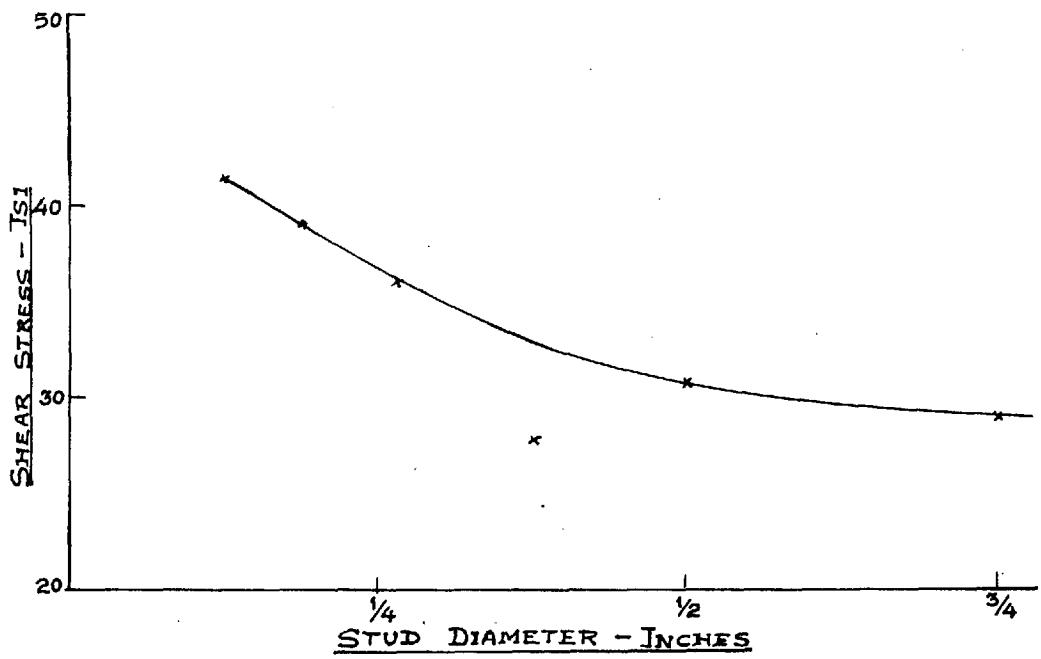


FIG. 38 SHEAR STRESS AT ULTIMATE LOAD IN PLAIN HEADED STUDS WITH VARYING STUD DIAMETER

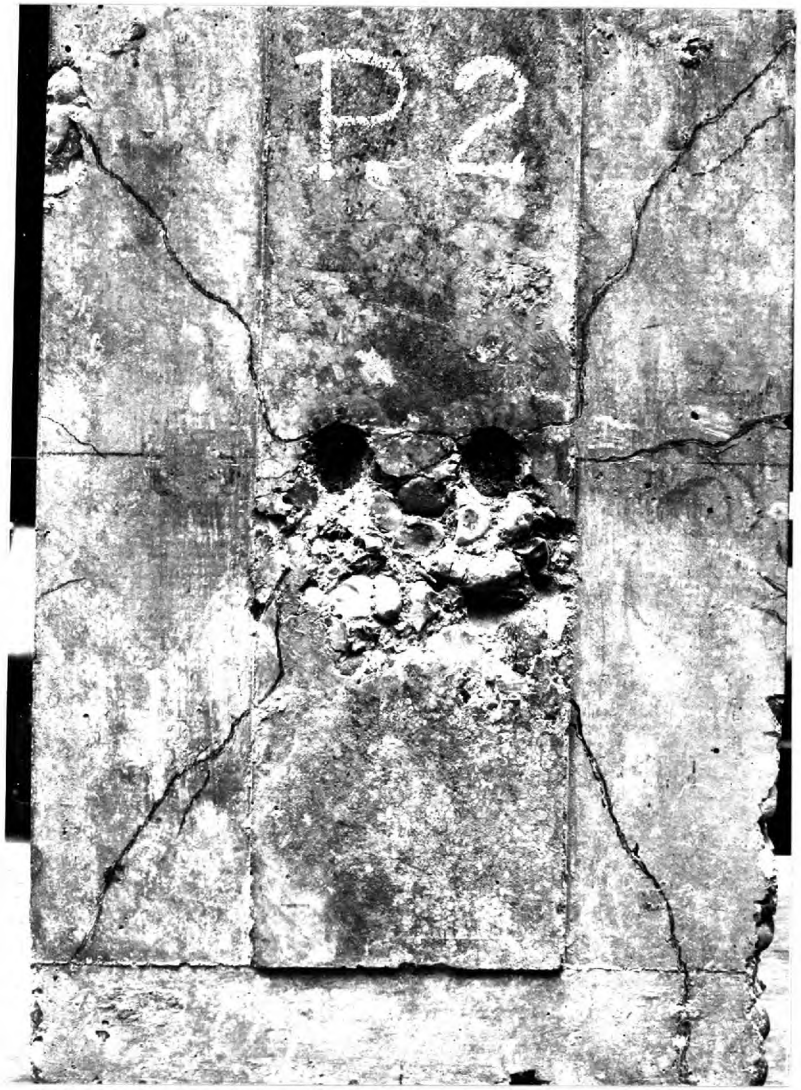


Figure 40. Concrete slab of a plain flanged full scale push-out specimen with $\frac{3}{4}$ in. dia. studs after failure



Figure 41. Concrete slab of a Durbar flanged full scale push-out specimen after failure (P12E1)

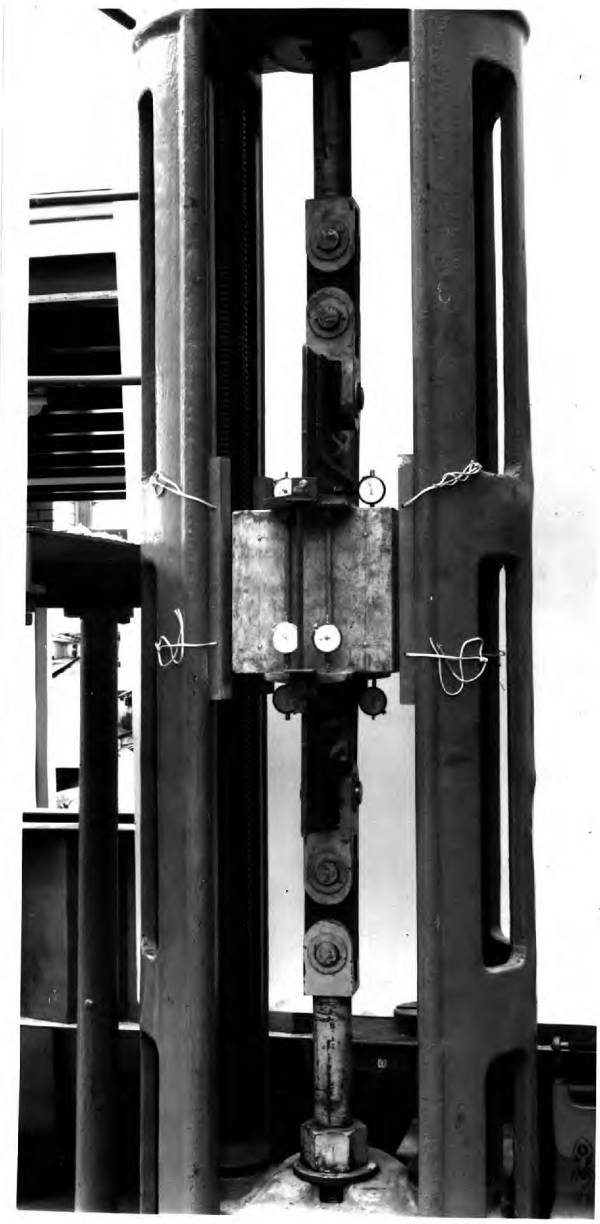
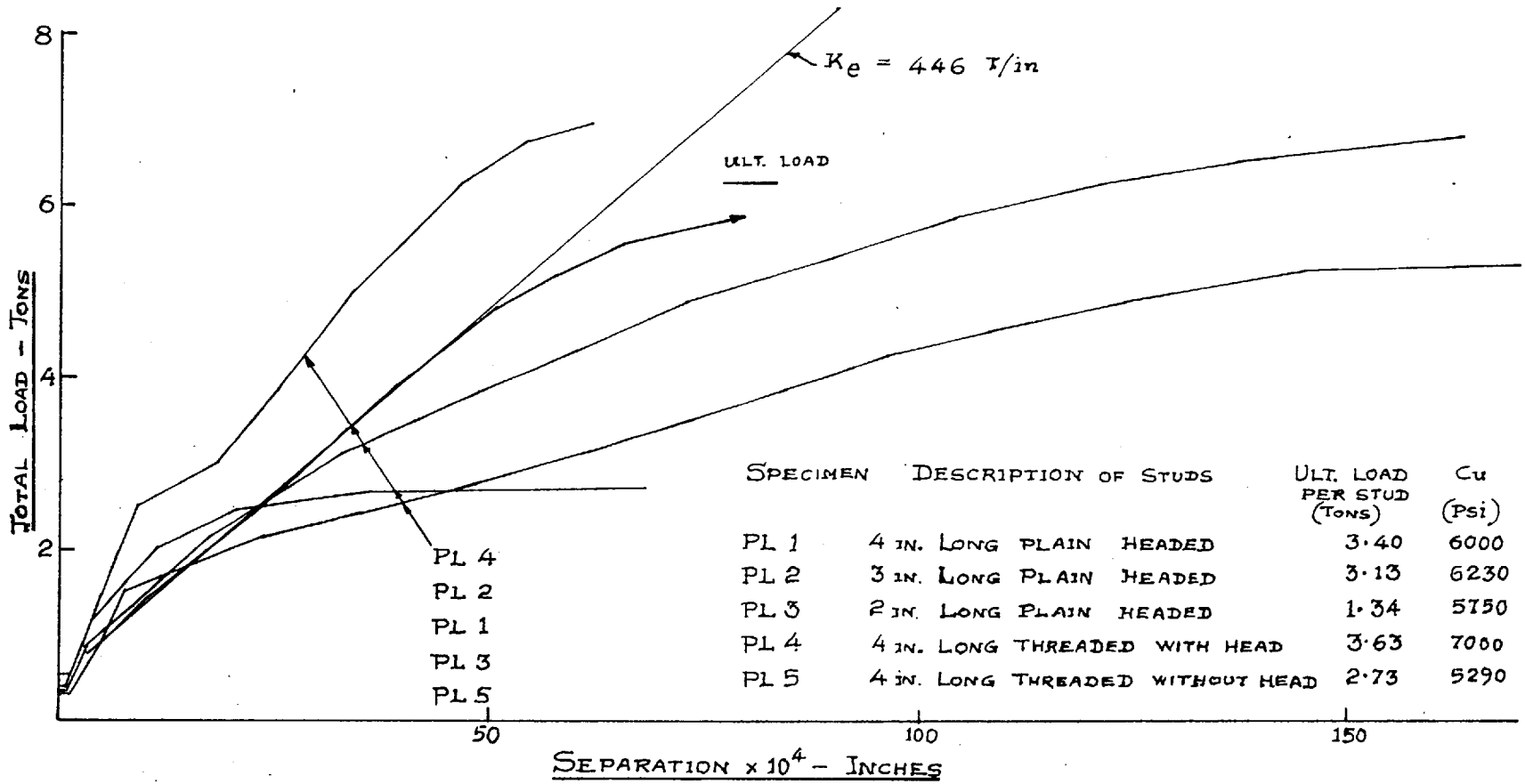
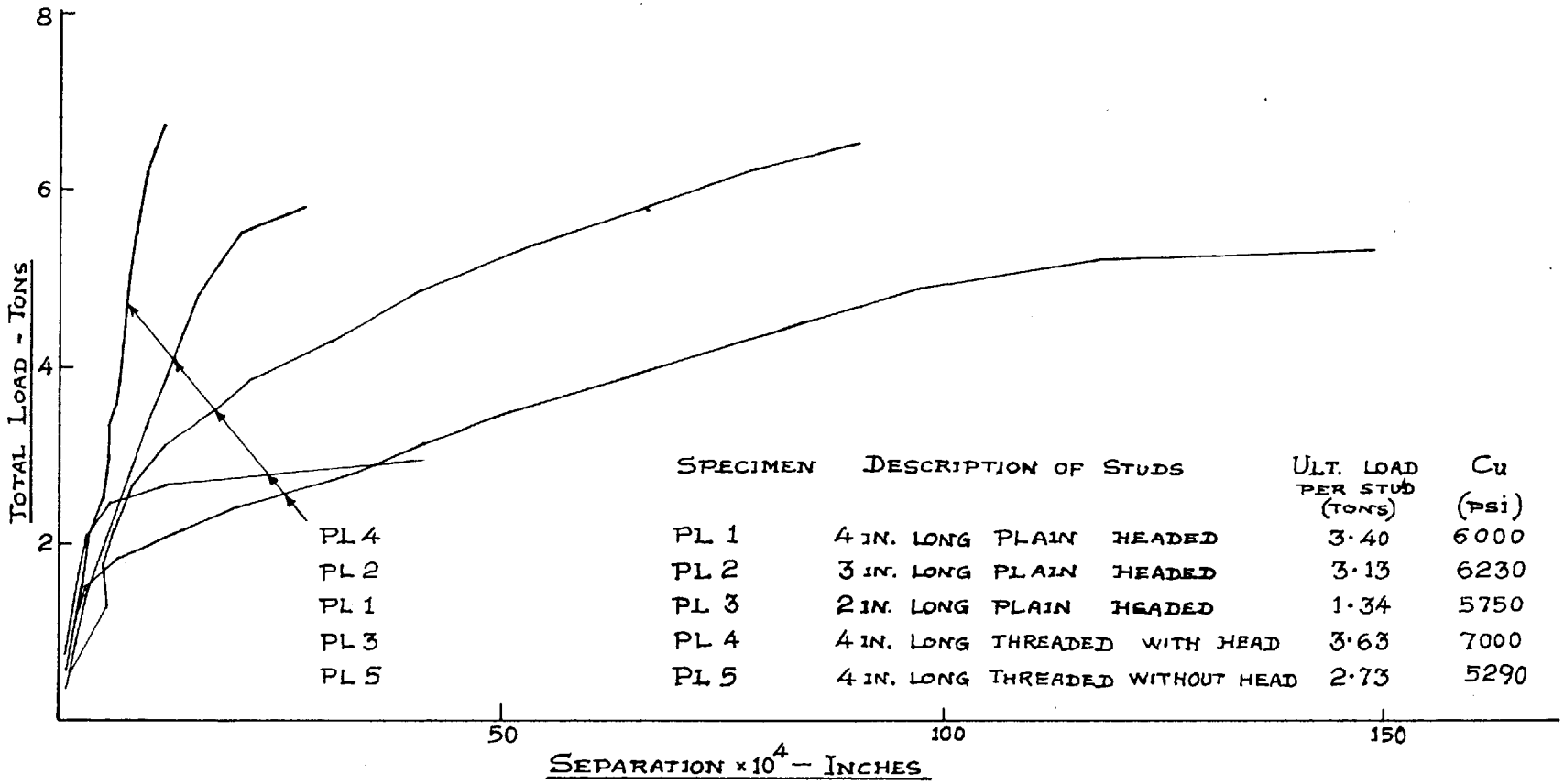


Figure 43. Set up for a pull-out test



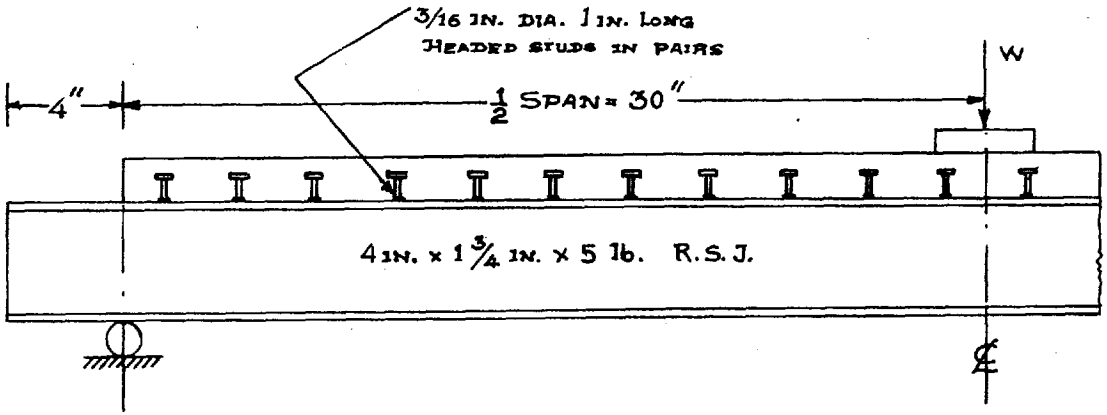
SPECIMEN	DESCRIPTION OF STUDS	ULT. LOAD PER STUD (TONS)	Cu (Psi)
PL 1	4 IN. LONG PLAIN HEADED	3·40	6000
PL 2	3 IN. LONG PLAIN HEADED	3·13	6230
PL 3	2 IN. LONG PLAIN HEADED	1·34	5750
PL 4	4 IN. LONG THREADED WITH HEAD	3·63	7000
PL 5	4 IN. LONG THREADED WITHOUT HEAD	2·73	5290

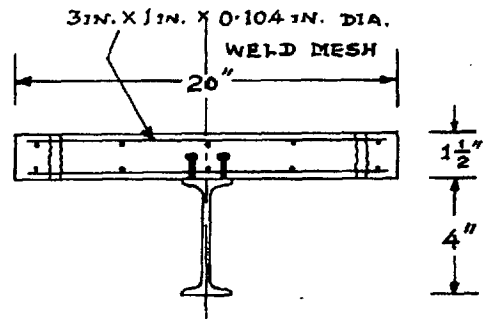
FIG. 44 TOTAL SEPARATIONS – PULL-OUT SPECIMENS WITH 3/4 IN. DIA. STUDS

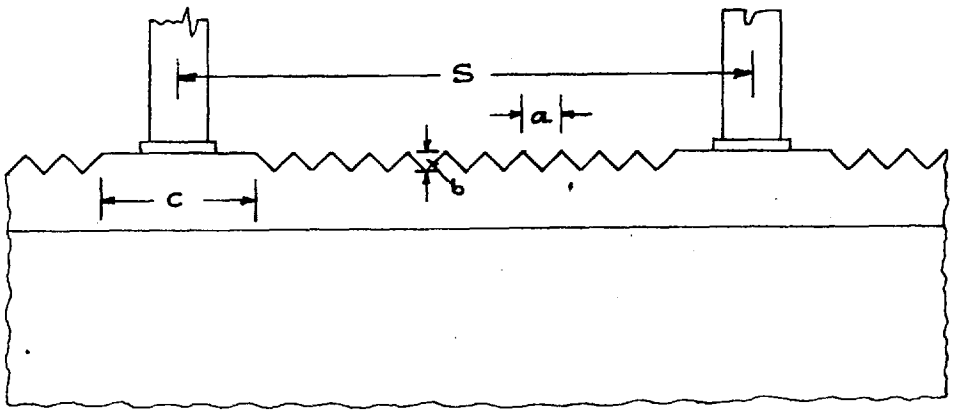


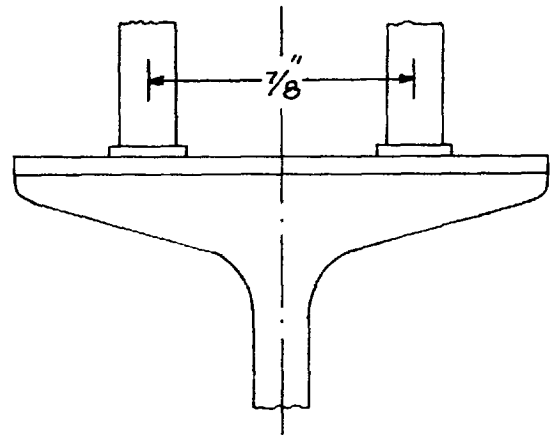
SPECIMEN	DESCRIPTION OF STUDS	ULT. LOAD PER STUD (TONS)	Cu (psi)
PL 1	4 IN. LONG PLAIN HEADED	3·40	6000
PL 2	3 IN. LONG PLAIN HEADED	3·13	6230
PL 3	2 IN. LONG PLAIN HEADED	1·34	5750
PL 4	4 IN. LONG THREADED WITH HEAD	3·63	7000
PL 5	4 IN. LONG THREADED WITHOUT HEAD	2·73	5290

FIG. 45 RESIDUAL SEPARATIONS — PULL-OUT SPECIMENS WITH 3/4 IN. DIA. STUDS









BEAMS	a IN.	b IN.	c IN.	S IN.
A1	1/8	1/16	5/8	3·75
A2	1/16	1/32	5/8	3·75
A3	1/32	1/64	5/8	3·75
B1	1/16	1/32	½	2·73
B2	1/32	1/64	½	2·73

B6 - DURBAR FLANGED

ALL OTHER BEAMS ARE PLAIN FLANGED

FIG. 47 DETAILS OF QUARTER SCALE BEAMS

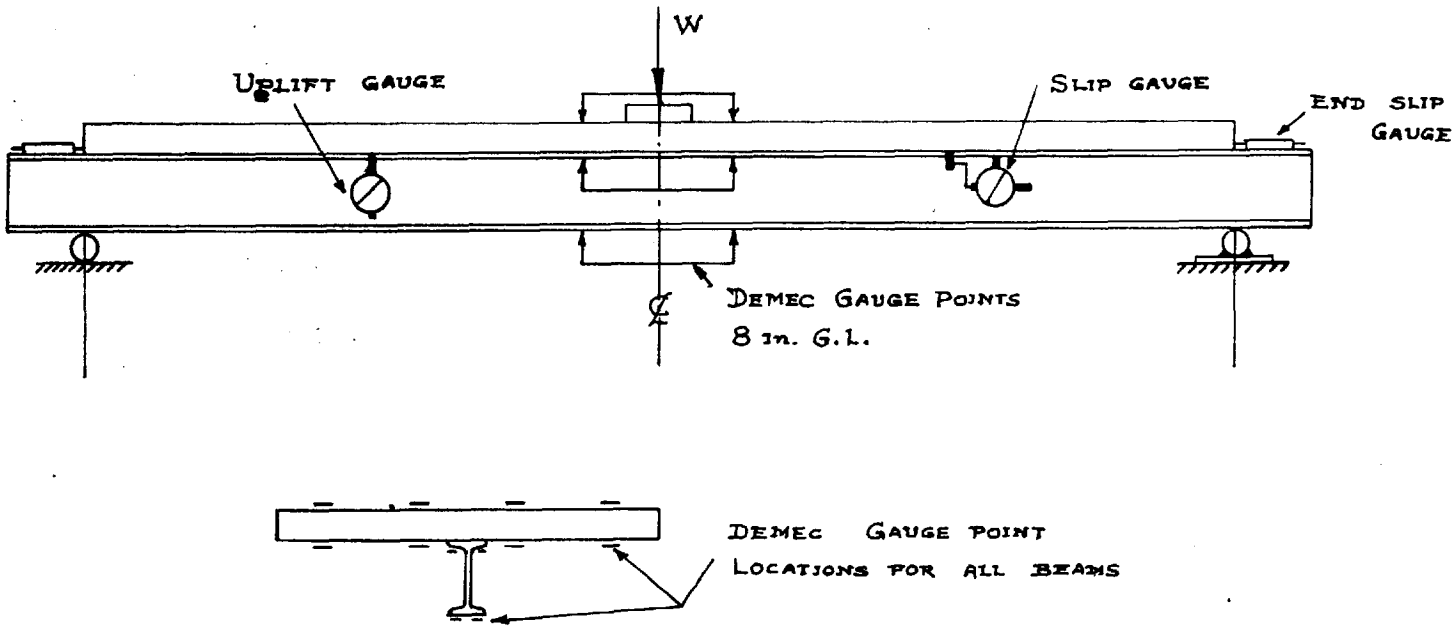


FIG. 48 GENERAL ARRANGEMENT FOR MEASUREMENTS IN QUARTER SCALE BEAMS

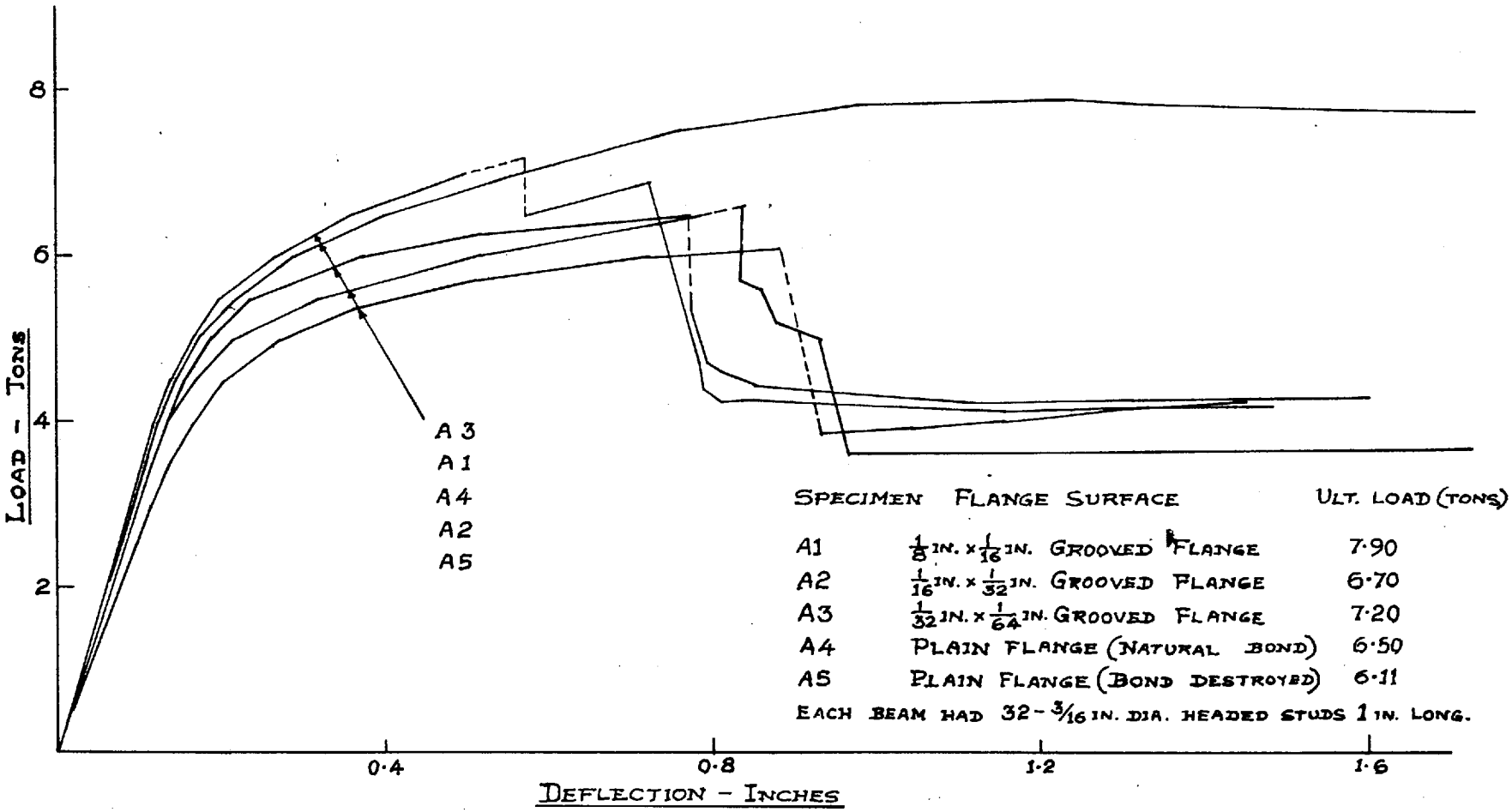


FIG. 49 MIDSPAN DEFLECTIONS - BEAMS OF GROUP A - POINT LOAD AT MIDSPAN.

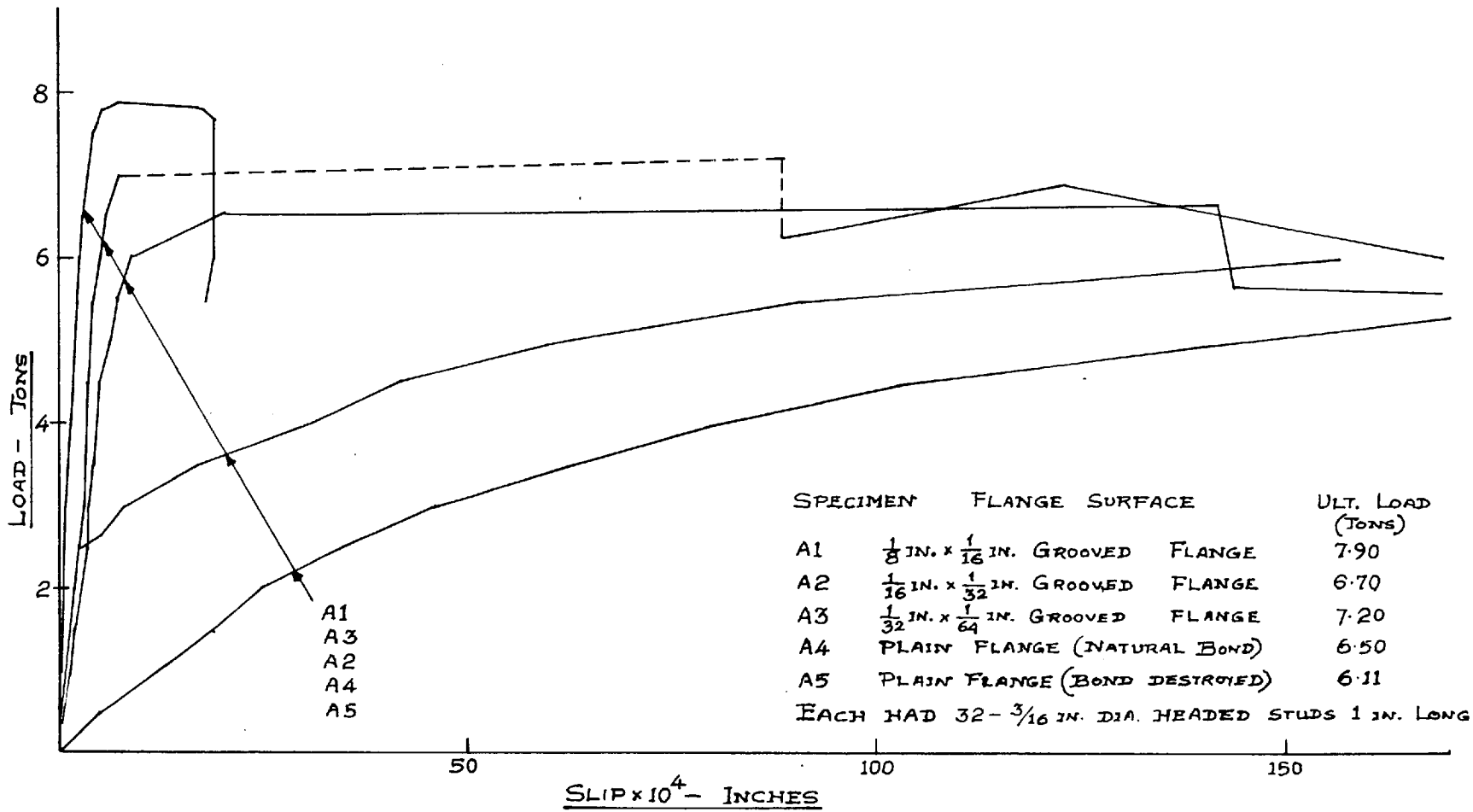


FIG. 50 AVERAGE END SLIPS - BEAMS OF GROUP A - POINT LOAD AT MIDSPAN

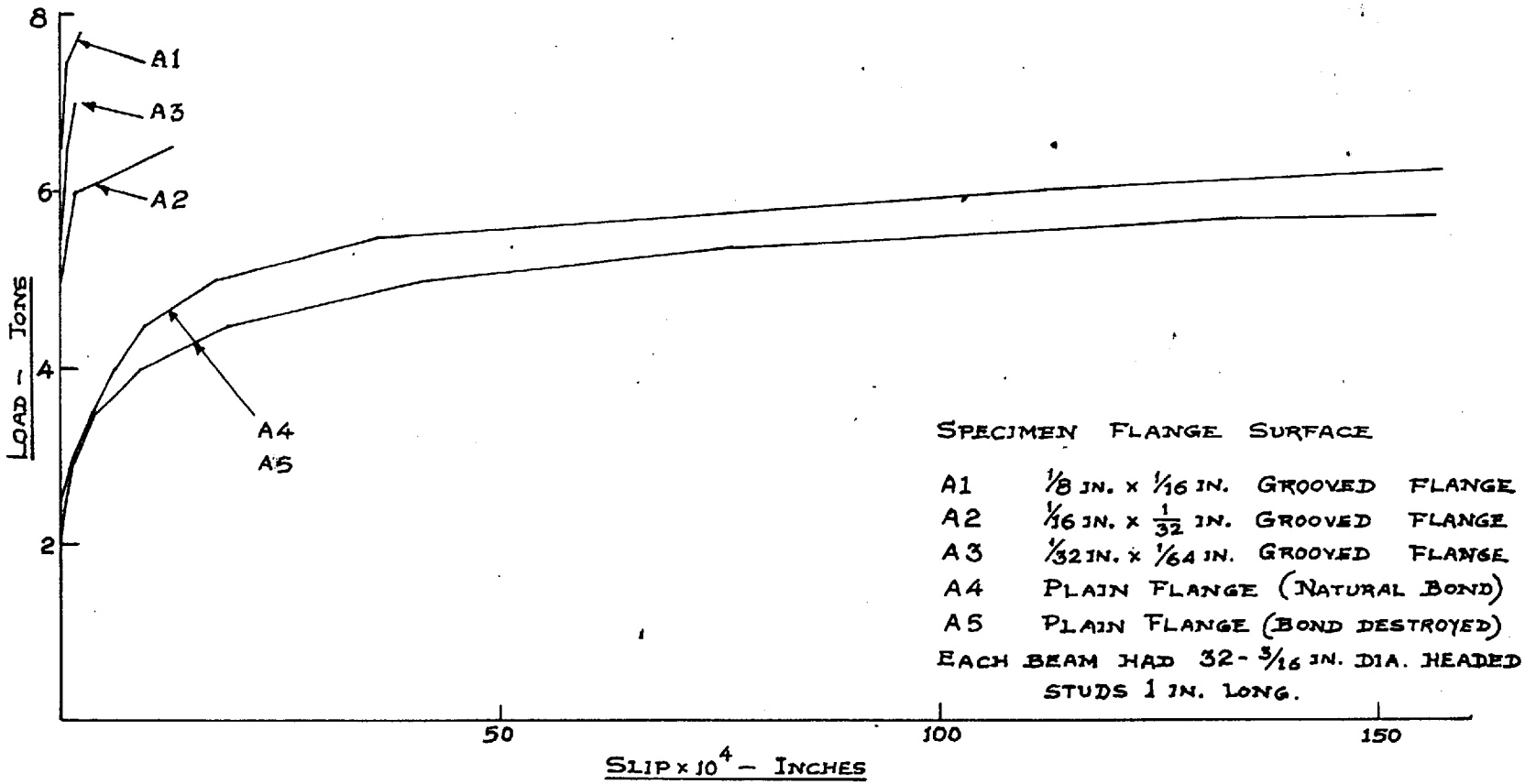


FIG. 51 AVERAGE RESIDUAL END SLIPS - BEAMS OF GROUP A - POIN LOAD AT MIDSPAN

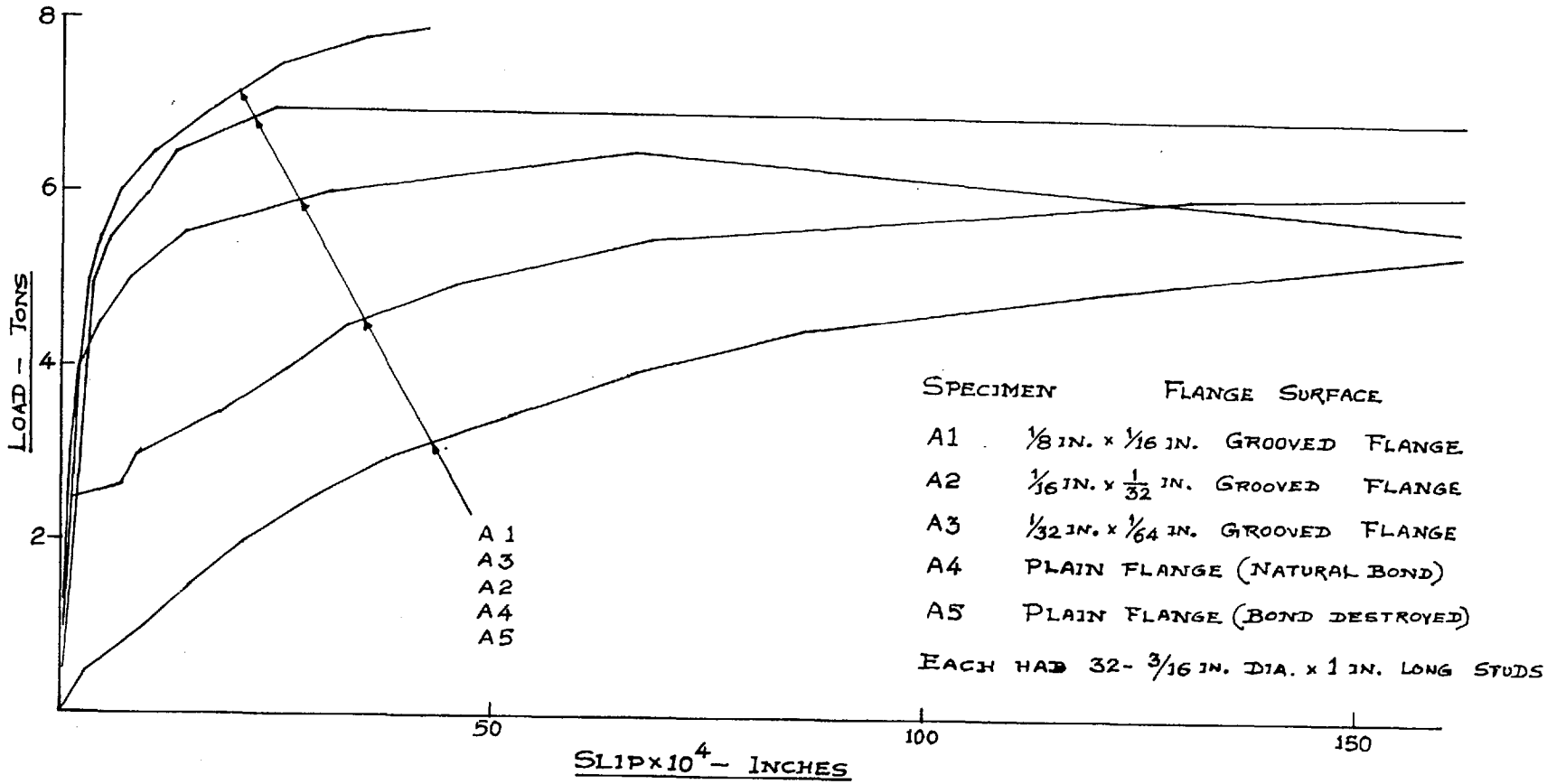


FIG. 52 AVERAGE SLIPS AT 1/4 SPAN — BEAMS OF GROUP A - POINT LOAD AT MIDSPAN

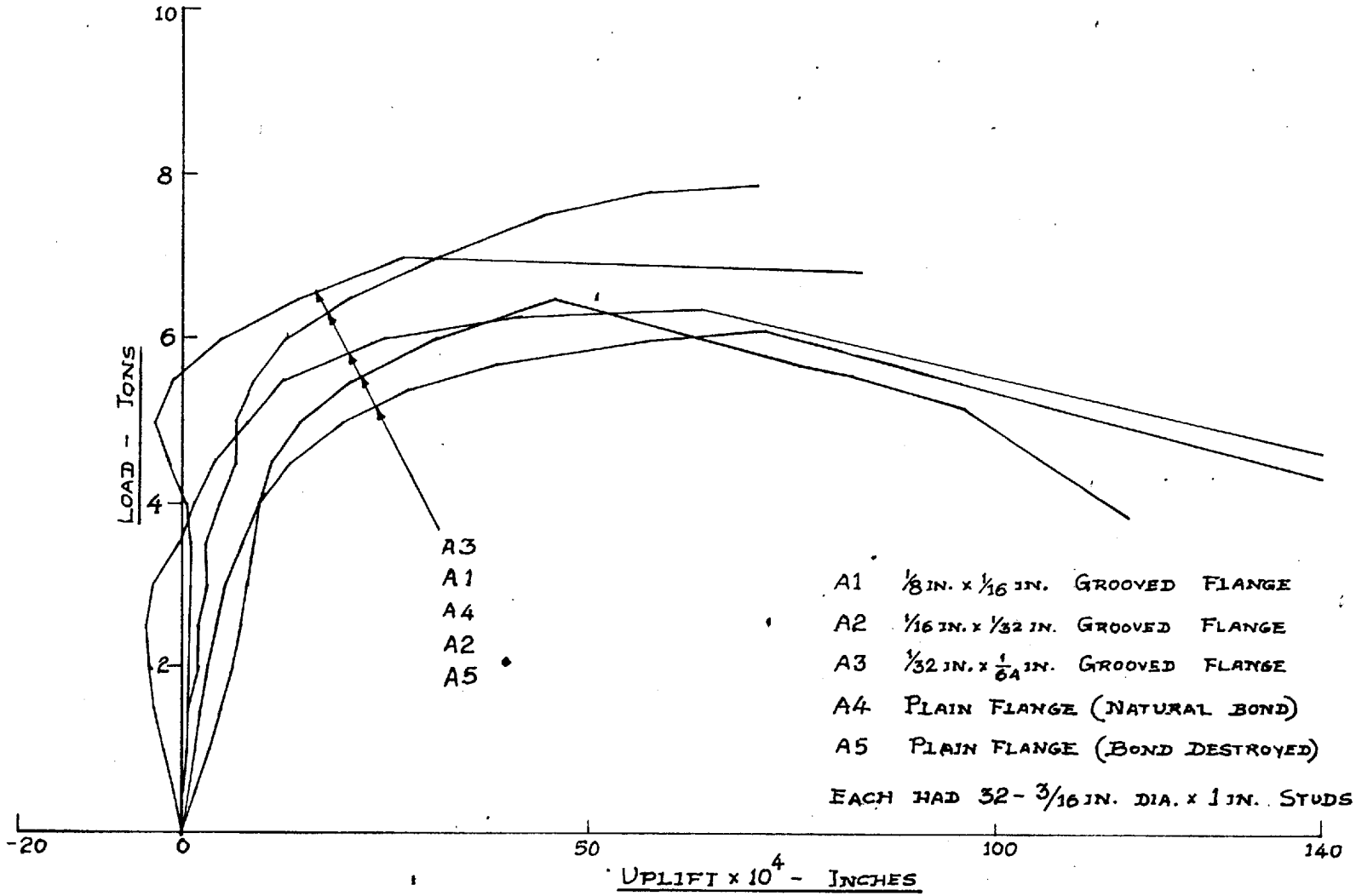


FIG. 53 AVERAGE UPLIFTS AT 1/4 SPAN —— BEAMS OF GROUP A - POINT LOAD AT MIDSPAN

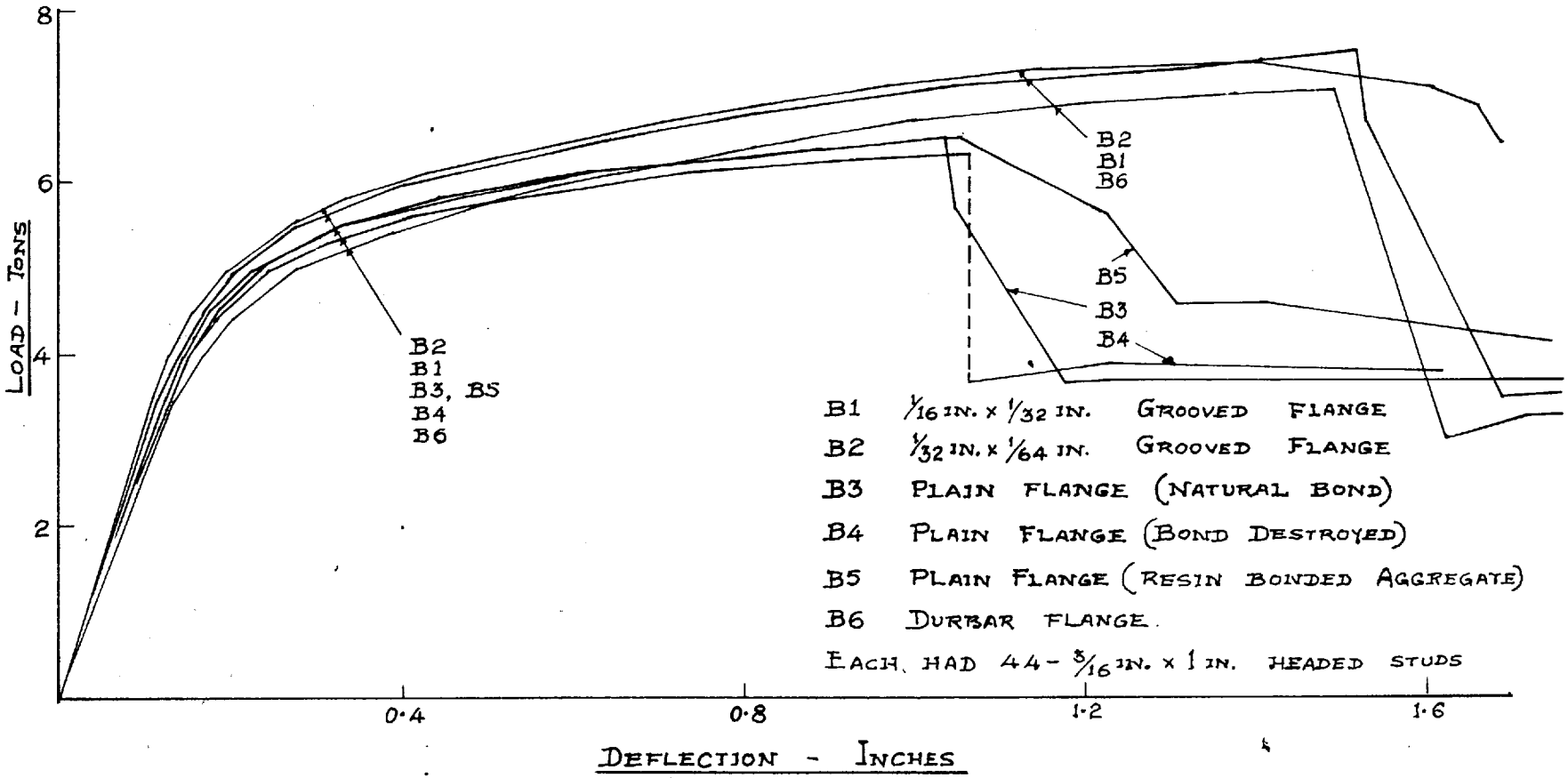


FIG. 54 MIDSPAN DEFLECTIONS - BEAMS OF GROUP B - POINT LOAD AT MIDSPAN

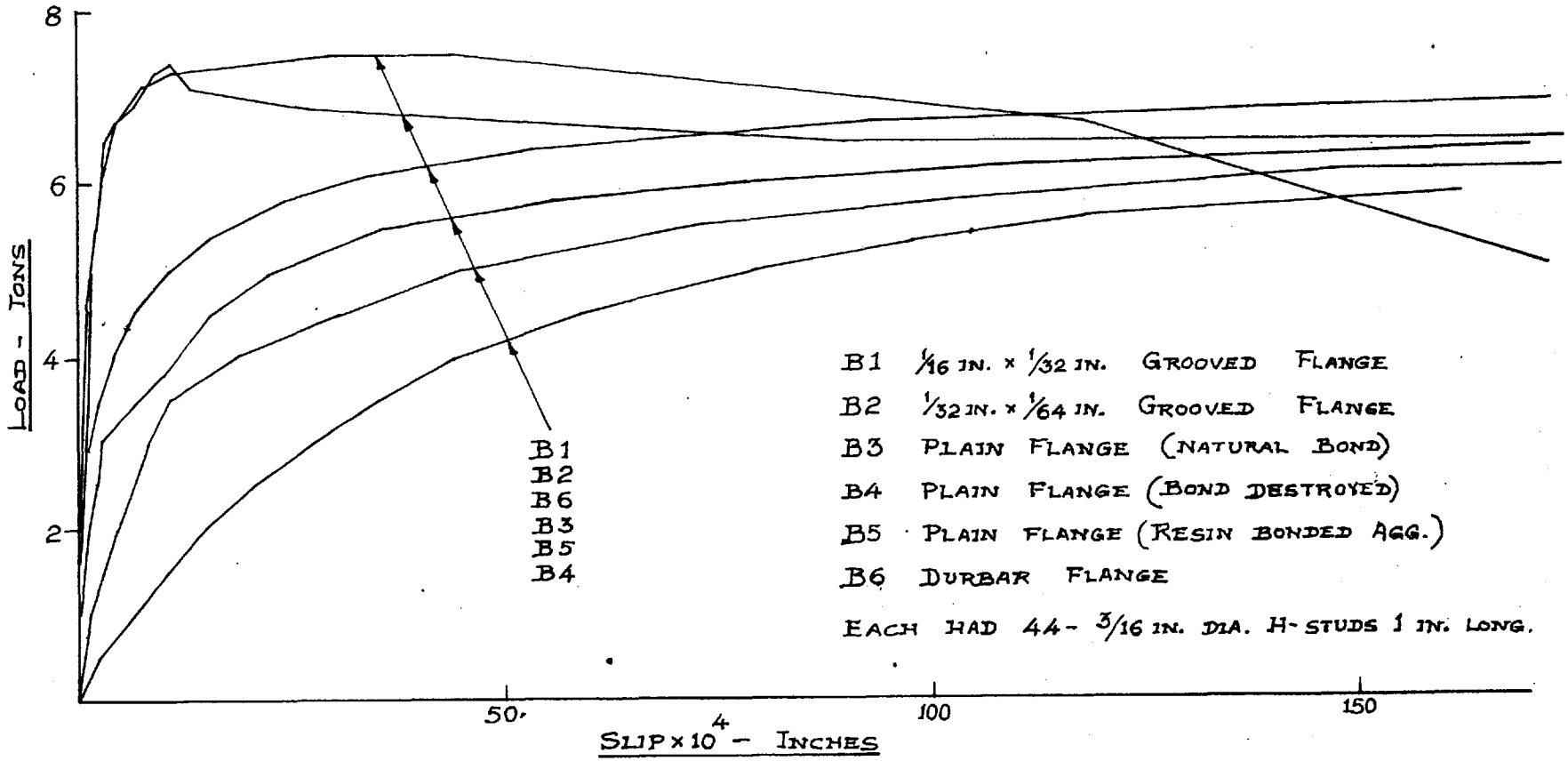


FIG. 55 AVERAGE END SLIPS - BEAMS OF GROUP B - POINT LOAD AT MIDSPAN

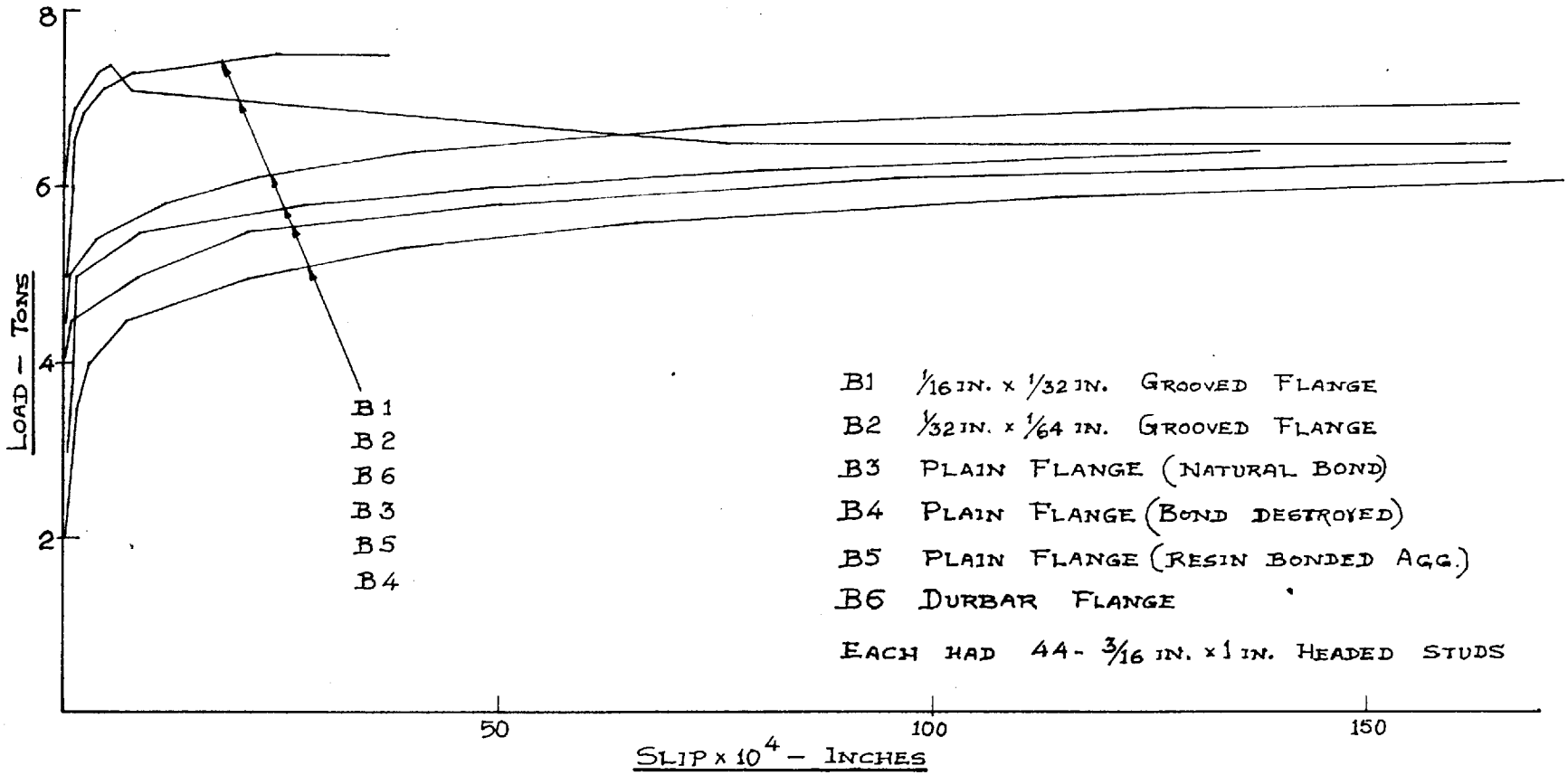


FIG. 56 AVERAGE RESIDUAL END SLIPS – BEAMS OF GROUP B – POINT LOAD AT MIDSPAN

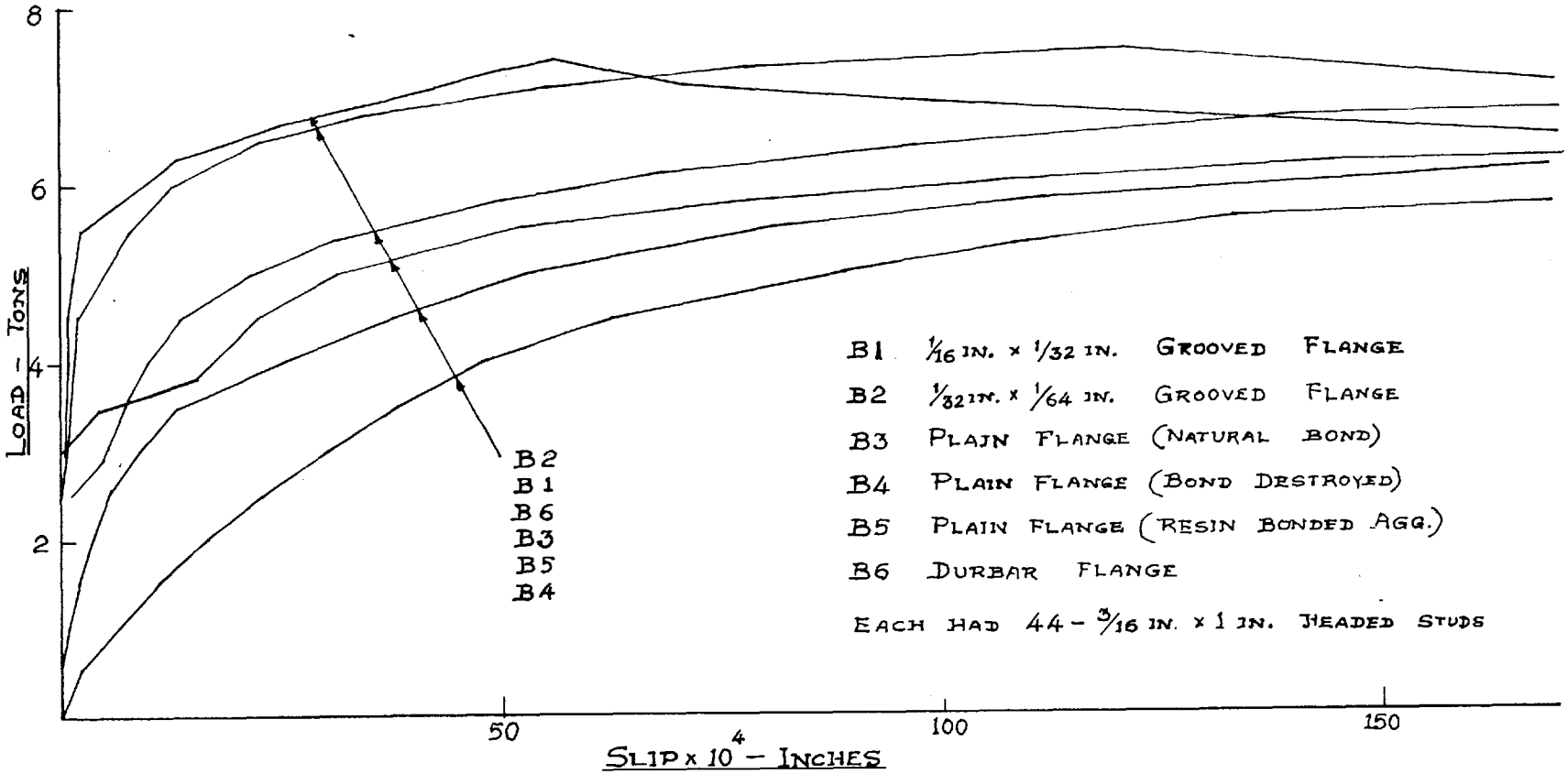


FIG. 57 AVERAGE SLIPS AT 1/4 SPAN —— BEAMS OF GROUP B - POINT LOAD AT MIDSPAN

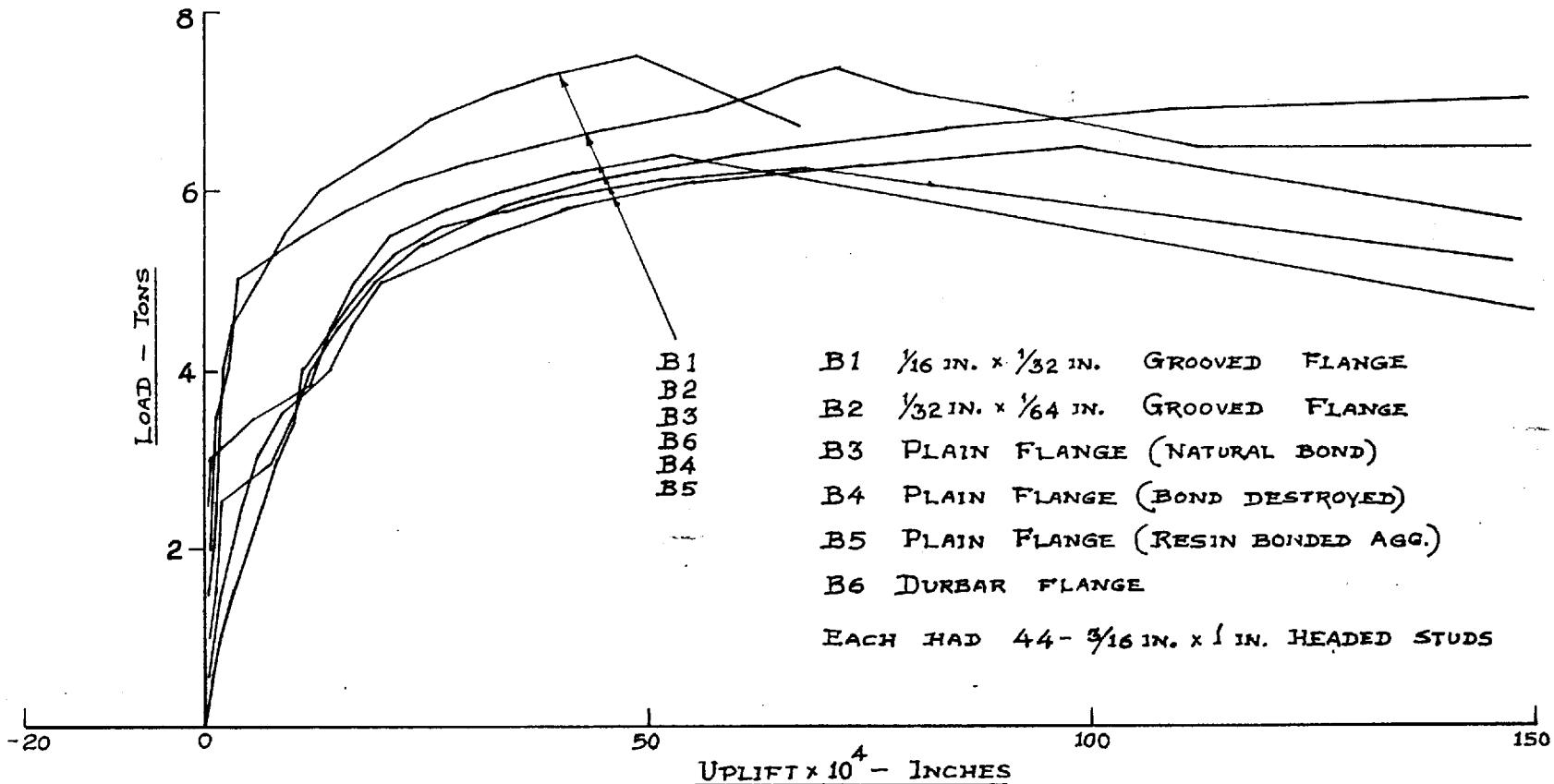


FIG. 58 AVERAGE UPLIFTS AT 1/4 SPAN —•— BEAMS OF GROUP B - POINT LOAD AT MIDSPAN

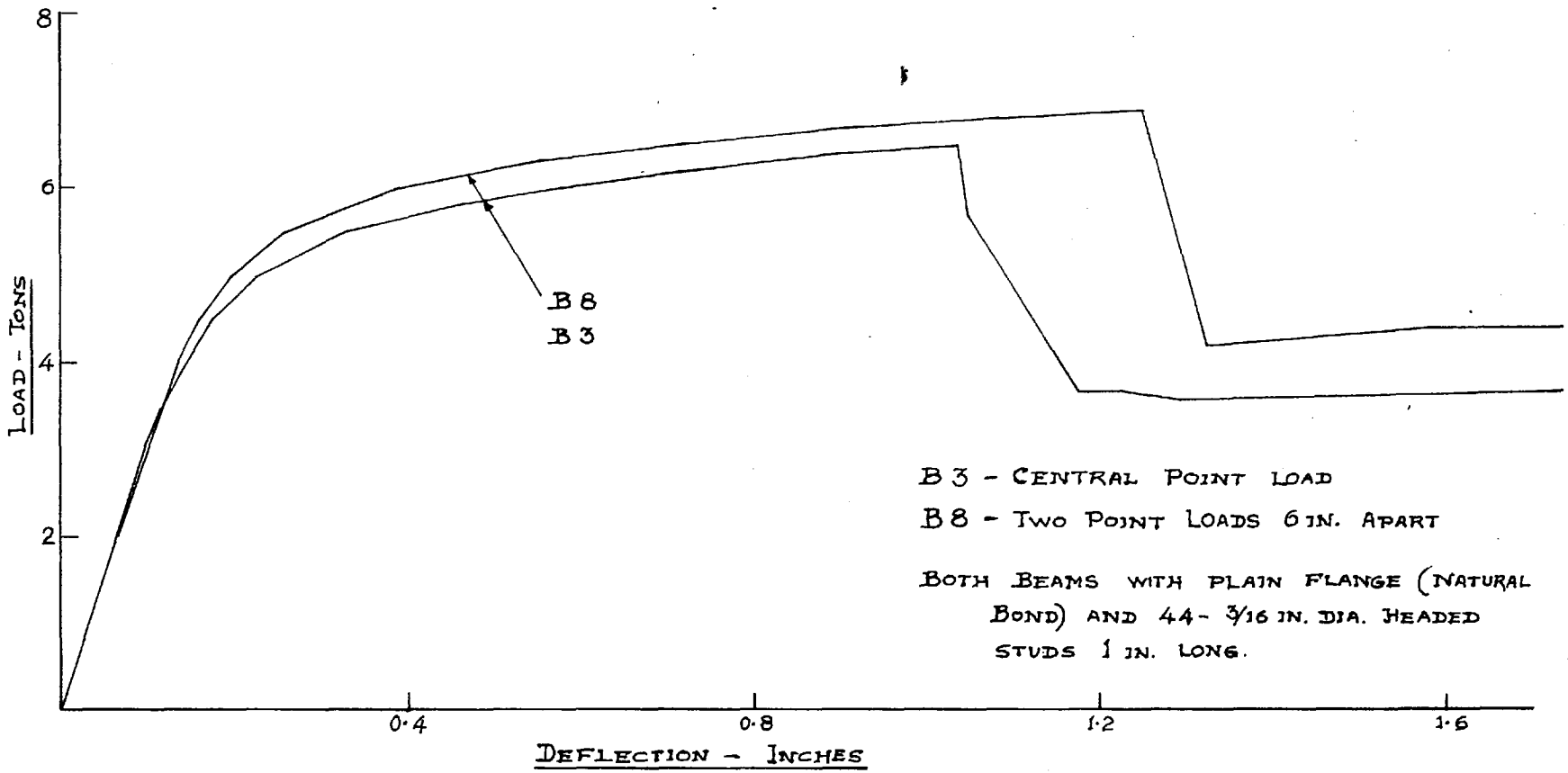


FIG. 59 MIDSPAN DEFLECTIONS - BEAMS B3 AND B8.

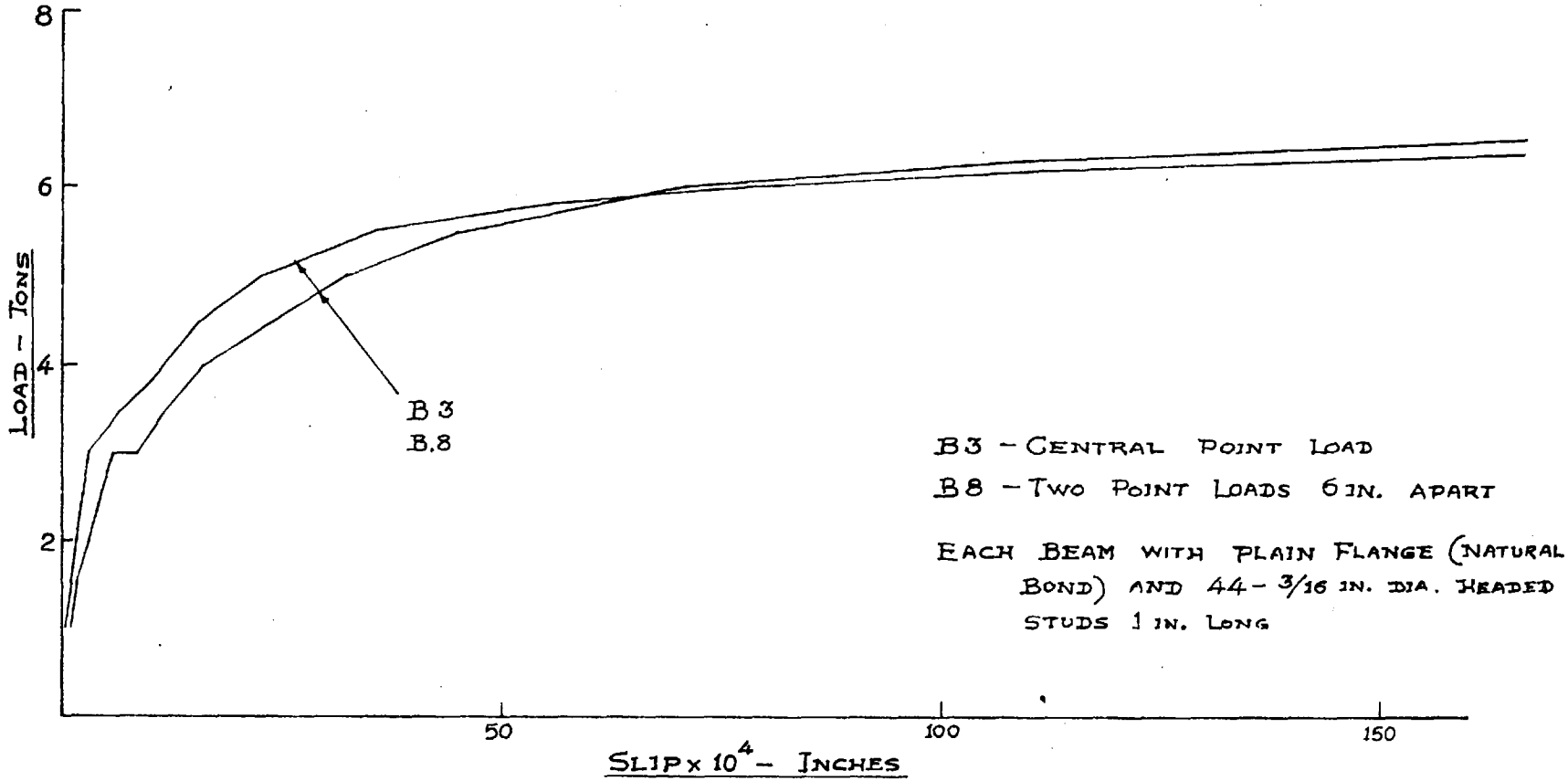


FIG. 60 . AVERAGE END SLIPS - BEAMS B3 AND B8

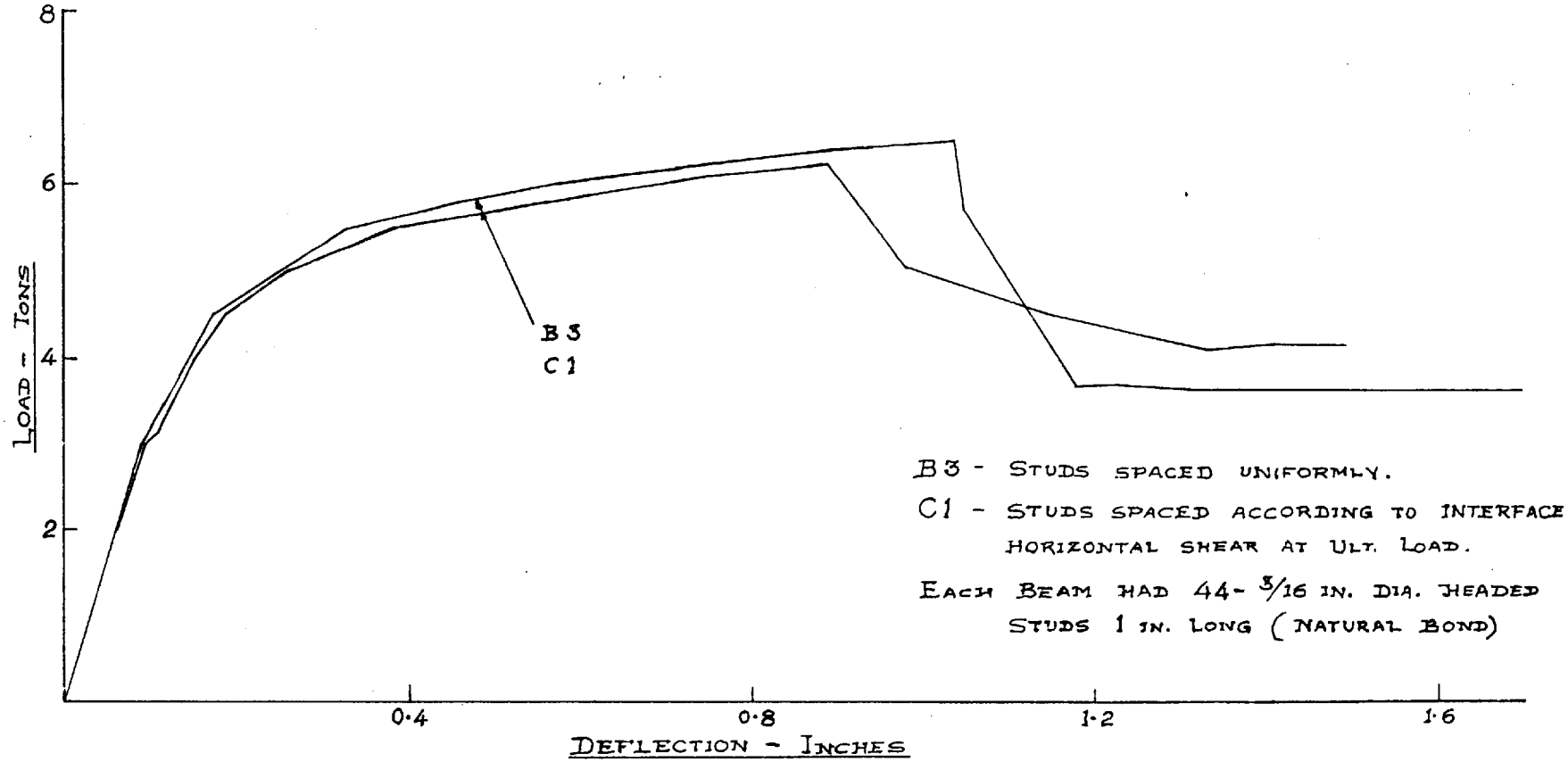


FIG. 61 MIDSPAN DEFLECTIONS - BEAMS B3 AND C1

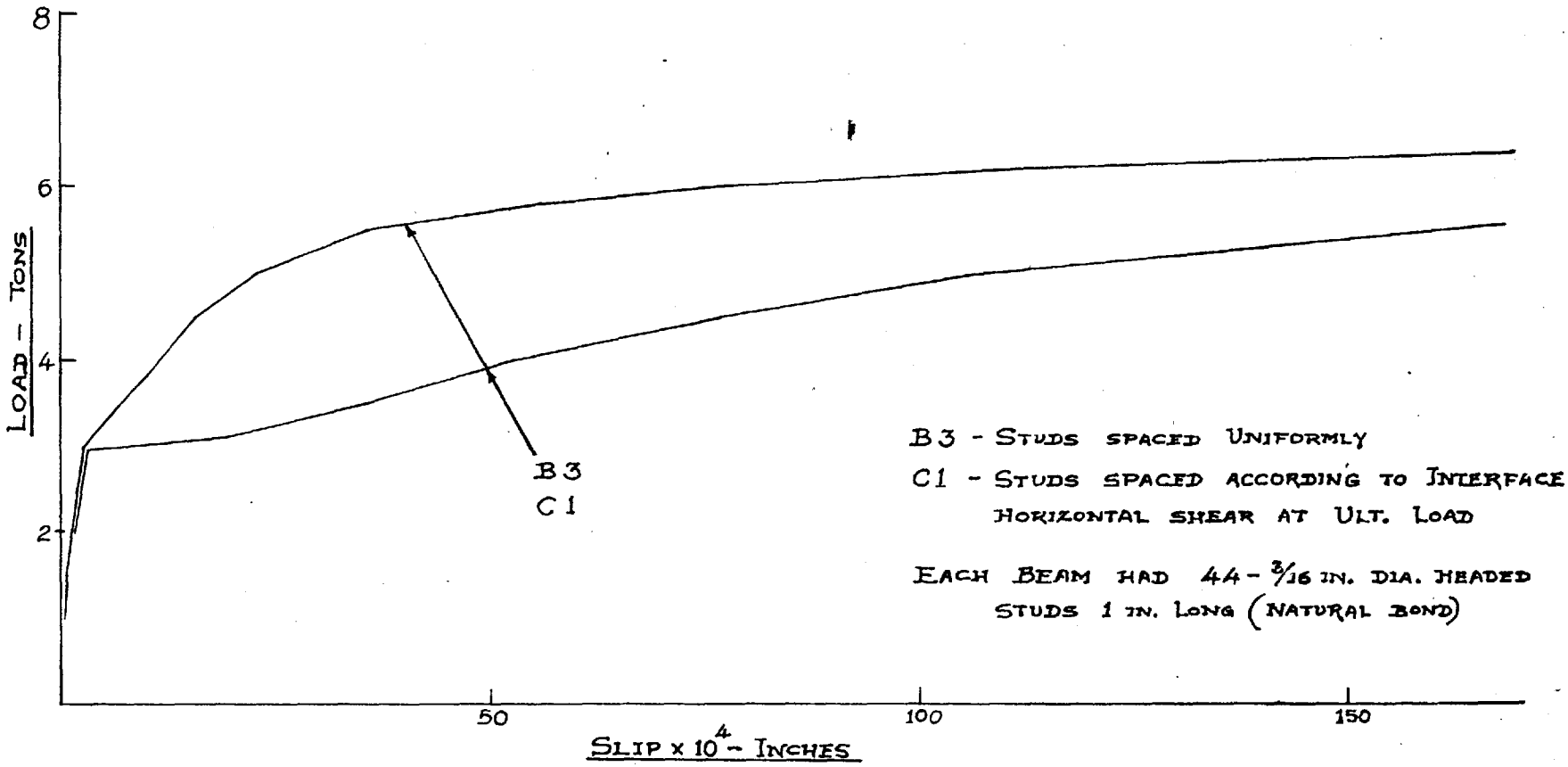


FIG. 62 AVERAGE END SLIPS — BEAMS B3 AND C1

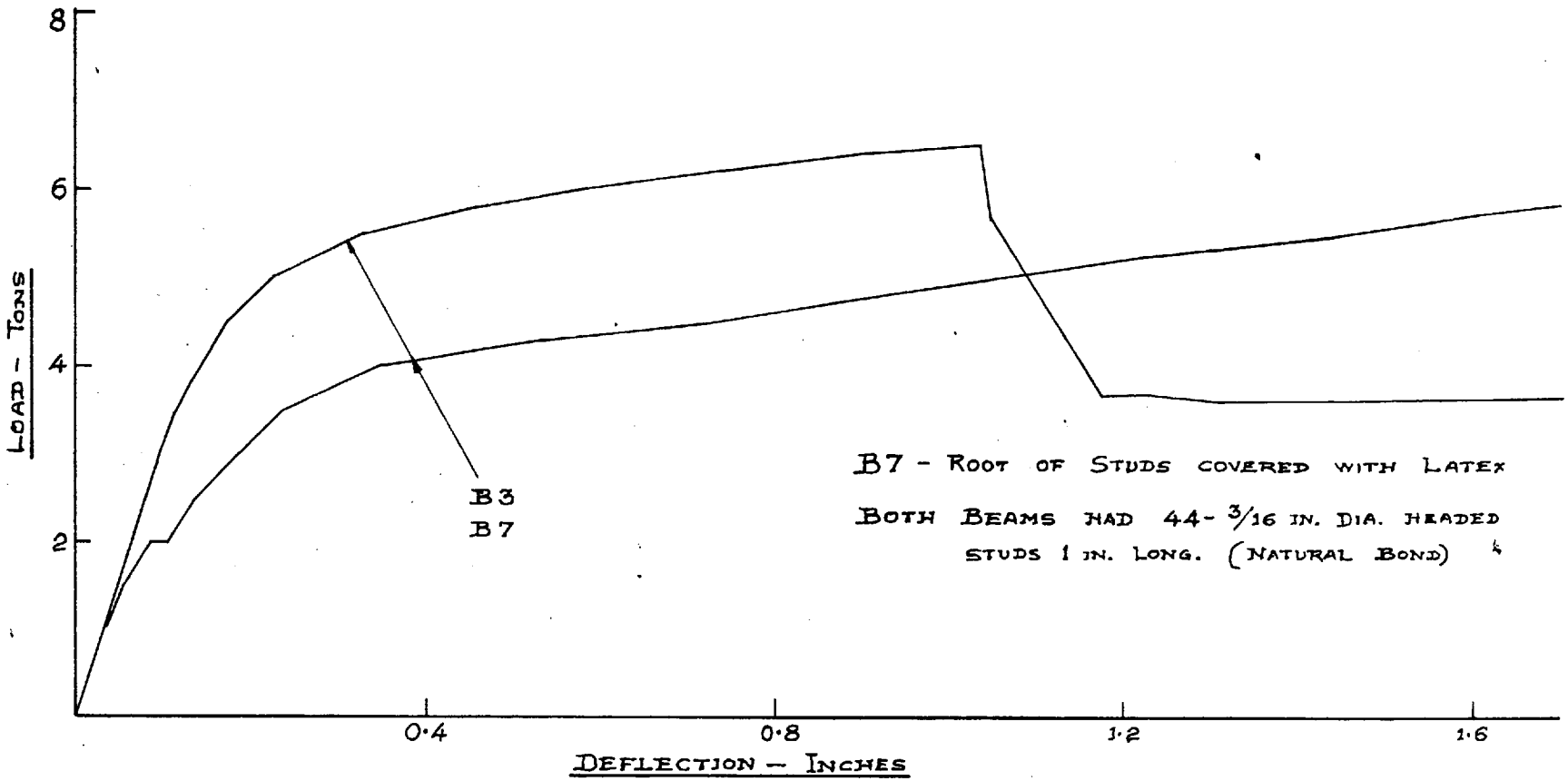


FIG. 63 MIDSPAN DEFLECTIONS - BEAMS B3 AND B7 - POINT LOAD AT MIDSPAN

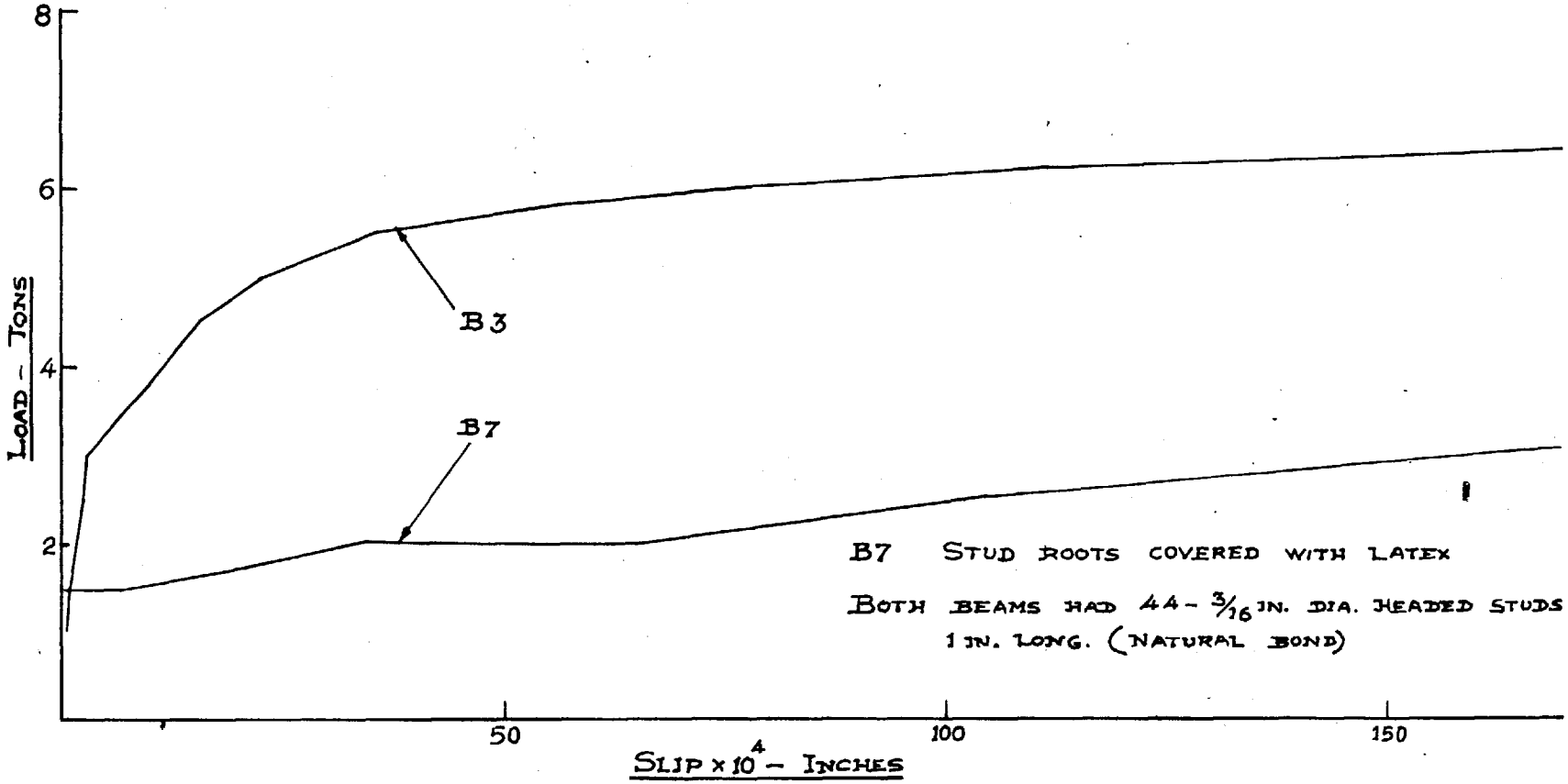


FIG. 64 AVERAGE END SLIPS - BEAMS B3 AND B7 - POINT LOAD AT MIDSPAN

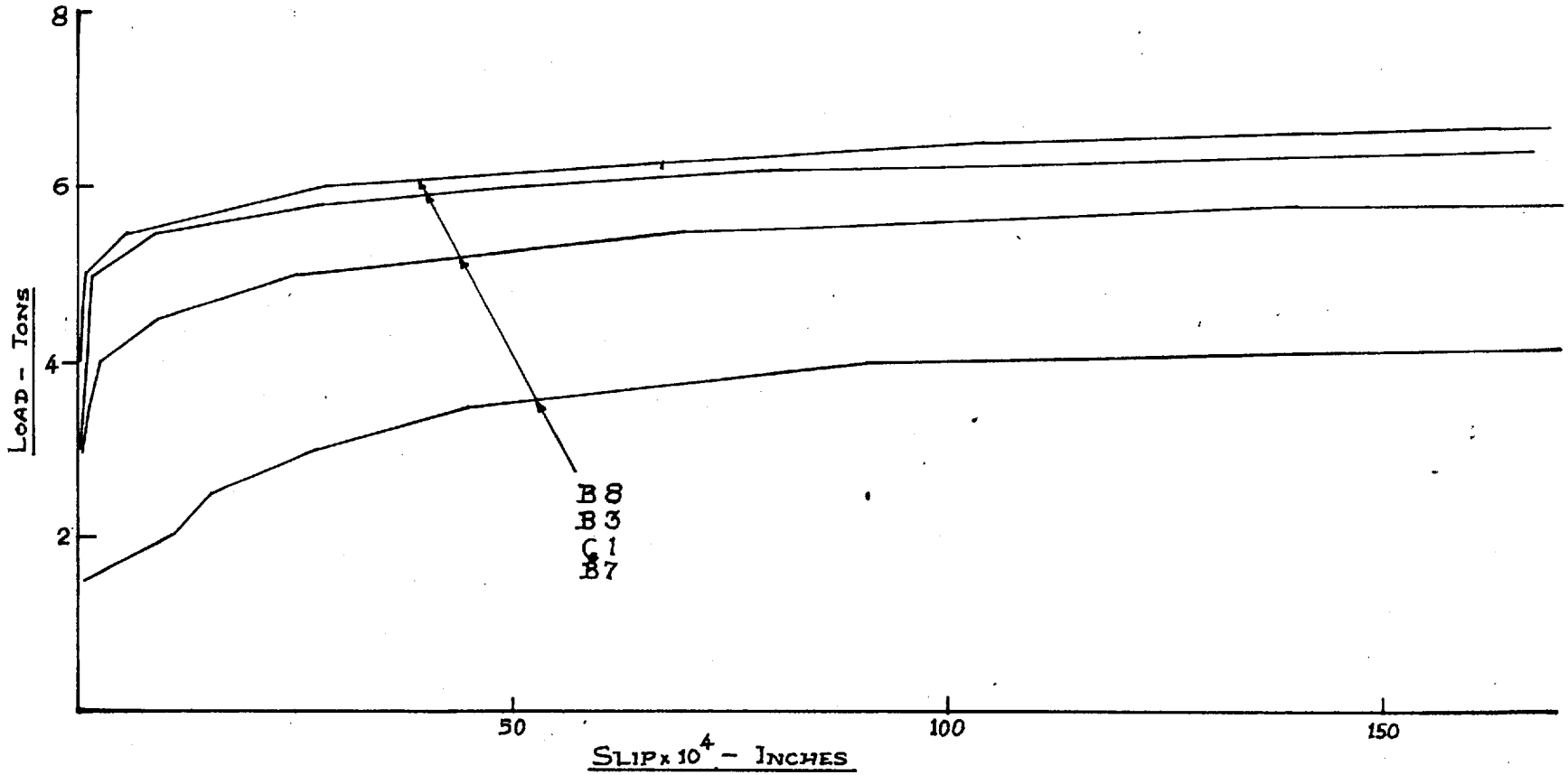


FIG. 65 AVERAGE RESIDUAL END SLIPS - BEAMS B3, B7, B8 AND C1 - EACH WITH 44 - 3/16 IN. DIA. HEADED STUDS 1 IN. LONG

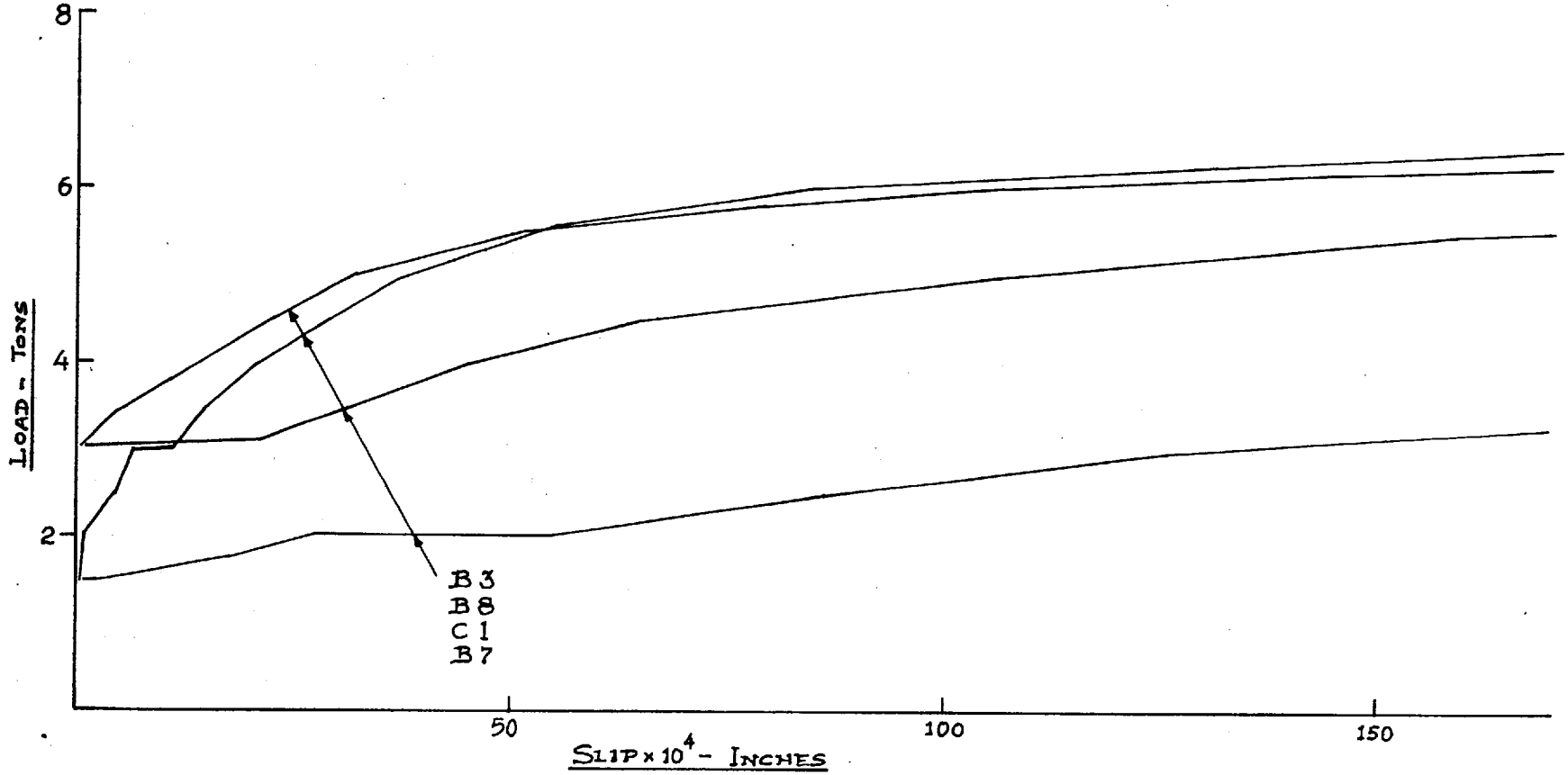


FIG. 66 AVERAGE SLIPS AT 1/4 SPAN —— BEAMS B3, B7, B8 AND C1 - EACH WITH 44 - 3/16 IN. DIA. HEADED STUDS 1 IN. LONG

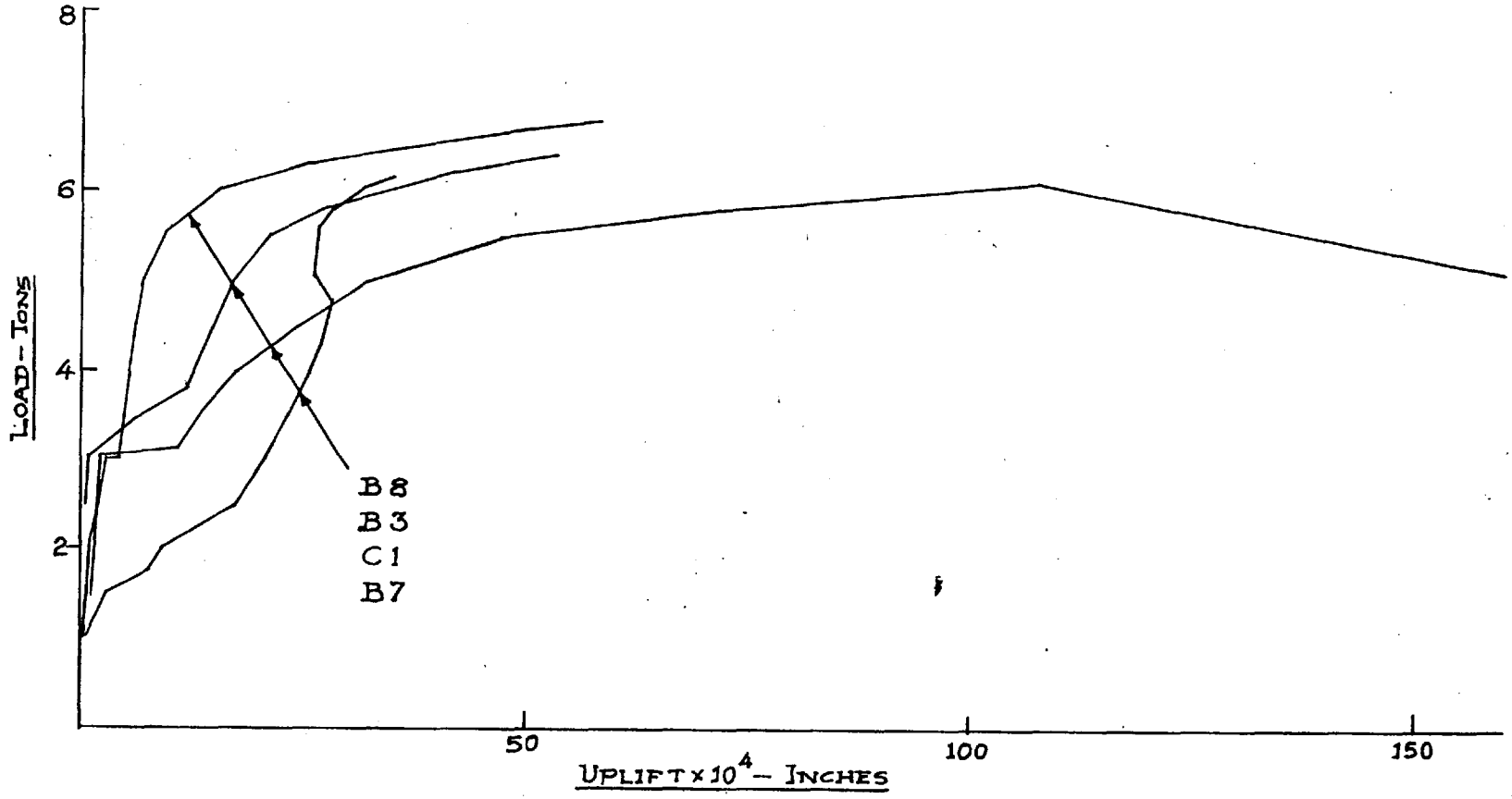


FIG. 67 AVERAGE UPLIFTS AT 1/4 SPAN —— BEAMS B3, B7, B8 AND C1 - EACH WITH 44 - 3/16 IN. DIA. HEADED STUDS 1 IN. LONG

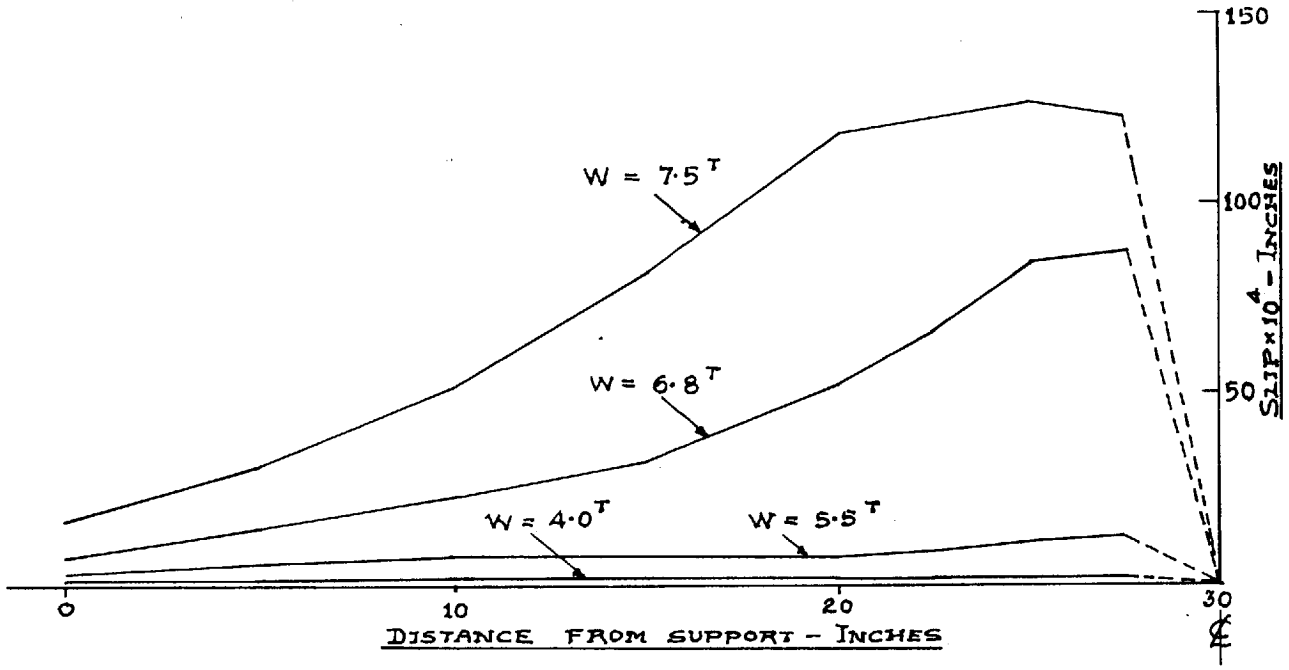


FIG. 68 SLIPS ALONG THE LENGTH – BEAM B1 WITH 1/16 IN. × 1/32 IN. GROOVED FLANGE AND 44 – 3/16 IN. DIA. × 1 IN. LONG H-STUDS

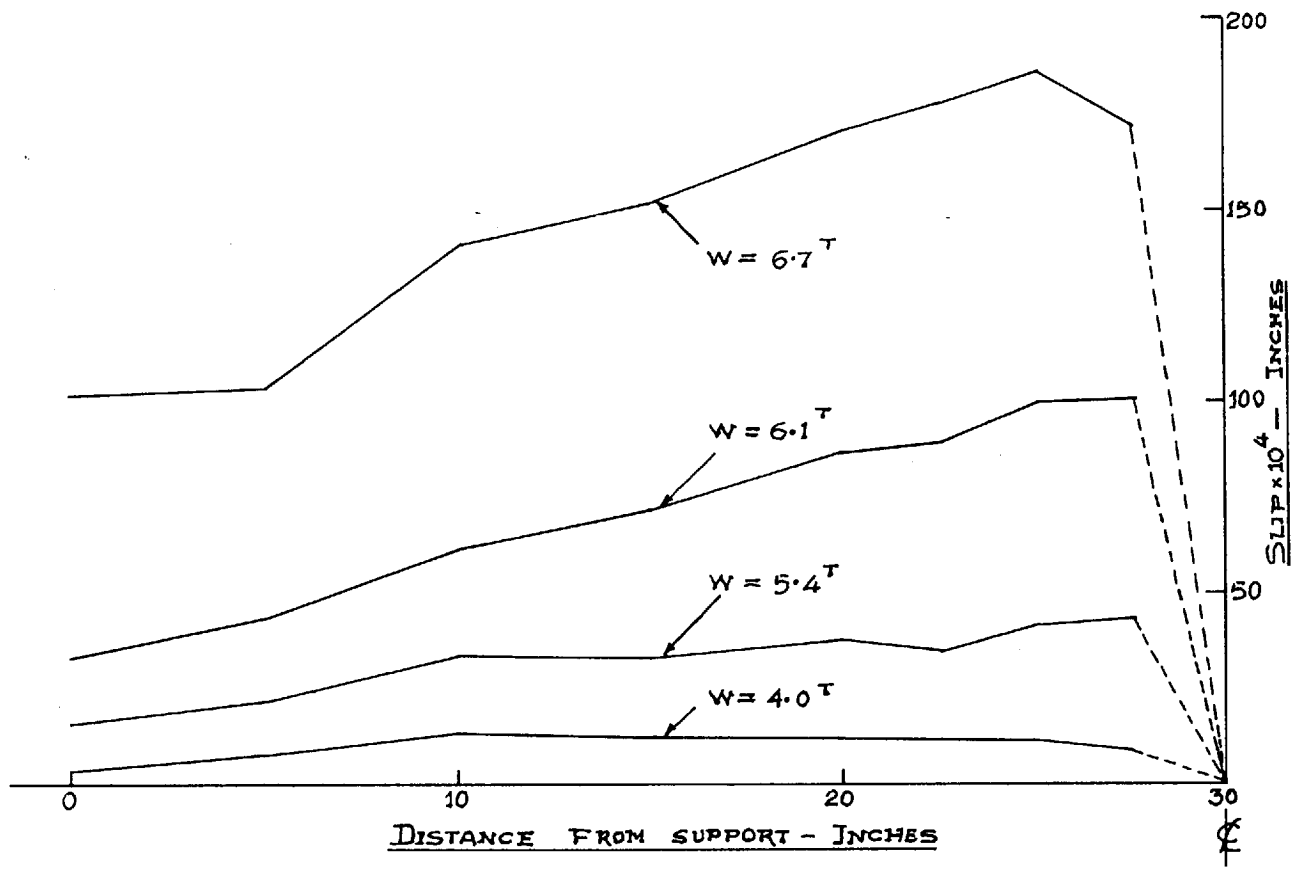


FIG. 69 SLIPS ALONG THE LENGTH – BEAM B6 WITH DURBAR FLANGE AND 44 – 3/16 IN. DIA. × 1 IN. LONG H-STUDS

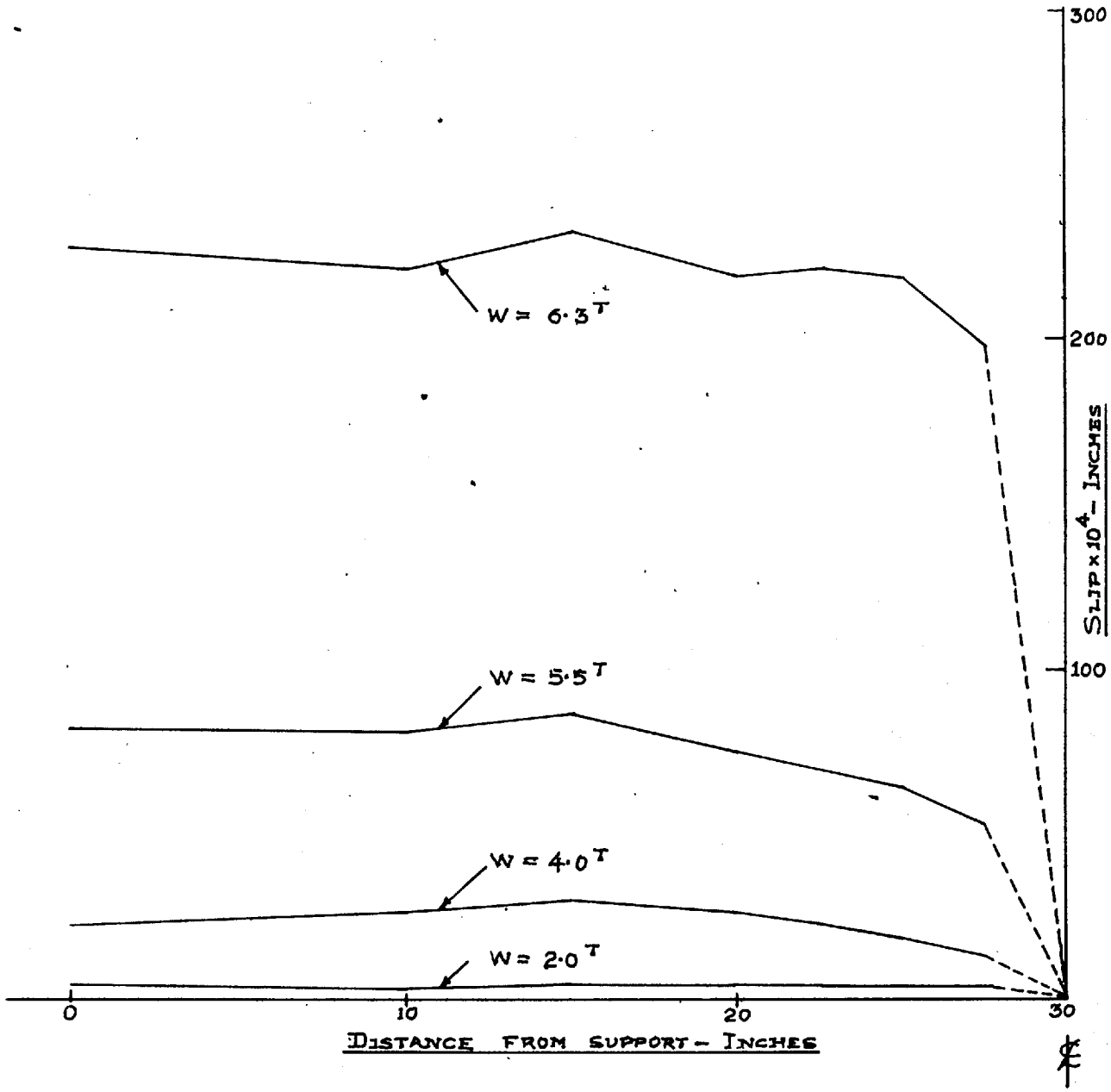


FIG. 70 SLIPS ALONG THE LENGTH — BEAM B5 WITH RESIN BONDED AGGREGATES AND 44-3/16 IN. DIA. x 1 IN. LONG HEADED STUDS

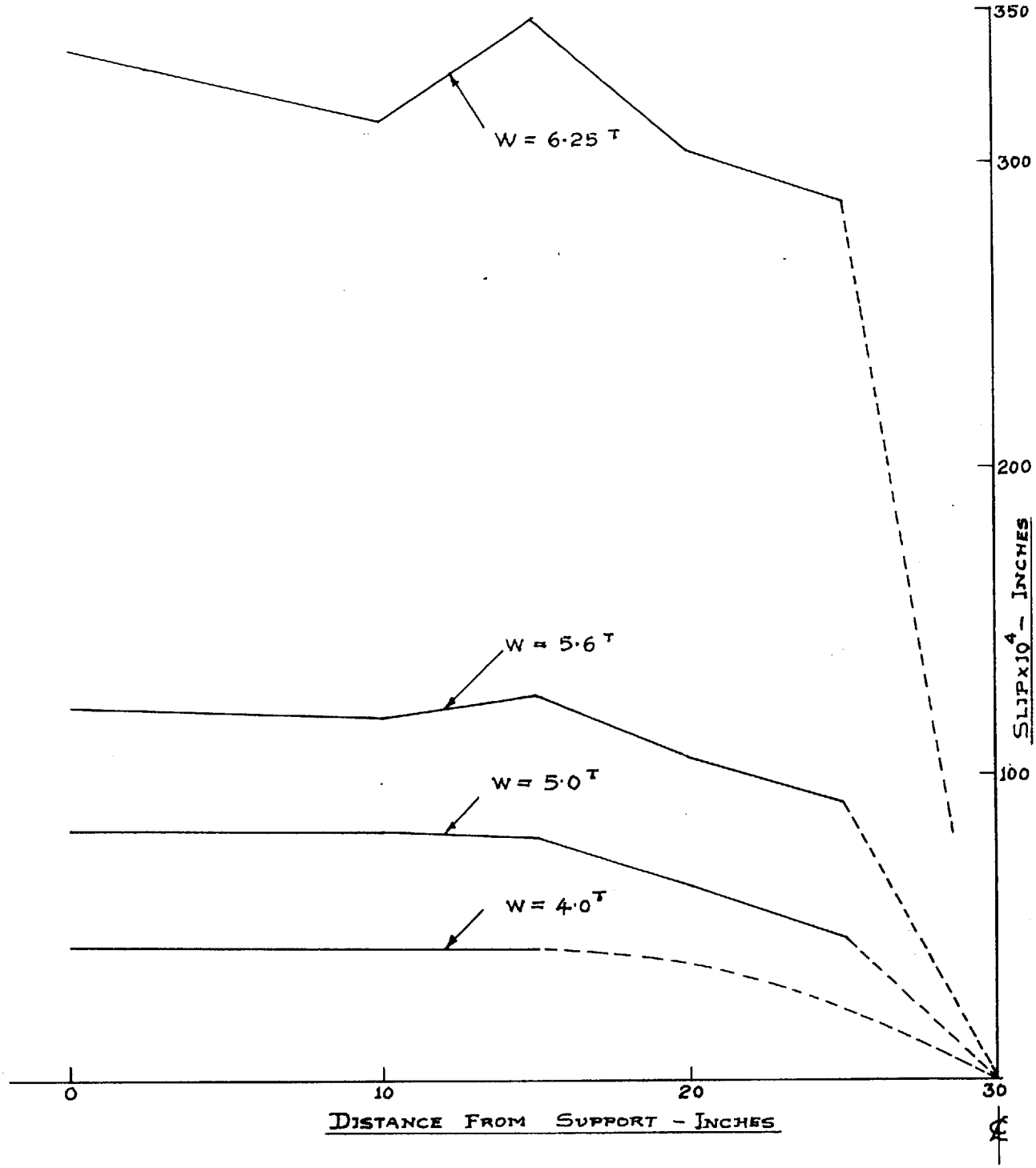


FIG. 71 SLIPS ALONG THE LENGTH - BEAM B4 WITH 44 - 3/16 IN. DIA. x 1 IN. LONG H-STUDS (BOND DESTROYED)

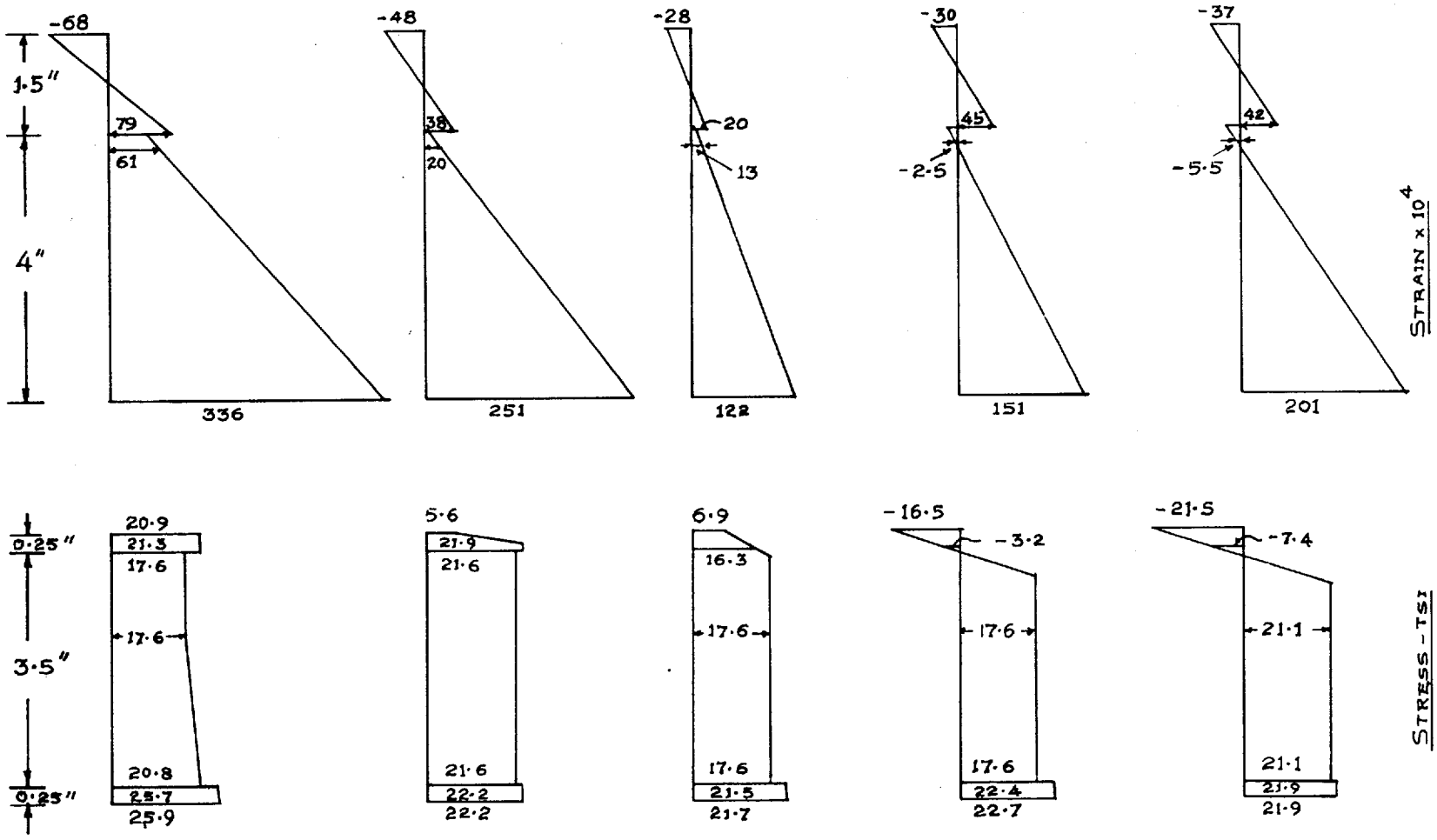


FIG. 72 MEASURED STRAINS AT MIDSPAN SECTION AT OR NEAR ULT. LOAD AND CORRESPONDING STRESSES IN STEEL BEAM — BEAMS OF GROUP A.

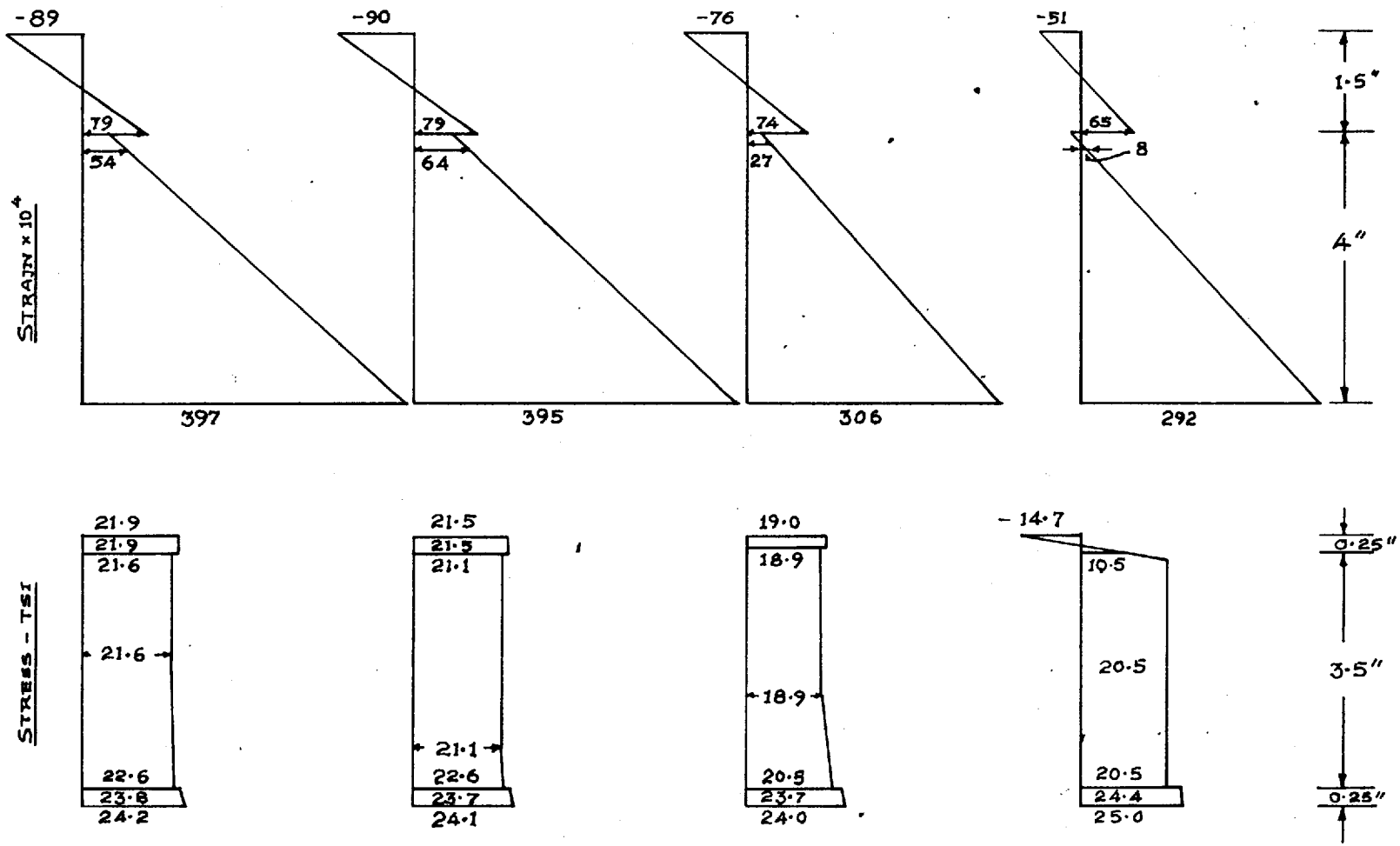


FIG. 73 MEASURED STRAINS AT MIDSPAN SECTION AT OR NEAR ULT. LOAD AND CORRESPONDING STRESSES IN THE STEEL BEAM — BEAMS OF GROUP B.

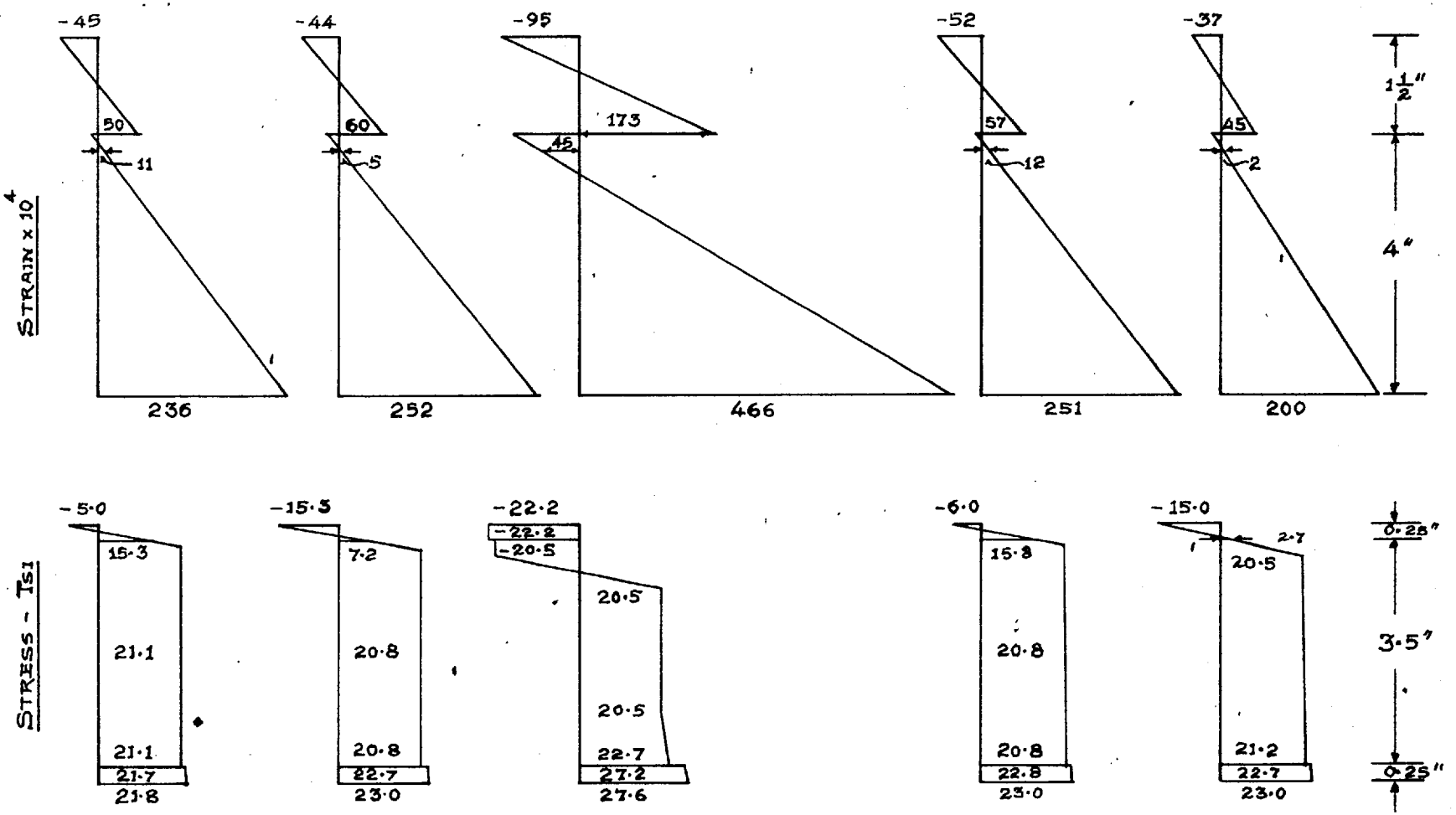


FIG. 73 (CONTD) MEASURED STRAINS AT MIDSPAN SECTION AT OR NEAR ULT. LOAD AND CORRESPONDING STRESSES IN STEEL BEAM - BEAMS OF GROUP B AND C1

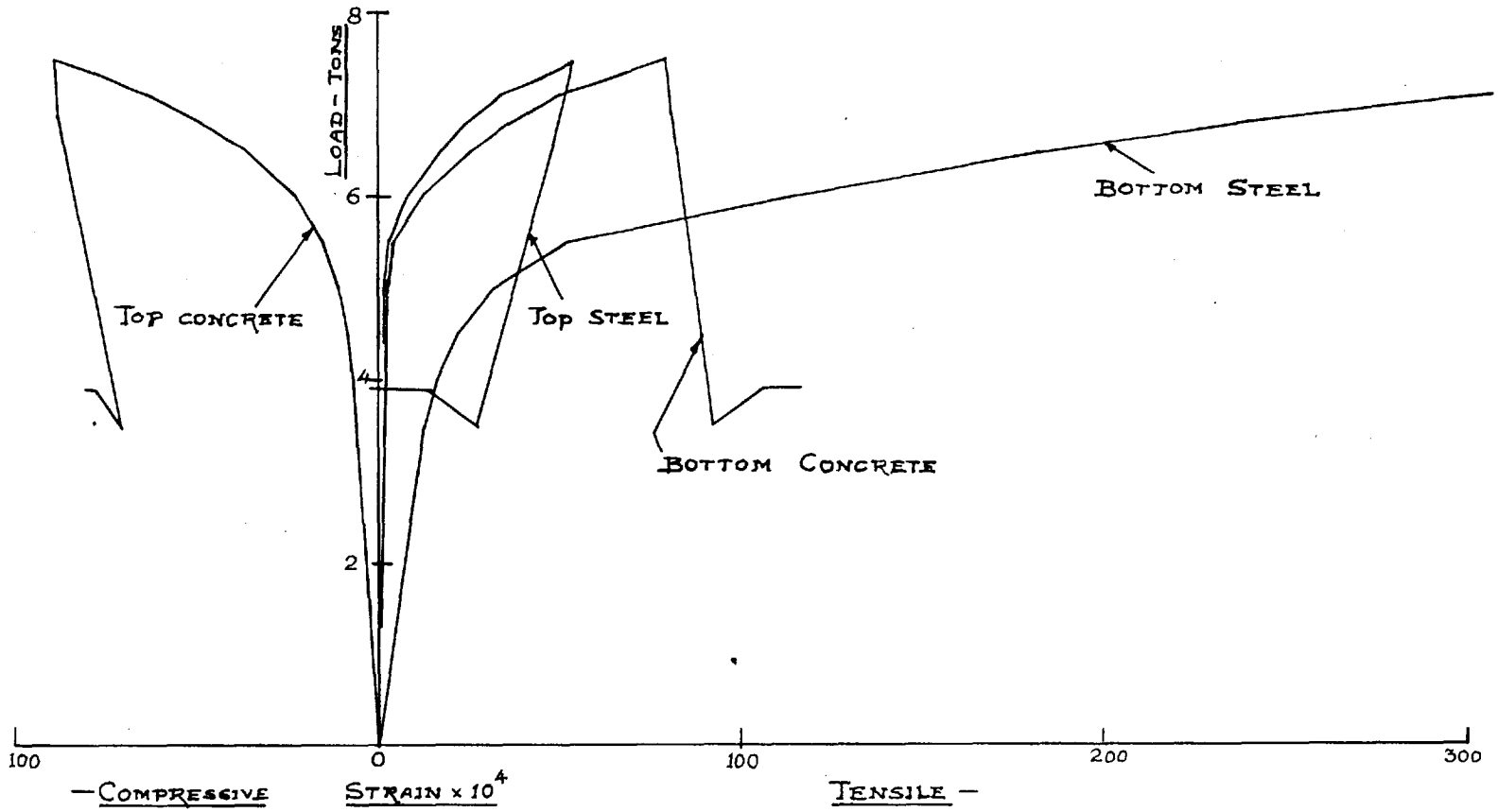


FIG. 74 STRAINS AT MIDSPAN SECTION - BEAM B1 WITH 1/16 IN. X 1/32 IN. GROOVES AND 44 - 3/16 IN. DIA. HEADED STUDS 1 IN. LONG.

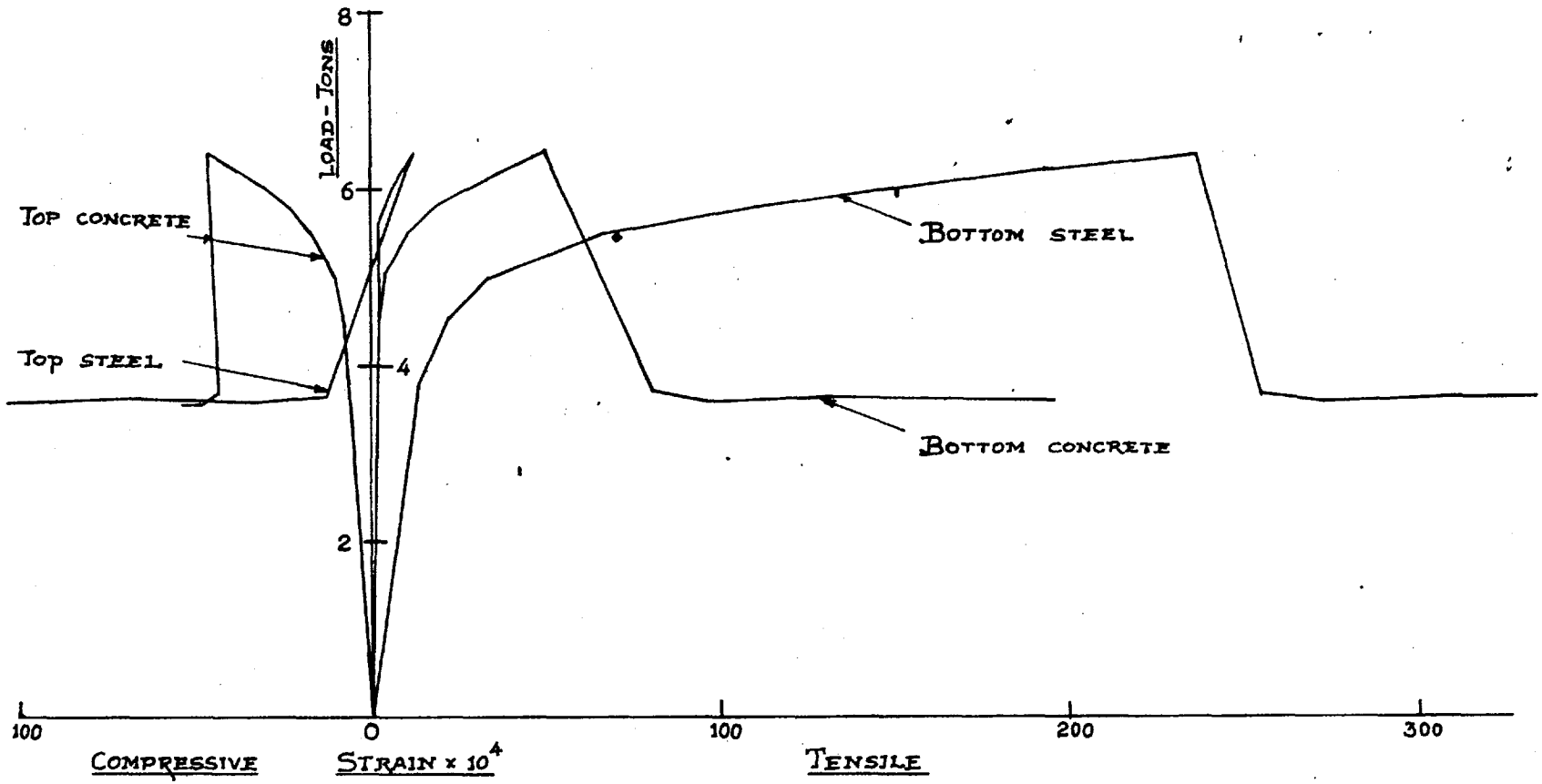


FIG. 75 STRAINS AT MIDSPAN SECTION - BEAM B3 WITH NATURAL BOND AND 44 - 5/16 IN. DIA. HEADED STUDS 1 IN. LONG

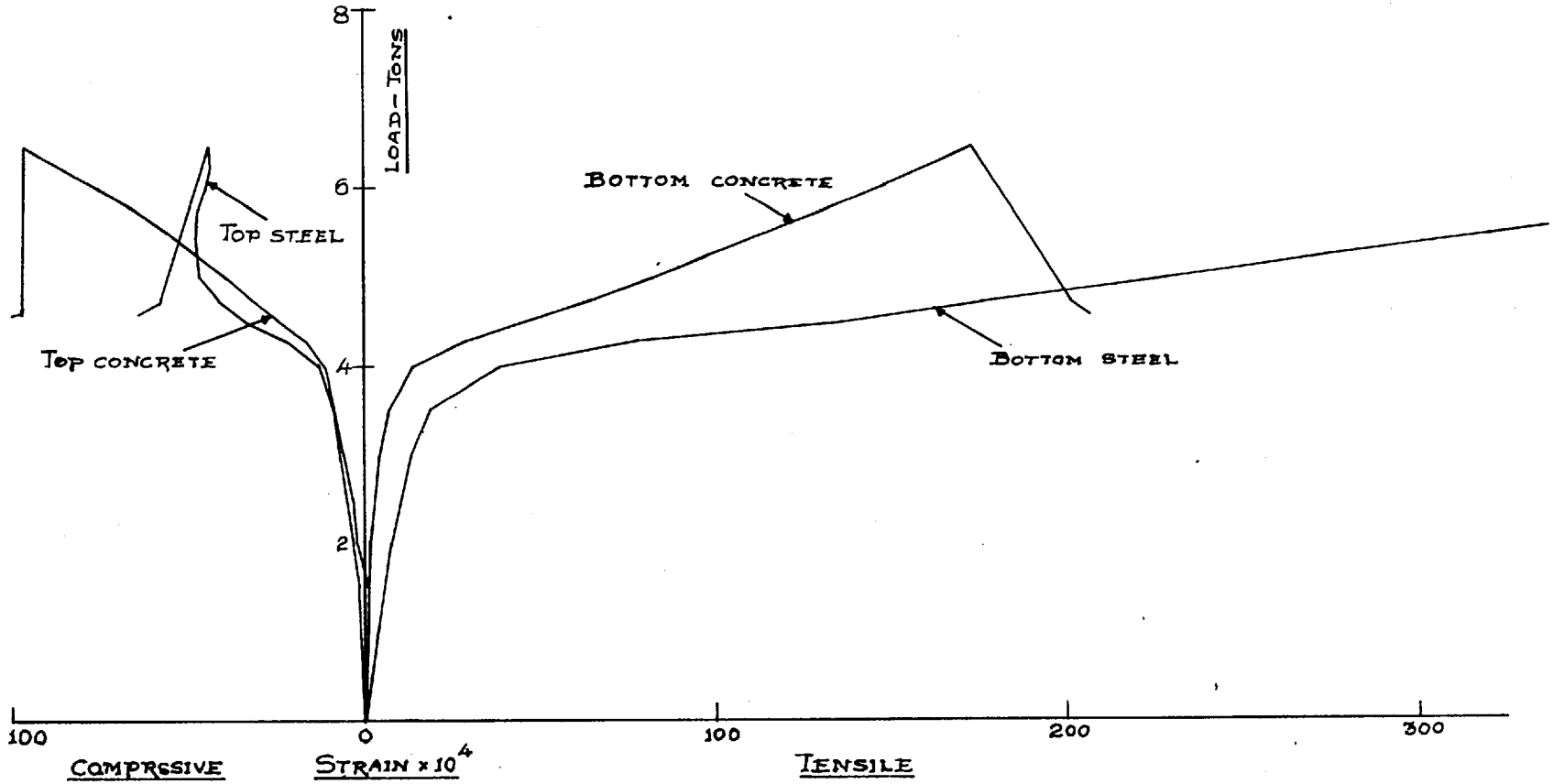


FIG. 76 STRAINS AT MIDSPAN SECTION - BEAM B7 WITH 44 - 3/16 IN. DIA. HEADED STUDS 1 IN. LONG. STUDS COVERED WITH LATEX AT BASE

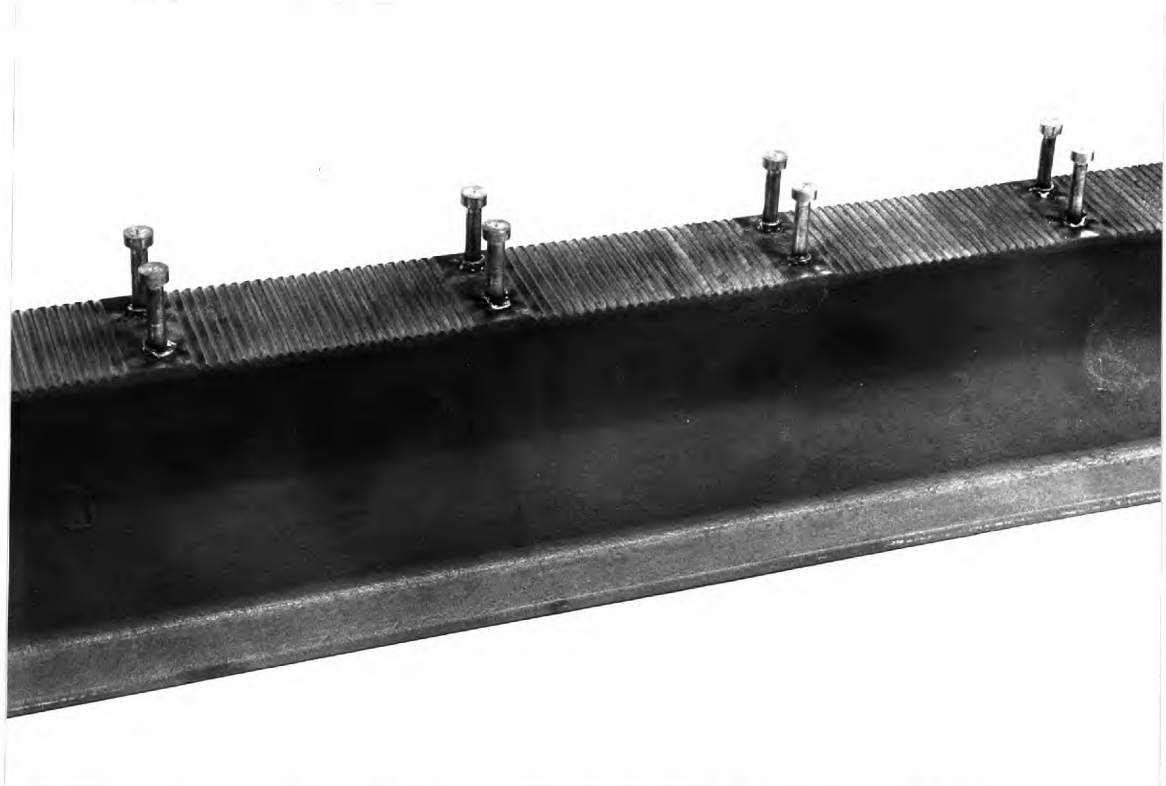


Figure 77. Beam with V-grooves on top flange (A1)

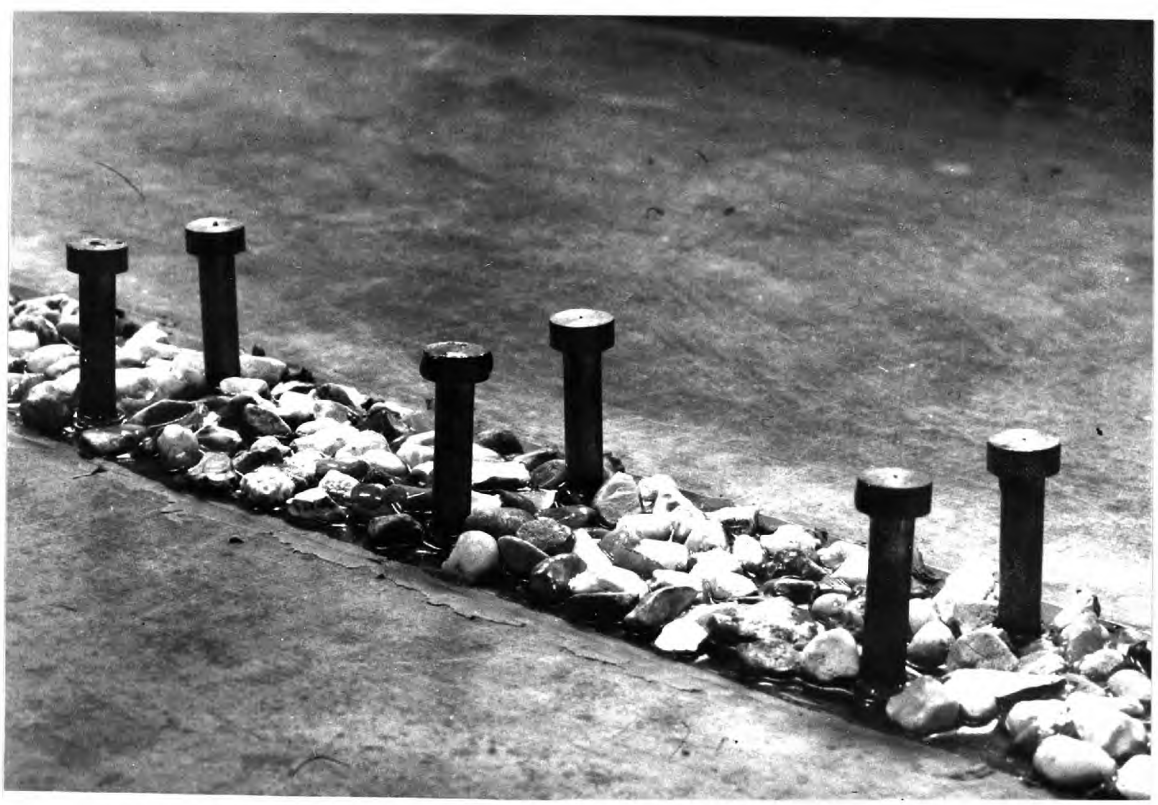


Figure 78. Resin bonded aggregates on top flange of beam B5

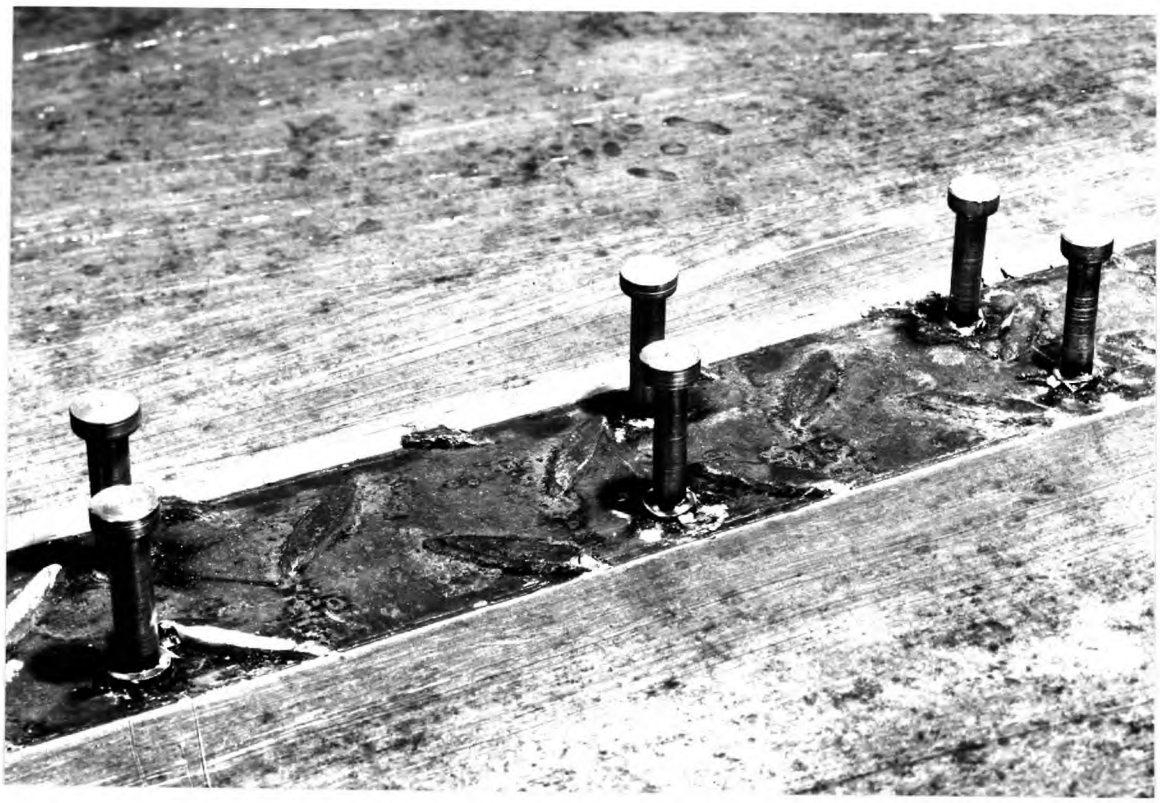


Figure 79. Beam with a Durbar plate as top flange (B6)

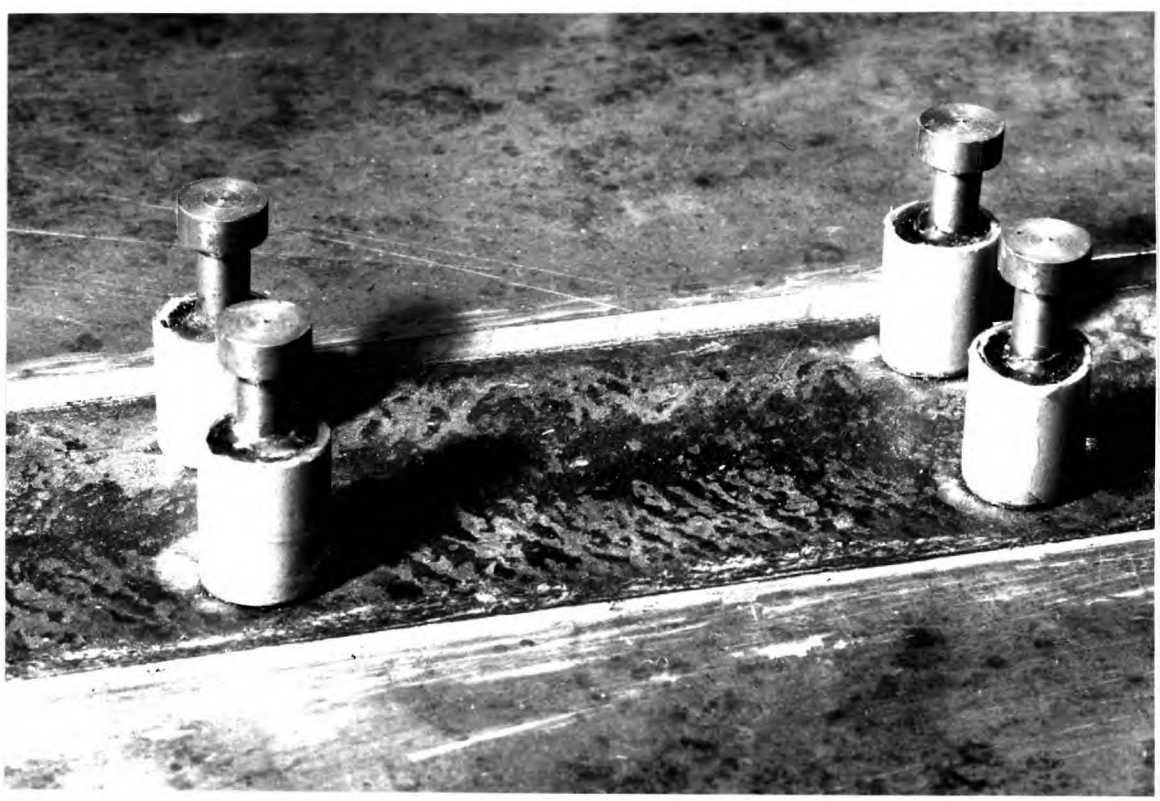


Figure 80. Beam with studs covered at the base with latex

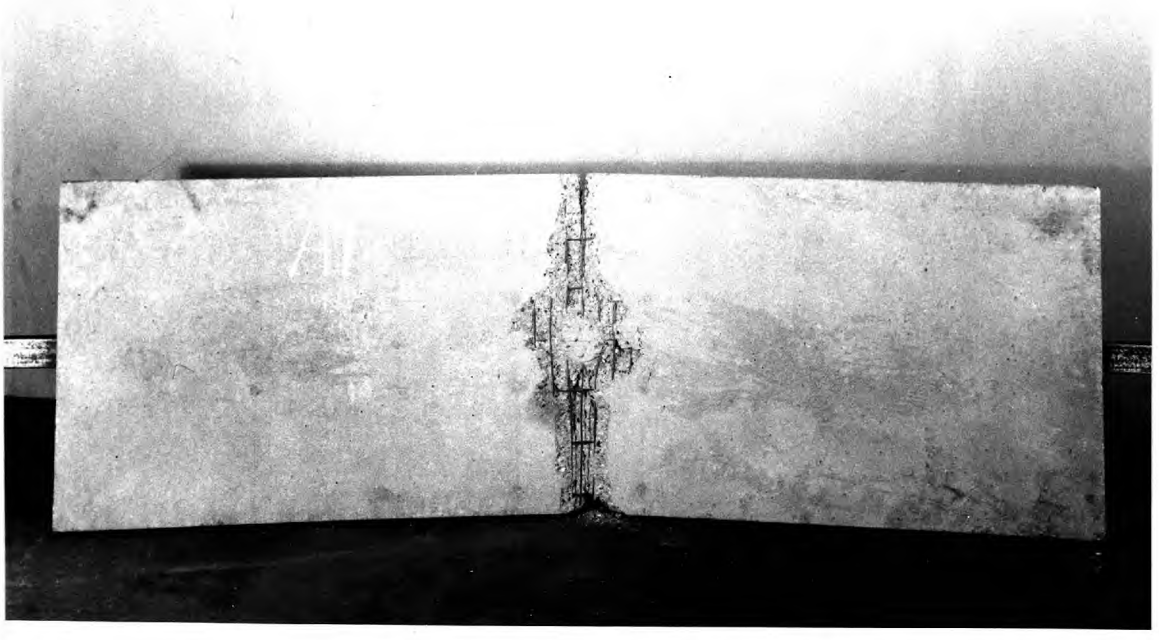


Figure 82. Crushing of concrete on top of the slab (Beam A1)

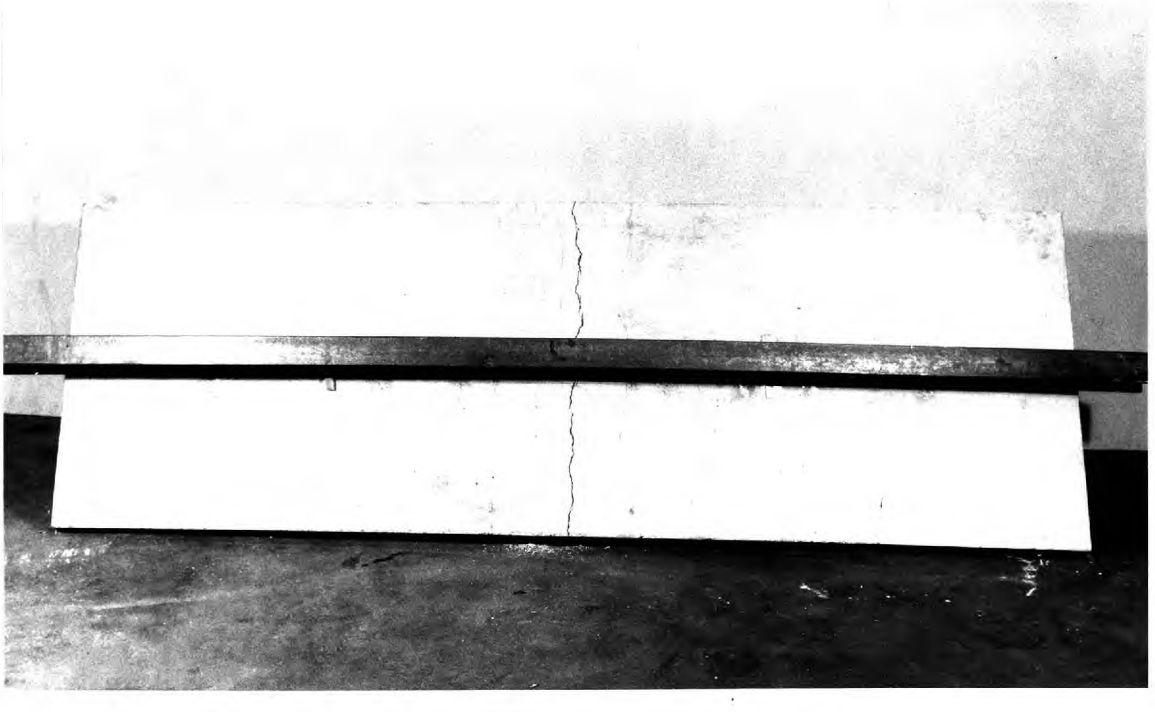


Figure 83. Typical transverse tension cracks at the bottom of the slab (Beam B4)

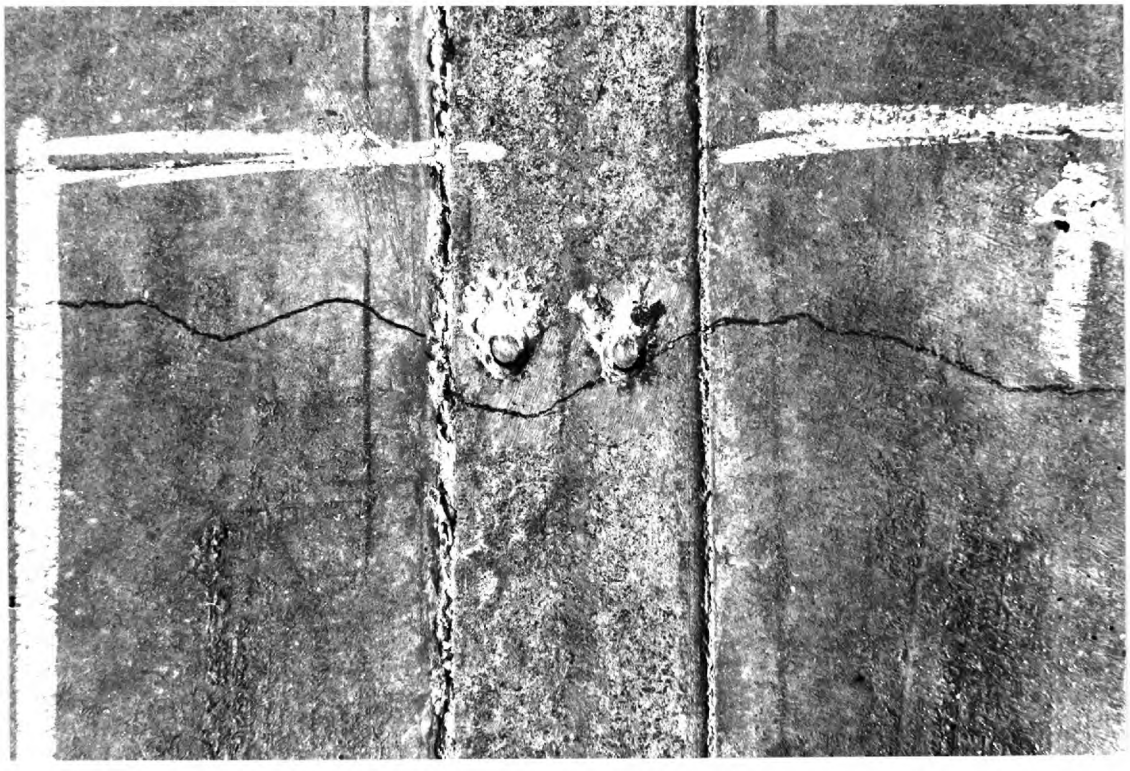


Figure 84. Underside of concrete slab near midspan of beam B4 after failure (steel beam removed)

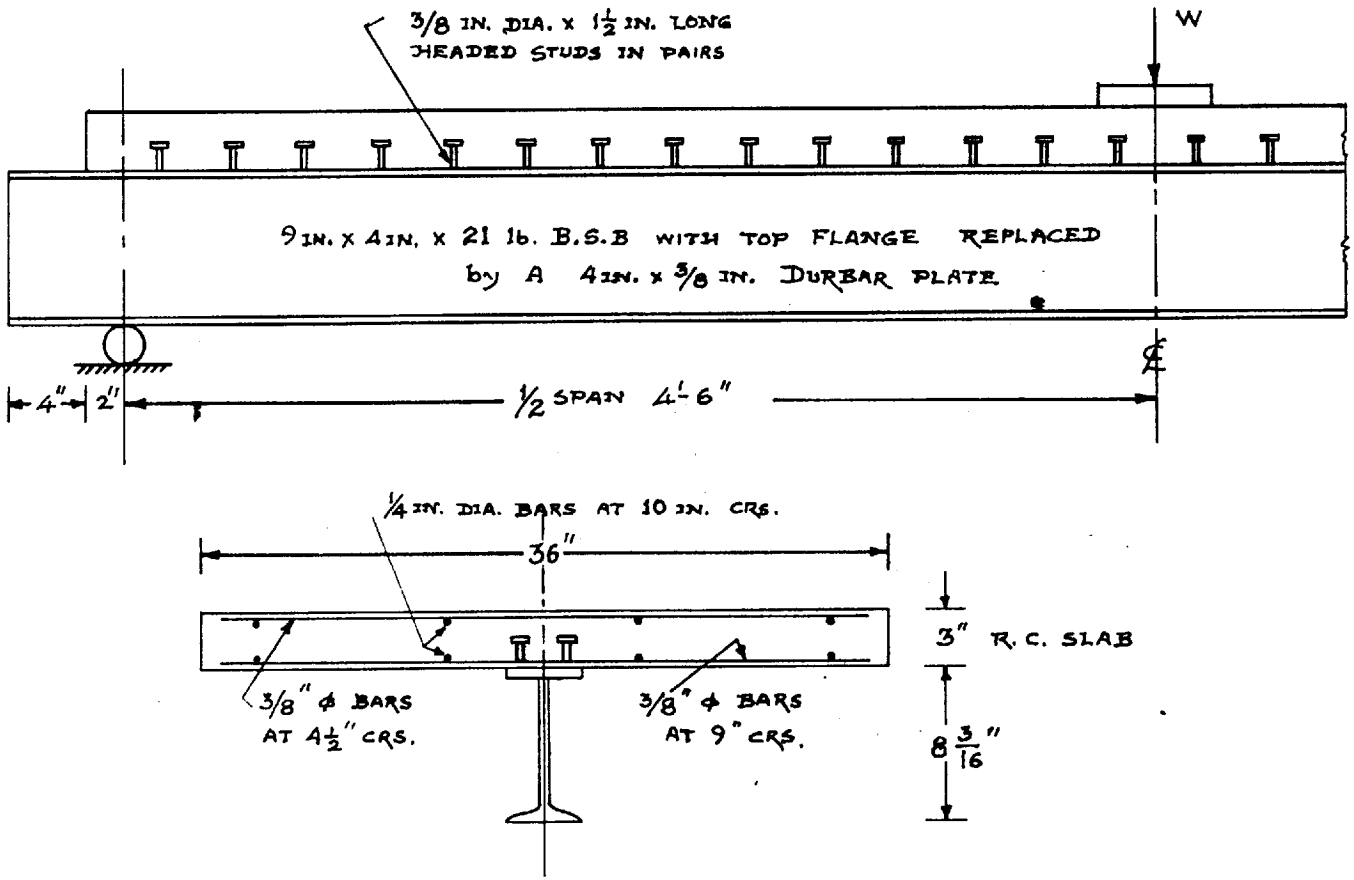


FIG. 85 DETAILS OF HALF SCALE COMPOSITE BEAMS - D1 AND D2

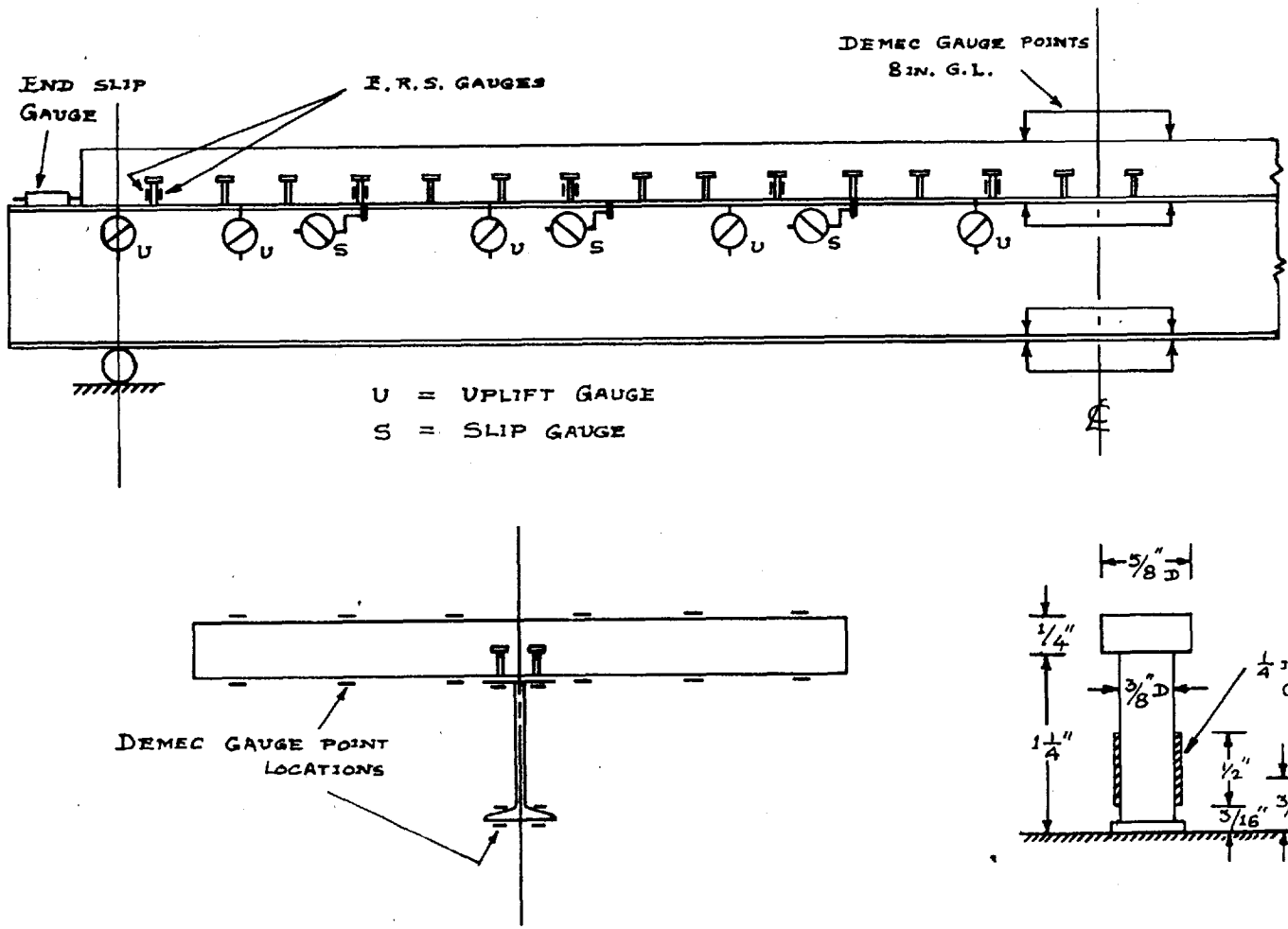


FIG. 86 GENERAL ARRANGEMENT FOR MEASUREMENT IN HALF SCALE BEAMS

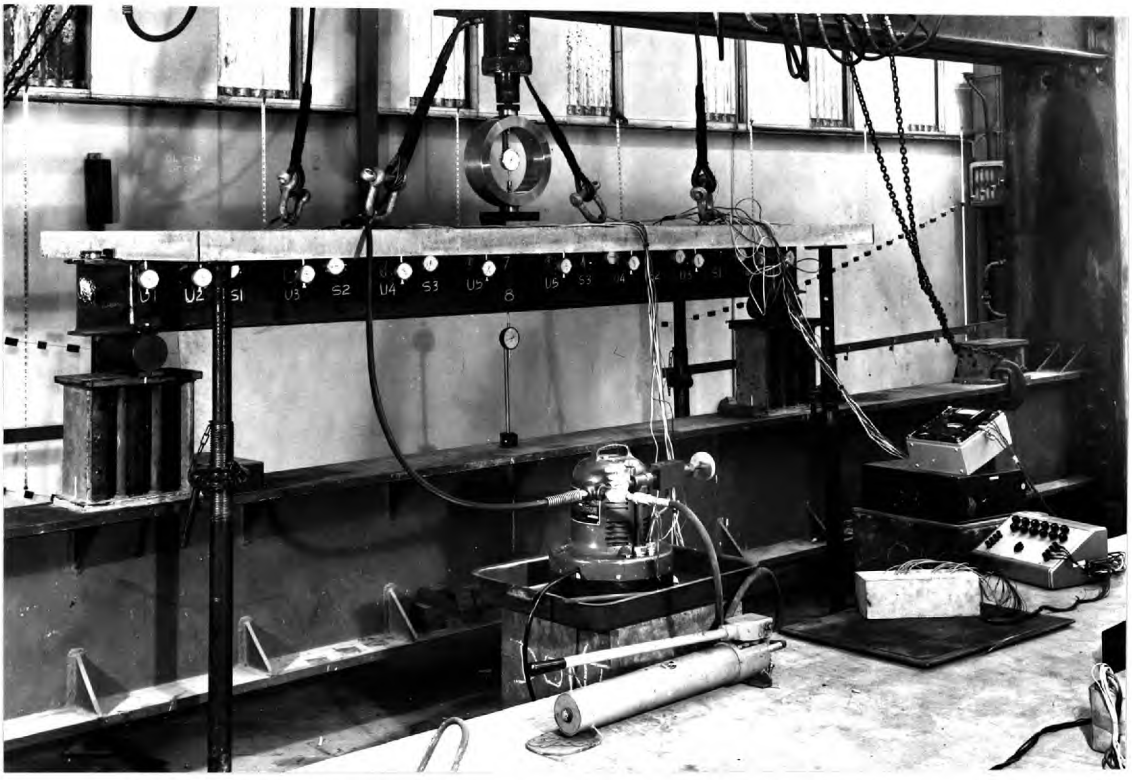


Figure 87. Set up of a half scale composite beam

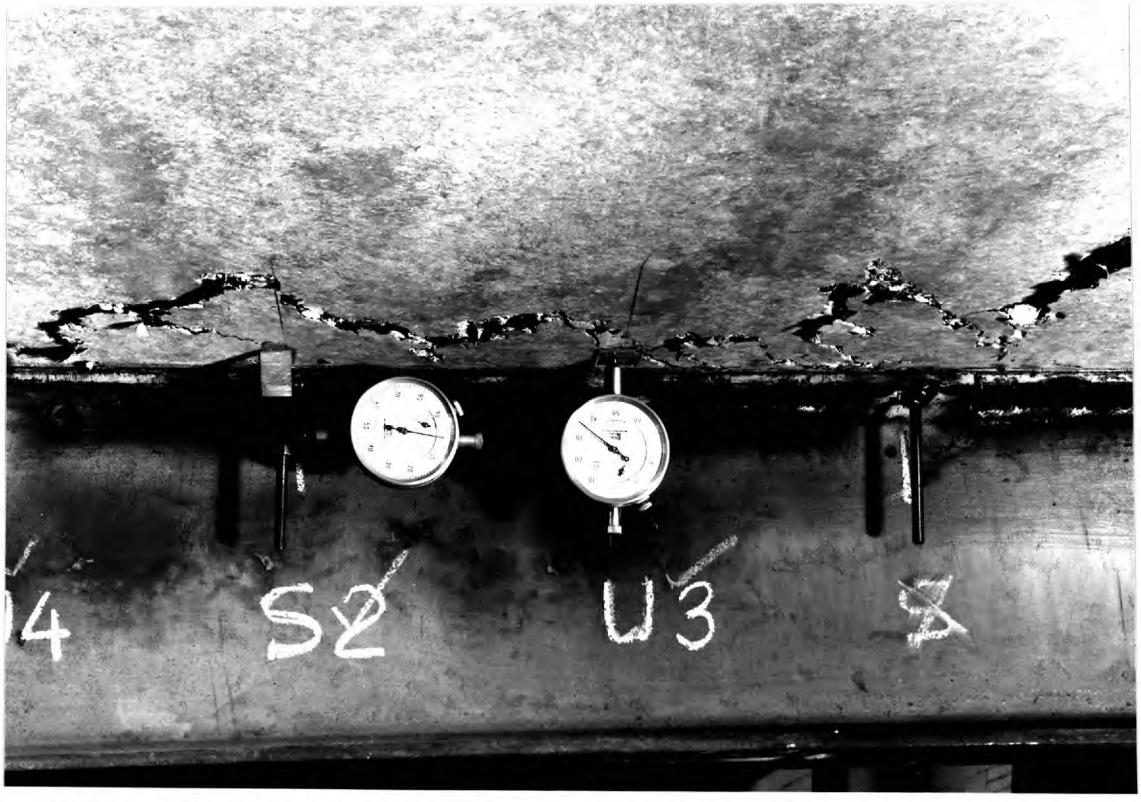


Figure 102. Failure of concrete around the studs in beam D2

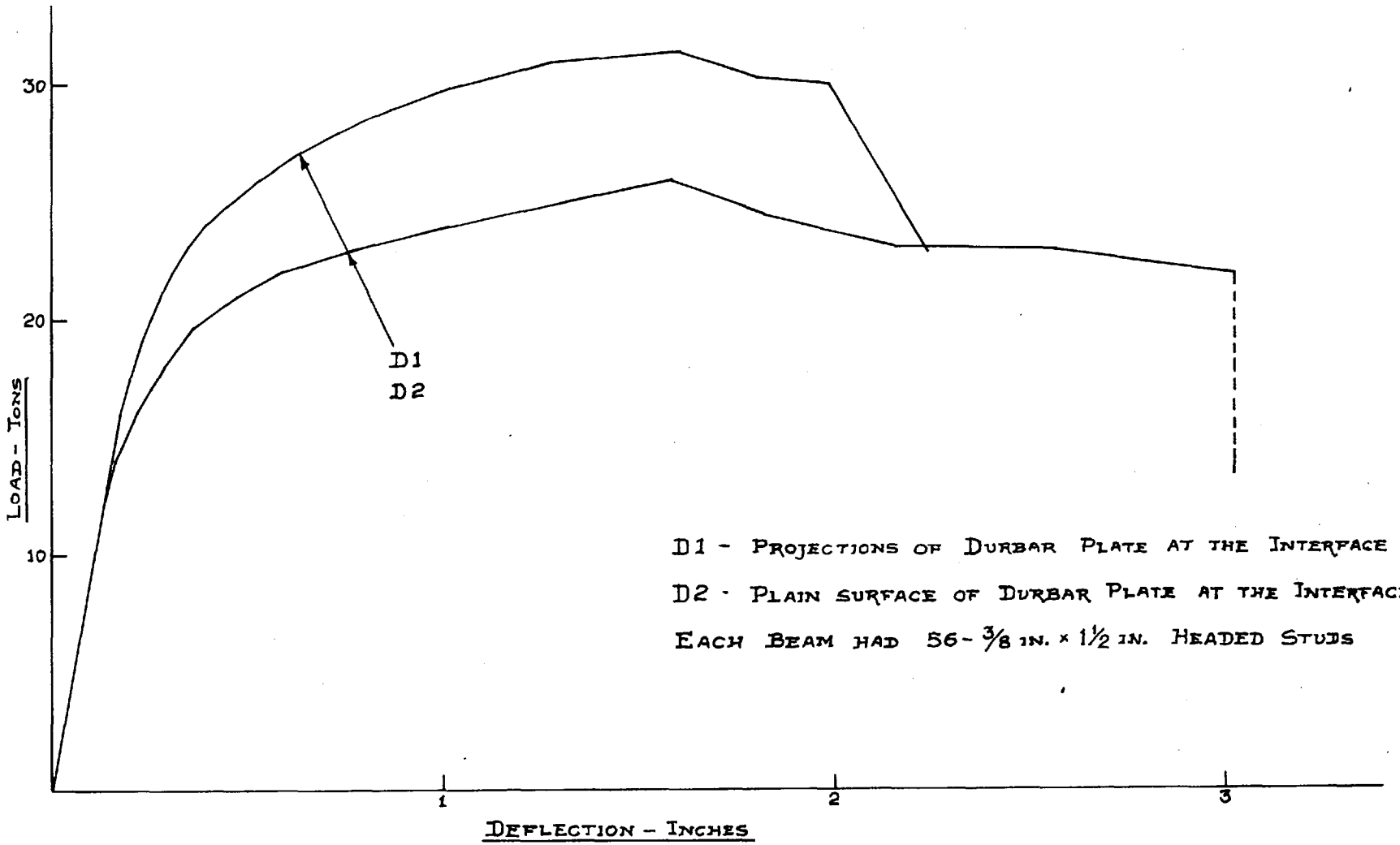


FIG. 88 MIDSPAN DEFLECTIONS - DURBAR FLANGED BEAMS - POINT LOAD AT MIDSPAN

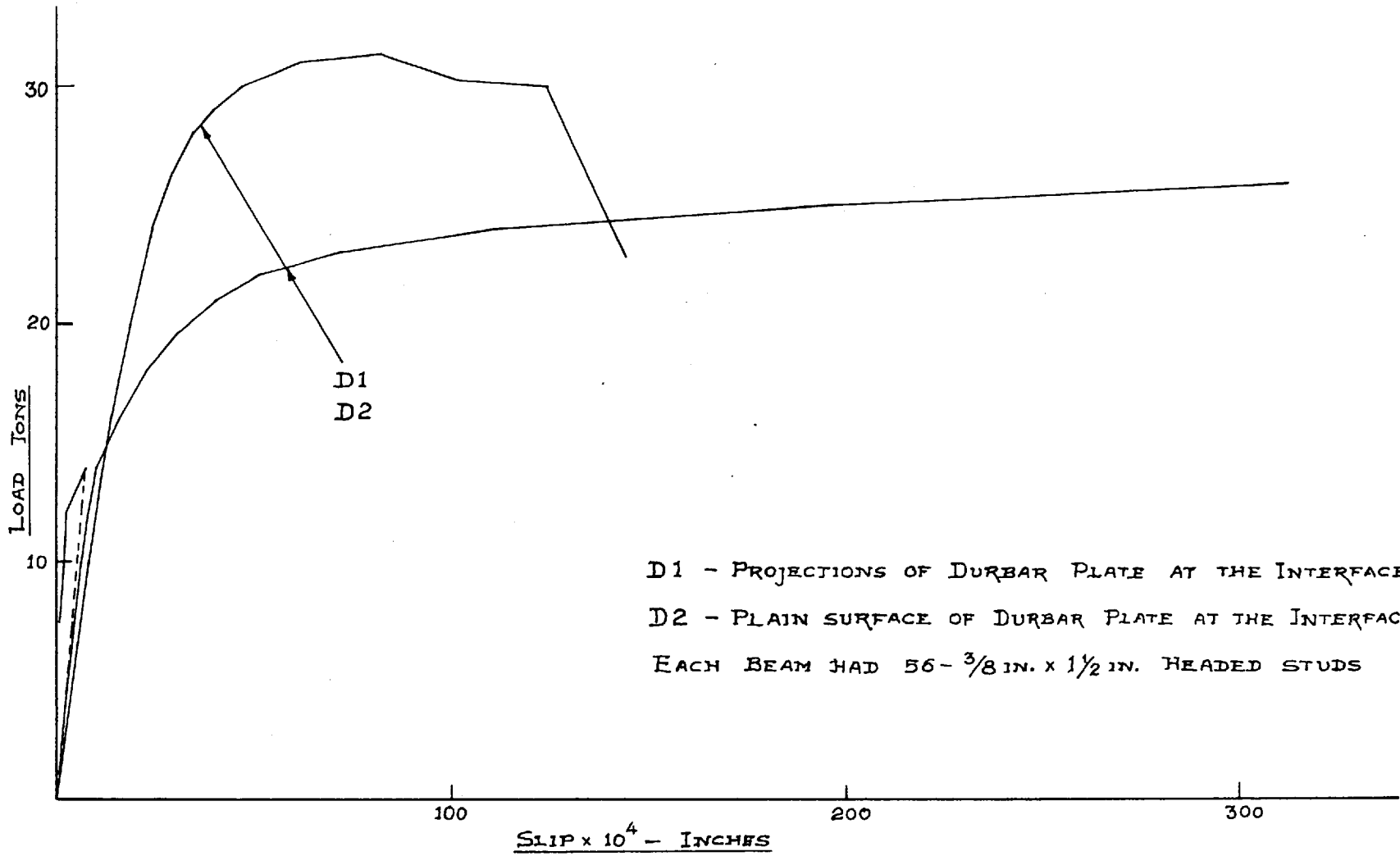


FIG. 89 AVERAGE END SLIPS - DURBAR FLANGED BEAMS - POINT LOAD AT MIDSPAN

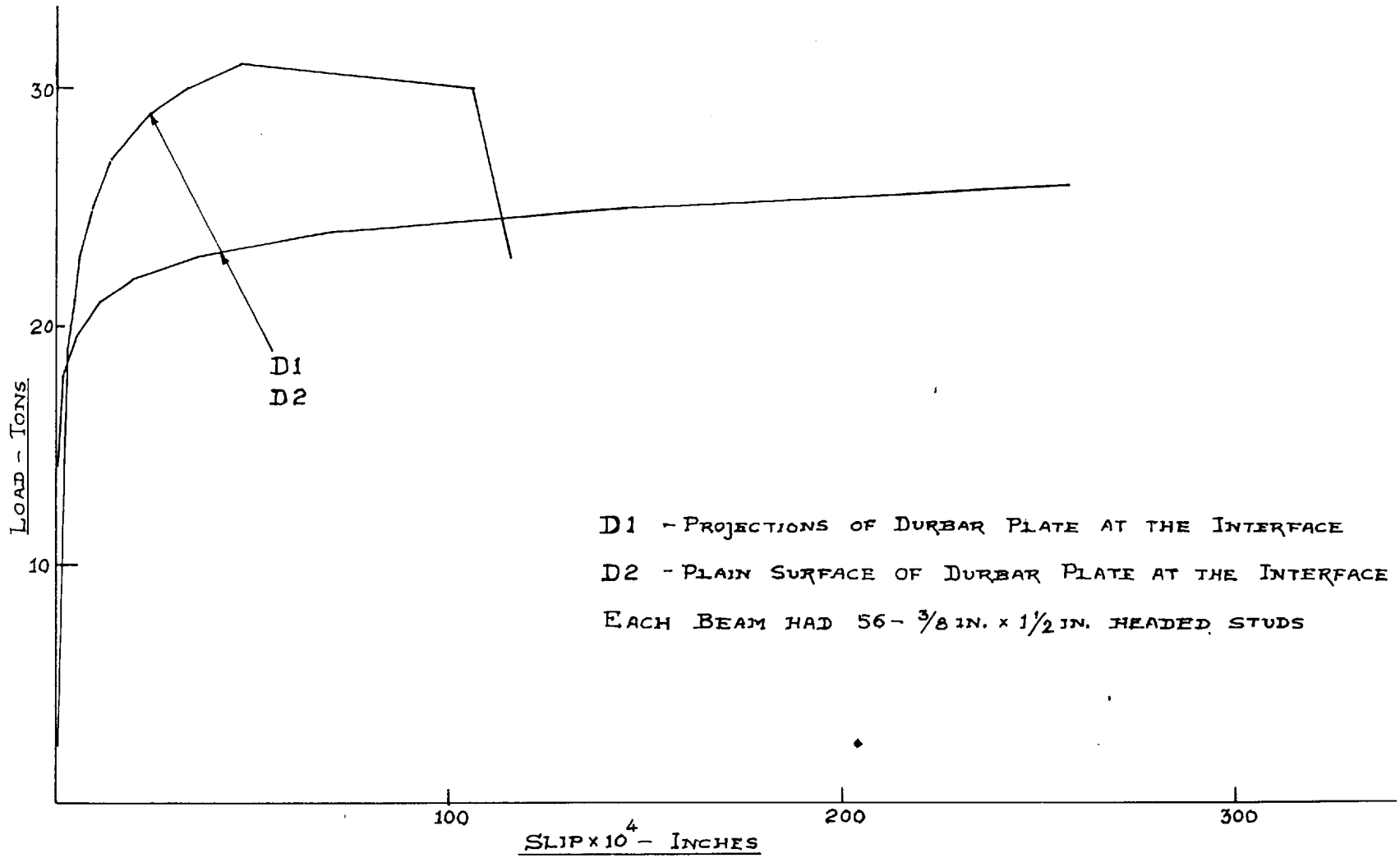


FIG. 90 AVERAGE RESIDUAL SLIPS - DURBAR FLANGED BEAMS - POINT LOAD AT MIDSPAN

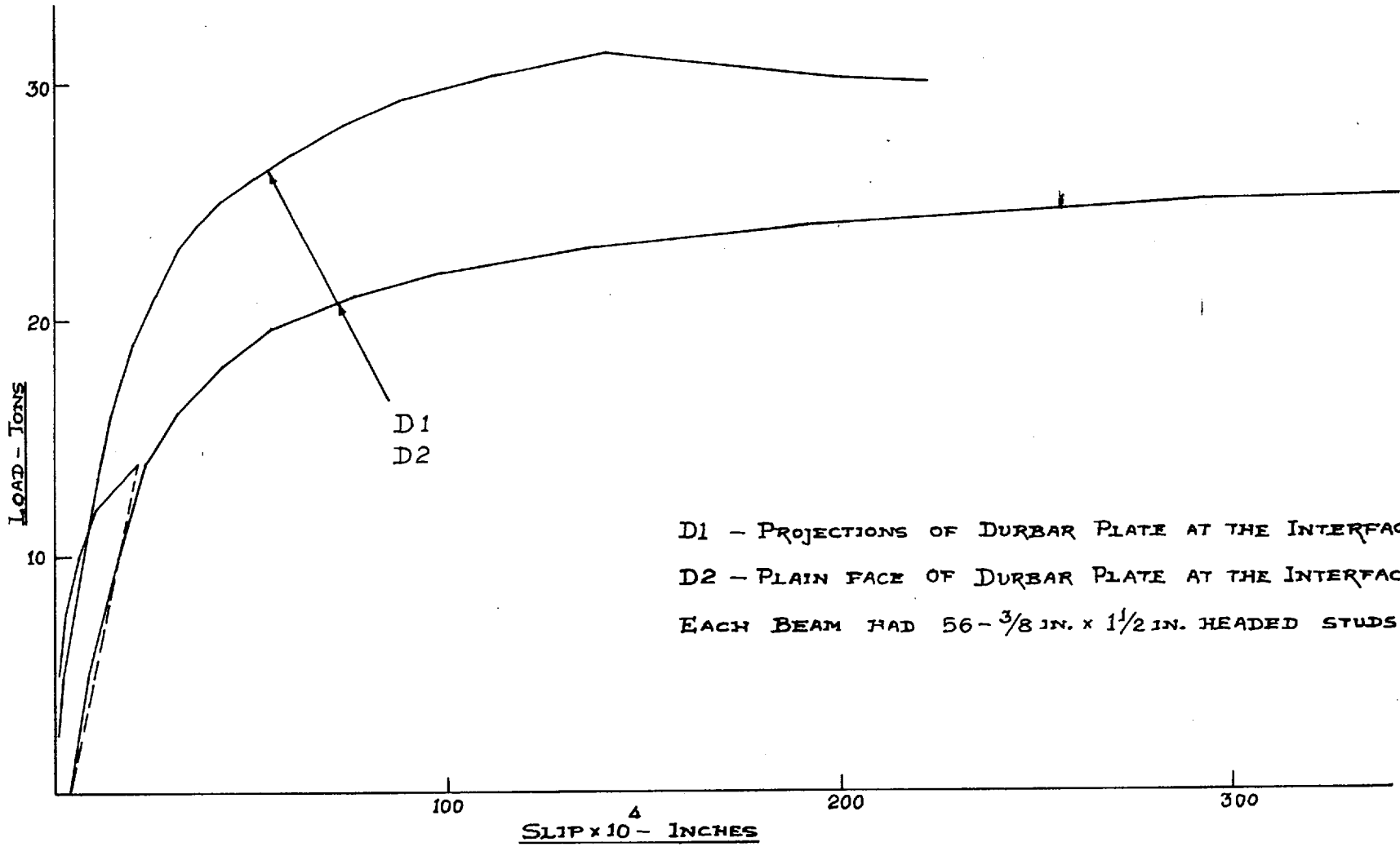


FIG. 91 AVERAGE SLIPS AT 1/4 SPAN — DURBAR FLANGED BEAMS - POINT LOAD AT MIDSPAN

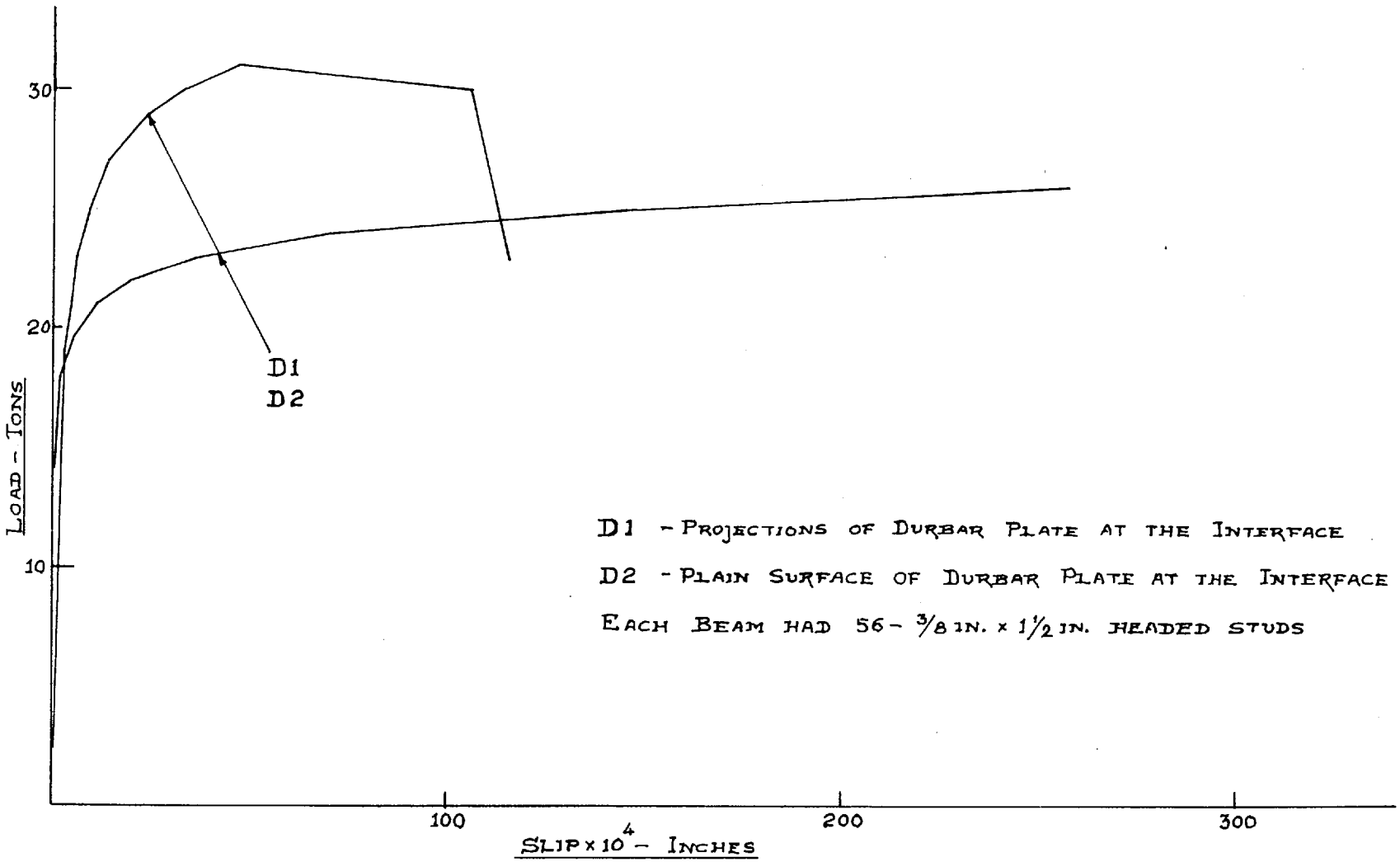


FIG. 90 AVERAGE RESIDUAL SLIPS - DURBAR FLANGED BEAMS - POINT LOAD AT MIDSPAN

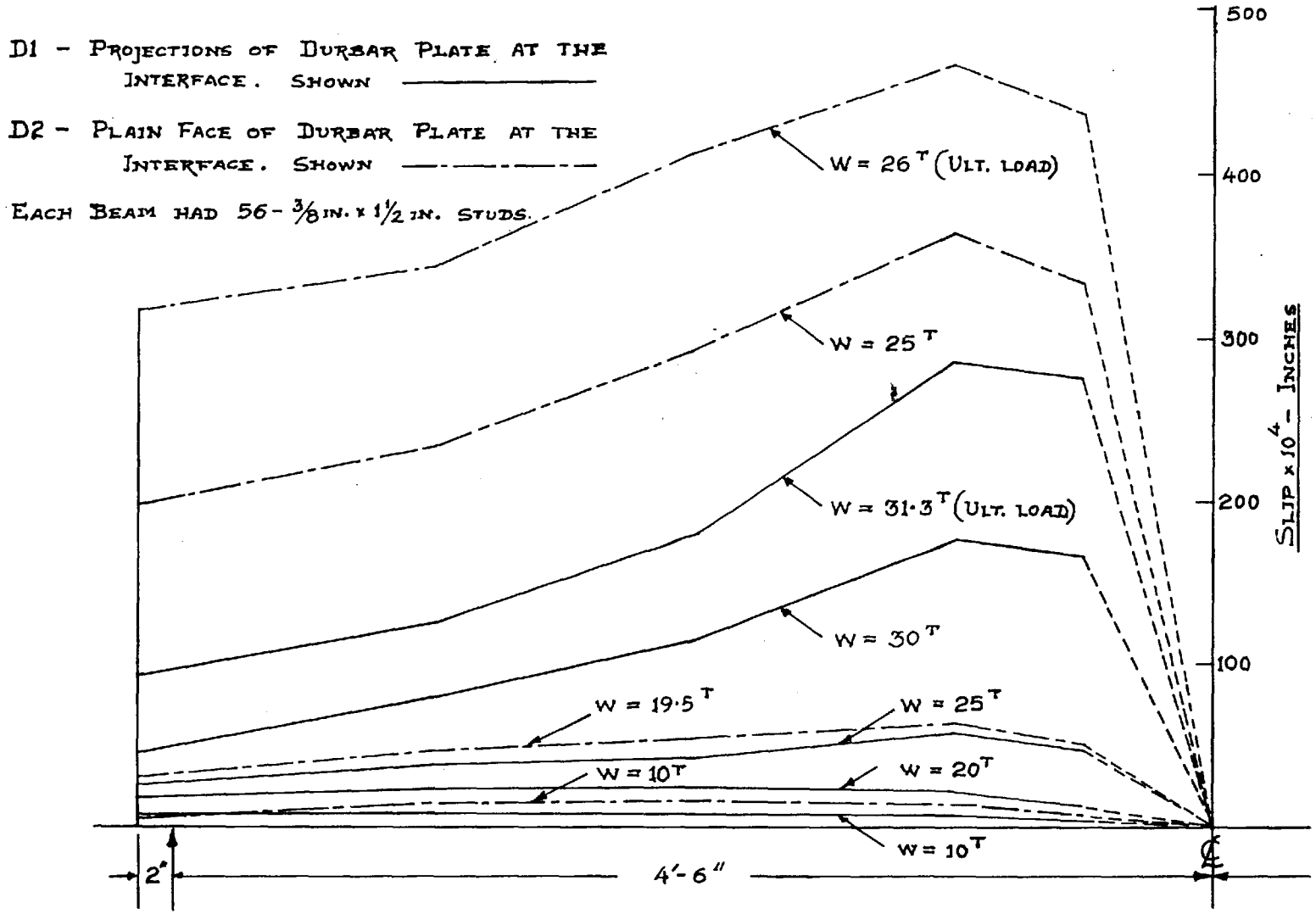


Fig. 92 Slips along the length - Durbar flanged beams - Point load at midspan

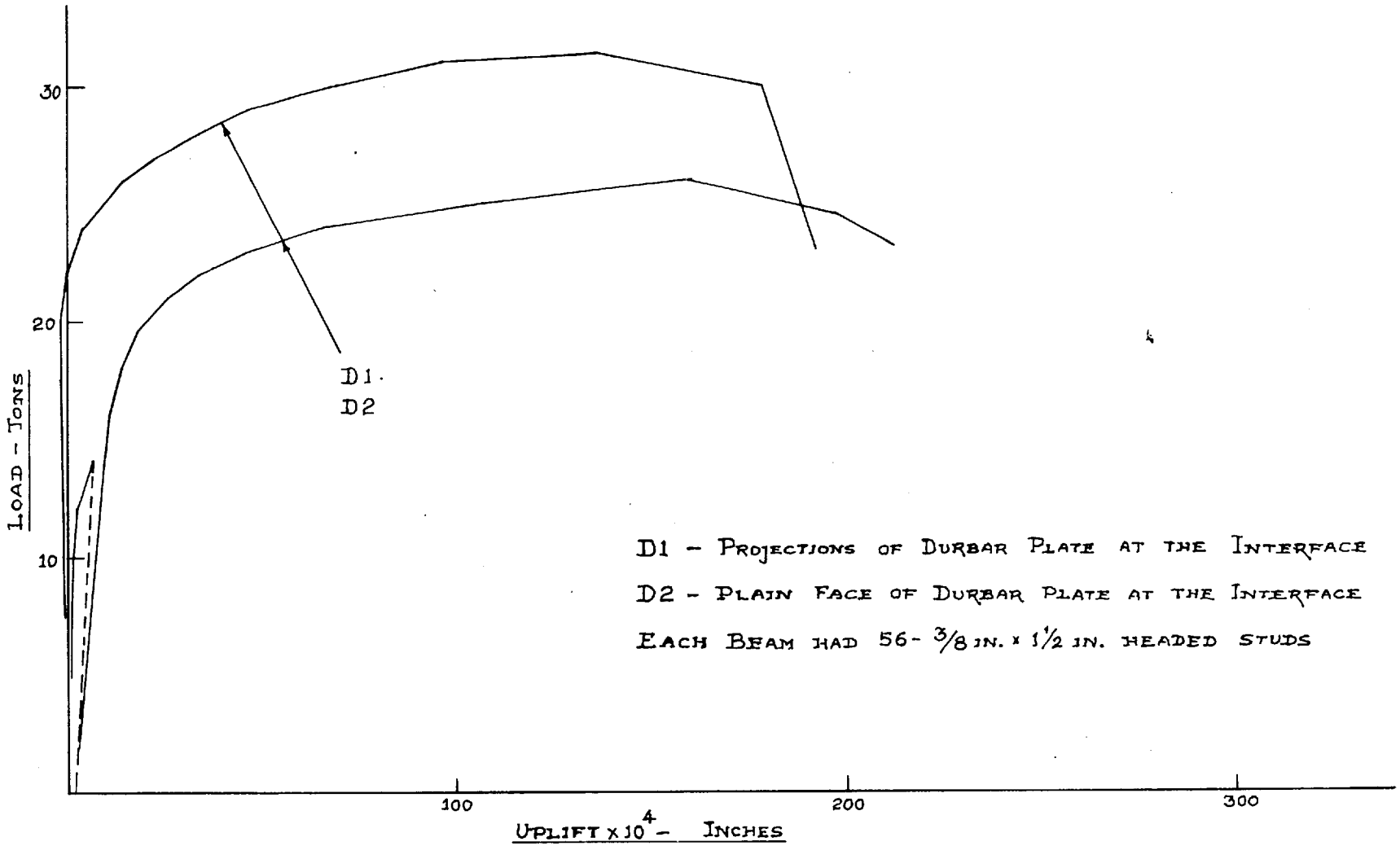


FIG. 93 AVERAGE UPLIFTS AT 1/4 SPAN —— DURBAR FLANGED BEAMS - POINT LOAD AT MIDSPAN

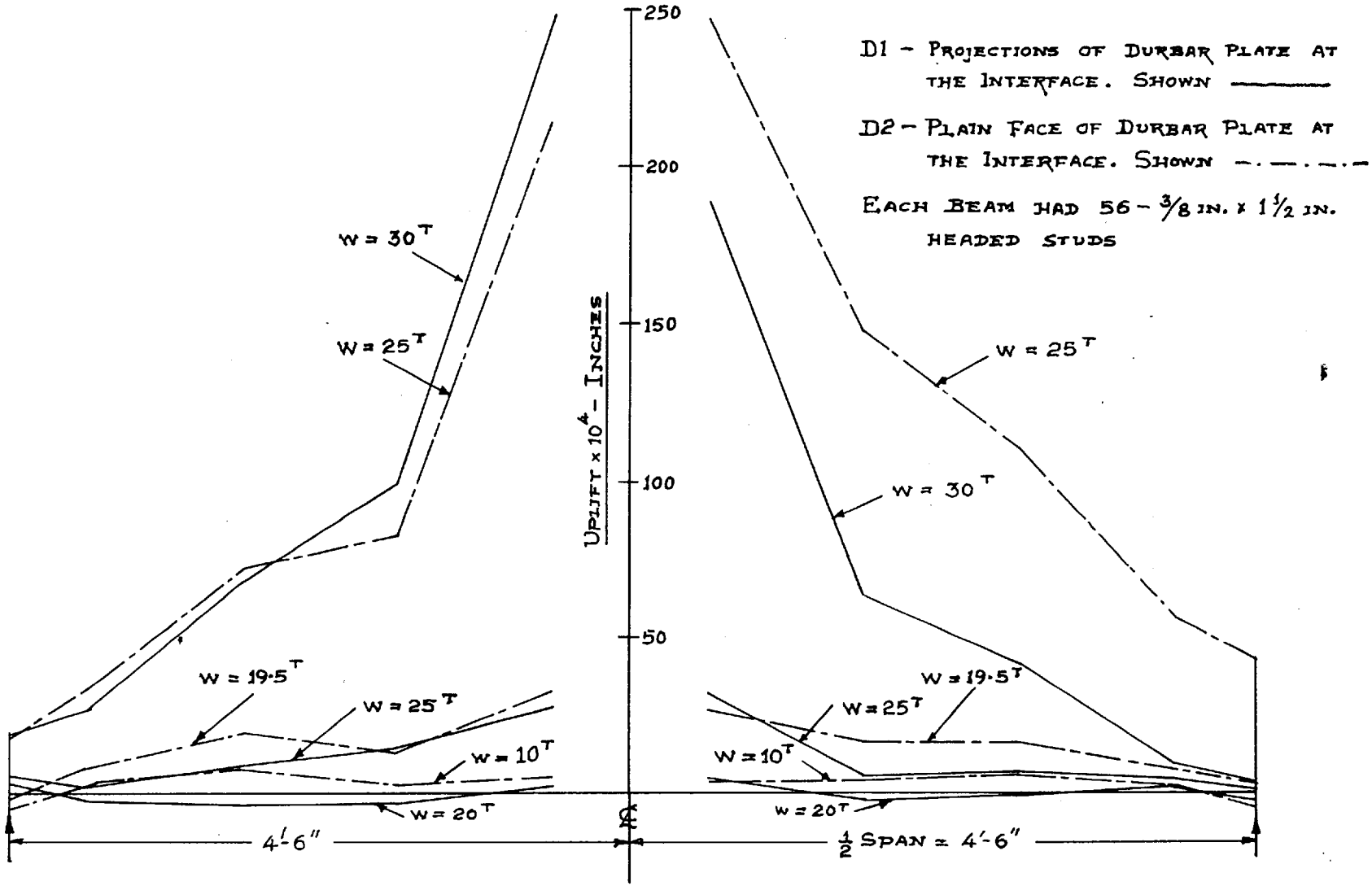


FIG. 94 UPLIFTS ALONG THE LENGTH - DURBAR FLANGED BEAMS - POINT LOAD AT MIDSPAN

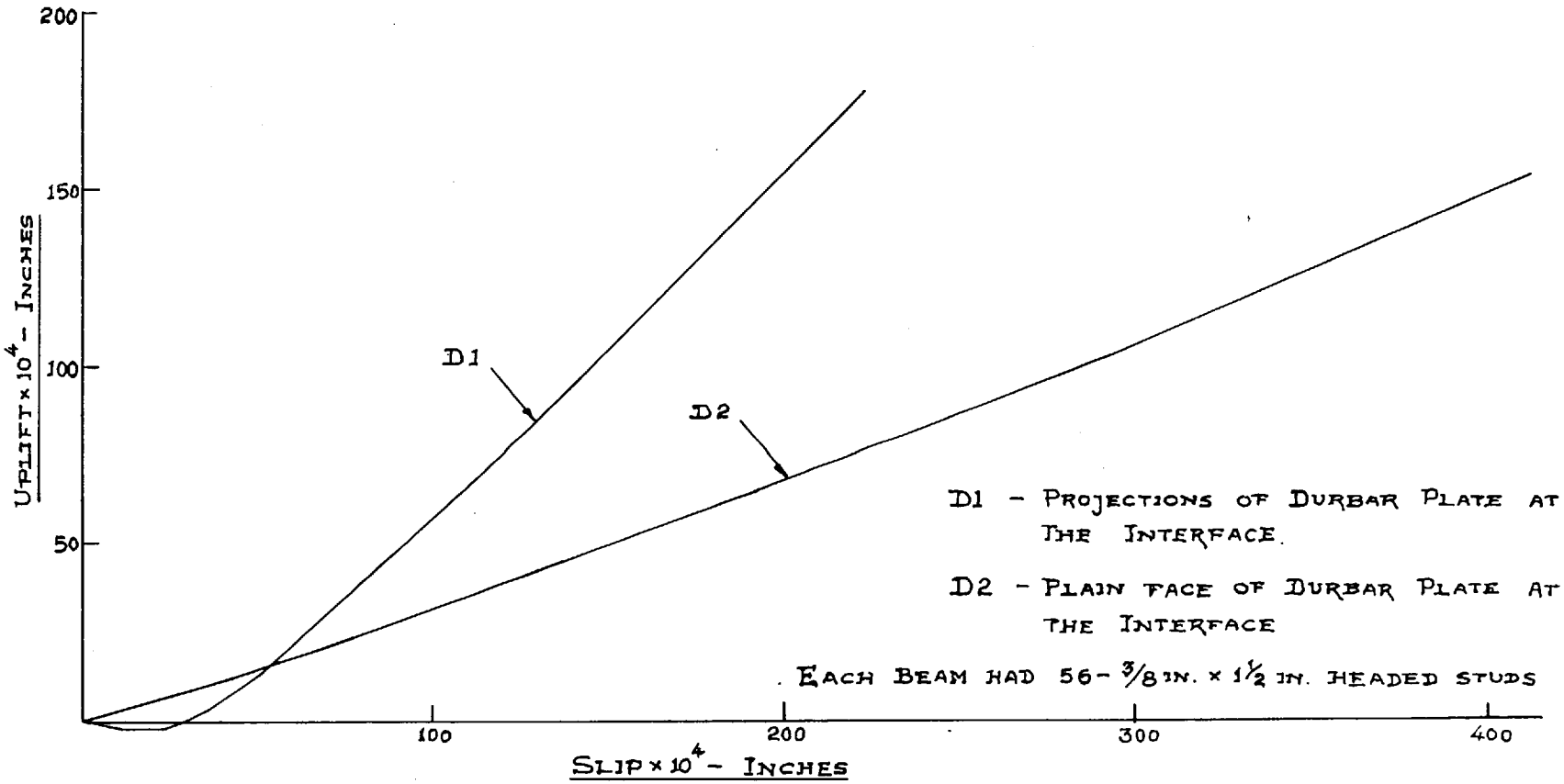


FIG. 95 UPLIFT-SLIP CURVES AT ¼ SPAN —— DURBAR FLANGED BEAMS
POINT LOAD AT MIDSPAN

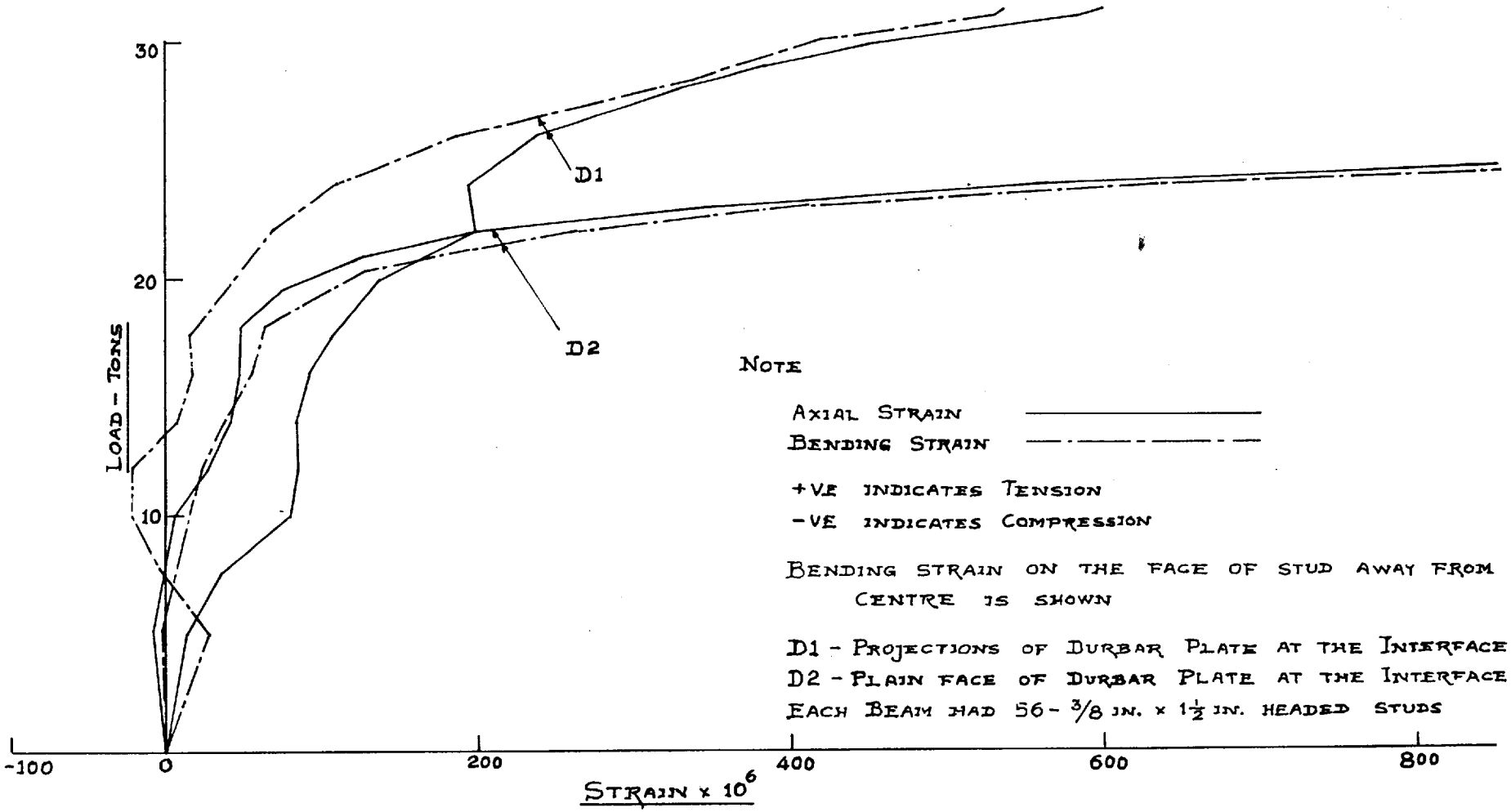


FIG. 96 AXIAL AND BENDING COMPONENTS OF MEASURED STRAINS IN STUDS AT ¼ SPAN POINT - DURBAR FLANGED BEAMS - POINT LOAD AT MIDSPAN

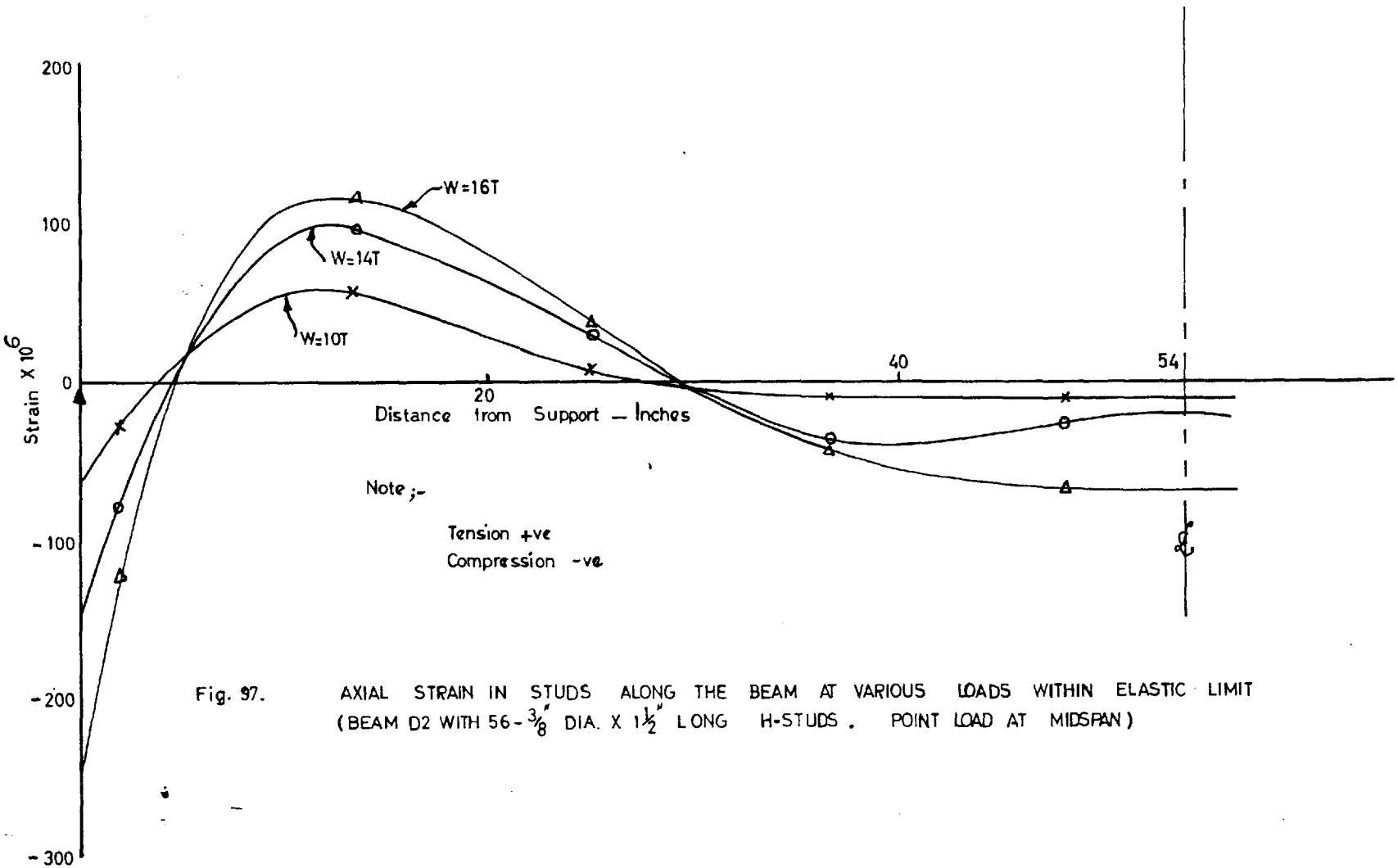
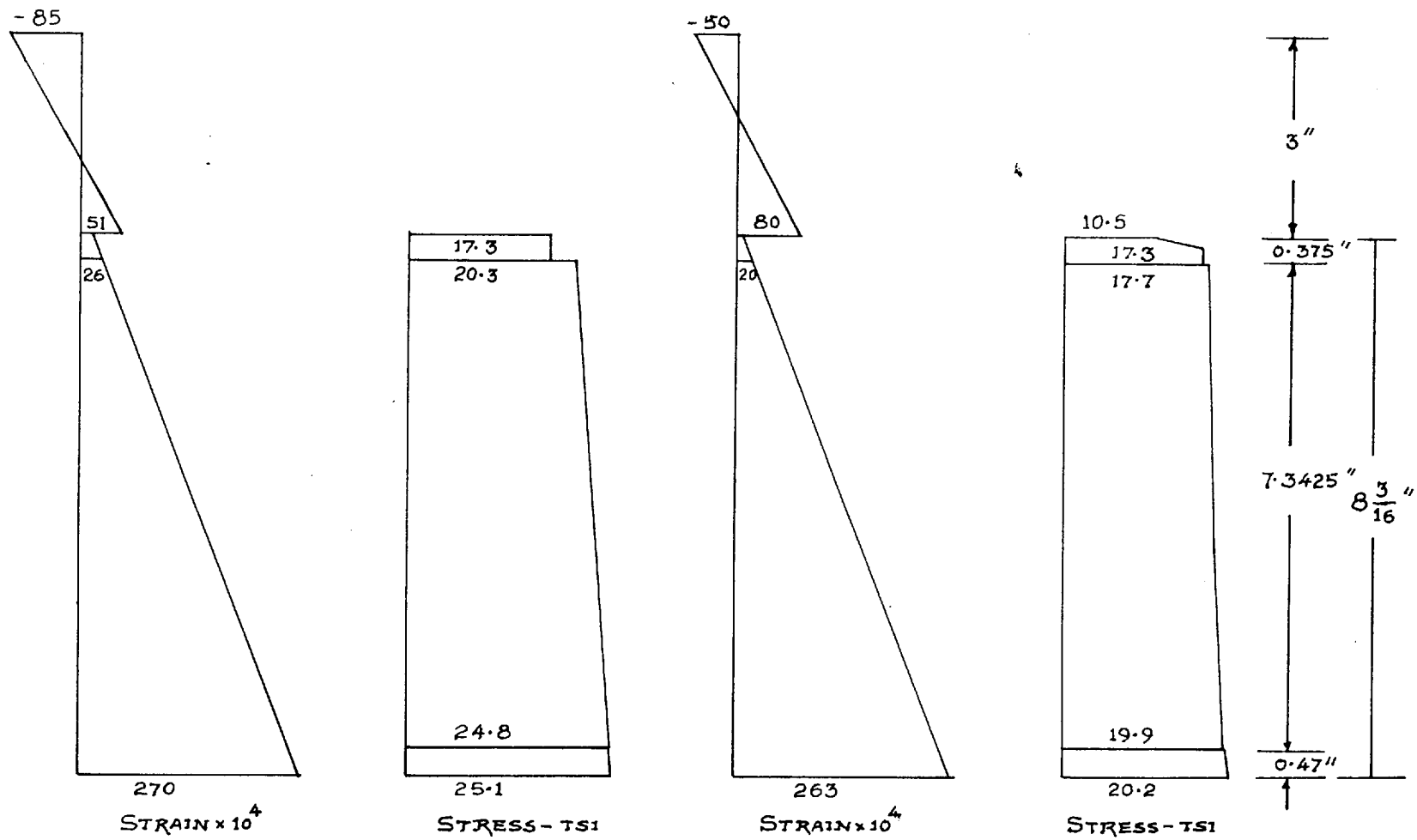


Fig. 97. AXIAL STRAIN IN STUDS ALONG THE BEAM AT VARIOUS LOADS WITHIN ELASTIC LIMIT (BEAM D2 WITH 56 - $\frac{3}{8}$" DIA. X $1\frac{1}{2}$" LONG H-STUDS . POINT LOAD AT MIDSPAN)



BEAM	D1	D2
FLANGE	ROUGH SURFACE AT THE INTERFACE	PLAIN SURFACE AT THE INTERFACE
LOAD - TONS	31·3	26·0

FIG. 98 MEASURED STRAINS AT MIDSPAN SECTION AT ULTIMATE LOAD AND CORRESPONDING STRESSES IN THE STEEL BEAMS - DURBAR FLANGED BEAMS.

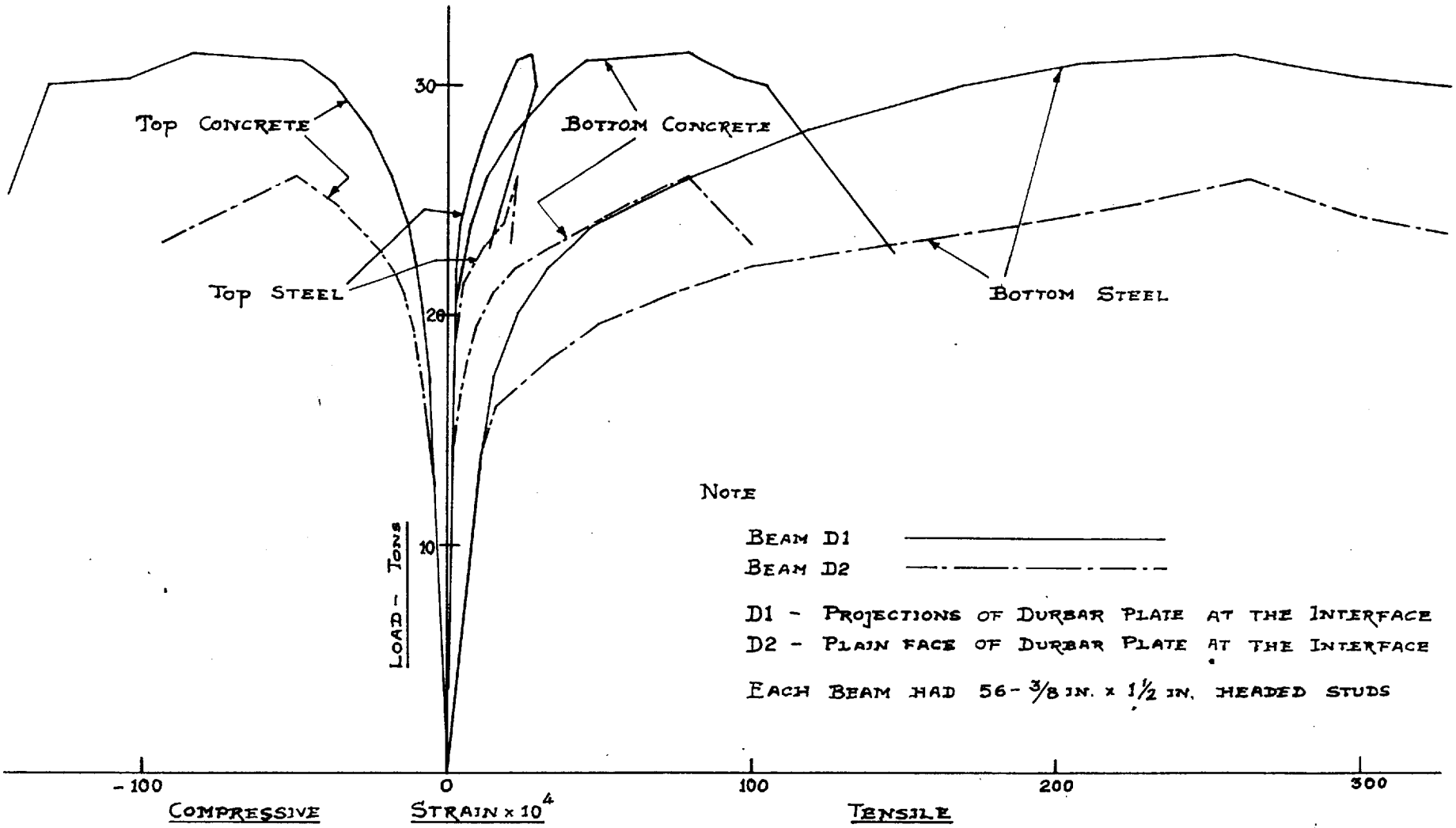


Fig. 99 Strains at Midspan Section - Durbar Flanged Beams - Point Load at Midspan

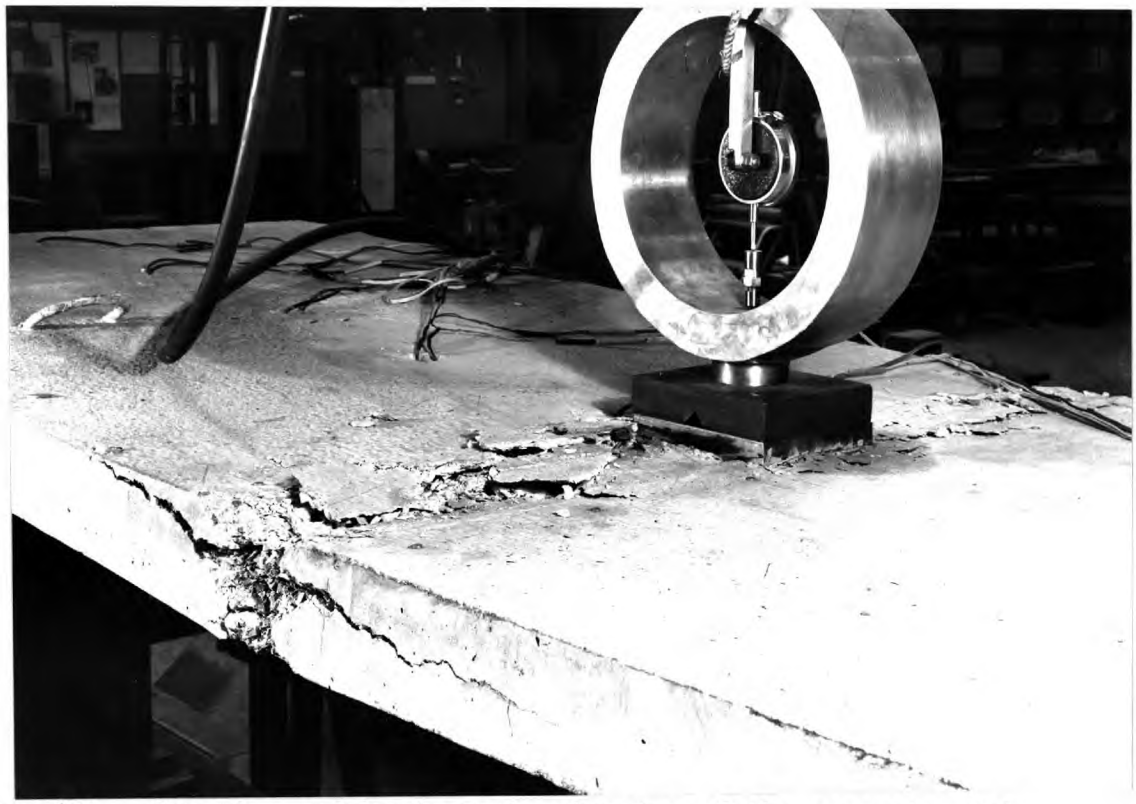
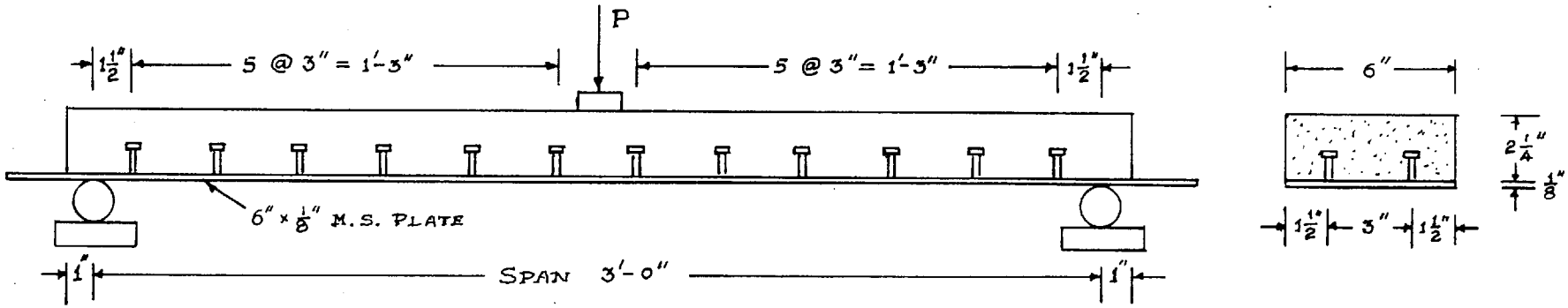


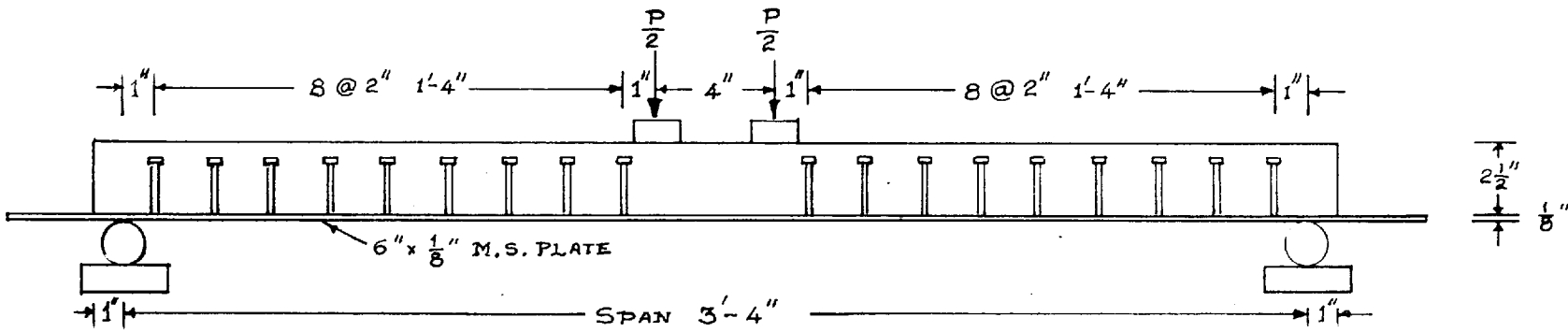
Figure 100. Crushing and horizontal splitting of the concrete slab after failure (Beam D1)

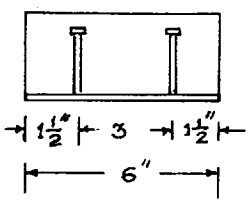


Figure 101. Tension cracks at the bottom of the concrete slab after failure (Beam D1)

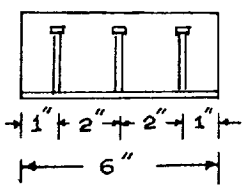


(a) PB2 AND PB3 — EACH WITH 24 - 3/16 IN. DIA. HEADED STUDS 1 IN. LONG.

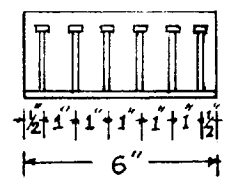




PB4 - 36 - ⅛ IN. DIA. x 2 IN. LONG STUDS

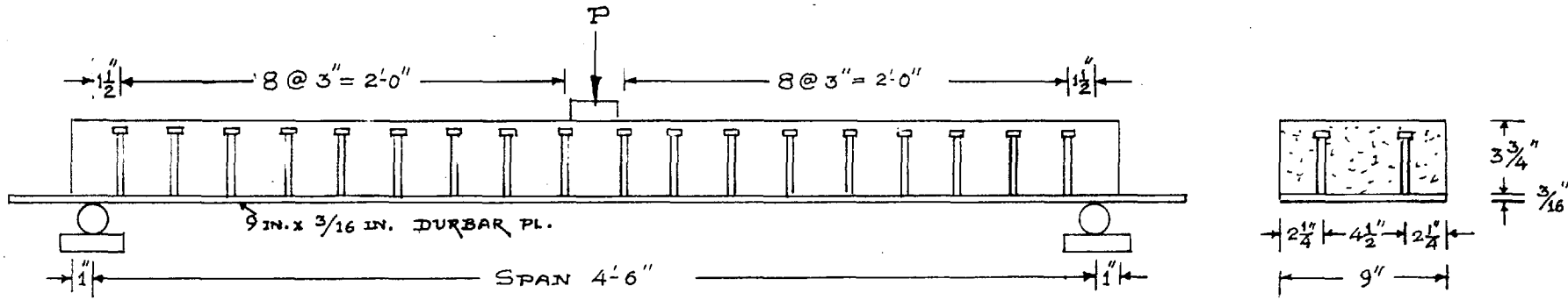


PB5 - 54 - ⅛ IN. DIA. x 2 IN. LONG STUDS



PB6 - 108 - ⅛ IN. DIA. x 2 IN. LONG STUDS.

FIG. 103 DETAILS OF PLATED BEAMS



PB7 AND PB8 - EACH WITH 36 - ¼ IN. DIA. HEADED STUDS 3½ IN. LONG.

FIG. 103 (CONTD) DETAILS OF PLATED BEAMS

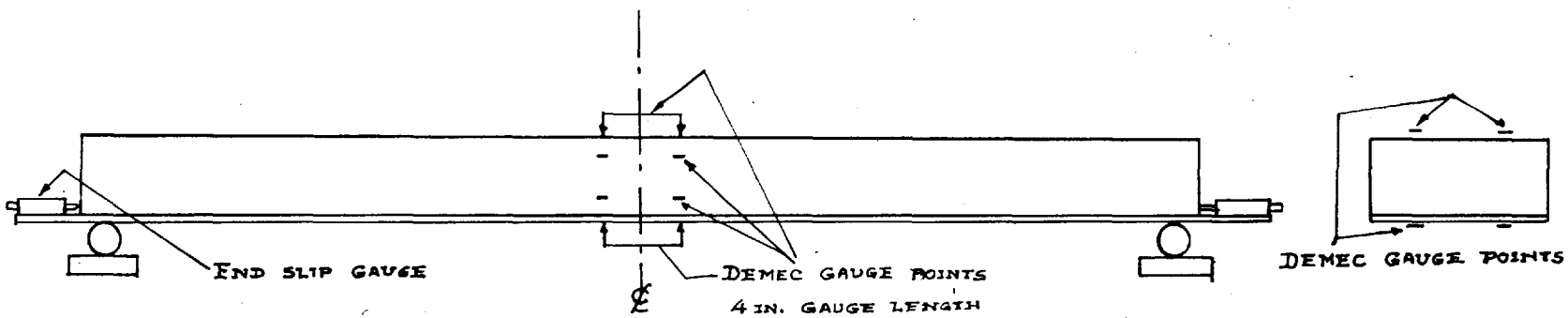


FIG. 104 GENERAL ARRANGEMENT FOR MEASUREMENTS IN PLATED BEAMS

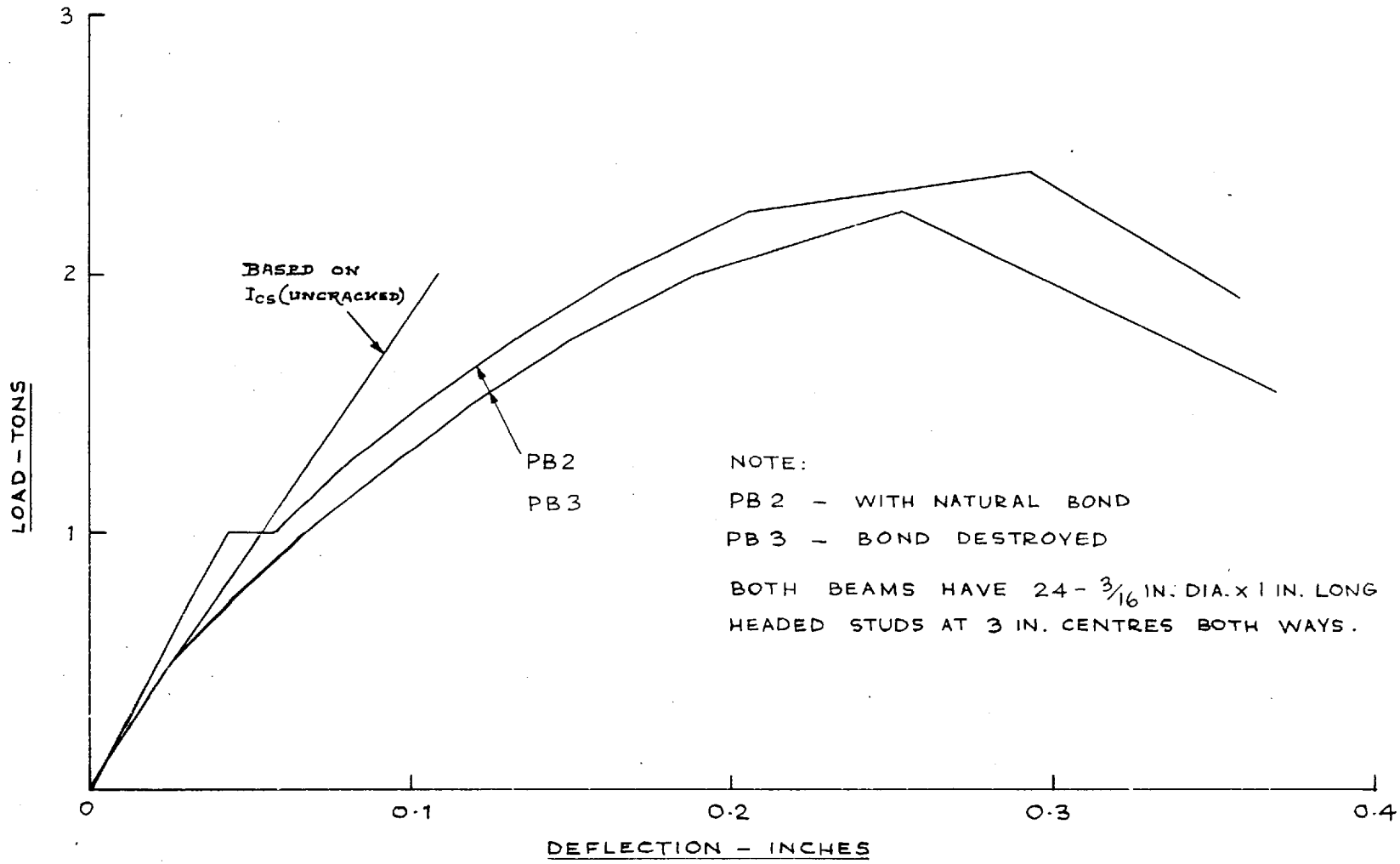


FIG. 105 MIDSPAN DEFLECTIONS — PLATED BEAMS PB2 AND PB3 — POINT LOAD AT MIDSPAN

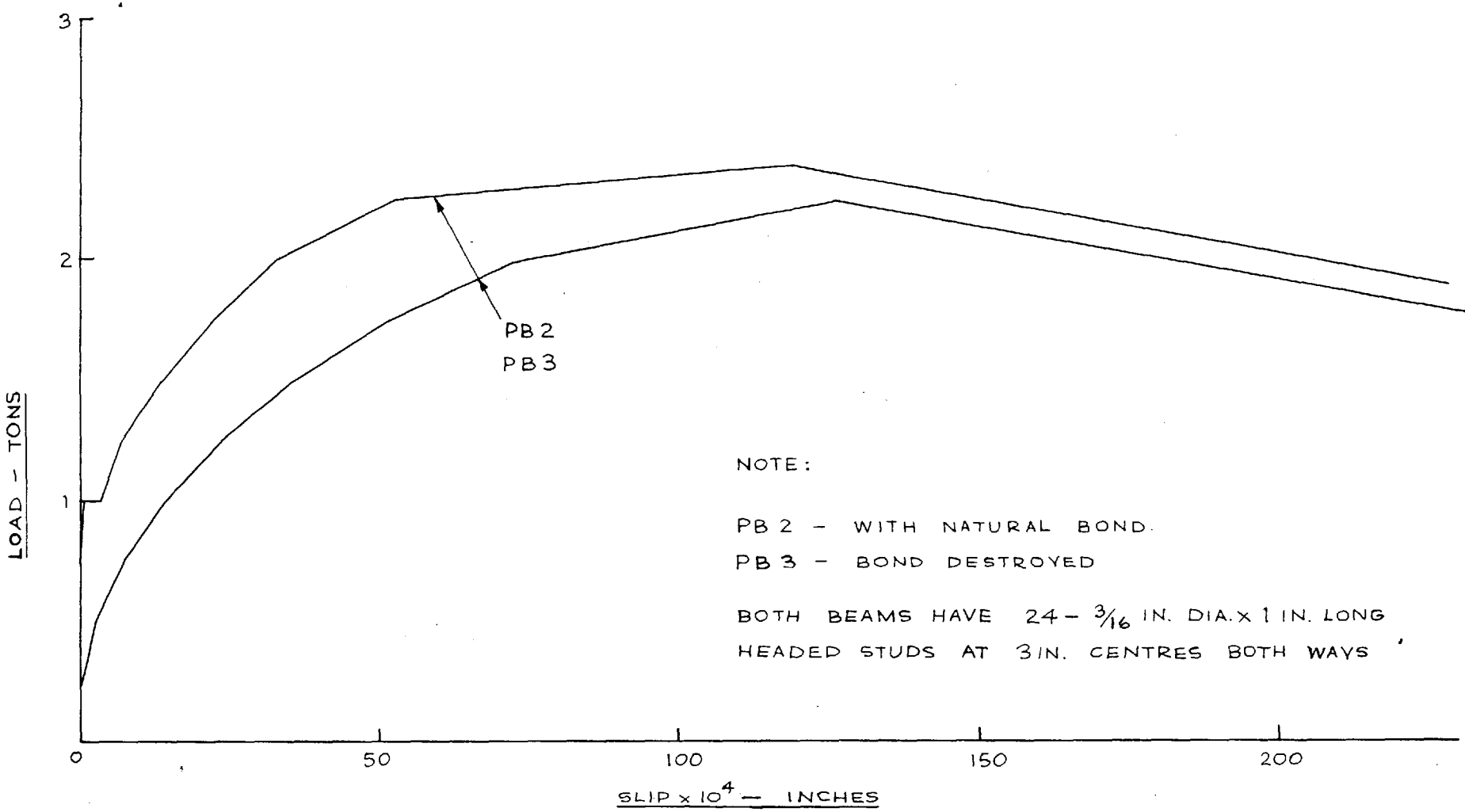


FIG. 106 AVERAGE END SLIPS — PLATED BEAMS PB 2 AND PB 3 — POINT LOAD AT MIDSPAN

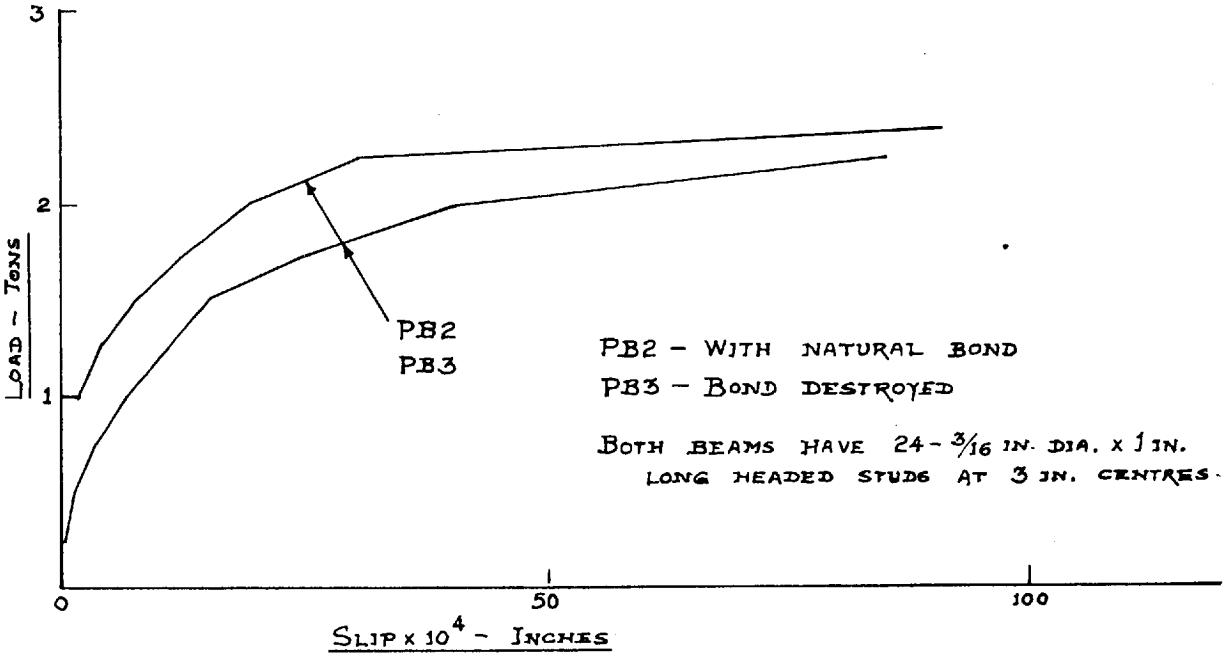


FIG. 107 AVERAGE RESIDUAL END SLIPS - PLATED BEAMS PB2 AND PB3 - POINT LOAD AT MIDSPAN

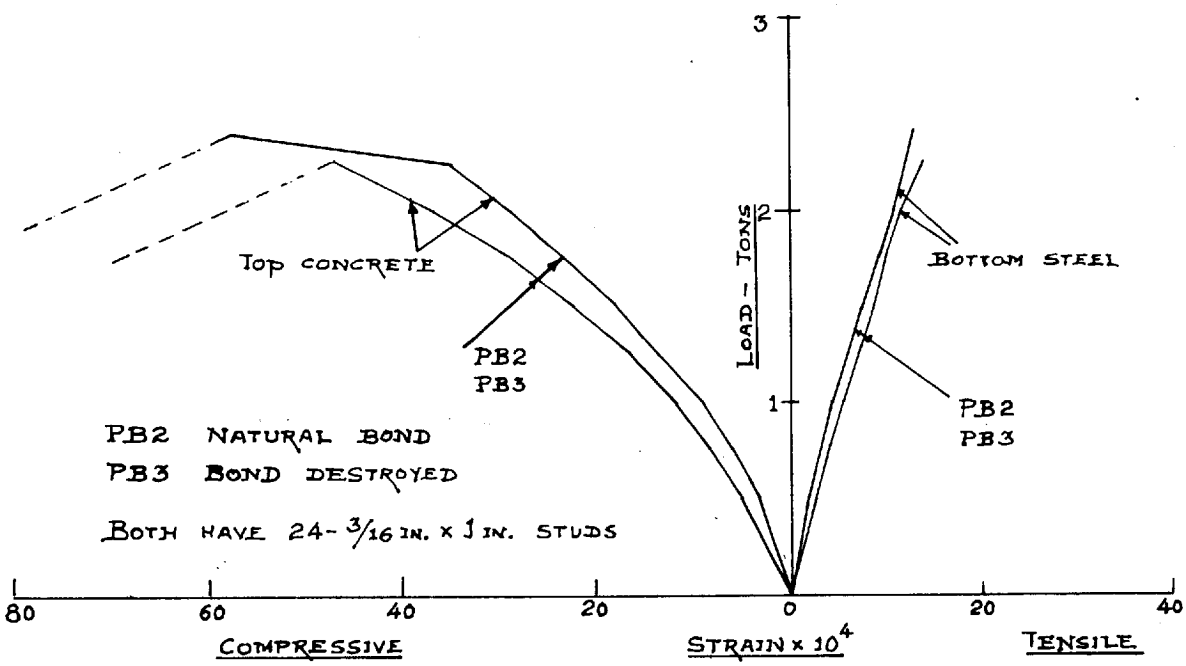


FIG. 108 STRAINS AT MIDSPAN SECTION - PLATED BEAMS PB2 AND PB3 - POINT LOAD AT MIDSPAN

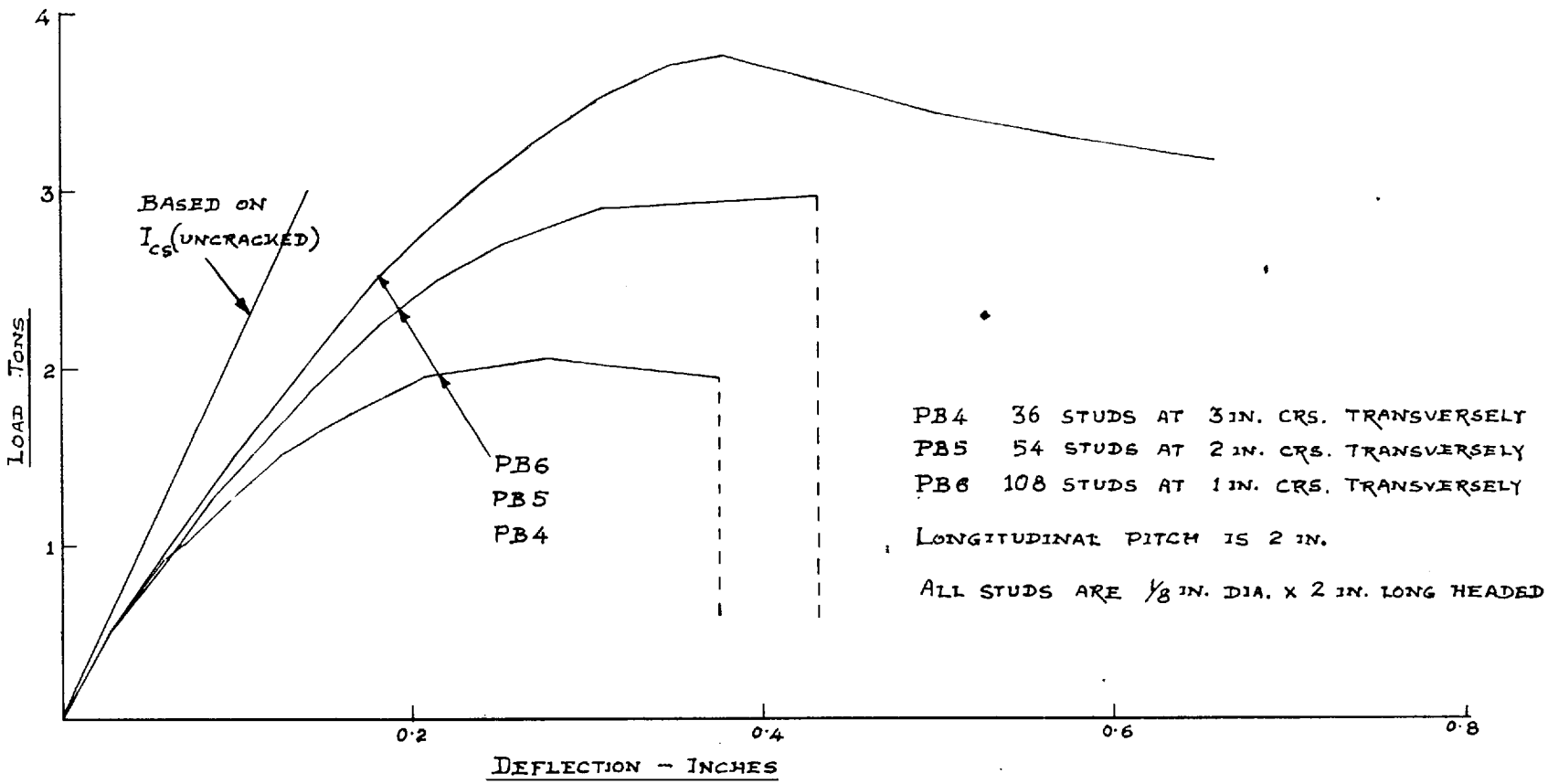


FIG. 109 MIDSPAN DEFLECTIONS – PLATED BEAMS PB4, PB5 AND PB6 – TWO POINT LOADS 4 IN. APART

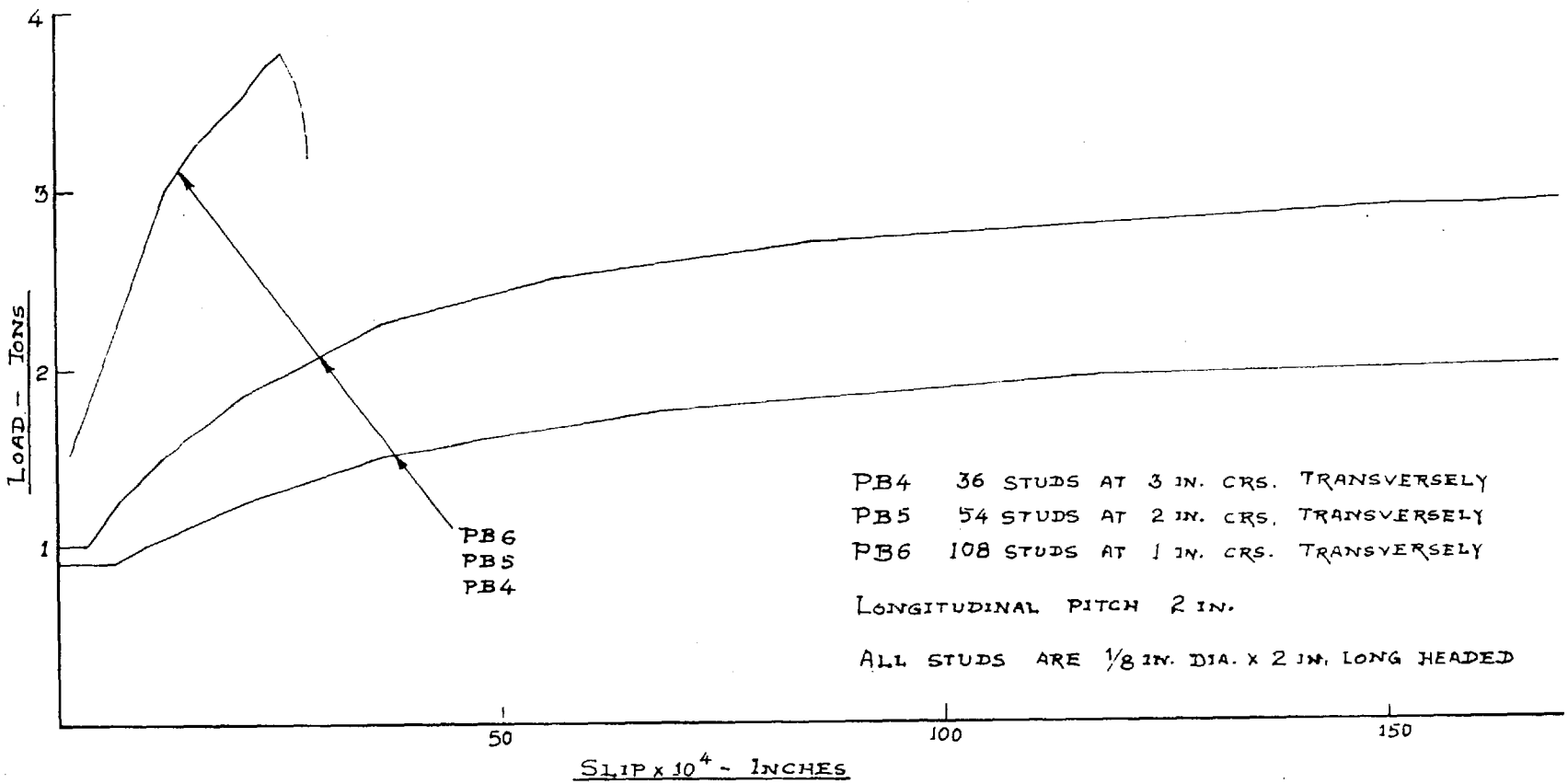


FIG. 110 AVERAGE END SLIPS PLATED BEAMS PB4, PB5 AND PB6 - TWO POINT LOADS 4 IN. APART

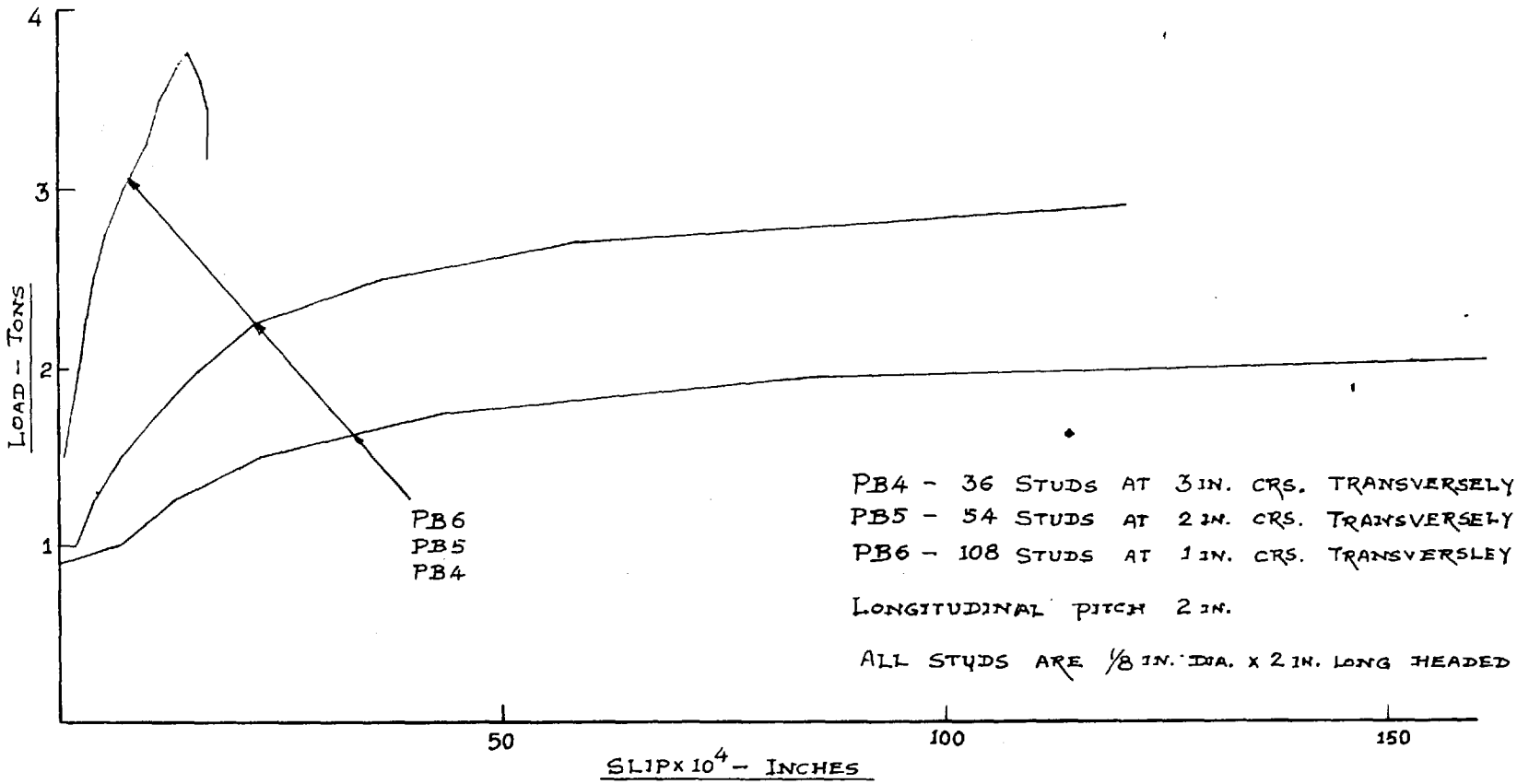


FIG. 111 AVERAGE RESIDUAL END SLIPS - PLATED BEAMS PB4, PB5 AND PB6 - TWO POINT LOADS 4 IN. APART

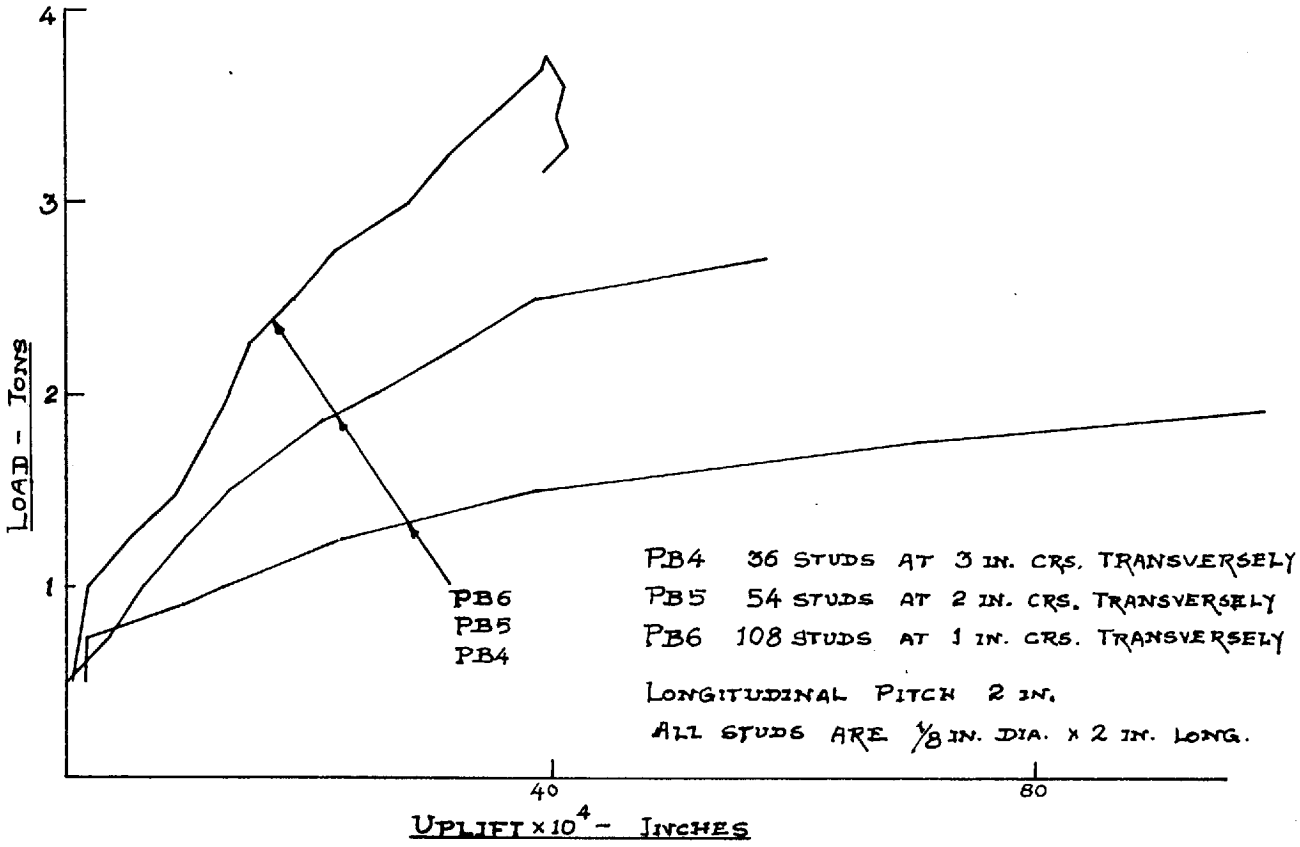


FIG. 113 AVERAGE UPLIFTS AT 1/4 SPAN - PLATED BEAMS PB4, 5 & 6.

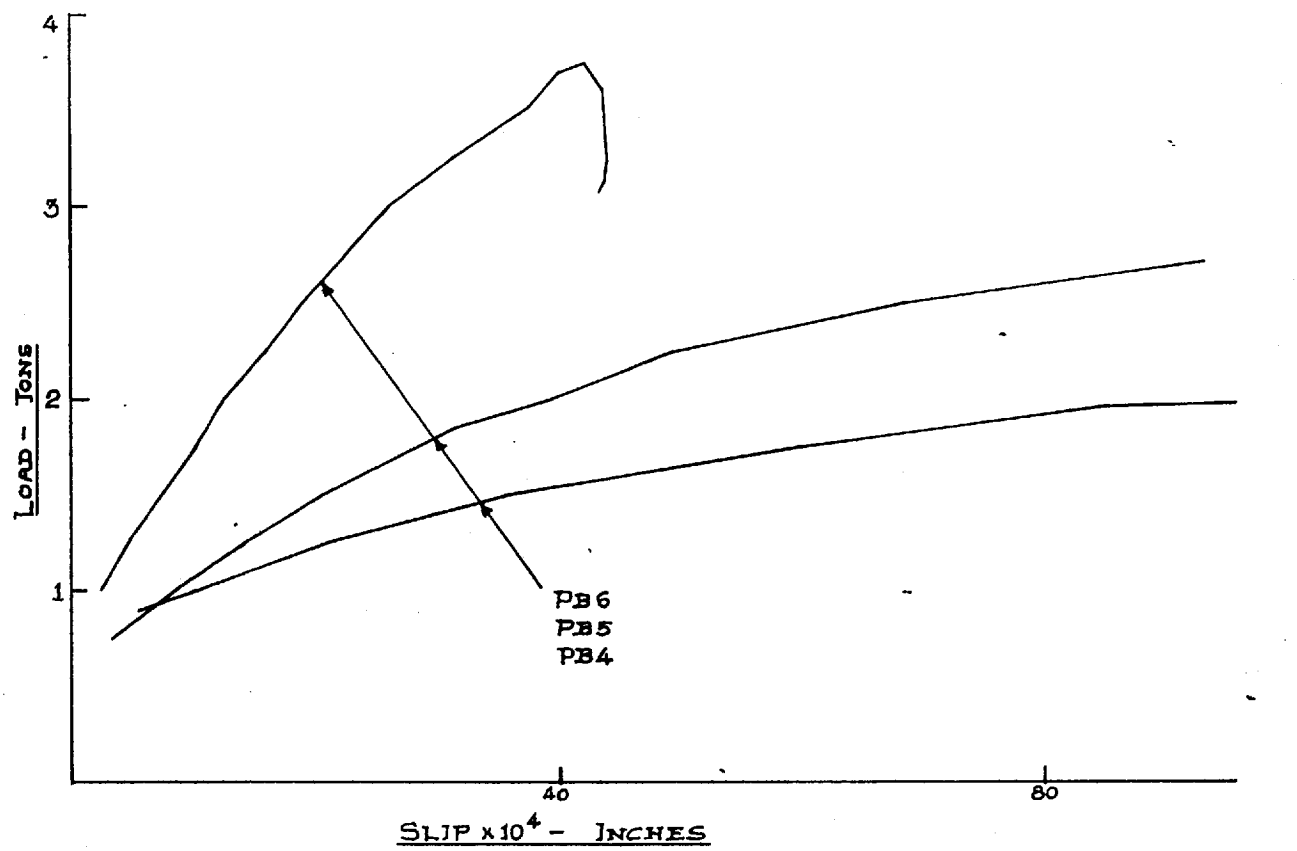
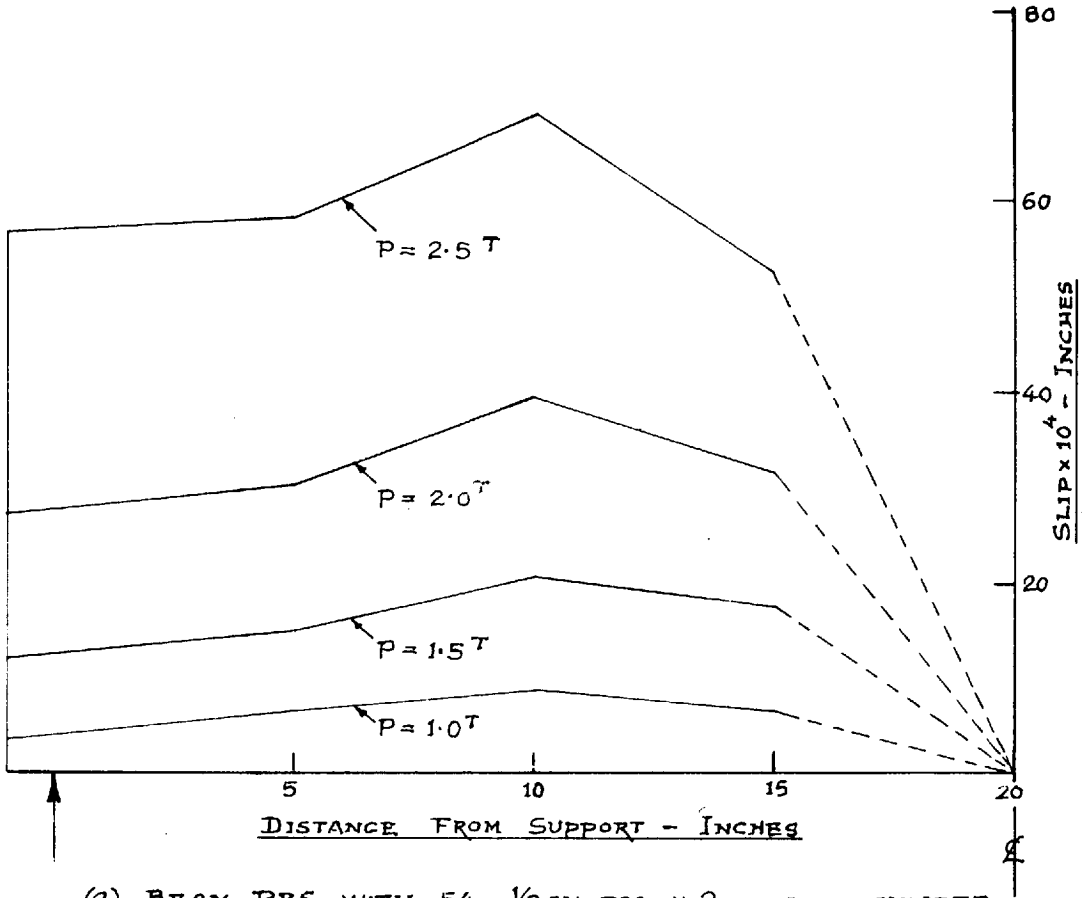
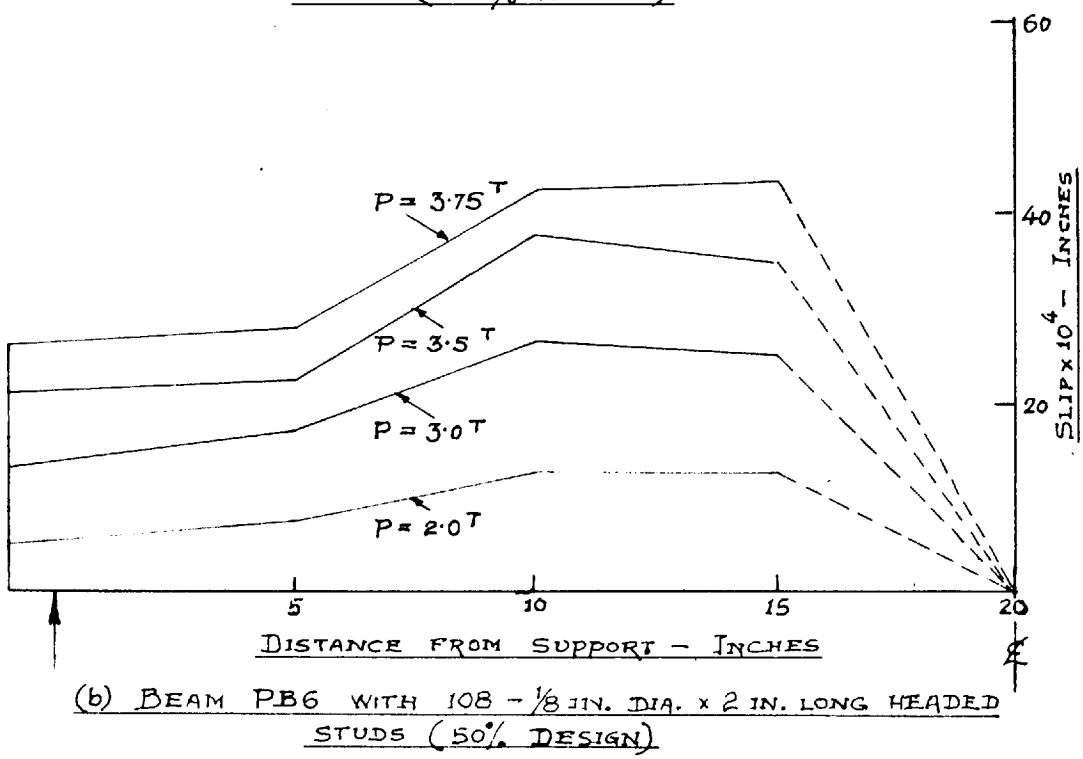


FIG 112 AVERAGE SLIPS AT 1/4 SPAN - PLATED BEAMS PB4, 5 & 6.



(a) BEAM PB5 WITH 54 - ⅛ IN. DIA. x 2 IN. LONG HEADED STUDS (100% DESIGN)



(b) BEAM PB6 WITH 108 - ⅛ IN. DIA. x 2 IN. LONG HEADED STUDS (50% DESIGN)

FIG. 114 SLIPS ALONG THE LENGTH OF PLATED BEAMS PB5 AND PB6

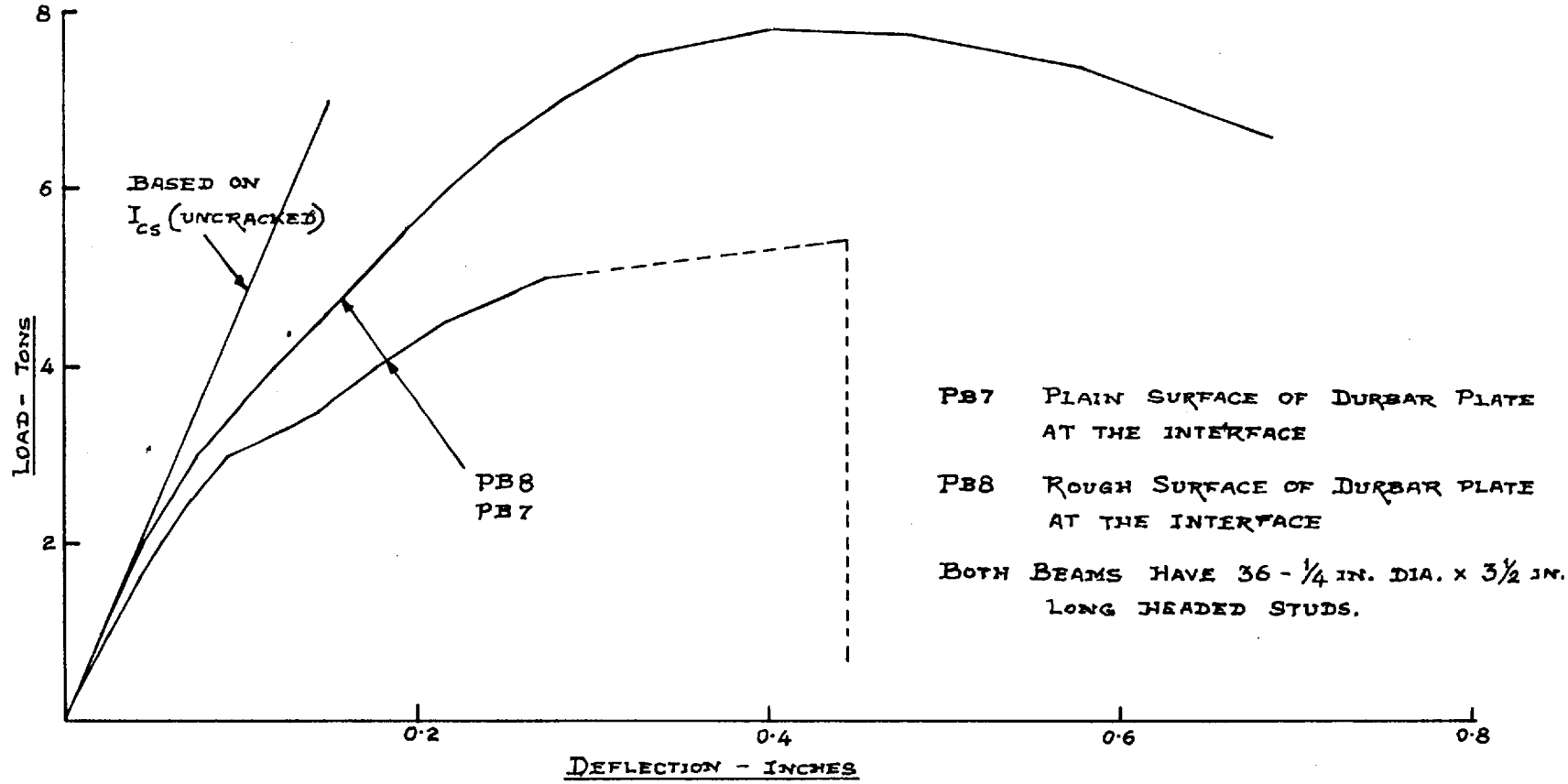


FIG. 115 MIDSPAN DEFLECTIONS - PLATED BEAMS WITH DURBAR PLATE - POINT LOAD AT MIDSPAN

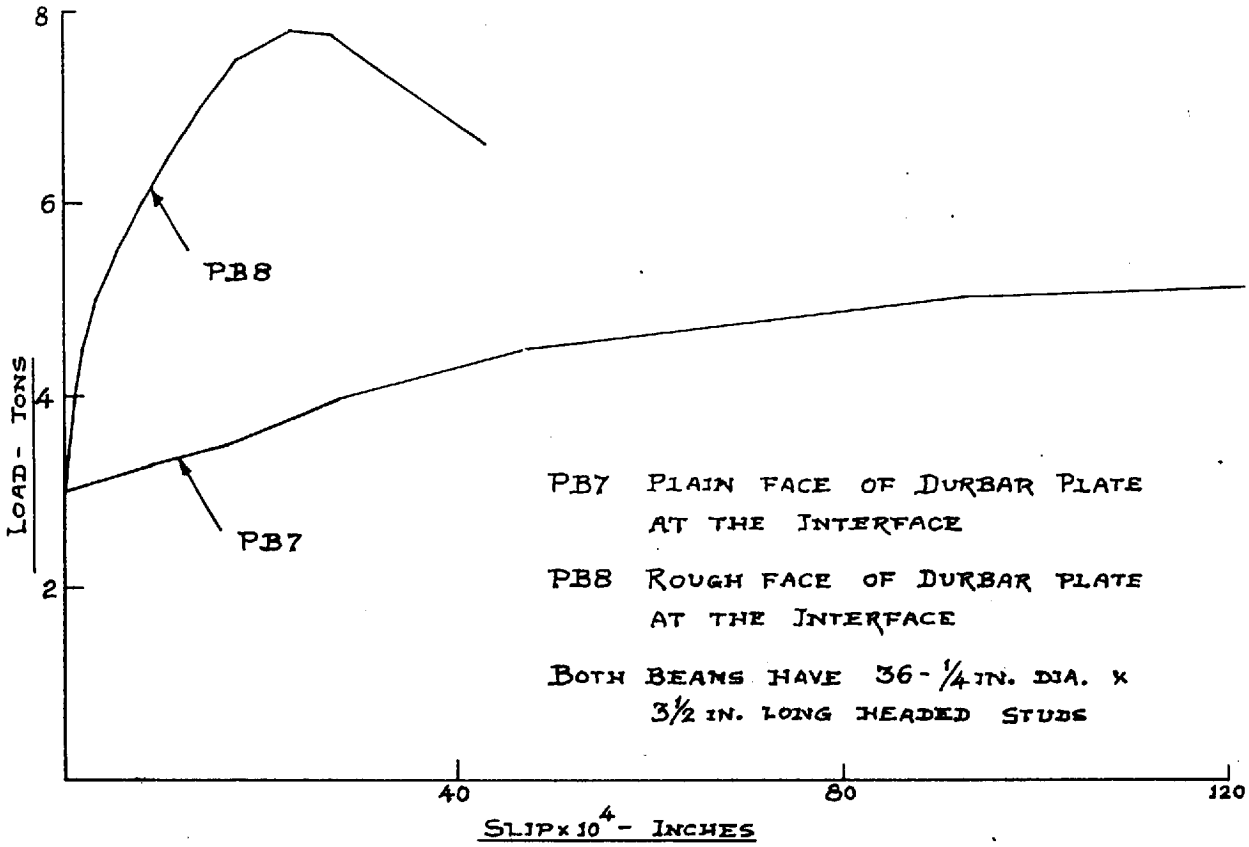


FIG. 116 AVERAGE END SLIPS - PLATED BEAMS WITH DURBAR PLATE - POINT LOAD AT MIDSPAN

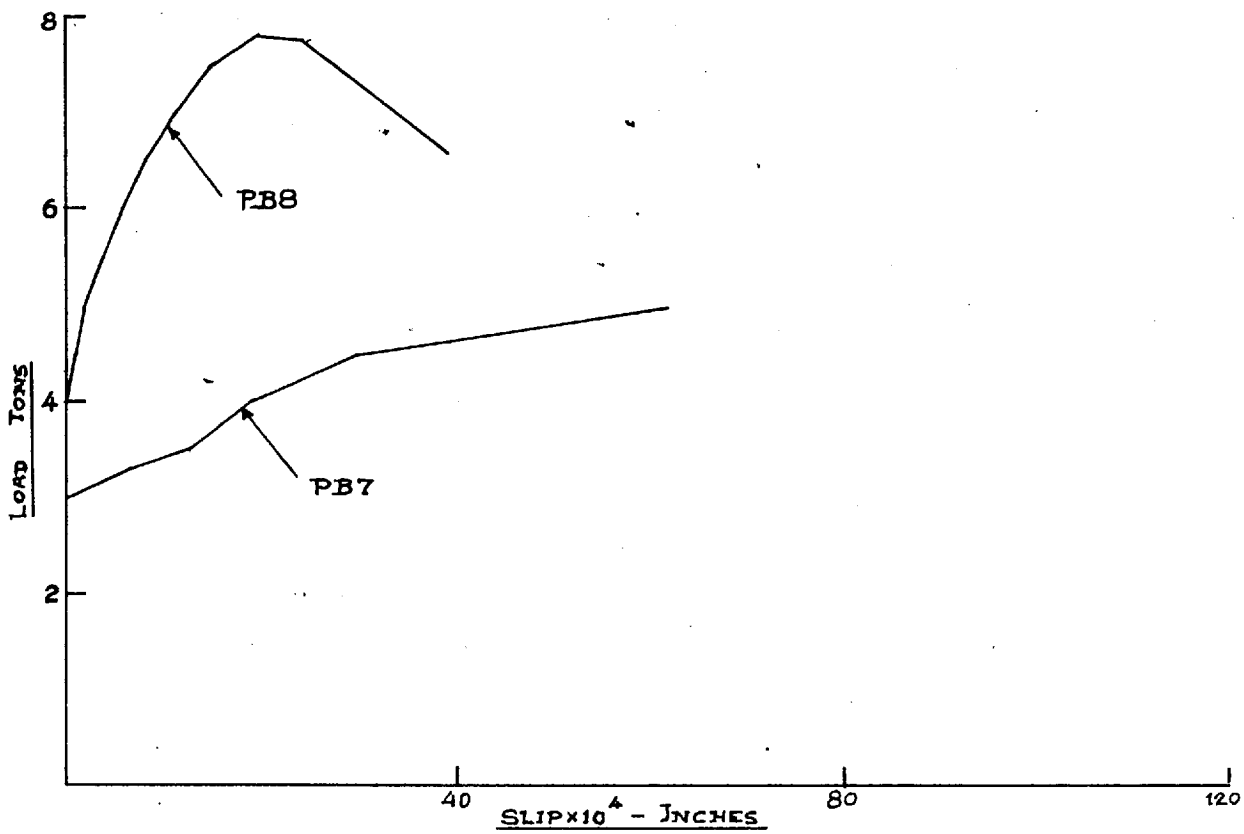


FIG. 117 AVERAGE RESIDUAL END SLIPS - PLATED BEAMS PB7 & 8.

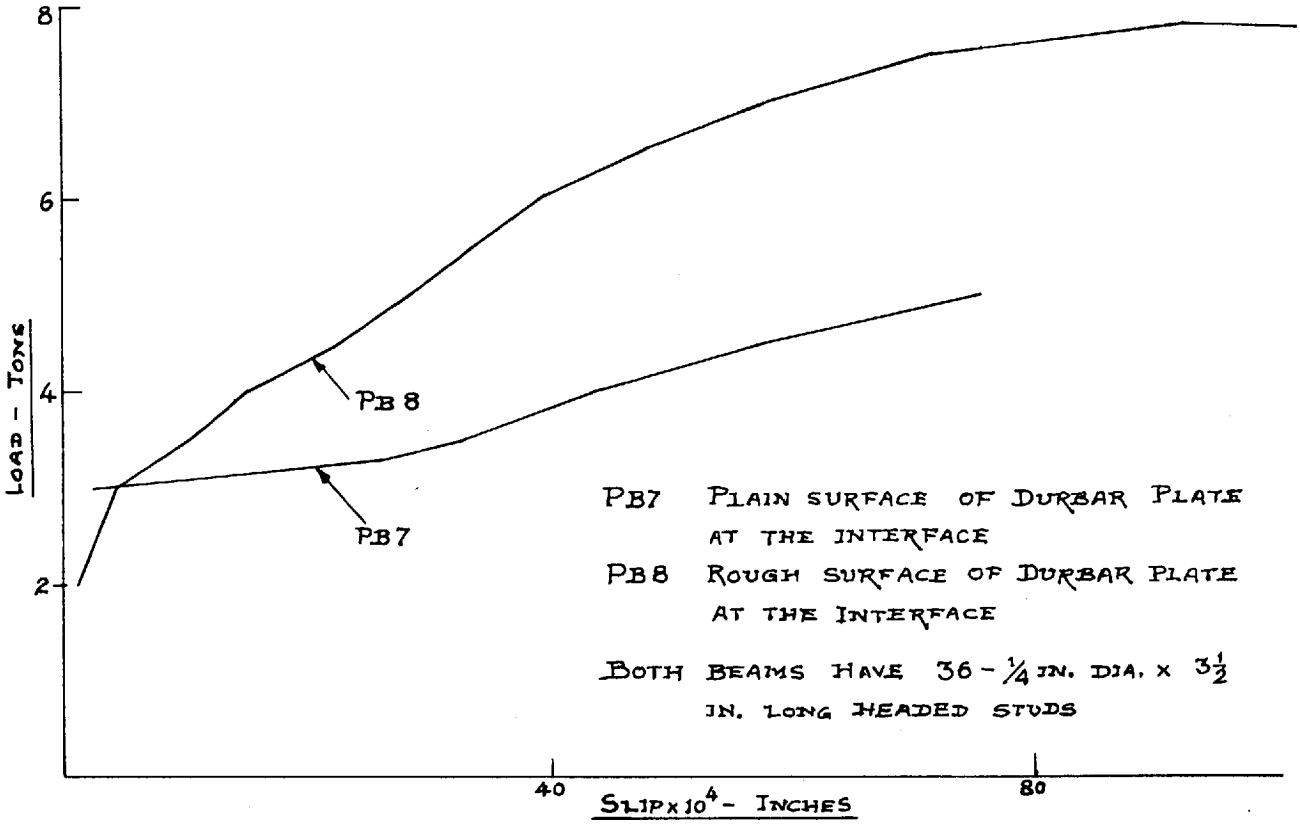


FIG. 118 AVERAGE SLIPS NEAR 1/3 SPAN - PLATED BEAMS WITH DURBAR PLATE - POINT LOAD AT MIDSPAN

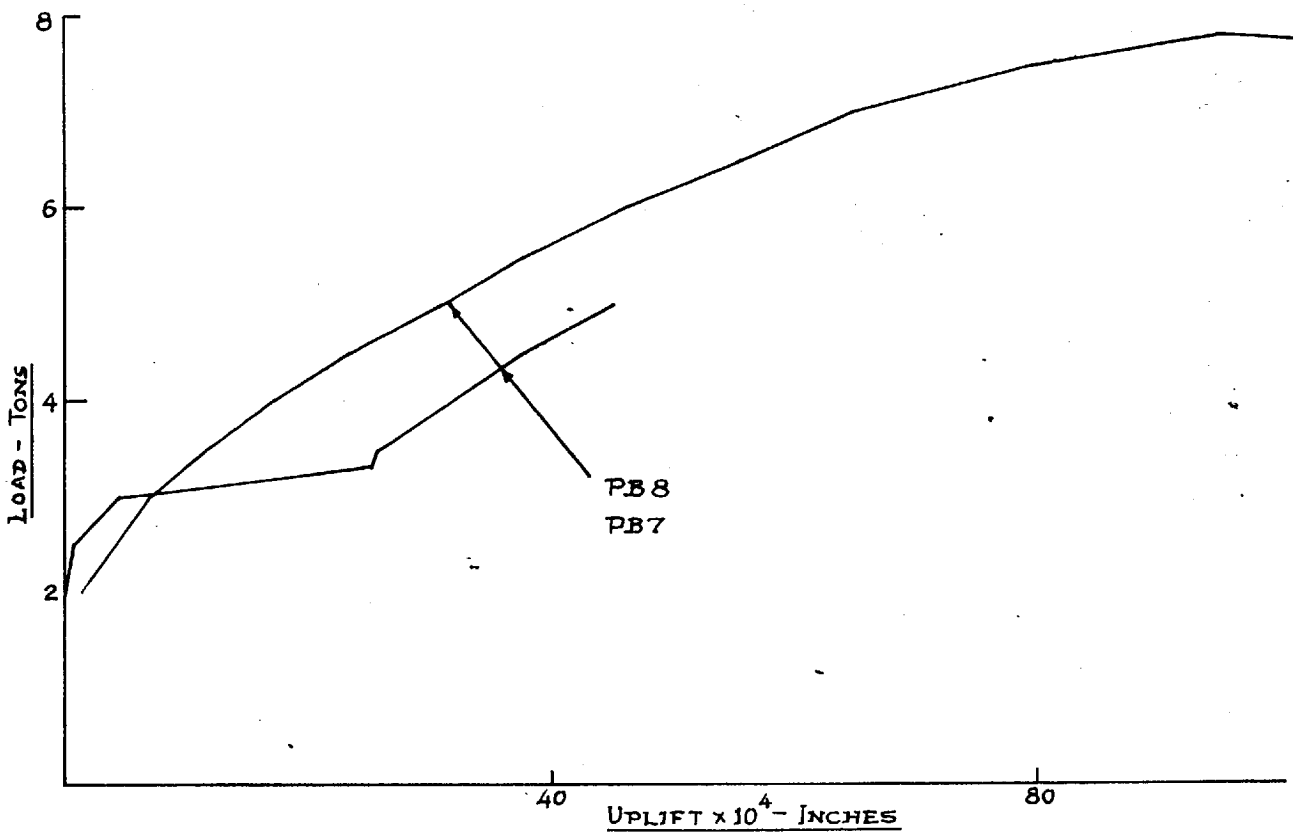
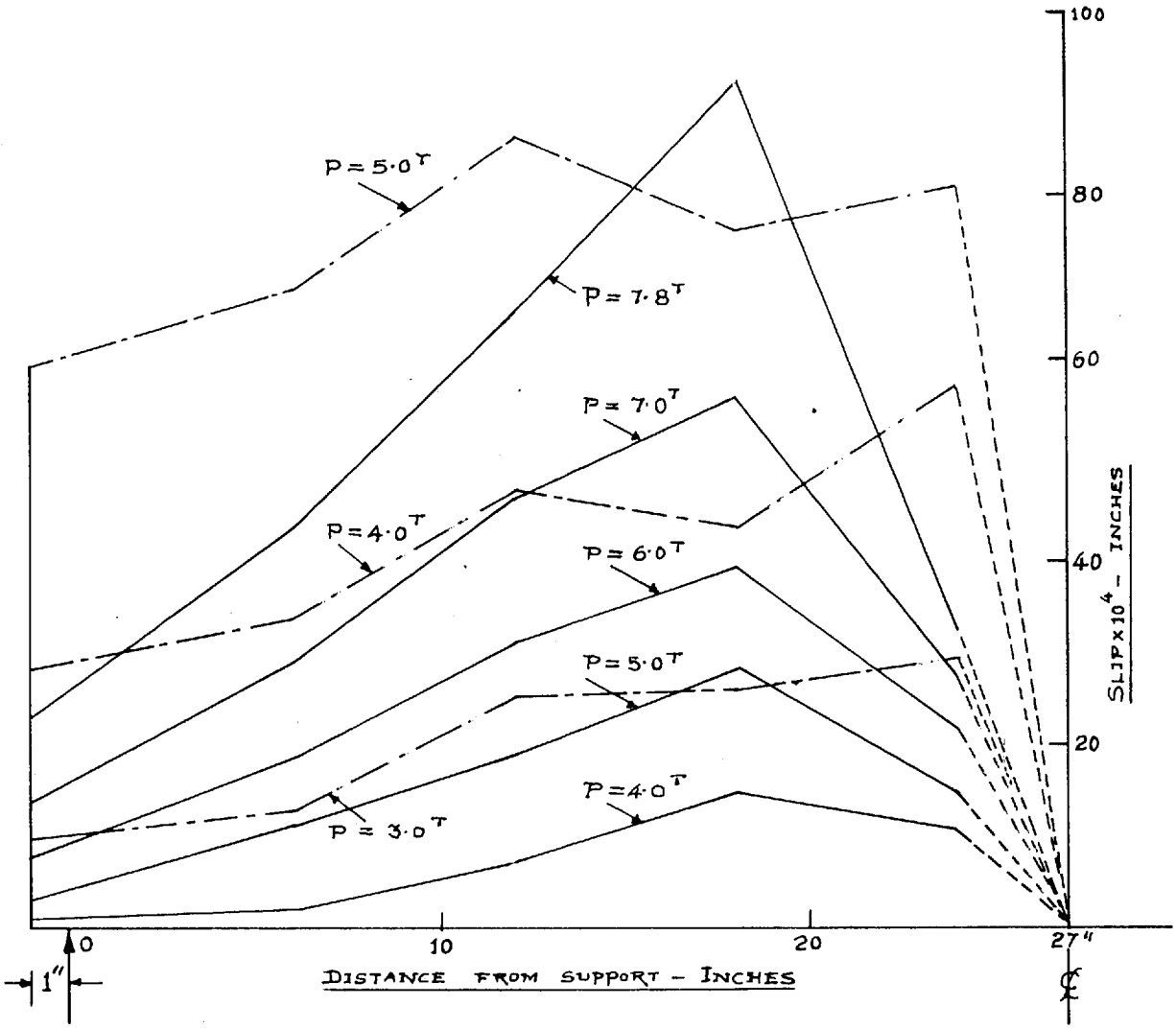


FIG. 119 AVERAGE UPLIFTS NEAR 1/3 SPAN - PLATED BEAMS PB7 & 8.



NOTE

PB7 ——·——·——·——

PB8 ————————

CONCRETE SLAB CAST ON PLAIN FACE OF DURBAR PLATE IN PB7 AND ON ROUGH FACE IN PB8.

FIG 120 SLIP DISTRIBUTION ALONG DURBAR PLATED BEAMS

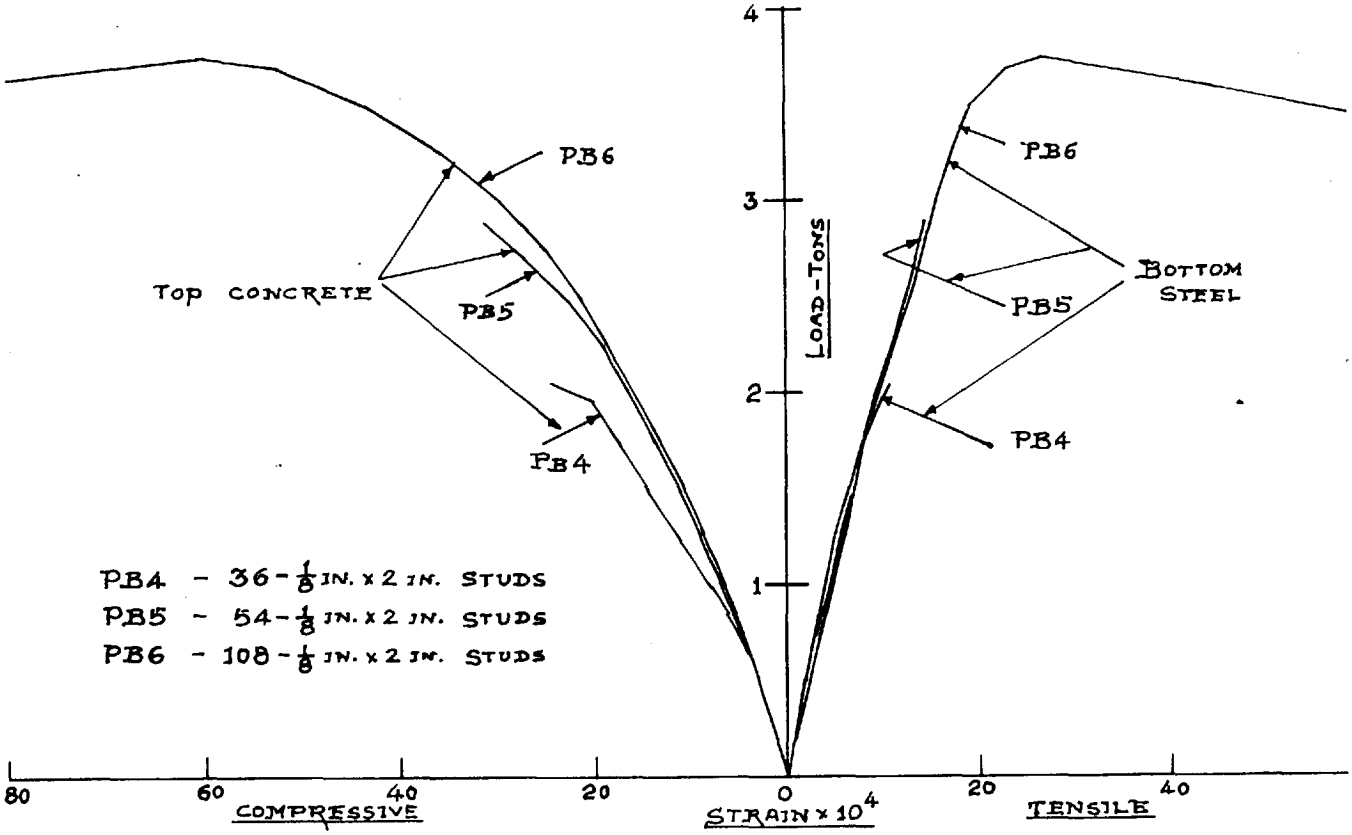


FIG. 121 STRAINS AT MIDSPAN SECTION - PLATED BEAMS PB4, 5 & 6.

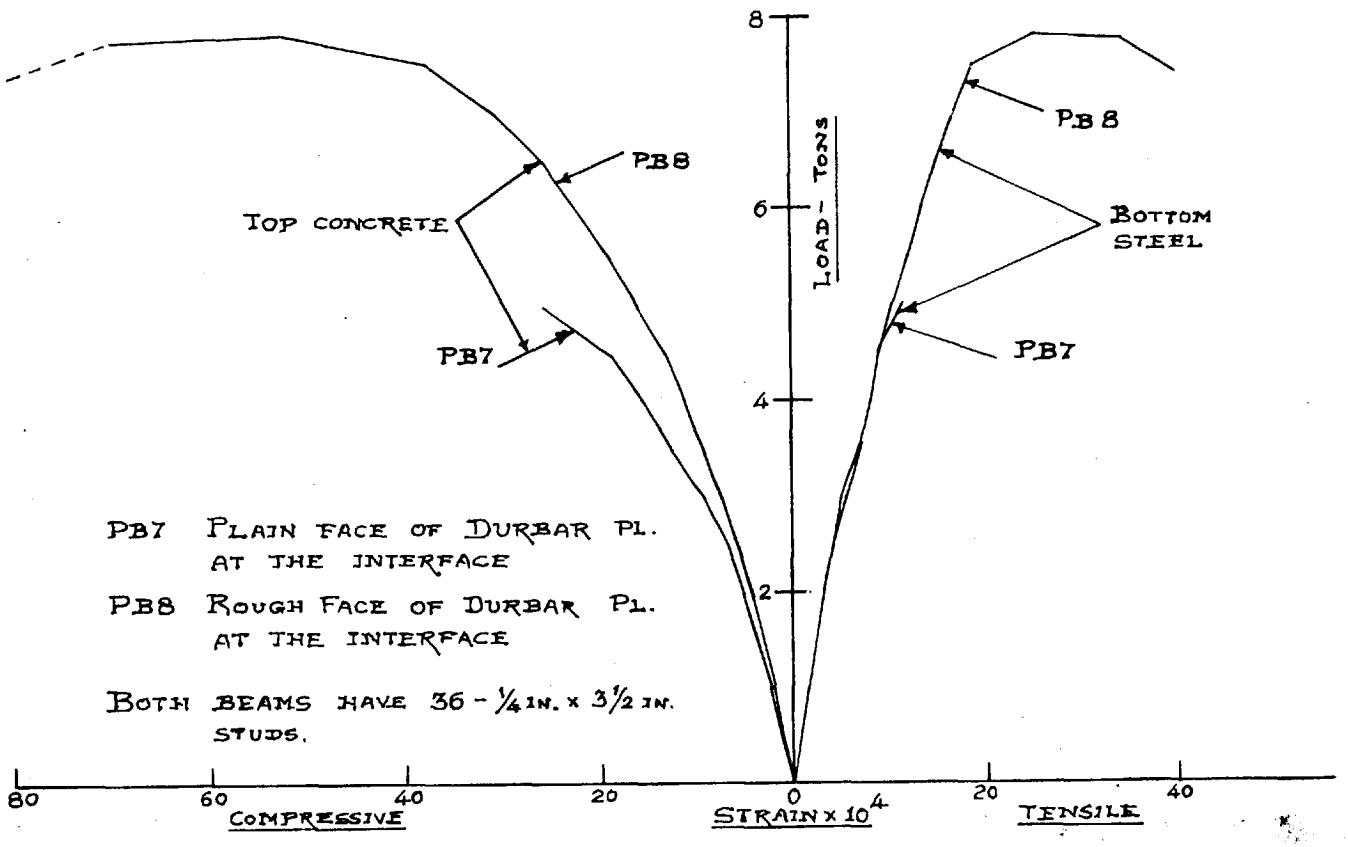


FIG. 122 STRAINS AT MIDSPAN SECTION - DURBAR PLATED BEAMS

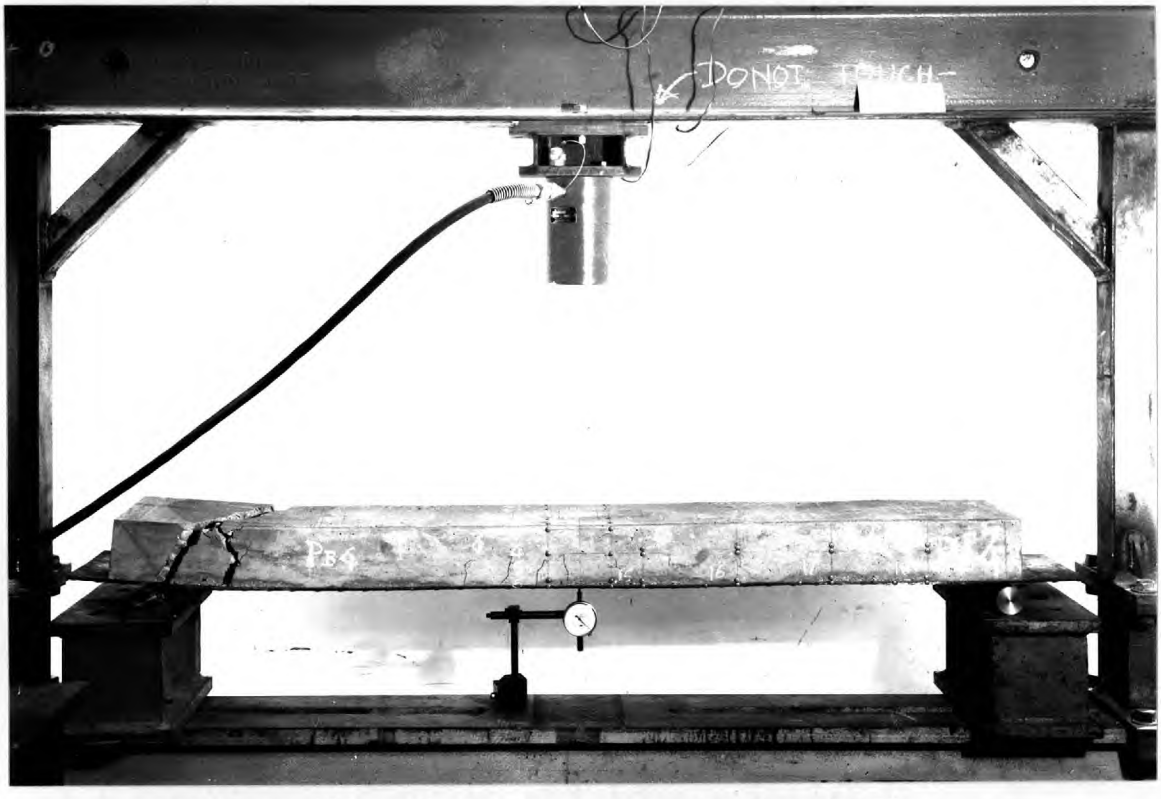


Figure 123. Plated beam after failure (PB7)

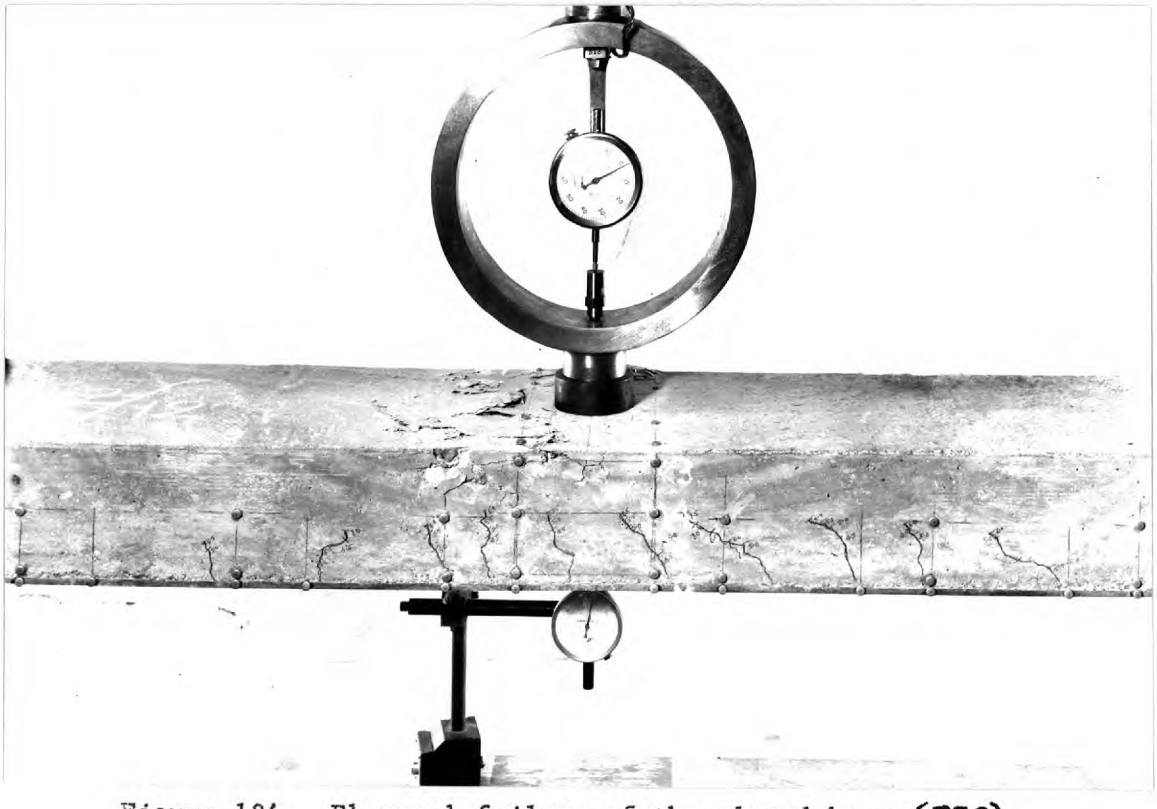


Figure 124. Flexural failure of the plated beam (PB8)

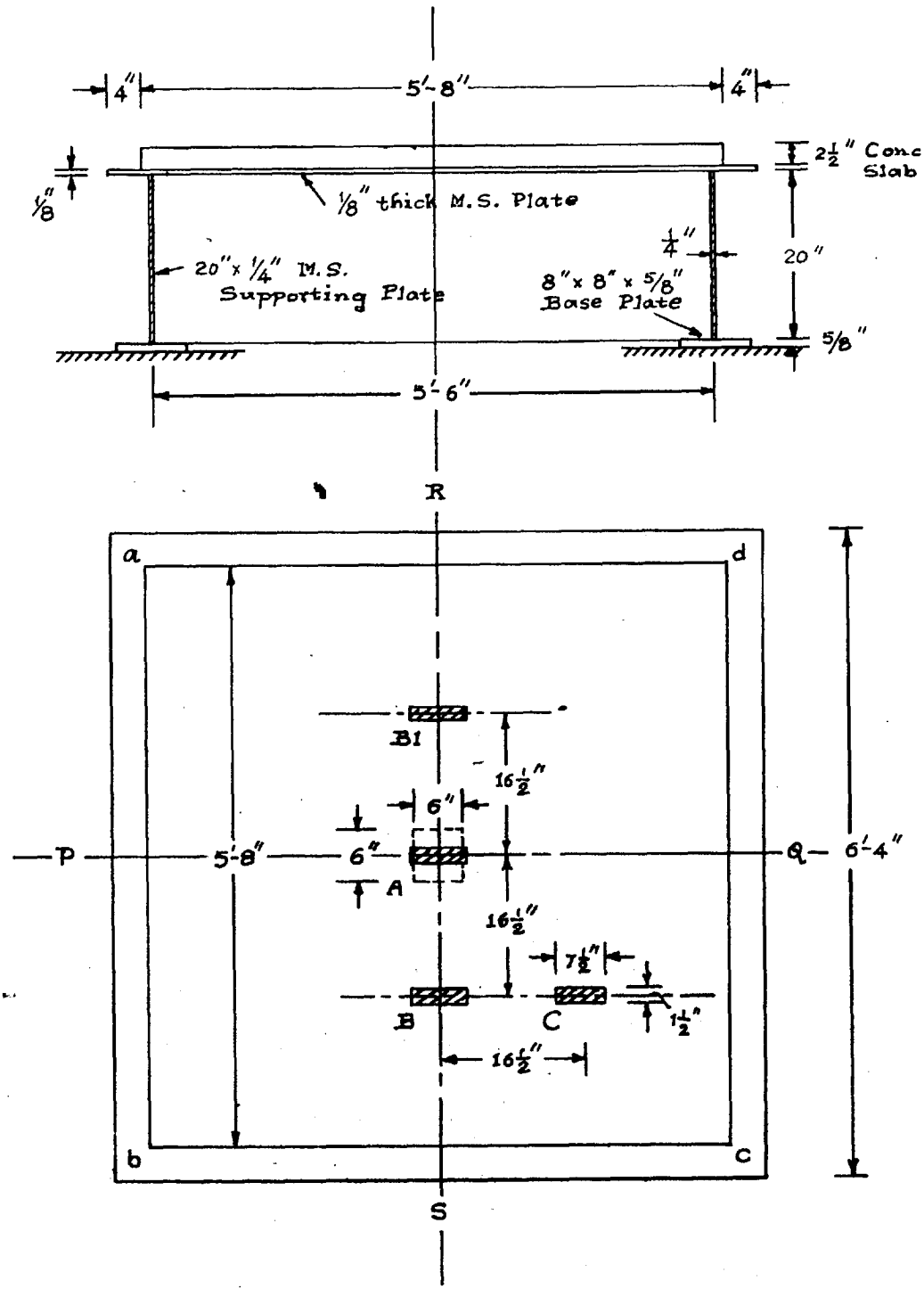
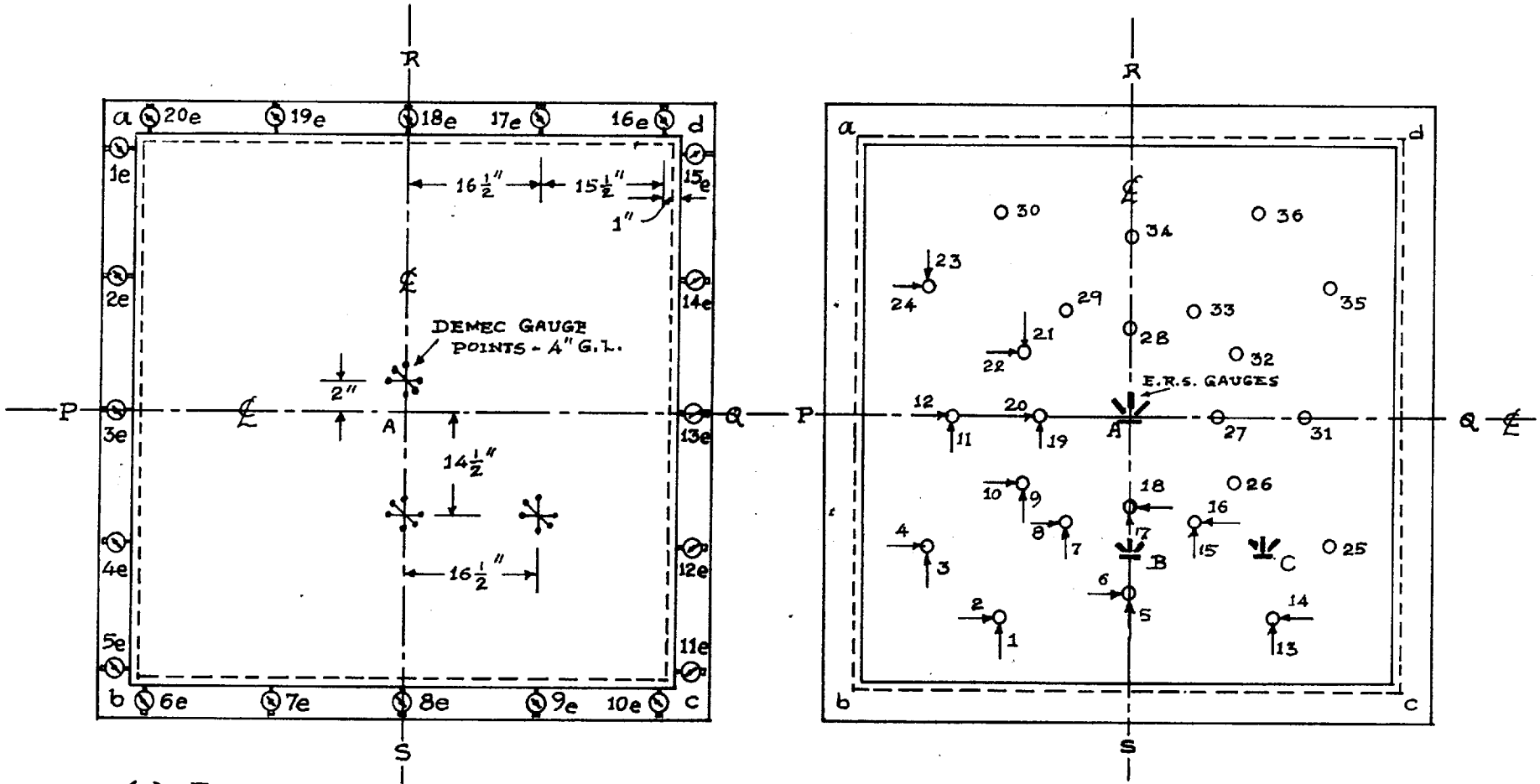


FIG. 125 DETAILS OF THE COMPOSITE PLATE - SHADED AREAS SHOW THE LOADED AREAS FOR DIFFERENT LOAD CONDITIONS



(a) TOP OF CONCRETE SLAB SHOWING POSITIONS OF END SLIP GAUGES AND DEMEC GAUGE POINTS.

(b) BOTTOM OF STEEL PLATE SHOWING SLIP GAUGE (1 to 24), UPLIFT GAUGE (25 to 36) AND E.R.S. GAUGE POSITIONS.

FIG. 126 GENERAL ARRANGEMENT FOR MEASUREMENTS IN THE COMPOSITE PLATE

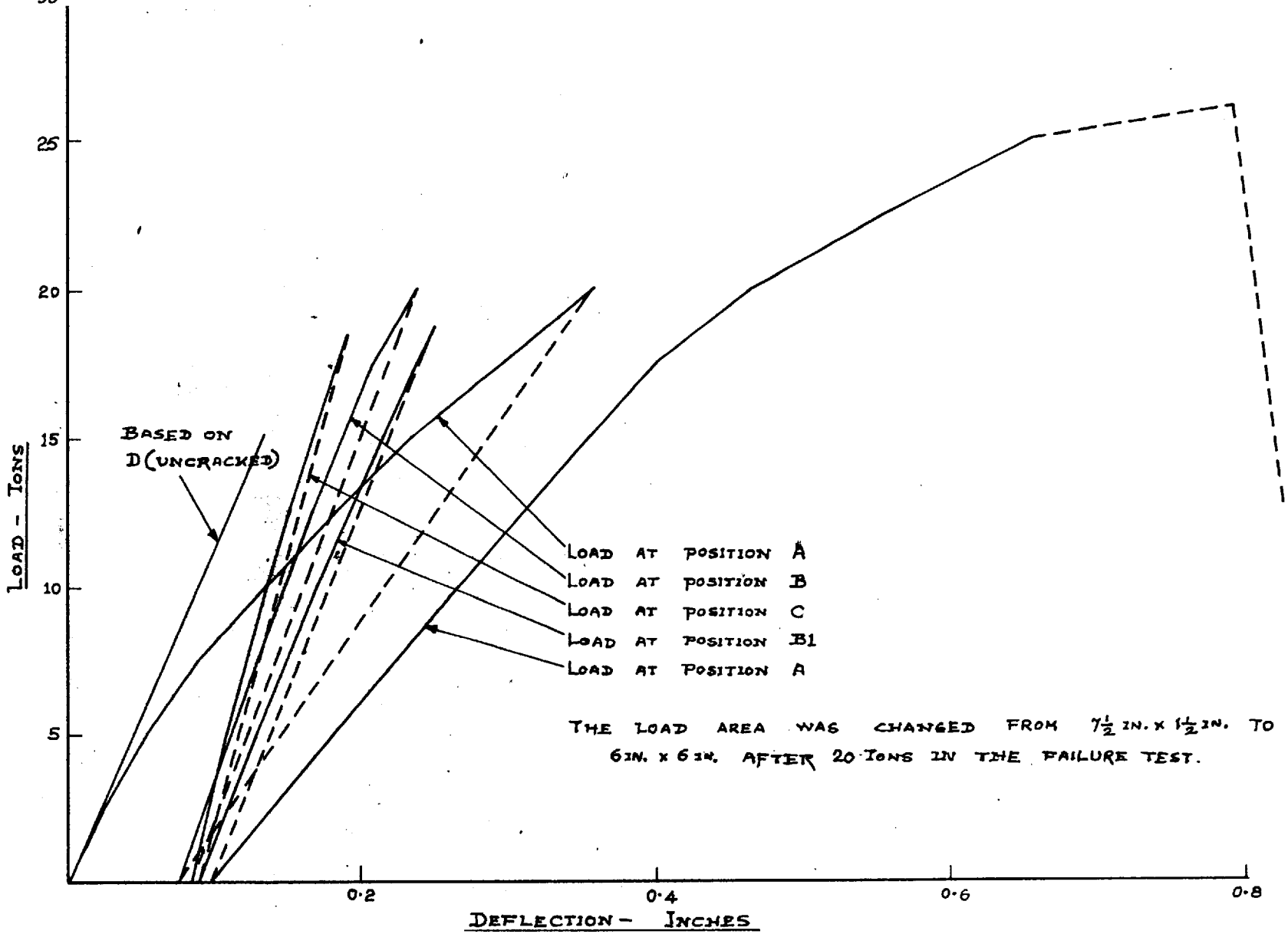


FIG. 127 CENTRAL DEFLECTIONS OF THE COMPOSITE PLATE FOR DIFFERENT LOAD POSITIONS

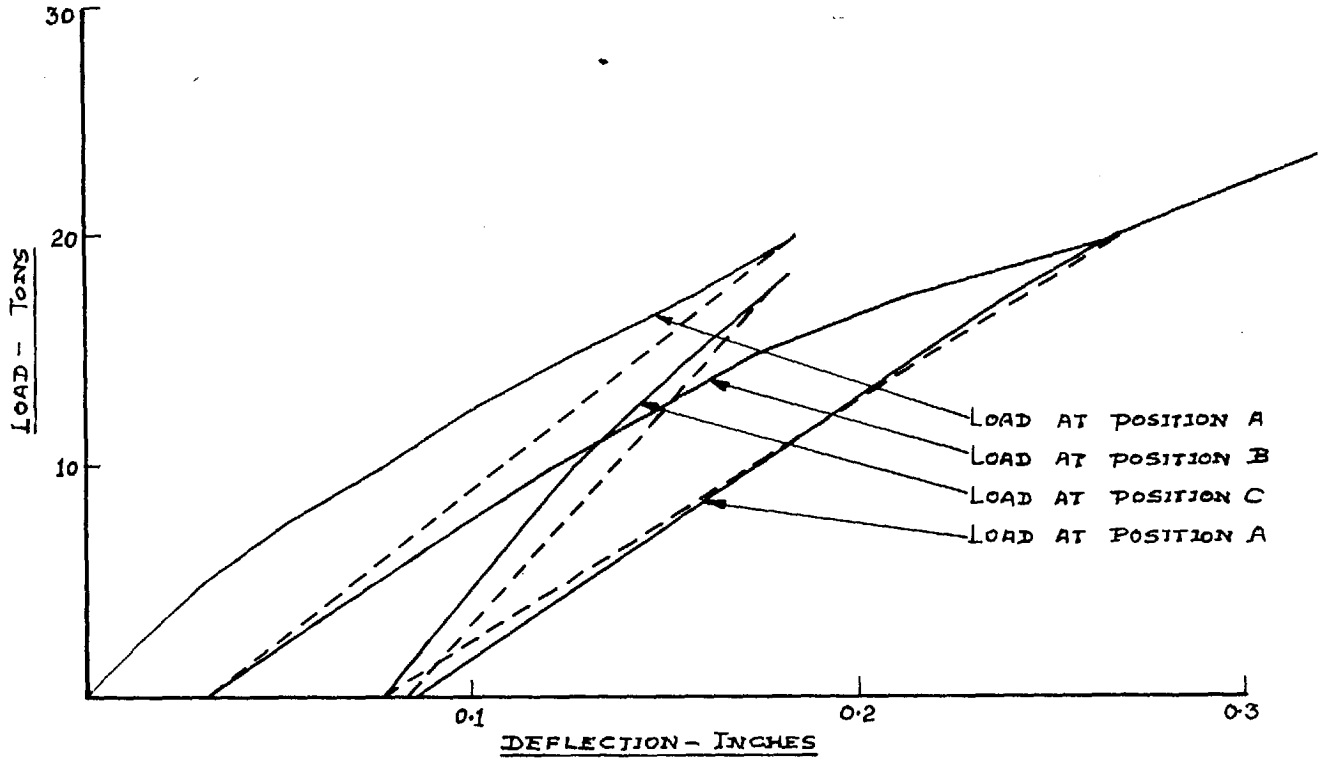


FIG. 128 DEFLECTIONS OF THE COMPOSITE PLATE AT B FOR DIFFERENT LOAD POSITIONS

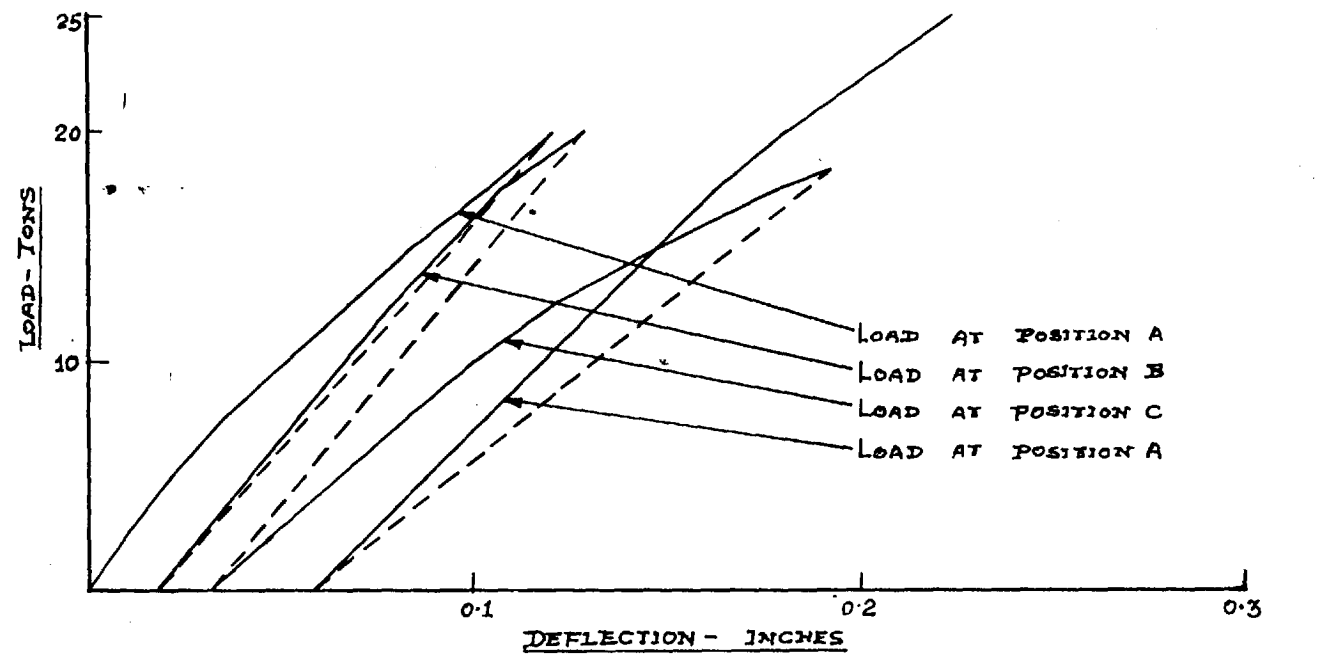
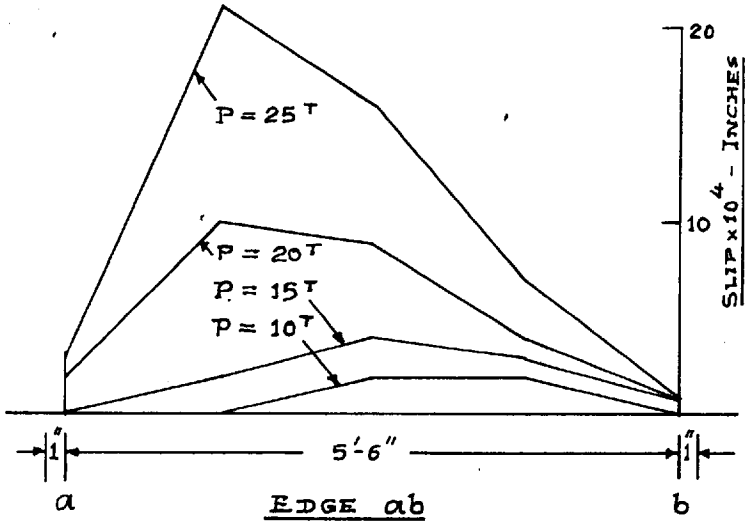
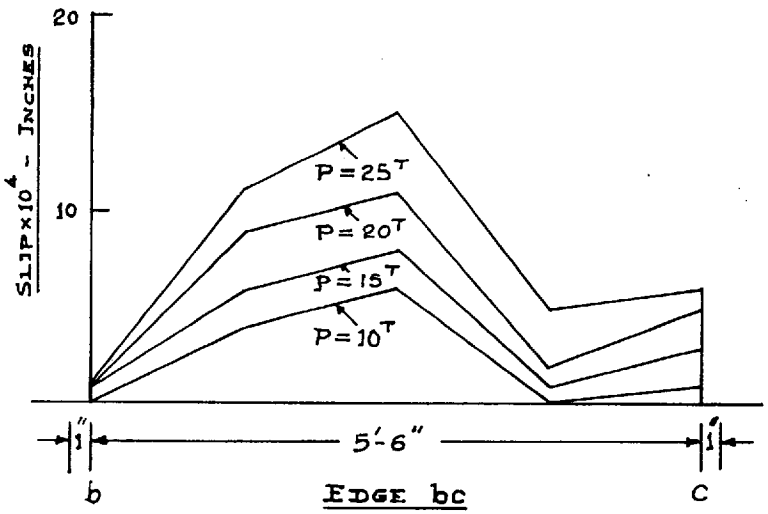
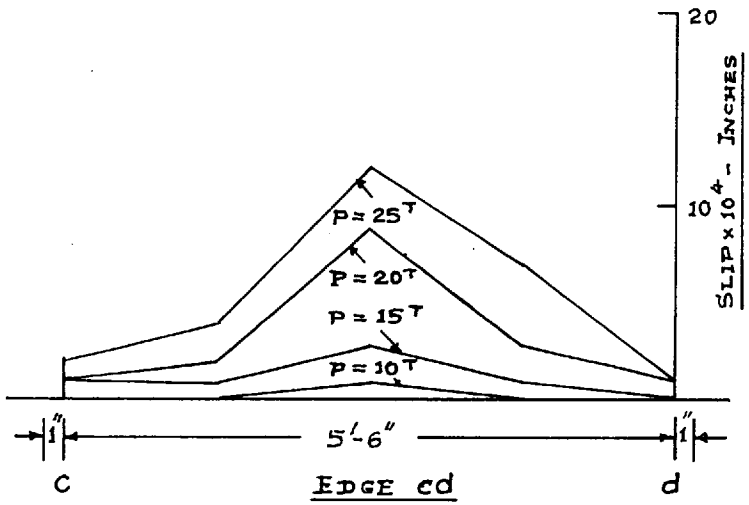


FIG. 129 DEFLECTIONS OF THE COMPOSITE PLATE AT C FOR DIFFERENT LOAD POSITIONS







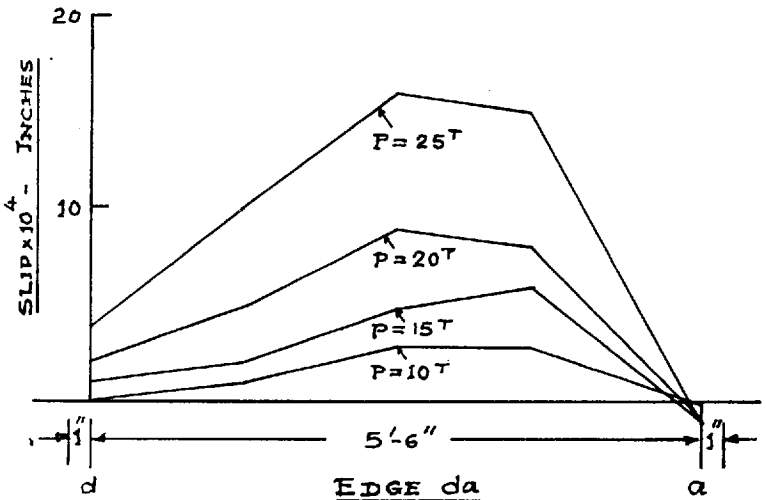
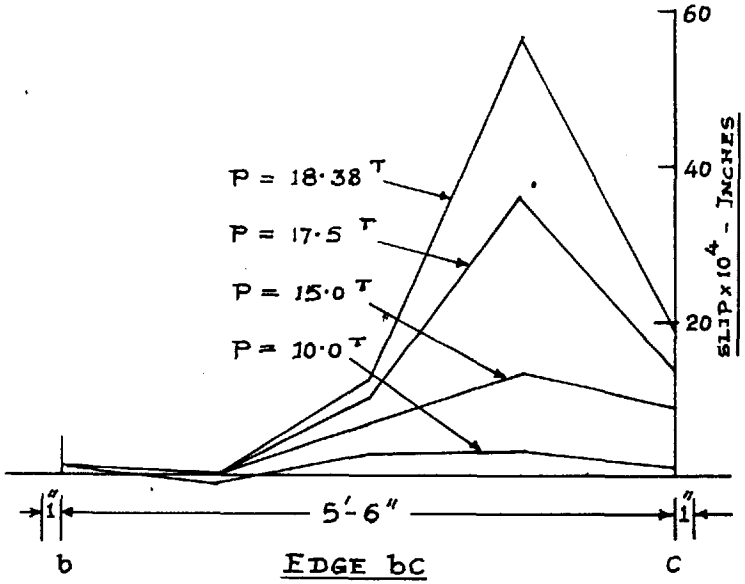


FIG. 130 END SLIPS ON FOUR EDGES OF THE COMPOSITE PLATE AT VARIOUS CENTRAL LOADS.



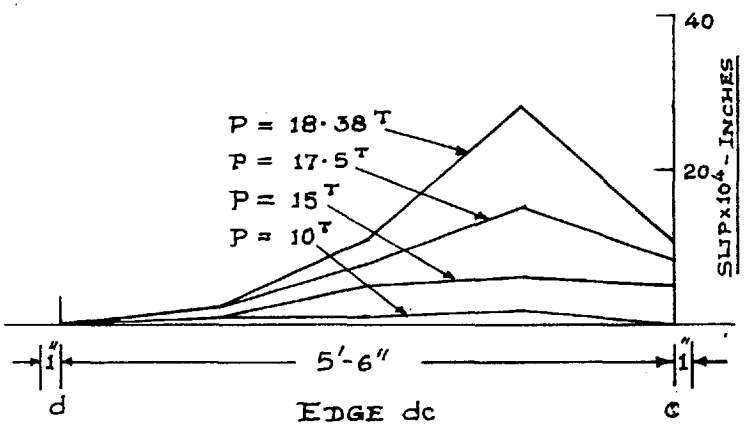


FIG. 131 END SLIPS ON EDGES bc AND dc FOR VARIOUS LOADS AT POSITION C

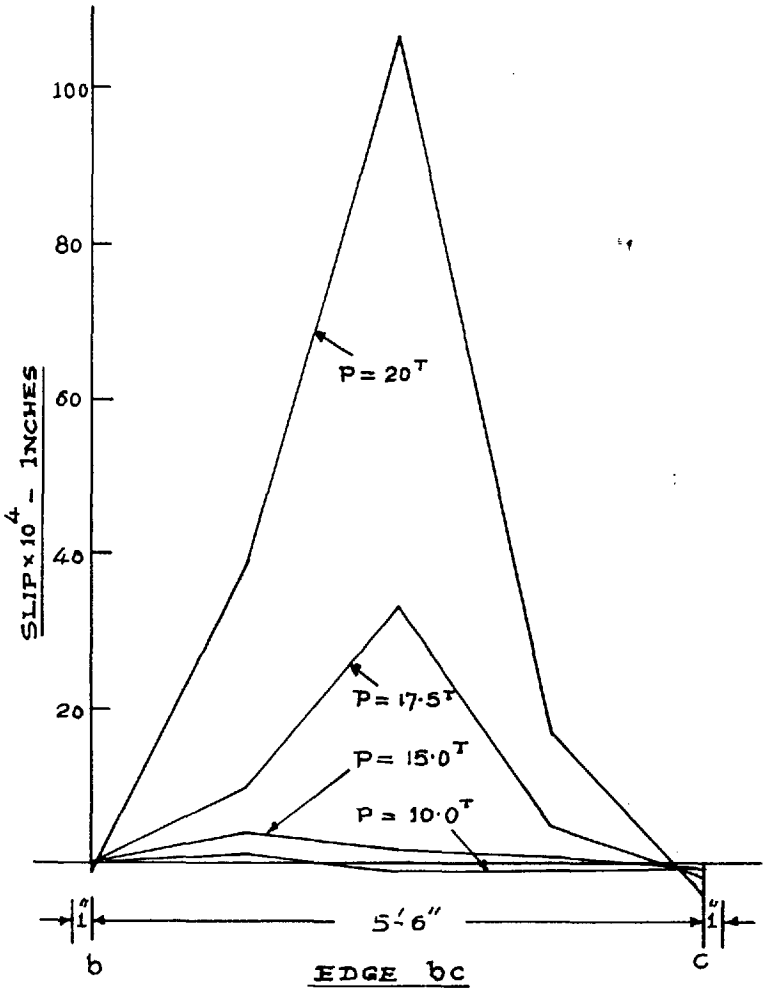


FIG. 132 END SLIPS ON EDGE bc FOR VARIOUS LOADS AT POSITION B

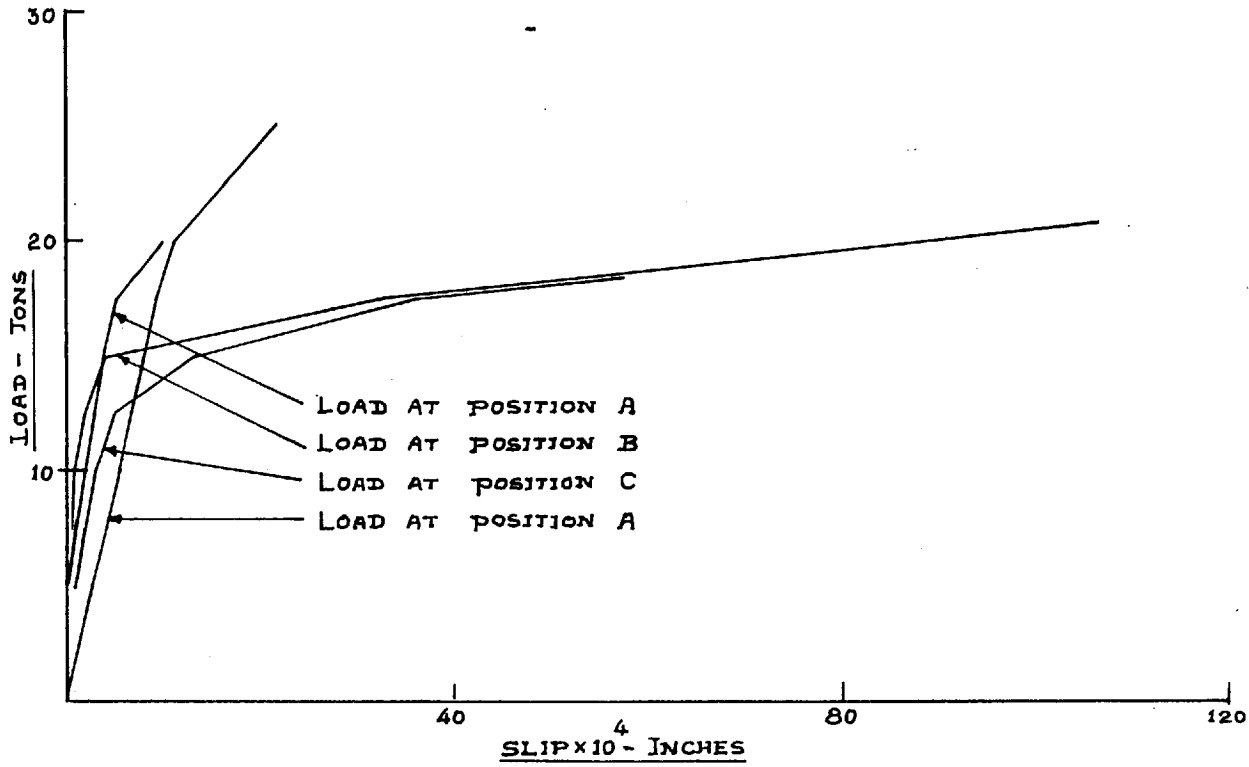


FIG. 133 MAXIMUM END SLIPS IN THE COMPOSITE PLATE FOR DIFFERENT LOAD POSITIONS

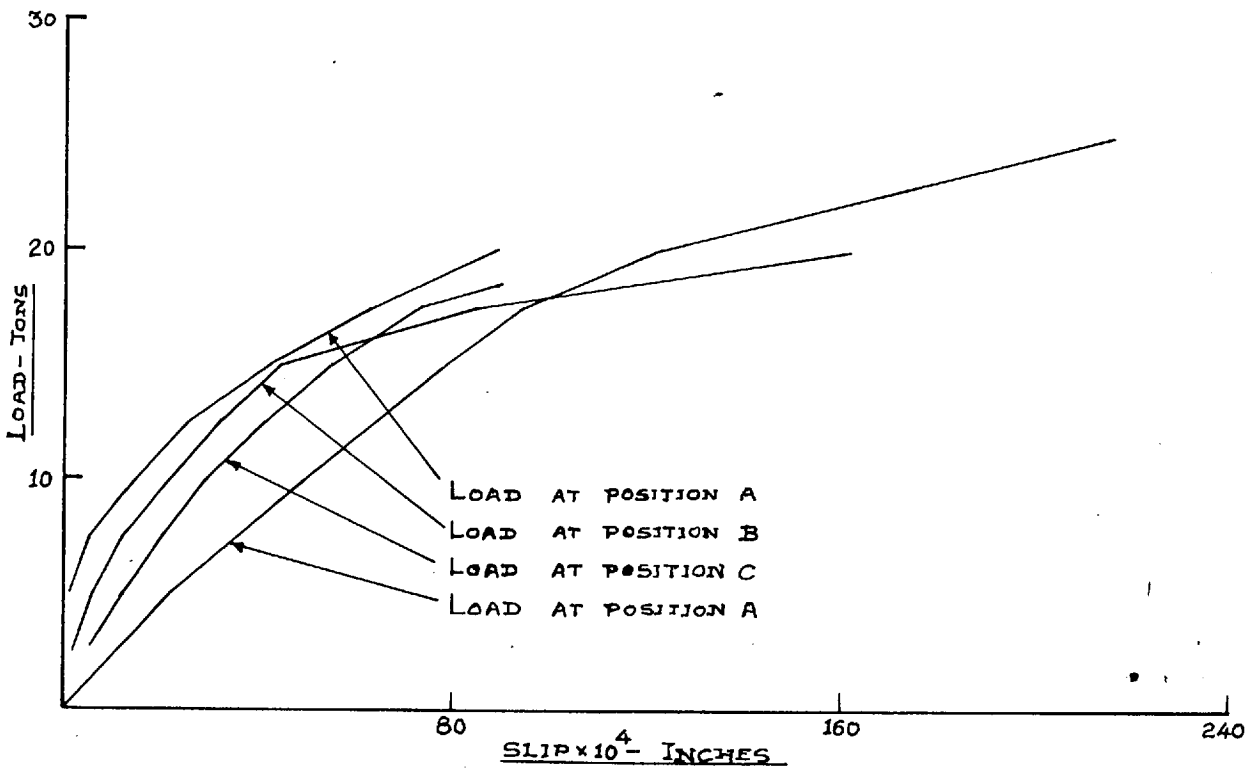


FIG. 134 MAXIMUM SLIPS IN THE PANEL OF THE COMPOSITE PLATE FOR DIFFERENT LOAD POSITIONS

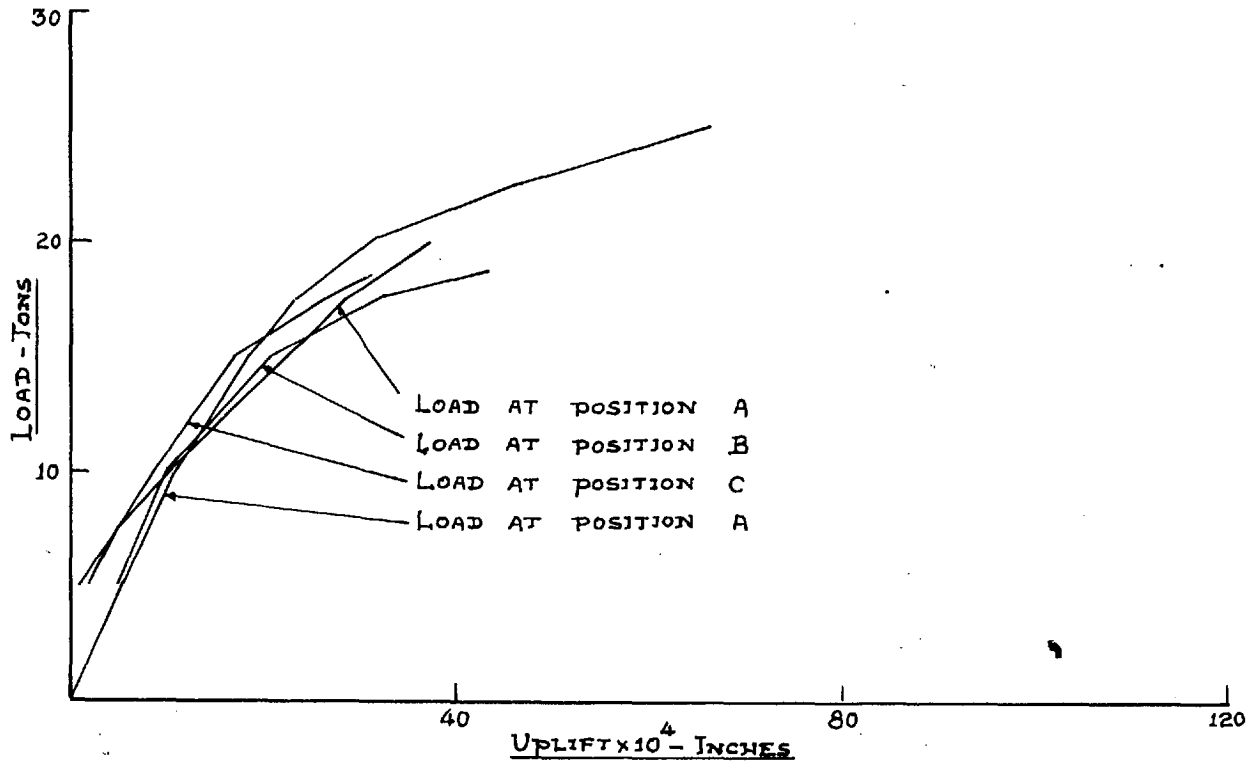


FIG. 135 MAXIMUM UPLIFTS IN THE PANEL OF THE COMPOSITE PLATE FOR VARIOUS LOAD POSITIONS

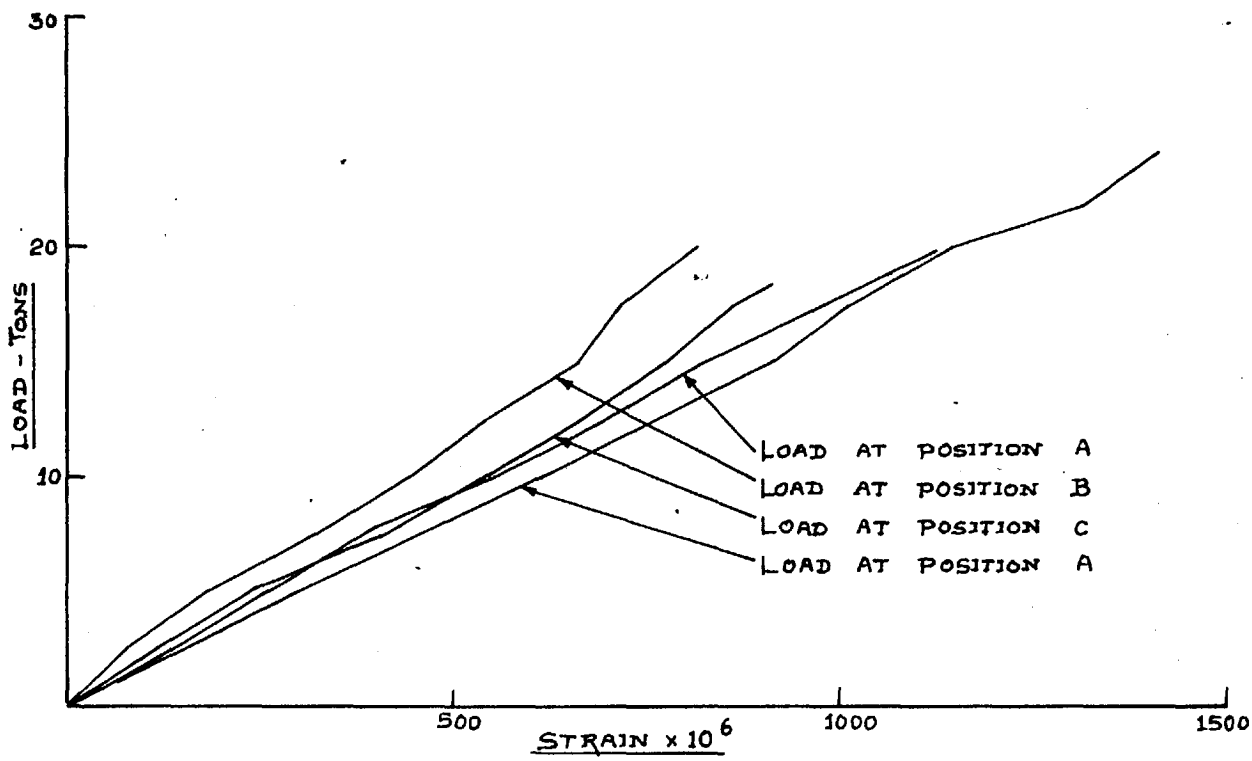
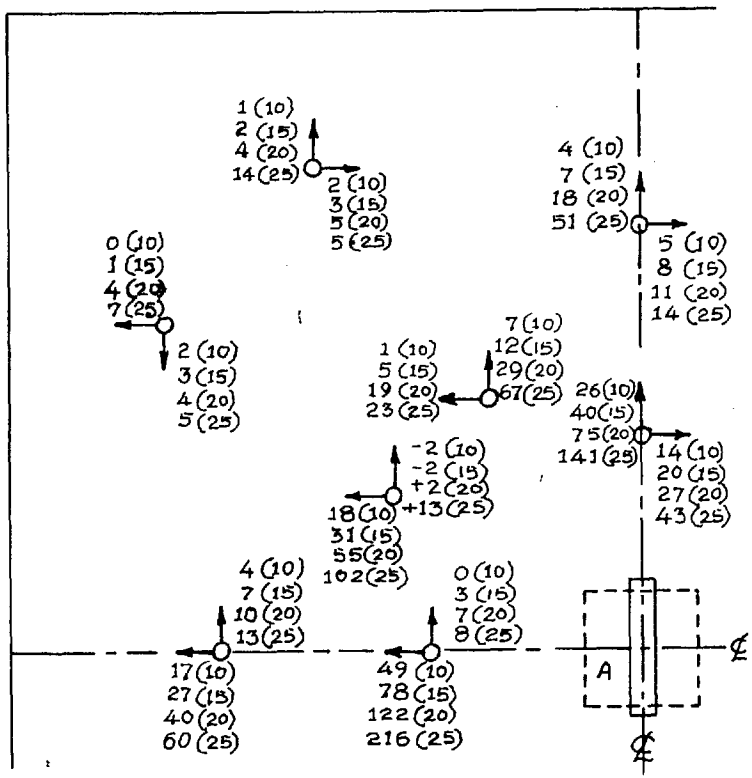
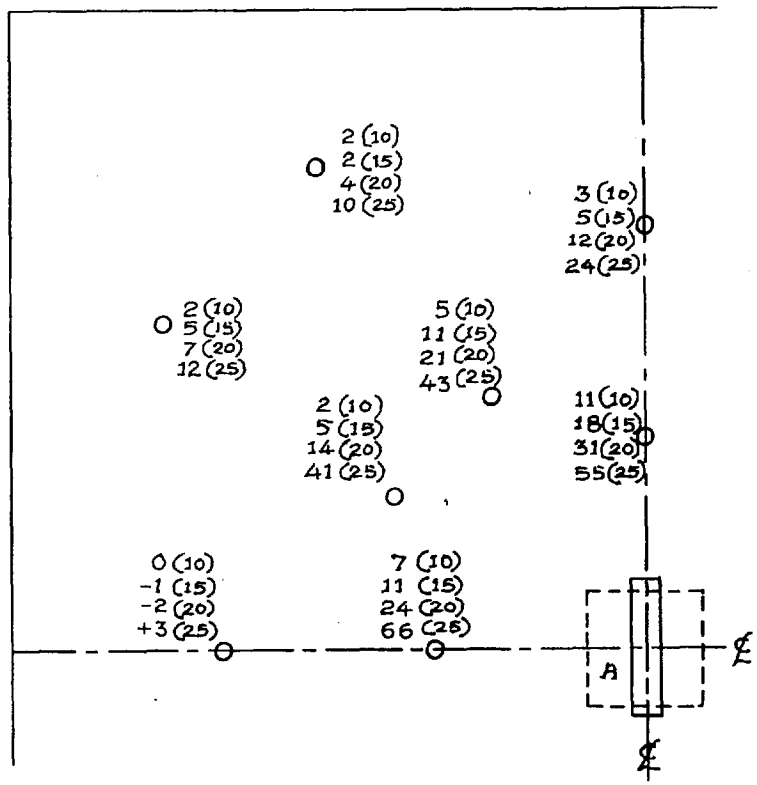


FIG. 136 MAXIMUM PRINCIPAL STRAINS IN THE STEEL PLATE UNDER THE LOAD FOR DIFFERENT LOAD POSITIONS



(a) SLIPS x 10^4 (INCHES) AT VARIOUS CENTRAL LOADS. ARROWS INDICATE DIRECTIONS



(b) UPLIFTS x 10^4 (INCHES) AT VARIOUS CENTRAL LOADS

FIG. 137 SLIPS AND UPLIFTS IN THE PANEL OF THE COMPOSITE PLATE FOR VARIOUS CENTRAL LOADS. CORRESPONDING LOADS IN TONS ARE SHOWN WITHIN BRACKETS. SQUARE LOADING PAD WAS USED AFTER 20 TONS

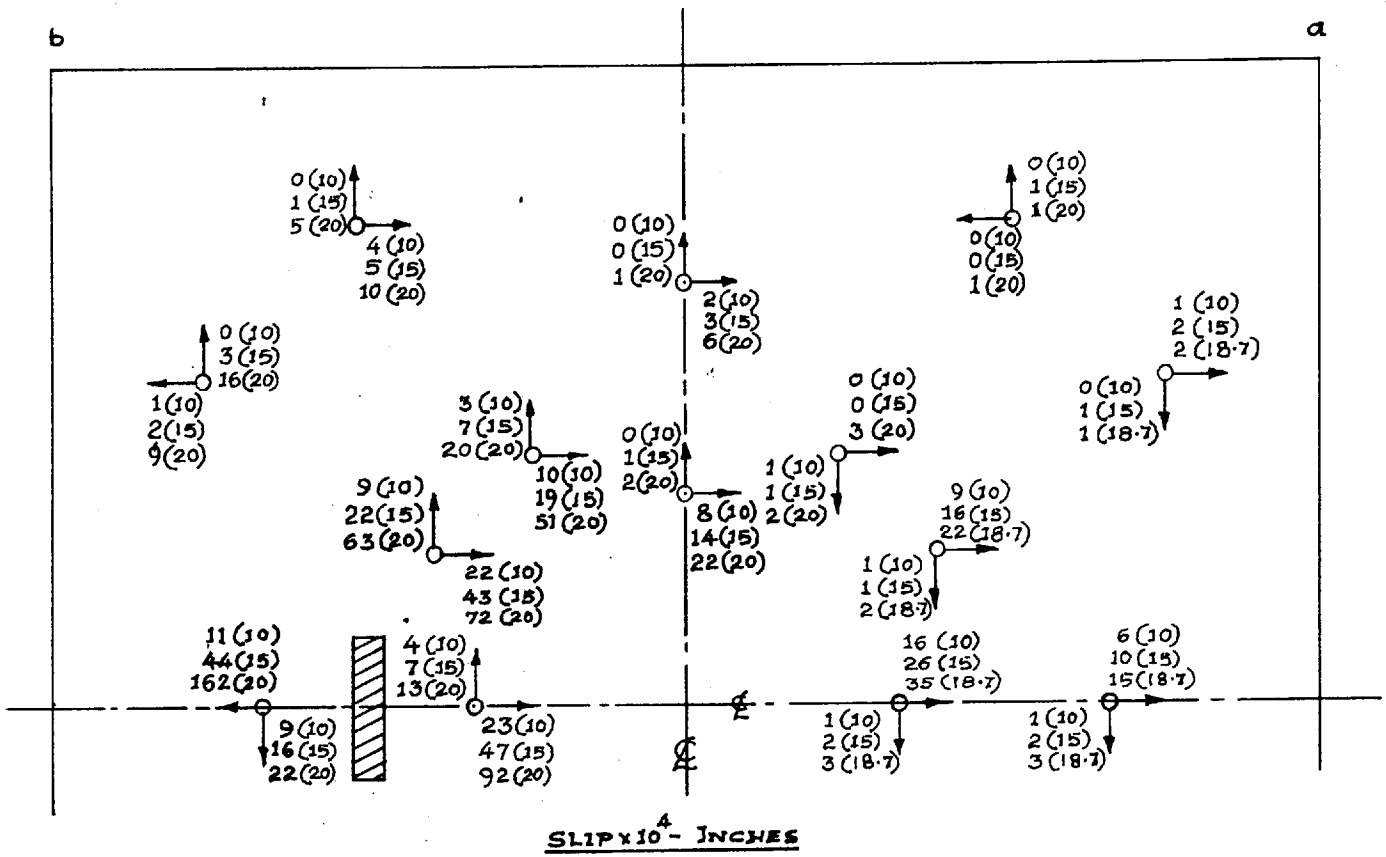


FIG. 138 SLIPS IN THE PANEL OF THE COMPOSITE PLATE FOR LOADS AT POSITION B. CORRESPONDING LOADS IN TONS ARE SHOWN IN BRACKETS. ARROWS INDICATE THE DIRECTIONS OF SLIP.

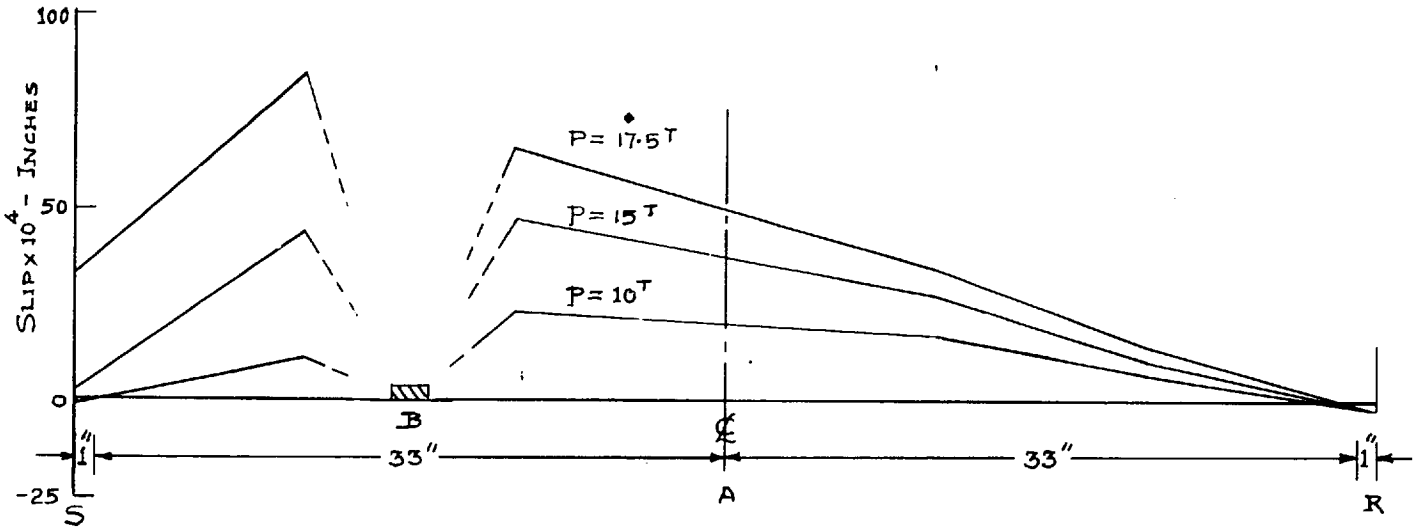


FIG. 139 SLIPS OF THE COMPOSITE PLATE ALONG SAR FOR VARIOUS LOADS AT POSITION B

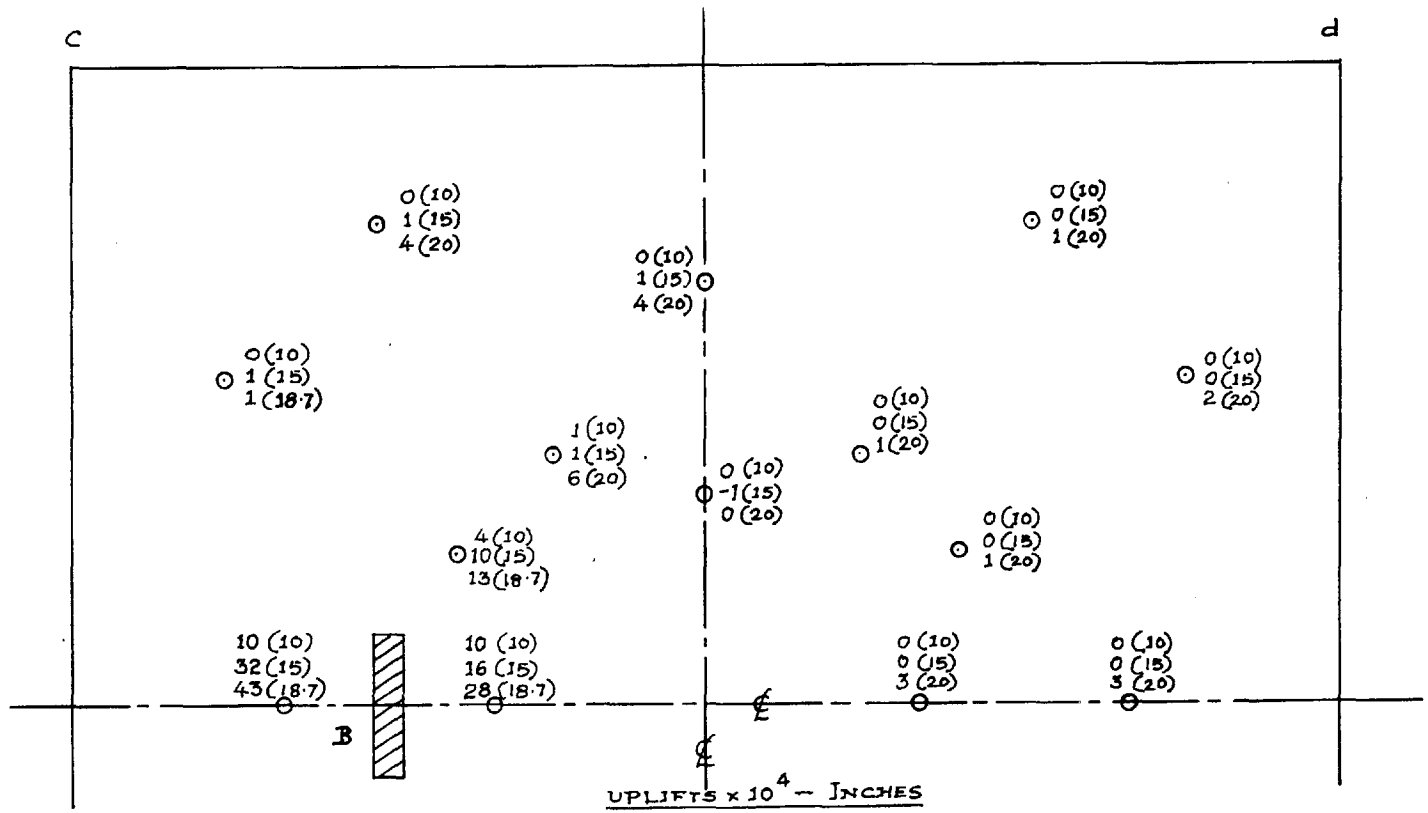


FIG. 140 UPLIFTS IN THE PANEL OF THE COMPOSITE PLATE FOR LOADS AT POSITION B. CORRESPONDING LOADS ARE SHOWN WITHIN BRACKETS

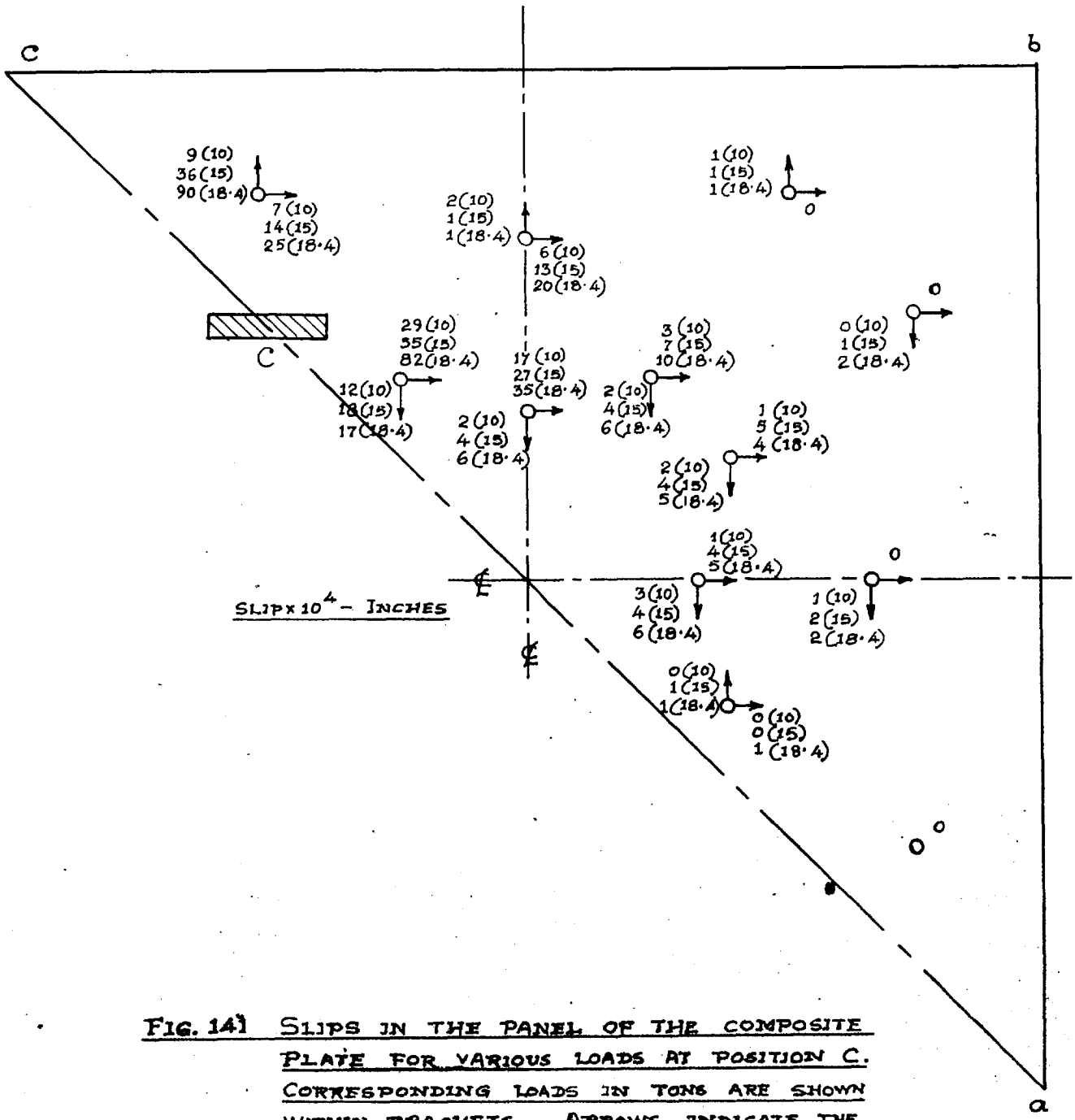


FIG. 141 SLIPS IN THE PANEL OF THE COMPOSITE PLATE FOR VARIOUS LOADS AT POSITION C. CORRESPONDING LOADS IN TONS ARE SHOWN WITHIN BRACKETS. ARROWS INDICATE THE DIRECTIONS OF SLIP.

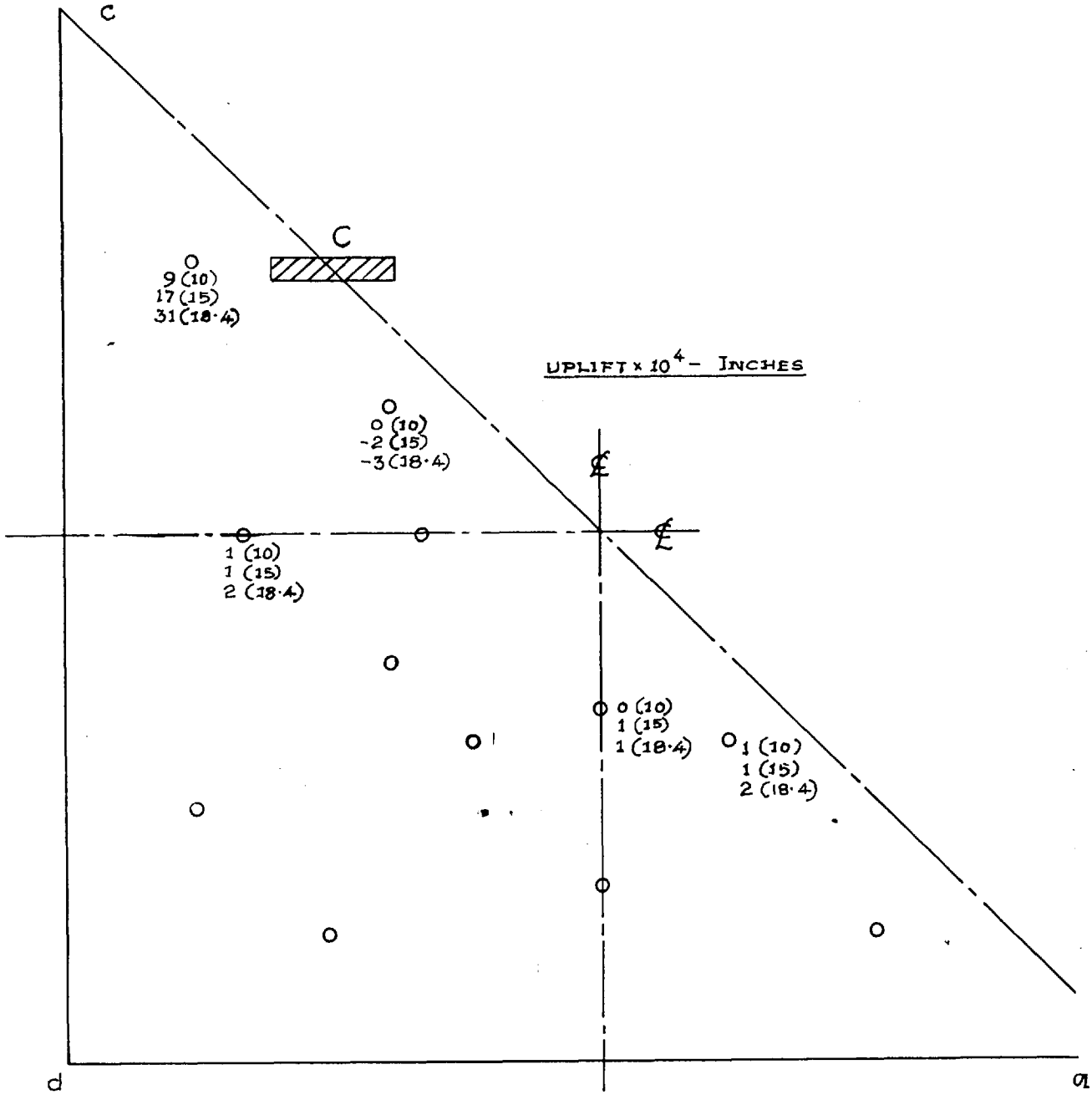


FIG. 142 UPLIFTS IN THE PANEL OF THE COMPOSITE PLATE FOR VARIOUS LOADS AT POSITION C. CORRESPONDING LOADS IN TONS ARE SHOWN WITHIN BRACKETS.



Figure 143. Set up of the composite plate



Figure 144. Underside of the composite plate showing gauges for measuring slip, uplift and deflections



Figure 145. Loaded area of the composite plate after failure

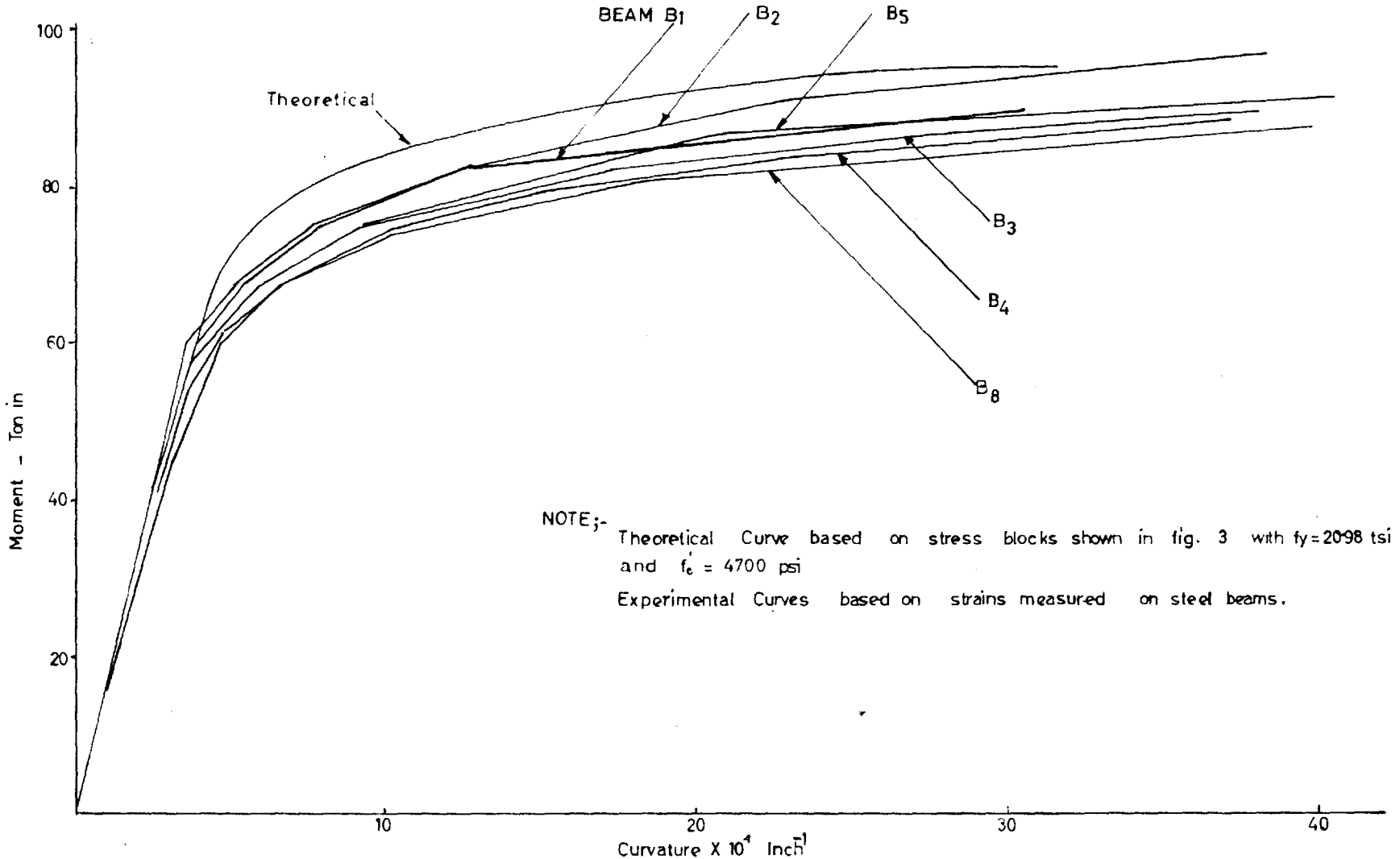


Fig. 146 MOMENT CURVATURE RELATION FOR QUARTER SCALE COMPOSITE BEAMS.

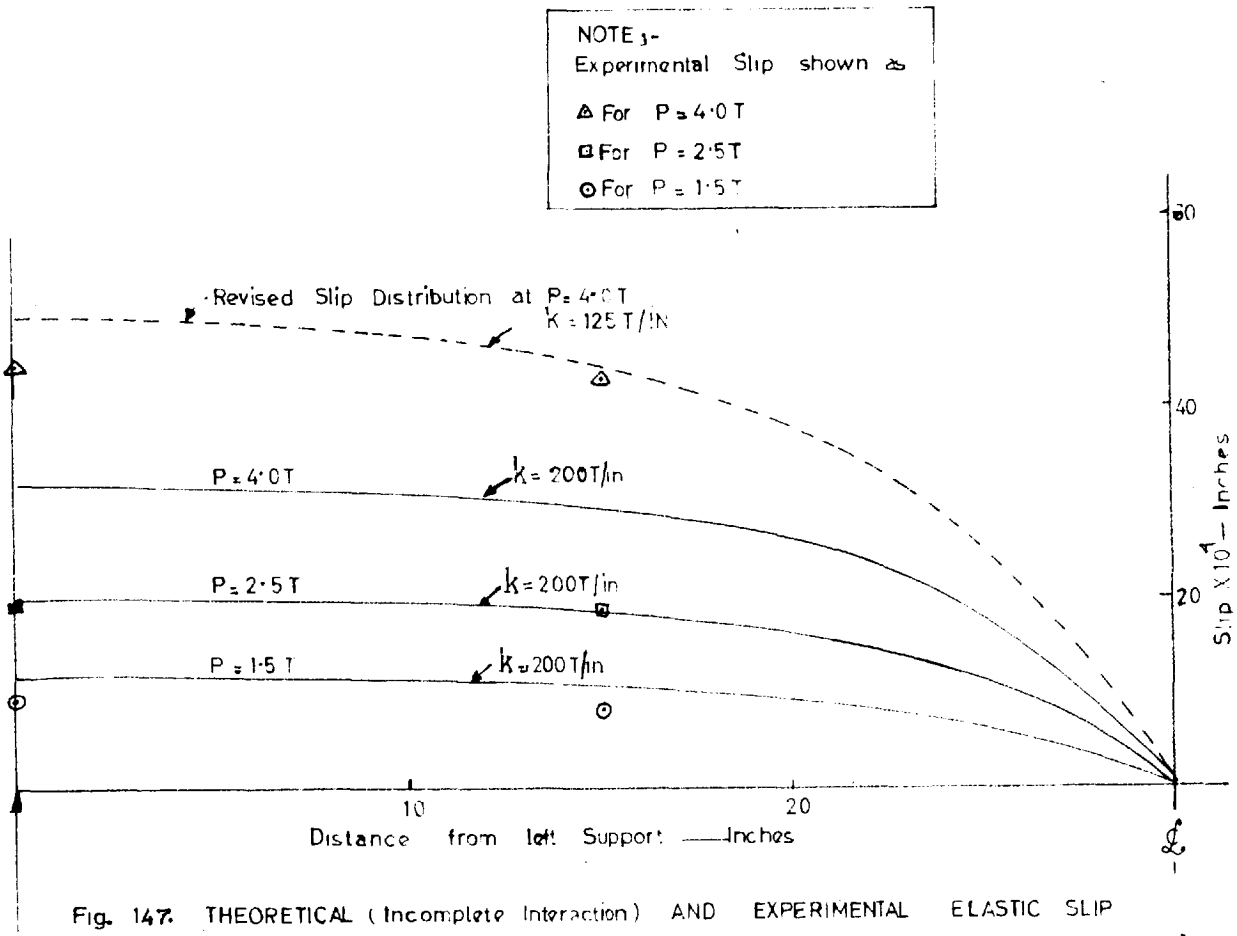


Fig. 147. THEORETICAL (Incomplete Interaction) AND EXPERIMENTAL ELASTIC SLIP DISTRIBUTION —— BEAM B4 WITH STUDS AT 100% (WITHOUT BOND)

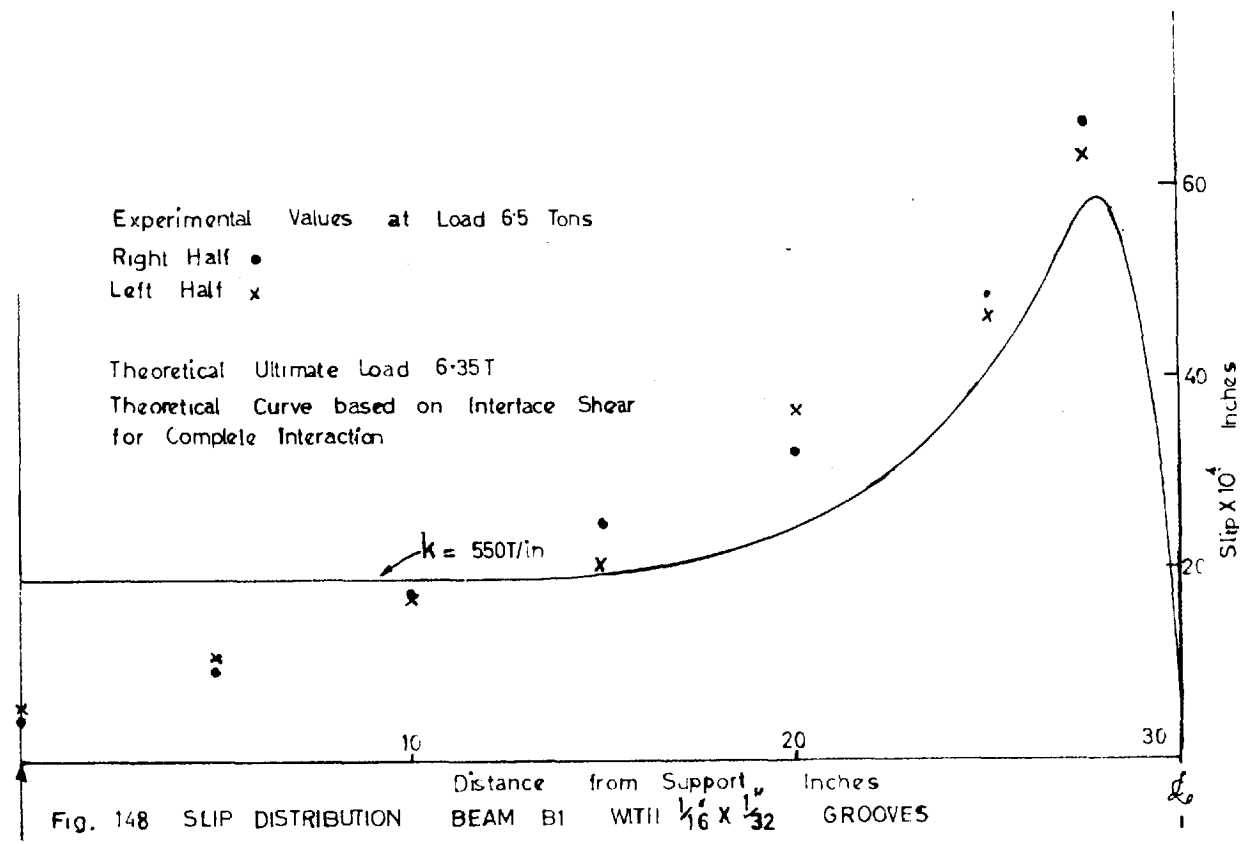


Fig. 148 SLIP DISTRIBUTION BEAM B1 WITH $\frac{1}{16}$" X $\frac{1}{32}$" GROOVES

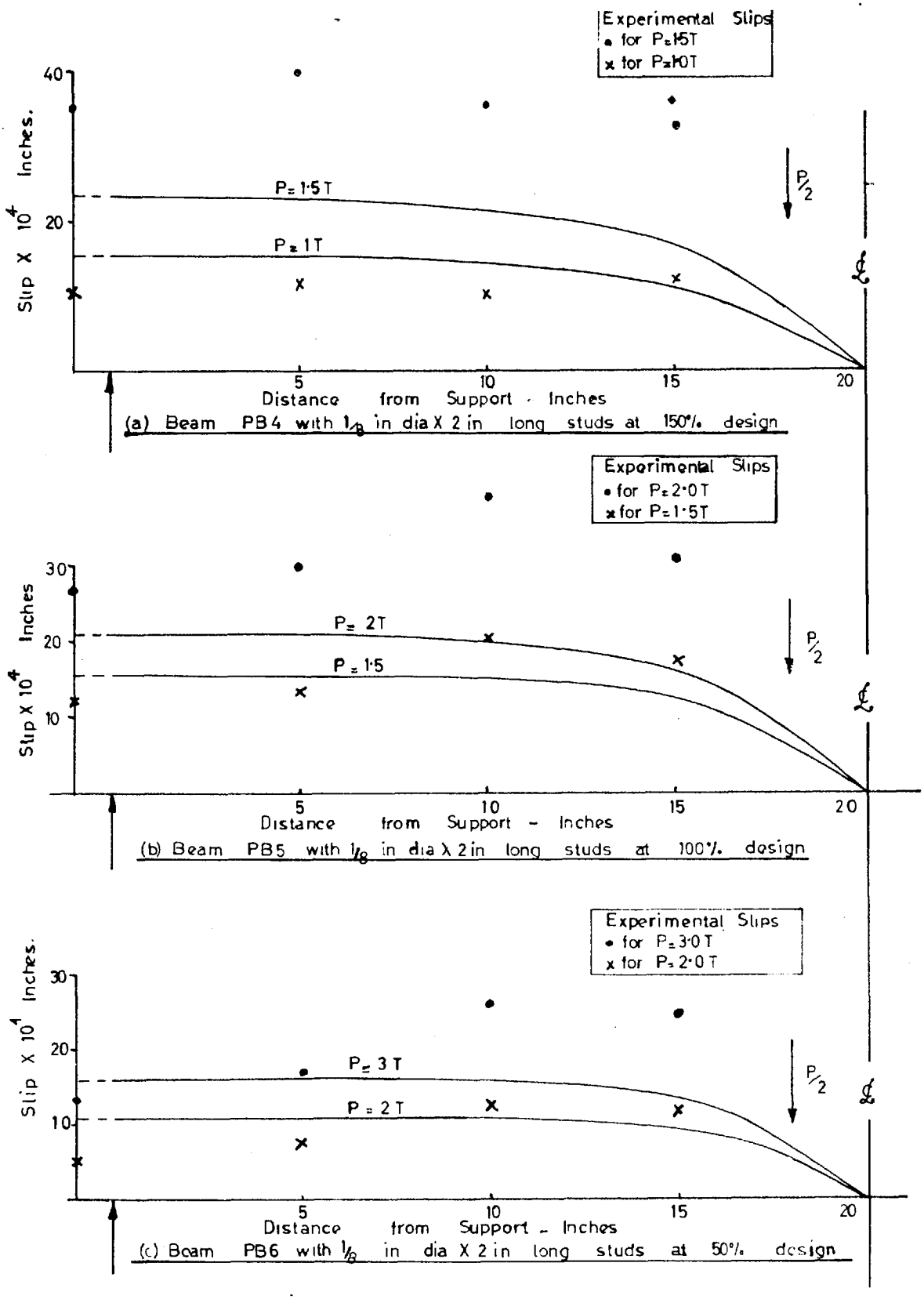
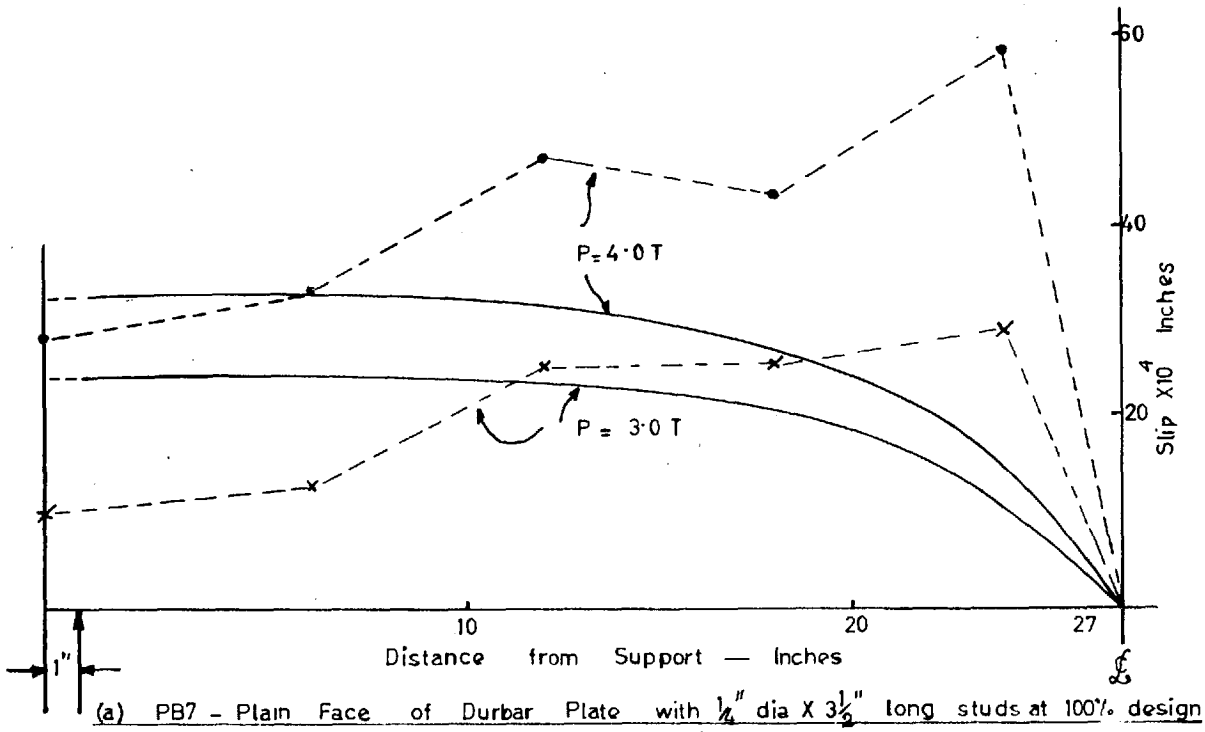
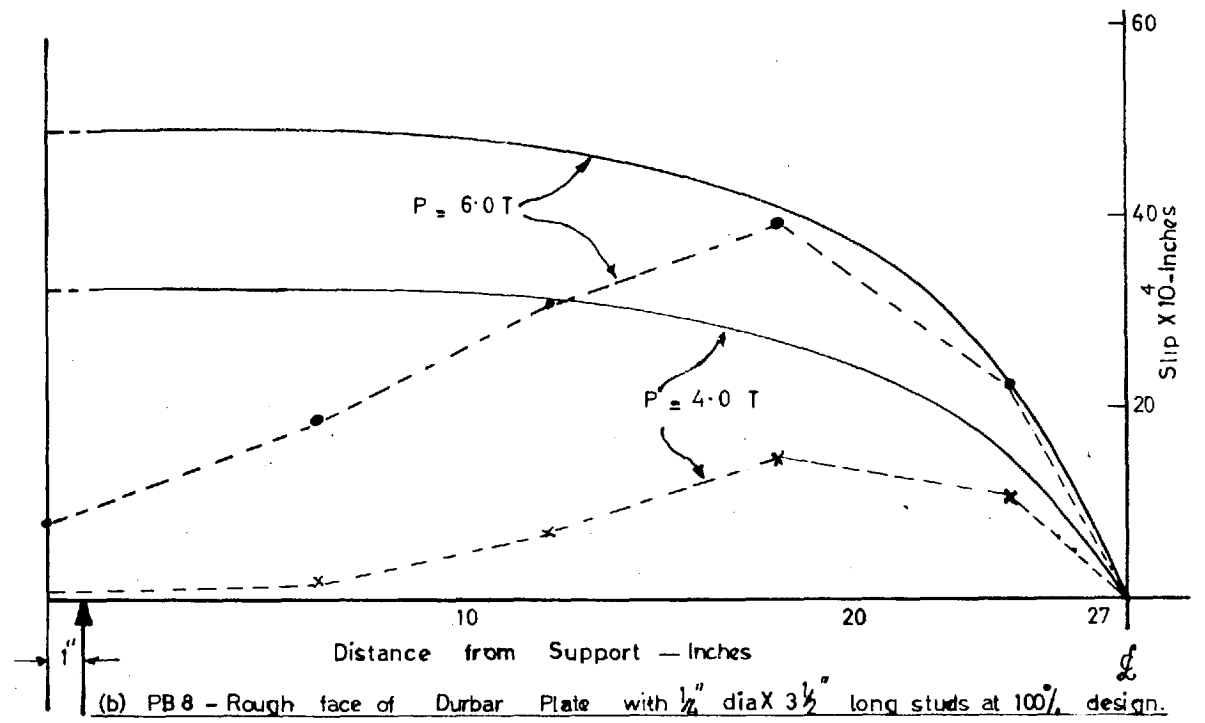


Fig. 149 THEORETICAL AND EXPERIMENTAL SLIP DISTRIBUTION IN SMALL SCALE PLATED BEAMS ($k = 150$ T/in)



(a) PB7 – Plain Face of Durbar Plate with ¼" dia X 3½" long studs at 100% design



(b) PB 8 – Rough face of Durbar Plate with ¼" dia X 3½" long studs at 100% design.

Fig. 150 THEORETICAL AND EXPERIMENTAL SLIP DISTRIBUTION IN PLATED BEAMS WITH DURBAR PLATE. POINT LOAD AT MIDSPAN, THEORETICAL CURVE SHOWN IN FIRM LINE AND EXPERIMENTAL CURVE SHOWN DOTTED $k = 290$ T/IN

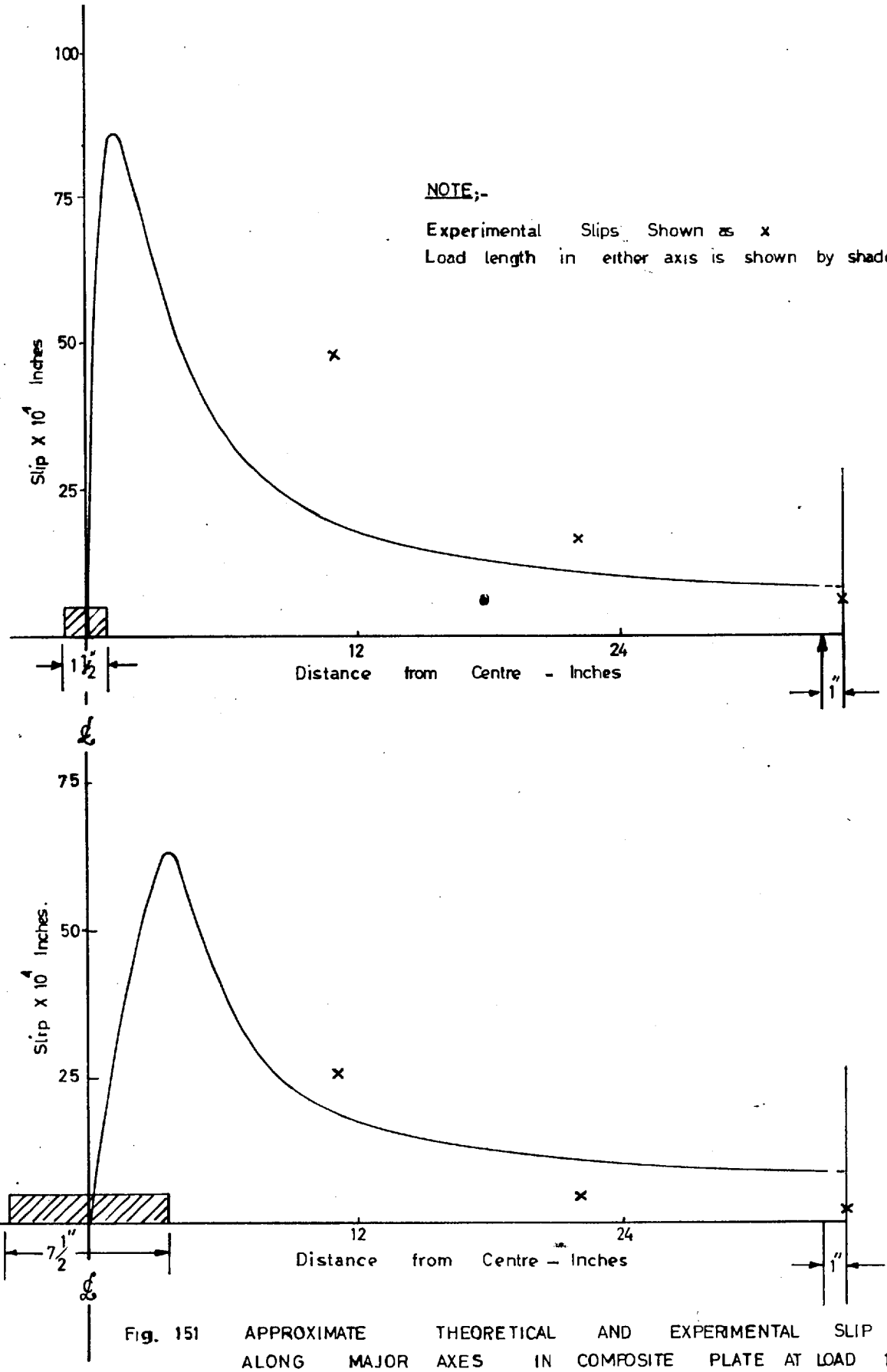


Fig. 151 APPROXIMATE THEORETICAL AND EXPERIMENTAL SLIP DISTRIBUTION ALONG MAJOR AXES IN COMPOSITE PLATE AT LOAD 10 TONS (k = 150 T/in)

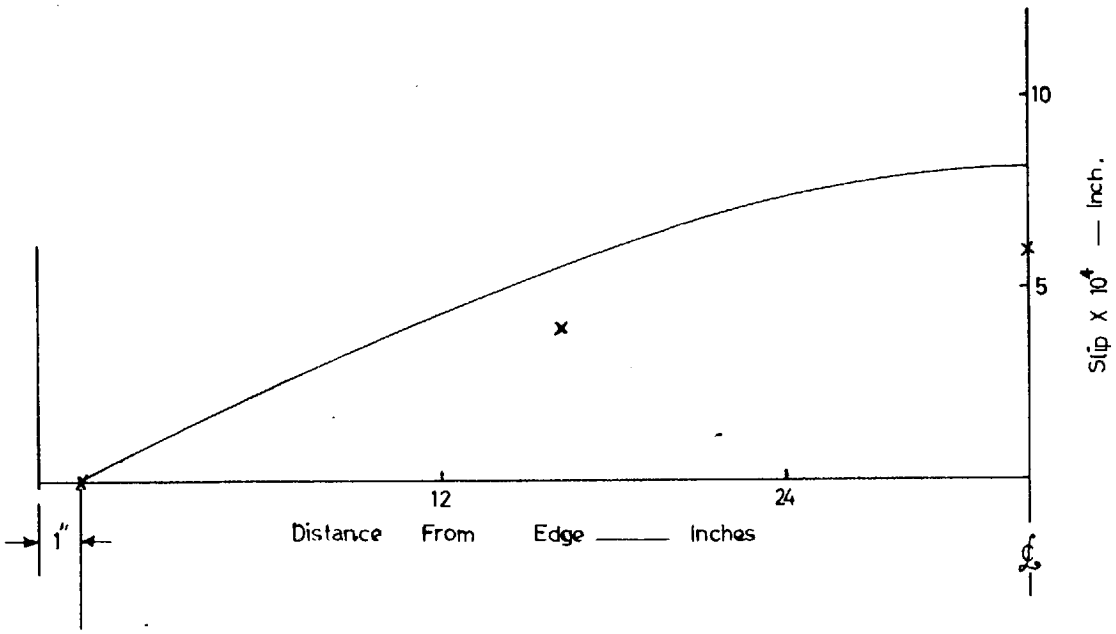


Fig. 152. APPROXIMATE THEORETICAL AND EXPERIMENTAL SLIPS IN COMPOSITE PLATE ALONG EDGE bc FOR LOAD 10 T AT CENTRE. (Experimental values are shown as x) k = 150 T/in

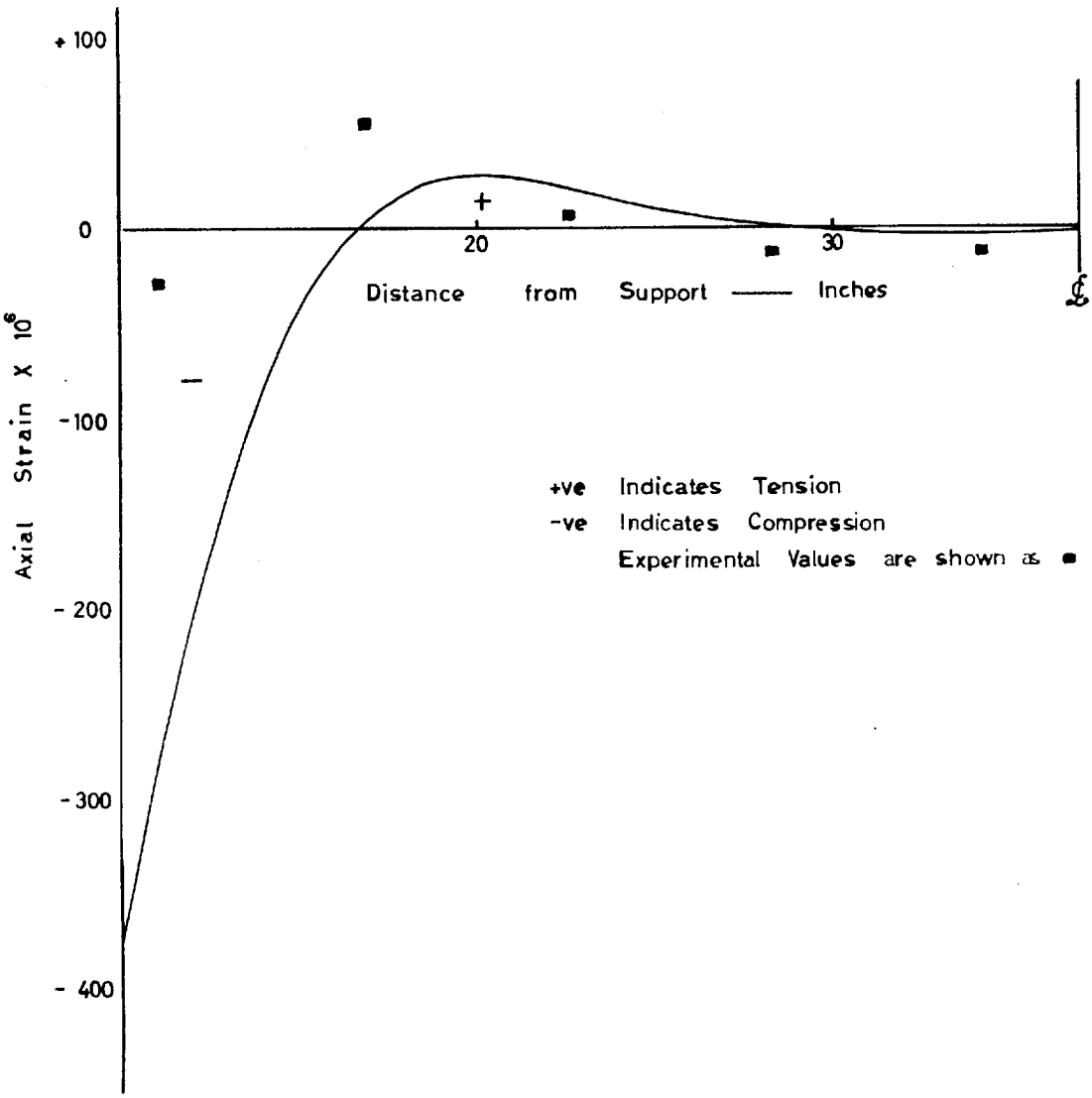


Fig. 153. THEORETICAL AND EXPERIMENTAL AXIAL STRAIN IN STUDS (Beam D_2 with plain face and 56 - $\frac{3}{8}$ in dia X $1\frac{1}{2}$ in long studs at 100% design. Assumed Foundation Modulus k = 115·5 T/in)

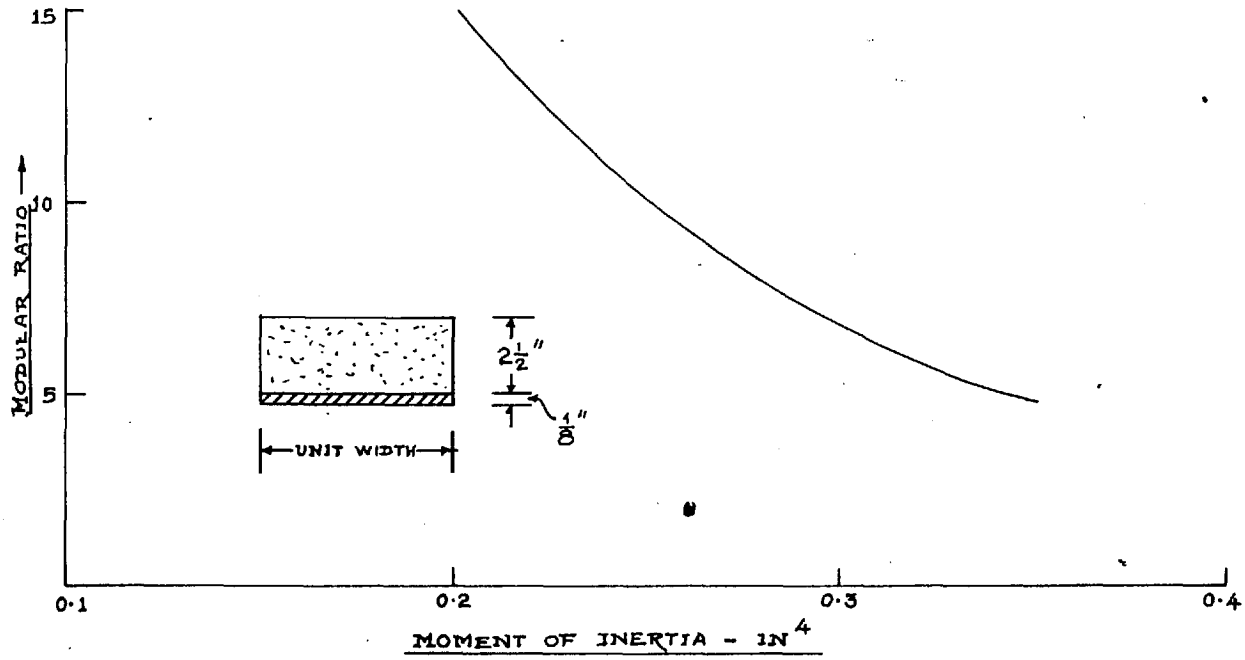
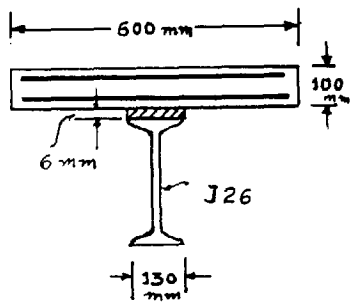


FIG. 154 VARIATION OF MOMENT OF INERTIA PER UNIT WIDTH OF EQUIVALENT SECTION OF A PLATED BEAM (SECTION AS SHOWN) WITH MODULAR RATIO. (CONCRETE IN TENSION NEGLECTED)

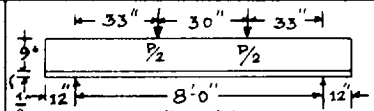
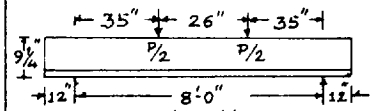
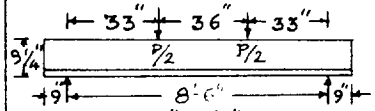
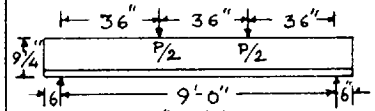
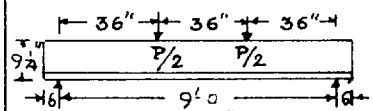
TABLE 1. SUMMARY OF THE RESULTS OF T-BEAMS TESTED BY G. WASTLUND AND L. OSTLUND

Section	Specimen	Shear connection	Load at which bond was exceeded (tons)	Total shear at load of column (4) (tons)	Shear stress at load of column (4) (psi)	Maximum load (tons)	Maximum shear stress (psi)	Concrete strength (psi)	Remark
1	2	3	4	5	6	7	8	9	10
 Span = 3000 mm. Two point loads at $\frac{1}{3}$ rd spans.	1	Plain flange No shear connector Natural bond	6	8	90	12	90	4420	Shear decreased after failure of bond
	2	Chequered plate No shear connector	18	30	334	22	334	3700	
	3	Chequered plate Two connectors on each half of beam	24	41	455	34	556	4380	

Note -

Results are taken from load-deflection, load-shear and shear slip curves.

TABLE 2. SUMMARY OF RESULT OF SOME OF THE PLATED BEAMS TESTED IN THE UNIVERSITY OF ILLINOIS

SPECIMEN	DETAILS OF SPECIMENS	STUD SHEAR CONNECTORS	NO. OF CONNECTORS ON SHEAR SPAN	LOAD/STUD AT FIRST SIGNIFICANT SLIP (kips)	CORRESPONDING BOND STRESS (psi)	BOND STRESS EXPRESSED IN Cy. STRENGTH	MAXIMUM LOAD (kips)	MAXIMUM SHEAR STRESS AT MAXM. LOAD (psi)	SHEAR STRESS EXPRESSED IN Cy. STRENGTH	MAXIMUM SLIP (inches)	CRITICAL LOAD PER STUD (kips)	AVERAGE LOAD PER STUD AT MAXM. LOAD (kips)	REMARK.
1	2	3	4	5	6	7	8	9	10	11	12	13	14
1		9 - ¾" × 4" @ 12" c/c at ℄ 1 stud/sft.	3	15·0	114	$0.019 f_c'$	28·5	149	$0.025 f_c'$	0·1567	16·0	19·6	SHEAR FAILURE
2		18 - ¾" × 4" @ 9" staggered pitch. 2 studs/sft.	6	8·0	114	$0.021 f_c'$	44·0	229	$0.042 f_c'$	0·0564	13·3	16·1	
3		36 - ¾" × 4" @ 6" bothways. 4 studs/sft.	12	4·0	121	$0.021 f_c'$	62·2	324	$0.056 f_c'$	0·0071	x	10·7	FLEXURAL FAILURE
4		24 - ⅝" × 4" @ 10" c/c in pairs 6" apart. 2·4 studs/sft.	8	4·4	92	$0.024 f_c'$	46·2	241	$0.063 f_c'$	0·0552	7·5	13·0	SHEAR FAILURE
5		34 - ½" × 4" @ 7" c/c in pairs 6" apart. 3·4 studs/6ft.	12	3·3	92	$0.021 f_c'$	47·1	246	$0.057 f_c'$	0·0807	5·4	8·8	

NOTE - (a) THE FIRST SIGNIFICANT SLIP HAS BEEN AS THE FIRST MEASURED SLIP OF 0·0006 IN.

(b) THE CRITICAL LOAD PER STUD IS THE LOAD AT WHICH THERE IS AN ABRUPT CHANGE IN THE RATE OF SLIP.

TABLE 3. TENSION TEST RESULTS

BEAM	SPECIMEN	E tsi	YIELD STRESS f_y (tsi)	ULT. STRESS f_u (tsi)	% ELONGATION OVER 10 IN. G.L.	% REDUCTION IN AREA OF X-SECTION	GRAPH TYPE	YIELD STRAIN $\varepsilon_y \times 10^{-4}$	STRAIN HARDENING STRAIN $\varepsilon_{SH} \times 10^{-4}$	$\frac{\varepsilon_{SH}}{\varepsilon_y}$	REMARK
A1, A3, A4	F	12970	20·85	29·69	22·2	52·5	2	16	38	2·4	
	W		17·60	26·60	26·5	54·9	1	14	140	10·0	
A2, B1	F	13720	21·93	29·20	23·5	56·9	1	16	197	12·3	
	W		21·60	28·40	25·5	56·2	1	16	197	12·3	
A5, B2, B3	F	13520	21·47	29·41	23·2	56·2	1	16	187	11·7	
	W		21·10	28·80	25·9	54·0	1	16	156	10·0	
B4, B8	F	13660	22·10	30·40	22·6	56·8	1	16	171	10·7	
	W		20·80	28·40	26·0	60·0	1	15	283	18·9	
B5, B7, C1	F	13360	22·20	31·40	21·8	53·0	1	17	172	10·1	
	W		20·50	28·50	26·0	54·0	1	15	317	21·1	
B6	F_t	13650	18·95	26·49	30·7	39·0	2	14	84	7·0	DURBAR PL.
	W		18·90	29·0	25·3	43·0	1	14	162	11·6	
	F_b	13660	22·10	30·40	22·6	56·8	1	16	171	10·7	
D1	F_t	13400	17·32	26·93	26·2	59·0	1	13	151	11·6	DURBAR PL.
	F_b	13000	20·31	30·13	22·5	53·7	2	16	30	1·9	
D2	F_t	13400	17·32	26·93	26·2	59·0	1	13	151	11·6	DURBAR PL.
	F_b	13000	17·70	28·50	27·8	54·0	3	14	197	14·1	
PB 1,2,3			22·20	31·90	24·6	48·0	1	16	212	13·3	
PB 4,5,6			22·70	31·70	25·2	49·0	1	17	256	15·0	
PB 7,8			19·82	28·47	19·6	50·0	3	15	256	17·1	FAILED OUTSIDE OF G.L.
S1		13630	18·73	25·83	27·5	54·2	1	14	306	21·8	

F = FLANGE W = WEB

Dia. of stud	Specimen number	Dia. of Specimen	area of cross-section ($in.^2$)	Yield load (tons)	Yield stress (t.s.i)	Ultimate load (tons)	Ultimate stress (t.s.i.)
$\frac{3}{16}$ in.	No. 1	0.1785	0.0250	0.770	30.8	0.870	34.8
	No. 2	0.1780	0.0249	0.782	31.4	0.886	35.6
$\frac{1}{4}$ in.	No. 1	0.1785	0.0250	0.755	30.2	0.880	35.2
	No. 2	0.1780	0.0249	0.740	29.7	0.880	35.3
$\frac{3}{8}$ in.	No. 1	0.1790	0.0252	0.810	32.1	0.856	34.0
	No. 2	0.1785	0.0250	0.810	32.4	0.862	34.5
$\frac{3}{4}$ in.	No. 1	0.1780	0.0249	0.755	30.3	0.840	33.7
	No. 2	0.1775	0.0247	0.785	31.8	0.948	38.4

TABLE 4. Properties of stud material

TABLE 5. Small scale push-out tests

Specimen	No. and dia. of stud	Description of flange surface	Useful capacity (tons)	Ultimate capacity (tons)	C_u (psi)	Nature of failure
POA1	0	$\frac{1}{8}$in. x $\frac{1}{16}$in. transverse triangular grooves	0	0	6890	One slab fell off before testing
P3A1	8 - $\frac{3}{16}$		1.75	1.84	6890	All eight studs sheared off
P3A2	8 - $\frac{3}{16}$		1.75	1.94	6440	
P3B1	8 - $\frac{3}{16}$	$\frac{1}{16}$in. x $\frac{1}{32}$in. transverse triangular grooves	1.31	1.56	6880	All four studs on one slab sheared off
P3B2	8 - $\frac{3}{16}$		1.41	1.50	6880	
P3C1	8 - $\frac{3}{16}$	$\frac{1}{32}$in. x $\frac{1}{64}$in. transverse triangular grooves	0.95	1.25	6440	All eight studs sheared off
P3D1	8 - $\frac{3}{16}$	Plain flange with natural bond	0.71	1.08	6490	All four studs on one slab sheared off
P3D2	8 - $\frac{3}{16}$		0.63	1.08	6490	
P3E1	8 - $\frac{3}{16}$	Durbar plated flange	0.92	1.63	6360	Four studs on one slab sheared off
P4E1	8 - $\frac{1}{4}$		1.12	2.00	5450	
P2E1	8 - $\frac{1}{8}$		0.48	0.94	6360	
P2E2	4 - $\frac{1}{8}$		0.50	1.25	5450	Load taken off just before failure
P4D1	8 - $\frac{1}{4}$	Plain flange with natural bond	0.92	1.75	6570	4 studs sheared off; slab cracked
P2D1	8 - $\frac{1}{8}$		0.33	0.51	6570	4 studs on one slab sheared off

Note: Useful capacity is the load on connector at 0.003in. residual slip.

C_u is the average of two 4in. cube strengths.

All connectors are 1in. long plain headed studs.

Specimen	Description of studs	Flange surface	Useful capacity (tons)	Ultimate capacity (tons)	C_u p.s.i.	Nature of failure
P6D1	4-$\frac{3}{8}$ dia. x 1$\frac{1}{2}$in. long plain headed	Plain flange (natural bond)	2.28	2.99	5880	All studs sheared off
P6D2			2.28	3.01	5880	
P12D(TH)	4-$\frac{3}{4}$in. dia. x 4in. long threaded, with head		6.75	13.4	6230	Two studs on one slab sheared off. Slab cracked.
P12D(T)	4-$\frac{3}{4}$in. dia. x 4in. long threaded, without head		6.50	12.5	6230	
P12E1	8-$\frac{3}{4}$in. dia. x 3in. long plain headed	Durbar flange	11.72	14.75	8960	Upper pairs sheared off. Concrete cracked.
P12E(DE)	Double-ended push-out. 16-$\frac{3}{4}$in. dia. x 4in. long plain headed		9.75		8010	

TABLE 6. Half Scale and Full Scale Push-out Test Results

Specimen	Description of studs	Flange surface	Load/stud at failure (tons)	C_u lb/in^2	Nature of failure
PL1	4-$\frac{3}{4}$in. dia. x 4in. long plain headed	Plain flange (natural bond)	3.40	6000	Concrete failed
PL2	4-$\frac{3}{4}$in. dia. x 3in. long plain headed		3.13	6230	Concrete failed
PL3	4-$\frac{3}{4}$in. dia. x 2in. long plain headed		1.34	5750	Concrete failed
PL4	4-$\frac{3}{4}$in. dia. x 4in. long threaded, with head		3.63	7000	Concrete failed
PL5	4-$\frac{3}{4}$in. dia. x 4in. long threaded, without head.		2.73	5290	Studs pulled out

TABLE 7. Full Scale Pull-out Test Results

TABLE 8. SUMMARY OF THE TEST RESULTS OF COMPOSITE BEAMS

SPECIMEN	SHEAR CONNECTION			AT FIRST SLIP SOUND		AT FIRST SIGNIFICANT SLIP		CALCULATED ULTIMATE LOAD		EXPERIMENTAL ULTIMATE LOAD (TONS)	EXPT. ULT. LOAD / CALC. ULT. LOAD		ULT. CAPACITY OF CONNECTORS		$\frac{Q_{uc}\ (beam)}{Q_{uc}\ (P.O.)}$	MAXIMUM END SLIPS AT/NEAR ULT. LOAD		MODE OF FAILURE
	FLANGE SURFACE	NO. OF CONNECTORS	PERCENTAGE DESIGN BASED ON $f_y = 16$ tsi.	LOAD (TONS)	BOND STRESS (PSI)	LOAD (TONS)	BOND STRESS (PSI)	BASED ON WHITNEY (TONS)	BASED ON CP 117 (TONS)		BASED ON WHITNEY	BASED ON CP 117	Q_{uc} (beam) (TONS)	Q_{uc} (P.O.) (TONS)		TOTAL (IN.)	RESIDUAL (IN.)	
1	2	3	4	5	6	7	8	9	10	11	12	13	14	15	16	17	18	19
A1	$\frac{1}{8}$ IN. x $\frac{1}{16}$ IN. GROOVES	32	138	NO SLIP SOUND		5·5	853	6·00	5·79	7·90	1·32	1·36	1·98	1·89	1·05	0·0008 (7·9)	0·0002 (7·91)	FLEXURAL FAILURE
A2	$\frac{1}{16}$ IN. x $\frac{1}{32}$ IN. GROOVES	32	138			4·5	800	6·61	6·30	6·70	1·01	1·06	1·84	1·53	1·20	0·0029 (6·5)	0·0018 (6·5)	
A3	$\frac{1}{32}$ IN. x $\frac{1}{64}$ IN. GROOVES	32	138			5·0	708	6·00	5·84	7·00	1·17	1·20	1·56	1·25	1·25	0·0007 (7·0)	0·0002 (7·0)	
A4	NATURAL BOND	32	138	2·63	401	2·63	401	6·02	5·77	6·50	1·08	1·13	0·96	1·08	0·89	0·0341 (6·4)	0·0256 (6·4)	
A5	BOND DESTROYED	32	138					6·47	6·15	6·10	0·94	0·99	0·88	1·00	0·88	0·0374 (6·0)	0·0261 (6·0)	
B1	$\frac{1}{16}$ IN. x $\frac{1}{32}$ IN. GROOVES	44	100	NO SLIP SOUND		5·0	860	6·60	6·32	7·50	1·14	1·19	1·51	1·53	0·99	0·0012 (7·3)	0·0008 (7·3)	
B2	$\frac{1}{32}$ IN. x $\frac{1}{64}$ IN. GROOVES	44	100			5·8	1009	6·64	6·38	7·40	1·11	1·16	1·48	1·25	1·18	0·0014 (7·4)	0·0008 (7·4)	
B3	NATURAL BOND	44	100	3·45	527	3·45	527	6·62	6·33	6·50	0·98	1·03	1·10	1·08	1·02	0·0337 (6·5)	0·0194 (6·4)	
B4	BOND DESTROYED	44	100					6·55	6·21	6·30	0·96	1·01	0·93	1·00	0·93	0·0338 (6·25)	0·0289 (6·25)	
B5	RESIN BONDED	44	100	NO SLIP SOUND		2·0	302	6·55	6·40	6·60	1·01	1·03	1·00	1·08	0·93	0·0326 (6·5)	0·0266 (6·5)	
B6	DURBAR FLANGE	44	100	2·9	493	2·9	493	6·27	6·10	7·05	1·12	1·16	1·29	1·63	0·79	0·0254 (7·0)	0·0232 (7·0)	
B7	STUD ROOT COVERED WITH LATEX	44	100	1·5	228	1·5	228	6·60	6·37	6·50	0·98	1·02	0·56	1·08	0·52	0·1312 (6·5)	0·1168 (6·5)	
B8	NATURAL BOND	44	100	2·5	378	2·5	378	7·25	6·94	6·96	0·96	1·00	1·11	1·08	1·03	0·0337 (6·8)	0·0280 (6·8)	
C1	NATURAL BOND	44	100	3·1	473	3·0	458	6·35	6·18	6·25	0·98	1·01	0·97	1·08	0·90	0·0373 (6·1)	0·0270 (6·1)	
D1	DURBAR FLANGE	56	100	NO SLIP SOUND		7·5	239	28·27	27·46	31·3	1·11	1·14	4·38	3·00	1·46	0·0116 (31·3)	0·0064 (31·0)	FLEXURAL FAILURE
D2	NATURAL BOND	56	100	14·0	444	10·0	317	25·05	24·57	26·0	1·04	1·06	3·66	3·00	1·21	0·0385 (26·0)	0·0322 (26·0)	CONC. AROUND STUDS FAILED.

NOTE (a) 3/16 IN. DIA. x 1 IN. LONG HEADED STUDS WERE USED IN ALL BEAMS EXCEPT D1 AND D2 WHERE 3/8 IN. DIA. x 1½ IN. LONG HEADED STUDS WERE USED.

(b) STUDS WERE SPACED UNIFORMLY IN ALL BEAMS EXCEPT C1 WHERE THE SPACING WAS ACCORDING TO THE INTERFACE SHEAR AT COLLAPSE

(c) FIRST SIGNIFICANT SLIP IS TAKEN AS THE FIRST MEASURED SLIP OF 0·0005 IN.

(d) CALCULATED ULT. LOAD IS BASED ON ACTUAL STEEL & CONC. STRENGTH.

(e) SLIPS OF COLUMNS 17 AND 18 WERE RECORDED AT LOADS IN TONS SHOWN WITHIN BRACKETS.

Table 9. Summary of results of material tests for composite beams

Beam	4in. cube psi	12" x 6" cylinder psi	E_c psi x10^6	Age at testing days	Yield stress t.s.i.		Ult. stress t.s.i.		Remark
					web	flange	web	flange	
A1	6890	4480	4.62	22	17.60	20.85	26.60	29.69	
A2	6800	4700	3.60	22	21.60	21.93	28.40	29.20	
A3	6560	4550	4.06	21	17.60	20.85	26.60	29.69	
A4	6750	4700	4.14	20	17.60	20.85	26.60	29.69	
A5	6580	4590	3.70	22	21.10	21.47	28.80	29.41	
B1	6900	4650	4.06	22	21.60	21.93	28.4	29.20	
B2	7890	5650	3.62	42	21.10	21.47	28.80	29.41	
B3	7650	5500	4.14	36	21.10	21.47	28.80	29.41	
B4	6570	4700	3.89	22	20.80	22.10	28.40	30.4	
B5	7850	4750	4.12	27	20.50	22.20	28.50	31.4	
B6	6360	- 4000	4.06	21	18.90	18.95 22.10	29.00	26.49 30.40	Durbar M.S.
B7	7600	5020	4.13	45	20.50	22.20	28.50	31.4	
B8	6750	4550	4.35	28	20.80	22.10	28.4	30.4	
C1	6480	3920	4.15	21	20.5	22.2	28.5	31.4	
D1	7880	5200	4.65	206	--	17.32 20.31	--	26,93 30.13	Durbar M.S.
D2	7870	4850	4.82	61	--	17.32 17.70	--	26.93 28.5	Durbar M.S.

TABLE 10. SUMMARY OF PLATED BEAM TEST RESULTS

Specimen	Shear Connection: Nature of Interface	Shear Connection: Number, Dia. and Length of Studs (in.)	Shear Connection: Longitudinal and Transverse Spacing (in.)	Shear Connection: Percentage Design Based on f_y = 16 tsi.	At First Significant Slip: Load (tons)	At First Significant Slip: Bond Stress (psi)	Calculated Ultimate Load: Based on Whitney (tons)	Calculated Ultimate Load: Based on CP 117 (tons)	Experimental Ult. Load (tons)	Expt. Ult. Load / Calc. Ult. Load: Based on Whitney	Expt. Ult. Load / Calc. Ult. Load: Based on CP 117	Maxm. Shear Stress at Ult. Load (psi)	Maxm. Shear Stress Expressed in Cylinder Strength	Average Load per Connector at Ult. Load (tons)	Col 15 / Q_{uc} (P.O.)	Maxm. End Slip at/near Ult. Load: Total (in.)	Maxm. End Slip at/near Ult. Load: Residual (in.)	Mode of Failure
1	2	3	4	5	6	7	8	9	10	11	12	13	14	15	16	17	18	19
PB2	Natural Bond	24 – 3/16" × 1"	3" × 3"	100	1·0	102	2·74	1·89	2·40	0·88	1·27	244	$0·057 f'_c$	0·85	0·79	0·0140	0·0111	Diagonal Tension
PB3	Bond Destroyed	24 – 3/16" × 1"	3" × 3"	100			2·63	2·04	2·25	0·86	1·10	228	$0·057 f'_c$	0·91	0·84	0·0148	0·0101	Diagonal Tension
PB4	Natural Bond	36 – 1/8" × 2"	2" × 3"	150	0·9	80	2·93	2·66	2·05	0·70	0·77	183	$0·050 f'_c$	0·49	0·96	0·0294	0·0246	Shearing of Studs
PB5	Natural Bond	54 – 1/8" × 2"	2" × 2"	100	1·0	89	2·81	2·53	2·97	1·06	1·17	256	$0·074 f'_c$	0·54	1·06	0·0280		Shearing of Studs
PB6	Natural Bond	108 – 1/8" × 2"	2" × 1"	50	1·25	111	3·04	2·73	3·75	1·23	1·37	333	$0·086 f'_c$	0·31	0·61	0·0026	0·0016	Flexural Failure
PB7	Plain Face of Durbar Plate	36 – 1/4" × 3 1/2"	3" × 4 1/2"	100	3·0	117	6·11	5·78	5·45	0·89	0·94	212	$0·060 f'_c$	1·66	0·95	0·0119		Shearing of Studs
PB8	Rough Face of Durbar Plate	36 – 1/4" × 3 1/2"	3" × 4 1/2"	100	3·0	117	6·05	6·03	7·80	1·29	1·29	302	$0·080 f'_c$	2·38	1·36	0·0028	0·0025	Flexural Failure

NOTE – First significant slip is taken as the first measured slip of 0·0005 in.
Calculated ultimate load is based on experimentel steel and concrete strength.

Beam No.	Steel		Concrete				
	yield stress t.s.i.	ultimate stress t.s.i.	4" cube strength p.s.i.	12" x 6" cylinder strength p.s.i.	E_c p.s.i.	Age at testing days	Remarks
PB1	22.2	31.9					Failed before testing
PB2	22.2	31.9	5450	4310	3.31×10^6	19	
PB3	22.2	31.9	5800	4030	3.44×10^6	15	
PB4	22.7	31.7	6160	3650	4.45×10^6	19	
PB5	22.7	31.7	5830	3450	4.25×10^6	16	
PB6	22.7	31.7	6350	3880	4.64×10^6	34	
PB7	19.82	28.47	6200	3560	4.52×10^6	21	Durbar plate $\frac{3}{16}$ in. thick
PB8	19.82	28.47	6660	3500	4.92×10^6	24	
S1	18.73	25.83	7470	4500	5.20×10^6	8 months	

TABLE 11. Summary of results of material tests for plated beams and composite plate